KU LEUVEN

ARENBERG DOCTORAL SCHOOL
Faculty of Engineering Science

Macro-Scale Flow and Heat Transfer in Systems with Periodic Solid Structures

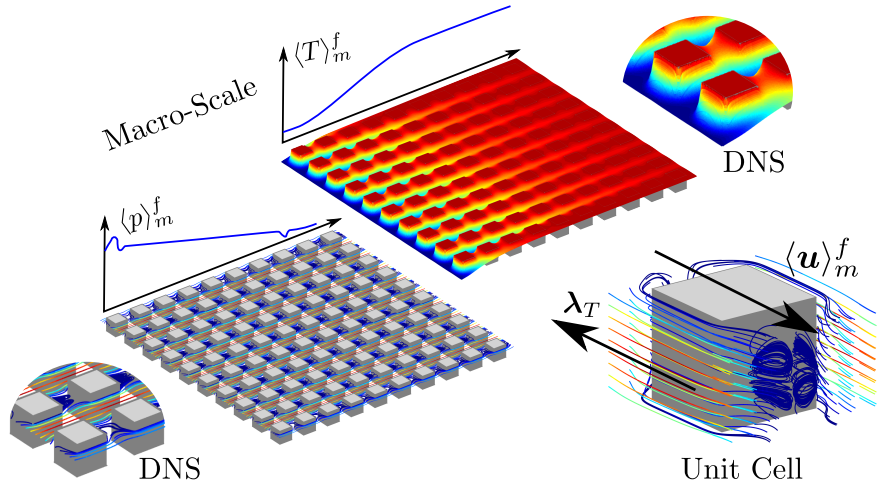

ir. Geert Buckinx

Supervisor:
Prof. dr. ir. Martine Baelmans

Dissertation presented in partial fulfillment of the requirements for the degree of Doctor of Engineering Science (PhD): Mechanical Engineering

January 2017

Macro-Scale Flow and Heat Transfer in Systems with Periodic Solid Structures

ir. Geert BUCKINX

Examination committee:
Prof. dr. ir. Hendrik Van Brussel, chair
Prof. dr. ir. Martine Baelmans, supervisor
Prof. dr. ir. Johan Meyers
Prof. dr. ir. Dirk Roose
Prof. dr. Michel Quintard
(Institut de Mécanique des Fluides de Toulouse)

Prof. dr. Anthony G. Straatman
(Western University, Canada)

Dissertation presented in partial fulfillment of the requirements for the degree of Doctor of Engineering Science (PhD): Mechanical Engineering

January 2017

Uitgegeven in eigen beheer, ir. Geert Buckinx, Celestijnenlaan 300A box 2421, B-3001 Leuven (Belgium)

PREFACE - VOORWOORD

Het is vrijdagavond. Onder mijn handpalmen ligt een dikke stapel papier met daarop de woorden *Macro-Scale Flow and Heat Transfer in Systems with Periodic Solid Structures*. Ook mijn naam staat erbij en de afkorting *ir.* gaat eraan vooraf. Het lijkt te suggereren dat deze dikke stapel papier mijn eigen werk is, al weet ik dat dat een leugen is. Dit werk was immers niet mogelijk geweest zonder alle mensen die naast mij hebben gestaan de afgelopen vijf jaar. Ik ben jullie, mijn collega's, familie en vrienden, daarom enorm dankbaar. Vond ik maar de juiste woorden om mijn dankbaarheid neer te schrijven in dit voorwoord ... Misschien kan ik jullie beter danken door samen een pint te klinken, het is tenslotte vrijdagavond.

Laat me eerst mijn promotor Tine Baelmans in het bijzonder danken. Tine, ik dank je voor alle kansen en vrijheid die je me in mijn onderzoek gegeven hebt. Je bent een onuitputtelijke bron van enthousiasme voor je onderzoeksgroep. Tijdens onze discussies waren jouw kennis en inzicht steeds waardevolle richtingwijzers voor mij. Ook buiten de muren van onze universiteit, denk maar aan de de Oude Markt van Leuven of de hotelbars in Kyoto en Atlanta, hebben we vaak gebabbeld over wat ons bezighoudt als onderzoeker. Gelukkig maakten onze serieuze gesprekken

ook vaak plaats voor verhalen en gelach die niets met ons onderzoek te maken hadden.

I would like to thank the jury members for critically reviewing the manuscript and making valuable suggestions to improve the text. In addition, I would like to thank each of the jury members for the interesting discussions before, during and after the preliminary defence.

Ik ben het Agentschap voor Innovatie door Wetenschap en Technologie (IWT) dankbaar voor de financiële steun van mijn doctoraatsonderzoek. Wat een geluk dat zulke beurzen bestaan en dat ik er een mocht krijgen! Bovendien was mijn onderzoek niet mogelijk geweest zonder de infrastructuur van het Vlaams Supercomputer Centrum, met steun van de Herculesstichting en de Vlaamse Overheid - departement EWI. Bedankt, Martijn Oldenhof, voor jouw waardevolle hulp bij het gebruik van de rekenclusters.

Daarnaast wil ik Frederik Rogiers, Tijs Van Oevelen en Ruben Gielen heel erg bedanken. Frederik, Tijs en Ruben, tijdens mijn doctoraat zijn jullie mijn mentors in de fluïdummechanica, warmteoverdracht en thermodynamica geweest. Ongetwijfeld zijn de ideeën die aan de grond liggen van dit werk mede het resultaat van jullie mentorschap. Frederik, ik wil je bedanken omdat je mijn doctoraatsonderzoek hebt helpen lanceren. Ik ben blij dat ik jouw geesteskind FVMLab tot een volwaardige CFD-code heb mogen verder ontwikkelen. Ruben, bedankt om zo een toffe collega, vriend en af en toe zelfs een moreel kompas te zijn. Ik kijk al uit naar jouw trouw dit jaar!

Ook de andere collega's van onze onderzoeksgroep wil ik hier even kort bedanken. Wouter Dekeyser en Tom Saenen, jullie hebben me veel geleerd, bijvoorbeeld dat kernfusie en tweefasenstromingen te complex zijn voor mij. Ik apprecieer jullie enorm, zowel als onderzoekers als collega's. Joris Coddé, Niels Horsten, Kristel Ghoos, Paul Lacko, Bart Peremans, Yang Zhou, Xu Huang and Tiwei Wei, it has been a pleasure to work with each of you. Paul, Bart and Yang, I hope to have been a mentor for you, hopefully even to the same extent as our older colleagues have been mentors for me. Nevertheless, I am convinced that you have so much potential that very soon I will have a lot to learn from you. Federica Maggioni, thank you for being such a friendly colleague, I really enjoyed our trips during the conference in Kyoto. Maarten Blommaert, met jou heb ik al meerdere vrijdagen (en weekdagen, als we eerlijk zijn) een pint

teveel gedronken. Ik zal daarom een andere manier bedenken om jou te danken.

Ik heb altijd graag de oefenzittingen thermodynamica gegeven met Anouk Bosmans en Tijs Van Oevelen, en later met Arnout Aertgeerts en Niels Horsten. Dankjewel, Anouk en Arnout, voor de vele persoonlijke gesprekken die we daarbij hadden. Met veel passie heb ik geprobeerd de oefenzittingen fluïdummechanica toegankelijker te maken voor onze ingenieursstudenten. Met veel minder passie heb ik de examens fluïdummechanica de afgelopen jaren verbeterd. Bedankt Joris Gillis, Damien Picard en Paul Lacko om achtereenvolgens me te helpen bij het verbeteren van die vijftig dozen examenvragen en de studenten steeds feedback te geven.

Considering that this work has been completed in our office room 01.51 at the department of mechanical engineering, I also owe my former office mates a debt of gratitude. Thank you, Jeroen Vandewalle, Anouk Bosmans, Eric Zhong, Shivanand Wasan and Ercan Atam, for making our office feel like a second home, although I am glad that we never had to sleep there. Furthermore, I would like to thank my current office mates, Kris Poncelet, Pieter Bauweraerts, Bram van der Heijde, Yang Zhou and Liang Fang, for the great atmosphere in our office. Yes, we still have the best office.

Bedankt Dieter Patteeuw, Brecht Baeten, Clara Verhelst, Roel De Coninck en Bart Saerens om mijn ecologisch bewustzijn te vergroten. Ik bewonder jullie idealisme en ben ervan overtuigd dat we met jullie ingesteldheid en expertise de klimaatsverandering kunnen keren. Dieter, het maakt me gelukkig zo een goede vriend als jou te hebben. Een reclamebord (voor warmtepompen) beter dan jou kan het westen van ons land zich niet wensen. Brecht, ik beloof voortaan terug de tonijn uit mijn voedselpiramide te schrappen, nog voor de laatste tonijn op aarde op mijn bord belandt.

Mijn dank gaat ook uit naar Dries Allaerts, die me steeds hielp met de pux 'n kux te bevoorraden. Tezamen met Ruben Gielen wisten we potentiële hongersnoden uit ons departement te bannen. Thomas Haas en Nicholas Agon, jullie zijn twee toffe kerels waar ik in de toekomst nog vaker mee hoop af te spreken. Maarten Vanierschot, het doet me plezier telkens weer van jou een vriendelijke goedendag te krijgen, zelfs al loop je daarna steeds snel van me weg. Bedankt ook, Andreas Belderbos, Mats Vande Cavey, Filip Jorissen, Mathias Hermans en Kenneth Vanden Bergh, voor

de animo op de werkvloer en op onze vele TME-activiteiten.

Verder ben ik dankbaar voor de uiterst plezante middaggesprekken, recepties en TME-weekends met collega's zoals Stefan Antonov, Nico Keyaerts, Jan Timmermans, Jan Hoogmartens, Daniël Walraven, Lieven Vervecken, Joachim Verhelst en Sarah Van Erdeweghe. De meesten van jullie hebben TME al even verlaten, maar onze goede herinneringen heb ik nog vaak opgehaald bij onze twee plezante anciens, Erik Delarue en Maarten Sourbron.

Wim Munters, Juliaan Bossuyt, Vahid Bokharaie, Jorge Mau and Thanos Vitsas, your names are forever connected to our happy hour tradition on Fridays. Thank you for all the fun we had those nights, were we in Leuven, Gent or even around Stuttgart.

Special thanks go to Asim Önder, Jay Goit and Vladimir Jovanovic, who I could bother with so many questions about CFD algorithms.

Juliana Zapata Riveros, gracias por tu amable sonrisa en los pasillos de nuestro departamento. Ana Luísa Rodrigues, obrigado por seu sorriso amigável nos corredores do nosso departamento. Alessia Arteconi, grazie per il suo sorriso amichevole nei corridoi del nostro reparto. Cornelia Nita, Sepideh Hosseinzadeh, Emre Yilmaz and Dejian Wu, thank you for being so kind to me every day.

Mijn oprechte dank gaat eveneens uit naar Valérie Karlshausen, Marina Siebens, Karin Dewit, Kathleen Coenen en Frieda Decoster, die steeds voor me klaar stonden om me te helpen met de organisatie van vergaderingen, examens, conferenties en uiteindelijk ook mijn doctoraatsverdediging. Eerlijk toegegeven, soms kwam ik ook wel eens langs omdat ik graag met jullie zever. Dat laatste geldt in het bijzonder voor Hans Van Eyken en Ivo Lamberts, onze twee beste werkmannen die me vaak met hun fratsen en (vuile) moppen aan het lachen brengen.

Tijdens mijn doctoraat heb ik veel plezier gehad in ons huisje in de Schepenenstraat met Britte Opdekamp, Jeroen Francois en Jan Boelanders. Bedankt ook Jan Boelanders, Sien Houbrechts en Kelly Hilven om zulke aangename huisgenoten te zijn in de Naamsestraat.

Een dikke merci is bestemd voor mijn favoriete drieling, Lien Brands, Lore Brands en Veerle Nijs, evenals mijn partner in crime, Hanne Snoeks, om me zo te steunen in de slotfase van mijn doctoraat (over alle jaren ervoor

ga ik hier niet uitwijden). Jort Moermans, Souz Vanhooymissen, Kenneth Bruninx, Nikki Janssens, Anne Dreesen en Dorien Martens, bedankt om me van onze middelbare-schooljaren tot universiteitsjaren als vriend te blijven appreciëren. Maak jullie maar klaar, want ik heb nu iets met jullie te vieren!

Hoewel dit voorwoord ondertussen een veel te lang stilistisch gedrocht geworden is, wil ik toch nog mijn burgiebuds Mathias Coomans, Jonas van den Heuvel, Dries Schreurs en Jan Vangenechten bedanken voor hun interesse in mijn vrije tijd en hun desinteresse in mijn onderzoek.

Mijn laatste dankwoord houd ik voor mijn ouders Xavier Buckinx en Chris Désiron, mijn zussen Eline en Hanne en onze kat Whiskers. Mijn grootste geluk is dat ik met jullie mijn leven kan delen. Ik ben trots op zo een warme familie. Al moet ik toegeven dat voorzetsels zoals *ir.* en binnenkort ook *dr. ir.* mij eerder onverschillig laten, ik hoop dat ze jullie ook een beetje trots op mij maken. Whiskers, jij bent het enige familielid dat deze stapel papier ondertussen in al zijn facetten doorgrond heeft. Ik zal daarom mijn toekomstige titel met je delen: Proficiat, dr. Whiskers!

ABSTRACT

This work treats the macro-scale description of flow and heat transfer in systems with spatially periodic solid structures, like compact heat exchangers and heat sinks with fin arrays or tube bundles. The presented macro-scale description allows us to extract the physically meaningful overall characteristics of the very detailed flow velocity, pressure and temperature fields in a heat transfer device. In that regard, it enables data reduction for the huge amount of detailed information which results after direct numerical simulation (DNS) of the Navier-Stokes flow and temperature equations for the device.

The presented macro-scale description also allows us to determine the macro-scale characteristics of the flow and temperature fields in the laminar periodically developed regime by solving a simple closure model on a unit cell of the solid structures. As the closure model for the flow and heat transfer within the unit cell is in exact agreement with DNS results for the entire array of solid structures, model reduction is achieved in a consistent manner with respect to DNS.

The model equations for the macro-scale flow and heat transfer are obtained by weighted spatial averaging, or filtering, of the Navier-Stokes

equations. It is shown that the macro-scale flow velocity and macro-scale pressure in the periodically developed flow regime must be defined through a double volume-average filter to ensure that the macro-scale flow velocity and macro-scale pressure gradient are spatially constant. In that case, also the interfacial force and the momentum dispersion source, which appear in the macro-scale flow equations, are spatially constant, so that they can be easily governed from the developed flow equations on a unit cell.

Furthermore, it is shown that the macro-scale temperature in the periodically developed heat transfer regime in isothermal solid structures is best defined through a filter that is matched to the temperature decay rate. With the matched filter, the macro-scale fluid temperature varies exponentially in the main flow direction and plays a role similar to that of the bulk temperature in developed duct flow. The matched filter also ensures that the macro-scale interfacial heat transfer between the flow and the solid structures can be represented by a spatially constant heat transfer coefficient. In addition, the matched filter defines a spatially constant thermal dispersion coefficient to represent the thermal dispersion source in the macro-scale temperature equation. Both coefficients are easily governed from the rescaled temperature on a unit cell.

Lastly, it is demonstrated that the appropriate definition of the macro-scale temperature in the periodically developed conjugate heat transfer regime again requires a double volume-average filter. The double volume-average filter yields a linearly changing macro-scale temperature and a constant macro-scale interfacial heat flux in the periodically developed conjugate heat transfer regime. Moreover, with the double volume average, the thermal dispersion source, the thermal tortuosity and the interfacial heat transfer coefficient all become spatially constant, so that they are easily governed from the periodic temperature part on a unit cell.

SAMENVATTING

Dit werk behandelt de macroschaal beschrijving van stroming en warmteoverdracht in systemen met ruimtelijk periodische vaste structuren, zoals compacte warmtewisselaars en koellichamen met vinnen en buizenbundels. De voorgestelde macroschaal beschrijving laat ons toe de fysisch betekenisvolle globale eigenschappen van de zeer gedetailleerde stromings- en temperatuurvelden in een warmteoverdrachtstoestel te extraheren. In dat opzicht laat de beschrijving datareductie toe voor de grote hoeveelheid gedetailleerde informatie die resulteert na directe numerieke simulatie (DNS) van de stromings- en temperatuursvergelijkingen (Navier-Stokesvergelijkingen) voor het toestel.

De voorgestelde macroschaal beschrijving laat ons eveneens toe de macroschaal eigenschappen van de stromings- en temperatuurvelden in het laminaire ontwikkelde regime te bepalen door het oplossen van een eenvoudig sluitingsmodel op een eenheidscel van de vaste structuren. Aangezien het sluitingsmodel voor de stroming en warmteoverdracht in de eenheidscel in exacte overeenstemming is met DNS-resultaten voor de gehele configuratie van vaste structuren, verkrijgen we modelreductie op een consistente manier ten opzichte van DNS.

De modelvergelijkingen voor de macroschaal stroming en warmteoverdracht worden verkregen door ruimtelijke uitmiddeling of het filteren van de Navier-Stokesvergelijkingen. We tonen aan dat de macroschaal stromingssnelheid en de macroschaal drukgradiënt in het periodisch ontwikkelde stromingsregime gedefinieerd moeten worden via een dubbele volumemiddelingsfilter om te verzekeren dat beide ruimtelijk constant zijn. In dat geval zijn ook de interfasekracht en de momentumdispersiebron, die verschijnen in de macroschaal stromingsvergelijkingen, ruimtelijk constant, zodat ze gemakkelijk verkregen kunnen worden uit de ontwikkelde stromingsvergelijkingen op een eenheidscel.

Verder wordt er aangetoond dat de macroschaal temperatuur in het periodisch ontwikkelde warmteoverdrachtsregime in isotherme vaste structuren het best gedefinieerd wordt via een filter die aangepast is aan de temperatuursafname. Met de aangepaste filter varieert de macroschaal fluïdumtemperatuur exponentieel in de globale stromingsrichting en speelt deze een rol vergelijkbaar met die van de bulktemperatuur in een ontwikkelde kanaalstroming. De aangepaste filter verzekert ook dat de macroschaal interfasewarmteoverdracht tussen de stroming en de vaste structuren voorgesteld kan worden met een ruimtelijk constante warmteoverdrachtscoëfficiënt. Bovendien definieert de aangepaste filter een ruimtelijk constante thermische dispersiecoëfficiënt om de thermische dispersiebron in de macroschaal temperatuursvergelijking voor te stellen. Beide coëfficiënten volgen eenvoudig uit de herschaalde temperatuur over de eenheidscel.

Ten slotte wordt er aangetoond dat de gepaste definitie van de macroschaal temperatuur in het periodisch ontwikkelde gekoppelde warmteoverdrachtsregime eveneens een dubbele volumemiddelingsfilter vereist. De dubbele volumemiddelingsfilter levert een lineair veranderende macroschaal temperatuur op, en een constante macroschaal interfasewarmteflux. Eveneens, met de dubbele volumemiddelingsfilter worden de thermische dispersiebron, de thermische tortuositeit en de interfasewarmteoverdrachtscoëfficiënt allemaal ruimtelijk constant, zodat ze eenvoudig verkregen worden uit het periodische temperatuursgedeelte op een eenheidscel.

LIST OF SYMBOLS

$\boldsymbol{\mathcal{B}}_{fs}$	weighted planar interfacial force (3.74)	$[N/m^3]$
$\mathcal{D}$	thermal dispersion source (4.18)	$[mK/s]$
$\mathcal{M}$	weighted planar momentum dispersion source (3.74)	$[m^2/s^2]$
$\boldsymbol{b}_{fs}$	weighted interfacial force (3.22)	$[N/m^3]$
$\boldsymbol{e}$	unit vector	$[-]$
$\boldsymbol{f}$	(gravitational body) force (3.5), (3.9)	$[N/m^3]$
$\boldsymbol{g}$	gravitational acceleration	$[m/s^2]$
$\boldsymbol{G}_m^{(n)}$	geometrical tensor (2.65)	
$\boldsymbol{I}$	unit tensor	$[-]$
$\boldsymbol{k}_d$	thermal dispersion coefficient (6.40)	$[m/s]$
$\boldsymbol{K}_m$	weighted permeability tensor (5.53)	$[m^2]$
$\boldsymbol{l}^{(j)}$	lattice vector of unit cell (5.1)	$[m]$
$\boldsymbol{M}$	weighted momentum dispersion source (3.22)	$[m^2/s^2]$
$\boldsymbol{n}$	normal unit vector of boundary	$[-]$

$\boldsymbol{r}$	position vector locating point within averaging domain	$[m]$
$\boldsymbol{S}$	double of strain rate tensor (3.3)	$[s^{-1}]$
$\boldsymbol{u}$	flow velocity (2.5)	$[m/s]$
$\boldsymbol{v}$	planar flow velocity (3.41)	$[m/s]$
$\boldsymbol{x}$	position vector (locating centroid of averaging domain)	$[m]$
$\boldsymbol{y}$	position vector relative to centroid of averaging domain	$[m]$
Δp	pressure drop over array of solid structures	$[Pa]$
$\dot{q}$	volumetric heat source	$[W/m^3]$
ℓ	characteristic small length scale	$[m]$
$\mathcal{P}$	planar pressure (3.42)	$[Pa]$
$\mathcal{T}$	planar temperature (4.50)	$[K]$
N	number of solid structures	$[-]$
Pr	Prandtl number	$[-]$
Re	Reynolds number	$[-]$
$\mathscr{L}$	characteristic length scale for filtered quantity	$[m]$
c	specific heat capacity (2.8)	$[J/kg\,K]$
C^∞	class of infinitely differentiable continuous functions	
d	diameter/ dimension	$[m]$
e	specific energy	$[J/kg]$
h	heat transfer coefficient (4.68), (6.45), (6.63),(7.38)	$[W/m^3K]$
I	interval	
k	thermal conductivity (2.8)	$[W/mK]$
m	normalized weighting function	$[m^{-3}]$
p	pressure (2.5)	$[Pa]$
q	heat flux (4.10),(4.16)	$[W/m^2]$
r_m	characteristic length scale for averaging domain (2.83)	$[m]$
s_0	position parameter first solid structure of array	$[m]$
s_x	horizontal spacing of solid structures	$[m]$
s_y	vertical spacing of solid structures	$[m]$
s_N	position parameter last solid structure of array	$[m]$

T	temperature (2.5)	$[K]$
t	time	$[s]$
u	specific internal energy	$[J/kg]$
V	volume of (part of) averaging domain (2.2), (2.3)	$[m^3]$

Greek Symbols

$\bar{\Gamma}$	boundary within averaging domain	
$\bar{\Omega}$	averaging domain, filter window	
$\boldsymbol{\mathfrak{T}}$	planar viscous stress tensor (3.74)	$[Pa]$
$\boldsymbol{\lambda}_T$	rescaled temperature gradient (6.6)	$[m^{-1}]$
$\boldsymbol{\phi}$	physical quantity (2.4)	
$\boldsymbol{\Psi}_3$	closure term planar momentum equation (3.55)	$[N/m^3]$
$\boldsymbol{\sigma}$	total stress tensor (4.1)	$[Pa]$
$\boldsymbol{\tau}$	viscous stress tensor (2.6), (3.3)	$[Pa]$
δ	Dirac distribution	$[m^{-1}]$
ϵ	filtered fluid or solid indicator	$[-]$
Γ	boundary	
γ	indicator (2.9)	$[-]$
λ_T	constant temperature decay rate (6.16)	$[m^{-1}]$
μ	viscosity (2.6)	$[Pa\,s]$
Ω	(part of) system domain	
ψ'_m	porosity-dependent thermal closure term (4.24)	$[W/m^3]$
ψ_3	closure term planar temperature equation (4.55)	$[W/m^3]$
ρ	mass density	$[kg/m^3]$
σ_T	source term rescaled temperature equation (6.5)	$[W/m^3]$
θ	rescaled temperature	$[-]$
φ_3	closure term planar continuity equation (3.54)	$[s^{-1}]$
$\zeta_{\boldsymbol{u}}$	velocity shape function (3.62)	$[-]$
ζ_θ	separable part of rescaled temperature (6.70)	$[-]$
ζ_T	temperature similarity profile (4.64)	$[-]$

Superscripts

$'$	intrinsic
$+$	dimensionless
$\star$	periodic
f	intrinsically averaged over fluid
s	intrinsically averaged over solid

Subscripts

λ	depending on temperature decay rate λ_T
f	fluid
fs	associated with fluid-solid interface
m	depending on weighting function m
s	solid
approx	approximative
b	bottom/bulk
int	internal
macro	macro-scale
ref	reference
t	top
tot	total
unit	unit cell
visc	viscous
w	wall

Abbreviations

DNS	direct numerical simulation
REV	representative elementary volume
VAT	volume-averaging technique

CONTENTS

LIST OF FIGURES

LIST OF TABLES

CHAPTER

1

INTRODUCTION

1.1 Introduction

In many areas of science and engineering, a profound understanding of flow and heat transfer through spatially periodic solid structures is of utmost importance. This is especially the case for the design and analysis of heat transfer devices, like compact heat exchangers and heat sinks, in which arrays of periodic fins are employed to enhance heat transfer. Macro-scale models describing the overall flow and temperature fields within such devices should enable model reduction (less computational work) and data reduction (less detailed information) with respect to direct numerical simulation of the Navier-Stokes flow and temperature equations. This work reformulates the existing macro-scale models for flow through porous media to present an exact macro-scale description of the developed laminar flow and heat transfer regimes in spatially periodic solid structures. The presented macro-scale description is obtained by spatial averaging of the Navier-Stokes flow and temperature equations [1, 2].

1.2 Heat Transfer Devices with Spatially Periodic Solid Structures

Spatially periodic structures are found, for example, in the form of fin arrays or tube bundles within the flow passages of heat transfer devices, such as heat sinks and heat exchangers.

A *heat sink* is a solid device that transfers the heat from a certain heat source towards a coolant fluid in motion. The heat source is often an electronic device, e.g. a central processing unit, a power transistor or a light emitting diode. The coolant fluid is mostly ambient air that is driven through the heat sink by means of a fan, but it can also be water or another liquid being pumped through the heat sink.

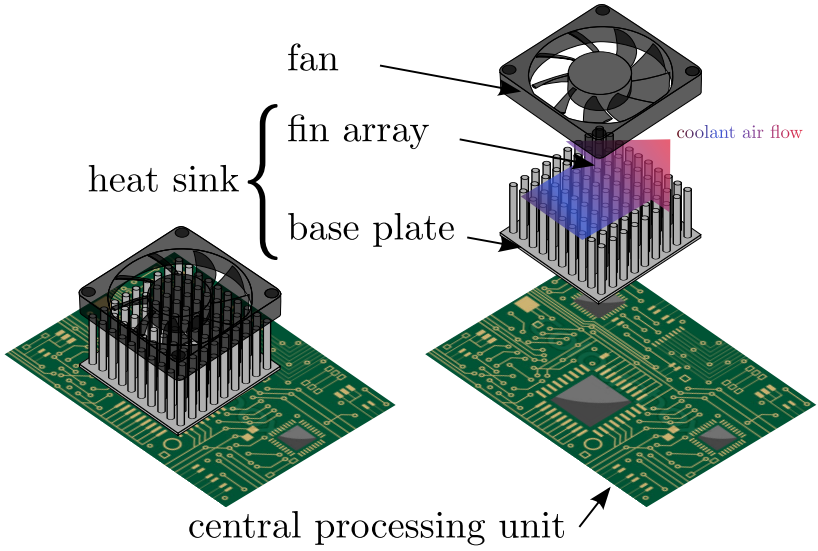

Figure 1.1: Heat sink with a pin-fin array on a central processing unit.

Contemporary heat sinks typically consist of an array of fins mounted on a base plate, which is attached to the heat source (see Figure 1.1). The cylindrical fins on Figure 1.1 are called *pin fins*, but in practise also many other beam-shaped fin geometries are employed. The fins and base plate form a large contact surface between the heat source and the coolant.

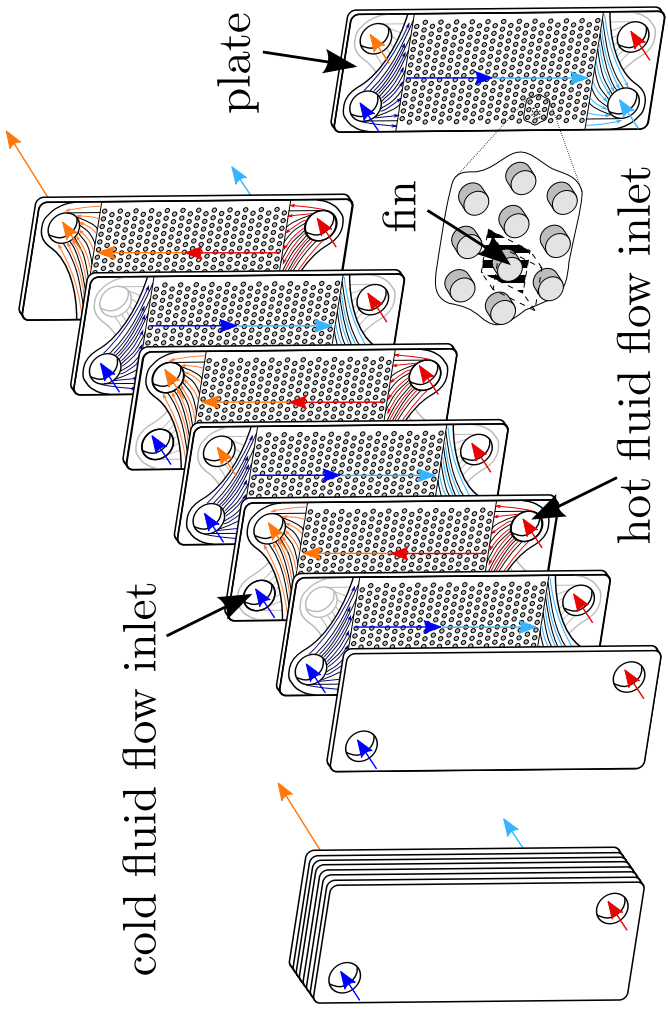

Figure 1.2: Plate-fin heat exchanger: The red-orange and dark-light blue arrows indicate the main flow direction of the hot and cold flow respectively.

They are made of a material with a high thermal conductivity, as their purpose is to conduct the heat away from the heat source towards the coolant without too much thermal resistance. That way, the heat sink maintains the temperature of the heat source within acceptable levels. Evidently, the overall temperature of the coolant increases as the coolant takes up heat while flowing over the fin array and base plate of the heat sink.

A *heat exchanger* is a solid device whose function is to transfer heat from a hot fluid to a cold fluid. Compact heat exchangers are often constructed as a stack of parallel plates with an array of fins in between (see Figure 1.2). The latter type of heat exchangers are called plate-fin heat exchangers. In a *plate-fin heat exchanger*, each pair of neighbouring plates forms a channel through which either hot or cold fluid flows in contact with the fins. Except for the top and bottom channel of the stack, each channel with hot fluid is adjacent to two channels with cold fluid and vice versa. The channel plates and fins form a large surface that conducts heat from the hot fluid towards the cold fluid. While the hot fluid flows through the heat exchanger and transfers heat towards the cold fluid, its overall temperature decreases from its inlet to its outlet. At the same time, the overall temperature of the cold fluid increases from its inlet to its outlet.

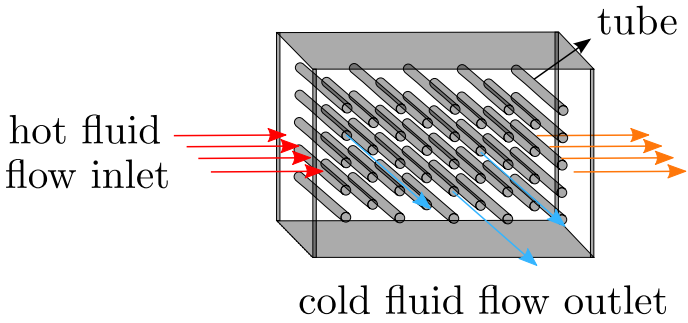

Figure 1.3: Tube bank heat exchanger.

Next to the previously discussed plate-fin heat exchangers, many other types of heat exchangers exist. For instance, heat exchangers can also be constructed as tube banks or plate-tube banks. In a *tube bank heat exchanger*, one fluid flows inside an array of tube channels, while the other fluid flows over the outer surface of these tube channels (see Figure 1.3).

The tube channels usually have a circular, elliptical or rectangular cross section. Sometimes additional fins are mounted along the outer surface of the tubes to increase the available heat transfer surface between the two fluids.

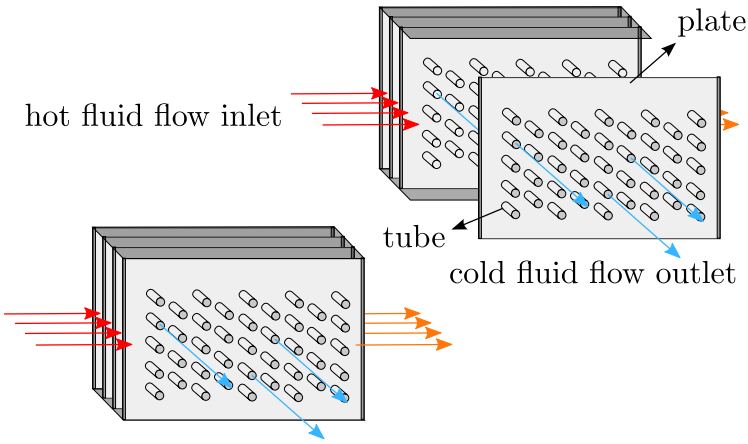

Figure 1.4: Plate-tube bank heat exchanger.

A *plate-tube bank heat exchanger* is in essence a tube bank heat exchanger in which additional parallel plates are mounted on the tube channels (see Figure 1.4). These parallel plates form different channels for the fluid that flows over the outer surface of the tubes.

The fins of a heat sink or a plate-fin heat exchanger and the tubes of a (plate-) tube bank heat exchanger are virtually always designed to have the same shape and placed in a periodic pattern: they are *spatially periodic solid structures*. The shape and configuration of these spatially solid structures should be designed in such a manner that they form a surface that ensures a large heat transfer rate on one hand, but does not cause too much friction with the fluid flow on the other hand.

Apart from heat transfer devices, spatially periodic solid structures are also present in chemical reactors and fuel cells, where the chemically reacting fluid typically passes through repetitive solid elements.

1.3 Challenges in Modelling of Heat Transfer Devices

The design and analysis of heat transfer devices with spatially periodic solid structures crucially depends on numerical models that describe the flow and heat transfer within these devices. In theory, the most accurate models rely on solving the detailed flow and temperature fields in the entire device through direct numerical simulation (DNS) of the Navier-Stokes equations. However, DNS modelling of an entire heat transfer device is in general not feasible, as it requires a huge amount of computational time and resources.

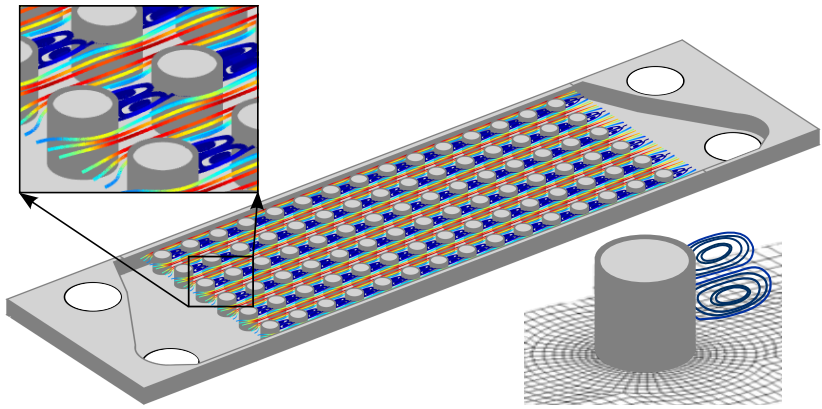

Figure 1.5: Flow streamlines through a channel with pin fins as calculated by a DNS simulation: red and blue color correspond to high and low flow speeds respectively (left). Part of the mesh around a single pin-fin (right).

To illustrate the computational time and resources required for DNS, we have applied DNS for visualizing the flow in just a single channel of a plate-fin heat exchanger. Figure 1.5 shows the streamlines of the steady flow through a plate channel with ninety equidistant cylindrical pin fins, calculated through DNS for a Reynolds number equal to hundred[1]. For an accurate resolution of the three-dimensional flow field near the boundary

[1]The Reynolds number is based on the overall pressure drop over the channel and the pin-fin diameter. The other parameters are the same as those given in Table 6.1.

of the fin and the wake behind the fin, as in Figure 1.5, the Navier-Stokes flow equations need to be discretized on a computational mesh of 250 000 to 1,500 000 grid cells per fin. A part of the computational mesh around a single fin is also depicted in Figure 1.5. Consequently, to obtain the velocity components in all three spatial directions as well as the pressure in each grid cell, a non-linear system of 90 million to 540 million flow variables has to be solved numerically. With the OpenFOAM® 2.3.1 software-package, this requires a simulation time of one to seven hours on one hundred processors[2].

Apart from the great amount of required computational time or resources, DNS modelling of the flow and heat transfer has still another consequence: it results in a huge amount of data. In the example of Figure 1.5, the simulation results contained 90 million to 540 million flow variables that had to be stored for further processing.

Therefore, a modelling approach different from DNS is necessary to reduce the computational effort and data involved in analysing the flow and heat transfer in devices with spatially periodic solid structures.

1.4 Macro-Scale Modelling of Flow and Heat Transfer in Solid Structures

For the design and analysis of heat transfer devices, information about the overall flow and temperature fields often suffices. Moreover, for a high number of periodic solid structures, simulation of the overall, averaged flow and temperature fields can be more computationally efficient than DNS of the detailed flow and temperature fields. Therefore, different mathematical equations have been proposed in the literature, that describe the flow and heat transfer in periodic solid structures in an averaged or global sense. These mathematical equations are called macro-scale models.

The adjective *macro-scale* is prone to subjective interpretation, as witnessed by its different meanings for each scientific domain. Mostly, the

[2]The 100 processors are of the type Intel® Ivy Bridge Xeon E5-2680v2 (2.8 GHz, 25 MB level 3 cache) and are part of ten 64 GB RAM nodes of the Flemish supercomputer centre.

word is used more or less as a synonym for averaged. For instance, in absence of a rigorous mathematical definition, *macro-scale temperature* just means the same as *averaged temperature*. The question then arises how *averaged* should be interpreted. Let us answer that question by explaining why there exists a necessity for defining macro-scale or averaged quantities in the first place. The invention of macro-scale quantities has two major reasons: the need for data reduction and the need for model reduction.

The *need for data reduction* is understood as follows. Physical quantities such as the temperature, velocity and pressure field in a flow through a device usually change from point to point (as well as in time). This was already clear from Figure 1.5. Consequently, a complete description of one of these physical quantities without loss of information comprises a huge amount of data: all of the quantity's point-wise values have to be stored, as we illustrated in the previous section. However, such detailed information is not always directly of interest, nor easy to interpret. Often, we are more interested in the overall or integral changes of a physical quantity. For example, we want to know the overall temperature difference between the inlet and the outlet of a device or we want to know how the temperature varies globally over the device, let's say in average sense from one fin to another. How the temperature varies locally, let's say from one specific spot on a fin to another spot on the same fin, is in that case irrelevant to us. The quantity that we call the *macro-scale temperature* represents this overall or average impression of the temperature data that we do have interest in. The former example illustrates that *a macro-scale quantity captures in an averaged way the most important patterns and spatial changes in the values* (data) of the original physical/mathematical quantity from which it is derived. It does not reflect all the point-wise variations in the values of the original quantity. Therefore, the macro-scale quantity itself can be described entirely by a smaller amount of data.

We already mentioned that the word *macro-scale* also has an interpretation in light of the need for model reduction. By *need for model reduction*, it is meant that we want to reduce the efforts involved for measuring a physically quantity, be it through a numerical simulation or real-word experiment. Because a physical quantity in a device typically changes from point to point, it is clear that for a complete description of the quantity, a lot of point-wise measurements would need to be collected, either via physical experiments or DNS. Obviously, such a detailed analysis is

mostly not desired, because in the previous section it was shown to be a time-consuming task which requires a lot of measuring equipment or computational resources. On the contrary, for a complete description of the corresponding macro-scale quantity, a smaller amount of measurements or computational resources is required. After all, the corresponding macro-scale quantity can be described by a smaller amount of data, as said before. Hence, model reduction can be achieved by measuring or simulating macro-scale quantities instead of original physical quantities.

The macro-scale models for heat transfer devices with periodic solid structures that have been proposed in the literature, attempt to predict the performance of the device through simplified equations for the macro-scale flow and temperature in the device. Solving these macro-scale models requires typically just a detailed simulation of the flow and temperature around a single solid structure of the device. In that regard, these macro-scale models are aimed to be a reduced model which avoids DNS of the flow through the entire array of solid structures.

Unfortunately, as it will be shown in the next chapters, the existing macro-scale models for heat transfer devices with periodic solid structures are in general not consistent with DNS results. Neither do they allow exact data reduction for the flow and temperature fields in heat transfer devices. The first reason is that most of these macro-scale models have been proposed empirically in accordance to experimental observations, so that they are prone to experimental errors and only applicable under the test conditions. The second reason is that the macro-scale models for periodic solid structures have been proposed heuristically from presumed analogies with porous media. Actually, the limited amount of theoretically supported macro-scale models for periodic solid structures are all derived from approximative macro-scale models for porous media. However, the geometry of porous media rarely resembles that of the periodic solid structures in heat transfer devices. In addition, the flow and heat transfer phenomena in porous media are very different. Therefore, also the empirical macro-scale models which are based on experimental observations in porous media are usually inaccurate for periodic solid structures.

In the next chapters, the shortcomings of the existing macro-scale models for heat transfer devices with periodic solid structures are examined in more detail. In the next two sections, the two technical approaches that have been used to develop theoretical macro-scale models for flow and heat transfer in porous media are discussed. These two approaches

are the *volume-averaging technique* [3, 4] and *asymptotic homogenization* [5]. The main features of the volume-averaging technique and asymptotic homogenization are illustrated in Appendix A, where the essential steps of each technique are applied on a simple one-dimensional steady heat conduction problem.

1.5 The Volume-Averaging Technique

The notion that a macro-scale quantity should capture in an averaged way the most important spatial changes of the quantity from which it is derived, has lead to the idea that a macro-scale quantity can be mathematically defined as a *volume-average*:

$$\langle \boldsymbol{\phi} \rangle|_{(\boldsymbol{x},t)} \triangleq \frac{1}{V} \int_{\boldsymbol{r} \in \bar{\Omega}(\boldsymbol{x})} \boldsymbol{\phi}(\boldsymbol{r},t)\, d\Omega(\boldsymbol{r})\,.$$

In this definition it can be recognized that the volume-averaged quantity $\langle \boldsymbol{\phi} \rangle$, at some point $\boldsymbol{x}$ within a medium, reflects an average of several pointwise values $\boldsymbol{\phi}(\boldsymbol{r},t)$ of the original quantity at some time instant t within some region of interest $\bar{\Omega}$, with volume V, centred around the point $\boldsymbol{x}$.

The volume-averaged quantity $\langle \boldsymbol{\phi} \rangle$ according to the former definition cannot directly be called a macro-scale quantity, unless we ensure that the volume-averaged quantity $\langle \boldsymbol{\phi} \rangle$ effectively represents only the most important patterns and spatial changes of the original quantity $\boldsymbol{\phi}$ that are of interest to us. Whether this requirement is fulfilled or not, depends on the choice of the averaging volume $\bar{\Omega}$ that defines the volume-averaged quantity $\langle \boldsymbol{\phi} \rangle$. The averaging volume has to be suitably chosen with respect to the type of medium over which the original quantity changes (the porous medium through which the flow occurs) and with respect to the physical processes that determine the original quantity (advection, diffusion, ...). In fact, it might not even be possible to find an averaging volume which recovers the most important patterns of $\boldsymbol{\phi}$ that we consider to be of interest, as this is a subjective matter.

The former definition of the macro-scale quantity $\langle \boldsymbol{\phi} \rangle$ and the existence of a suitable averaging volume $\bar{\Omega}$ are the main foundations of the *volume-averaging technique* (VAT). In VAT, the partial differential equations that model some physical quantities are averaged over a suitable volume to

obtain macro-scale equations which govern the corresponding volume-averaged quantities. The macro-scale equations contain so-called *closure terms*, which are terms arising due to the averaging procedure that still depend on the original non-averaged quantities. Therefore, the closure terms require additional modelling in order to solve the macro-scale equations. The aim of VAT is to express the closure terms in terms of solely volume-averaged quantities, through a so-called *closure model* that can be solved on just a part of the (porous) medium under consideration. This part of the medium is thought to be representative for the entire (porous) medium and is usually of the same size as the averaging volume. For that reason it is called a *representative elementary volume* (REV). To develop a closure model that is solvable on a REV of the medium, various approximations and assumptions need to be made. A common assumption is that the medium is composed of many REV's in a periodic configuration. One of the most recurring assumptions in the literature on porous media, is that the porous medium consists of pores or flow channels of a characteristic width that is much smaller than the overall distances over which the volume-averaged quantities change significantly. The validity of these assumptions is often difficult to verify a priori and typically holds only for some specific classes of porous media or composite materials.

1.6 Asymptotic Homogenization

The viewpoint that a macro-scale quantity should be an overall approximation of the original quantity, no longer containing the local changes of the original quantity over a relatively small spatial distance, has lead to the idea that a macro-scale quantity can also be defined as an *asymptotic approximation*:

$$\boldsymbol{\phi}_0|_{(\boldsymbol{x},t)} \triangleq \lim_{\varepsilon \to 0} \boldsymbol{\phi}_\varepsilon \left(\boldsymbol{x}, \frac{\boldsymbol{x}}{\varepsilon}, t \right) \qquad \text{where} \qquad \varepsilon \ll 1 \,.$$

In this definition, the small parameter ε represents the ratio of the smallest spatial distance of interest to the largest spatial distance of interest, so that the macro-scale quantity $\boldsymbol{\phi}_0$ is the limit of an asymptotic approximation $\boldsymbol{\phi}_\varepsilon$ for the original quantity $\boldsymbol{\phi}$ that is found when ε approaches zero. In the context of porous media, ε usually represents the ratio of the characteristic width of the pores to the characteristic size of the entire porous medium.

The equations of classical continuum mechanics that govern a physical quantity in a medium composed of different materials (e.g. fluid and solid) which succeed each other over a short distance, are typically partial differential equations with rapidly oscillating coefficients. From a mathematical point of view, the coefficients oscillate rapidly over space, because they depend on the so-called micro-scale coordinate $\boldsymbol{x}/\varepsilon$ and not just on the so-called macro-scale coordinate $\boldsymbol{x}$. *Asymptotic homogenization* is a mathematical method to transform a partial differential equation with a highly oscillatory coefficient into a new partial differential equation of the same form, but with a homogeneous, i.e. spatially uniform, coefficient. The homogeneous coefficient then represents an *effective material property* of the entire medium, e.g. fluid and solid together. The partial differential equation with the homogeneous coefficient is considered a macro-scale equation and its solution governs the corresponding macro-scale quantity.

1.7 Contributions of this Work

In the near future, DNS of the flow and heat transfer in large arrays of periodic solid structures will still require a huge amount of computational time and resources. Reduced models for the flow and heat transfer in spatially periodic solid structures are thus of crucial importance to analyse and further improve compact heat transfer devices. Moreover, even when DNS will have finally become feasible, data reduction for detailed DNS results will still be necessary.

Therefore, the aim of this work is to develop a physically meaningful macro-scale description of the flow and heat transfer in spatially periodic solid structures, which enables model reduction and data reduction in exact agreement with DNS. The presented macro-scale description should replace the existing macro-scale models for heat transfer devices with periodic solid structures, which are theoretically inconsistent with DNS results and not generally applicable.

The macro-scale description presented in this work is based on a *spatial filter technique* or *weighted spatial averaging* and relies on a more general reformulation of the VAT models for porous media. A reformulation of the existing VAT models for porous media is necessary for spatially periodic structures, because of the following three reasons.

First, the existing macro-scale flow and heat transfer equations for porous media have been derived by VAT under the assumption that some approximations called *length-scale constraints* are satisfied and that the spatial moments of the medium under consideration are zero. Although most length-scale approximations seem reasonable for different transport regimes in a broad class of porous media, their validity is not ensured for the flow and heat transfer regimes in spatially periodic structures. Besides, the validity of these length-sale constraints is difficult to verify without DNS information. Furthermore, it has been shown that for solid structures with a spatially periodic solid-fluid interface, the spatial moments often cannot be neglected, so that the existing VAT equations are inaccurate for spatially periodic structures [1, 2].

Second, when the existing VAT macro-scale models are applied to model channels with spatially periodic solid structures, their physical interpretation is not straightforward, as these models do not respect any analogies with the existing models for flow and heat transfer in channels without solid structures.

Lastly, the current VAT closure models for porous media do not yield exact closure terms for the developed flow regime and the developed heat transfer regimes. While the developed flow and heat transfer regimes do not occur in porous media like aquifers and soils, they are the fundamental (idealized) physical regimes that occur in arrays of spatially periodic solid structures like fins and tubes in heat transfer devices.

In accordance with the former shortcomings of the existing VAT models for describing the macro-scale flow and heat transfer in spatially periodic solid structures, the contributions of this work are

1) the mathematical formulation of spatially averaged flow and temperature equations describing the macro-scale flow and heat transfer in channels with periodic solid structures, without any ad hoc assumptions regarding length scales or spatial moments;

2) the development of spatial averaging operators to recover physically meaningful macro-scale quantities for the developed flow and heat transfer regimes, which respect many analogies with the models for channels without solid structures;

3) the derivation of simple closure models for the developed flow and heat transfer regimes that are in exact agreement with DNS results.

While the first two contributions enable data reduction, the third contribution leads to model reduction with respect to DNS.

More specifically, the former contributions are restrictively accomplished by

1) reformulating the Navier-Stokes flow and temperature equations within the theory of mathematical distributions and applying the spatial filter technique employed by Quintard and Whitaker [1, 2];

2) proposing some new weighting functions for spatial filtering;

3) extending Patankar's description of the periodically flow and heat transfer regimes in ducts with a varying cross section [6] to channels with spatially periodic solid structures.

The focus of this work lies on the *laminar* developed flow and heat transfer regimes. The laminar regime is characterised by a type of layered flow in which the fluid tends to flow in parallel layers with no disruption between the layers. The laminar flow regime typically occurs at low flow speeds when the flow channels and solid structures are relatively small, like in compact heat transfer devices with fin diameters below one millimetre and above a few micrometres, as in Figure 1.6. Also when the fluid has a high viscosity, e.g. high-viscosity lubricating oils and food streams, the flow often remains laminar.

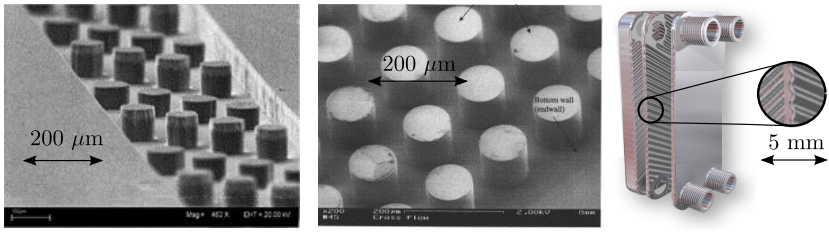

Figure 1.6: Channel with micro pin fins [7] (left), close-up of a bank of micro pin fins [8] (mid), compact chevron-type plate-fin heat exchanger [9] (right).

As a last remark, it should be mentioned that the suitability of asymptotic homogenization for the macro-scale description of flow and heat transfer

in periodic solid structures has been left unexplored in this work. One of the difficulties involved with asymptotic homogenization is the choice of the small parameter ε, as alternative choices for ε lead to different macro-scale descriptions [10]. Another concern is the practical measurement of macro-scale quantities defined by a limit operator.

1.8 Outline

This work first examines the main concepts of the weighted spatial averaging technique in Chapter 2. In the next chapter, Chapter 3, the spatially averaged flow equations are presented for an incompressible viscous fluid flowing through solid structures. In Chapter 3, the spatially averaged temperature equations for the incompressible fluid and the solid structures are derived. Subsequently, Chapter 5 gives a macro-scale description of periodically developed flow. A macro-scale description of the periodically developed heat transfer regime in isothermal solids is elaborated in Chapter 6. Chapter 7 treats the macro-scale description of the periodically developed conjugate heat transfer regime. Finally, Chapter 8 summarizes the main conclusions of this work and provides some recommendations for further research.

Bibliography

[1] M. Quintard and S. Whitaker, "Transport in ordered and disordered porous media I: The cellular average and the use of weighting functions," *Transport in Porous Media*, vol. 14, no. 2, pp. 163–177, 1994.

[2] M. Quintard and S. Whitaker, "Transport in ordered and disordered porous media II: Generalized volume averaging," *Transport in Porous Media*, vol. 14, no. 2, pp. 179–206, 1994.

[3] S. Whitaker, *The Method of Volume Averaging (Theory and Applications of Transport in Porous Media)*. Kluwer Academic Publishers, Boston, 1999.

[4] S. Whitaker, *Fluid Transport in Porous Media*, ch. 1: Volume Averaging of Transport Equations, pp. 1–60. Computational Mechanics Publications, 1997.

[5] A. Bensoussan, J. Lions, and G. Papanicolaou, *Asymptotic analysis for periodic structures, Studies in Mathematics and its Applications 5*. North-Holland Publishing Company, Amsterdam, 1978.

[6] S. V. Patankar, C. H. Liu, and E. M. Sparrow, "Fully Developed Flow and Heat Transfer in Ducts Having Streamwise-Periodic Variations of Cross-Sectional Area," *Journal of Heat Transfer*, vol. 99, no. 2, p. 180, 1977.

[7] S. G. Kandlikar and W. J. Grande, "Evaluation of single phase flow in microchannels for high heat flux chip cooling - thermohydraulic performance enhancement and fabrication technology," *Heat Transfer Engineering*, vol. 25, no. 8, pp. 5–16, 2004.

[8] A. Kosar, C. Mishra, and Y. Peles, "Laminar flow across a bank of low aspect ratio micro pin fins," *Journal of Fluids Engineering*, vol. 127, no. 3, pp. 419–430, 2005.

[9] C. S. Fernandes, R. P. Dias, J. M. Nóbrega, and J. M. Maia, "Laminar flow in chevron-type plate heat exchangers: CFD analysis of tortuosity, shape factor and friction factor," *Chemical Engineering and Processing: Process Intensification*, vol. 46, no. 9, pp. 825 – 833, 2007. Selected Papers from the European Process Intensification Conference (EPIC), Copenhagen, Denmark, September 19-20, 2007.

[10] Y. Davit, C. G. Bell, H. M. Byrne, L. A. C. Chapman, L. S. Kimpton, G. E. Lang, K. H. L. Leonard, J. M. Oliver, N. C. Pearson, R. J. Shipley, S. L. Waters, J. P. Whiteley, B. D. Wood, and M. Quintard, "Homogenization via formal multiscale asymptotics and volume averaging: How do the two techniques compare?," *Advances in Water Resources*, vol. 62, Part B, pp. 178 – 206, 2013.

CHAPTER

2

CONCEPTS OF THE SPATIAL AVERAGING TECHNIQUE

2.1 Introduction

This chapter introduces the concepts of the spatial averaging technique as formulated by Quintard and Whitaker in their series of papers [1–5]. The definitions and notations of the spatial averaging operators within their framework have largely been adopted in this text. However, some modifications to the original formulation have been made to pursue more mathematical transparency and conciseness. Especially the definition of a macro-scale quantity and the definition of a length scale are carefully re-examined.

2.2 Historical Background

Definitions of Spatially Averaged Quantities

The earliest ideas underlying the volume-averaging technique (VAT) and related spatial averaging techniques date from the 1960s. The pioneering steps go back to the work of Marle [6], who defined macro-scale quantities for porous media in terms of (weighted) volume-averages of micro-scale quantities compatible with the principles of thermodynamics:

$$\boldsymbol{\phi}_{\text{macro}} \triangleq \frac{\displaystyle\int_V \rho\boldsymbol{\phi}\,\Upsilon\,dV}{\displaystyle\int_V \rho\Upsilon\,dV} = \frac{\displaystyle\iiint \rho\boldsymbol{\phi}\,\Upsilon(a,b,c)\,da\,db\,dc}{\displaystyle\iiint \rho\Upsilon(a,b,c)\,da\,db\,dc}\,.$$

According to Marle's definition, the macro-scale quantity $\boldsymbol{\phi}_{\text{macro}}$ is the average of the original or *micro-scale* quantity $\boldsymbol{\phi}$ within a unitary volume V of fluid or solid with density ρ. The weighting factor Υ in Marle's definition equals one when the original quantity $\boldsymbol{\phi}$ is an extensive or additive quantity, like the internal energy u or entropy s of the fluid or solid. When the original quantity is an intensive quantity, like the fluid temperature or fluid pressure, the weighting factor Υ is chosen such that the macro-scale quantity satisfies some specified thermodynamic relationship. For instance, the macro-scale temperature T_{macro} and macro-scale pressure p_{macro} of the fluid are defined by weighting factors, such that they satisfy Gibbs' relation $du_{\text{macro}} = p_{\text{macro}}\,dV + T_{\text{macro}}\,ds$.

The use of the convolution product to define macro-scale quantities as smooth spatial averages of distributions was introduced in Marle's subsequent work [7]:

$$\boldsymbol{\phi}_{\text{macro}} \triangleq \int \boldsymbol{\phi}(\boldsymbol{x}+\boldsymbol{x}', t+t')\,m(-\boldsymbol{x}', -t')\,d\boldsymbol{x}'\,dt' \triangleq \boldsymbol{\phi} * m\,.$$

The weighting function m in this definition depends on the degree of detail that one desires to keep in the macro-scale description. Marle suggested that for a non-additive quantity $\boldsymbol{\phi}$, such as the flow velocity through a porous medium, the former definition of a macro-scale quantity should be replaced by

$$\boldsymbol{\phi}_{\text{macro}} \triangleq \frac{(\rho\boldsymbol{\phi}) * m}{\rho * m}\,,$$

provided that $\rho\boldsymbol{\phi}$ is an additive quantity. The conviction that the spatial average of a non-additive quantity has no precise physical significance would persist at least until the end of the 1980s [8].

The standard volume-averaging technique, by which macro-scale quantities are obtained as a local average of a physical quantity over a representative elementary volume (REV) V:

$$\boldsymbol{\phi}_{\text{macro}} \triangleq \frac{1}{V}\int_V \boldsymbol{\phi}\, dV \triangleq \langle\boldsymbol{\phi}\rangle\,,$$

was developed independently from Marle by Slattery [9], Whitaker [10] and Bear [11] to describe isothermal Stokes flow through porous media. The definition of the volume-averaging operator $\langle\,\rangle$, as well as the definitions of the mass-averaging and area-averaging operators, were extended in the work of Hassanizadeh and Gray [12] to define macro-scale quantities for multiphase flow through heterogeneous porous media. The extension required the introduction of a phase indicator within the volume-integral to indicate whether a point within the REV belongs to a certain phase or not. The REV in the standard VAT framework corresponds to the smallest averaging domain for which the macro-scale quantities are independent of the magnitude, shape and orientation of the averaging domain [11]. Another viewpoint is that the REV represents any averaging domain for which the postulated form of (the closure terms in) the macro-scale equations that govern the macro-scale quantity holds [10, 12].

The convolution product of Marle [7] was adopted by Baveye and Sposito [13] in the following form:

$$\boldsymbol{\phi}_{\text{macro}}(\boldsymbol{x},t) \triangleq \int \boldsymbol{\phi}(\boldsymbol{y},t)\, m(\boldsymbol{x}-\boldsymbol{y},\boldsymbol{x},t)\, d^3y \triangleq \boldsymbol{\phi} * m\,.$$

Baveye and Sposito proposed to formulate macro-scale quantities in a porous medium as convolution products of microscopic quantities with a weighting function m representing the appropriate measuring instrument. This interpretation of the weighting function is called the relativist concept, because the explicit dependence of the weighting function on the time instant t and position $\boldsymbol{x}$ of the measurement reflects the influence of the instantaneous and local presence of the experimentalist through his or her measuring instrument. In the relativist concept of Baveye and Sposito, the averaging domain corresponds to the support of the weighting function (or measuring instrument), which is not necessarily an REV.

The spatial averaging technique of Marle [7] and the idea of media-specific weighting functions according to Baveye and Spositio [13] were picked up by Quintard and Whitaker in the 1990s [1–5] to develop a *local*[1] macro-scale equation for Stokes flow in ordered and disordered media for which the closure terms can be solved on some representative region of the medium. In the work of Quintard and Whitaker [1–5], the macro-scale quantities are defined through a convolution product with a time-independent weighting function:

$$\boldsymbol{\phi}_{\text{macro}} \triangleq \int_{\mathbb{R}^3} m(\boldsymbol{x}-\boldsymbol{r})\,\boldsymbol{\phi}(\boldsymbol{r},t)\,dV_r \triangleq \langle\boldsymbol{\phi}\rangle_m \triangleq m * \boldsymbol{\phi}\,.$$

The series of five papers of Quintard and Whitaker forms the first work in which a specific weighting function is proposed to define macro-scale quantities in flow through *ordered* or *spatially periodic* structures. The specific weighting function of Quintard and Whitaker for ordered media has been named the *cellular average* and is equivalent to a double volume-average. Quintard and Whitaker have also derived some constraints for a suitable weighting function in spatially aperiodic disordered media. As the main purpose of the weighting function in the work of Quintard and Whitaker is to ensure the validity of the local macro-scale equation and the local closure problem, the weighting function in the averaging operator $\langle\,\rangle_m$ has a role similar to that of the REV in the volume-averaging operator $\langle\,\rangle$. Therefore, there is no difference between the form of the macro-scale equations obtained by the weighted spatial averaging technique of Quintard and Whitaker or the standard volume-averaging technique, although the interpretation of the averaging operator differs for both techniques [2].

Currently, the use of weighting functions for spatial averaging is less common than the standard volume-averaging technique in the field of macro-scale modelling of transport through porous media and spatially periodic solid structures. Nevertheless, some recent exceptions exist which have applied the weighted spatial averaging technique to connect theoretically derived macro-scale models to experimental measurements [14, 15]. Probably, the sporadic use of weighting functions can be explained by the fact that it is always possible to reinterpret the meaning of the standard volume-averaging operator in the VAT macro-scale equations in light of the weighting functions of Quintard and Whitaker. Another explanation

[1] A partial differential equation is called *local* when it contains only derivatives but no integrals of its solution.

seems that the mathematical framework of the weighted spatial averaging technique is rather complex and leads to tedious derivations of the macro-scale equations.

The standard volume-average as well as the weighted spatial average according to Quintard and Whitaker [1–5] are closely related to the filter used in large-eddy simulation (LES) for turbulent flows [16, 17]. In the LES framework, which was developed simultaneously but independently from the VAT framework, an LES *filter* $\langle\,\rangle$ is defined as

$$\langle \boldsymbol{\phi} \rangle|_{(\boldsymbol{x},t)} \triangleq \int_{\mathbb{R}} \int_{\mathbb{R}^3} G(\boldsymbol{x}-\boldsymbol{r}, t-t')\, \boldsymbol{\phi}(\boldsymbol{r},t')\, d\boldsymbol{r}\, dt' \triangleq G * \boldsymbol{\phi}\,.$$

For instance, when the kernel or weighting function G of the LES filter is a time-independent box filter of width Δ, i.e. $G(\boldsymbol{x}-\boldsymbol{r}) = \frac{1}{\Delta}$ if $\|\boldsymbol{x}-\boldsymbol{r}\| \leq \frac{\Delta}{2}$ and $G(\boldsymbol{x}-\boldsymbol{r}) = 0$ otherwise, we retrieve the standard volume-average over a cuboid averaging domain of side Δ. In LES, the spatial averaging operator usually acts as a low-pass filter, which means that the spatial filter width Δ corresponds to the largest length scale of the turbulent flow phenomena that are not resolved, so that the phenomena occurring over a length scale smaller than Δ are filtered away. Mostly, the spatial filter width or cut-off length equals the typical size of a single grid cell used in the discretisation of the filtered Navier-Stokes flow equations. Only in a limited number of studies of turbulent flow through an array of solid structures, e.g. [18], the spatial filter width of the LES filter actually corresponds to a unit cell of the solid structures.

Spatial Averaging Theorems

Together with the development of VAT, also the theorems which relate volume-averages of derivatives to derivatives of volume-averaged quantities were formulated and gradually more rigorously proven. The volume-averaging gradient theorem for an averaging volume that is invariant in space and orientation was first presented by Anderson and Jackson [19], Slattery [9] and Whitaker [20]. Different proofs of the volume-averaging gradient theorem were given by Bachmat [21] and Gray and Lee [22], Cushman [23] and later by Howes and Whitaker [24].

The gradient theorem and the time-derivative theorem in VAT for a time- and space-dependent averaging volume have been explored by Gray [25] and Cushman [26]. The gradient theorem and time-derivative theorem for the weighted spatial averaging technique were first given in [2] and follow directly from the distribution theory of Schwarz [27, 28].

All of the former theorems are analogous, but not necessarily equivalent to the commutation rules for the spatial gradient and time derivative of LES filters with a uniform filter width [29] or spatially dependent filter width [30].

2.3 System Domain and Averaging Domain

We consider a system (Figure 2.1), for instance a heat sink or a channel of a heat exchanger, as a two- or three-dimensional continuum domain Ω which consists of subregions of fluid (Ω_f) and solid (Ω_s). The fluid and solid domain have an interface boundary Γ_{fs}. The solid domain is assumed to be composed of solid structures whose characteristic size is small in comparison to the global domain size of the system. The boundary of the continuum domain is denoted $\Gamma = \partial\Omega$ and can be of any shape.

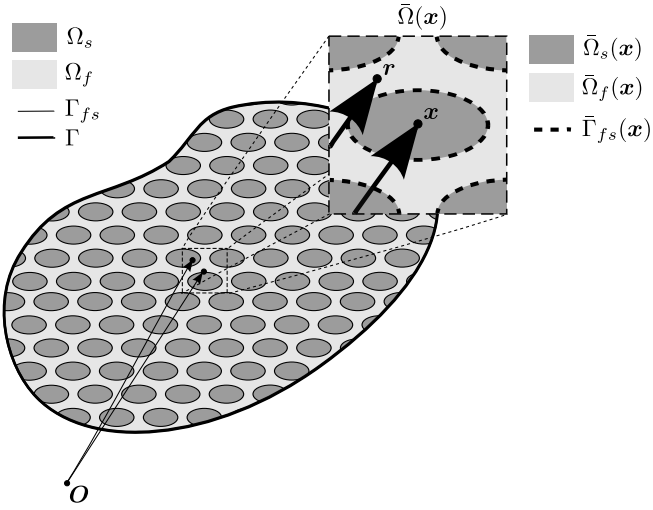

Figure 2.1: Two-dimensional continuum domain, averaging domain and interface boundaries.

The system domain Ω comprises many points. A single point of the domain Ω is identified by its position vector $\boldsymbol{x}$ with respect to a fixed ref-

erence point $\boldsymbol{O}$, the origin. With every point $\boldsymbol{x}$ we now associate an *averaging domain* $\bar{\Omega}(\boldsymbol{x})$. The averaging domain $\bar{\Omega}(\boldsymbol{x})$ is a set of points in a closed region of fixed shape and orientation around $\boldsymbol{x}$, such that $\boldsymbol{x}$ is the geometrical centroid of $\bar{\Omega}$. A single point within this averaging domain $\bar{\Omega}(\boldsymbol{x})$ is on its turn identified by the position vector $\boldsymbol{r}$. The centroid of the averaging domain thus determines the location and orientation of the averaging domain via

$$\boldsymbol{x} = \frac{1}{V} \int_{\boldsymbol{r} \in \bar{\Omega}(\boldsymbol{x})} \boldsymbol{r} \, d\Omega(\boldsymbol{r}) \,, \tag{2.1}$$

where the volume V of the averaging domain is given by

$$V = \int_{\boldsymbol{r} \in \bar{\Omega}(\boldsymbol{x})} d\Omega(\boldsymbol{r}) \,. \tag{2.2}$$

The fact that the location and orientation of an averaging domain of fixed shape should be identified by an arbitrary fixed reference point is discussed by Wood [31].

The size of the averaging domain is chosen small compared to the size of the system domain. However, the averaging domain is much larger than the differential domain $d\Omega$, which is the smallest (infinitesimal) domain element in the continuum approach. Obviously, for the continuum assumption to hold, the differential domain on its turn should be large enough with respect to the molecular transport scale within the fluid and solid, which is characterized by the mean free path.

The parts of the averaging domain that match with the fluid and solid regions are denoted $\bar{\Omega}_f(\boldsymbol{x})$ and $\bar{\Omega}_s(\boldsymbol{x})$ respectively. Their respective volumes are

$$V_f = \int_{\boldsymbol{r} \in \bar{\Omega}_f(\boldsymbol{x})} d\Omega(\boldsymbol{r}) \quad \text{and} \quad V_s = \int_{\boldsymbol{r} \in \bar{\Omega}_s(\boldsymbol{x})} d\Omega(\boldsymbol{r}) \,. \tag{2.3}$$

The interface boundary between the solid and fluid within $\bar{\Omega}(\boldsymbol{x})$ is further denoted by $\bar{\Gamma}_{fs}(\boldsymbol{x})$.

Topology of the System Domain and Averaging Domain
In the previously discussed literature on spatial averaging techniques, the mathematical topology of the system domain and averaging domain are seldom discussed, although some information about the topology can be found in the theorems from Cushman [23]. In this work, the mathematical topology is specified in such a manner that a practically useful theory of distributions [27, 28] can be formulated on these domains.

The system domain is considered a connected open subset of the real space $\mathbb{R}^2$ or $\mathbb{R}^3$, i.e. $\Omega \subset \mathbb{R}^d$ with $d = 2$ or $d = 3$. The assumption that the system domain Ω is a *connected* set means that this set cannot be represented as the union of two or more disjoint non-empty open subsets. The assumption that Ω is an *open* set means that it contains none of its boundary points: $\Omega \cap \Gamma = \emptyset$. The boundary $\Gamma = \partial\Omega$ of the system domain is assumed to be a *piecewise smooth orientable* surface in $\mathbb{R}^d$.

Further, the fluid domain and the solid domain are considered disjoint subsets of the system domain such that $\Omega = \Omega_f \cup \Omega_s \cup \Gamma_{fs}$ with $\Omega_f \cap \Omega_s = \emptyset$ and $\Gamma_{fs} \cap \Gamma = \emptyset$. The fluid-solid interface is defined by $\Gamma_{fs} = \partial\Omega_f \cap \partial\Omega_s$, where $\partial\Omega_f$ and $\partial\Omega_s$ denote the boundary of Ω_f and Ω_s respectively. Just like in the proofs of the spatial averaging theorems by Cushman [23], we will treat both Ω_f and Ω_s as *open* sets, so $\Omega_f \cap \Gamma_{fs} = \emptyset$ and $\Omega_s \cap \Gamma_{fs} = \emptyset$. The latter property implies that Ω_f, Ω_s and Γ_{fs} form a *partition* of Ω, which makes it possible to define so-called *jump distributions* and *indicators* on Ω having Γ_{fs} as discontinuity surface in agreement with [27, 28].

The fluid part and solid part of the local averaging domain and the fluid-solid interface contained within the averaging domain are respectively defined as $\bar{\Omega}_f = \bar{\Omega} \cap \Omega_f$, $\bar{\Omega}_s = \bar{\Omega} \cap \Omega_s$ and $\bar{\Gamma}_{fs} = \Gamma_{fs} \cap \bar{\Omega}$. They are supposed to form a partition of $\bar{\Omega} = \bar{\Omega}_f \cup \bar{\Omega}_s \cup \bar{\Gamma}_{fs}$, respecting $\bar{\Omega}_s \cap \bar{\Omega}_f = \emptyset$ and $\bar{\Omega}_f \cap \bar{\Gamma}_{fs} = \emptyset$. Consequently, the averaging domain in our work satisfies $\bar{\Omega}(\boldsymbol{x}) = \mathrm{cl}(\bar{\Omega}_f(\boldsymbol{x})) \cup \mathrm{cl}(\bar{\Omega}_s(\boldsymbol{x}))$, just like in [26], provided that $\boldsymbol{x}$ lies sufficiently far from Γ so that $\partial\bar{\Omega}_f \cap \Gamma = \emptyset$ and $\partial\bar{\Omega}_s \cap \Gamma = \emptyset$. Here, the *closure* of a set is denoted by cl, which is the union of this set and its boundary, e.g. $\mathrm{cl}(\bar{\Omega}_f) = \Omega_f \cap \partial\Omega_f$.

2.4 Physical Quantities as Distributions

To facilitate the theorems of the spatial averaging technique, a space- and time-dependent physical quantity is described as a *mathematical distribution* [1, 27, 28] over the solid and fluid regions. We suppose that every physical quantity of interest can be represented as a tensor distribution $\boldsymbol{\phi}$ whose function representation is

$$\boldsymbol{\phi}(\boldsymbol{x}, t) = \begin{cases} \boldsymbol{\phi}_f(\boldsymbol{x}, t) & \text{in } \Omega_f \\ \boldsymbol{\phi}_s(\boldsymbol{x}, t) & \text{in } \Omega_s \end{cases} . \tag{2.4}$$

Hereby it is understood that the distribution $\boldsymbol{\phi}$ is defined on Ω, while the functions $\boldsymbol{\phi}_f$ and $\boldsymbol{\phi}_s$ are defined on some neighbourhood of Ω_f and Ω_s respectively. For convenience, we will say that $\boldsymbol{\phi}_f$ is defined for $\boldsymbol{x} \in \mathrm{cl}(\Omega_f)$ and $\boldsymbol{\phi}_f$ is defined for $\boldsymbol{x} \in \mathrm{cl}(\Omega_s)$. In general, $\boldsymbol{\phi}$ should be treated as a *jump distribution*, which means that $\boldsymbol{\phi}$ might be discontinuous at the boundary Γ_{fs}, because its function value $\boldsymbol{\phi}_f$ at Γ_{fs} might differ from its function value $\boldsymbol{\phi}_s$ at Γ_{fs}.

Some physical quantities such as the velocity field $\boldsymbol{u}$, pressure field p, stress field $\boldsymbol{\tau}$ and the space dependent viscosity μ have physical meaning in the fluid domain only. For these quantities the extension of their definition towards a mathematical distribution is possible as follows;

$$\boldsymbol{u} = \begin{cases} \boldsymbol{u}_f & \text{in } \Omega_f \\ 0 & \text{in } \Omega_s \end{cases}, \quad p = \begin{cases} p_f & \text{in } \Omega_f \\ 0 & \text{in } \Omega_s \end{cases}, \tag{2.5}$$

$$\mu = \begin{cases} \mu_f & \text{in } \Omega_f \\ 0 & \text{in } \Omega_s \end{cases}, \quad \boldsymbol{\tau} = \begin{cases} \boldsymbol{\tau}_f & \text{in } \Omega_f \\ 0 & \text{in } \Omega_s \end{cases}. \tag{2.6}$$

Likewise, a physical quantity that physically exists only for the solid region, can be described by a mathematical distribution $\boldsymbol{\phi}$ when we take $\boldsymbol{\phi}_f = 0$.

Physical quantities such as the temperature T, the thermal conductivity k, the density ρ and the specific heat capacity c are defined on both the solid and fluid region:

$$T = \begin{cases} T_f & \text{in } \Omega_f \\ T_s & \text{in } \Omega_s \end{cases}, \quad \rho = \begin{cases} \rho_f & \text{in } \Omega_f \\ \rho_s & \text{in } \Omega_s \end{cases}, \tag{2.7}$$

$$k = \begin{cases} k_f & \text{in } \Omega_f \\ k_s & \text{in } \Omega_s \end{cases}, \quad c = \begin{cases} c_f & \text{in } \Omega_f \\ c_s & \text{in } \Omega_s \end{cases}. \tag{2.8}$$

For these kind of quantities, the part of the distribution on the fluid domain can be distinguished from the part on the solid domain by introducing the *fluid indicator* γ_f and *solid indicator* γ_s [1, 28]:

$$\gamma_f = \begin{cases} 1 & \text{in } \Omega_f \\ 0 & \text{in } \Omega_s \end{cases}, \quad \gamma_s = \begin{cases} 1 & \text{in } \Omega_s \\ 0 & \text{in } \Omega_f \end{cases}. \tag{2.9}$$

With the aid of the fluid and solid indicators, any jump distribution $\boldsymbol{\phi}$ can be decomposed as

$$\boldsymbol{\phi} = \boldsymbol{\phi}\gamma_f + \boldsymbol{\phi}\gamma_s \,, \tag{2.10}$$

because $\gamma_f = 1 - \gamma_s$ in $\Omega \setminus \Gamma_{fs}$. The latter decomposition should be interpreted as an equality in the sense of a distribution, but not as point-wise equality, since the fluid and solid indicators are discontinuous at Γ_{fs}. It is assumed that the products $\boldsymbol{\phi}\gamma_f$ and $\boldsymbol{\phi}\gamma_s$ exist for the function representation of (2.4), although a complete general definition of the product of arbitrary distributions is not possible [28]. Furthermore, it should be noted that a distribution cannot be decomposed as $\boldsymbol{\phi} = \boldsymbol{\phi}_f\gamma_f + \boldsymbol{\phi}_s\gamma_s$, as done in [2], when $\boldsymbol{\phi}_f$ and $\boldsymbol{\phi}_s$ are functions defined on $\mathrm{cl}(\Omega_f)$ and $\mathrm{cl}(\Omega_s)$ instead of Ω or $\mathbb{R}^d$.

2.5 Spatial Averaging Operators

With every detailed physical quantity (2.4), we will now associate a corresponding spatially averaged quantity for our macro-scale description. Hereto, we use the concept of a *linear spatial averaging operator* or *filter* $\langle\,\rangle_m$ which acts on a distribution $\boldsymbol{\phi}$ through a convolution and governs the spatial average $\langle\boldsymbol{\phi}\rangle_m$ of this distribution.

Convolution Product

The *convolution product* [1, 7, 27] of a distribution $\boldsymbol{\phi}$, with a compactly supported smooth *test* or *weighting function* $m : \mathbb{R}^d \to \mathbb{R}$ is defined as

$$m * \boldsymbol{\phi}|_{(\boldsymbol{x},t)} \triangleq \int_{\boldsymbol{r}\in\mathbb{R}^d} m(\boldsymbol{x}-\boldsymbol{r})\,\boldsymbol{\phi}(\boldsymbol{r},t)\,d\Omega(\boldsymbol{r})\,. \tag{2.11}$$

Here *smooth* means that m is infinitely differentiable, $m \in C^\infty$, and *compactly supported* means that m is exactly zero outside some closed set. The existence of this convolution product requires that $\boldsymbol{\phi}$ be defined on $\mathbb{R}^d$ instead of $\Omega \subset \mathbb{R}^d$. The extension of the definition domain of $\boldsymbol{\phi}$ from Ω to $\mathbb{R}^d$ in order to evaluate the convolution integral will be discussed in §2.15. For now, it suffices to note that it is always possible to set $\boldsymbol{\phi} = 0$ in $\mathbb{R}^d \setminus \Omega$.

Because the integral operator $\langle\,\rangle_m$ of (2.12) transforms the distribution $\boldsymbol{\phi}$ into its filtered counterpart $\langle\boldsymbol{\phi}\rangle_m$, the weighting function m can also be called the *kernel* of the filter, according to the theory of integral transformations.

Superficial Spatial Average

The *weighted superficial average* of a distribution $\boldsymbol{\phi}$ is defined as the convolution of this distribution with a *normalized* weighting function m satisfying $m(\boldsymbol{x}-\boldsymbol{r})=0$ for $\boldsymbol{r}\notin\bar{\Omega}(\boldsymbol{x})$:

$$\langle\boldsymbol{\phi}\rangle_m|_{(\boldsymbol{x},t)} \triangleq \int_{\boldsymbol{r}\in\bar{\Omega}(\boldsymbol{x})} m(\boldsymbol{x}-\boldsymbol{r})\,\boldsymbol{\phi}(\boldsymbol{r},t)\,d\Omega(\boldsymbol{r}) \triangleq m*\boldsymbol{\phi}|_{(\boldsymbol{x},t)}\,. \tag{2.12}$$

By this notation it is understood that the weighted superficial average is evaluated at position $\boldsymbol{x}$, while the integration is carried out over all points having a position vector $\boldsymbol{r}$ within the averaging domain $\bar{\Omega}$.

The superficial spatial average can be decomposed into two separate integrals, one over the solid domain and one over the fluid domain, because the discontinuity surface $\bar{\Gamma}_{fs}$ of the distribution can be left out of the integration domain $\bar{\Omega}=\bar{\Omega}_f\cup\bar{\Omega}_s\cup\bar{\Gamma}_{fs}$ according to [28]:

$$\begin{aligned}\langle\boldsymbol{\phi}\rangle_m|_{(\boldsymbol{x},t)} &\triangleq \int_{\boldsymbol{r}\in\bar{\Omega}_f(\boldsymbol{x})} m(\boldsymbol{x}-\boldsymbol{r})\,\boldsymbol{\phi}_f(\boldsymbol{r},t)\,d\Omega(\boldsymbol{r}) \\ &\quad+\int_{\boldsymbol{r}\in\bar{\Omega}_s(\boldsymbol{x})} m(\boldsymbol{x}-\boldsymbol{r})\,\boldsymbol{\phi}_s(\boldsymbol{r},t)\,d\Omega(\boldsymbol{r}) \\ &\triangleq \langle\boldsymbol{\phi}_f\rangle_m\big|_{(\boldsymbol{x},t)}+\langle\boldsymbol{\phi}_s\rangle_m|_{(\boldsymbol{x},t)}\,.\end{aligned} \tag{2.13}$$

We note that the second integral over Ω_s in (2.13) does not appear in the weighted spatial averaging technique of Quintard and Whitaker [1–5], as only flow quantities are considered in the latter study.

In the last line of (2.13), we have introduced the notational convention that the integral operator $\langle\,\rangle_m$ works over the part of the averaging domain on which its argument is defined. This means that the integration is carried out over $\bar{\Omega}$ when its argument is the *distribution* $\boldsymbol{\phi}$, but $\bar{\Omega}_f$ or $\bar{\Omega}_s$, when its argument is one of the *functions* $\boldsymbol{\phi}_f$ or $\boldsymbol{\phi}_s$ respectively. This notational convention is equivalent to the definitions

$$\langle\boldsymbol{\phi}_f\rangle_m \triangleq \langle\boldsymbol{\phi}\gamma_f\rangle_m \quad\text{and}\quad \langle\boldsymbol{\phi}_s\rangle_m \triangleq \langle\boldsymbol{\phi}\gamma_s\rangle_m\,. \tag{2.14}$$

In the work of Quintard and Whitaker [1–5], no distinct notation is employed for the distribution $\boldsymbol{\phi}$ of a flow quantity on Ω and its function part $\boldsymbol{\phi}_f$ on $\mathrm{cl}(\Omega_f)$. The absence of this distinction is sometimes confusing, but with the convention (2.14), the spatial averages in their work can be mostly unambiguously interpreted.

Intrinsic Spatial Average

The *weighted intrinsic average* [2] of $\boldsymbol{\phi}$ *over the fluid or solid domain*, are respectively defined as

$$\langle \boldsymbol{\phi} \rangle_m^f \triangleq \epsilon_{fm}^{-1} \langle \boldsymbol{\phi} \gamma_f \rangle_m \quad \text{and} \quad \langle \boldsymbol{\phi} \rangle_m^s \triangleq \epsilon_{sm}^{-1} \langle \boldsymbol{\phi} \gamma_s \rangle_m \,, \tag{2.15}$$

where the functions ϵ_{fm} and ϵ_{sm} are the weighted superficial average of the fluid and solid indicators:

$$\epsilon_{fm} \triangleq \langle \gamma_f \rangle_m \quad \text{and} \quad \epsilon_{sm} \triangleq \langle \gamma_s \rangle_m \,. \tag{2.16}$$

Following the notational convention for the superficial averaging operator, one can also introduce the notations

$$\langle \boldsymbol{\phi} \rangle_m^f \triangleq \langle \boldsymbol{\phi}_f \rangle_m^f \quad \text{and} \quad \langle \boldsymbol{\phi} \rangle_m^s \triangleq \langle \boldsymbol{\phi}_s \rangle_m^s \tag{2.17}$$

for the intrinsic weighted average. The latter notation will be used to express the link between the weighted intrinsic averages in this work and the intrinsic volume-averages in e.g. [2].

The weighted superficial and intrinsic average are related through the following identity

$$\langle \boldsymbol{\phi} \rangle_m = \epsilon_{fm} \langle \boldsymbol{\phi} \rangle_m^f + \epsilon_{sm} \langle \boldsymbol{\phi} \rangle_m^s \,, \tag{2.18}$$

which follows directly from (2.10).

Fully Separable filter

The spatial averaging operator $\langle\,\rangle_m$ is called a *(fully) separable filter* with respect to the linearly independent vectors $\boldsymbol{e}^{(j)}$ that form a basis for $\mathbb{R}^d$, if this filter can be transformed into a d-fold iterated integral of the form

$$\begin{aligned} \langle \boldsymbol{\phi} \rangle_m|_{(\boldsymbol{x},t)} &= \int_{\boldsymbol{y} \in I_1 \times \cdots \times I_d} m(-\boldsymbol{y})\, \boldsymbol{\phi}(\boldsymbol{x}+\boldsymbol{y},t)\, d\Omega(\boldsymbol{y}) \\ = \int_{y_1 \in I_1} m_1'(-y_1) \cdots \int_{y_d \in I_d} & m_d'(-y_d)\, \boldsymbol{\phi}(x_1+y_1,\ldots,x_d+y_d,t)\, dy_d \cdots dy_1 \,, \\ \text{with} \qquad x_j \triangleq \boldsymbol{x} \cdot \boldsymbol{e}^{(j)} \qquad & \text{and} \quad y_j \triangleq \boldsymbol{y} \cdot \boldsymbol{e}^{(j)} \,. \end{aligned} \tag{2.19}$$

According to its definition, a fully separable filter thus has a filter window which coincides with the following Cartesian product of closed intervals $I_j \subset \mathbb{R}$:

$$\boldsymbol{r} \in \bar{\Omega}(\boldsymbol{x}) \Leftrightarrow \boldsymbol{y} \triangleq \boldsymbol{r} - \boldsymbol{x} \in I_1 \times \cdots \times I_d \Leftrightarrow y_j \triangleq \boldsymbol{y} \cdot \boldsymbol{e}^{(j)} \in I_j \,. \tag{2.20}$$

In order to be separable, the filter kernel m must be expressible as a product of functions m_j, each equal to zero outside the corresponding interval I_j:

$$m(-\boldsymbol{y}) = \prod_{j=1}^{d} m_j(-y_j) \qquad \text{with} \qquad m_j(-y_j) = 0 \qquad \text{for } y_j \notin I_j \,. \tag{2.21}$$

Moreover, a filter operator can only be separable w.r.t. a basis in $\mathbb{R}^d$ that has a metric which allows the elementary integration domain $d\Omega$ to be parametrized as

$$d\Omega(\boldsymbol{y}) = d\Omega(y_1, \ldots, y_d) = \prod_{j=1}^{d} g_j(y_j)\, dy_j \,, \tag{2.22}$$

so that the filter has a separable kernel m'_j in (2.19):

$$m'_j(-y_j) \triangleq m_j(-y_j)\, g_j(y_j) \,. \tag{2.23}$$

The product form of $d\Omega$ (2.22) does not necessarily exist for an arbitrary basis. For an arbitrary basis $\boldsymbol{e}^{(j)} = \frac{\partial \boldsymbol{r}}{\partial y_j}$, the elementary integration domain satisfies

$$d\Omega(\boldsymbol{r}) = \begin{cases} \left| \left(\frac{\partial \boldsymbol{r}}{\partial y_1} \times \frac{\partial \boldsymbol{r}}{\partial y_2} \right) \right| dy_1\, dy_2 & \text{if } d = 2 \\ \left\| \frac{\partial \boldsymbol{r}}{\partial y_1} \cdot \left(\frac{\partial \boldsymbol{r}}{\partial y_2} \times \frac{\partial \boldsymbol{r}}{\partial y_3} \right) \right\| dy_1\, dy_2\, dy_3 & \text{if } d = 3 \end{cases} . \tag{2.24}$$

In shorthand notation, a fully separable filter is denoted as

$$\langle \boldsymbol{\phi} \rangle_m = \begin{cases} \langle \langle \boldsymbol{\phi} \rangle_1 \rangle_2 & \text{if } d = 2 \\ \langle \langle \langle \boldsymbol{\phi} \rangle_1 \rangle_2 \rangle_3 & \text{if } d = 3 \end{cases} , \tag{2.25}$$

where the one-dimensional convolution product $\langle \boldsymbol{\phi} \rangle_j$ is defined in analogy to (2.11):

$$\begin{aligned} \langle \boldsymbol{\phi} \rangle_j |_{(\boldsymbol{x},t)} &\triangleq \int_{y_j \in I_j} m'_j(-y_j)\, \boldsymbol{\phi}(x_j + y_j, \ldots, t)\, dy_j \\ &\triangleq m'_j * \boldsymbol{\phi} \big|_{(\boldsymbol{x},t)} \,. \end{aligned} \tag{2.26}$$

Partly Separable filter

The spatial averaging operator $\langle\ \rangle_m$ is called a *(partly) separable filter* with respect to the single basis vector $\boldsymbol{e}^{(3)}$ in $\mathbb{R}^3$, if this filter can be transformed into an iterated integral of the form

$$\langle\boldsymbol{\phi}\rangle_m|_{(\boldsymbol{x},t)} = \int_{\boldsymbol{y}\in\times\bar{\Omega}_{1,2}\times I_3} m(-\boldsymbol{y})\,\boldsymbol{\phi}(\boldsymbol{x}+\boldsymbol{y},t)\,d\Omega(\boldsymbol{y})$$

$$= \int_{\boldsymbol{y}_{1,2}\in\bar{\Omega}_{1,2}} m_{1,2}(-\boldsymbol{y}_{1,2}) \int_{y_3\in I_3} m_3'(-y_3)\,\boldsymbol{\phi}(\boldsymbol{x}_{1,2}+\boldsymbol{y}_{1,2}, x_3+y_3, t)\,dy_3\,d\Omega_{1,2}(\boldsymbol{y}_{1,2})\,,$$

$$\text{with} \qquad \boldsymbol{x}_{1,2} \triangleq x_1\boldsymbol{e}^{(1)} + x_2\boldsymbol{e}^{(2)} \qquad \text{and} \qquad x_j \triangleq \boldsymbol{y}\cdot\boldsymbol{e}^{(j)}\,,$$
$$\boldsymbol{y}_{1,2} \triangleq y_1\boldsymbol{e}^{(1)} + y_2\boldsymbol{e}^{(2)} \qquad \text{and} \qquad y_j \triangleq \boldsymbol{y}\cdot\boldsymbol{e}^{(j)}\,. \tag{2.27}$$

The filter window of a partly separable filter coincides with the following Cartesian product of a closed interval $I_3 \subset \mathbb{R}$ and a set $\bar{\Omega}_{1,2} \subset \mathbb{R}^2$:

$$\begin{aligned} \boldsymbol{r}\in\bar{\Omega}(\boldsymbol{x}) \quad &\Leftrightarrow \quad \boldsymbol{y}\in\bar{\Omega}_{1,2}\times I_3 \\ &\Leftrightarrow \quad \boldsymbol{y}_{1,2} \triangleq y_1\boldsymbol{e}^{(1)} + y_2\boldsymbol{e}^{(2)} \in \bar{\Omega}_{1,2} \qquad y_3\in I_3\,. \end{aligned} \tag{2.28}$$

The kernel m of a partly separable filter can be written as a product of the form

$$\begin{aligned} m(-\boldsymbol{y}) &= m_{1,2}(-\boldsymbol{y}_{1,2})\,m_3(-y_3)\,, \\ \text{with} \qquad m_{1,2}(-\boldsymbol{y}_{1,2}) &= 0 \qquad \text{for } \boldsymbol{y}_{1,2}\notin\bar{\Omega}_{1,2}\,, \\ m_3(y_3) &= 0 \qquad \text{for } y_3\notin I_3\,, \end{aligned} \tag{2.29}$$

while the integration domain is

$$d\Omega(\boldsymbol{y}) = d\Omega_{1,2}(\boldsymbol{y}_{1,2})\,g_3(y_3)\,dy_3\,, \tag{2.30}$$

so that

$$m_3'(-y_3) \triangleq m_3(-y_3)\,g_3(y_3)\,. \tag{2.31}$$

By definition, a partly separable filter can be evaluated as a repeated integral:

$$\langle\boldsymbol{\phi}\rangle_m = \langle\langle\boldsymbol{\phi}\rangle_{1,2}\rangle_3 = \langle\langle\boldsymbol{\phi}\rangle_3\rangle_{1,2}\,, \tag{2.32}$$

where the two-dimensional convolution product $\langle\boldsymbol{\phi}\rangle_{1,2}$ is defined in analogy to (2.11):

$$\begin{aligned} \langle\boldsymbol{\phi}\rangle_{1,2}|_{(\boldsymbol{x},t)} &\triangleq \int_{\boldsymbol{y}_{1,2}\in\bar{\Omega}_{1,2}} m_{1,2}(-\boldsymbol{y}_{1,2})\,\boldsymbol{\phi}(\boldsymbol{x}_{1,2}+\boldsymbol{y}_{1,2},x_3,t)\,d\Omega_{1,2}(\boldsymbol{y}_{1,2}) \\ &\triangleq m_{1,2} * \boldsymbol{\phi}|_{(\boldsymbol{x},t)}\,. \end{aligned} \tag{2.33}$$

Lastly, we remark that by definition, a filter that is fully separable filter with respect to a vector basis, is always partly separable with respect to each individual basis vector.

2.6 Volume-Averaging Operators

A special type of weighting function is the one used for volume averaging:

$$m_V(\boldsymbol{x}-\boldsymbol{r}) \triangleq \begin{cases} \frac{1}{V} & \boldsymbol{r} \in \bar{\Omega}(\boldsymbol{x}) \\ 0 & \text{elsewhere} \end{cases} . \tag{2.34}$$

In VAT for porous media, the averaging domain is usually considered a sphere of radius r_0: $\bar{\Omega}(\boldsymbol{x}) = \{\forall \boldsymbol{r} \,|\, r_0 \geq \|\boldsymbol{x}-\boldsymbol{r}\|\}$ [2]. Although $m_V \notin C^\infty$, it has been shown that m_V in practise satisfies the same theorems as a smooth weighting function [21–24].

Superficial Volume Average

When the weighting function m_V is chosen, the subscript m from the averaging operator $\langle\,\rangle_m$ will be dropped for convenience so that the *superficial volume average* [1, 2] of a distribution $\boldsymbol{\phi}$ is denoted by

$$\langle\boldsymbol{\phi}\rangle|_{(\boldsymbol{x},t)} \triangleq \frac{1}{V}\int_{\boldsymbol{r}\in\bar{\Omega}(\boldsymbol{x})} \boldsymbol{\phi}(\boldsymbol{r},t)\, d\Omega(\boldsymbol{r}) \triangleq m_V * \boldsymbol{\phi}\,. \tag{2.35}$$

Because of (2.13), this definition of the superficial volume average is equivalent to

$$\begin{aligned} \langle\boldsymbol{\phi}\rangle|_{(\boldsymbol{x},t)} &\triangleq \frac{1}{V}\int_{\boldsymbol{r}\in\bar{\Omega}_f(\boldsymbol{x})} \boldsymbol{\phi}_f(\boldsymbol{r},t)\, d\Omega(\boldsymbol{r}) + \frac{1}{V}\int_{\boldsymbol{r}\in\bar{\Omega}_s(\boldsymbol{x})} \boldsymbol{\phi}_s(\boldsymbol{r},t)\, d\Omega(\boldsymbol{r}) \\ &\triangleq \langle\boldsymbol{\phi}_f\rangle + \langle\boldsymbol{\phi}_s\rangle\,, \end{aligned} \tag{2.36}$$

where $\langle\boldsymbol{\phi}_f\rangle$ and $\langle\boldsymbol{\phi}_s\rangle$ are respectively called the *superficial volume average over the fluid* and the *superficial volume average over the solid.*

Intrinsic Volume Average

In accordance with the definition of the weighted intrinsic average, the *intrinsic volume average* [1, 2] is obtained by averaging a distribution *over the solid or fluid region* through the operators $\langle\,\rangle^f$ and $\langle\,\rangle^s$:

$$\begin{aligned} \langle\boldsymbol{\phi}\rangle^f\big|_{(\boldsymbol{x},t)} &\triangleq \frac{1}{V_f}\int_{\boldsymbol{r}\in\bar{\Omega}_f(\boldsymbol{x})} \boldsymbol{\phi}(\boldsymbol{r},t)\, d\Omega(\boldsymbol{r}) \triangleq \epsilon_f^{-1}\, m_V * (\boldsymbol{\phi}\gamma_f) \\ &\triangleq \epsilon_f^{-1}\langle\boldsymbol{\phi}_f\rangle \triangleq \langle\boldsymbol{\phi}_f\rangle^f\,. \end{aligned} \tag{2.37}$$

As already explained, the last two equalities are rather a matter of short hand notation. Likewise, we can express the intrinsic volume average over the solid domain as

$$\begin{aligned}\langle\boldsymbol{\phi}\rangle^s\big|_{(\boldsymbol{x},t)} &\triangleq \frac{1}{V_s}\int_{\boldsymbol{r}\in\bar{\Omega}_s(\boldsymbol{x})}\boldsymbol{\phi}(\boldsymbol{r},t)\,d\Omega(\boldsymbol{r}) \triangleq \epsilon_s^{-1}\,m_V*(\boldsymbol{\phi}\gamma_s)\\ &\triangleq \epsilon_s^{-1}\langle\boldsymbol{\phi}_s\rangle \triangleq \langle\boldsymbol{\phi}_s\rangle^s\,. \end{aligned} \tag{2.38}$$

Note that the intrinsic volume average of quantity with a constant value over the f- or s-region yields this constant again.

The functions ϵ_f and ϵ_s, relating the superficial and intrinsic volume average, are derived from ϵ_{fm} and ϵ_{sm} (cf. (2.16)) replacing m by m_V:

$$\epsilon_f \triangleq \langle\gamma_f\rangle = \tfrac{V_f}{V} \quad \text{and} \quad \epsilon_s \triangleq \langle\gamma_s\rangle = \tfrac{V_s}{V}\,. \tag{2.39}$$

From (2.39) it is clear that ϵ_f represents the *volume fraction* of the fluid, which is also called the *porosity*.

Cellular Average

The *cellular average* is the spatial average of $\boldsymbol{\phi}$ that results from the weighting function $m = m_V * m_V$, which can easily be computed through repeated volume averaging. We remark that $m = m_V * m_V \notin C^\infty$, but $m = m_V * m_V$ does satisfy all of the averaging theorems in this work.

Sometimes the following definition is used for the cellular average [1, 2]:

$$\frac{1}{V}\int_{\boldsymbol{r}\in\bar{\Omega}(\boldsymbol{x})}\langle\boldsymbol{\phi}_f\rangle^f\big|_{(\boldsymbol{r},t)}\,d\Omega(\boldsymbol{r}) \triangleq m_V*\left(\epsilon_f^{-1}\,m_V*(\boldsymbol{\phi}\gamma_f)\right)\,. \tag{2.40}$$

When $\epsilon_f \triangleq m_V*\gamma_f$ is constant, the last expression for the cellular average becomes equivalent to the former definition:

$$\frac{1}{V}\int_{\boldsymbol{r}\in\bar{\Omega}(\boldsymbol{x})}\langle\boldsymbol{\phi}_f\rangle^f\big|_{(\boldsymbol{r},t)}\,d\Omega(\boldsymbol{r}) = \frac{m_V*m_V*(\boldsymbol{\phi}\gamma_f)}{m_V*\gamma_f} \tag{2.41}$$

$$= \frac{m_V*m_V*(\boldsymbol{\phi}\gamma_f)}{m_V*m_V*\gamma_f} \tag{2.42}$$

$$\triangleq \langle\boldsymbol{\phi}\rangle_m^f \qquad \text{with } m = m_V*m_V\,, \tag{2.43}$$

because of $\epsilon_{fm} = \epsilon_f$ in that case (see §5.6).

2.7 Gradient and Averaging Theorems

Gradient and Divergence of a Distribution

The *gradient in the sense of a distribution* [1, 27, 28] as in (2.4) is given by

$$\nabla \boldsymbol{\phi} = \nabla^{\nu} \boldsymbol{\phi} - \boldsymbol{n}_{fs} (\boldsymbol{\phi}_f - \boldsymbol{\phi}_s) \delta_{fs} \,. \tag{2.44}$$

In the equation above, the unit normal vector $\boldsymbol{n}_{fs}$ at the fluid-solid interface Γ_{fs} points from the f-region toward the s-region. The symbol δ_{fs} denotes the Dirac distribution associated with the fluid-solid interface Γ_{fs}, which in $\mathbb{R}^d$ corresponds to the line ($d = 2$) or surface ($d = 3$) at which $\boldsymbol{\phi}$ can be discontinuous.

The *Dirac surface distribution* δ_{fs} is defined by the integral property

$$\int_{\boldsymbol{r} \in \mathbb{R}^d} f(\boldsymbol{r}) \delta_{fs}(\boldsymbol{r}) \, d\Omega(\boldsymbol{r}) \triangleq \int_{\boldsymbol{r} \in \Gamma_{fs}} f(\boldsymbol{r}) \, d\Gamma(\boldsymbol{r}) \,, \tag{2.45}$$

for any compactly supported smooth function $f : \mathbb{R}^d \to \mathbb{R}$. The Dirac surface distribution is in fact the inward normal derivative of the indicator distribution: $\delta_{fs}(\boldsymbol{x}) = -\boldsymbol{n}_{fs}(\boldsymbol{x}) \cdot \nabla \gamma_f(\boldsymbol{x})$.

The *gradient in the usual sense* [1, 27, 28] on the other hand is given the symbol $\nabla^{\nu} \boldsymbol{\phi}$ such that

$$\nabla^{\nu} \boldsymbol{\phi} \triangleq \begin{cases} \nabla \boldsymbol{\phi}_f & \text{in } \Omega_f \\ \nabla \boldsymbol{\phi}_s & \text{in } \Omega_s \end{cases} \,. \tag{2.46}$$

In a similar fashion to (2.44), the *divergence in the sense of a distribution* is given by

$$\nabla \cdot \boldsymbol{\phi} = \nabla^{\nu} \cdot \boldsymbol{\phi} - \boldsymbol{n}_{fs} \cdot (\boldsymbol{\phi}_f - \boldsymbol{\phi}_s) \delta_{fs} \,. \tag{2.47}$$

The divergence in the usual sense is defined in the same way as the gradient in the usual sense.

Spatial-Averaging Gradient Theorem

An important gradient theorem [2] for the spatial averaging operator is

$$\nabla \langle \boldsymbol{\phi} \rangle_m = \langle \nabla^{\nu} \boldsymbol{\phi} \rangle_m - \langle \boldsymbol{n}_{fs} (\boldsymbol{\phi}_f - \boldsymbol{\phi}_s) \delta_{fs} \rangle_m \,. \tag{2.48}$$

For the divergence operator the generalized spatial averaging theorem states

$$\nabla \cdot \langle \boldsymbol{\phi} \rangle_m = \langle \nabla^{\nu} \cdot \boldsymbol{\phi} \rangle_m - \langle \boldsymbol{n}_{fs} \cdot (\boldsymbol{\phi}_f - \boldsymbol{\phi}_s) \delta_{fs} \rangle_m \,. \tag{2.49}$$

These equalities can be proven from (2.46) and the theorem

$$\nabla(m * \boldsymbol{\phi}) = (\nabla m) * \boldsymbol{\phi} = m * (\nabla \boldsymbol{\phi})\,. \tag{2.50}$$

The last term in (2.48) can also be expressed as follows by definition of the surface Dirac distribution:

$$\begin{aligned}\langle \boldsymbol{n}_{fs}(\boldsymbol{\phi}_f - \boldsymbol{\phi}_s)\delta_{fs}\rangle_m &= \int_{\boldsymbol{r}\in\Gamma_{fs}} m(\boldsymbol{x}-\boldsymbol{r})\,\boldsymbol{n}_{fs}(\boldsymbol{r})\big(\boldsymbol{\phi}_f(\boldsymbol{r},t) - \boldsymbol{\phi}_s(\boldsymbol{r},t)\big)\,d\Gamma(\boldsymbol{r}) \\ &= \int_{\boldsymbol{r}\in\bar{\Gamma}_{fs}(\boldsymbol{x})} m(\boldsymbol{x}-\boldsymbol{r})\,\boldsymbol{n}_{fs}(\boldsymbol{r})\,\big(\boldsymbol{\phi}_f(\boldsymbol{r},t) - \boldsymbol{\phi}_s(\boldsymbol{r},t)\big)\,d\Gamma(\boldsymbol{r})\,. \end{aligned} \tag{2.51}$$

Here the fact that $m(\boldsymbol{x}-\boldsymbol{r}) = 0$ for $\boldsymbol{r} \notin \bar{\Omega}(\boldsymbol{x})$ was used to restrict the integration surface from Γ_{fs} to $\bar{\Gamma}_{fs}$. Because of the former property the term $\langle \boldsymbol{n}_{fs}(\boldsymbol{\phi}_f - \boldsymbol{\phi}_s)\delta_{fs}\rangle_m$ is sometimes called the *surface filter*.

Volume-Averaging Gradient Theorem

Provided the averaging domain is spatially and time-invariant, i.e. $\bar{\Omega}$ has the same volume V for all points $\boldsymbol{x}$ of the system domain and the orientation of $\bar{\Omega}$ remains unchanged with respect to an inertial reference frame, irrespective of time, the *volume-averaging gradient theorem* [9, 19, 20, 24] holds for the function $\boldsymbol{\phi}_f$ if $\boldsymbol{\phi}_s = 0$:

$$\langle \nabla \boldsymbol{\phi}_f\rangle\big|_{(\boldsymbol{x},t)} = \nabla\langle \boldsymbol{\phi}_f\rangle\big|_{(\boldsymbol{x},t)} + \frac{1}{V}\int_{\boldsymbol{r}\in\bar{\Gamma}_{fs}(\boldsymbol{x})} \boldsymbol{n}_f(\boldsymbol{r})\,\boldsymbol{\phi}_f(\boldsymbol{r},t)\,d\Gamma(\boldsymbol{r})\,. \tag{2.52}$$

The volume averaging theorem is a special case of the spatial averaging gradient theorem (2.48). The unit normal $\boldsymbol{n}_f$ at the fluid solid interface boundary in the averaging volume points outside the fluid region f. The interface surface integral in (2.52) holds the information that would be lost when the average of a derivative was taken to be the derivative of the average. Not seldom this integral is the dominant contribution in the right-hand-side of (2.52).

Time-Derivative Theorem

The *time derivative in the usual sense* [1, 28] is the distribution which takes the form

$$\frac{\partial^\nu \boldsymbol{\phi}}{\partial t} \triangleq \begin{cases} \frac{\partial \boldsymbol{\phi}_f}{\partial t} & \text{in } \Omega_f \\ \frac{\partial \boldsymbol{\phi}_s}{\partial t} & \text{in } \Omega_s \end{cases}\,. \tag{2.53}$$

The time derivative of a spatially averaged distribution is given by

$$\frac{\partial\langle \boldsymbol{\phi}\rangle_m}{\partial t} = \left\langle \frac{\partial^\nu \boldsymbol{\phi}}{\partial t}\right\rangle_m + \langle \boldsymbol{n}_{fs}\cdot\boldsymbol{w}\,(\boldsymbol{\phi}_f - \boldsymbol{\phi}_s)\delta_{fs}\rangle_m\,. \tag{2.54}$$

The last term in the former equation is zero when the singularity surface between the s- and f-region is stationary and thus has no speed of displacement $\boldsymbol{w}$.

Geometrical Theorem

In [2] the following geometrical theorem is proven for $n \geq 0$:

$$\begin{aligned}&\int_{\boldsymbol{r}\in\mathbb{R}^d} m(\boldsymbol{x}-\boldsymbol{r})\,\boldsymbol{n}_{fs}(\boldsymbol{r})\,(\boldsymbol{r}-\boldsymbol{x})^{\otimes n}\delta_{fs}(\boldsymbol{r})\,d\Omega(\boldsymbol{r})\\&= -\nabla\int_{\boldsymbol{r}\in\mathbb{R}^d} m(\boldsymbol{x}-\boldsymbol{r})\,\gamma_f(\boldsymbol{r})\,(\boldsymbol{r}-\boldsymbol{x})^{\otimes n}\,d\Omega(\boldsymbol{r})\,.\end{aligned} \tag{2.55}$$

More precisely, the identity $\nabla\langle\gamma_f\boldsymbol{y}^{\otimes n}\rangle_m = \langle(\nabla\gamma_f)\boldsymbol{y}^{\otimes n}\rangle_m$ is proven in [2]. Equation (2.55) follows from this proof through substitution of $\nabla\gamma_f = -\nabla\gamma_s = -\boldsymbol{n}_{fs}\delta_{fs}$. In (2.55), $\otimes n$ denotes the n^{th} tensor power of a tensor, which is the n-fold tensor product of this tensor with itself (see for instance [31]).

For notational simplicity, this geometrical theorem is from here on expressed as

$$\langle\boldsymbol{n}_{fs}\boldsymbol{y}^{\otimes n}\delta_{fs}\rangle_m = -\nabla\langle\gamma_f\boldsymbol{y}^{\otimes n}\rangle_m = \nabla\langle\gamma_s\boldsymbol{y}^{\otimes n}\rangle_m\,, \tag{2.56}$$

where the position vector $\boldsymbol{y}(\boldsymbol{r})|_{\boldsymbol{x}} \triangleq \boldsymbol{r}-\boldsymbol{x}$ locates points relative to the centroid of the averaging domain.

As a special case for $n = 0$ we retrieve the equality

$$\langle\boldsymbol{n}_{fs}\delta_{fs}\rangle_m = -\nabla\epsilon_{fm} = \nabla\epsilon_{sm}\,. \tag{2.57}$$

2.8 Taylor Series of a Spatially Averaged Distribution

The Taylor series representation of a spatially averaged distribution around the point $\boldsymbol{x}$ has the form

$$\begin{aligned}\langle\boldsymbol{\phi}\rangle_m|_{(\boldsymbol{r},t)} = {}& \langle\boldsymbol{\phi}\rangle_m|_{(\boldsymbol{x},t)} + (\boldsymbol{r}-\boldsymbol{x})\cdot\nabla\langle\boldsymbol{\phi}\rangle_m|_{(\boldsymbol{x},t)}\\&+\frac{1}{2}(\boldsymbol{r}-\boldsymbol{x})(\boldsymbol{r}-\boldsymbol{x})\cdot\cdot\nabla\nabla\langle\boldsymbol{\phi}\rangle_m|_{(\boldsymbol{x},t)}+\ldots\end{aligned} \tag{2.58}$$

In short hand notation, this Taylor series will be further represented as

$$\langle \boldsymbol{\phi} \rangle_m |_{(\boldsymbol{r},t)} = \sum_{n=0}^{\infty} \frac{1}{n!} (\boldsymbol{r} - \boldsymbol{x})^{\otimes n} \underbrace{\cdot\cdot}_{n\text{-times}} \nabla^{\otimes n} \langle \boldsymbol{\phi} \rangle_m \big|_{(\boldsymbol{x},t)} \,. \tag{2.59}$$

The n-times repeated dot operator $\cdot$ is the inner product of two n^{th} rank tensors, creating a scalar.

2.9 Decomposition of a Distribution

The spatial averaging technique allows the *decomposition of a distribution* into a spatially averaged part over the fluid and solid regions and a deviation part:

$$\boldsymbol{\phi} = \langle \boldsymbol{\phi} \rangle_m^f \gamma_f + \langle \boldsymbol{\phi} \rangle_m^s \gamma_s + \widetilde{\boldsymbol{\phi}} \,, \tag{2.60}$$

where the deviation part $\widetilde{\boldsymbol{\phi}}$ has the function representation:

$$\widetilde{\boldsymbol{\phi}} \triangleq \begin{cases} \widetilde{\boldsymbol{\phi}}_f = \boldsymbol{\phi}_f - \left\{ \langle \boldsymbol{\phi} \rangle_m^f \right\}_f & \text{in } \Omega_f \\ \widetilde{\boldsymbol{\phi}}_s = \boldsymbol{\phi}_s - \left\{ \langle \boldsymbol{\phi} \rangle_m^s \right\}_s & \text{in } \Omega_s \end{cases} . \tag{2.61}$$

Here $\{\,\}_f$ and $\{\,\}_s$ denote the part of the distribution in the f- and s-region respectively. This decomposition differs from the work of Quintard and Whitakter [2] and traditional VAT, because we also consider distributions which are non-zero over the solid domain.

The presence of the indicators γ_f and γ_s in (2.60) ensures that $\widetilde{\boldsymbol{\phi}}_f = 0$ when $\boldsymbol{\phi}_f = 0$ and $\widetilde{\boldsymbol{\phi}}_s = 0$ when $\boldsymbol{\phi}_s = 0$. In general, when $\boldsymbol{\phi}_s = 0$, $\langle \boldsymbol{\phi} \rangle_m^f$ might be non-zero in Ω_s within some distance R away from the interface boundary Γ_{fs}. Likewise, when $\boldsymbol{\phi}_f = 0$, it might be that $\langle \boldsymbol{\phi} \rangle_m^s |_{(\boldsymbol{x},t)} \neq 0$ in Ω_f, for $\boldsymbol{r} \in \Gamma_{fs}$ and $\|\boldsymbol{x} - \boldsymbol{r}\| = R > 0$.

Lastly, we give an expression for the gradient in the usual sense of a distribution:

$$\begin{aligned} \nabla^\nu \boldsymbol{\phi} &= \nabla^\nu (\langle \boldsymbol{\phi} \rangle_m^f \gamma_f + \langle \boldsymbol{\phi} \rangle_m^s \gamma_s) + \nabla^\nu \widetilde{\boldsymbol{\phi}} \\ &= \gamma_f \nabla \langle \boldsymbol{\phi} \rangle_m^f + \gamma_s \nabla \langle \boldsymbol{\phi} \rangle_m^s + \nabla^\nu \widetilde{\boldsymbol{\phi}} \,, \end{aligned} \tag{2.62}$$

where it was taken into account that $\nabla^\nu \gamma_f = \nabla^\nu \gamma_s = 0$ and $\nabla^\nu \langle \boldsymbol{\phi} \rangle_m^f = \nabla \langle \boldsymbol{\phi} \rangle_m^f$, $\nabla^\nu \langle \boldsymbol{\phi} \rangle_m^s = \nabla \langle \boldsymbol{\phi} \rangle_m^s$ because $\langle \boldsymbol{\phi} \rangle_m^f$ and $\langle \boldsymbol{\phi} \rangle_m^s$ are free of discontinuities at Γ_{fs}.

2.10 Decomposition of the Surface Filter

The surface filter arises in expressions for spatially averaged gradients via the spatial gradient theorem. Because the Dirac distribution at the interface boundary merely selects the value of the functions $\boldsymbol{\phi}_f$ and $\boldsymbol{\phi}_s$ at the singularity surface Γ_{fs}, the following statement holds for the surface filter:

$$\begin{aligned}\langle \boldsymbol{n}_{fs}(\boldsymbol{\phi}_f - \boldsymbol{\phi}_s)\delta_{fs}\rangle_m &= \langle \boldsymbol{n}_{fs}\big[\big\{\langle\boldsymbol{\phi}\rangle_m^f\big\}_f + \widetilde{\boldsymbol{\phi}}_f - \big\{\langle\boldsymbol{\phi}\rangle_m^s\big\}_s - \widetilde{\boldsymbol{\phi}}_s\big]\delta_{fs}\rangle_m \\ &= \langle \boldsymbol{n}_{fs}(\langle\boldsymbol{\phi}\rangle_m^f - \langle\boldsymbol{\phi}\rangle_m^s)\delta_{fs}\rangle_m + \langle \boldsymbol{n}_{fs}(\widetilde{\boldsymbol{\phi}}_f - \widetilde{\boldsymbol{\phi}}_s)\delta_{fs}\rangle_m \,. \end{aligned} \tag{2.63}$$

Using the Taylor series representation (cf. (2.59)), the surface filter in (2.63) can be decomposed in the following way

$$\begin{aligned}\langle \boldsymbol{n}_{fs}(\boldsymbol{\phi}_f - \boldsymbol{\phi}_s)\delta_{fs}\rangle_m = &\sum_{n=0}^{\infty} \boldsymbol{G}_m^{(n)} \underbrace{\cdot\cdot}_{n\text{-times}} \nabla^{\otimes n}\langle\boldsymbol{\phi}\rangle_m^f - \sum_{n=0}^{\infty} \boldsymbol{G}_m^{(n)} \underbrace{\cdot\cdot}_{n\text{-times}} \nabla^{\otimes n}\langle\boldsymbol{\phi}\rangle_m^s \\ &+ \langle \boldsymbol{n}_{fs}(\widetilde{\boldsymbol{\phi}}_f - \widetilde{\boldsymbol{\phi}}_s)\delta_{fs}\rangle_m \,, \end{aligned} \tag{2.64}$$

where the geometrical tensors $\boldsymbol{G}_m^{(n)}$ are defined as

$$\begin{aligned}\boldsymbol{G}_m^{(n)} &\triangleq \frac{1}{n!}\langle \boldsymbol{n}_{fs}\boldsymbol{y}^{\otimes n}\delta_{fs}\rangle_m \\ &= -\frac{1}{n!}\nabla\langle\gamma_f\boldsymbol{y}^{\otimes n}\rangle_m = -\frac{1}{n!}\nabla(\epsilon_{fm}\langle\boldsymbol{y}^{\otimes n}\rangle_m^f) \,. \end{aligned} \tag{2.65}$$

This last identity results from the geometrical theorem (2.56).

Later on, we will also make use of the related geometrical tensors $\boldsymbol{G}_m^{\prime(n)}$, which we define as

$$\boldsymbol{G}_m^{\prime(n)} \triangleq \epsilon_{fm}^{-1}\boldsymbol{G}_m^{(n)} \,. \tag{2.66}$$

In the original work of Whitaker and Quintard [2], the decomposition of the surface filter is performed in a questionable manner, leading to geometrical tensors of the form $\langle \boldsymbol{n}_{fs}\boldsymbol{y}^{\otimes n}\gamma_f\delta_{fs}\rangle_m$. This form is not only incorrect, but also ambiguous [32] as it requires a definition of the product $\gamma_f\delta_{fs}$ (e.g. [33]).

2.11 Filter Properties

Fundamental Properties of the Weighting Function

Although the weighting function m is in principle of arbitrary choice, it should at the very least satisfy three properties [2] to result in a continuous and compact filter operator:

P1. The weighting function is smooth:
$m \in C^\infty$

P2. The weighting function has compact support over $\mathbb{R}^d$:
$m(\boldsymbol{x}-\boldsymbol{r}) = 0$ for $\boldsymbol{r} \notin \bar{\Omega}(\boldsymbol{x})$

P3. The weighting function is normalized:
$$\int_{\boldsymbol{r}\in\mathbb{R}^d} m(\boldsymbol{x}-\boldsymbol{r})\, d\Omega(\boldsymbol{r}) = \int_{\boldsymbol{r}\in\bar{\Omega}(\boldsymbol{x})} m(\boldsymbol{x}-\boldsymbol{r})\, d\Omega(\boldsymbol{r}) = 1$$

The first condition (**P**1) gives rise to average quantities that are smooth or infinitely differentiable. The second condition (**P**2) means that $m = 0$ everywhere except in a compact set and implies the average is taken over a finite averaging domain or filter window $\bar{\Omega}$, which contains a part $\bar{\Gamma}_{fs}$ of the complete interface boundary Γ_{fs}. The normalization property (**P**3) is necessary to have a filter which is idempotent with respect to a constant.

Idempotence Property

In order to construct a spatial averaging operator $\langle\ \rangle_m$ which yields a meaningful average, the weighting function should ensure that the average remains approximately unaltered after repeated averaging. Therefore, we require the filter $\langle\ \rangle_m$ to be based on a weighting function which satisfies, apart from the three fundamental properties (**P**1-**P**3), the idempotence property (**P**4):

P4. (version A) – The filter approximately preserves idempotence:

$$\langle\langle\boldsymbol{\phi}\rangle_m\rangle_m \simeq \langle\boldsymbol{\phi}\rangle_m\,. \tag{2.67}$$

The idempotence property for the superficial spatial average (2.67) is also formulated as: If m gives rise to an idempotent filter operator, also $m * m$ gives rise to an idempotent spatial filter operator.

The fact that the idempototence property for the superficial spatial average (**P**4 version A) in general can only be satisfied approximately, follows from the Taylor-series representation for the averaged distribution (cf.(2.59)):

$$\langle\langle\boldsymbol{\phi}\rangle_m\rangle_m\big|_{(\boldsymbol{x},t)} = \langle\boldsymbol{\phi}\rangle_m\big|_{(\boldsymbol{x},t)} + \sum_{n=1}^{\infty}\frac{1}{n!}\,\langle\boldsymbol{y}^{\otimes n}\rangle_m\big|_{\boldsymbol{x}}\underbrace{\cdot\cdot}_{n\text{-times}}\nabla^{\otimes n}\langle\boldsymbol{\phi}\rangle_m\big|_{(\boldsymbol{x},t)}\,. \tag{2.68}$$

Hence, (**P**4 version A) implies the following constraint on the weighting function m:

P4. (version A) – The weighting function suppresses the effect of gradients and other higher-order derivatives of the filtered distribution:

$$\langle\boldsymbol{\phi}\rangle_m \gg \sum_{n=1}^{\infty}\frac{1}{n!}\langle\boldsymbol{y}^{\otimes n}\rangle_m\underbrace{\cdot\cdot}_{n\text{-times}}\nabla^{\otimes n}\langle\boldsymbol{\phi}\rangle_m\,, \tag{2.69}$$

or, if the higher-order derivatives are not dominating:

$$\langle\boldsymbol{\phi}\rangle_m \gg \langle\boldsymbol{y}\rangle_m\cdot\nabla\langle\boldsymbol{\phi}\rangle_m\,. \tag{2.70}$$

The specific mathematical conditions for the idempotence property for the volume average are discussed in e.g. [10, 34].

The idempotence property of the intrinsic spatial average is expressed by the statement:

P4. (version B) – The filter approximately preserves idempotence for the intrinsic spatial averages:

$$\langle\langle\boldsymbol{\phi}\rangle_m^f\rangle_m^f \simeq \langle\boldsymbol{\phi}\rangle_m^f \qquad \text{and} \qquad \langle\langle\boldsymbol{\phi}\rangle_m^s\rangle_m^s \simeq \langle\boldsymbol{\phi}\rangle_m^s\,. \tag{2.71}$$

When the intrinsic spatial averages are expressed in terms of a Taylor series similar to (2.68), it follows that (**P**4 version B) is equivalent to

P4. (version B) – The weighting function must suppress the derivatives of the intrinsic spatial averages within the filter window:

$$\langle\gamma_f\rangle_m\langle\boldsymbol{\phi}\rangle^f_m \gg \sum_{n=1}^{\infty}\frac{1}{n!}\langle\gamma_f\boldsymbol{y}^{\otimes n}\rangle_m \underbrace{\cdot\cdot}_{n\text{-times}} \nabla^{\otimes n}\langle\boldsymbol{\phi}\rangle^f_m\,,$$
$$\langle\gamma_s\rangle_m\langle\boldsymbol{\phi}\rangle^s_m \gg \sum_{n=1}^{\infty}\frac{1}{n!}\langle\gamma_s\boldsymbol{y}^{\otimes n}\rangle_m \underbrace{\cdot\cdot}_{n\text{-times}} \nabla^{\otimes n}\langle\boldsymbol{\phi}\rangle^s_m\,. \tag{2.72}$$

The idempotence property (**P**4 version B) can also be formulated in another way:

P4. (version B) – The weighting function must suppress the deviation part of the distribution:

$$\langle\widetilde{\boldsymbol{\phi}}\rangle_m \simeq 0\,. \tag{2.73}$$

To prove the equivalence between (2.72) and (2.73), we express the Taylor series of (2.68) in terms of the intrinsic averages:

$$\begin{aligned}\langle\boldsymbol{\phi}\rangle_m &= \langle\langle\boldsymbol{\phi}\rangle^f_m\gamma_f\rangle_m + \langle\langle\boldsymbol{\phi}\rangle^s_m\gamma_s\rangle_m + \langle\widetilde{\boldsymbol{\phi}}\rangle_m\\ &= \langle\gamma_f\rangle_m\langle\boldsymbol{\phi}\rangle^f_m + \langle\gamma_f\boldsymbol{y}\rangle_m\cdot\nabla\langle\boldsymbol{\phi}\rangle^f_m + \frac{1}{2}\langle\gamma_f\boldsymbol{y}\boldsymbol{y}\rangle_m\cdot\cdot\nabla\nabla\langle\boldsymbol{\phi}\rangle^f_m + \ldots\\ &\quad + \langle\gamma_s\rangle_m\langle\boldsymbol{\phi}\rangle^s_m + \langle\gamma_s\boldsymbol{y}\rangle_m\cdot\nabla\langle\boldsymbol{\phi}\rangle^s_m + \frac{1}{2}\langle\gamma_s\boldsymbol{y}\boldsymbol{y}\rangle_m\cdot\cdot\nabla\nabla\langle\boldsymbol{\phi}\rangle^s_m + \ldots\\ &\quad + \langle\widetilde{\boldsymbol{\phi}}\rangle_m\,,\end{aligned} \tag{2.74}$$

where it is understood that $\langle\boldsymbol{\phi}\rangle^f_m$, $\langle\boldsymbol{\phi}\rangle^s_m$ and all their derivatives are eval-

uated at the centroid $\boldsymbol{x}$ of $\bar{\Omega}$. From the last result, we find that

$$\langle\widetilde{\boldsymbol{\phi}}\rangle_m = \sum_{n=1}^{\infty} \frac{1}{n!} \langle \gamma_f \boldsymbol{y}^{\otimes n} \rangle_m \underbrace{\ddots}_{n\text{-times}} \nabla^{\otimes n} \langle \boldsymbol{\phi} \rangle_m^f + \sum_{n=1}^{\infty} \frac{1}{n!} \langle \gamma_s \boldsymbol{y}^{\otimes n} \rangle_m \underbrace{\ddots}_{n\text{-times}} \nabla^{\otimes n} \langle \boldsymbol{\phi} \rangle_m^s \,. \tag{2.75}$$

A comparison of this result with (2.72) confirms that $\langle\widetilde{\boldsymbol{\phi}}\rangle_m = 0$ (cf. (2.73)) when $\langle\langle\boldsymbol{\phi}\rangle_m^f\rangle_m^f = \langle\boldsymbol{\phi}\rangle_m^f$ and $\langle\langle\boldsymbol{\phi}\rangle_m^s\rangle_m^s = \langle\boldsymbol{\phi}\rangle_m^s$ (cf. (2.71)).

Finally, we give yet another equivalent version of the idempotence property:

P4. (version B) – The weighting function ensures that variations of the filtered distributions $\langle\boldsymbol{\phi}\rangle_m^f$ and $\langle\boldsymbol{\phi}\rangle_m^s$ within an averaging window $\bar{\Omega}$ can be neglected, such that

$$\begin{array}{l} \langle\langle\boldsymbol{\phi}\rangle_m^f \gamma_f\rangle_m \simeq \epsilon_{fm} \langle\boldsymbol{\phi}\rangle_m^f \\ \langle\langle\boldsymbol{\phi}\rangle_m^s \gamma_s\rangle_m \simeq \epsilon_{sm} \langle\boldsymbol{\phi}\rangle_m^s \end{array} \quad \Rightarrow \quad \begin{array}{l} \langle\boldsymbol{\phi}\rangle_m \simeq \langle\langle\boldsymbol{\phi}\rangle_m^f \gamma_f\rangle_m + \langle\langle\boldsymbol{\phi}\rangle_m^s \gamma_s\rangle_m \\ \langle\widetilde{\boldsymbol{\phi}}\rangle_m = \langle\widetilde{\boldsymbol{\phi}}_f\rangle_m + \langle\widetilde{\boldsymbol{\phi}}_s\rangle_m \simeq 0 \end{array} \tag{2.76}$$

The final version (2.76) is obtained after combination of (2.72) and (2.74).

2.12 Macro- and Micro-Scale Quantities

In Chapter 1, we have defined a macro-scale quantity as a quantity that captures in an averaged way the most important patterns and spatial changes of the original quantity from which it is derived. Therefore, $\langle\boldsymbol{\phi}\rangle_m^f$ and $\langle\boldsymbol{\phi}\rangle_m^s$ are called *macro-scale quantities*, if they undergo significant spatial changes (gradients) over a length scale $\mathscr{L}_\phi$ much larger than the spatial scale ℓ_ϕ over which the original distribution $\boldsymbol{\phi}$ undergoes significant changes. If $\langle\boldsymbol{\phi}\rangle_m^f$ and $\langle\boldsymbol{\phi}\rangle_m^s$ are macro-scale quantities, the deviation part $\widetilde{\boldsymbol{\phi}}$ is called a *micro-scale* quantity and $\widetilde{\boldsymbol{\phi}}$ changes significantly over a length scale $\ell_{\widetilde{\phi}}$ that is smaller than $\mathscr{L}_\phi$.

In symbolic notation, the former definition becomes:

$\langle\boldsymbol{\phi}\rangle_m^f$ and $\langle\boldsymbol{\phi}\rangle_m^s$ are macro-scale quantities and $\widetilde{\boldsymbol{\phi}}$ is a micro-scale quantity if and only if

$$\underbrace{\boldsymbol{\phi}}_{} = \underbrace{\langle\boldsymbol{\phi}\rangle_m^f\gamma_f + \langle\boldsymbol{\phi}\rangle_m^s\gamma_s}_{} + \underbrace{\widetilde{\boldsymbol{\phi}}}_{}$$
$$\ell_\phi \ll \mathscr{L}_\phi \gg \ell_{\widetilde{\phi}}. \tag{2.77}$$

When the condition for *scale separation* (2.77) is met through a proper choice of the weighting function and averaging domain of the filter, the spatial decomposition (2.60) reflects a separation between the micro- and macro-scale level.

2.13 Characteristic Length Scales

Illustration of Length Scales

In physics, a *length scale* is a particular length or spatial distance that is used to characterize some physical quantity or physical process. Often a length scale is not represented by a precise number, but rather by a number of which only the order of magnitude is specified.

The meaning of a length scale in this work is illustrated in Figure 2.2. Figure 2.2 gives a hypothetical example of a scalar flow quantity ϕ_f which varies with the spatial coordinate x. Also the corresponding volume-averaged quantity $\langle\phi_f\rangle^f$ and its deviation field $\widetilde{\phi}_f$ are displayed as functions of the coordinate x. In the neighbourhood of the point ⓐ, the original flow quantity ϕ_f varies continuously, but only at a distance ℓ_ϕ from ⓐ, the relative changes in ϕ_f are considered to become significant. Therefore we say that ℓ_ϕ is the characteristic length scale for (the gradients of) this flow quantity at this point. As it can be observed in Figure 2.2, the characteristic length scale usually depends on the position. For instance, near the point ⓑ, ϕ_f changes relatively less in comparison to near the point ⓐ or ⓒ. Therefore, ℓ_ϕ is larger at ⓑ than at ⓐ or ⓒ. Figure 2.2 also shows the length scale $\mathscr{L}_{\phi,f}$ for $\langle\phi_f\rangle^f$ and the length scale $\ell_{\widetilde{\phi}}$ for $\widetilde{\phi}_f$ at positions ⓐ, ⓑ and ⓒ. In this example, the length scale for the volume-averaged

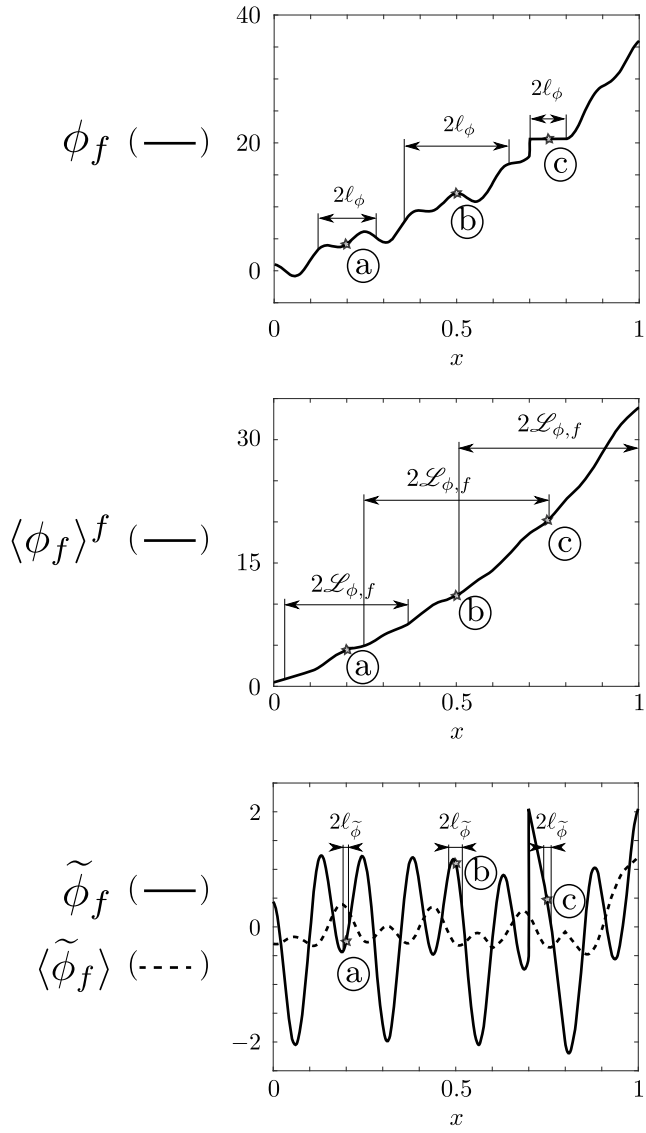

Figure 2.2: Illustration of the length scale ℓ_ϕ of a flow quantity ϕ_f, the length scale $\mathscr{L}_{\phi,f}$ of its volume average $\langle\phi_f\rangle^f$ and the length scale $\ell_{\widetilde{\phi}}$ of its deviation part $\widetilde{\phi}_f$.

quantity is larger than the length scale of the original quantity or the length scale of the deviation part: $\mathscr{L}_{\phi,f} > \ell_\phi$ and $\mathscr{L}_{\phi,f} > \ell_{\widetilde{\phi}}$ at ⓐ,ⓑ and ⓒ. The latter observations are a consequence of the fact that the filter radius r_0 of the averaging volume is larger than ℓ_ϕ for most locations x. In this figure, an averaging volume $\bar{\Omega}(x) = \{\forall r | r \in (x - r_0/2, x + r_0/2)\}$ with $r_0 = 0.2$ was chosen. However, whether $\mathscr{L}_{\phi,f} > \ell_\phi$ depends not just on the relative size r_0/ℓ_ϕ or $r_0/\mathscr{L}_{\phi,f}$ of the filter window, but also on the profile of the physical quantity $\phi_f(x)$.

Definition of Length Scales

In this work, the length scale $\mathcal{L}_{\phi,f}$ for the quantity $\langle \boldsymbol{\phi} \rangle^f_m$ around some point of interest $\boldsymbol{x}$ at a time-instant t, is defined as the largest constant $\mathcal{L}_{\phi,f} = \max \mathcal{L}^\star_{\phi,f}$ such that

$$O\left(\frac{\|\boldsymbol{y} \cdot \nabla \langle \boldsymbol{\phi} \rangle^f_m\big|_{(\boldsymbol{x},t)}\|}{\|\langle \boldsymbol{\phi} \rangle^f_m|_{(\boldsymbol{x},t)}\|}\right) \leq O\left(\frac{\|\boldsymbol{y}\|}{\mathscr{L}^\star_{\phi,f}}\right), \qquad \forall \boldsymbol{y} \,|\, \mathscr{L}^\star_{\phi,f} \geq \|\boldsymbol{y}\|\,. \tag{2.78}$$

The *order of magnitude* of a quantity $\boldsymbol{a}$ is defined as $O(\boldsymbol{a}) \triangleq \lfloor \log_{10} \|\boldsymbol{a}\| \rfloor$.

In an analogous manner to (2.78), we define the length scales $\mathscr{L}_{\phi,s}$, ℓ_ϕ and $\ell_{\widetilde{\phi}}$ for the quantities $\langle \boldsymbol{\phi} \rangle^s_m$, $\boldsymbol{\phi}$ and $\widetilde{\boldsymbol{\phi}}$ respectively. The common length scale $\mathscr{L}_\phi$ for both $\langle \boldsymbol{\phi} \rangle^f_m$ and $\langle \boldsymbol{\phi} \rangle^s_m$ is defined as $\mathscr{L}_\phi \triangleq \min(\mathscr{L}_{\phi,f}, \mathscr{L}_{\phi,s})$.

Interpretation of Length Scales

The interpretation of the former definitions is that the original quantity and the filtered quantities can be treated as approximately constant respectively within a radius $R \ll \ell_\phi$ and $R \ll \mathscr{L}_\phi$ around some point of interest $\boldsymbol{x}$. This interpretation can be understood from Taylor's inequality which implies that

$$\begin{aligned} \langle \boldsymbol{\phi} \rangle^f_m\big|_{(\boldsymbol{r},t)} &= \langle \boldsymbol{\phi} \rangle^f_m\big|_{(\boldsymbol{x},t)} + \Delta\langle \boldsymbol{\phi} \rangle^f_m\big|_{(\boldsymbol{x},\boldsymbol{r},t)} \qquad \text{with} \\ O\left(\frac{\|\,\Delta\langle \boldsymbol{\phi} \rangle^f_m\big|_{(\boldsymbol{x},\boldsymbol{r},t)}\|}{\|\langle \boldsymbol{\phi} \rangle^f_m|_{(\boldsymbol{x},t)}\|}\right) &\leq O\left(\frac{\|\boldsymbol{r} - \boldsymbol{x}\|}{\mathscr{L}_{\phi,f}}\right) \qquad \text{for} \qquad \|\boldsymbol{r} - \boldsymbol{x}\| \leq \mathscr{L}_{\phi,f}\,, \end{aligned} \tag{2.79}$$

provided that the length scale $\mathscr{L}_{\phi,f}$ exists. Hence, we can use the approximation

$$\langle \boldsymbol{\phi} \rangle^f_m\big|_{(\boldsymbol{r},t)} \simeq \langle \boldsymbol{\phi} \rangle^f_m\big|_{(\boldsymbol{x},t)} \qquad \text{if} \qquad \frac{R}{\mathscr{L}_\phi} \triangleq \frac{\|\boldsymbol{r} - \boldsymbol{x}\|}{\mathscr{L}_\phi} \ll 1\,. \tag{2.80}$$

In this regard, the spatial changes or gradients of the quantity $\langle\boldsymbol{\phi}\rangle_m^f$ are considered *significant* only at a distance $R = O(\mathscr{L}_\phi)$ away from the point $\boldsymbol{x}$, because then a gradient term and possibly other higher-order derivatives must be taken into account in the Taylor series similar to (2.58):

$$\langle\boldsymbol{\phi}\rangle_m^f\big|_{(\boldsymbol{r},t)} \simeq \langle\boldsymbol{\phi}\rangle_m^f\big|_{(\boldsymbol{x},t)} + \boldsymbol{y}\cdot\nabla\,\langle\boldsymbol{\phi}\rangle_m^f\big|_{(\boldsymbol{x},t)} + \ldots \text{ if } \quad R = O(\mathscr{L}_\phi)\ . \tag{2.81}$$

According to the former definitions, the length scales still may vary in space and time and depend on the physical transport process for the quantity ϕ, like the gradients $\nabla\langle\boldsymbol{\phi}\rangle_m^f$, $\nabla\langle\boldsymbol{\phi}\rangle_m^s$ and $\nabla\widetilde{\boldsymbol{\phi}}$ do. In Chapters 5, 6 and 7, we will use the definitions according to (2.78) to quantify the length scales for the developed flow and heat transfer regimes.

Length Scales as Order-of-Magnitude Estimates

The definitions of the length scales $\mathscr{L}_\phi$ and ℓ_ϕ in this work can be used to estimate the order of magnitude of the gradients of the spatially averaged quantities and their deviation fields through the following *order-of-magnitude estimates*:

$$\nabla\langle\boldsymbol{\phi}\rangle_m^f = \mathcal{O}\left(\frac{\langle\boldsymbol{\phi}\rangle_m^f}{\mathscr{L}_\phi}\right), \qquad \nabla\widetilde{\boldsymbol{\phi}}_f = \mathcal{O}\left(\frac{\widetilde{\boldsymbol{\phi}}_f}{\ell_\phi}\right),$$
$$\nabla\langle\boldsymbol{\phi}\rangle_m^s = \mathcal{O}\left(\frac{\langle\boldsymbol{\phi}\rangle_m^s}{\mathscr{L}_\phi}\right), \qquad \nabla\widetilde{\boldsymbol{\phi}}_s = \mathcal{O}\left(\frac{\widetilde{\boldsymbol{\phi}}_s}{\ell_\phi}\right). \tag{2.82}$$

These estimates are based on the assumption that the order of magnitude of the remainder term in (2.79) is determined by the gradient, but not the higher-order derivatives: $\Delta\langle\boldsymbol{\phi}\rangle_m^f\big|_{(\boldsymbol{x},\boldsymbol{r},t)} \simeq (\boldsymbol{r}-\boldsymbol{x})\cdot\nabla\,\langle\boldsymbol{\phi}\rangle_m^f\big|_{(\boldsymbol{x},t)}$. Furthermore, these estimates assume $\mathscr{L}_{\phi,f} \simeq \mathscr{L}_\phi$ and $\ell_{\widetilde{\phi}} \simeq \ell_\phi$.

In the length-scale analysis that is used in the VAT models for porous media, order-of-magnitude estimates similar to (2.82) actually serve as definitions for the length scales. However, the order-of-magnitude estimates (2.82) cannot be used to define $\mathscr{L}_\phi$ and ℓ_ϕ, because these estimates are prone to subjective interpretation for the following two reasons.

To start, an order-of-magnitude estimate written in the form $\boldsymbol{b} = \mathcal{O}(\boldsymbol{a})$ reflects the idea that the order of magnitude of $\boldsymbol{a}$ is an *estimate* or a *guess* for the order of magnitude of $\boldsymbol{b}$, so one writes $\boldsymbol{b} = \mathcal{O}(\boldsymbol{a})$ while one means something like $O(\boldsymbol{b}) \simeq O(\boldsymbol{a})$. However, as an order-of-magnitude estimate

represents just an estimate, but not the order of magnitude itself, it is not clear how the symbol $\mathcal{O}$ is defined. Unless one properly defines the symbol $\mathcal{O}$ by specifying an objective criterion to measure how close $\mathcal{O}(\boldsymbol{a})$ should match $O(\boldsymbol{a})$, the length scales in (2.82) are ill-defined.

Secondly, even if the order-of-magnitude estimate in (2.82) would be no longer prone to subjective interpretation or if one would use the true order of magnitude instead, one must be aware that each of the length scales in (2.82) cannot be quantified by a single number, because for every $\boldsymbol{b}$ there exist many $\boldsymbol{a}$ such that $\boldsymbol{b} = O(\boldsymbol{a})$. On the contrary, the definition of a length scale in this work (2.78) does allow to quantify a length scale by a unique number: the length scale $\mathcal{L}_{\phi,f}$ for instance is the largest number of all length scale numbers $\mathcal{L}^{\star}_{\phi,f}$ satisfying (2.78).

Because of the former two reasons, we conclude that a length scale is not a well-defined, quantifiable concept in the literature on VAT, so that its interpretation in the literature strongly depends on the context.

Length-Scale Constraint for Idempotence

The support $\bar{\Omega}$ of the weighting function is characterized by the length scale r_m, which can be defined in a number of ways, e.g.

$$r_m \triangleq \langle \|\boldsymbol{y}\| \rangle_m \qquad \text{or} \qquad r_m \triangleq \sqrt[d]{V} \qquad \text{or} \qquad r_m \triangleq r_0\,, \tag{2.83}$$

While the last definition in (2.83) is suitable for a spherical averaging domain with radius r_0, $\bar{\Omega}(\boldsymbol{x}) = \{\forall \boldsymbol{r} \,|\, r_0 \geq \|\boldsymbol{y}\|\}$, the other two definitions are suitable for an averaging domain with a more complex shape in $\mathbb{R}^d$.

The length scale r_m of the filter represents the width of the filter window. It characterizes the distance $\|\boldsymbol{y}\| \triangleq \|\boldsymbol{r} - \boldsymbol{x}\|$ between the centroid of the averaging domain and the other points within the averaging domain. When this distance r_m is much smaller than the length scale $\mathscr{L}_\phi$ for the filtered quantities, the filtered quantities can be treated as constant within the averaging domain (cf. (2.80)). Therefore, the filter is idempotent when the support of the weighting function satisfies the following length-scale constraint:

P4. (version C) – A filter is (approximately) idempotent when the support of its weighting function m is constrained by the length-scale inequality

$$r_m \ll \mathscr{L}_\phi\,. \tag{2.84}$$

The length-scale constraint (2.84) permits the simplification

$$\langle \boldsymbol{\phi} \rangle_m \simeq \langle \gamma_f \rangle_m \langle \boldsymbol{\phi} \rangle_m^f + \langle \gamma_s \rangle_m \langle \boldsymbol{\phi} \rangle_m^s + \langle \widetilde{\boldsymbol{\phi}} \rangle_m = \langle \boldsymbol{\phi} \rangle_m + \langle \widetilde{\boldsymbol{\phi}} \rangle_m \,, \qquad (2.85)$$

from which it automatically follows that $\langle \widetilde{\boldsymbol{\phi}} \rangle_m \simeq 0$. In Figure 2.2 for example, we have chosen an averaging radius which does not strictly respect $r_m = r_0 \ll \mathscr{L}_{\phi,f}$ everywhere. Therefore, the approximation $\langle \widetilde{\phi}_f \rangle \simeq 0$ holds just very roughly. However, the idempotence of the volume-averaging operator for ϕ_f would be easier to judge if the difference between $\langle \phi_f \rangle^f$ and $\langle \langle \phi_f \rangle^f \rangle^f$ had been shown in the figure.

In the VAT theory for porous media [10, 34], the length-scale constraint (2.84) for the idempotence property is usually derived from the order-of-magnitude estimate

$$\langle \langle \boldsymbol{\phi} \rangle_m \rangle_m = \langle \boldsymbol{\phi} \rangle_m + \mathcal{O}\left(\langle \boldsymbol{\phi} \rangle_m \frac{r_m}{\mathscr{L}_\phi} \right) . \qquad (2.86)$$

This order-of-magnitude estimate is based on the assumption that the importance of the derivatives in (2.69) and (2.72) can be estimated via

$$\begin{aligned} \nabla^{\otimes n} \langle \boldsymbol{\phi} \rangle_m^f &= \mathcal{O}\left(\frac{\langle \boldsymbol{\phi} \rangle_m^f}{\mathscr{L}_\phi^n} \right) , \qquad & \nabla^{\otimes n} \langle \boldsymbol{\phi} \rangle_m^s &= \mathcal{O}\left(\frac{\langle \boldsymbol{\phi} \rangle_m^s}{\mathscr{L}_\phi^n} \right) , \\ \nabla^{\otimes n} \langle \boldsymbol{\phi} \rangle_m &= \mathcal{O}\left(\frac{\langle \boldsymbol{\phi} \rangle_m}{\mathscr{L}_\phi^n} \right) , \qquad & \nabla^{\otimes n} \widetilde{\boldsymbol{\phi}} &= \mathcal{O}\left(\frac{\widetilde{\boldsymbol{\phi}}}{\ell_\phi^n} \right) . \end{aligned} \qquad (2.87)$$

Moreover, the estimate (2.86) takes the characteristic size r_m of the filter window $\bar{\Omega}$ into account to estimate the geometrical moments in (2.69) and (2.72):

$$\langle \gamma_f \boldsymbol{y}^{\otimes n} \rangle_m = \mathcal{O}\left(\epsilon_{fm} r_m^n \right) , \quad \langle \gamma_s \boldsymbol{y}^{\otimes n} \rangle_m = \mathcal{O}\left(\epsilon_{sm} r_m^n \right) , \quad \langle \boldsymbol{y}^{\otimes n} \rangle_m = \mathcal{O}\left(r_m^n \right) . \qquad (2.88)$$

For any weighting function of the form $m = m_G * m_V$ with $m_G \in C^\infty$ it holds that $\langle \boldsymbol{y} \rangle_m = 0$, as $\boldsymbol{x}$ is the centroid of $\bar{\Omega}$ and $\boldsymbol{y} \triangleq \boldsymbol{r} - \boldsymbol{x}$. Consequently, for $m = m_G * m_V$, the estimates (2.87) and (2.88) lead to the estimate

$$\langle \langle \boldsymbol{\phi} \rangle_m \rangle_m = \langle \boldsymbol{\phi} \rangle_m + \mathcal{O}\left(\langle \boldsymbol{\phi} \rangle_m \frac{r_m^2}{\mathscr{L}_\phi^2} \right) , \qquad (2.89)$$

instead of (2.86).

Length Scale Constraint for Macro-Scale Quantities

To obtain a meaningful macro-scale quantity, the averaging operator must not only respect the definition of a macro-scale quantity (2.77), but also be idempotent (2.86), hence $\ell_\phi \ll \mathscr{L}_\phi$ and $r_m \ll \mathscr{L}_\phi$. In practise, $\mathscr{L}_\phi > \ell_\phi$ is achieved by choosing a sufficiently large filter width $r_m \geq \ell_\phi$. Thus, an averaging operator whose weighting function satisfies (**P**1-**P**4), defines a meaningful macro-scale quantity, if the support of m also satisfies the following property (**P**5):

P5. The characteristic filter width r_m of the filter is at least as large as the characteristic length scale of the original quantity:

$$r_m \geq \ell_\phi \,, \tag{2.90}$$

so that if the filter is (approximately) idempotent,

$$\ell_\phi \leq r_m \ll \mathscr{L}_\phi \,. \tag{2.91}$$

The length-scale constraint (2.91) is a criterion to check whether the filtered quantities are macro-scale quantities. However, one must keep in mind that this criterion can only be used a posteriori, i.e. after filtering, as $\mathscr{L}_\phi$ depends on r_m. On the other hand, ℓ_ϕ is independent of the filter size r_m because it is the scale of the original distribution $\boldsymbol{\phi}$.

Degree of Scale Separation

Although we have explained that the scale $\mathscr{L}_\phi$ over which the filtered quantity varies, should be much larger than the scale ℓ_ϕ over which the original quantity varies, we have not explained *how much larger* $\mathscr{L}_\phi$ should be *in comparison to* ℓ_ϕ in order to call the filtered quantity a meaningful macro-scale quantity and its deviation part a micro-scale quantity. *How much larger in comparison to*, the symbol $\ll$ in (2.77) and (2.91) means, remains however a subjective choice.

In the first place, the interpretation of the inequality sign in (2.77) and (2.91) depends on the degree of detail of the original quantity that one subjectively desires to keep in the macro-scale quantity [7]. The macro-scale quantity becomes more detailed when it has significant spatial gradients over a shorter length scale, hence when the difference between $\mathscr{L}_\phi$ and ℓ_ϕ becomes smaller. In VAT for instance, the volume-averaged quantities are

expected to become less detailed over space, as a larger radius $r_m = r_0$ of the averaging domain is chosen.

In the VAT models for porous media, the idempotence of the averaging operator and the scale-separation condition (2.77) are usually postulated as the fundamental assumptions in the derivation of the volume-averaged transport equations. Therefore, the difference between $\mathscr{L}_\phi$ and ℓ_ϕ in these VAT models is constrained by the validity of the volume-averaged transport equations and the validity of the closure problem on the REV of the porous medium. As a consequence, the macro-scale quantities in the VAT models for porous media are actually defined in agreement with the approximations in the volume-averaged model equations.

In this work, the spatially averaged flow and temperature equations will be derived from the Navier-Stokes equations using a general filter, hence without requiring the idempotence of the filter or scale separation. That way, we will define the macro-scale quantities directly from the quantities in the original Navier-Stokes equations, without imposing any constraints that are prone to subjective interpretation. Our definitions are based on very specific weighting functions and lead to a clear physical interpretation of the macro-scale quantities. The scale-separation condition (2.77) itself is considered of secondary importance in this work, as it will be merely the result of our choice of weighting functions. Moreover, in this work, the weighting function guarantees the exactness of our simplified closure problems. The exactness of our macro-scale description is entirely owing to the spatial periodicity of the solid structures.

2.14 Filtered Product of Two Macro-Scale Quantities

When the filter has the properties (**P**1-**P**5) with respect to two distributions $\boldsymbol{\phi}_1$ and $\boldsymbol{\phi}_2$, so $r_m \geq \max(\ell_{\phi_1}, \ell_{\phi_2})$, the filtered product of the two distributions can be approximated as

$$\begin{aligned}\langle \boldsymbol{\phi}_1 \boldsymbol{\phi}_2 \rangle_m &= \langle \langle \boldsymbol{\phi}_1 \rangle_m^f \boldsymbol{\phi}_2 \gamma_f + \langle \boldsymbol{\phi}_1 \rangle_m^s \boldsymbol{\phi}_2 \gamma_s + \langle \widetilde{\boldsymbol{\phi}}_1 \boldsymbol{\phi}_2 \rangle_m \\ &\simeq \epsilon_{fm} \langle \boldsymbol{\phi}_1 \rangle_m^f \langle \boldsymbol{\phi}_2 \rangle_m^f + \epsilon_{sm} \langle \boldsymbol{\phi}_1 \rangle_m^s \langle \boldsymbol{\phi}_2 \rangle_m^s + \langle \widetilde{\boldsymbol{\phi}}_1 \widetilde{\boldsymbol{\phi}}_2 \rangle_m \,. \end{aligned} \tag{2.92}$$

In case $\{\boldsymbol{\phi}_1\}_f$ and $\{\boldsymbol{\phi}_1\}_s$ both are constant within $\bar{\Omega}$, the former result gives

$$\langle \boldsymbol{\phi}_1 \boldsymbol{\phi}_2 \rangle_m \simeq \epsilon_{fm} \{\boldsymbol{\phi}_1\}_f \langle \boldsymbol{\phi}_2 \rangle_m^f + \epsilon_{sm} \{\boldsymbol{\phi}_1\}_s \langle \boldsymbol{\phi}_2 \rangle_m^s \,. \tag{2.93}$$

The equation above is also a good approximation when gradients of $\{\boldsymbol{\phi}_1\}_f$ over $\bar{\Omega}_f$ as well as gradients of $\{\boldsymbol{\phi}_1\}_s$ over $\bar{\Omega}_s$ are small, although discontinuities of $\boldsymbol{\phi}_1$ at Γ_{fs} might be present. Note that when (2.93) is used as approximation, point-values of $\{\boldsymbol{\phi}_1\}_f$ and $\{\boldsymbol{\phi}_1\}_s$ are used to evaluate $\langle \boldsymbol{\phi}_1 \boldsymbol{\phi}_2 \rangle_m$ at position $\boldsymbol{x}$. When $\boldsymbol{x}$ lies within the s-region, the value of $\{\boldsymbol{\phi}_1\}_f |_{\boldsymbol{x}}$ is not defined and a suitable representative value of $\{\boldsymbol{\phi}_1\}_f$ within $\bar{\Omega}(\boldsymbol{x})$ should be used. A similar remark can be made when $\boldsymbol{x}$ is located in the f-region.

2.15 Extension of a Distribution Outside of the System Domain

In this one but last section, we return back to the convolution product (2.11), whose evaluation requires that the distribution $\boldsymbol{\phi}$ is defined on $\mathbb{R}^d$ instead of $\Omega \subset \mathbb{R}^d$. The extension of the distribution, $\boldsymbol{\phi}(\boldsymbol{x}, t) = \boldsymbol{\phi}_e(\boldsymbol{x}, t)$ for $\boldsymbol{x} \in \mathbb{R}^d \setminus \Omega$ is of arbitrary choice, but it must be constructed in a manner that Γ_{fs} is the only discontinuity surface of $\boldsymbol{\phi}$ in $\mathbb{R}^d$. Otherwise the commutativity of the convolution operator and the gradient operator (cf. (2.50)) is not guaranteed, so that the gradient theorems (2.44) and (2.48) no longer hold.

When the distribution satisfies a specific physical boundary condition at the boundary of the system domain, $\boldsymbol{\phi}(\boldsymbol{x}, t) = \boldsymbol{\phi}_\Gamma(\boldsymbol{x}, t)$ for $\boldsymbol{x} \in \Gamma$, the extension must thus satisfy $\boldsymbol{\phi}_e \in C^\infty$ for $\boldsymbol{x} \in \mathbb{R}^d \setminus \Omega$ and $\boldsymbol{\phi}_e(\boldsymbol{x}, t) = \boldsymbol{\phi}_\Gamma(\boldsymbol{x}, t)$ for $\boldsymbol{x} \in \Gamma$. If $\boldsymbol{\phi}_e \in C^\infty$ for $\boldsymbol{x} \in \mathbb{R}^d \setminus \Omega$, but $\boldsymbol{\phi}(\boldsymbol{x}, t) \neq \boldsymbol{\phi}_\Gamma(\boldsymbol{x}, t)$ for $\boldsymbol{x} \in \Gamma$, the expression for the gradient in the sense of distribution (2.44) would have to be modified into

$$\nabla \boldsymbol{\phi} = \nabla^\nu \boldsymbol{\phi} - \boldsymbol{n}_{fs}(\boldsymbol{\phi}_f - \boldsymbol{\phi}_s)\delta_{fs} - \boldsymbol{n}(\boldsymbol{\phi}_\Gamma - \boldsymbol{\phi}_e)\delta_\Gamma \,, \tag{2.94}$$

where δ_Γ and $\boldsymbol{n}$ are respectively the Dirac distribution associated with the system boundary Γ and the normal vector at Γ pointing outward of Ω.

In this work, the convolution product near Γ is always evaluated by extending $\boldsymbol{\phi}$ in a continuous way outside of Ω, that way the commutation error $\boldsymbol{n}(\boldsymbol{\phi}_\Gamma - \boldsymbol{\phi}_e)\delta_\Gamma$ does not have to be dealt with.

2.16 Time-Averaging Operator

To close this chapter, we give the definition of the *time average* of a distribution over a time-interval τ:

$$\overline{\boldsymbol{\phi}}\big|_{(\boldsymbol{x},t)} \triangleq \frac{1}{\tau}\int_{t-\frac{\tau}{2}}^{t+\frac{\tau}{2}} \boldsymbol{\phi}(\boldsymbol{x},t')\,dt'\,. \tag{2.95}$$

For a time-periodic distribution $\boldsymbol{\phi}(\boldsymbol{x},t) = \boldsymbol{\phi}(\boldsymbol{x},t+\tau)$ with period τ, the former time average is independent of time: $\overline{\boldsymbol{\phi}}(\boldsymbol{x})$.

Bibliography

[1] M. Quintard and S. Whitaker, "Transport in ordered and disordered porous media I: The cellular average and the use of weighting functions," *Transport in Porous Media*, vol. 14, no. 2, pp. 163–177, 1994.

[2] M. Quintard and S. Whitaker, "Transport in ordered and disordered porous media II: Generalized volume averaging," *Transport in Porous Media*, vol. 14, no. 2, pp. 179–206, 1994.

[3] M. Quintard and S. Whitaker, "Transport in ordered and disordered porous media III: Closure and comparison between theory and experiment," *Transport in Porous Media*, vol. 15, no. 1, pp. 31–49, 1994.

[4] M. Quintard and S. Whitaker, "Transport in ordered and disordered porous media IV: Computer generated porous media for three-dimensional systems," *Transport in Porous Media*, vol. 15, no. 1, pp. 51–70, 1994.

[5] M. Quintard and S. Whitaker, "Transport in ordered and disordered porous media V: Geometrical results for two-dimensional systems," *Transport in Porous Media*, vol. 15, no. 2, pp. 183–196, 1994.

[6] C. M. Marle, "Application de la méthode de la thermodynamique des processus irréversible à l'écoulement d'un fluide à travers un milieux poreux," *Bulletin RILEM*, vol. 29, pp. 1066–1071, 1965.

[7] C. M. Marle, "Ecoulements monophasiques en milieu poreux," *Revue de l'Institut Français du Pétrole*, vol. 22, no. 10, pp. 1471–1509, 1967.

[8] S. Whitaker, "The role of the volume-averaged temperature in the analysis of nonisothermal, multiphase transport phenomena," *Chemical Engineering Communications*, vol. 58, no. 1-6, pp. 171–183, 1987.

[9] J. C. Slattery, "Flow of viscoelastic fluids through porous media," *AIChE Journal*, vol. 13, no. 6, pp. 1066–1071, 1967.

[10] S. Whitaker, "Advances in theory of fluid motion in porous media," *Industrial & Engineering Chemistry Research*, vol. 61, no. 12, pp. 14–28, 1969.

[11] J. Bear, *Dynamics of Fluids in Porous Media.* Elsevier, New York, 1972.

[12] M. Hassanizadeh and W. G. Gray, "General conservation equations for multi-phase systems: 1. Averaging procedure," *Advances in Water Resources*, vol. 2, pp. 131–144, 1979.

[13] P. Baveye and G. Sposito, "The operational significance of the continuum hypothesis in the theory of water movement through soils and aquifers," *Water Resources Research*, vol. 20, pp. 521–530, 1984.

[14] S. R. Pride and J. G. Berryman, "Connecting theory to experiment in poroelasticity," *Journal of the Mechanics and Physics of Solids*, vol. 46, pp. 719–747, 1998.

[15] Y. Davit, G. Debenest, B. D. Wood, and M. Quintard, "Modeling non-equilibrium mass transport in biologically reactive porous media," *Advances in Water Resources*, vol. 33, pp. 1075–1093, 2010.

[16] S. B. Pope, *Turbulent flows.* Cambridge University Press, 2000.

[17] P. Sagaut, *Large Eddy Simulation for Incompressible Flows.* Springer-Verlag, Berlin Heidelberg New York, 2001.

[18] F.-S. Lien and E. Yee, "Numerical modelling of the turbulent flow developing within and over a 3-D building array, part III:: a distributed drag force approach, its implementation and application," *Boundary-Layer Meteorology*, vol. 114, no. 2, pp. 287–313, 2005.

[19] T. B. Anderson and R. Jackson, "Fluid mechanical description of fluidized beds. equations of motion," *Industrial & Engineering Chemistry Fundamentals*, vol. 6, no. 4, pp. 527–539, 1967.

[20] S. Whitaker, "Diffusion and dispersion in porous media," *AIChE Journal*, vol. 13, pp. 420–427, 1967.

[21] Y. Bachmat, "Spatial macroscopization of processes in heterogeneous systems," *Israel Journal of Technology*, vol. 10, pp. 391–403, 1972.

[22] W. G. Gray and P. C. Y. Lee, "On the theorems for local volume averaging of multiphase systems," *International Journal of Multiphase Flow*, vol. 3, pp. 333–340, 1977.

[23] J. H. Cushman, "Proofs of the volume averaging theorems for multiphase flow," *Advances in Water Resources*, vol. 5, no. 4, pp. 248 – 253, 1982.

[24] F. A. Howes and S. Whitaker, "The spatial averaging theorem revisited," *Chemical Engineering Science*, vol. 40, no. 8, pp. 1387–1392, 1985.

[25] W. G. Gray, "Local volume averaging of multiphase systems using a non-constant averaging volume," *International Journal of Multiphase Flow*, vol. 9, no. 6, pp. 755 – 761, 1983.

[26] J. H. Cushman, "Multiphase transport equations: I - general equation for macroscopic statistical, local space-time homogeneity," *Transport Theory and Statistical Physics*, vol. 12, no. 1, pp. 35–71, 1983.

[27] L. Schwartz, *Théorie des Distributions*. Hermann, Paris, 1978.

[28] R. J. Gagnon, "Distribution theory of vector fields," *American Journal of Physics*, vol. 38, no. 7, pp. 879–891, 1970.

[29] S. Ghosal and P. Moin, "The basic equations for the large eddy simulation of turbulent flows in complex geometry," *Journal of Computational Physics*, vol. 118, no. 1, pp. 24 – 37, 1995.

[30] O. V. Vasilyev, T. S. Lund, and P. Moin, "A General Class of Commutative Filters for LES in Complex Geometries," *Journal of Computational Physics*, vol. 146, no. 1, pp. 82 – 104, 1998.

[31] B. D. Wood, "Technical note: Revisiting the geometric theorems for volume averaging," *Advances in Water Resources*, vol. 62, pp. 340–352, 2013.

[32] D. Griffiths, "Dirac deltas and discontinuous functions," *American Journal of Physics*, vol. 67, no. 5, p. 446, 1999.

[33] C. K. Raju, "Products and compositions with the Dirac delta function," *Journal of Physics A: Mathematical and General*, vol. 15, no. 2, pp. 381–396, 1982.

[34] B. D. Wood, "Volume averaging for determining the effective dispersion tensor: Closure using periodic unit cells and comparison with ensemble averaging," *Water Resources Research*, vol. 39, no. 8, p. 1210, 2003.

CHAPTER

3

SPATIALLY AVERAGED FLOW EQUATIONS

3.1 Introduction

This chapter presents spatially averaged Navier-Stokes equations for modelling the macro-scale flow in devices with solid structures. The form of the macro-scale flow equations presented here is generally valid for an incompressible Newtonian fluid, as long as the viscosity of the fluid changes gradually over the device domain. No assumptions about the flow regime or the topology of the solid structures are incorporated in the flow equations. To describe the mainly two-dimensional flow through small channels with solid structures, so-called macro-scale planar flow equations are proposed in this chapter.

3.2 Outline

In this chapter, first a historical overview is given of the development of spatially averaged flow equations describing the macro-scale flow in solid media. In addition, the need for a reformulation of the existing macro-scale flow equations for spatially periodic solid structures is explained. In the next section, Section 4, the Navier-Stokes flow equations for an incompressible Newtonian fluid are reformulated within the theory of mathematical distributions, so that they become compatible with the spatial averaging technique of the previous chapter. In Section 5, the boundary conditions for the flow in a heat transfer device are discussed. Section 6 presents the exact form of the spatially averaged Navier-Stokes flow equations. In the same section, also the differences with the macro-scale flow equations from the literature are clarified. The boundary conditions for the spatially averaged Navier-Stokes flow equations are the topic of Section 7. In Section 8, the global closure problem for the closure terms in the macro-scale flow equations is given. The boundary conditions for the global closure problem follow in Section 9. In Section 10, the planar flow equations are developed by averaging the Navier-Stokes equations over the height of the flow domain. The boundary conditions for the planar flow equations are obtained in Section 11. Subsequently, Section 12 gives an approximate closure method for the planar flow equations. Finally, in the last section, the spatially averaged planar flow and their boundary conditions are presented.

3.3 Historical Background

The spatially averaged flow equations presented in the literature have been developed for solid media like rocks, sandstones and other porous materials which one encounters in geosciences and petroleum engineering. As porous media have a complex and spatially aperiodic fluid-solid interface whose precise shape is in practise unknown, DNS of the very detailed flow phenomena around the interface of the entire porous medium is in practise impossible. Therefore, the spatially averaged flow equations presented in the literature all incorporate certain (length-scale) approximations which enable us to deal with the complex fluid-solid interface and detailed flow phenomena on just an REV of the porous medium.

It will be shown that most of the work in the literature is aimed at defining the permeability and Forchheimer tensor, which characterize the macro-scale flow through a porous medium, via REV-based closure models. In that perspective, spatial averaging of the flow equations has been used as a method to define approximative effective properties of a porous medium (i.e. approximative homogenization), rather than to obtain exact model reduction and data reduction.

Furthermore, it will appear that a lot of studies concern the spatial averaging of the Stokes flow equations, which describe steady incompressible viscous flow in absence of inertial effects. Less studies are available which treat the spatial averaging of the Navier-Stokes equations for inertial flow. Lastly, it will become clear that the macro-scale description of turbulent flow still faces a lot of challenges.

Spatially Averaged Stokes Flow Equations

The macro-scale description of Stokes flow through a porous medium was one of the first problems to be investigated by means of spatial averaging techniques, at the end of the 1960s [1–4]. The volume-averaged form of the Stokes momentum equation was shown to approximate *Darcy's law*:

$$\nabla\langle p\rangle \simeq -\mu_f \boldsymbol{K}^{-1} \cdot \langle \boldsymbol{u}\rangle \,.$$

Darcy's law states that the relation between the volume-averaged flow velocity $\langle \boldsymbol{u}\rangle$ and the gradient of the volume-averaged pressure $\nabla\langle p\rangle$ is determined by the permeability tensor $\boldsymbol{K}$ of the porous medium.

One of the earliest derivations of Darcy's law was established by Marle [1], who used a weighted averaging technique to justify Darcy's law from the principles of irreversible thermodynamics and Onsager's reciprocal relations. Other early derivations of Darcy's law were obtained by the volume-averaging technique. The early VAT derivations are either based on several constitutive assumptions about the porous medium and restricted to homogeneous porous media, e.g. the work of Slattery [2] and Whitaker [3], or restricted to spatially periodic solid media in which the volume-averaged velocity remains constant, e.g. the work of Brenner [5]. A summary of these earliest derivations can be found in the work of [4].

The first derivation of Darcy's law by means of VAT without constitutive assumptions was carried out by Whitaker in 1986 [6]. Whitaker simplified the volume-averaged Stokes momentum equation under different length-

scale constraints into the form

$$-\nabla\langle p\rangle^f+\rho_f\boldsymbol{g}+\boldsymbol{b}'_{fs}=0 \quad \text{with} \quad \boldsymbol{b}'_{fs}\simeq\frac{\mu_f}{V_f}\int_{A_{fs}}\boldsymbol{n}_{fs}\cdot(-\widetilde{p}_f\boldsymbol{I}+\mu_f\nabla\widetilde{\boldsymbol{u}}_f)\;dA\,.$$

Here $\langle p\rangle^f$ denotes the intrinsically volume-averaged pressure, while $\rho_f\boldsymbol{g}$ denotes the gravitational body force on the fluid. In Whitaker's analysis, the interfacial force $\boldsymbol{b}'_{fs}$ is assumed to result from the stresses due to the deviation pressure $\widetilde{p}_f$ and deviation velocity $\widetilde{\boldsymbol{u}}_f$ at the fluid-solid surface A_{fs} in the averaging volume V_f. To determine the interfacial force, Whitaker postulated an approximate closure problem of which the solution consists of the closure variables $\boldsymbol{B}$ and $\boldsymbol{b}$:

$$\widetilde{\boldsymbol{u}}_f=\boldsymbol{B}\cdot\langle\boldsymbol{u}\rangle^f \quad \text{and} \quad \widetilde{p}_f=\mu_f\boldsymbol{b}\cdot\langle\boldsymbol{u}\rangle^f\,.$$

The closure variables $\boldsymbol{B}$ and $\boldsymbol{b}$ yield the deviation velocity and deviation pressure within the porous medium and therefore also the interfacial force. Because the closure variables are assumed to be periodic over an REV of the porous medium, the closure problem of Whitaker is a *local closure problem* that can be solved on an REV. The local closure problem of Whitaker governs the permeability of the porous medium in the Stokes flow regime through the relation

$$\boldsymbol{b}'_{fs}\simeq\mu_f\boldsymbol{K}^{-1}\cdot\langle\boldsymbol{u}\rangle \quad \text{where} \quad \boldsymbol{K}^{-1}\triangleq\epsilon_f^{-1}\frac{1}{V_f}\int_{A_{fs}}\boldsymbol{n}_{fs}\cdot(-\boldsymbol{b}+\nabla\boldsymbol{B})\;dA\,.$$

The former expression shows that the interfacial force is an integral of the closure variables, so that Whitaker's local closure problem consists of an integro-differential equation.

An equivalent local closure problem for the volume-averaged Stokes equations was given by Barrère in 1992 [7]. This equivalent closure problem determines the closure variables $\boldsymbol{D}$ and $\boldsymbol{d}$ on an REV of the porous medium:

$$\widetilde{\boldsymbol{u}}_f=\boldsymbol{D}\cdot(\nabla\langle p\rangle^f-\rho_f\boldsymbol{g}) \quad \text{and} \quad \widetilde{p}_f=\mu_f\boldsymbol{D}\cdot(\nabla\langle p\rangle^f-\rho_f\boldsymbol{g})\,,$$

Furthermore, it governs the Darcy permeability via the simple expression

$$\boldsymbol{K}=-\epsilon_f\langle\boldsymbol{D}\rangle^f\,.$$

While the closure problem of Whitaker [6] for Stokes flow is an integro-differential equation, the equivalent closure problem of Barrère is a differential equation similar to the Stokes momentum equation.

The exact form of the spatially averaged Stokes momentum equation that holds for an arbitrary weighting function m had not been presented in the literature until the work of Quintard and Whitaker in 1994 [8] appeared:

$$-\nabla\langle p\rangle_m + \rho_f \boldsymbol{g}\epsilon_{fm} + \mu_f\nabla^2\langle \boldsymbol{u}\rangle_m + \boldsymbol{b}_{fs} = 0\,,$$

where the viscous term $\mu_f\nabla^2\langle \boldsymbol{u}\rangle_m$ is called the *Brinkman correction* and the weighted porosity ϵ_{fm} of the medium might be space-dependent. Quintard and Whitaker showed that the weighted interfacial force[1] not only consists of a surface integral of the pressure and viscous deviation stresses along the fluid-solid interface, but also an infinite number of higher-order terms which are disregarded in all VAT derivations:

$$\begin{aligned}\boldsymbol{b}_{fs} = m * \left[\boldsymbol{n}_{fs}\cdot(-\widetilde{p}_f\boldsymbol{I} + \mu_f\nabla^2\widetilde{\boldsymbol{u}}_f)\delta_{fs}\right] + \nabla(m*\gamma_f)\langle p\rangle_m^f \\ + \nabla\left[m*(\boldsymbol{y}\gamma_f)\right]\cdot\nabla\langle p\rangle_m^f + \nabla\left[m*(\boldsymbol{y}\boldsymbol{y}\gamma_f)\right]\cdot\cdot\nabla\nabla\langle p\rangle_m^f + \ldots \\ - \nabla(m*\gamma_f)\cdot\mu_f\nabla\langle \boldsymbol{u}\rangle_m^f - \nabla\left[m*(\boldsymbol{y}\gamma_f)\right]\cdot\cdot\mu_f\nabla\nabla\langle \boldsymbol{u}\rangle_m^f + \ldots\,.\end{aligned}$$

The infinite number of higher-order terms make the spatially averaged momentum equation a *non-local* partial differential equation, so they inhibit the development of a local closure problem that governs the interfacial force $\boldsymbol{b}_{fs}$ on an REV of the medium. The higher-order terms appear when the spatial moments of medium, $m*\gamma_f, m*(\boldsymbol{y}\gamma_f), m*(\boldsymbol{y}\boldsymbol{y}\gamma_f)$ etc., are nonzero.

It was demonstrated by Quintard and Whitaker [8] that the spatial moments of a spatially periodic solid medium can be made to vanish with the specific weighting $m = m_V * m_V$ which defines the cellular average. For spatially aperiodic porous media, Quintard and Whitaker proposed to use a weighting function which approximately suppresses the infinite number of higher-order terms in the macro-scale Stokes equation. Whether such a weighting function can be found, still remains a partly unanswered question, but Quintard and Whitaker argued that it may be sufficient that the weighting function just ensures that the first-order spatial moment be small:

$$\nabla\left[m*(\boldsymbol{y}\gamma_f)\right] \ll \boldsymbol{I}\,.$$

A spatially aperiodic porous medium that satisfies the condition above with respect to some weighting function has been called a *disordered* porous medium by Quintard and Whitaker.

[1] In the work of Quintard and Whitaker [6, 8], the different terms in the averaged Stokes equation are never collected into a single term called the interfacial force. The latter term is actually a re-interpretation of their work.

The local closure problem for the weighted averaged Stokes equations of Quintard and Whitaker[8] has been given in [9] under the assumption that the spatial moments of the medium are zero for the chosen weighting function. The latter closure problem has the same form as the closure problem for the volume-averaged Stokes equations in [6] and finally leads to the same form of Darcy's law as VAT.

An extension of the volume-averaged Stokes equations for slightly compressible flow can be found in Quintard's study from 1996 [10] and in Lasseux's study from 2014 [11]. Both studies present a closure problem for the interfacial force in compressible Stokes flow, which is in essence based on the same closure variables as for the incompressible case [6, 7]. However, both studies differ from each other in one major aspect. The closure problem in Quintard's work incorporates a no-slip condition for the flow velocity at the fluid-solid interface, while the closure problem in Lasseux's work takes gas-rarefaction into account via a velocity slip condition.

The volume-averaged Stokes equations for a power-law fluid flowing through a porous medium were derived by Wang et al. in 2014 [12]. A power-law fluid is a fluid whose viscous stress tensor is of the form

$$\boldsymbol{\tau} = \mu_f \|\boldsymbol{A}\|^{n-1}\boldsymbol{A} \qquad \text{with} \qquad \boldsymbol{A} \triangleq \nabla\boldsymbol{u} + (\nabla\boldsymbol{u})^{\intercal} \ .$$

In the study of Wang et al., the closure problem for a power-law fluid flow is assumed to be analogous to that of a Newtonian fluid flow. Under that assumption, the relation between the interfacial force and the volume-averaged velocity can be transformed in a power law:

$$\boldsymbol{b}'_{fs} \simeq \mu_f \|\langle\boldsymbol{u}\rangle\|^{n-1}\boldsymbol{K}_n^{-1} \cdot \langle\boldsymbol{u}\rangle \, ,$$

where the apparent permeability tensor $\boldsymbol{K}_n$ is very similar in nature to the Darcy permeability.

In 2016, Minale [13] used VAT to derive the macro-scale equation for Stokes flow of a visco-elastic second-order fluid in a porous medium. The viscous stress tensor of a visco-elastic second-order fluid has the form

$$\boldsymbol{\tau} = \mu_f\boldsymbol{A} + 4\beta_1\boldsymbol{A}\cdot\boldsymbol{A} + \beta_2\left((\nabla\boldsymbol{u})^{\intercal}\cdot\boldsymbol{A} + \boldsymbol{A}\cdot\nabla\boldsymbol{u}\right) \, .$$

In Minale's local closure problem, the interfacial force is partly represented by a Darcy permeability tensor $\boldsymbol{K}_{\mathrm{N}}$ and partly by a non-Newtonian third-order tensor $\boldsymbol{K}_{\mathrm{nN}}$. The non-Newtonian third-order tensor corrects Darcy's

law for visco-elastic effects:

$$\boldsymbol{b}'_{fs} \simeq \mu_f \boldsymbol{K}_{\mathrm{N}}^{-1} \cdot \langle \boldsymbol{u} \rangle + \boldsymbol{K}_{\mathrm{nN}}^{-1} \cdot \cdot \langle \boldsymbol{u} \rangle \langle \boldsymbol{u} \rangle \, .$$

Spatially Averaged Navier-Stokes Flow Equations

The spatially averaged form of the flow equations for a general fluid can be traced back to the work of Marle [14] in 1967. Marle reformulated the continuity and momentum equations within the theory of distributions of Schwarz [15] to average them through a convolution product with a weighting function m:

$$\frac{\partial \rho_{fm}}{\partial t} + \nabla \cdot (\rho_{fm} \boldsymbol{u}_m) = 0 \, ,$$

$$\frac{\partial (\rho_{fm} \boldsymbol{u}_m)}{\partial t} + \nabla \cdot (\rho_{fm} \boldsymbol{u}_m \boldsymbol{u}_m + p_m \boldsymbol{I} - \boldsymbol{M} - \boldsymbol{\tau}_m) = \rho_{fm} \boldsymbol{X} + \boldsymbol{b}_{fs} \, .$$

In Marle's macro-scale continuity and momentum equations, the spatially averaged density $\rho_{fm} \triangleq m * \rho_f$ and flow velocity $\boldsymbol{u}_m \triangleq (\rho_f \boldsymbol{u}) * m / \rho_{fm}$, as well as the spatially averaged viscous stress tensor $\boldsymbol{\tau}_m$ and pressure p_m can be recognized. The closure term $\boldsymbol{b}_{fs} \triangleq [\boldsymbol{n}_{fs} \cdot (p\boldsymbol{I} - \boldsymbol{\tau}) \delta_{fs})] * m$ represents the weighted interfacial force. The closure term $\boldsymbol{M}$ represents the exchange of momentum between macro-scale streamlines due to fluctuations of the micro-scale velocity: $\boldsymbol{M} \triangleq -[\rho_f (\boldsymbol{u} - \boldsymbol{u}_m)(\boldsymbol{u} - \boldsymbol{u}_m)] * m$. The spatially constant body force is denoted by $\boldsymbol{X}$ in Marle's work.

One of the first volume-averaged forms of the Navier-Stokes equations appears in the work of Whitaker in 1969 [3], where the macro-scale equations for an incompressible viscous flow are written as

$$\nabla \cdot \langle \boldsymbol{u} \rangle = 0 \, ,$$

$$\rho_f \left(\frac{\partial \langle \boldsymbol{u} \rangle}{\partial t} + \langle \boldsymbol{u} \rangle \cdot \nabla \langle \boldsymbol{u} \rangle \right) = -\nabla \langle p \rangle + \boldsymbol{R} \cdot \langle \boldsymbol{u} \rangle \, .$$

The total resistance tensor $\boldsymbol{R} \triangleq \mu_f \langle \nabla^2 \boldsymbol{M} \rangle + \boldsymbol{A}$ arises in the macro-scale flow equations of Whitaker [3] from the assumption that there exists a non-linear mapping $\boldsymbol{M}$ between the original flow velocity and the volume-averaged velocity, as well as a mapping $\boldsymbol{A}$ from the macro-scale velocity to the following volume-averaged terms:

$$\boldsymbol{u} = \boldsymbol{M} \cdot \langle \boldsymbol{u} \rangle \, ,$$

$$\frac{1}{V} \int_{A_{fs}} \boldsymbol{n}_{fs} p_f \, dA - \rho_f \nabla \cdot \langle \widetilde{\boldsymbol{u}} \widetilde{\boldsymbol{u}} \rangle = \boldsymbol{A} \cdot \langle \boldsymbol{u} \rangle \, .$$

A more profound derivation of the volume-averaged Navier-Stokes for incompressible flow was elaborated by Whitaker in 1996 [16]. In the latter study, Whitaker introduces many length-scale approximations to arrive at the following momentum equation:

$$\rho_f \frac{\partial \langle \boldsymbol{u} \rangle^f}{\partial t} + \rho_f \langle \boldsymbol{u} \rangle^f \cdot \nabla \langle \boldsymbol{u} \rangle^f + \rho_f \epsilon_f^{-1} \nabla \cdot \langle \widetilde{\boldsymbol{u}} \widetilde{\boldsymbol{u}} \rangle = -\nabla \langle p \rangle^f + \rho_f \boldsymbol{g} + \mu_f \nabla^2 \langle \boldsymbol{u} \rangle^f + \boldsymbol{b}'_{fs} \, .$$

In this momentum equation, an inertial closure term $\rho_f \epsilon_f^{-1} \nabla \cdot \langle \widetilde{\boldsymbol{u}} \widetilde{\boldsymbol{u}} \rangle$ shows up, which Whitaker identified as the *volume filter*. The interfacial force or *surface filter* $\boldsymbol{b}'_{fs}$ in the former momentum equation is approximated in the same way as in Whitaker's preceding work on Stokes flow [6].

Whitaker's study [16] presents two closure problems to determine the surface filter and volume filter on a REV of the porous medium. The first of these closure problems yields the surface filter and volume filter via the closure variables $\boldsymbol{b}$ and $\boldsymbol{B}$:

$$\boldsymbol{b}'_{fs} \simeq \left[\frac{\mu_f}{V_f} \int_{A_{fs}} \boldsymbol{n}_{fs} \cdot (-\boldsymbol{b} + \nabla \boldsymbol{B}) \, dA \right] \cdot \langle \boldsymbol{u} \rangle \, ,$$
$$\langle \widetilde{\boldsymbol{u}} \widetilde{\boldsymbol{u}} \rangle \simeq \langle \boldsymbol{u} \rangle^f \cdot \langle \boldsymbol{B}^\intercal \boldsymbol{B} \rangle \cdot \langle \boldsymbol{u} \rangle^f \, .$$

The closure variables $\boldsymbol{b}$ and $\boldsymbol{B}$ map the volume-averaged velocity $\langle \boldsymbol{u} \rangle^f$ into the deviation velocity and pressure, just like in the local closure problem for the volume-averaged Stokes equations [6]. Of course, $\boldsymbol{b}$ and $\boldsymbol{B}$ are defined differently from the Stokes closure problem in [6], as the first closure problem of [16] also includes inertial terms. The closure variables of the first closure problem determine the apparent permeability [17] of the porous medium. In contrast to the Darcy permeability, the apparent permeability is not a geometric property of the porous medium, because it also depends on the volume-averaged flow velocity.

The second closure problem in [16] only holds when the volume filter and macro-scale advection terms are neglected in the macro-scale momentum equation. It defines the closure variables $\boldsymbol{B}$ and $\boldsymbol{b}$ as the solution of the Stokes closure problem in [6] and introduces the additional closure variables $\boldsymbol{C}$ and $\boldsymbol{c}$ to account for the inertial terms in the Navier-Stokes equations:

$$\widetilde{\boldsymbol{u}}_f = \boldsymbol{B} \cdot \langle \boldsymbol{u} \rangle^f + \boldsymbol{C} \cdot \langle \boldsymbol{u} \rangle^f \quad \text{and} \quad \widetilde{p}_f = \mu_f \boldsymbol{b} \cdot \langle \boldsymbol{u} \rangle^f + \mu_f \boldsymbol{c} \cdot \langle \boldsymbol{u} \rangle^f \, .$$

When the second closure problem is solved, the surface filter in the volume-averaged Navier-Stokes momentum equation can be transformed into

$$\boldsymbol{b}'_{fs} \simeq \mu_f \boldsymbol{K}^{-1} \cdot \langle \boldsymbol{u} \rangle - \mu_f \boldsymbol{K}^{-1} \cdot \boldsymbol{F} \cdot \langle \boldsymbol{u} \rangle \,,$$

where $\boldsymbol{K}$ is the Darcy permeability tensor for the volume-averaged Stokes equations and $\boldsymbol{F}$ is the *Forchheimer correction tensor*, which is defined by

$$\boldsymbol{F} \triangleq -\epsilon_f^{-1} \boldsymbol{K} \cdot \left[\frac{1}{V_f} \int_{A_{fs}} \boldsymbol{n}_{fs} \cdot (-\boldsymbol{c} + \nabla \boldsymbol{C}) \, dA \right] .$$

Finally, we remark that modifications of the volume-averaged Navier-Stokes equations have been presented to incorporate Non-Newtonian behaviour [18] or the presence of a moving solid boundary [19]. Apparently, a local closure problem for the flow of a Non-Newtonian fluid or for the flow near a solid boundary moving with a non-constant velocity has not been investigated yet in the literature [18, 19].

Spatially Averaged Turbulent Flow Equations

To derive macro-scale equations for turbulent flow in porous media, two main approaches have been followed in the literature. The first approach consists of first time-averaging the Navier-Stokes flow equations to apply volume-averaging afterwards. As the time-averaged Navier-Stokes equations, or RANS equations as they are also called, contain a Reynolds stress tensor,

$$\boldsymbol{\tau}_{\mathrm{Re}} \triangleq \rho_f \left(\overline{\boldsymbol{u}\boldsymbol{u}} - \overline{\boldsymbol{u}}\,\overline{\boldsymbol{u}} \right) \simeq \rho_f \overline{\boldsymbol{u}'\boldsymbol{u}'} \qquad \text{with} \qquad \boldsymbol{u}' \triangleq \boldsymbol{u} - \overline{\boldsymbol{u}},$$

also the volume-average of this stress tensor has to be properly derived within this approach. Usually, the Reynolds stress tensor is expressed as a function of the time-averaged velocity gradients through a coefficient μ_t called the *(turbulence) eddy viscosity* [20]:

$$\boldsymbol{\tau}_{\mathrm{Re}} \simeq \mu_t \left(\nabla \overline{\boldsymbol{u}} + (\nabla \overline{\boldsymbol{u}})^{\intercal} \right) + \frac{2}{3} \rho_f \kappa \boldsymbol{I} \,.$$

The eddy viscosity on its turn can be predicted through κ-ϵ-equations, which yield the turbulence kinetic energy $\kappa = \frac{1}{2} \overline{\boldsymbol{u}' \cdot \boldsymbol{u}'}$ and its dissipation rate ϵ [20]. Therefore, the first approach typically proceeds by volume-averaging the κ-ϵ-equations to arrive at a macro-scale turbulence model.

The first approach was initially examined in the work of Masuoka and Takatsu in 1996 [21], albeit without consideration of the κ-ϵ-equations. Instead, this work postulates an equation for the eddy viscosity in which the permeability and Forchheimer coefficient of the porous medium appear from the misconception that the Forchheimer flow resistance is caused mainly by turbulent mixing. Therefore, the theoretical foundations and the form of the macro-scale turbulent flow equations in this work are questionable [22].

A volume-averaged form of the κ-ϵ-equations to model macro-scale turbulence was first derived by Nakayama and Kuwahara in 1996 [23]. The derivation of the volume-averaged κ-ϵ-equations and the volume-averaged RANS equations was further formalized with the double decomposition of Pedras and de Lemos from 2001 [24]. According to the double decomposition, every flow quantity is first decomposed into its volume-average and its deviation part and afterwards decomposed into a time-average and a time-fluctuating part.

A major difficulty with the first approach is that after volume-averaging of the RANS equations and κ-ϵ-equations, many closure terms appear, for which no general (local) closure models are available. Only heuristic/empirical closure models have been proposed, which need to be tuned to the specific turbulent flow conditions and the morphology of the porous medium. Examples of such heuristic/empirical closure models can be found for non-isotropic porous media e.g. in the work of Catton and Travkin (1993) [25] and in the work of Pinson et al. (2006) [26]. Heuristic/empirical closure models have also been adapted to longitudinal flows in channels, pipes and rod bundles in the work of Chandesris, Sagaut et al. (2006) [27], as well as the studies of Nakayama et al. (2008) [28] and Drouin et al. (2013) [29].

The second approach to model turbulent flow through porous media involves time-averaging of the volume-averaged flow equations. In the second approach, the interfacial force in the volume-averaged flow equations is usually modelled through a Darcy term and a Forchheimer term, the latter depending on the volume-averaged velocity in a non-linear way. The non-linearity of this Forcheimer term and the convection terms in the volume-averaged flow equations complicates the time-averaging procedure, so that many approximations are made in the second approach.

Time-averaging after volume-averaging of the Navier-Stokes equations

seems to have been applied for the first time by Wang and Takle [30, 31] in 1995 to study flow over canopies, which they modelled as flow through porous media.

Another pioneering study on the second approach was that of Atohe and Lage [32] in 1997. The flow equations in their study contain a Darcy and a Forchheimer term, so that they can be interpreted as volume-averaged flow equations. The coefficient of the Forchheimer term was treated as a constant in their study. Furthermore, in their time-averaging procedure, Atohe and Lage kept only the linear velocity terms in the expansion of Forchheimer term. As a consequence of these approximations, the final macro-scale turbulent flow equations in their work contain just a single closure term. To model the remaining closure term, Atohe and Lage introduced a macro-scale eddy viscosity and macro-scale turbulence kinetic energy in analogy to the κ-ϵ-equations. If we interpret the velocity in their work as the volume-averaged velocity through the porous medium, the macro-scale eddy viscosity $\mu_{t,\mathrm{macro}}$ and macro-scale turbulence kinetic energy κ_{macro} are defined by

$$\rho_f \overline{\langle \boldsymbol{u} \rangle' \langle \boldsymbol{u} \rangle}' \simeq \mu_{t,\mathrm{macro}} \left(\nabla \overline{\langle \boldsymbol{u} \rangle} + \left(\nabla \overline{\langle \boldsymbol{u} \rangle} \right)^{\intercal} \right) + \frac{2}{3} \rho_f \kappa_{\mathrm{macro}} \boldsymbol{I} \,,$$

where $\langle \boldsymbol{u} \rangle' \triangleq \langle \boldsymbol{u} \rangle - \overline{\langle \boldsymbol{u} \rangle}$ and $\kappa_{\mathrm{macro}} \triangleq \frac{1}{2} \overline{\langle \boldsymbol{u} \rangle' \cdot \langle \boldsymbol{u} \rangle}'$. The equations for the macro-scale turbulence kinetic energy as derived in the work of Atohe and Lage are very similar to the κ-ϵ-equations for the Reynolds stress tensor, apart from the fact that they contain contributions of the Darcy and Forchheimer terms.

The macro-scale turbulence model of Atohe and Lage [32] was further refined by Getachew et al. in 2000 [33] by including some second-order correlations to approximate the Forchheimer term in the time-averaged volume-averaged momentum equation.

Theoretically, both approaches to derive macro-scale models for turbulent flow through porous media can lead to the same mathematical equations, as the order of volume-averaging and time-averaging operations is mathematically interchangeable [34]. However, the previously discussed studies all introduce different approximations and assumptions at different steps in their derivation, so that the obtained models also differ in form and interpretation. As a result, there is no consensus in the research community as to which approach to model turbulent flow in porous media is most suitable [34–36].

Next to the two main approaches explained above, also some alternative approaches have been proposed. A first alternative approach is based on the decomposition of fluid quantities into a space-time average in addition to a fluctuation. This approach was introduced by Teruel et al. in 2009 [36] and leads to a natural construction of micro- and macro-scale κ-ϵ-equations for rigid and isotropic porous media, in which in all the turbulent kinetic energy (filtered and non-filtered) is modelled.

A second alternative approach has been developed by Soulaine and Quintard in 2016 [37]. The latter approach starts by volume-averaging a modified form of the Navier-Stokes equations, in which the momentum equation contains a spatially variable viscosity and a turbulent pressure term to describe the localized turbulent flow phenomena. After invoking some length-scale approximations, Soulaine and Quintard retrieve a simplified closure problem for the turbulent interfacial force on an REV of the porous medium. This closure problem shares many similarities with the closure problem for laminar inertial flow and is solved with a similar closure mapping as in [16]. Soulaine and Quintard also show that their approach allows to represent the interfacial force in the localized turbulent flow regime by means of an apparent permeability tensor.

Spatially Averaged Multi-Phase Equations

The formulation of spatially averaged flow equations has benefited from the developments in the macro-scale description of multiphase flow, especially the work of Hassanizadeh and Gray around 1980. Hassanizadeh and Gray [38] transformed the conservation law for a thermodynamic property $\boldsymbol{\psi}$ having a surface flux $\boldsymbol{i}$, an external supply $\boldsymbol{f}$ and a net production $\boldsymbol{G}$, into a macro-scale conservation law for the macro-scale property $\overline{\boldsymbol{\psi}}^{\alpha}$ having a surface flux $\boldsymbol{i}_{\alpha}$:

$$\frac{\partial(\langle\rho\rangle_{\alpha}\overline{\boldsymbol{\psi}}^{\alpha})}{\partial t} + \nabla\cdot(\langle\rho\rangle_{\alpha}\overline{\boldsymbol{v}}_{\alpha}\overline{\boldsymbol{\psi}}^{\alpha}) - \nabla\cdot\boldsymbol{i}_{\alpha} - \langle\rho\rangle_{\alpha}\overline{\boldsymbol{f}}^{\alpha} = \langle\rho\rangle_{\alpha}\overline{\boldsymbol{\psi}}^{\alpha}e^{\alpha}(\rho\boldsymbol{\psi}) + \langle\rho\rangle_{\alpha}\overline{\boldsymbol{G}}^{\alpha} - \langle\rho\rangle_{\alpha}\hat{\boldsymbol{I}}^{\alpha}\,.$$

In the macro-scale conservation law of [38], $e^{\alpha}(\rho\boldsymbol{\psi})$ and $\hat{\boldsymbol{I}}^{\alpha}$ denote the density functions for exchange of $\boldsymbol{\psi}$ with other phases due to phase changes and due to mechanical interactions respectively. The macro-scale description of Hassanizadeh and Gray is based on a combination of mass-averaged quantities, defined by the mass-averaging operator $\_^{\alpha}$, and volume-averaged quantities over the α-phase, defined by the operator $\langle\,\rangle_{\alpha}$.

The theoretical framework of Hassanizadeh and Gray [38] lies on the basis of *the theory of mixtures* [39], which has been clarified and extended by Achanta [40] and Bennethum [41] around 1995. The theory of mixtures is however fundamentally different from the volume-averaging technique applied by Quintard and Whitaker. VAT is usually applied on transport equations which include some constitutive models, like the Navier-Stokes equations which include Newton's law of viscosity. On the contrary, the theory of mixtures involves volume-averaging of general conservation laws and then obtaining restrictions on the form of closure and constitutive equations by applying the second law of thermodynamics on the volume-averaged equations.

Open Research Questions in the Literature

Virtually all the macro-scale flow equations from the literature have been derived via VAT under the assumption that several length-scale approximations hold and the assumption that the spatial moments of the solid medium are negligible. However, for flow through spatially periodic solid structures, the validity of these VAT assumptions is not ensured [42]. Consequently, the existing macro-scale flow equations impede exact model reduction and data reduction for the flow in heat transfer devices with periodic solid structures. The question which exact form the macro-scale flow equations have without these VAT assumptions should thus be answered first to develop the macro-scale description envisaged in this work.

The only study in which the spatial moments of the solid medium have been taken into account, seems to be the macro-scale treatment of Stokes flow in solid media presented by Quintard and Whitaker [8]. In heat transfer devices with periodic solid structures, the flow usually becomes periodically developed with significant inertial effects, so that the flow is governed by the Navier-Stokes equations instead of the Stokes equations. Therefore, the remainder of this chapter is devoted to the exact averaging of the Navier-Stokes flow equations.

As the spatial moments of periodic solid structures can be suppressed by a suitable choice of weighting function like in the work of Quintard and Whitaker [8], the exact macro-scale flow equations will be derived with the weighted spatial averaging technique from the previous chapter. This requires us first to generalize the Navier-Stokes equations within the theory of mathematical distributions. The generalized Navier-Stokes equations are the topic of the next section.

3.4 Generalized Navier-Stokes Equations

In this work, the fluid flow through the system under consideration (§2.3) is described by the Navier-Stokes flow equations [43] for an incompressible Newtonian fluid. When the velocity field and pressure of the flow are represented by distributions as in (2.5), the Navier-Stokes flow equations take the following form in the system domain Ω:

$$\nabla^\nu \cdot \boldsymbol{u} = 0 \qquad \text{in } \Omega\,, \tag{3.1}$$

$$\rho_f \frac{\partial^\nu \boldsymbol{u}}{\partial t} + \rho_f \nabla^\nu \cdot (\boldsymbol{u}\boldsymbol{u}) = -\nabla^\nu p + \nabla^\nu \cdot \boldsymbol{\tau} + \boldsymbol{f} \qquad \text{in } \Omega\,. \tag{3.2}$$

The continuity equation (3.1) and momentum equation (3.2) are called the *generalized Navier-Stokes (flow) equations*, because they also hold within the solid domain and not just within the fluid domain. When the inertial or advection term $\nabla^\nu \cdot (\boldsymbol{u}\boldsymbol{u})$ in (3.2) is neglected, the generalized Stokes equations of [8] are retrieved[2].

The deformation stress tensor $\boldsymbol{\tau}$ in the generalized flow equations is defined such that $\boldsymbol{n} \cdot \boldsymbol{\tau}$ represents the viscous stress exerted on a surface element with outward pointing normal vector $\boldsymbol{n}$. Because the velocity field is divergence-free for incompressible flow and the fluid is assumed to be Newtonian, the viscous stress tensor equals

$$\boldsymbol{\tau} \triangleq \mu \boldsymbol{S} \triangleq 2\mu\boldsymbol{\epsilon} \triangleq \mu \left(\nabla^\nu \boldsymbol{u} + (\nabla^\nu \boldsymbol{u})^\intercal\right)\,, \tag{3.3}$$

where the strain rate tensor $\boldsymbol{\epsilon}$ is related to the velocity gradient tensor $\nabla^\nu \boldsymbol{u}$ via the viscosity μ. In the case that the viscosity μ_f is constant over Ω_f, we have:

$$\nabla^\nu \cdot \boldsymbol{\tau} = \mu \nabla^{\nu\,2} \boldsymbol{u}\,. \tag{3.4}$$

In this work, the only body force $\boldsymbol{f}$ considered is gravity;

$$\boldsymbol{f} = \rho_f \boldsymbol{g} \gamma_f\,, \tag{3.5}$$

and the gravitational acceleration $\boldsymbol{g}$ is constant over Ω.

[2] In the work of Quintard and Whitaker [8] the generalized Stokes equations are formulated on $\mathbb{R}^3$ instead of Ω though.

The velocity distribution $\boldsymbol{u}$ satisfies the zero-velocity (no-slip) condition [44] at the rigid fluid-solid interface,

$$\boldsymbol{u}(\boldsymbol{x},t) = 0 \qquad \boldsymbol{x} \in \Gamma_{fs}\,. \tag{3.6}$$

The no-slip condition for the velocity (3.6) is taken into account implicitly in the flow equations with the aid of an additional force term $\boldsymbol{f}_{fs}$:

$$\nabla \cdot \boldsymbol{u} = 0 \qquad \text{in } \Omega\,, \tag{3.7}$$

$$\rho_f \frac{\partial \boldsymbol{u}}{\partial t} + \rho_f \nabla \cdot (\boldsymbol{u}\boldsymbol{u}) = -\nabla p + \nabla \cdot \boldsymbol{\tau} + \boldsymbol{f} + \boldsymbol{f}_{fs}\,. \qquad \text{in } \Omega\,. \tag{3.8}$$

The expression for the interfacial force term $\boldsymbol{f}_{fs}$ associated with the no-slip condition is

$$\boldsymbol{f}_{fs} \triangleq \boldsymbol{n}_{fs} \cdot (-p_f \boldsymbol{I} + \boldsymbol{\tau}_f)\delta_{fs}\,, \tag{3.9}$$

where $\boldsymbol{I}$ denotes the unit tensor. This expression is obtained by replacing the gradient in the usual sense in (3.1) and (3.2) by the gradient in the sense of a distribution. Note that, for instance, the velocity gradient tensor is given by

$$\nabla^{\nu} \boldsymbol{u} = \nabla \boldsymbol{u}\,, \tag{3.10}$$

as follows from (2.44) and (3.6).

The generalized flow equations (3.7) and (3.8) with the interfacial force term (3.9) can be solved over the fluid-solid domain Ω with immersed boundary methods [45]. Equation (3.9) shows however the true mathematical form of the interfacial force, which in some immersed boundary methods, especially those used for topology optimization [46, 47], has been replaced by a scalar permeability K_{IBM}: $\boldsymbol{f}_{fs} \simeq K_{\mathrm{IBM}}^{-1}\boldsymbol{u}$.

The generalized continuity equation, (3.1) or (3.7), and momentum equation, (3.2) (3.8), are suitable for use with the convolution product in Ω. In other words, we can apply a spatial averaging operator on this flow problem, because all the physical quantities are defined as distributions over both the f- and s-region.

3.5 Flow Boundary Conditions

The generalized flow equations are to be solved for some prescribed boundary and initial conditions. In this work, the boundary of the system, for example a channel of a heat transfer device, is either a flow inlet, a flow outlet or a solid wall. In order to clarify the appropriate boundary conditions for the flow equations, a clear distinction is made between different parts of these boundaries (see Figure 3.1).

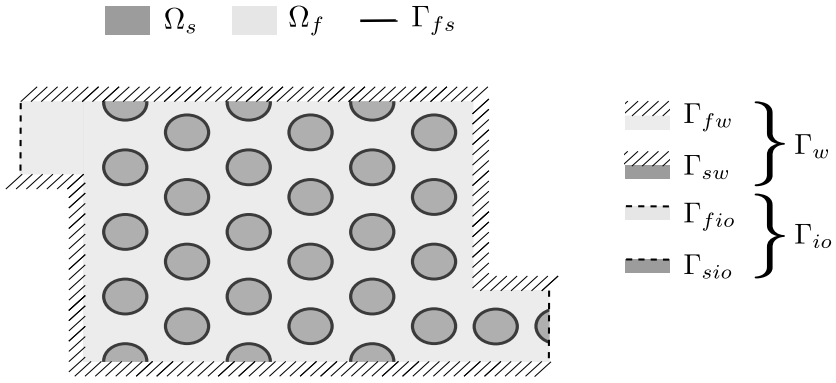

Figure 3.1: Two-dimensional continuum domain and its boundaries.

We already defined Γ as the boundary of the system domain: $\Gamma = \partial\Omega$. This boundary Γ can be further divided into two complementary parts: $\Gamma = \Gamma_f \cup \Gamma_s$. The boundary parts Γ_s and Γ_f form outer restrictions on the solid and fluid domain Ω_s and Ω_f respectively. Γ_f can further be subdivided as $\Gamma_f = \Gamma_{fio} \cup \Gamma_{fw}$, where Γ_{fio} is the part of Γ_f that allows for fluid flow over the boundary (i.e. an inlet or outlet) and Γ_{fw} is the part of Γ_f where fluid flow is blocked by the presence of a wall. The outer boundary of the solid Γ_s is likewise subdivided into two complementary parts: $\Gamma_s = \Gamma_{sio} \cup \Gamma_{sw}$. Γ_{sio} is the part of Γ_s where some inflow or outflow boundary, part of Γ_{fio}, is present in some neighbourhood. The part $\Gamma_{sw} = \Gamma_s \setminus \Gamma_{sio}$ is then allocated to the boundary region where a wall is in some neighbourhood.

Finally, the macro-scale boundaries Γ_{io} and Γ_w are defined as the unions of previous boundary parts: $\Gamma_{io} = \Gamma_{sio} \cup \Gamma_{fio}$ represents the macro-scale

inflow or outflow boundary, while $\Gamma_w = \Gamma_{sw} \cup \Gamma_{fw}$ represents the macro-scale wall boundary. By these definitions the boundary of the system domain satisfies $\Gamma = \Gamma_{io} \cup \Gamma_w$, with $\Gamma_{io} \cap \Gamma_w = \emptyset$. The macro-scale boundaries Γ_{io} and Γ_w will be used to impose boundary conditions on the macro-scale flow problem (see §3.7).

In this work we will mainly focus on the following boundary and initial conditions for the pressure and velocity distributions:

$$\boldsymbol{u}(\boldsymbol{x}, t) = 0 \qquad \boldsymbol{x} \in \Gamma_{fs} \cup \Gamma_{fw}\,, \tag{3.11}$$

$$p(\boldsymbol{x}, t) = p_{io}(\boldsymbol{x}) \qquad \boldsymbol{x} \in \Gamma_{fio}\,. \tag{3.12}$$

3.6 Macro-Scale Flow Equations

Superficially Averaged Flow Equations

In their generalized form, the flow equations (3.1) and (3.2) are spatially filtered over the entire system domain Ω to find the following macro-scale flow equations in Ω:

$$\nabla \cdot \langle \boldsymbol{u} \rangle_m = 0\,, \tag{3.13}$$

$$\rho_f \frac{\partial \langle \boldsymbol{u} \rangle_m}{\partial t} + \rho_f \nabla \cdot \left(\epsilon_{fm}^{-1} \langle \boldsymbol{u} \rangle_m \langle \boldsymbol{u} \rangle_m \right) = -\nabla \langle p \rangle_m + \nabla \cdot \langle \boldsymbol{\tau} \rangle_m + \boldsymbol{b}_{fs} - \rho_f \nabla \cdot \boldsymbol{M} + \langle \boldsymbol{f} \rangle_m\,, \tag{3.14}$$

where

$$\langle \boldsymbol{\tau} \rangle_m = \mu_f \left(\nabla \langle \boldsymbol{u} \rangle_m + (\nabla \langle \boldsymbol{u} \rangle_m)^\intercal \right) \quad \text{and} \quad \langle \boldsymbol{f} \rangle_m = \rho_f \boldsymbol{g} \epsilon_{fm}\,,$$

$$\boldsymbol{b}_{fs} \triangleq \langle \boldsymbol{n}_{fs} \cdot (-p_f \boldsymbol{I} + \boldsymbol{\tau}_f)\, \delta_{fs} \rangle_m \quad \text{and} \quad \boldsymbol{M} \triangleq \langle \boldsymbol{u}\boldsymbol{u} \rangle_m - \epsilon_{fm}^{-1} \langle \boldsymbol{u} \rangle_m \langle \boldsymbol{u} \rangle_m\,.$$

The derivation of the spatially averaged flow equations is explained in Appendix B. It should be noted that for a constant viscosity μ_f we can use the expressions

$$\nabla \cdot \langle \boldsymbol{\tau} \rangle_m = \mu_f \nabla^2 \langle \boldsymbol{u} \rangle_m\,, \quad \boldsymbol{b}_{fs} = \langle \boldsymbol{n}_{fs} \cdot (-p_f \boldsymbol{I} + \mu_f \nabla \boldsymbol{u}_f)\, \delta_{fs} \rangle_m\,, \tag{3.15}$$

because $\langle \boldsymbol{u} \rangle_m$ is divergence-free and the no-slip condition holds at Γ_{fs}[3]

[3] See Appendix B, (B.22).

Intrinsically Averaged Flow Equations

The macro-scale flow equations can also be formulated in terms of the intrinsically averaged velocity $\langle \boldsymbol{u} \rangle_m^f$ and pressure $\langle p \rangle_m^f$:

$$\nabla \cdot \langle \boldsymbol{u} \rangle_m^f = -\epsilon_{fm}^{-1} \nabla \epsilon_{fm} \cdot \langle \boldsymbol{u} \rangle_m^f \,, \tag{3.16}$$

$$\begin{aligned} \rho_f \frac{\partial \langle \boldsymbol{u} \rangle_m^f}{\partial t} + \rho_f \nabla \cdot \left(\langle \boldsymbol{u} \rangle_m^f \langle \boldsymbol{u} \rangle_m^f \right) &= -\nabla \langle p \rangle_m^f + \nabla \cdot \mu_f \boldsymbol{S}'_m \\ &\quad + \boldsymbol{b}'_{fs} - \rho_f \nabla \cdot \boldsymbol{M}' + \langle \boldsymbol{f} \rangle_m^f + \boldsymbol{\Psi}'_m \,, \end{aligned} \tag{3.17}$$

where

$$\boldsymbol{S}'_m \triangleq \nabla \langle \boldsymbol{u} \rangle_m^f + (\nabla \langle \boldsymbol{u} \rangle_m^f)^\intercal \qquad \text{and} \qquad \langle \boldsymbol{f} \rangle_m^f = \rho_f \boldsymbol{g} \,,$$

$$\boldsymbol{b}'_{fs} \triangleq \epsilon_{fm}^{-1} \boldsymbol{b}_{fs} \qquad \text{and} \qquad \boldsymbol{M}' \triangleq \epsilon_{fm}^{-1} \boldsymbol{M} \,.$$

Due to possible presence of gradients of the weighted porosity, the term $\boldsymbol{\Psi}'_m$ appears in the intrinsically averaged macro-scale flow equations:

$$\begin{aligned} \boldsymbol{\Psi}'_m \triangleq \epsilon_{fm}^{-1} \nabla \epsilon_{fm} \cdot \left(-\langle p \rangle_m^f \boldsymbol{I} + \langle \boldsymbol{\tau} \rangle_m^f - \boldsymbol{M}' - \langle \boldsymbol{u} \rangle_m^f \langle \boldsymbol{u} \rangle_m^f \right) \\ + \nabla \cdot \mu_f \left(\epsilon_{fm}^{-1} \nabla \epsilon_{fm} \langle \boldsymbol{u} \rangle_m^f + \langle \boldsymbol{u} \rangle_m^f \epsilon_{fm}^{-1} \nabla \epsilon_{fm} \right) \,. \end{aligned} \tag{3.18}$$

Intrinsically Averaged Flow Equations: Constant Viscosity

When the viscosity μ_f is constant over the fluid domain, equation (3.15) holds and the intrinsically averaged flow equations take the form

$$\nabla \cdot \langle \boldsymbol{u} \rangle_m^f = -\epsilon_{fm}^{-1} \nabla \epsilon_{fm} \cdot \langle \boldsymbol{u} \rangle_m^f \,, \tag{3.19}$$

$$\begin{aligned} \rho_f \frac{\partial \langle \boldsymbol{u} \rangle_m^f}{\partial t} + \rho_f \nabla \cdot \left(\langle \boldsymbol{u} \rangle_m^f \langle \boldsymbol{u} \rangle_m^f \right) &= -\nabla \langle p \rangle_m^f + \mu_f \nabla^2 \langle \boldsymbol{u} \rangle_m^f \\ &\quad + \boldsymbol{b}'_{fs} - \rho_f \nabla \cdot \boldsymbol{M}' + \langle \boldsymbol{f} \rangle_m^f + \boldsymbol{\Psi}^{0\,\prime}_m \,. \end{aligned} \tag{3.20}$$

The term $\boldsymbol{\Psi}^{0\,\prime}_m$ due to porosity changes, which appears in the intrinsically averaged flow equations for a constant viscosity, is given by

$$\begin{aligned} \boldsymbol{\Psi}^{0\,\prime}_m = \epsilon_{fm}^{-1} \nabla \epsilon_{fm} \cdot \left(-\langle p \rangle_m^f \boldsymbol{I} + 2\mu_f \nabla \langle \boldsymbol{u} \rangle_m^f - \boldsymbol{M}' - \langle \boldsymbol{u} \rangle_m^f \langle \boldsymbol{u} \rangle_m^f \right) \\ + \mu_f (\epsilon_{fm}^{-1} \nabla^2 \epsilon_{fm}) \langle \boldsymbol{u} \rangle_m^f \,. \end{aligned} \tag{3.21}$$

Macro-Scale Flow Assumptions

The first requirement for the validity of the macro-scale flow equations is that the no-slip condition (3.6) holds at the boundary whose normal $\boldsymbol{n}_{fs}$ and Dirac distribution δ_{fs} appear in the closure term $\boldsymbol{b}_{fs}$.

The second requirement is that of a spatially constant viscosity. In Appendix B, it is shown that this requirement for (3.14) and (3.17) can be relaxed into the requirement that the viscosity be approximately constant within the local averaging domain.

Macro-Scale Flow Problem

The macro-scale flow equations differ from the original incompressible Navier-Stokes equations in four important aspects. First, the macro-scale flow equations do not longer contain $\boldsymbol{u}$ and p as the unknowns, but they allow to solve the filtered pressure and velocity distributions, $\langle p \rangle_m$ and $\langle \boldsymbol{u} \rangle_m$, when the appropriate boundary conditions for $\langle p \rangle_m$ and $\langle \boldsymbol{u} \rangle_m$ are known.

A second key difference is the presence of two momentum closure terms in the filtered flow equations:

$$\boldsymbol{M} \triangleq \langle \boldsymbol{u}\boldsymbol{u} \rangle_m - \epsilon_{fm}^{-1} \langle \boldsymbol{u} \rangle_m \langle \boldsymbol{u} \rangle_m \qquad \text{and} \qquad \boldsymbol{b}_{fs} \triangleq \langle \boldsymbol{f}_{fs} \rangle_m \,. \tag{3.22}$$

The first term is the *weighted momentum dispersion source* $\boldsymbol{M}$, which adds momentum contained in the deviation velocity field $\widetilde{\boldsymbol{u}}$ that is not captured by the advective acceleration term of the filtered flow field. The second term is the *weighted interfacial force* $\boldsymbol{b}_{fs}$, which is the local surface integral of the pressure and viscous stresses acting on the fluid-solid interface $\bar{\Gamma}_{fs}$ in $\bar{\Omega}(\boldsymbol{x})$. This surface filter is introduced via the spatial averaging gradient theorem (2.48)) and ensures that the effect of the interfacial forces $\boldsymbol{f}_{fs}$ within the averaging domain is taken into account in the macro-scale flow equations. We remark that in the filtered flow equations for LES models, the interfacial force only appears if the commutation error of the gradient and filter operator near the solid boundary is taken into account [48].

A third difference is that the macro-scale flow equations should be solved on the entire system domain Ω, because the spatially averaged fields $\langle p \rangle_m$ and $\langle \boldsymbol{u} \rangle_m$ are defined on Ω_f as well as Ω_s. Furthermore, whereas solving the original Navier-Stokes equations would require the specification of the no-slip condition at the solid-fluid interface, this boundary condition is already implicitly incorporated in the spatially averaged flow equations.

Lastly, the macro-scale flow equations are non-local transport equations, as some terms involve a surface filter in which the full pressure and velocity field, including $\langle p \rangle_m$ and $\langle \boldsymbol{u} \rangle_m$, are evaluated at points other than the centroid located by $\boldsymbol{x}$.

Apart from the presence of these two momentum closure terms, the macro-scale flow equations resemble the original incompressible Navier-Stokes flow equations. Therefore, if the momentum closure terms are known in advance, these macro-scale equations can be solved numerically using the same discretization techniques as available for the original Navier-Stokes equations. However, when only the macro-scale flow is of interest, it is more advantageous to solve the macro-scale flow equations as they require less computational resources in comparison to the original flow equations.

Indeed, provided that the filter size r_m satisfies

$$\ell_p \leq r_m \ll \mathscr{L}_p \qquad \text{and} \qquad \ell_{\boldsymbol{u}} \leq r_m \ll \mathscr{L}_{\boldsymbol{u}}\,, \tag{3.23}$$

the intrinsically averaged pressure $\langle p \rangle_m^f$ and velocity field $\langle \boldsymbol{u} \rangle_m^f$ vary over length scales $\mathscr{L}_p$ and $\mathscr{L}_{\boldsymbol{u}}$ larger than the scales ℓ_p and $\ell_{\boldsymbol{u}}$ of the non-filtered pressure and velocity field. This means that for numerically solving the former macro-scale equations, a coarser mesh over the system domain Ω can be used, oblivious of the solid distribution (e.g. fins). In other words, the reduction in computational effort is a consequence of the fact that the mesh does not need to capture small-scale effects related to geometric intricacies of the solid-fluid interface (and the associated no-slip boundary condition, which is implicitly incorporated in the macro-scale flow equations) over the entire fluid domain.

Approximative Forms of the Macro-Scale Flow Problem
The form of the macro-scale flow equations presented here omits the simplifications that are incorporated in the derivation of the volume-averaged Navier-Stokes equations [16] in the literature. Another difference with the literature is that the macro-scale Navier-Stokes equations in this work are embedded in the theory of mathematical distributions, like in [8].

The volume-averaged Stokes or Navier-Stokes equations in the literature only hold for a constant viscosity and typically contain the following approximations. First, some contributions in the interfacial force due to the geometrical tensors (or spatial moments) are disregarded [8, 16]. For instance, the pressure contribution in the interfacial force, which can be

decomposed according to (2.64) and (2.65), is approximated as

$$\begin{aligned}
\boldsymbol{b}'^{\,p}_{fs} &\triangleq -\epsilon_{fm}^{-1}\langle \boldsymbol{n}_{fs}\cdot p_f \boldsymbol{I}\delta_{fs}\rangle_m \\
&= \epsilon_{fm}^{-1}\nabla\epsilon_{fm}\cdot\langle \boldsymbol{p}\rangle_m^f \boldsymbol{I} - \sum_{n=1}^{\infty} \boldsymbol{G'}_m^{(n)} \underbrace{\cdot\cdot}_{n\text{-times}} \nabla^{\otimes n}\langle \boldsymbol{p}\rangle_m^f \\
&\quad - \epsilon_{fm}^{-1}\langle \boldsymbol{n}_{fs}\cdot \widetilde{p}_f \boldsymbol{I}\delta_{fs}\rangle_m \\
&\simeq \epsilon_{fm}^{-1}\nabla\epsilon_{fm}\cdot\langle \boldsymbol{p}\rangle_m^f \boldsymbol{I} - \epsilon_{fm}^{-1}\langle \boldsymbol{n}_{fs}\cdot \widetilde{p}_f \boldsymbol{I}\delta_{fs}\rangle_m \,. \qquad (3.24)
\end{aligned}$$

Similarly, the viscous contribution in the interfacial force (3.15) is approximated as[4]

$$\begin{aligned}
\boldsymbol{b}'^{\,\tau}_{fs} &\triangleq \epsilon_{fm}^{-1}\langle \boldsymbol{n}_{fs}\cdot \mu_f\nabla \boldsymbol{u}_f\delta_{fs}\rangle_m \\
&= \epsilon_{fm}^{-1}\langle \boldsymbol{n}_{fs}\cdot \mu_f\nabla\langle \boldsymbol{u}\rangle_m^f\delta_{fs}\rangle_m + \epsilon_{fm}^{-1}\langle \boldsymbol{n}_{fs}\cdot \mu_f\nabla\widetilde{\boldsymbol{u}}_f\delta_{fs}\rangle_m \\
&= -\epsilon_{fm}^{-1}\nabla\epsilon_{fm}\cdot\mu_f\nabla\langle \boldsymbol{u}\rangle_m^f + \mu_f\sum_{n=1}^{\infty} \boldsymbol{G'}_m^{(n)} \underbrace{\cdot\cdot}_{n\text{-times}} \nabla^{\otimes(n+1)}\langle \boldsymbol{u}\rangle_m^f \\
&\quad + \epsilon_{fm}^{-1}\langle \boldsymbol{n}_{fs}\cdot \mu_f\nabla\widetilde{\boldsymbol{u}}_f\delta_{fs}\rangle_m \\
&\simeq -\epsilon_{fm}^{-1}\nabla\epsilon_{fm}\cdot\mu_f\nabla\langle \boldsymbol{u}\rangle_m^f + \epsilon_{fm}^{-1}\langle \boldsymbol{n}_{fs}\cdot \mu_f\nabla\widetilde{\boldsymbol{u}}_f\delta_{fs}\rangle_m \,. \qquad (3.25)
\end{aligned}$$

Second, in the literature [16], the spatial changes of the filtered velocity within the averaging domain are often neglected for evaluating the momentum dispersion source $\boldsymbol{M}$:

$$\boldsymbol{M} \simeq \langle \widetilde{\boldsymbol{u}}\widetilde{\boldsymbol{u}}\rangle_m \,. \qquad (3.26)$$

This approximation is justified when the characteristic size r_m of the averaging domain $\bar{\Omega}$ is small with respect to the length scale $\mathscr{L}_{\boldsymbol{u}}$ over which the average velocity changes: $r_m \ll \mathscr{L}_{\boldsymbol{u}}$. However, we must note that $\mathscr{L}_{\boldsymbol{u}}$ always depends on r_m, so that this condition cannot be checked a priori, i.e. before choosing a specific filter size r_m to calculate $\langle \boldsymbol{u}\rangle_m^f$.

Moreover, although the terms related to porosity changes are virtually always neglected for homogeneous media, some authors [6, 8, 16] have approximated the last term in (3.20) as

$$\boldsymbol{\Psi}_m^{0\,\prime} \simeq \epsilon_{fm}^{-1}\nabla\epsilon_{fm}\cdot\left(-\langle p\rangle_m^f \boldsymbol{I} + 2\mu_f\nabla\langle \boldsymbol{u}\rangle_m^f\right) + \mu_f(\epsilon_{fm}^{-1}\nabla^2\epsilon_{fm})\langle \boldsymbol{u}\rangle_m^f \,. \qquad (3.27)$$

[4] In [8], the interfacial force is decomposed in a less rigorous manner, so that $\boldsymbol{b}'^{\,\tau}_{fs}$ contains a term $\langle \boldsymbol{n}_{fs}\cdot\mu_f\nabla\langle \boldsymbol{u}\rangle_m^f\gamma_f\delta_{fs}\rangle_m$ instead of $\langle \boldsymbol{n}_{fs}\cdot\mu_f\nabla\langle \boldsymbol{u}\rangle_m^f\delta_{fs}\rangle_m$.

3.7 Macro-Scale Flow Boundary Conditions

The boundary conditions for the macro-scale flow equations can be specified in terms of the intrinsically averaged velocity and pressure:

$$\langle \boldsymbol{u} \rangle_m^f = \boldsymbol{f}_{\boldsymbol{u}}(\boldsymbol{x}, t) \qquad \boldsymbol{x} \in \Gamma_w \,, \tag{3.28}$$

$$\langle p \rangle_m^f = f_p(\boldsymbol{x}, t) \qquad \boldsymbol{x} \in \Gamma_{fio} \,. \tag{3.29}$$

However, the appropriate boundary values $\boldsymbol{f}_{\boldsymbol{u}}$ and f_p are in practise unknown. They can only be calculated by filtering the original velocity and pressure distributions near the boundaries, which necessitates solving the original flow equations. Besides, near the boundaries, the filter window $\bar{\Omega}$ can contain points that do not belong to the domain Ω, so that $\boldsymbol{u}$ and p at these points outside of Ω must be specified, before $\langle \boldsymbol{u} \rangle_m^f = \boldsymbol{f}_{\boldsymbol{u}}$ and $\langle p \rangle_m^f = f_p$ can be calculated. One way to determine $\langle \boldsymbol{u} \rangle_m^f = \boldsymbol{f}_{\boldsymbol{u}}$ and $\langle p \rangle_m^f = f_p$ once the original flow equations have been solved, is through extrapolation of $\boldsymbol{u}$ and p near the boundary.

Extrapolation in the normal direction of the boundary Γ means that

$$\boldsymbol{u}(\boldsymbol{r}, t) = \boldsymbol{u}(\boldsymbol{x}^\star, t) \,, \quad p(\boldsymbol{r}, t) = p(\boldsymbol{x}^\star, t) \,, \quad \text{if } \boldsymbol{r} \in \bar{\Omega}(\boldsymbol{x}),\, \boldsymbol{r} \notin \Omega \,, \tag{3.30}$$

where $\boldsymbol{x}^\star$ is the nearest orthogonal projection of $\boldsymbol{r}$ at Γ:

$$\boldsymbol{x}^\star = \underset{\boldsymbol{z} \in \Gamma, (\boldsymbol{z}-\boldsymbol{r}) \times \boldsymbol{n}_{fs}(\boldsymbol{z}) = 0}{\arg\min} \| \boldsymbol{z} - \boldsymbol{r} \| \,. \tag{3.31}$$

Often, the curvature of the boundary Γ is such that $\boldsymbol{x}^\star$ is a unique point. When multiple $\boldsymbol{x}^\star$ satisfy (3.31), the boundary conditions (3.11) and (3.12) are usually such that the values $\boldsymbol{u}(\boldsymbol{x}^\star, t)$ and $p(\boldsymbol{x}^\star, t)$ are the same for all of these points $\boldsymbol{x}^\star$. In other cases, the point $\boldsymbol{x}^\star$ of (3.31) must be chosen uniquely with an additional criterion.

In order to supply boundary conditions for the macro-scale flow problem without solving the original flow equations, we suggest to take the boundary values on Γ_{io} and Γ_w equal to the boundary values (3.11) and (3.12) of the original flow problem:

$$\langle \boldsymbol{u} \rangle_m^f \simeq 0 \qquad \boldsymbol{x} \in \Gamma_w \,, \tag{3.32}$$

$$\langle p \rangle_m^f \simeq p_{io}(\boldsymbol{x}) \qquad \boldsymbol{x} \in \Gamma_{fio} \,. \tag{3.33}$$

The suggested boundary conditions (3.32) and (3.33) are often a good approximation for (3.28 when the velocity and pressure distributions are extrapolated outside of Ω in accordance with (3.30).

3.8 Global Closure for Macro-Scale Flow

In order to model the macro-scale flow in a system via the spatially averaged flow equations, one must somehow know the weighted interfacial force $\boldsymbol{b}_{fs}$ and the weighted momentum dispersion source $\boldsymbol{M}$ a priori. However, the dependence of $\boldsymbol{b}_{fs}$ and $\boldsymbol{M}$ on the full velocity $\boldsymbol{u}$ and pressure distribution p (cf. (3.22)), including their deviation parts $\widetilde{\boldsymbol{u}}$ and $\widetilde{p}$, inhibits solving the macro-scale flow equations. Thus, the macro-scale flow equations themselves are not closed.

For closure, the deviation distributions could be obtained in any point of the fluid domain by solving the following global closure problem[5] in Ω_f:

$$\nabla \cdot \widetilde{\boldsymbol{u}}_f = \epsilon_{fm}^{-1} \nabla \epsilon_{fm} \cdot \langle \boldsymbol{u} \rangle_m^f \,, \tag{3.34}$$

$$\begin{aligned} \rho_f \frac{\partial \widetilde{\boldsymbol{u}}_f}{\partial t} + \rho_f \boldsymbol{u}_f \cdot \nabla \widetilde{\boldsymbol{u}}_f = &-\nabla \widetilde{p}_f + \nabla \cdot \mu \big\{ \widetilde{\boldsymbol{S}}_m \big\}_f - \big\{ \boldsymbol{b}'_{fs} \big\}_f + \rho_f \nabla \cdot \big\{ \boldsymbol{M}' \big\}_f \\ &+ \widetilde{\boldsymbol{f}}_f - \rho_f \cdot \nabla \cdot \Big(\widetilde{\boldsymbol{u}}_f \big\{ \langle \boldsymbol{u} \rangle_m^f \big\}_f \Big) - \big\{ \boldsymbol{\Psi}'_m \big\}_f \,, \end{aligned} \tag{3.35}$$

where

$$\widetilde{\boldsymbol{S}}_m \triangleq \nabla \widetilde{\boldsymbol{u}} + (\nabla \widetilde{\boldsymbol{u}})^{\mathsf{T}} \quad \text{and} \quad \widetilde{\boldsymbol{f}}_f = 0 \,,$$

$$\boldsymbol{b}'_{fs} \triangleq \epsilon_{fm}^{-1} \boldsymbol{b}_{fs} \quad \text{and} \quad \boldsymbol{M}' \triangleq \epsilon_{fm}^{-1} \boldsymbol{M} \,.$$

This system of equations for the deviation quantities $\widetilde{p}$ and $\widetilde{\boldsymbol{u}}$ is obtained by subtracting the filtered flow equations (3.16 and (3.17) from the original flow equations (3.1) and (3.2) on the f-region. It is important to note that these closure equations are restricted to the fluid domain. In the fluid domain, the gravitational body force has no deviation part and the velocity field is given by $\boldsymbol{u}_f = \big\{ \langle \boldsymbol{u} \rangle_m^f \big\}_f + \widetilde{\boldsymbol{u}}_f$.

The former closure equations are not only quite complex, but also very expensive to solve. In the first place, they contain all deviation quantities throughout the whole device domain. As the length scale of a deviation quantity usually has the same magnitude as the length scale of the original flow quantity, solving the closure problem is expected to require the same

[5] See Appendix C for a derivation.

mesh resolution as needed for solving the original flow equations.

Moreover, there is a strong coupling between the closure problem and the filtered flow equations: the filtered quantities and the deviation quantities need to be solved simultaneously in order to resolve the coupling terms.

At first sight, determining the closure terms $\boldsymbol{b}_{fs}$ and $\boldsymbol{M}$ thus seems to require even more computational effort than solving the original Navier-Stokes equations. However, in Chapter 5, we will present practical strategies to determine these closure terms a priori for periodically developed flow through spatially periodic solid structures.

Approximative Forms of the Global Closure Problem
In the literature [8, 16], the global closure problem of the volume-averaged flow equations for incompressible viscous flow through porous media is further simplified.

To begin, the global closure problem is simplified under the quasi-steady approximation. That means that the local acceleration term $\frac{\partial \widetilde{\boldsymbol{u}}_f}{\partial t}$ is dropped in the global closure problem.

Also the momentum dispersion source is neglected in the closure problem, because it is assumed that $\nabla \cdot \left\{\boldsymbol{M}'\right\}_f \ll \boldsymbol{u}_f \cdot \nabla \widetilde{\boldsymbol{u}}_f$.

Furthermore, for a homogeneous porous medium, the gradients of the porosity are neglected, so that $\nabla \cdot \widetilde{\boldsymbol{u}}_f \simeq 0$, $\nabla \cdot \left(\widetilde{\boldsymbol{u}}_f \left\{\langle \boldsymbol{u} \rangle_m^f\right\}_f\right) \simeq 0$ and $\left\{\boldsymbol{\Psi}'_m\right\}_f \simeq 0$.

Finally, the interfacial force is assumed to stem just from the deviation stresses at the fluid-solid interface: $\boldsymbol{b}'_{fs} \simeq \langle \boldsymbol{n}_{fs} \cdot (-\widetilde{p}_f \boldsymbol{I} + \mu_f \nabla \widetilde{\boldsymbol{u}}_f) \delta_{fs} \rangle_m$.

3.9 Boundary Conditions for Global Closure

For the global closure problem, the following boundary conditions are suitable:

$$\widetilde{\boldsymbol{u}} = -\langle \boldsymbol{u} \rangle_m^f \gamma_f \qquad \boldsymbol{x} \in \Gamma_{fs}\,, \tag{3.36}$$

$$\widetilde{\boldsymbol{u}} = -\boldsymbol{f}_{\boldsymbol{u}}(\boldsymbol{x}, t) \gamma_f(\boldsymbol{x}) \simeq 0 \qquad \boldsymbol{x} \in \Gamma_{fw}\,, \tag{3.37}$$

$$\widetilde{p} = p_{io}(\boldsymbol{x}) - f_p(\boldsymbol{x}, t) \gamma_f(\boldsymbol{x}) \simeq 0 \qquad \boldsymbol{x} \in \Gamma_{fio}\,. \tag{3.38}$$

These boundary conditions ensure compatibility between the original flow boundary conditions and the macro-scale boundary conditions. Due to the no-slip boundary condition at the solid-fluid interface, the intrinsic spatially averaged velocity acts as a source term for $\widetilde{\boldsymbol{u}}$ at the interface boundary. Note that the boundary conditions (3.37) and (3.38) are in practise unknown [16].

3.10 Planar Flow Equations

Definition of planar flow

When the system domain Ω is three-dimensional and partly bounded by two parallel planar surfaces (solid or fictitious) which are separated over a relatively small distance, so that the flow transport happens mainly in the directions parallel to both planar surfaces, we will speak of *planar flow*. In planar flow, the average flow field parallel to both planar surfaces can be described via the two-dimensional planar flow equations presented in this section. The planar flow equations, as presented here, are valid under the assumption that the solid structures as well as the domain boundary have the same cross-sectional shape in every plane parallel to the two confining planar surfaces.

Suppose that l_3 corresponds to the distance between the upper and bottom planar surface, as in Figure 3.2) and let $\boldsymbol{e}^{(3)}$ be a basis vector with its direction orthogonal to both planar surfaces, then the domain Ω under consideration is constrained in the x_3-coordinate as follows:

$$\forall \boldsymbol{x} \in \Omega : x_3 = \boldsymbol{x} \cdot \boldsymbol{e}^{(3)} \in I_3 = \left[-\frac{l_3}{2}, \frac{l_3}{2} \right] . \tag{3.39}$$

The middle plane $\Omega_{x_3=0}$ between the two parallel planar surfaces is thus located at $x_3 = 0$:

$$\Omega_{x_3=0} \triangleq \left\{ \boldsymbol{x} \in \Omega | x_3 = \boldsymbol{x} \cdot \boldsymbol{e}^{(3)} = 0 \right\} . \tag{3.40}$$

The middle plane serves as the definition domain for the planar flow velocity and pressure, as we define the planar flow velocity $\boldsymbol{v}$ and pressure $\mathcal{P}$ as the weighted average of the original flow and pressure distribution over the x_3- coordinate perpendicular to the middle plane.

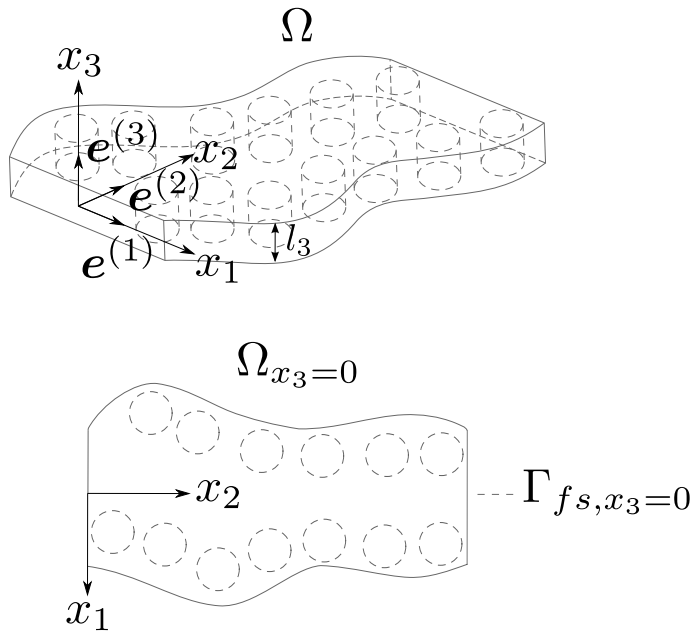

Figure 3.2: System domain for planar flow: a parallel-plate channel with cylindrical pin fins.

Mathematically, the planar flow velocity and pressure are expressed by a one-dimensional convolution product (2.26):

$$\boldsymbol{v} \triangleq \langle \boldsymbol{u}_{1,2} \rangle_3 |_{(\boldsymbol{x}_{1,2}, x_3=0, t)} \triangleq \int_{y_3 \in I_3} m_3'(-y_3)\, \boldsymbol{u}_{1,2}(\boldsymbol{x}_{1,2}, y_3, t)\, dy_3 \,, \tag{3.41}$$

$$\mathcal{P} \triangleq \langle p \rangle_3 |_{(\boldsymbol{x}_{1,2}, x_3=0, t)} \triangleq \int_{y_3 \in I_3} m_3'(-y_3)\, p(\boldsymbol{x}_{1,2}, y_3, t)\, dy_3 \,, \tag{3.42}$$

where $\boldsymbol{u}_{1,2}$ and $\boldsymbol{x}_{1,2}$ are respectively the part of velocity vector $\boldsymbol{u}$ and position vector $\boldsymbol{x}$ parallel to the middle plane $\Omega_{x_3=0}$:

$$\boldsymbol{u} = \boldsymbol{u}_{1,2} + \boldsymbol{u}_3 \qquad \text{with} \qquad \boldsymbol{u}_3 \triangleq \boldsymbol{u} \cdot \boldsymbol{e}^{(3)} \boldsymbol{e}^{(3)} \,, \tag{3.43}$$

$$\boldsymbol{x} = \boldsymbol{x}_{1,2} + \boldsymbol{x}_3 \qquad \text{with} \qquad \boldsymbol{x}_3 \triangleq \boldsymbol{x} \cdot \boldsymbol{e}^{(3)} \boldsymbol{e}^{(3)} \,. \tag{3.44}$$

The definition of the planar flow velocity and pressure is based on the one-dimensional convolution product (2.26) in $\Omega_{x_3=0}$.

When the solid structures have a shape which does not vary over the x_3-direction, it holds that

$$\Gamma_{fs} = \left\{ \boldsymbol{x} \,\middle|\, \boldsymbol{x}_{1,2} \in \Gamma_{fs,x_3=0}\,, x_3 \in \left]-\frac{l_3}{2}, \frac{l_3}{2}\right[\right\}, \tag{3.45}$$

where $\Gamma_{fs,x_3=0} \triangleq \Gamma_{fs} \cap \Omega_{x_3=0}$ represents the intersection line of the solid structures with the middle plane of the domain. Likewise, when the shape of the domain boundary does not vary over the x_3-direction, it holds that

$$\Gamma = \left\{ \boldsymbol{x} \,\middle|\, \boldsymbol{x}_{1,2} \in \Gamma_{x_3=0}\,, x_3 \in \left]-\frac{l_3}{2}, \frac{l_3}{2}\right[\right\} \cup \left\{ \boldsymbol{x} \in \Omega | x_3 = \pm\frac{l_3}{2} \right\}, \tag{3.46}$$

where $\Gamma_{x_3=0} \triangleq \partial\Omega_{x_3=0} = \Gamma \cap \Omega_{x_3=0}$ is the intersection between the middle plane and the system boundary.

Under the conditions of (3.45) and (3.46), the fluid and solid indicators depend only on the position $\boldsymbol{x}_{1,2}$ with respect to the middle plane:

$$\gamma_f = \gamma_f(\boldsymbol{x}_{1,2}) \qquad \text{and} \qquad \gamma_s = \gamma_s(\boldsymbol{x}_{1,2})\,, \tag{3.47}$$

insofar that we leave the boundary of Ω out of consideration, hence insofar that $x_3 \in \left]-\frac{l_3}{2}, \frac{l_3}{2}\right[$. Consequently, the normal vector at the fluid-solid indicator satisfies

$$\boldsymbol{n}_{fs} = \boldsymbol{n}_{fs}(\boldsymbol{x}_{1,2}) \qquad \text{and} \qquad \boldsymbol{n}_{fs} \cdot \boldsymbol{e}^{(3)} = 0\,. \tag{3.48}$$

From (3.47) it automatically follows that the planar velocity and pressure distributions can be represented as two-dimensional distributions over the fluid and solid regions of the middle plane $\Omega_{x_3=0}$:

$$\boldsymbol{v} = \begin{cases} \boldsymbol{v}_f(\boldsymbol{x}_{1,2}, t) & \text{in } \Omega_{f,x_3=0} \\ 0 & \text{in } \Omega_{s,x_3=0} \end{cases}, \quad \mathcal{P} = \begin{cases} \mathcal{P}_f(\boldsymbol{x}_{1,2}, t) & \text{in } \Omega_{f,x_3=0} \\ 0 & \text{in } \Omega_{s,x_3=0} \end{cases}. \tag{3.49}$$

Moreover, the weighted planar velocity distribution $\boldsymbol{v}$ then implicitly satisfies the following no-slip boundary:

$$\boldsymbol{v} = 0 \qquad \text{at } \Gamma_{fs,x_3=0}\,, \tag{3.50}$$

where $\Gamma_{fs,x_3=0}$ has an associated Dirac line distribution $\delta_{fs,x_3=0}$ and normal vector $\boldsymbol{n}_{fs,x_3=0} = \boldsymbol{n}_{fs}(\boldsymbol{x}_{1,2})$. It should be remarked that for solid structures of which the shape does vary in the x_3-direction, the planar flow cannot be represented in the form (3.49) while satisfying (3.50).

Planar Flow Equations

The continuity and momentum equation for incompressible planar flow are derived[6] from the generalized flow equations (3.1) and (3.2). In $\Omega_{x_3=0} = \Omega_{f,x_3=0} \cup \Omega_{s,x_3=0}$ they are given by:

$$\nabla^\nu \cdot \boldsymbol{v} = \varphi_3 \,, \tag{3.51}$$

$$\rho_f \frac{\partial^\nu \boldsymbol{v}}{\partial t} + \rho_f \nabla^\nu \cdot (\boldsymbol{v}\boldsymbol{v}) = -\nabla^\nu \mathcal{P} + \nabla^\nu \cdot \mu \big[\nabla^\nu \boldsymbol{v} + (\nabla^\nu \boldsymbol{v})^\intercal \big] + \langle \boldsymbol{f}_{1,2} \rangle_3 + \boldsymbol{\Psi}_3 \,. \tag{3.52}$$

We note that the gradient and time derivative in the planar flow equations are defined with respect to the two-dimensional regions $\Omega_{f,x_3=0}$ and $\Omega_{s,x_3=0}$ instead of the original three-dimensional regions Ω_f and Ω_s. The symbol $\boldsymbol{f}_{1,2}$ in (3.52) denotes the part of the body force vector that is parallel to the middle plane, similar as in (3.43).

The planar flow equations are based on the assumption that the viscosity and density do not vary significantly over the interval $x_3 \in \big[-\frac{l_3}{2}, \frac{l_3}{2}\big]$, so that we can use the representations

$$\mu = \begin{cases} \mu_f(\boldsymbol{x}_{1,2}) & \text{in } \Omega_{f,x_3=0} \\ 0 & \text{in } \Omega_{s,x_3=0} \end{cases} \,, \quad \rho = \begin{cases} \rho_f(\boldsymbol{x}_{1,2}) & \text{in } \Omega_{f,x_3=0} \\ \rho_s(\boldsymbol{x}_{1,2}) & \text{in } \Omega_{s,x_3=0} \end{cases} \,. \tag{3.53}$$

The closure term φ_3 in the planar continuity equation is defined as

$$\varphi_3 \triangleq -\langle (\boldsymbol{e}^{(3)} \cdot \nabla)(\boldsymbol{u} \cdot \boldsymbol{e}^{(3)}) \rangle_3 \,. \tag{3.54}$$

The closure term $\boldsymbol{\Psi}_3$ in the planar momentum equation consists of three parts:

$$\boldsymbol{\Psi}_3 \triangleq \boldsymbol{\Psi}_3^{\mathrm{I}} + \boldsymbol{\Psi}_3^{\mathrm{II}} + \boldsymbol{\Psi}_3^{\mathrm{III}} \,. \tag{3.55}$$

The first part represents the advective momentum fluxes in the directions parallel to the middle-plane that are not carried by the planar flow velocity:

$$\boldsymbol{\Psi}_3^{\mathrm{I}} \triangleq \rho_f \nabla^\nu \cdot \big(\boldsymbol{v}\boldsymbol{v} - \langle \boldsymbol{u}_{1,2} \boldsymbol{u}_{1,2} \rangle_3 \big) \,. \tag{3.56}$$

The second part contains the advective momentum fluxes at the two confining planar surfaces, as well as the advective momentum fluxes in the

[6] The derivation can be found in Appendix D.

direction normal to the planar velocity:

$$\boldsymbol{\Psi}_3^{\mathrm{II}} \triangleq -\langle (\boldsymbol{e}^{(3)} \cdot \nabla)\big(\boldsymbol{u} \cdot \boldsymbol{e}^{(3)} \boldsymbol{u}_{1,2}\big)\rangle_3 \,. \tag{3.57}$$

The third part stems from the shear stresses, i.e. viscous friction due to velocity gradients, at the two confining planar surfaces, as well as the residual shear stresses due to the averaging procedure:

$$\boldsymbol{\Psi}_3^{\mathrm{III}} \triangleq \langle \nabla_3^\nu \cdot \mu \left(\nabla_3^\nu \boldsymbol{u}_{1,2} + \big(\nabla_{1,2}^\nu \boldsymbol{u}_3\big)^{\mathsf{T}} \right) \rangle_3 \,, \tag{3.58}$$

where $\nabla_{1,2}^\nu$ and ∇_3^ν denote the component of the gradient operator in the usual sense respectively orthogonal and parallel to $\boldsymbol{e}^{(3)}$.

3.11 Planar Flow Boundary Conditions

For planar flow through a channel consisting of two parallel plates with solid structures in between, the no-slip condition holds at the bottom and top plate:

$$\boldsymbol{u} = 0 \qquad\qquad \text{at } x_3 = \pm \tfrac{l_3}{2} \,. \tag{3.59}$$

and the following boundary conditions for the planar velocity and pressure are consistent with (3.11) and (3.12):

$$\boldsymbol{v} = 0 \qquad\qquad \boldsymbol{x} \in \Gamma_{fs,x_3=0} \cup \Gamma_{fw,x_3=0} \,, \tag{3.60}$$

$$\mathcal{P} = \langle p_{io} \rangle_3 \qquad\qquad \boldsymbol{x} \in \Gamma_{fio,x_3=0} \,. \tag{3.61}$$

3.12 Closure of Planar Flow Equations

The closure terms φ_3 and $\boldsymbol{\Psi}_3$ in the planar flow equations are not known a priori. But if one is willing to accept a modelling error, the closure terms can be estimated by modelling the velocity distribution as a separable function of the x_3-coordinate along the channel height [47, 49]:

$$\boldsymbol{u}(\boldsymbol{x}_{1,2}, x_3, t) \simeq \boldsymbol{v}(\boldsymbol{x}_{1,2}, t) \zeta_{\boldsymbol{u}}(x_3) \qquad \text{so } \boldsymbol{u}_3 = 0 \,. \tag{3.62}$$

By definition of the planar velocity (3.41), the velocity shape function $\zeta_{\boldsymbol{u}}(x_3)$ must be normalized:

$$\langle \zeta_{\boldsymbol{u}} \rangle_3 = 1 \,. \tag{3.63}$$

The velocity shape function must also satisfy the no-slip condition at both plates:

$$\zeta_{\boldsymbol{u}} = 0 \qquad \text{at } x_3 = \pm\tfrac{l_3}{2}\,. \tag{3.64}$$

From (3.62) it follows that wherever $\boldsymbol{u} = 0$ holds, also $\boldsymbol{v} = 0$ holds. Therefore, the former assumption makes only sense for solid structures of which the shape does not change in the x_3-direction, or equivalently, for which (3.47) and (3.49) are justified.

Because of the assumption that $\boldsymbol{u}_3 = 0$, the closure term for the planar continuity equation vanishes:

$$\varphi_3 \simeq 0\,. \tag{3.65}$$

Using (3.62), the expression for $\boldsymbol{\Psi}_3^{\mathrm{I}}$ simplifies to

$$\boldsymbol{\Psi}_3^{\mathrm{I}} \simeq \big(1 - \langle\zeta_{\boldsymbol{u}}^2\rangle_3\big)\rho_f \nabla^\nu \cdot (\boldsymbol{v}\boldsymbol{v})\,. \tag{3.66}$$

The closure term $\boldsymbol{\Psi}_3^{\mathrm{II}}$ must also vanish when $\boldsymbol{u}_3 = 0$:

$$\boldsymbol{\Psi}_3^{\mathrm{II}} \simeq 0\,. \tag{3.67}$$

Furthermore, by (3.62) the shear stress contributions in the flow domain at the upper and bottom plate can be simplified into

$$\tau_{1,3} \simeq \mu\frac{\partial u_1}{\partial x_3} \simeq \mu v_1 \frac{\partial \zeta_{\boldsymbol{u}}}{\partial x_3}\,, \tag{3.68}$$

$$\tau_{2,3} \simeq \mu\frac{\partial u_2}{\partial x_3} \simeq \mu v_2 \frac{\partial \zeta_{\boldsymbol{u}}}{\partial x_3}\,. \tag{3.69}$$

This result gives as approximation for $\boldsymbol{\Psi}_3^{\mathrm{III}}$:

$$\boldsymbol{\Psi}_3^{\mathrm{III}} \simeq \mu\boldsymbol{v}\left\langle \frac{\partial^2 \zeta_{\boldsymbol{u}}}{\partial x_3^2} \right\rangle_3\,. \tag{3.70}$$

In case $m_3'(-y_3) = \frac{1}{l_3}$ is chosen and a parabolic velocity profile is assumed, $\zeta_{\boldsymbol{u}}(x_3)$ is given by

$$\zeta_{\boldsymbol{u}}(x_3) = 6\left[\frac{1}{4} - \left(\frac{x_3}{l_3}\right)^2\right]\,, \tag{3.71}$$

and the closure coefficients are

$$\big\langle\zeta_{\boldsymbol{u}}^2\big\rangle_3 = \frac{6}{5} \qquad \text{and} \qquad \left\langle \frac{\partial^2 \zeta_{\boldsymbol{u}}}{\partial x_3^2} \right\rangle_3 = \frac{12}{l_3^2}\,. \tag{3.72}$$

3.13 Macro-Scale Planar Flow Equations

When the solid structures have a shape which does not depend on the x_3-coordinate in the direction normal to the bottom and upper wall plate of the channel, the planar velocity and pressure can be represented as two-dimensional distributions of a form (cf. (3.49)) which respects the no-slip condition (3.50). This makes it possible to apply the spatial averaging technique on the two-dimensional domain $\Omega_{x_3=0}$ in the same way as we did for the three-dimensional generalized Navier-Stokes equations.

Superficially Averaged Planar Flow Equations
The superficially averaged planar flow equations look like:

$$\nabla \cdot \langle \boldsymbol{v} \rangle_m = 0 \,, \tag{3.73}$$

$$\rho_f \frac{\partial \langle \boldsymbol{v} \rangle_m}{\partial t} + \rho_f \nabla \cdot \left(\epsilon_{fm}^{-1} \langle \boldsymbol{v} \rangle_m \langle \boldsymbol{v} \rangle_m \right) = -\nabla \langle \mathcal{P} \rangle_m + \nabla \cdot \langle \boldsymbol{\mathcal{T}} \rangle_m + \boldsymbol{\mathcal{B}}_{fs} - \rho_f \nabla \cdot \boldsymbol{\mathcal{M}} + \langle \boldsymbol{\Psi}_3 \rangle_m \,, \tag{3.74}$$

where

$$\boldsymbol{\mathcal{T}} \triangleq \mu \left[\nabla^\nu \boldsymbol{v} + (\nabla^\nu \boldsymbol{v})^\intercal \right] \quad \text{and} \quad \boldsymbol{\mathcal{B}}_{fs} \triangleq \langle \boldsymbol{n}_{fs} \cdot (-\mathcal{P}_f \boldsymbol{I} + \boldsymbol{\mathcal{T}}_f) \, \delta_{fs} \rangle_m$$

$$\langle \boldsymbol{\mathcal{T}} \rangle_m = \mu \left[\nabla \langle \boldsymbol{v} \rangle_m + (\nabla \langle \boldsymbol{v} \rangle_m)^\intercal \right] \quad \text{and} \quad \boldsymbol{\mathcal{M}} \triangleq \langle \boldsymbol{v}\boldsymbol{v} \rangle_m - \epsilon_{fm}^{-1} \langle \boldsymbol{v} \rangle_m \langle \boldsymbol{v} \rangle_m \,.$$

Just like the gradient ∇ is defined with respect to the domain $\Omega_{x_3=0} \subset \mathbb{R}^2$ and corresponds to the operator $\nabla_{1,2}$ in $\Omega \subset \mathbb{R}^3$, also $\boldsymbol{n}_{fs}$ and δ_{fs} are defined here with respect to the solid-fluid interface $\Gamma_{x_3=0}$ within $\Omega_{x_3=0}$, so they correspond to $\boldsymbol{n}_{fs,x_3=0}$ and $\delta_{fs,x_3=0}$ in Ω.

In Appendix E, it is shown that if $\boldsymbol{u} \cdot \boldsymbol{e}^{(3)} = 0$, the macro-scale velocity of (3.14) corresponds to the macro-scale planar velocity of (3.74):

$$\langle \boldsymbol{u} \rangle_m^f = \langle \boldsymbol{v} \rangle_m^f \,, \tag{3.75}$$

provided that the filter in (3.14) is partly separable with respect to $\boldsymbol{e}^{(3)}$ and its convolution product is evaluated at $\boldsymbol{x} \cdot \boldsymbol{e}^{(3)} = 0$. Under the same assumptions, also the macro-scale pressure corresponds to the macro-scale planar pressure:

$$\langle p \rangle_m^f = \langle \mathcal{P} \rangle_m^f \,. \tag{3.76}$$

In laminar flow through small channels, it can be expected that the solid structures in many cases will not induce a three-dimensional velocity field if their shape satisfies (3.45), so that the planar flow is effectively characterized by $\boldsymbol{u} \cdot \boldsymbol{e}^{(3)} = 0$.

Closure Terms in Macro-Scale Planar Flow Equations

In apppendix E, it is shown that when the filter in (3.14) is partly separable with respect to $\boldsymbol{e}^{(3)}$ and its convolution product is evaluated at $\boldsymbol{x} \cdot \boldsymbol{e}^{(3)} = 0$, the planar interfacial force $\boldsymbol{\mathcal{B}}_{fs}$ equals the interfacial force of the three-dimensional macro-scale flow equations:

$$\boldsymbol{\mathcal{B}}_{fs} = \boldsymbol{b}_{fs} \,, \tag{3.77}$$

at least if $\boldsymbol{u} \cdot \boldsymbol{e}^{(3)} = 0$. In that case, also the divergence of the planar momentum dispersion source is directly related to the divergence of the momentum dispersion source of the three-dimensional macro-scale flow equations via:

$$\nabla \cdot \boldsymbol{\mathcal{M}} = \nabla \cdot \boldsymbol{M} + \langle \boldsymbol{\Psi}_3^{\mathrm{I}} \rangle_m + \langle \boldsymbol{\Psi}_3^{\mathrm{II}} \rangle_m \,. \tag{3.78}$$

If we use (3.66), (3.67) and (3.70) as an approximation for the planar flow equations, the closure terms in the macro-scale planar flow equations are estimated by

$$\langle \boldsymbol{\Psi}_3^{\mathrm{I}} \rangle_m \simeq \big(1 - \langle \zeta_{\boldsymbol{u}}^2 \rangle_3\big) \rho_f \nabla \cdot \left(\langle \boldsymbol{v} \rangle_m \langle \boldsymbol{v} \rangle_m + \boldsymbol{\mathcal{M}} \right) \,, \tag{3.79}$$

$$\langle \boldsymbol{\Psi}_3^{\mathrm{II}} \rangle_m \simeq 0 \tag{3.80}$$

and

$$\langle \boldsymbol{\Psi}_3^{\mathrm{III}} \rangle_m \simeq \mu \langle \boldsymbol{v} \rangle_m \left\langle \frac{\partial^2 \zeta_{\boldsymbol{u}}}{\partial x_3^2} \right\rangle_3 \,. \tag{3.81}$$

Macro-Scale Planar Flow Boundary conditions

By analogy to the original macro-scale flow, the boundary conditions for the macro-scale planar flow are stated in the form

$$\langle \boldsymbol{v} \rangle_m^f = \boldsymbol{f}_{\boldsymbol{v}}(\boldsymbol{x}) \simeq 0 \qquad \text{on } \Gamma_{w,x_3=0} \,, \tag{3.82}$$

$$\langle \mathcal{P} \rangle_m^f = f_{\mathcal{P}}(\boldsymbol{x}) \simeq \langle p_{io} \rangle_3 \qquad \text{on } \Gamma_{fio,x_3=0} \,. \tag{3.83}$$

The functions $\boldsymbol{f}_{\boldsymbol{v}}$ and $f_{\mathcal{P}}$ are again unknown since the actual value of a filtered quantity on the boundary depends on the point values contained in the averaging domain around the boundary point considered.

Global Closure for Macro-Scale Planar Flow Equations
A comparison of the planar macro-scale flow equations (3.73), (3.74) and (3.82) with the macro-scale flow system of (3.13),(3.14) and (3.28) reveals that both equation sets are very similar in nature. It appears that the planar flow quantities $\boldsymbol{v}$, $\mathfrak{T}$ and $\mathcal{P}$ respectively have replaced $\boldsymbol{u}$, $\boldsymbol{\tau}$ and p in the macro-scale equations. Therefore, the global closure problem for the macro-scale planar flow is not shown here.

As a matter of fact, the planar global closure problem would look similar to (3.34) and (3.35), except that the additional term $\boldsymbol{\Psi}_3 - \langle \boldsymbol{\Psi}_3 \rangle_m$ would appear on the right hand side of the momentum equation of the former closure problem (3.35).

Bibliography

[1] C. M. Marle, "Application de la méthode de la thermodynamique des processus irréversible à l'écoulement d'un fluide à travers un milieux poreux," *Bulletin RILEM*, vol. 29, pp. 1066–1071, 1965.

[2] J. C. Slattery, "Flow of viscoelastic fluids through porous media," *AIChE Journal*, vol. 13, no. 6, pp. 1066–1071, 1967.

[3] S. Whitaker, "Advances in theory of fluid motion in porous media," *Ind. Eng. Chem.*, vol. 61, pp. 14–28, 1969.

[4] J. Bear, *Dynamics of Fluids in Porous Media*. Elsevier, New York, 1972.

[5] P. M. Adler, *Porous media: Geometry and transport*. Butterworth-Heinemann, Stoneham, 1992.

[6] S. Whitaker, "Flow in porous media I: A theoretical derivation of Darcy's law," *Transport in Porous Media*, vol. 1, no. 1, pp. 3–25, 1986.

[7] J. Barrere, O. Gipouloux, and S. Whitaker, "On the closure problem for darcy's law," *Transport in Porous Media*, vol. 7, no. 3, pp. 209–222, 1992.

[8] M. Quintard and S. Whitaker, "Transport in ordered and disordered porous media II: Generalized volume averaging," *Transport in Porous Media*, vol. 14, no. 2, pp. 179–206, 1994.

[9] M. Quintard and S. Whitaker, "Transport in ordered and disordered porous media III: Closure and comparison between theory and experiment," *Transport in Porous Media*, vol. 15, no. 1, pp. 31–49, 1994.

[10] M. Quintard and S. Whitaker, "Transport in chemically and mechanically heterogeneous porous media. I: Theoretical development of region-averaged equations for slightly compressible single-phase flow," *Advances in Water Resources*, vol. 19, no. 1, pp. 29 – 47, 1996.

[11] D. Lasseux, F. J. Valdes Parada, J. A. Ochoa Tapia, and B. Goyeau, "A macroscopic model for slightly compressible gas slip-flow in homogeneous porous media," *Physics of Fluids*, vol. 26, no. 5, 2014.

[12] X.-H. Wang, J.-T. Jia, Z.-F. Liu, and L.-D. Jin, "Derivation of the darcy-scale filtration equation for power-law fluids with the volume-averaging method," *Journal of Porous Media*, vol. 17, no. 8, pp. 741–750, 2014.

[13] M. Minale, "Modelling the flow of a second order fluid through and over a porous medium using the volume averages. i. the generalized brinkman's equation," *Physics of Fluids*, vol. 28, no. 2, 2016.

[14] C. M. Marle, "Ecoulements monophasiques en milieu poreux," *Revue de l'Institut Français du Pétrole*, vol. 22, no. 10, pp. 1471–1509, 1967.

[15] L. Schwartz, *Théorie des Distributions*. Hermann, Paris, 1978.

[16] S. Whitaker, "The Forchheimer equation: A theoretical development," *Transport in Porous Media*, vol. 25, no. 1, pp. 27–61, 1996.

[17] D. Lasseux, A. A. Abbasian Arani, and A. Ahmadi, "On the stationary macroscopic inertial effects for one phase flow in ordered and disordered porous media," *Physics of Fluids*, vol. 23, no. 7, 2011.

[18] D. Getachew, W. Minkowycz, and D. Poulikakos, "Macroscopic equations of non-newtonian fluid flow and heat transfer in a porous matrix," *Journal of Porous Media*, 1998.

[19] L. Wang, L.-P. Wang, Z. Guo, and J. Mi, "Volume-averaged macroscopic equation for fluid flow in moving porous media," *International Journal of Heat and Mass Transfer*, vol. 82, pp. 357 – 368, 2015.

[20] S. B. Pope, *Turbulent flows*. Cambridge University Press, 2000.

[21] T. Masuoka and Y. Takatsu, "Turbulence model for flow through porous media," *International Journal of Heat and Mass Transfer*, vol. 39, no. 13, pp. 2803 – 2809, 1996.

[22] D. Nield, "Comments on turbulence model for flow through porous media," *International Journal of Heat and Mass Transfer*, vol. 40, no. 10, pp. 2499 –, 1997.

[23] A. Nakayama and F. Kuwahara, "A macroscopic turbulence model for flow in a porous medium," *Journal of Fluids Engineering*, vol. 121, no. 2, pp. 427–433., 1996.

[24] M. H. Pedras and M. J. de Lemos, "Macroscopic turbulence modeling for incompressible flow through undeformable porous media," *International Journal of Heat and Mass Transfer*, vol. 44, no. 6, pp. 1081 – 1093, 2001.

[25] V. S. Travkin, I. Catton, and L. Gratton, "Single-phase turbulent transport in prescribed non-isotropic and stochastic porous media," *Heat Transfer in Porous Media, ASME–HTD–240*, pp. 43–48., 1993.

[26] F. Pinson, O. Grégoire, and O. Simonin, "Macro-scale modeling of turbulence based on a two scale analysis in porous media," *International Journal of Heat and Fluid Flow*, vol. 27, no. 5, pp. 955 – 966, 2006. Special issue of the 6th International Symposium on Engineering Turbulence Modelling and Measurements ETMM6.

[27] M. Chandesris, G. Serre, and P. Sagaut, "A macroscopic turbulence model for flow in porous media suited for channel, pipe and rod bundle flows," *International Journal of Heat and Mass Transfer*, vol. 49, no. 1516, pp. 2739 – 2750, 2006.

[28] A. Nakayama and F. Kuwahara, "A general macroscopic turbulence model for flows in packed beds, channels, pipes, and rod bundles," *Journal of Fluids Engineering*, vol. 130, no. 10, p. 101205, 2008.

[29] M. Drouin, O. Grgoire, and O. Simonin, "A consistent methodology for the derivation and calibration of a macroscopic turbulence model for flows in porous media," *International Journal of Heat and Mass Transfer*, vol. 63, pp. 401 – 413, 2013.

[30] H. Wang and E. S. Takle, "Boundary-layer flow and turbulence near porous obstacles," *Boundary–Layer Meteorology*, vol. 74, no. 1, pp. 73–88, 1995.

[31] H. Wang, E. S. .Takle, and J. Shen, "Shelterbelts and windbreaks: Mathematical modeling and computer simulations of turbulent flows," *Annual Review of Fluid Mechanics*, vol. 33, no. 1, pp. 549–586, 2001.

[32] B. Antohe and J. Lage, "A general two-equation macroscopic turbulence model for incompressible flow in porous media," *International Journal of Heat and Mass Transfer*, vol. 40, no. 13, pp. 3013 – 3024, 1997.

[33] D. Getachew, W. Minkowycz, and J. Lage, "A modified form of the $k-\epsilon$ model for turbulent flows of an incompressible fluid in porous media," *International Journal of Heat and Mass Transfer*, vol. 43, no. 16, pp. 2909 – 2915, 2000.

[34] M. de Lemos and M. Pedras, "Recent mathematical models for turbulent flow in saturated rigid porous media," *Journal of Fluids Engineering*, vol. 123, no. 4, pp. 935–940, 2001.

[35] V. S. Travkin, "Discussion: Alternative Models of Turbulence in a Porous Medium, and Related Matters (D. A. Nield, 2001, ASME J. Fluids Eng., 123, pp. 928931)," *Journal of Fluids Engineering*, vol. 123, no. 4, pp. 931–934., 2001.

[36] F. E. Teruel and Rizwan-uddin, "A new turbulence model for porous media flows. Part I: Constitutive equations and model closure," *International Journal of Heat and Mass Transfer*, vol. 52, no. 1920, pp. 4264 – 4272, 2009.

[37] C. Soulaine and M. Quintard, "On the use of a darcy-forchheimer like model for a macro-scale description of turbulence in porous media and its application to structured packings," *International Journal of Heat and Mass Transfer*, vol. 74, pp. 88 – 100, 2014.

[38] M. Hassanizadeh and W. G. Gray, "General conservation equations for multiphase systems: 2. Mass, momenta, energy, and entropy equations," *Advances in Water Resources*, vol. 2, pp. 191–208, 1979.

[39] M. Hassanizadeh and W. G. Gray, "General conservation equations for multiphase systems: 3. Constitutive theory for porous media," *Advances in Water Resources*, vol. 3, pp. 25–40., 1980.

[40] S. Achanta, J. H. Cushman, and M. R. Okos, "On multicomponent, multiphase thermomechanics with interfaces," *International Journal of Engineering Science*, vol. 32, pp. 1717– 1738, 1994.

[41] L. S. Bennethum and J. H. Cushman, "Multiscale, hybrid mixture theory for swelling systems i: balance laws," *International Journal of Engineering Science*, vol. 34, no. 2, pp. 125 – 145, 1996.

[42] M. Quintard and S. Whitaker, "Transport in ordered and disordered porous media I: The cellular average and the use of weighting functions," *Transport in Porous Media*, vol. 14, no. 2, pp. 163–177, 1994.

[43] F. M. White, *Viscous fluid flow*. New York: McGraw-Hill., 1974.

[44] J. Neustupa and P. Penel, "Incompressible viscous fluid flows and the generalized impermeability boundary conditions," *IASME Transactions 7*, vol. 2, pp. 1254–1261, 2005.

[45] R. Mittal and G. Iaccarino, "Immersed boundary methods," *Annual Review of Fluid Mechanics*, vol. 37, no. 1, pp. 239–261, 2005.

[46] T. Borrvall and J. Petersson, "Topology optimization of fluids in stokes flow," *International Journal for Numerical Methods in Fluids*, vol. 41, no. 1, pp. 77–107, 2003.

[47] T. Van Oevelen, *Optimal Heat Sink Design for Liquid Cooling of Electronics*. PhD thesis, Arenberg Doctoral School, Faculty of Engineering, KULeuven, 2014.

[48] A. Dunca, V. John, and W. J. Layton, "The commutation error of the space averaged navier-stokes equations on a bounded domain," *Journal of Mathematical Fluid Mechanics*, vol. 1, no. 3, pp. 273–283, 2003.

[49] M. Lyytikäinen, T. Hämäläinen, and J. Hämäläinen, "A fast modelling tool for plate heat exchangers based on depth-averaged equations," *International Journal of Heat and Mass Transfer*, vol. 52, no. 56, pp. 1132 – 1137, 2009.

CHAPTER

4

SPATIALLY AVERAGED TEMPERATURE EQUATIONS

4.1 Introduction

This chapter presents spatially averaged temperature equations for modelling the macro-scale heat transfer in devices with solid structures. The form of the macro-scale flow equations presented here is generally valid for an incompressible Newtonian fluid, as long as the thermal and hydraulic properties of the fluid change gradually over the device domain. No assumptions about the heat transfer regime or the topology of the solid structures are incorporated in the temperature equations. To describe the heat transfer in a mainly two-dimensional flow through a small channel with solid structures, so-called macro-scale planar temperature equations are proposed in this chapter.

4.2 Outline

This chapter begins with a brief overview of the historical development of the spatially averaged temperature equations describing macro-scale heat transfer in two-phase and three-phase media. After this historical background, the energy and temperature equations for flow through a solid medium are generalized within the theory of mathematical distributions to make them compatible with the spatial averaging technique of chapter 2. In Section 5, the boundary conditions for the generalized temperature equations in a heat transfer device are set down. Subsequently, in Section 6, the generalized temperature equations are spatially averaged to obtain the macro-scale temperature equations of the fluid and the solid. In Section 7, the boundary conditions for the macro-scale temperature are given. In Section 8, the global closure problem for the closure terms in the macro-scale temperature equations is explained. The boundary conditions for the global closure problem follow in Section 9. In Section 10, the planar temperature equations are derived by averaging the generalized temperature equations over the height of the domain. The appropriate boundary conditions for the planar temperature equations are stated in Section 11. Section 12 contains an approximative method to determine the closure terms in the planar temperature equation. Finally, the macro-scale planar temperature equations are the topic of the last section.

4.3 Historical Background

In this section, it will be shown that the spatially averaged temperature equations in the literature have been developed mainly with the objective of defining effective thermal properties of porous media, like the effective thermal conductivity. In order to obtain closure models for the effective thermal properties which can be solved on an REV of the porous medium, different (length-scale) approximations have been introduced.

Spatially Averaged Heat Conduction Equations

The volume-averaged temperature equations that describe the macro-scale temperature field in a two-phase system in which only heat conduction takes place, were derived by Carbonell, Whitaker and Nozad in 1984 [1, 2]. The volume-averaged heat conduction equation for the phase s in their

work has the form

$$\epsilon_s(\rho c)_s \frac{\partial \langle T_s \rangle^s}{\partial t} \simeq \nabla \cdot (\epsilon_s k_s \nabla \langle T_s \rangle^s) + \nabla \cdot \frac{1}{V_s} \int_{A_{sf}} \boldsymbol{n}_{sf} \widetilde{T}_s \, dA + \frac{1}{V} \int_{A_{sf}} \boldsymbol{n}_{sf} \cdot k_s \nabla T_s \, dA \,.$$

This equation contains two closure terms: one that depends on the deviation temperature and another that depends on the heat flux at the boundary surface A_{sf} between the two phases s and f. Carbonell, Whitaker and Nozad showed that under the assumption of local thermal equilibrium, when both phases have the same macro-scale temperature $\langle T_s \rangle^s = \langle T_f \rangle^f$, macro-scale heat conduction is described by the following *one-equation model*:

$$\langle \rho \rangle c_{\text{eff}} \frac{\partial \langle T \rangle}{\partial t} \simeq \boldsymbol{K}_{\text{eff}} \cdot\cdot \nabla \nabla \langle T \rangle \,.$$

The effective heat capacity c_{eff} in the one-equation model corresponds to the mass-fraction weighted sum of the heat capacities of the individual phases:

$$\langle \rho \rangle c_{\text{eff}} \triangleq \epsilon_s (\rho c)_s + \epsilon_f (\rho c)_f \,,$$

The effective conductivity $\boldsymbol{K}_{\text{eff}}$ of the two-phase system is defined as

$$\boldsymbol{K}_{\text{eff}} \triangleq (\epsilon_s k_s + \epsilon_f k_f) \boldsymbol{I} + \frac{k_f - k_s}{V} \int_{A_{sf}} \frac{1}{2} \left(\boldsymbol{n}_{sf} \boldsymbol{d} + \boldsymbol{d} \boldsymbol{n}_{sf} \right) \, dA$$

and contains the closure variable $\boldsymbol{d}$, which links the deviation temperature to the superficially averaged temperature:

$$\widetilde{T}_s = \boldsymbol{d} \cdot \nabla \langle T \rangle \,.$$

As the closure variable $\boldsymbol{d}$ is the solution of a local closure problem on an REV of the system [1], the effective conductivity $\boldsymbol{K}_{\text{eff}}$ depends just on the geometry of the REV and the conductivity ratio k_f/k_s.

While the latter studies of Carbonell, Whitaker and Nozad [1, 2] mainly concerned quasi-steady heat conduction in two-phase systems, the transient problem was further studied by Levec and Carbonell [3]. In the work of Levec and Carbonell, the spatially averaged temperature equations of the two phases are coupled by convective and dispersive coupling terms.

Such coupling terms also arise in the *two-equation model* of Quintard and Whitaker of 1993 [4], where the following form of the macro-scale temperature equation for the phase s is derived:

$$\epsilon_{sm}(\rho c)_s \frac{\partial \langle T_s \rangle_m^s}{\partial t} \simeq \nabla \cdot \left(\boldsymbol{K}_{sf} \cdot \nabla \langle T_f \rangle_m^f + \boldsymbol{K}_{ss} \cdot \nabla \langle T_s \rangle_m^s \right) + \boldsymbol{u}_{sf} \cdot \nabla \langle T_f \rangle_m^f + \boldsymbol{u}_{ss} \cdot \nabla \langle T_s \rangle_m^s - a_v h_{fs} \left(\langle T_s \rangle_m^s - \langle T_f \rangle_m^f \right) ,$$

and a similar equation is proposed for the fluid. The coupling closure coefficients, $\boldsymbol{K}_{sf}$, $\boldsymbol{K}_{ss}$, $\boldsymbol{u}_{sf}$ and $\boldsymbol{u}_{ss}$, as well as the interfacial heat transfer coefficient h_{fs}, arise from the assumption that the temperature deviation fields can be represented in a form like

$$\widetilde{T}_s = \boldsymbol{b}_{sf} \cdot \nabla \langle T_s \rangle_m^f + \boldsymbol{b}_{ss} \cdot \nabla \langle T_s \rangle_m^s + s_s \left(\langle T_s \rangle_m^s - \langle T_f \rangle_m^f \right) + \xi_s ,$$

where $\boldsymbol{b}_{sf}$, $\boldsymbol{b}_{ss}$, s_s and ξ_s satisfy coupled periodic partial differential equations on an REV of the two-phase system. The convolution product $\langle \, \rangle_m$ in the former two-equation model [4] corresponds to a volume average in the case of a disordered two-phase system and a cellular average in the case of an ordered two-phase system.

Whereas the two-equation model of Quintard and Whitaker is only applicable under quasi-steady state conditions, the two-equation model of Moyne in 1997 [5] treats macro-scale heat conduction under unsteady conditions. Moyne extended the macro-scale heat conduction equation for the phase s of a two-phase system as

$$\begin{aligned} \epsilon_s(\rho c)_s \frac{\partial \langle T_s \rangle^s}{\partial t} \simeq{}& \nabla \cdot (\epsilon_s k_s \nabla \langle T_s \rangle^s) + \nabla \cdot \left(\frac{k_s}{k_f} \boldsymbol{f} \star \frac{\partial}{\partial t} \left(\nabla \langle T_s \rangle^s \right) \right) \\ & - \nabla \cdot \left(\boldsymbol{f} \star \frac{\partial}{\partial t} \left(\nabla \langle T_f \rangle^f \right) \right) - h_{fs} \star \frac{\partial}{\partial t} \left(\langle T_s \rangle^s - \langle T_f \rangle^f \right) \\ & + (k_s \boldsymbol{g} - k_s \boldsymbol{s}) \star \cdot \frac{\partial}{\partial t} \left(\nabla \langle T_s \rangle^s \right) + (k_s \boldsymbol{g} - k_f \boldsymbol{s}) \star \cdot \frac{\partial}{\partial t} \left(\nabla \langle T_f \rangle^f \right) . \end{aligned}$$

Moyne's two-equation model is in form similar to that of Quintard and Whitaker [4], except that it contains a temporal convolution $\star$ due to the time dependency of the interfacial heat transfer coefficient h_{fs} and the other closure coefficients $\boldsymbol{f}$, $\boldsymbol{g}$ and s. These closure coefficients in Moyne's two-equation model are derived from the closure variables $\boldsymbol{v}$, $\boldsymbol{w}$ and u for the deviation temperature:

$$\widetilde{T}_s = \boldsymbol{v}_f \star \cdot \nabla \langle T_s \rangle^f + \boldsymbol{w}_s \star \cdot \nabla \langle T_s \rangle^s + u_s \star \left(\langle T_s \rangle^s - \langle T_f \rangle^f \right) .$$

Because the closure variables are all assumed to be spatially periodic over an REV of the system, the closure coefficients are constant over any REV.

Under the assumption of local thermal equilibrium, the former two-equation models for macro-scale heat conduction can all be simplified into a one-equation model. The (length-scale) constraints that must be satisfied in order that the principle of local thermal equilibrium be valid, have been re-examined by Quintard in 1995 [6].

In the previous studies, the macro-scale heat conduction equation incorporates the continuity of the heat flux and temperature at the boundary between the two phases. On the other hand, Gobbé et al. [7, 8] have investigated macro-scale heat conduction under the presence of a temperature jump at the interface boundary between the two phases f and s, caused by a thermal resistance barrier R:

$$\boldsymbol{n}_{fs} \cdot k_s \nabla T_s = \boldsymbol{n}_{fs} \cdot k_f \nabla T_f = \frac{1}{R} \left(T_s - T_f \right) .$$

In their study, the presence of a thermal resistance barrier is taken into account in the two-equation model of Quintard and Whitaker [4] without adapting its form.

Spatially Averaged Heat Convection Equations

The macro-scale heat transfer between a flow and a solid porous medium is not just the result of heat conduction in the fluid and solid phase, but also advection of thermal energy by the fluid flow. Macro-scale heat convection, encompassing both conduction and advection, in a flow through a porous medium can be described by the volume-averaged temperature equations presented by Quintard, Kaviany and Whitaker in 1991 [9]. The volume-averaged temperature equation for the fluid flow in [9] is given by

$$\epsilon_f (\rho c)_f \frac{\partial \langle T_f \rangle^f}{\partial t} + \epsilon_f (\rho c)_f \langle \boldsymbol{u}_f \rangle^f \cdot \nabla \langle T_f \rangle^f \simeq \nabla \cdot \left(\epsilon_f k_f \nabla \langle T_f \rangle^f \right)$$
$$- \epsilon_f (\rho c)_f \nabla \cdot \langle \widetilde{u}_f \widetilde{T}_f \rangle + \nabla \cdot \frac{1}{V_s} \int_{A_{fs}} \boldsymbol{n}_{fs} \widetilde{T}_f \, dA + \frac{1}{V} \int_{A_{fs}} \boldsymbol{n}_{fs} \cdot k_f \nabla T_f \, dA .$$

This volume-averaged temperature equation can be regarded as a special case of the macro-scale energy equation for a fluid that was already derived by Marle in 1967 [10] using weighted spatial averaging:

$$\frac{\partial (\rho_{fm} e_{fm})}{\partial t} + \nabla \cdot \left((\rho_f e_f \boldsymbol{u}) * m + \boldsymbol{q}_f * m \right) - (\boldsymbol{q}_f \cdot \boldsymbol{n}_{fs} \delta_{fs}) * m = \zeta_{fm} .$$

In Marle's work $\zeta_{fm} \triangleq [(-p\boldsymbol{I} + \boldsymbol{\tau}) \cdot\cdot \nabla \boldsymbol{u}] * m$ corresponds to the mechanical energy dissipated by stresses and $\boldsymbol{q}_f \triangleq -k_f \nabla T$ denotes the heat flux in the fluid.

Quintard, Kaviany and Whitaker [9] also derived a one-equation model for macro-scale convective transport of thermal energy in a flow through a porous medium, which reads

$$\langle\rho\rangle c_{\text{eff}} \frac{\partial \langle T\rangle}{\partial t} + \epsilon_f (\rho c)_f \langle \boldsymbol{u}_f\rangle^f \cdot \nabla \langle T\rangle \simeq \nabla \cdot ((\boldsymbol{K}_{\text{eff}} + \boldsymbol{K}_D) \cdot \nabla \langle T\rangle) + \epsilon_s \langle q_s\rangle^s + a_V \langle Q_{fs}\, \delta_{fs}\rangle \,.$$

Here, Q_{fs} is the heterogeneous heat source at the fluid-solid interface and q_s is the heat source within the solid medium. The thermal dispersion tensor in their one-equation model is defined as

$$\boldsymbol{K}_D \triangleq -(\rho c)_f \langle \widetilde{\boldsymbol{u}}_f \boldsymbol{f}\rangle$$

with $\boldsymbol{f}$ being a closure variable for the deviation temperature of the fluid:

$$\widetilde{T}_f = \boldsymbol{f} \cdot \nabla \langle T\rangle + h_f \langle Q_{fs}\, \delta_{fs}\rangle + \psi + \frac{1}{2}\left(\langle T_s\rangle^s - \langle T_f\rangle^f\right) .$$

The closure variables $\boldsymbol{f}$, h_f and ψ for the deviation temperature in [9] are all the solution of a periodic closure problem on an REV of the porous medium, which holds under local thermal equilibrium and various other length-scale approximations.

A two-equation model for macro-scale heat convection was presented in a subsequent study of Quintard, Kaviany and Whitaker [11]. This two-equation model is based on the following two volume-averaged temperature equations for the fluid and solid phase respectively:

$$\epsilon_f (\rho c)_f \frac{\partial \langle T_f\rangle^f}{\partial t} + \epsilon_f (\rho c)_f \langle \boldsymbol{u}_f\rangle^f \cdot \nabla \langle T_f\rangle^f \simeq \boldsymbol{u}_{ff} \cdot \nabla \langle T_f\rangle^f + \boldsymbol{u}_{fs} \cdot \nabla \langle T_s\rangle^s + \nabla \cdot \left(\boldsymbol{K}_{ff} \nabla \langle T_f\rangle^f\right) + \nabla \cdot (\boldsymbol{K}_{fs} \nabla \langle T_s\rangle^s) - a_{\text{v}} h_{fs} \left(\langle T_f\rangle^f - \langle T_s\rangle^s\right) ,$$

$$\epsilon_s (\rho c)_s \frac{\partial \langle T_s\rangle^f}{\partial t} \simeq \boldsymbol{u}_{sf} \cdot \nabla \langle T_f\rangle^f + \boldsymbol{u}_{ss} \cdot \nabla \langle T_s\rangle^s + \nabla \cdot \left(\boldsymbol{K}_{sf} \nabla \langle T_f\rangle^f\right) + \nabla \cdot (\boldsymbol{K}_{ss} \nabla \langle T_s\rangle^s) - a_{\text{v}} h_{fs} \left(\langle T_s\rangle^s - \langle T_f\rangle^f\right) .$$

The closure coefficients in the two-equation model of [11], e.g. $\boldsymbol{u}_{fs}$ and $\boldsymbol{K}_{ff}$, are to be governed from a closure problem consisting of three integro-differential equations on an REV of the porous medium. This closure problem can be transformed into a system of six differential equations with spatially periodic boundary conditions.

In 2000, Quintard, Ladevie and Whitaker [12] generalized the two-equation model of [11] and its closure problem to include the presence of a homogeneous heat source in the solid and a heterogeneous heat source at the fluid-solid interface. When a heterogeneous heat source Q_{fs} is present, the following boundary condition at the fluid-solid interface must be incorporated in the volume-averaged temperature equations:

$$\boldsymbol{n}_{fs} k_s \nabla T_s = \boldsymbol{n}_{fs} k_f \nabla T_f + Q_{fs} \, .$$

The two-equation model of Quintard, Ladevie and Whitaker [12] extends the one-equation model of [9] for situations when thermal equilibrium does not occur.

A more complete form of the volume-averaged heat convection equations which includes radiation transfer, has been deduced by Leroy, Goyeay and Taine in 2013 [13]. In the work of Leroy and his co-authors, the statistical radiation field is homogenized through a radiative intrinsic averaging operator and a radiative interface average to define a radiative flux and radiative conductivity, which are isotropic and vary continuously through the porous medium. The radiative flux at the fluid-solid interface leads to an additional closure term in the macro-scale temperature equations for the fluid and solid. The radiative conductivity appears in the macro-scale temperature equation via the macro-scale radiative energy generation rate. The closure problem for the macro-scale temperature equation in [13] differs whether the solid is transparent or semi-transparent.

Spatially Averaged Concentration Equations

The development of the former one-equation and two-equation temperature models has benefited a lot from the progression of macro-scale models for species transport in two-phase systems. This should be no surprise, since the form of the temperature equation strongly resembles that of a species concentration equation and both belong to the class of (advection-) diffusion equations. As a matter of fact, one of the earliest problems to be studied by means of VAT was the concentration equation for diffusion and dispersion of a single species in a flow through a porous medium.

The volume-averaged concentration equation for a nonreacting, nonadsorbing single species in an incompressible laminar flow in a porous medium dates back from 1967 and was derived by Whitaker [14]. The early work of Whitaker [14] and the work of Ryan in 1981 [15] on macro-scale diffusion and reaction in porous media would form the foundations for the one-equation heat conduction model.

Also in the work of Carbonell and Whitaker of 1984 [1], the development of the volume-averaged heat conduction equation is preceded by a derivation of the volume-averaged concentration equation for pure diffusion of a single species in a porous medium. In their work [1], a first-order irreversible reaction with a heterogeneous reaction source at the interface boundary is assumed. Therefore, their work shows many similarities with later studies [9, 12], which consider heat convection under the presence of a heterogeneous heat source at the interface of the porous medium.

The basic steps in the derivation of the two-equation model for macro-scale heat convection in a porous medium and its closure problem were laid down in the work of Zanotti and Carbonell in 1984 [16]. Zanotti and Carbonell did not investigate macro-scale heat convection on itself, but did derive the volume-averaged concentration equation for a solute being distributed between two phases by convection, diffusion and interfacial transport.

The one-equation model for macro-scale heat conduction in a two-phase system is strongly connected to the one-equation model for macro-scale diffusion and reaction in heterogeneous two-phase media, which has been treated e.g. in the work of Ochoa, Stroeve and Whitaker in 1986 [17].

On the other hand, the one-equation model for macro-scale heat convection in a porous medium and its closure problem have been developed in parallel with the one-equation model for macro-scale convection and dispersion of a species in a porous medium. The macro-scale convection-dispersion problem was for instance the subject of Plumb's work in 1988 [18] as well as Quintard's work of 2001 [19].

The literature on macro-scale concentration models is very broad and falls beyond the scope of this work. However, it must be remarked that also one-equation and two equation concentration models have been developed which rely on weighted averaging instead of volume-averaging, e.g. by Davit et al. in 2010 [20].

Spatially Averaged Three-Phase Equations
In the literature also macro-scale models for two-phase flows with phase-change in porous media have been developed. The macro-scale model of Duval et al. [21] consists of the volume-averaged flow equations for the gas and liquid phase and the three volume-averaged temperature equations for the liquid, gas and solid. Hence, this macro-scale model provides a three-phase description. Furthermore, Duval et al. have derived a closed form of the evaporation rate at the macroscopic level, which depends on the macro-scale temperatures and the effective properties of the three-phase system.

Open Research Questions in the Literature
The (length-scale) approximations that are incorporated in the macro-scale temperature equations from the literature impede exact model reduction and data reduction for the heat transfer regimes in heat transfer devices with spatially periodic structures. In view of the macro-scale description envisaged in this work, an exact formulation of the macro-scale temperature equations is needed.

As the complete procedure for the exact filtering of the temperature equations has not been presented in the literature, we consider it an open research question which we will address in the remainder of this chapter. The next section gives the first step of the procedure, which is the reformulation of the energy and temperature equations for the flow in a solid medium within the theory of mathematical distributions.

4.4 Generalized Energy Equations

In this work, the fluid flow and solid structures which form the system under consideration (§2.3) are regarded as a single continuum whose energy and temperature are described by a single energy conservation equation.

Conservation of Total Energy
Conservation of energy for the fluid and the solid structures is expressed by the generalized energy conservation equation in Ω:

$$\rho \frac{\partial^\nu e_{\mathrm{tot}}}{\partial t} + \rho \nabla^\nu \cdot (\boldsymbol{u} e_{\mathrm{tot}}) = \nabla^\nu \cdot (\boldsymbol{\sigma} \cdot \boldsymbol{u}) + \boldsymbol{f} \cdot \boldsymbol{u} + \nabla^\nu \cdot (k \nabla^\nu T) + \dot{q} \,. \tag{4.1}$$

Here, the total energy e_{tot} of the fluid-solid continuum and its internal energy u_{int} are mathematical distributions over the system domain, as is the total stress tensor $\boldsymbol{\sigma}$:

$$e_{\text{tot}} \triangleq u_{\text{int}} + \frac{||\boldsymbol{u}||^2}{2} \qquad \text{and} \qquad \boldsymbol{\sigma} \triangleq -p\boldsymbol{I} + \boldsymbol{\tau}\,. \tag{4.2}$$

The generalized energy equation (4.1) states that the change of total energy, consisting of the internal energy and kinetic energy, is balanced by the rate of work done on the continuum by body forces and surface forces, the heat transfer rate by thermal conduction in the continuum and the volumetric heat addition $\dot{q}$ into the continuum.

Mechanical Energy Equation

The equation for the kinetic or mechanical energy of the fluid is governed by taking the inner product of the velocity distribution with each term of the momentum equation (3.2):

$$\rho\frac{\partial^\nu}{\partial t}\left(\frac{||\boldsymbol{u}||^2}{2}\right) + \rho\nabla^\nu\cdot\left(\boldsymbol{u}\,\frac{||\boldsymbol{u}||^2}{2}\right) = (\nabla^\nu\cdot\boldsymbol{\sigma})\cdot\boldsymbol{u} + \boldsymbol{f}\cdot\boldsymbol{u} \qquad \text{in } \Omega\,. \tag{4.3}$$

Internal Energy Equation

The equation for the internal energy results from subtracting the mechanical energy equation (4.3) from the generalized energy conservation equation (4.1):

$$\rho\frac{\partial^\nu u_{\text{int}}}{\partial t} + \rho\nabla^\nu\cdot(\boldsymbol{u}u_{\text{int}}) = \boldsymbol{\sigma}\cdot\cdot\nabla^\nu\boldsymbol{u} + \nabla^\nu\cdot(k\,\nabla^\nu T) + \dot{q} \qquad \text{in } \Omega\,. \tag{4.4}$$

Thermal Energy Equation

When the fluid is incompressible, the work done by the stresses is given by $\boldsymbol{\sigma}\cdot\cdot\nabla^\nu\boldsymbol{u} = -p\nabla^\nu\cdot\boldsymbol{u} + \boldsymbol{\tau}\cdot\cdot\nabla^\nu\boldsymbol{u} = \boldsymbol{\tau}\cdot\cdot\nabla^\nu\boldsymbol{u}$. Furthermore, if the fluid is incompressible and the solid structures are rigid bodies, the internal energy is given by $u_{\text{int}} = cT$. Consequently, the thermal energy equation for the incompressible fluid and the rigid solid structures looks like

$$\rho\frac{\partial^\nu(cT)}{\partial t} + \rho\nabla^\nu\cdot(\boldsymbol{u}cT) = \nabla^\nu\cdot(k\,\nabla^\nu T) + \dot{q} + \dot{q}_{\text{visc}} \qquad \text{in } \Omega\,. \tag{4.5}$$

For ease of notation, the viscous dissipation term in the thermal energy equation has been given a separate symbol:

$$\dot{q}_{\text{visc}} \triangleq \boldsymbol{\tau}\cdot\cdot\nabla^\nu\boldsymbol{u}\,. \tag{4.6}$$

In the fluid region Ω_f, equation (4.5) takes the form

$$\rho_f \frac{\partial\,(c_f T_f)}{\partial t} + \rho \nabla \cdot (\boldsymbol{u}_f c_f T_f) = \nabla \cdot (k_f\, \nabla T_f) + \dot{q}_f + \dot{q}_{\mathrm{visc},f}\,, \tag{4.7}$$

while in the solid Ω_s, the equation for the temperature is given by

$$\rho_s \frac{\partial\,(c_s T_s)}{\partial t} = \nabla \cdot (k_s\, \nabla T_s) + \dot{q}_s\,. \tag{4.8}$$

The temperature is supposed to be continuous at the fluid-solid interface:

$$T_f(\boldsymbol{x}, t) = T_s(\boldsymbol{x}, t) \qquad\qquad \boldsymbol{x} \in \Gamma_{fs}\,. \tag{4.9}$$

The interfacial heat flux q_{fs} from the fluid to the solid is also assumed to be continuous and is given by Fourier's law:

$$q_{fs}(\boldsymbol{x}, t) = -\boldsymbol{n}_{fs} \cdot k_f\, \nabla T_f = -\boldsymbol{n}_{fs} \cdot k_s\, \nabla T_s \qquad \boldsymbol{x} \in \Gamma_{fs}\,, \tag{4.10}$$

because we consider the energy transfer at the fluid-solid interface solely due to thermal conduction.

If the gradient in the usual sense in (4.5) is replaced by the gradient in the sense of a distribution, the interfacial heat source $\dot{q}_{fs}$ appears in the thermal energy equation:

$$\rho \frac{\partial\,(cT)}{\partial t} + \rho \nabla \cdot (\boldsymbol{u} c T) = \nabla \cdot (k\, \nabla T) + \dot{q} + \dot{q}_{\mathrm{visc}} + \dot{q}_{fs} \qquad \text{in } \Omega\,. \tag{4.11}$$

The interfacial heat source $\dot{q}_{fs}$ in (4.11) originates from the gradient theorem (2.44) and is given by

$$\begin{aligned} \dot{q}_{fs} &\triangleq \boldsymbol{n}_{fs} \cdot (k_f\, \nabla T_f - k_s\, \nabla T_s)\delta_{fs} \\ &\qquad + \nabla \cdot (\boldsymbol{n}_{fs}(k_f T_f - k_s T_s)\delta_{fs}) \qquad (4.12) \\ &= \nabla \cdot (\boldsymbol{n}_{fs}(k_f T_f - k_s T_s)\delta_{fs})\,, \qquad (4.13) \end{aligned}$$

because of (4.10). The single-temperature equations for fluid-solid continua in the literature [22, 23] neglect the interfacial heat source. From a theoretical point of view, this term should be taken into account due to the discontiuity of the heat conduction coefficient at the fluid-solid interface, for instance via the method described in [24].

4.5 Temperature Boundary Conditions

In this work we will assume that the inlet temperature T_i of the fluid is known and steady. At the flow outlets Γ_{fo}, a zero-gradient boundary condition for the temperature is imposed. Further, it is assumed that at the wall boundary of the system domain, either its steady temperature T_w or the heat flux q_w is known. The boundary conditions for the temperature distribution are then:

$$T(\boldsymbol{x},t) = T_i(\boldsymbol{x}) \qquad \boldsymbol{x} \in \Gamma_{fi}\,, \tag{4.14}$$

$$\boldsymbol{n}\cdot\nabla^{\nu}T = 0 \qquad \boldsymbol{x} \in \Gamma_{fo}\,, \tag{4.15}$$

$$T(\boldsymbol{x},t) = T_w(\boldsymbol{x}) \quad \text{or} \quad \boldsymbol{n}\cdot k\nabla^{\nu}T = q_w(\boldsymbol{x},t) \qquad \boldsymbol{x} \in \Gamma_{w}\,. \tag{4.16}$$

Here $\boldsymbol{n}$ is the normal vector at Γ which points out of the system domain Ω, so that q_w is the heat flux from the wall to the fluid and solid.

4.6 Macro-Scale Temperature Equations

Superficially Averaged Fluid-Solid Temperature Equation In its generalized form, the temperature equation (4.5) can be spatially filtered over the entire system domain Ω to find the following macro-scale temperature equation in Ω:

$$\begin{aligned}\rho_f\epsilon_{fm}\frac{\partial\left(c_f\langle T\rangle_m^f\right)}{\partial t} + \rho_s\epsilon_{sm}\frac{\partial\left(c_s\langle T\rangle_m^s\right)}{\partial t} + \rho_f\nabla\cdot\left(c_f\epsilon_{fm}\langle\boldsymbol{u}\rangle_m^f\langle T\rangle_m^f\right) = \\ \nabla\cdot k_f\nabla\left(\epsilon_{fm}\langle T\rangle_m^f\right) + \nabla\cdot k_s\nabla\left(\epsilon_{sm}\langle T\rangle_m^s\right) + \nabla\cdot k_f\langle\boldsymbol{n}_{fs}T_f\delta_{fs}\rangle_m - \\ \nabla\cdot k_s\langle\boldsymbol{n}_{fs}T_s\delta_{fs}\rangle_m - \rho_f\nabla\cdot(c_f\boldsymbol{\mathcal{D}}) + \langle\dot{q}\rangle_m + \langle\dot{q}_{\text{visc}}\rangle_m\,.\end{aligned} \tag{4.17}$$

The derivation of the spatially averaged temperature equation is elaborated in Appendix G.

The thermal closure term $\boldsymbol{\mathcal{D}}$ in the macro-scale temperature equation is called the *thermal dispersion source* and is defined as

$$\boldsymbol{\mathcal{D}} \triangleq \langle\boldsymbol{u}T\rangle_m - \epsilon_{fm}\langle\boldsymbol{u}\rangle_m^f\langle T\rangle_m^f\,. \tag{4.18}$$

Separate Superficially Averaged Temperature Equations

The filtered thermal energy equation (4.17) is in matter of fact the sum of two independent equations expressing energy conservation at the macro-scale level for the fluid and solid region respectively. Energy conservation for the fluid at the macro-scale level determines the macro-scale temperature of the fluid:

$$\rho_f \epsilon_{fm} \frac{\partial \left(c_f \langle T \rangle_m^f\right)}{\partial t} + \rho_f \nabla \cdot \left(c_f \epsilon_{fm} \langle \boldsymbol{u} \rangle_m^f \langle T \rangle_m^f\right) = \nabla \cdot k_f \nabla \left(\epsilon_{fm} \langle T \rangle_m^f\right) + \nabla \cdot k_f \langle \boldsymbol{n}_{fs} T_f \delta_{fs} \rangle_m + \langle \boldsymbol{n}_{fs} \cdot (k_f \nabla T_f) \delta_{fs} \rangle_m - \rho_f \nabla \cdot (c_f \mathfrak{D}) + \epsilon_{fm} \langle \dot{q} \rangle_m^f + \epsilon_{fm} \langle \dot{q}_{\text{visc}} \rangle_m^f \,. \tag{4.19}$$

The macro-scale temperature of the solid, $\langle T \rangle_m^s$, follows from the following equation:

$$\rho_s \epsilon_{sm} \frac{\partial \left(c_s \langle T \rangle_m^s\right)}{\partial t} = \nabla \cdot k_s \nabla \left(\epsilon_{sm} \langle T \rangle_m^s\right) - \nabla \cdot k_s \langle \boldsymbol{n}_{fs} T_s \delta_{fs} \rangle_m - \langle \boldsymbol{n}_{fs} \cdot (k_s \nabla T_s) \delta_{fs} \rangle_m + \epsilon_{sm} \langle \dot{q} \rangle_m^s \,. \tag{4.20}$$

The former two equations can be directly proven by multiplying equation (4.5) with γ_f and γ_s respectively and taking the weighted spatial average of the individual terms as performed in Appendix G.

Intrinsically Averaged Temperature Equations

For further analysis, the macro-scale temperature equations are formulated here in terms of the intrinsically averaged temperatures over the fluid and solid. The intrinsic macro-scale thermal energy equation for the fluid is

$$\rho_f \frac{\partial \left(c_f \langle T \rangle_m^f\right)}{\partial t} + \rho_f \nabla \cdot \left(c_f \langle \boldsymbol{u} \rangle_m^f \langle T \rangle_m^f\right) = \nabla \cdot k_f \nabla \langle T \rangle_m^f + \epsilon_{fm}^{-1} \nabla \cdot k_f \langle \boldsymbol{n}_{fs} T_f \delta_{fs} \rangle_m + \epsilon_{fm}^{-1} \langle \boldsymbol{n}_{fs} \cdot (k_f \nabla T_f) \delta_{fs} \rangle_m - \rho_f \nabla \cdot \left(c_f \mathfrak{D}'\right) + \langle \dot{q} \rangle_m^f + \langle \dot{q}_{\text{visc}} \rangle_m^f + \{\psi'_m\}_f \,. \tag{4.21}$$

The intrinsic thermal energy equation for the solid looks like

$$\rho_s \frac{\partial \left(c_s \langle T \rangle_m^s\right)}{\partial t} = \nabla \cdot k_s \nabla \langle T \rangle_m^s - \epsilon_{sm}^{-1} \nabla \cdot k_s \langle \boldsymbol{n}_{fs} T_s \delta_{fs} \rangle_m - \epsilon_{sm}^{-1} \langle \boldsymbol{n}_{fs} \cdot (k_s \nabla T_s) \delta_{fs} \rangle_m + \langle \dot{q} \rangle_m^s + \{\psi_m'\}_s \,. \tag{4.22}$$

The definition of the thermal closure term $\mathcal{D}'$ in (4.21) is

$$\mathcal{D}' \triangleq \epsilon_{fm}^{-1} \mathcal{D} \,. \tag{4.23}$$

The term ψ_m' in the intrinsically averaged temperature equations is defined as

$$\begin{aligned} \psi_m' \triangleq\ & \epsilon_{fm}^{-1} \nabla \epsilon_{fm} \cdot \left(c_f \langle \boldsymbol{u} \rangle_m^f \langle T \rangle_m^f + c_f \mathcal{D}' + \nabla \left(k_f \langle T \rangle_m^f\right)\right) \gamma_f \\ & + \epsilon_{fm}^{-1} \left(\nabla \cdot k_f \nabla \epsilon_{fm}\right) \langle T \rangle_m^f \gamma_f + \epsilon_{sm}^{-1} \left(\nabla \cdot k_f \nabla \epsilon_{sm}\right) \langle T \rangle_m^s \gamma_s \\ & + \epsilon_{fm}^{-1} \nabla \left(k_f \nabla \epsilon_{fm}\right) \cdot \nabla \langle T \rangle_m^f \gamma_f + \epsilon_{sm}^{-1} \nabla \left(k_s \nabla \epsilon_{sm}\right) \cdot \nabla \langle T \rangle_m^s \gamma_s \\ & + \epsilon_{sm}^{-1} \nabla \epsilon_{sm} \cdot \nabla \left(k_s \langle T \rangle_m^s\right) \gamma_s \,, \end{aligned} \tag{4.24}$$

and is only present in the intrinsically averaged temperature equations when there exists a gradient of the weighted porosity.

Macro-Scale Temperature Assumptions

The macro-scale temperature equations (4.17)-(4.22) are valid as long as the specific heat capacities and conductivities of the fluid and solid (c_f, k_f, c_s and k_s) are quasi spatially constant over the local averaging domains $\bar{\Omega}_f$ and $\bar{\Omega}_s$.

The macro-scale temperature equation for the fluid-solid continuum (4.17) incorporates the continuity of the heat flux at the fluid-solid interface (4.10). On the contrary, the separate macro-scale temperature equations for the fluid and solid, (4.19) -(4.22), remain valid even without the interface conditions (4.9) and (4.10).

Macro-Scale Temperature Problem

The macro-scale temperature equations contain three closure terms, which depend on the full temperature distribution, hence both the intrinsically averaged temperature of the fluid and solid and the temperature deviation part. The first closure term is the *weighted interfacial heat transfer*:

$$\langle q_{fs} \delta_{fs} \rangle_m = -\langle \boldsymbol{n}_{fs} \cdot (k_f \nabla T_f) \delta_{fs} \rangle_m = -\langle \boldsymbol{n}_{fs} \cdot (k_s \nabla T_s) \delta_{fs} \rangle_m \,, \tag{4.25}$$

which is the heat transfer by conduction from the fluid to the solid at the solid-fluid interface contained within the averaging domain.

The second closure term is given by

$$\langle \boldsymbol{n}_{fs} T_f \delta_{fs} \rangle_m = \langle \boldsymbol{n}_{fs} T_s \delta_{fs} \rangle_m \tag{4.26}$$

because of (4.9) and is called the *weighted thermal tortuosity*. The thermal tortuosity represents the effect at the macro-scale level of heat transfer by conduction at the fluid-solid interface due the fact that this interface forms a tortuous flow path and heat transfer surface.

The last closure term is the *weighted thermal dispersion source*

$$\mathfrak{D} \triangleq \langle \boldsymbol{u} T \rangle_m - \epsilon_{fm} \langle \boldsymbol{u} \rangle_m^f \langle T \rangle_m^f \,. \tag{4.27}$$

Thermal dispersion is the heat transfer due to hydrodynamic mixing of the fluid at the micro-scale level, thus the convective spreading of heat caused by local variations in fluid velocity on top of the macro-scale flow.

Knowledge of the relation of the interfacial heat transfer, the thermal tortuosity and thermal dispersion source with respect to the filtered temperature and velocity is an absolute requirement for solving the macro-scale temperature equations.

We emphasize that the term '*macro-scale* energy equation' implies that the filtered temperature and filtered velocity can be justifiably called a meaningful macro-scale temperature and macro-scale velocity. Therefore, it is assumed that the following length-scale requirements are satisfied:

$$\ell_T \leq r_m \ll \mathscr{L}_T \qquad \text{and} \qquad \ell_{\boldsymbol{u}} \leq r_m \ll \mathscr{L}_{\boldsymbol{u}} \,. \tag{4.28}$$

By choosing the weighting function m and the size r_m of the averaging window so as to satisfy (4.28), the macro-scale temperature and velocity fields will vary over length scales $\mathscr{L}_T$ and $\mathscr{L}_{\boldsymbol{u}}$ larger than the scales ℓ_T and $\ell_{\boldsymbol{u}}$ over which the original temperature and velocity fields change. As a consequence, the macro-scale temperature equations can be discretized and solved on a coarser mesh than the one needed for a direct numerical simulation of the temperature through (4.7) and (4.8). This consequence can also be understood by noting that the mesh no longer has to capture the small-scale temperature deviation $\widetilde{T}$ over the entire fluid domain.

Approximative Forms of the Macro-Scale Thermal Problem

In contrast to the macro-scale equations for convective heat transfer in porous media, the macro-scale temperature equations presented in this work contain all terms which appear due to the averaging procedure. In the literature, a number of terms in the macro-scale temperature equations have been neglected.

For instance, the thermal dispersion source is as a rule, see e.g. [9, 16], approximated as

$$\mathcal{D} \simeq \mathcal{D}_{\text{approx}} \triangleq \langle \widetilde{\boldsymbol{u}} \widetilde{T} \rangle_m \qquad \text{and} \qquad \mathcal{D}' \simeq \langle \widetilde{\boldsymbol{u}} \widetilde{T} \rangle_m^f \,. \tag{4.29}$$

In Appendix G, after (G.7), it shown that the former approximation is justified when the filter window is small in comparison to the characteristic length scale over which the filtered velocity and temperature change: $r_m \ll \mathscr{L}_{\boldsymbol{u}}$ and $r_m \ll \mathscr{L}_T$.

Also, the geometrical tensors (or spatial moments) in the expression for the thermal tortuosity are virtually always neglected [1, 2, 9, 16]:

$$\begin{aligned} \langle \boldsymbol{n}_{fs} T_f \delta_{fs} \rangle_m &= \sum_{n=0}^{\infty} \boldsymbol{G}_m^{(n)} \underbrace{\cdot\cdot}_{n\text{-times}} \nabla^{\otimes n} \langle T \rangle_m^f + \langle \boldsymbol{n}_{fs} \widetilde{T}_f \delta_{fs} \rangle_m \\ &\simeq \langle \boldsymbol{n}_{fs} \widetilde{T}_f \delta_{fs} \rangle_m \,. \end{aligned} \tag{4.30}$$

Furthermore, the interfacial heat transfer term is sometimes approximated as [16]:

$$\begin{aligned} \langle \boldsymbol{n}_{fs} \cdot k_f \nabla T_f \delta_{fs} \rangle_m &= \langle \boldsymbol{n}_{fs} \cdot k_f \nabla \widetilde{T}_f \delta_{fs} \rangle_m - \nabla \epsilon_{fm} \cdot k_f \nabla \langle T \rangle_m^f + \\ &\quad + k_f \sum_{n=1}^{\infty} \boldsymbol{G}_m^{(n)} \underbrace{\cdot\cdot}_{n\text{-times}} \nabla^{\otimes (n+1)} \langle T \rangle_m^f \\ &\simeq -\nabla \epsilon_{fm} \cdot k_f \nabla \langle T \rangle_m^f + \langle \boldsymbol{n}_{fs} \cdot k_f \nabla \widetilde{T}_f \delta_{fs} \rangle_m \,. \end{aligned} \tag{4.31}$$

Lastly, in most studies, the terms containing gradients of the porosity are neglected [1, 2, 9, 16]: $\psi_m' \simeq 0$ and $\nabla \epsilon_{fm} \simeq 0$.

Instead of the preceding approximative forms from the literature, the exact form of the macro-scale equations will be used in chapters 6 and 7 to obtain exact closure for the heat transfer regimes in spatially periodic structures.

4.7 Macro-Scale Temperature Boundary Conditions

Just like the macro-scale flow boundary conditions are in practise not known, also the intrinsically filtered temperature and its gradient are unknown functions at the macro-scale boundaries of the domain:

$$\langle T\rangle_m^f = f_{Tf}(\boldsymbol{x},t) \qquad \boldsymbol{x}\in\Gamma_{fi}\cup\Gamma_w\,, \tag{4.32}$$

$$\langle T\rangle_m^s = f_{Ts}(\boldsymbol{x},t) \qquad \boldsymbol{x}\in\Gamma_{fi}\cup\Gamma_w\,, \tag{4.33}$$

$$\boldsymbol{n}\cdot k_f\nabla\langle T\rangle_m^f = f_{\nabla Tf}(\boldsymbol{x},t) \qquad \boldsymbol{x}\in\Gamma_{fo}\cup\Gamma_w\,, \tag{4.34}$$

$$\boldsymbol{n}\cdot k_s\nabla\langle T\rangle_m^s = f_{\nabla Ts}(\boldsymbol{x},t) \qquad \boldsymbol{x}\in\Gamma_{fo}\cup\Gamma_w\,. \tag{4.35}$$

Therefore, we propose to use the boundary conditions of the original temperature problem as approximative boundary conditions for the macro-scale temperature problem:

$$\langle T\rangle_m^f \simeq \langle T\rangle_m^s \simeq T_i(\boldsymbol{x}) \qquad \boldsymbol{x}\in\Gamma_{fi}\,, \tag{4.36}$$

$$\langle T\rangle_m^f \simeq \langle T\rangle_m^s \simeq T_w(\boldsymbol{x}) \qquad \boldsymbol{x}\in\Gamma_w\,, \tag{4.37}$$

$$\boldsymbol{n}\cdot\nabla\langle T\rangle_m^f \simeq \boldsymbol{n}\cdot\nabla\langle T\rangle_m^s \simeq 0 \qquad \boldsymbol{x}\in\Gamma_{fo}\,, \tag{4.38}$$

$$\boldsymbol{n}\cdot k_f\nabla\langle T\rangle_m^f \simeq \boldsymbol{n}\cdot k_s\nabla\langle T\rangle_m^s \simeq q_w(\boldsymbol{x},t) \qquad \boldsymbol{x}\in\Gamma_w\,. \tag{4.39}$$

4.8 Global Closure for Macro-Scale Temperature Equations

The macro-scale temperature equations cannot be directly solved for some prescribed boundary conditions if the closure terms (the thermal dispersion term, the thermal tortuosity term and interfacial heat transfer term) are unknown. The relation between these unknown closure terms and the macro-scale temperature of the fluid and solid can be sought by determining the deviation temperature. The global closure problem which governs the deviation temperature is obtained by subtracting the filtered temperature equations (4.21) and (4.22) from the generalized temperature equation (4.5). In this section just the final result is shown, the derivation of the global closure problem can be found in Appendix H.

The global closure problem consists of the following closure equation for the fluid deviation temperature:

$$\rho_f \frac{\partial\left(c_f \tilde{T}_f\right)}{\partial t} + \rho_f \nabla \cdot \left(\boldsymbol{u}_f c_f \tilde{T}_f\right) = \nabla \cdot k_f \nabla \tilde{T}_f - \epsilon_{fm}^{-1} \nabla \cdot k_f \langle \boldsymbol{n}_{fs} T_f \delta_{fs} \rangle_m - \epsilon_{fm}^{-1} \langle \boldsymbol{n}_{fs} \cdot (k_f \nabla T_f) \delta_{fs} \rangle_m + \rho_f \nabla \cdot c_f \boldsymbol{\mathcal{D}}_f' - \rho_f \nabla \cdot \left(\widetilde{\boldsymbol{u}}_f c_f \left\{ \langle T \rangle_m^f \right\}_f\right) \widetilde{\dot{q}}_f + \widetilde{\dot{q}}_{\mathrm{visc},f} - \{\psi_m'\}_f \qquad \text{in } \Omega_f \tag{4.40}$$

and the following closure equation for the solid deviation temperature:

$$\rho_s \frac{\partial\left(c_s \widetilde{T}_s\right)}{\partial t} = \nabla \cdot k_s \nabla \widetilde{T}_s + \epsilon_{sm}^{-1} \nabla \cdot k_s \langle \boldsymbol{n}_{fs} T_s \delta_{fs} \rangle_m^s + \epsilon_{sm}^{-1} \langle \boldsymbol{n}_{fs} \cdot (k_s \nabla T_s) \delta_{fs} \rangle_m^s + \widetilde{\dot{q}}_s - \{\psi_m'\}_s \qquad \text{in } \Omega_s\,. \tag{4.41}$$

The closure equations for the deviation temperature of the fluid (4.40) and the deviation temperature of the solid (4.41) can only be solved together with the filtered temperature equations (4.21) and (4.22). Moreover, the closure equations (4.40) and (4.41) can only be solved once the complete velocity field $\boldsymbol{u}$ is known.

The coupling between the global closure problem and the macro-scale temperature equations and the fact that the deviation temperature contains all small-scale details of the temperature distribution, make the global closure problem only of theoretical interest. In Chapters 6 and 7, practical strategies are proposed to determine the thermal closure terms in the developed heat transfer regimes in spatially periodic solid structures.

Approximative Forms of the Global Closure Problem

In the literature [9, 11, 12], the global closure problem for the volume-averaged temperature equations of the fluid and solid is further simplified through the following approximations.

First, the global closure problem is reduced to its quasi-steady form through the simplifications $\frac{\partial\left(c_f \widetilde{T}_f\right)}{\partial t} \simeq 0$ and $\frac{\partial\left(c_s \widetilde{T}_s\right)}{\partial t} \simeq 0$.

Second, the thermal tortuosity term in the global closure problem is approximated as $\langle \boldsymbol{n}_{fs} T_f \delta_{fs} \rangle_m \simeq \langle \boldsymbol{n}_{fs} \widetilde{T}_f \delta_{fs} \rangle_m$. Similarly, the thermal heat transfer term in the global closure problem is approximated as $\langle \boldsymbol{n}_{fs} \cdot k_f \nabla T_f \delta_{fs} \rangle_m \simeq \langle \boldsymbol{n}_{fs} \cdot k_f \nabla \widetilde{T}_f \delta_{fs} \rangle_m$.

Moreover, the advection terms for the internal energy in the global closure problem are only partly taken into account, as it is assumed that $\mathcal{D}'_f \simeq 0$ and $\nabla \cdot \left(\widetilde{\boldsymbol{u}}_f c_f \left\{ \langle T \rangle^f_m \right\}_f \right) \simeq c_f \widetilde{\boldsymbol{u}}_f \cdot \nabla \langle T \rangle^f_m$.

Lastly, the literature mainly addresses the closure problem for heat transfer in homogeneous porous media, in which gradients of the porosity can be neglected, so that also $\psi'_m \simeq 0$ is assumed in the global closure problem.

The fact that the global closure problem in this work avoids any of the approximations from the literature makes it exact. In chapter 6 and 7, exact solutions of the exact global closure problem will be derived for the periodically developed heat transfer regimes in periodic solid structures.

4.9 Boundary Conditions for Global Closure

Theoretically, the appropriate boundary conditions for the global closure problem need to be derived from (4.14)-(4.16) and (4.32)-(4.35):

$$\widetilde{T}(\boldsymbol{x},t) = -f_{Tf}(\boldsymbol{x},t)\gamma_f(\boldsymbol{x}) - f_{Ts}(\boldsymbol{x},t)\gamma_s(\boldsymbol{x}) - T_i(\boldsymbol{x}) \qquad \boldsymbol{x} \in \Gamma_{fi}\,, \quad (4.42)$$

$$\boldsymbol{n} \cdot k \nabla^\nu \widetilde{T} = -f_{\nabla Tf}(\boldsymbol{x},t)\gamma_f(\boldsymbol{x}) - f_{\nabla Ts}(\boldsymbol{x},t)\gamma_s(\boldsymbol{x}) \qquad \boldsymbol{x} \in \Gamma_{fo}\,, \quad (4.43)$$

$$\widetilde{T}(\boldsymbol{x},t) = -f_{Tf}(\boldsymbol{x},t)\gamma_f(\boldsymbol{x}) - f_{Ts}(\boldsymbol{x},t)\gamma_s(\boldsymbol{x}) - T_w(\boldsymbol{x}) \qquad \boldsymbol{x} \in \Gamma_w\,, \quad (4.44)$$

$$\boldsymbol{n} \cdot k \nabla^\nu \widetilde{T} = -f_{\nabla Tf}(\boldsymbol{x},t)\gamma_f(\boldsymbol{x}) - f_{\nabla Ts}(\boldsymbol{x},t)\gamma_s(\boldsymbol{x}) + q_w \quad \boldsymbol{x} \in \Gamma_w\,. \quad (4.45)$$

With the approximate boundary conditions for the macro-scale temperature (4.36)-(4.39), the boundary conditions for the global closure problem thus become

$$\widetilde{T}(\boldsymbol{x},t) \simeq 0 \qquad\qquad\qquad\qquad \boldsymbol{x} \in \Gamma_{fi} \cup \Gamma_w\,, \quad (4.46)$$

$$\boldsymbol{n} \cdot \nabla^\nu \widetilde{T} \simeq 0 \qquad\qquad\qquad\qquad \boldsymbol{x} \in \Gamma_{fo}\,, \quad (4.47)$$

$$\boldsymbol{n} \cdot \nabla^\nu \widetilde{T} \simeq 0 \qquad \text{or} \qquad \widetilde{T}(\boldsymbol{x},t) \simeq 0 \qquad \boldsymbol{x} \in \Gamma_w\,. \quad (4.48)$$

4.10 Planar Temperature Equation

If the flow is planar, also the three-dimensional temperature equations for the fluid and solid structures can be reduced to a two-dimensional form. Hereto we introduce the planar temperature $\mathcal{T}$:

$$\mathcal{T} \triangleq \langle T \rangle_3|_{(\boldsymbol{x}_{1,2}, x_3=0, t)} \triangleq \int_{y_3 \in I_3} m_3'(-y_3)\, T(\boldsymbol{x}_{1,2}, y_3, t)\, dy_3\,, \tag{4.49}$$

The notational conventions in the definition above are the same as those used for the description of planar flow (cf. §3.10). The planar temperature is a measure for the average temperature of the fluid and solid structures in the direction perpendicular to the planar flow direction.

We assume that the shape of the boundary of the flow domain and the solid structures only depends on the position vector $\boldsymbol{x}_{1,2}$ within the plane of the planar flow. In that case, equations (3.45), (3.46) and (3.47) hold, so that the planar temperature can be represented as a two-dimensional distribution over the middle plane of the flow domain:

$$\mathcal{T} = \begin{cases} \mathcal{T}_f(\boldsymbol{x}_{1,2}, t) & \text{in } \Omega_{f,x_3=0} \\ \mathcal{T}_s(\boldsymbol{x}_{1,2}, t) & \text{in } \Omega_{s,x_3=0} \end{cases}\,. \tag{4.50}$$

Moreover, the planar temperature then satisfies the following boundary conditions on the solid-fluid interface line:

$$\langle q_{fs} \rangle_3 = -\boldsymbol{n}_{fs} \cdot k_f\, \nabla \mathcal{T}_f = -\boldsymbol{n}_{fs} \cdot k_s\, \nabla \mathcal{T}_s \qquad \boldsymbol{x}_{1,2} \in \Gamma_{fs,x_3=0}\,, \tag{4.51}$$

$$\mathcal{T}_f = \mathcal{T}_s \qquad \boldsymbol{x}_{1,2} \in \Gamma_{fs,x_3=0}\,, \tag{4.52}$$

because we can take $\boldsymbol{n}_{fs,x_3=0} = \boldsymbol{n}_{fs}(\boldsymbol{x}_{1,2})$ by (3.48).

Planar Temperature Equation

The planar temperature equation which governs the planar temperature in $\Omega_{x_3=0} = \Omega_{f,x_3=0} \cup \Omega_{s,x_3=0}$ is given by

$$\rho \frac{\partial^\nu (c\mathcal{T})}{\partial t} + \rho \nabla^\nu \cdot (\boldsymbol{v} c \mathcal{T}) = \nabla^\nu \cdot (k\, \nabla^\nu \mathcal{T}) + \langle \dot{q} \rangle_3 + \langle \dot{q}_{\text{visc}} \rangle_3 + \psi_3\,. \tag{4.53}$$

The derivation of the planar temperature equation is included in Appendix F.

We remark that the gradient and the time derivative in (4.53) are defined with respect to the two-dimensional regions $\Omega_{f,x_3=0}$ and $\Omega_{s,x_3=0}$ instead of the original three-dimensional regions Ω_f and Ω_s.

The planar temperature equation (4.53) is only valid when the fluid and solid properties do not vary in the direction perpendicular to the planar flow, so that they have equivalent two-dimensional representations, e.g.:

$$c = \begin{cases} c_f(\boldsymbol{x}_{1,2}) & \text{in } \Omega_{f,x_3=0} \\ c_s(\boldsymbol{x}_{1,2}) & \text{in } \Omega_{s,x_3=0} \end{cases}, \quad k = \begin{cases} k_f(\boldsymbol{x}_{1,2}) & \text{in } \Omega_{f,x_3=0} \\ k_s(\boldsymbol{x}_{1,2}) & \text{in } \Omega_{s,x_3=0} \end{cases}. \tag{4.54}$$

The closure term ψ_3 in the planar temperature equation is the sum of three different contributions:

$$\psi_3 \triangleq \psi_3^{\mathrm{I}} + \psi_3^{\mathrm{II}} + \psi_3^{\mathrm{III}}. \tag{4.55}$$

The first contribution, ψ_3^{I} corrects for the advective thermal energy transport which is present in the original flow, although not captured by advection with the planar flow field solely:

$$\psi_3^{\mathrm{I}} \triangleq \rho\nabla^\nu \cdot (\boldsymbol{v}c\mathcal{T}) - \rho\nabla^\nu \cdot \langle \boldsymbol{u}_{1,2}cT\rangle_3 . \tag{4.56}$$

In (4.56), $\boldsymbol{u}_{1,2}$ is the part of the velocity vector $\boldsymbol{u}$ parallel to the planar velocity $\boldsymbol{v}$.

The second contribution to the closure term ψ_3 represents the overall advection of thermal energy perpendicular to the planar velocity:

$$\psi_3^{\mathrm{II}} \triangleq -\rho\langle\nabla_3^\nu \cdot (\boldsymbol{u}_3 cT)\rangle_3 . \tag{4.57}$$

Here ∇_3^ν and $\boldsymbol{u}_3$ denote the gradient operator and velocity part perpendicular to $\boldsymbol{v}$.

The third contribution, ψ_3^{III} is related to the overall heat conducted in the direction perpendicular to the planar flow:

$$\psi_3^{\mathrm{III}} \triangleq \langle\nabla_3^\nu \cdot (k\nabla_3^\nu T)\rangle_3 . \tag{4.58}$$

Actually, the third planar thermal closure term ψ_3^{III} contains the heat flux at the planar surfaces which confine the planar flow domain.

4.11 Planar Temperature Boundary Conditions

For planar flow through a channel consisting of two parallel plates (or planes) with solid structures in between, we can assume that either the temperature or heat flux at the bottom and top plate (or plane) are known:

$$T(\boldsymbol{x},t) = T_{wt}(x_3) \quad \text{or} \quad k\frac{\partial T}{\partial x_3} = q_{wt}(\boldsymbol{x},t) \quad \text{at} \quad x_3 = \frac{l_3}{2}\,, \tag{4.59}$$

$$T(\boldsymbol{x},t) = T_{wb}(x_3) \quad \text{or} \quad -k\frac{\partial T}{\partial x_3} = q_{wb}(\boldsymbol{x},t) \quad \text{at} \quad x_3 = -\frac{l_3}{2}\,. \tag{4.60}$$

We note that we could have replaced the position vector $\boldsymbol{x}$ in (4.59) and (4.60) by $\boldsymbol{x}_{1,2}$, as this is just a matter of equivalent notation.

The following boundary conditions for the planar temperature are consistent with (4.14), (4.15), (4.16) respectively:

$$\mathcal{T}(\boldsymbol{x},t) = \langle T_i\rangle_3 \qquad \boldsymbol{x} \in \Gamma_{fi,x_3=0}\,, \tag{4.61}$$

$$\boldsymbol{n}\cdot\nabla\mathcal{T} = 0 \qquad \boldsymbol{x} \in \Gamma_{fo,x_3=0}\,, \tag{4.62}$$

$$\mathcal{T}(\boldsymbol{x},t) = \langle T_w\rangle_3 \quad \text{or} \quad \boldsymbol{n}\cdot\nabla\mathcal{T} = \langle q_w\rangle_3 \qquad \boldsymbol{x} \in \Gamma_{w,x_3=0}\,. \tag{4.63}$$

4.12 Closure of Planar Temperature Equation

The closure term ψ_3 in the planar temperature equations can be modelled in approximative way, if we assume that the upper and bottom plate (plane) of the channel have the same known (wall) temperature $T_w(\boldsymbol{x}_{1,2}) = T_{wt} = T_{wb}$. We can then postulate the existence of the following similarity profile for the temperature [23]:

$$\zeta_T(x_3) \simeq \frac{T(\boldsymbol{x}_{1,2},x_3) - T_w(\boldsymbol{x}_{1,2})}{\mathcal{T}(\boldsymbol{x}_{1,2}) - T_w(\boldsymbol{x}_{1,2})} = \begin{cases} \zeta_{T,f} \simeq \frac{T_f - T_w}{\mathcal{T}_f - T_w} & \boldsymbol{x} \in \Omega_f \\ \zeta_{T,s} \simeq \frac{T_s - T_w}{\mathcal{T}_s - T_w} & \boldsymbol{x} \in \Omega_s \end{cases}, \tag{4.64}$$

where we have used the spatial decomposition $\boldsymbol{x} = \boldsymbol{x}_{1,2} + x_3\boldsymbol{e}^{(3)}$, as in (3.44).

When we substitute the former temperature similarity profile (4.64) together with the velocity shape function of (3.62) into the expression for ψ_3^{I}, we find the following approximation for this closure term:

$$\psi_3^{\mathrm{I}} \simeq \rho_f \left(1 - \langle \zeta_{\boldsymbol{u}} \zeta_{T,f} \rangle_3\right) \nabla \cdot \left(c\boldsymbol{v}\mathcal{T} - c\boldsymbol{v}T_w\right) . \tag{4.65}$$

The approximation of (3.62) implies that the velocity has no component $\boldsymbol{u}_3$, so that

$$\psi_3^{\mathrm{II}} \simeq 0 . \tag{4.66}$$

With the temperature similarity profile (4.64), the third closure term becomes

$$\psi_3^{\mathrm{III}} \simeq h_w \left(T_w - \mathcal{T}\right) . \tag{4.67}$$

For this last representation of ψ_3^{III}, we define the heat transfer coefficient h_w between wall and fluid or solid as

$$h_w \triangleq -k \left\langle \frac{d^2\zeta_T}{dx_3^2} \right\rangle_3 \triangleq \begin{cases} -k_f \left\langle \frac{d^2\zeta_{T,f}}{dx_3^2} \right\rangle_3 \triangleq h_{w,f} & \text{in } \Omega_{f,x_3=0} \\ -k_s \left\langle \frac{d^2\zeta_{T,s}}{dx_3^2} \right\rangle_3 \triangleq h_{w,s} & \text{in } \Omega_{s,x_3=0} \end{cases} . \tag{4.68}$$

With (4.64, the heat flux at the top and bottom plate of the channel (cf. (4.59) and (4.60)) are approximated as

$$q_{wt} \simeq h_{wt} \left(T_w - \mathcal{T}\right) \qquad \text{and} \qquad q_{wb} \simeq h_{wb} \left(T_w - \mathcal{T}\right) , \tag{4.69}$$

where

$$h_{wt} = -k \frac{1}{l_3} \left.\frac{d\zeta_T}{dx_3}\right|_{x_3=\frac{l_3}{2}} \qquad \text{and} \qquad h_{wb} = k \frac{1}{l_3} \left.\frac{d\zeta_T}{dx_3}\right|_{x_3=\frac{-l_3}{2}} . \tag{4.70}$$

When the weighting function is $m_3'(-y_3) = \frac{1}{l_3}$, it holds that

$$\begin{array}{ll} \psi_3^{\mathrm{III}} & = \frac{1}{l_3} \left(q_{wt} + q_{wb}\right) \\ h_w & = h_{wt} + h_{wb} \end{array} \qquad \Leftrightarrow \qquad m_3'(-y_3) = \frac{1}{l_3} . \tag{4.71}$$

This equality can be readily verified from (4.68) through partial integration (see Appendix F).

We add that the wall temperature of both plates can be modelled approximatively through the following two-dimensional heat conduction equation in the plate domain $\Omega_w \triangleq \left\{\boldsymbol{x} \in \Omega | x_3 = \pm\frac{l_3}{2}\right\}$:

$$\rho_w \frac{\partial \left(c_w T_w\right)}{\partial t} = \nabla \cdot \left(k_w \nabla T_w\right) + h_w \left(T_w - \mathcal{T}\right) + \dot{q}_w \qquad \text{in } \Omega_w \,, \tag{4.72}$$

where $\dot{q}_w$ represents the external heat source in or at the surface of the plate wall. The approximate equation (4.72) for the wall temperature is based on the assumption that the physical wall has a sufficiently small thickness, so that any variations of the physical wall temperature perpendicular to the wall can be neglected.

4.13 Macro-Scale Planar Temperature Equations

If the shape of the solid structures does not change in the direction normal to the bottom and top wall of the channel, the planar temperature has the form (4.50) and satisfies the continuity conditions (4.51) at the fluid-solid interface. In that case, the planar temperature equation (4.53) can be spatially averaged to obtain the macro-scale planar temperature equations.

Superficially Averaged Planar Temperature Equations
The equation for the macro-scale planar temperature of the fluid has the form

$$\begin{aligned}\rho_f \epsilon_{fm} \frac{\partial \left(c_f \langle \mathcal{T} \rangle_m^f\right)}{\partial t} + \rho_f \nabla \cdot \left(c_f \epsilon_{fm} \langle \boldsymbol{u} \rangle_m^f \langle \mathcal{T} \rangle_m^f\right) = \nabla \cdot k_f \nabla \left(\epsilon_{fm} \langle \mathcal{T} \rangle_m^f\right) + \\ \nabla \cdot k_f \langle \boldsymbol{n}_{fs} \mathcal{T}_f \delta_{fs} \rangle_m + \langle \boldsymbol{n}_{fs} \cdot (k_f \nabla \mathcal{T}_f) \delta_{fs} \rangle_m - \rho_f \nabla \cdot (c_f \boldsymbol{\mathcal{D}}) + \\ \epsilon_{fm} \langle \langle \dot{q} \rangle_3 \rangle_m^f + \epsilon_{fm} \langle \langle \dot{q}_{\text{visc}} \rangle_3 \rangle_m^f + \epsilon_{fm} \langle \psi_3 \rangle_m^f \,.\end{aligned} \tag{4.73}$$

Here, the *planar weighted thermal dispersion source* is defined as

$$\boldsymbol{\mathcal{D}} \triangleq \langle \boldsymbol{v} T \rangle_m - \epsilon_{fm} \langle \boldsymbol{v} \rangle_m^f \langle T \rangle_m^f \,. \tag{4.74}$$

The equation for the macro-scale planar temperature of the solid has the form

$$\rho_s \epsilon_{sm} \frac{\partial \left(c_s \langle \mathcal{T} \rangle_m^s\right)}{\partial t} = \nabla \cdot k_s \nabla \left(\epsilon_{sm} \langle \mathcal{T} \rangle_m^s\right) - \nabla \cdot k_s \langle \boldsymbol{n}_{fs} \mathcal{T}_s \delta_{fs} \rangle_m - \langle \boldsymbol{n}_{fs} \cdot \left(k_s \nabla \mathcal{T}_s\right) \delta_{fs} \rangle_m + \epsilon_{sm} \langle \langle \dot{q} \rangle_3 \rangle_m^s + \epsilon_{sm} \langle \psi_3 \rangle_m^s \ . \tag{4.75}$$

The gradient ∇ in (4.73) and (4.75) is defined with respect to the domain $\Omega_{x_3=0} \subset \mathbb{R}^2$ and corresponds to the operator $\nabla_{1,2}$ in $\Omega \subset \mathbb{R}^3$, also $\boldsymbol{n}_{fs}$ and δ_{fs} are defined here with respect to the solid-fluid interface $\Gamma_{x_3=0}$ within $\Omega_{x_3=0}$, so they correspond to $\boldsymbol{n}_{fs,x_3=0}$ and $\delta_{fs,x_3=0}$ in Ω.

When the filter in (4.73) and (4.75) is partly separable with respect to $\boldsymbol{e}^{(3)}$ and its convolution product is evaluated at $\boldsymbol{x} \cdot \boldsymbol{e}^{(3)} = 0$, the macro-scale temperature and the macro-scale planar temperature are equal:

$$\langle T \rangle_m^f = \langle \mathcal{T} \rangle_m^f \qquad \text{and} \qquad \langle T \rangle_m^s = \langle \mathcal{T} \rangle_m^s \, . \tag{4.76}$$

Closure Terms in Macro-Scale Planar Temperature Equations – As we have assumed that $\boldsymbol{n}_{fs} \cdot \boldsymbol{e}^{(3)} = 0$ when planar flow occurs (cf. (3.48)), the interfacial heat transfer term in the macro-scale planar temperature equations is given by

$$\langle \boldsymbol{n}_{fs} \cdot k_f \nabla \mathcal{T}_f \delta_{fs} \rangle_m = \langle \boldsymbol{n}_{fs} \cdot k_f \nabla T_f \delta_{fs} \rangle_m \, , \tag{4.77}$$

provided that the filter is separable with respect to $\boldsymbol{e}^{(3)}$ and evaluated at $\boldsymbol{x} \cdot \boldsymbol{e}^{(3)} = 0$.

Similarly, the thermal tortuosity in the macro-scale planar temperature equations equals

$$\langle \boldsymbol{n}_{fs} \mathcal{T}_f \delta_{fs} \rangle_m = \langle \boldsymbol{n}_{fs} T_f \delta_{fs} \rangle_m \, . \tag{4.78}$$

The divergence of the planar weighted thermal dispersion source $\boldsymbol{\mathcal{D}}$ is related to the divergence of the thermal dispersion source $\boldsymbol{\mathcal{D}}$ via the relationship

$$\rho_f \nabla \cdot \left(c_f \boldsymbol{\mathcal{D}}\right) = \rho_f \nabla \cdot \left(c_f \boldsymbol{\mathcal{D}}\right) + \langle \psi_3^{\mathrm{I}} \rangle_m + \langle \psi_3^{\mathrm{II}} \rangle_m + \rho_f \nabla \cdot \left(c_f \epsilon_{fm} \langle \boldsymbol{u}_3 \rangle_m^f \langle T \rangle_m^f\right) \, . \tag{4.79}$$

When the planar closure term ψ_3^{I} is modelled as in (4.65), we have

$$\begin{aligned}\epsilon_{fm}\langle\psi_3^{\mathrm{I}}\rangle_m^f \simeq (1-\langle\zeta_{\boldsymbol{u}}\zeta_{T,f}\rangle_3)\,\nabla\cdot\left(c_f\epsilon_{fm}\langle\boldsymbol{v}\rangle_m^f\langle\mathcal{T}\rangle_m^f + c_f\boldsymbol{\mathcal{D}}\right)\\ -(1-\langle\zeta_{\boldsymbol{u}}\zeta_{T,f}\rangle_3)\,\nabla\cdot\left(c_f\langle\boldsymbol{v}T_w\rangle_m\right)\,.\end{aligned} \tag{4.80}$$

The term $\langle\boldsymbol{v}T_w\rangle_m$ must be further approximated to obtain closure, for instance by assuming that $\langle\boldsymbol{v}T_w\rangle_m \simeq \langle\boldsymbol{v}\rangle_m\langle T_w\rangle_m^f$, so that

$$\epsilon_{fm}\langle\psi_3^{\mathrm{I}}\rangle_m^f \simeq (1-\langle\zeta_{\boldsymbol{u}}\zeta_{T,f}\rangle_3)\,\nabla\cdot\left(c_f\epsilon_{fm}\langle\boldsymbol{v}\rangle_m^f\left(\langle\mathcal{T}\rangle_m^f-\langle T_w\rangle_m^f\right)+c_f\boldsymbol{\mathcal{D}}\right)\,. \tag{4.81}$$

Furthermore, with the approximative models of (4.66) and (4.67), we have

$$\langle\psi_3^{\mathrm{II}}\rangle_m^f \simeq 0 \tag{4.82}$$

and

$$\langle\psi_3^{\mathrm{III}}\rangle_m^f \simeq h_{w,f}\left(\langle T_w\rangle_m^f-\langle\mathcal{T}\rangle_m^f\right)\,, \tag{4.83}$$

$$\langle\psi_3^{\mathrm{III}}\rangle_m^s \simeq h_{w,s}\left(\langle T_w\rangle_m^s-\langle\mathcal{T}\rangle_m^s\right) \tag{4.84}$$

respectively.

We remark that if the macro-scale plate wall temperature satisfies local thermal equilibrium: $\langle T_w\rangle_m^f \simeq \langle T_w\rangle_m^s = T_W$, spatial averaging of (4.72) yields the following single equation for the macro-scale wall temperature:

$$\rho_w\frac{\partial\left(c_wT_W\right)}{\partial t} = \nabla\cdot k_s\nabla T_W + h_{w,f}\left(\langle\mathcal{T}\rangle_m^f-T_W\right)+h_{w,s}\left(\langle\mathcal{T}\rangle_m^s-T_W\right)\,. \tag{4.85}$$

Macro-Scale Planar Temperature Boundary conditions

By analogy with the original macro-scale temperature boundary conditions, the boundary conditions for the macro-scale planar can be approximated as

$$\langle\mathcal{T}\rangle_m^f \simeq \langle\mathcal{T}\rangle_m^s \simeq \langle T_i\rangle_3 \qquad \boldsymbol{x}\in\Gamma_{fi}\,, \tag{4.86}$$

$$\langle\mathcal{T}\rangle_m^f \simeq \langle\mathcal{T}\rangle_m^s \simeq T_w(\boldsymbol{x}) \qquad \boldsymbol{x}\in\Gamma_w \tag{4.87}$$

$$\boldsymbol{n}\cdot\nabla\langle\mathcal{T}\rangle_m^f \simeq \boldsymbol{n}\cdot\nabla\langle\mathcal{T}\rangle_m^s \simeq 0 \qquad \boldsymbol{x}\in\Gamma_{fo}\,, \tag{4.88}$$

$$\boldsymbol{n}\cdot\nabla\langle\mathcal{T}\rangle_m^f \simeq \boldsymbol{n}\cdot\nabla\langle\mathcal{T}\rangle_m^s \simeq \langle q_w\rangle_3 \qquad \boldsymbol{x}\in\Gamma_w\,. \tag{4.89}$$

Global Closure for Macro-Scale Planar Temperature Equations
The global closure problem for the macro-scale planar temperature equations would look similar to (4.40) and (4.41), except that the variable T would have to be replaced by $\mathcal{T}$ and the additional term $\psi_3 - \langle\psi_3\rangle_m$ would have to be taken into account.

Bibliography

[1] R. G. Carbonell and S. Whitaker, *Fundamentals of Transport Phenomena in Porous Media, eds J. Bear and M. Y. Corapcioglu. Martinus Nijhof*, ch. Heat and mass transfer in porous media, pp. 121–198. Dordrecht: Springer Netherlands, 1984.

[2] I. Nozad, R. Carbonell, and S. Whitaker, "Heat conduction in multiphase systems I: Theory and experiment for two-phase systems," *Chemical Engineering Science*, vol. 40, no. 5, pp. 843 – 855, 1985.

[3] J. Levec and R. G. Carbonell, "Longitudinal and lateral thermal dispersion in packed beds. Part I: Theory," *AIChE Journal*, vol. 31, no. 4, pp. 581–590, 1985.

[4] M. Quintard and S. Whitaker, "One– and two–equation models for transient diffusion processes in two-phase systems," vol. 23 of *Advances in Heat Transfer*, pp. 369–464, Elsevier, 1993.

[5] C. Moyne, "Advances in heat transfer in porous media two-equation model for a diffusive process in porous media using the volume averaging method with an unsteady-state closure," *Advances in Water Resources*, vol. 20, no. 2, pp. 63 – 76, 1997.

[6] M. Quintard and S. Whitaker, "Local thermal equilibrium for transient heat conduction: theory and comparison with numerical experiments," *International Journal of Heat and Mass Transfer*, vol. 38, no. 15, pp. 2779 – 2796, 1995.

[7] C. Gobbé and M. Quintard, "Macroscopic description of unsteady heat transfer in heterogeneous media," *High Temperatures–High Pressures*, vol. 26, pp. 1–14, 1994.

[8] C. Gobbé, L. Ramond, and M. Quintard, "Macroscopic description of unsteady heat transfer in heterogeneous media with consideration

of interfacial thermal barriers," *High Temperatures–High Pressures*, vol. 30, no. 3, pp. 365–372, 1998.

[9] S. Whitaker, "Improved constraints for the principle of local thermal equilibrium," *Industrial & Engineering Chemistry Research*, vol. 30, no. 5, pp. 983–997, 1991.

[10] C. M. Marle, "Ecoulements monophasiques en milieu poreux," *Revue de l'Institut Français du Pétrole*, vol. 22, no. 10, pp. 1471–1509, 1967.

[11] M. Quintard, M. Kaviany, and S. Whitaker, "Advances in heat transfer in porous media two-medium treatment of heat transfer in porous media: numerical results for effective properties," *Advances in Water Resources*, vol. 20, no. 2, pp. 77 – 94, 1997.

[12] M. Quintard, B. Ladevie, and S. Whitaker, "Effect of homogeneous and heterogeneous source terms on the macroscopic description of heat transfer in porous media," *Energy Engineering*, vol. 2, pp. 482–489, 2000.

[13] V. Leroy, B. Goyeau, and J. Taine, "Coupled upscaling approaches for conduction, convection, and radiation in porous media: Theoretical developments," *Transport in Porous Media*, vol. 98, no. 2, pp. 323–347, 2013.

[14] S. Whitaker, "Diffusion and dispersion in porous media," *AIChE Journal*, vol. 13, no. 3, pp. 420–427, 1967.

[15] D. Ryan, R. G. Carbonell, and S. Whitaker, "A theory of diffusion and reaction in porous media,," *AIChE Symposium Series*, vol. 77, no. 202, 1981.

[16] F. Zanotti and R. Carbonell, "Development of transport equations for multiphase system–I: General Development for two phase system," *Chemical Engineering Science*, vol. 39, no. 2, pp. 263 – 278, 1984.

[17] J. Ochoa, P. Stroeve, and S. Whitaker, "Diffusion and reaction in cellular media," *Chemical Engineering Science*, vol. 41, no. 12, pp. 2999 – 3013, 1986.

[18] O. A. Plumb and S. Whitaker, "Dispersion in heterogeneous porous media: 1. local volume averaging and large-scale averaging," *Water Resources Research*, vol. 24, no. 7, pp. 913–926, 1988.

[19] M. Quintard, F. Cherblanc, and S. Whitaker, "Dispersion in heterogeneous porous media: One-equation non-equilibrium model," *Transport in Porous Media*, vol. 44, no. 1, pp. 181–203, 2001.

[20] Y. Davit, G. Debenest, B. D. Wood, and M. Quintard, "Modeling non-equilibrium mass transport in biologically reactive porous media," *Advances in Water Resources*, vol. 33, no. 9, pp. 1075 – 1093, 2010.

[21] F. Duval, F. Fichot, and M. Quintard, "A local thermal non-equilibrium model for two-phase flows with phase-change in porous media," *International Journal of Heat and Mass Transfer*, vol. 47, no. 3, pp. 613 – 639, 2004.

[22] D. Lopez Penha, S. Stolz, J. Kuerten, M. Nordlund, A. Kuczaj, and B. Geurts, "Fully-developed conjugate heat transfer in porous media with uniform heating," *Int. J. Heat Fluid Flow*, vol. 38, pp. 94–106, 2012.

[23] T. Van Oevelen, *Optimal Heat Sink Design for Liquid Cooling of Electronics*. PhD thesis, Arenberg Doctoral School, Faculty of Engineering, KULeuven, 2014.

[24] C. Schroeder, A. Stomakhin, R. Howes, and J. Teran, "A second order virtual node algorithm for Navier–Stokes flow problems with interfacial forces and discontinuous material properties," *J. Comp. Phys.*, vol. 265, pp. 221 – 245, 2014.

CHAPTER

5

MACRO-SCALE DESCRIPTION OF PERIODICALLY DEVELOPED FLOW

5.1 Introduction

This chapter gives an exact and physically meaningful macro-scale description of the laminar periodically developed flow regime, which occurs in spatially periodic solid structures at low flow speeds. Parts of this chapter are published in [1, 2]. In this chapter, the macro-scale properties of steady and unsteady periodically developed flow are investigated to assess different strategies for determining the closure terms in the macro-scale flow equations. It is shown that the spatial averaging technique requires a double volume-averaging operator [3] to ensure that the closure terms are spatially constant for periodically developed flow. Moreover, via the double volume average, the closure terms can be obtained by solving a local closure problem on a unit cell of the periodic structures. The theoretical framework of this chapter is applied to model the macro-scale flow through an array of cylindrical tubes.

5.2 Outline

This chapter first gives a qualitative description of (periodically) developed flow in heat transfer devices with spatially periodic structures. Afterwards, in Section 4, the literature on (periodically) developed flow and macro-scale flow models for heat transfer devices with periodic solid structures is briefly reviewed. In the next section, Section 5, it is explained what we consider to be a unit cell of spatially periodic structures. In Section 6, some filters that are suitable for filtering spatially periodic quantities are presented. Subsequently, Section 7 gives a mathematical definition of periodically developed flow. Section 8 investigates the macro-scale properties of this regime. The periodic flow equations are further elaborated in Section 9 to obtain closure for periodically developed flow. In Section 10, the choice of the weighting function for spatial averaging is discussed. It is shown that a double volume average strongly simplifies the closure terms in the case of periodically developed flow. Alternative closure strategies for periodically developed flow and their connection with the choice of weighting function are explored in Section 11. The representation of the closure terms in the periodically developed flow regime is the subject of Section 12. Section 13 extends the preceding results to planar periodically developed flow. Finally, in the last section, the spatial averaging technique is applied to numerically model the flow around an array of cylindrical tubes.

5.3 Developed Flow in Heat Transfer Devices

The flow through compact heat transfer devices with spatially periodic solid structures is often laminar, as these devices usually operate at rather low flow speeds and their flow channels have quite small dimensions (cf. §1.7). Laminar flow in compact heat transfer devices typically becomes *periodically developed* after a certain number of solid structures from the flow inlet. This means that the flow patterns or streamlines around the solid structures become periodically similar in the downstream direction. The periodic flow patterns only break up near walls outside the array of solid structures and near the flow outlet, so that the periodically developed flow regime often extends over the largest part of the channel.

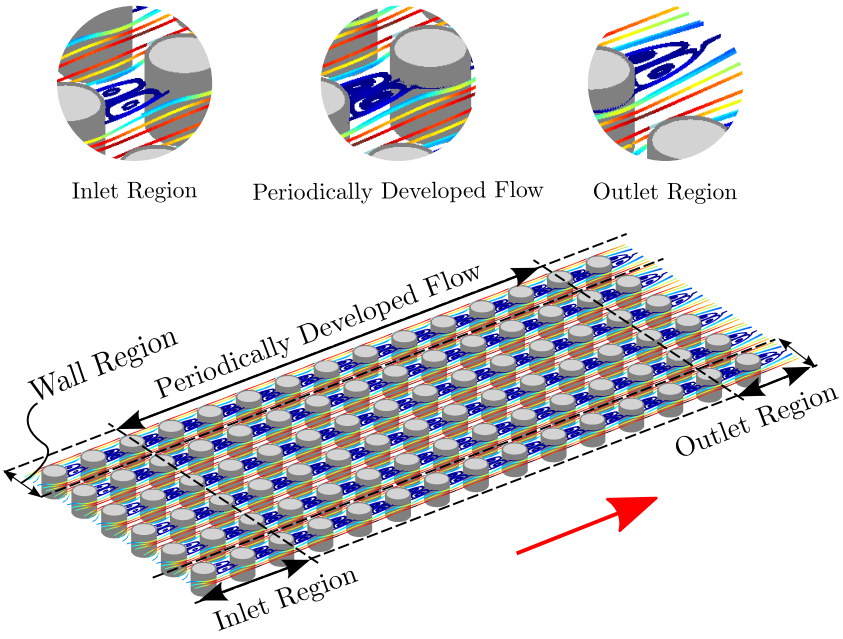

Figure 5.1: Streamlines in the inlet region, outlet region, wall region and periodically developed flow region within the channel of Figure 1.5 from §1.3. The red arrow indicates the main flow direction.

Figure 5.1 shows again the streamlines around the solid structures in the channel of Figure 1.5 from §1.3. The flow field within the channel can be divided into four regions. First, we have the inlet region, where the fluid enters the channel and the flow is not yet periodically developed. Second, we can identify the core of the channel, where the streamline patterns repeat themselves in a periodic fashion from one pin fin to another, so that we call this the periodically developed flow region. Further, the outlet region can be recognized, where the fluid flow leaves the channel and the flow is no longer periodically developed. Lastly, the fourth region is called the wall region, as it extends over the outer rows of the pin fin array which are adjacent to the channel walls. In the wall region, the streamline patterns differ from those in the periodically developed flow region, because the flow in the wall region is only partly surrounded by pin fins.

At relatively low flow speeds, periodically developed flow is characterized by steady flow patterns. At higher flow speeds, time-periodic flow oscillations set in, once a certain Reynolds number is reached [4, 5]. It has been observed that in the unsteady periodically developed regime, time-periodic vortices occur first within the array of solid structures and then move upstream into the inlet region [6]. When the flow speed and Reynolds number are further increased, the unsteady periodically developed regime is eventually replaced by chaotic flow phenomena as transition towards turbulent flow sets in.

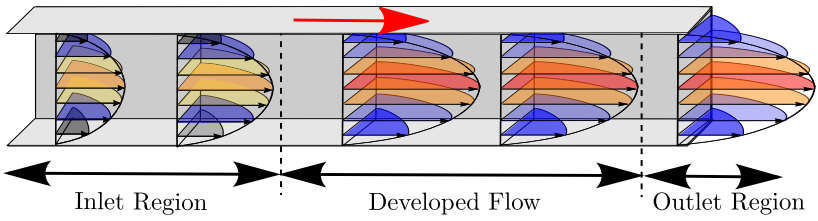

Figure 5.2: Steady velocity profiles in the inlet region, outlet region and fully developed flow region within a rectangular channel. The flow speed is the highest in the center of the channel and the lowest near the solid wall. The red arrow indicates the main flow direction.

The periodically developed flow regime is a generalization of the *fully developed flow regime*, which occurs when the spatially periodic structures form duct walls of which the cross-sectional shape does not change in the main flow direction. Figure 5.2 illustrates the steady fully developed flow regime in a solid duct with a rectangular cross section [7]. The fully developed flow regime is characterized by a flow velocity profile over the cross section of the duct which does not change in the downstream direction. Another feature of the fully developed flow regime, is that the pressure gradient remains constant. Although the laminar fully developed flow regime is usually steady in compact heat transfer devices, also unsteady, oscillatory flow phenomena can occur [8, 9].

5.4 Historical Background

Given its importance for compact heat transfer devices, the literature on developed flow is reviewed first in this section, at least for the most commonly applied periodic solid structures. Afterwards, the literature on macro-scale flow models for periodic solid structures is reviewed. We establish that the macro-scale flow models from the literature are all heuristic and often empirical and that an exact macro-scale description of the periodically developed flow regime has not been presented.

Developed Flow in Periodic Solid Structures
The governing equations for the periodically developed flow regime were described for the first time by Patankar, Liu and Sparrow [10] in 1977. Patankar et al. considered two-dimensional steady developed flow through ducts with a periodically varying cross section in the main flow direction. In that case, the velocity components u and v are streamwise-periodic over the period length L of the cross-sectional variations:

$$u(x,y) = (x+L,y) \qquad \text{and} \qquad v(x,y) = (x+L,y) \ .$$

Patankar and his co-workers showed that the pressure in the steady periodically developed regime consists of a linear term and a periodic contribution:

$$p(x,y) = -\beta x + P(x,y) \qquad \text{with} \qquad P(x,y) = (x+L,y) \ .$$

Here, the constant pressure gradient β is related to the total mass flow rate through the duct, while $P(x,y)$ is related to the detailed local flow motions. Since their formulation, the flow equations of Patankar et al. have been used extensively to numerically calculate the developed flow field in spatially periodic duct units for an imposed pressure gradient.

In its original form, the formulation of Patankar et al. [10] is only applicable to ducts in which the main flow direction and the constant pressure gradient are aligned. This is for instance the case when the spatially periodic solid structures form wavy or corrugated fins, like in Figure 5.3. For corrugated fins, the steady periodically developed flow equations of [10] were solved numerically by Yutaka et al. in 1988 [11]. For wavy fins, steady periodically developed flow solutions were reported by Zhang, Manglik, Metwally and their co-workers between 2004 and 2007 [12–16].

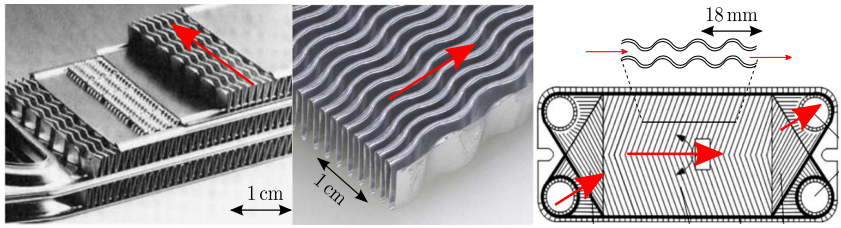

Figure 5.3: Compact plate-fin heat exchanger channel with wavy fins [14] (left), close-up of a wavy fin array [12] (mid), plate-fin heat exchanger with corrugated fins, adapted from [17] (right). The main flow direction of the fluid is indicated by the red arrow.

Steady developed flow results for cross-wavy and cross-corrugated fins, which are variants of wavy and corrugated fins, were obtained earlier by Utriainen and Sunden in 2000 [18, 19] and further investigated by Zhou et al. in 2014 [20]. In the latter studies, also the relation between the average flow speed and the constant pressure drop in the steady laminar periodically developed regime was correlated.

Patankar's equations for steady periodically developed flow [10] were extended towards unsteady flow, for example by Wang et al. in 1995 [21]. In the study of Wang et al., it was found that self-sustained time-periodic oscillations in wavy fins start to form at a Reynolds number, based on the average interwall-spacing, around 180. In the work of Comini et al. [6, 22] on corrugated (or wavy) fins, unsteady laminar solutions of the periodically developed flow equations were found up to a Reynolds number, based on twice the fin height, close to 1000. Unsteady laminar periodically developed flow solutions for cross-wavy or cross-corrugated fins are available in the work of Ciofalo et al. [23] from 1996.

For offset-strip fins, which are one of the most common types of spatially periodic structures in compact heat transfer devices (see Figure 5.4), almost no numerical solutions for the laminar periodically developed regime are available in the literature. In 2009, Bhowmik and Lee [27] presented correlations for the total pressure drop and the average flow speed through an entire array of offset-strip fins. However, it seems that their results also include flow effects in the inlet region and not just in the periodically developed region. In the work of Kim et al. [28] from 2011, the relation between the total pressure drop and the average flow speed is numerically

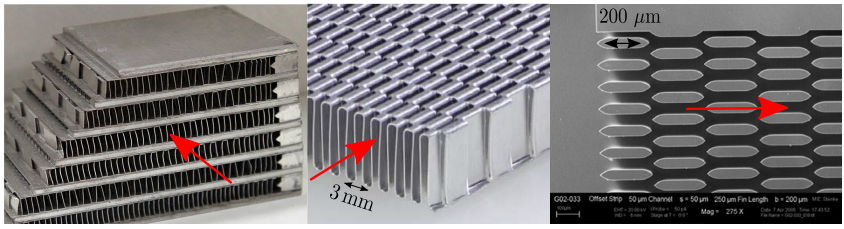

Figure 5.4: Compact plate-fin heat exchanger with offset-strip fins [24] (left), close-up of an array of offset-strip fins [25] (mid), heat sink with rectangular micro fins [26] (right). The main flow direction of the fluid is indicated by the red arrow.

calculated by simulating the flow over a single offset-strip fin unit. It is not clear whether their results in the laminar regime are consistent with the governing equations for periodically developed flow from Patankar et al. [10].

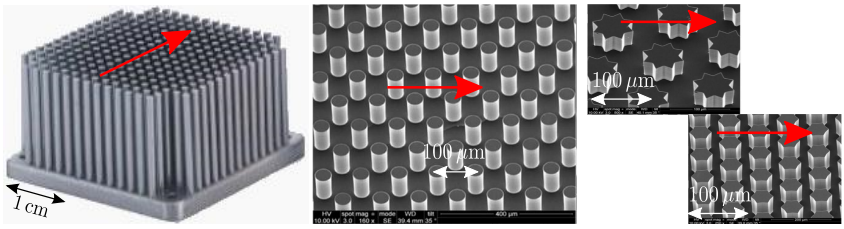

Figure 5.5: Heat sink with pin fins with a diameter of 1 mm and a fin spacing of 2 mm, in which the coolant air flow is laminar at speeds below 5 m/s [29] (left), close-up of a cylindrical pin fin array in a micro heat sink (mid), variants of pin fin geometries (right). The main flow direction of the fluid is indicated by the red arrow.

Laminar periodically developed flow around two-dimensional solid structures like circles and squares, which is of importance for compact heat transfer devices with tube banks or arrays of (long) pin fins (see Figure 5.5), has been studied intensively. Most of the work has been performed with the objective of determining the apparent permeability for arrays of cylinders and square rods.

The apparent permeability in the periodically developed regime is defined as a scalar K which relates the magnitude of the constant pressure gradient ∇P (or flow resistance force F) to the volume-averaged velocity U over a unit cell of the array:

$$U = -\frac{\mu_f}{K}\nabla P \qquad \text{where} \qquad \nabla P = F\,.$$

The apparent permeability of an array of cylinders in steady periodically developed flow was first studied by Edwards et al. in 1990 [30] and by Martin et al. [31] in 1997. Afterwards, their results have been re-evaluated and extended by Papathanasiou et al. [32] in 2001. Correlations for the apparent permeability of a cylinder array in the unsteady regime can be found in the work of Ghaddar et al. [33] from 1995 and more complete data are given in the work of Koch et al. [5] from 1997. Also, some data on the apparent permeability of cylinders have been reported by Hellström et al. [34], Tamayol et al. [35] and Mattis et al. [36] between 2006 and 2012.

The apparent permeability of an array of square rods in steady periodically developed flow was investigated by Kuwahara, Nakayama et al. [37, 38] in 2002 and 2004. Kuwahara, Nakayama et al. numerically correlated the constant pressure gradient in the developed regime with respect to the volume-averaged velocity on a unit cell of the array by means of a Darcy permeability and a Forchheimer coefficient. Their correlation takes different overall flow directions, Reynolds numbers and porosities into account. A correlation which includes the unsteady periodically developed flow regime in the same rod configuration, was presented by Alshare, Strykowski and Simon [39] in 2010.

Apart from wavy fins, corrugated fins, offset strip fins and pin fins also rectangular fins as in Figure 5.6 are commonly applied in compact heat transfer devices. The fully developed laminar flow solutions for rectangular fins and other ducts with a constant cross section can be found as analytical formulas for instance in [42] and many standard works [7, 43, 44].

Macro-Scale Modelling of Flow in Periodic Solid Structures —
In §1.3, it was explained that DNS of the flow through heat transfer devices with periodic solid structures is often not feasible, because it requires a huge amount of computational time and resources. For this reason, macro-scale flow models have been proposed which are computationally

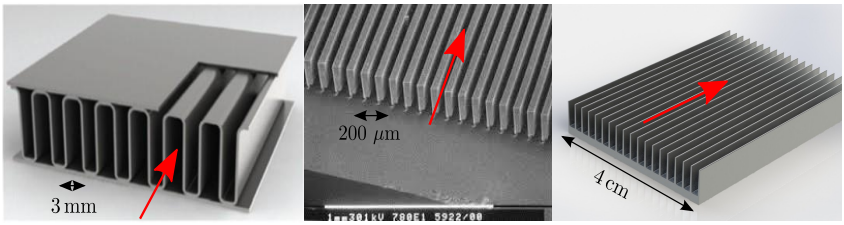

Figure 5.6: Part of a channel with rectangular fins in a compact plate-fin heat exchanger [40] (left), close-up of a heat sink with micro offset strip fins [41] (mid), heat sink with rectangular fins (right). The main flow direction of the fluid is indicated by the red arrow.

less expensive in comparison to DNS, albeit they are not in exact agreement with DNS results due to their heuristic and/or empirical nature.

In many cases, these macro-scale flow models can be called heuristic, because they treat the array of solid structures as a porous medium whose effective parameters depend only the geometry of the solid structures. The heuristic macro-scale flow models based on such a porous medium approach attempt to predict the relationship between the total pressure drop and mass flow rate in the entire device from the geometry of a single solid structure. For instance, the pressure drop over the core and the mean flow velocity through the core of a finned heat sink are often assumed to satisfy a relationship similar to the Darcy-Forchheimer law for a porous medium. The Darcy permeability and Forchheimer coefficient are then determined from the fin geometry through simplified analytical expressions. Examples of such analytical macro-scale flow models can be found in the work of Kim et al. [45] from 2000, as well as in the work of Chen et al. [46] from 2007. Some researchers, like Jeng and his co-workers [47, 48], have governed the Darcy permeability and Forchheimer coefficient for a finned heat sink by combining analytical expressions with experimental data. In the latter study, the Darcy permeability and Forchheimer coefficient just serve as empirical parameters which relate the measured pressure drop over the entire core (for a given flow rate) to the geometric parameters of a single fin.

In a number of studies, the macro-scale flow models for periodic solid structures are heuristically obtained from the volume-averaged flow equa-

tions that describe the macro-scale flow through a porous medium. These macro-scale flow models contain the interfacial force exerted by the solid structures on the flow. Mostly, the interfacial force in the volume-averaged flow equations is assumed to equal the gradient of the volume-averaged pressure. The gradient of the volume-averaged pressure on its turn is calculated from the pressure drop over a unit cell of the solid structures or the flow resistance force experienced by a single solid structure, under the assumption that the flow in the unit cell is laminar and periodically developed. Often, the relationship between the pressure drop and the volume-averaged flow velocity on a unit cell of the solid structures is then again expressed with the aid of an apparent permeability or in the form of the Darcy-Forchheimer law.

The latter approach seems to have been initiated in the 1990's by Edwards, Martin and others [30, 31] to evaluate the macro-scale flow in periodic cylinder arrays under laminar conditions. For instance, in the work of Martin, Saltiel and Shyy [31], the macro-scale pressure gradient is treated as a scalar quantity and expressed as

$$-\nabla\langle p_f\rangle^f \simeq \frac{\mu_f}{K}\langle u_f\rangle + \frac{F\rho_f}{\sqrt{K}}\langle u_f\rangle|\langle u_f\rangle|\,,$$

where u_f denotes the velocity in the streamwise direction. The so-called Darcy permeability K and the Forchheimer coefficient F in this work are actually calculated from the pressure drop Δp between two adjacent cylinder rows when the flow in the array is periodically developed:

$$-\frac{\Delta p}{c} = \frac{\mu_f}{K}\langle u_f\rangle + \frac{F\rho_f}{\sqrt{K}}\langle u_f\rangle|\langle u_f\rangle|\,.$$

The same approach has been followed by Kuwahara, Nakayama et al. [37, 38] and Alshare et al. [39], who used the VAT framework to model a uniform macro-scale flow through a bank of spatially periodic square rods.

Also in the work of Horvat and Catton [49] from 2003, the volume-averaged flow equations for porous media are used to model uniform macro-scale flow through spatially periodic structures. Horvat and Catton modelled the unidirectional macro-scale flow through a heat sink consisting of pin fins on a solid base-plate. The interfacial force in their macro-scale flow model is represented with the aid of a local drag force coefficient,

which is obtained from experimental correlations. In a related study [50] from 2005, Horvat and Mavko calculated this local drag coefficient for a single pin fin by solving the periodically flow equations on a unit cell of the pin fin array. In both of the latter studies [49, 50], the VAT model predicts the total pressure drop of the whole pin fin section in the heat sink in good agreement with experimental results.

In the work of Alshare, Strykowski and Simon [51] from 2010, the volume-averaged flow equations were solved numerically to simulate the macro-scale velocity field in a serpentine heat exchanger. To model the interfacial force in the volume-averaged flow equations, the permeability correlation from their previous work [39] was used. Their work offers a case study which is used to discuss in depth the accuracy of the macro-scale flow model in comparison to DNS.

We add that empirical VAT models for turbulent flow in heat sinks with circular and square pin fins were developed by Catton [52] in 2006. More recently, empirical VAT models have also been applied to turbulent flow in circular tube-fin heat exchangers [53] as well as heat sinks with elliptic scale-roughened surfaces [54].

Open Research Questions in the Literature

From this brief historical overview, it is concluded that the volume-averaged flow equations for porous media have been applied to model the macro-scale flow through spatially periodic solid structures in a heuristic approach or on empirical grounds. Due to this heuristic and empirical modelling, some fundamental questions have been left unanswered in the literature. A first fundamental question is whether the volume-averaging technique is actually capable of giving a physically meaningful macro-scale description of flow through periodic solid structures. More specifically, one can raise the question whether VAT at least yields a physically meaningful macro-scale description of the periodically developed flow regime.

Secondly, the volume-averaged flow equations for porous media are not exact model equations, in the sense that they are derived from the Navier-Stokes flow equations under the assumption that the spatial moments of the solid medium are zero and the assumption that some length-scale approximations are satisfied (cf. §3.6). Therefore, a second fundamental question is whether an exact macro-scale description of the periodically developed flow regime can be developed from the spatially averaged flow equations given in Chapter 3.

Furthermore, above it was explained that in the literature, the interfacial force is rarely distinguished from the macro-scale pressure gradient in the volume-averaged flow equations. Neither a distinction is made between the macro-scale pressure gradient and the constant pressure gradient in the periodically developed flow regime. A third question is thus whether this lack of distinction is really mathematically founded or if it introduces modelling errors.

Lastly, it is not immediately clear from the literature how the apparent permeability in the periodically developed regime is connected to the permeability tensor for the volume-averaged flow equations. In other words, the question remains how the periodically developed flow equations from Patankar et al. [10] are mathematically connected to the closure equations derived by Whitaker [55].

In the following part of this chapter, these questions will be answered one after the other, but first we will clarify the concept of a unit cell and introduce some filters which are needed to develop a macro-scale description of the periodically developed flow regime.

5.5 Unit Cell

When the domain Ω is a device covered by a periodic distribution of solid structures of the same shape and size, the fluid and solid indicators are periodic in the sense that for any position $\boldsymbol{x}$ sufficiently far from the external boundaries of Ω, there exist some *lattice vectors* $\boldsymbol{l}^{(j)}$ [56] such that

$$\gamma_f(\boldsymbol{x}) = \gamma_f\left(\boldsymbol{x} + \boldsymbol{l}^{(j)}\right) = 1 - \gamma_s(\boldsymbol{x}) = 1 - \gamma_s\left(\boldsymbol{x} + \boldsymbol{l}^{(j)}\right) . \tag{5.1}$$

Therefore, an array of spatially periodic solid structures is characterized by the existence of a local *unit cell* for any position $\boldsymbol{x}$ sufficiently far from the external boundaries of Ω:

$$\Omega_{\text{unit}}(\boldsymbol{x}) \triangleq \left\{ \boldsymbol{r} \,|\, \exists\, c_j \in \left[-\frac{1}{2}, \frac{1}{2}\right] \Leftrightarrow \boldsymbol{r} = \boldsymbol{x} + \sum_{j=1}^{\mathrm{n}_j} c_j \boldsymbol{l}^{(j)} \right\} . \tag{5.2}$$

An illustration of a unit cell for a tube bank and an array of cylinders is given in Figure 5.7. In (5.2) the number n_j of lattice vectors spanning

the domain of the two- or three-dimensional unit cell equals the maximal number of linearly independent lattice vectors $\boldsymbol{l}^{(j)}$ which can be found to satisfy (5.1).

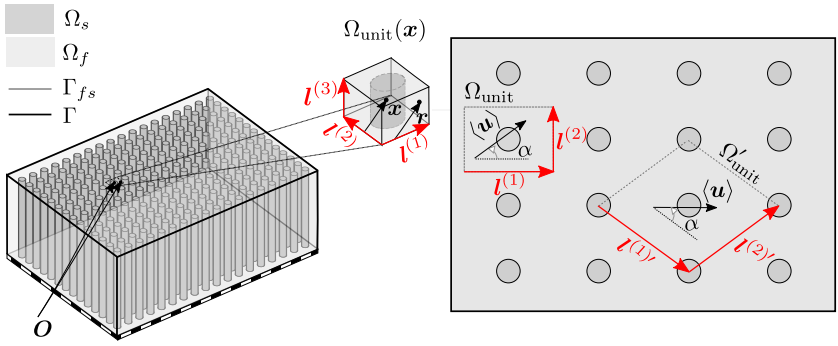

Figure 5.7: Example of a local unit cell (dashed lines) and its lattice vectors in a cylindrical tube bank (left). Two unit cells in a two-dimensional array of cylinders, where the volume-averaged velocity over the unit cell makes an angle α with respect to the cylinders (right).

According to its definition (5.2), a unit cell contains all geometric information of the array of solid structures and (5.2) many unit cells exist. In this work, always the lattice vectors with the smallest non-zero magnitude are chosen to define a unit cell.

This definition of a unit cell should not be confused with the concept of a representative elementary volume (REV) as used for porous media. An REV is usually regarded as an averaging domain which by definition satisfies the length-scale constraint (2.91) with respect to a volume-averaging operator and, if existent, gives rise to meaningful macro-scale properties of the porous medium.

In the following sections, we will often use the volume of the unit cell of (5.2), which equals

$$V_{\mathrm{unit}} \triangleq \int_{\boldsymbol{r}\in\Omega_{\mathrm{unit}}(\boldsymbol{x})} d\Omega(\boldsymbol{r}) = \begin{cases} \left\| \boldsymbol{l}^{(1)} \times \boldsymbol{l}^{(2)} \right\| & \text{if } \mathrm{n}_j = 2\,, \\ \left| \boldsymbol{l}^{(1)} \cdot \left(\boldsymbol{l}^{(2)} \times \boldsymbol{l}^{(3)} \right) \right| & \text{if } \mathrm{n}_j = 3 \end{cases} . \quad (5.3)$$

5.6 Filters Suitable for Spatial Periodicity

For averaging physical quantities over a spatially periodic solid-fluid domain, filters based on the weighting function for volume-averaging have some suitable properties. In particular, it is worth to explore the properties of filters with a weighting function of the form $m = m_G * m_V$, where the function m_G is arbitrary and the filter window of m_V matches a unit cell of the domain, $\bar{\Omega} = \Omega_{\text{unit}}$;

$$m_V(\boldsymbol{r}) \triangleq \begin{cases} \frac{1}{V_{\text{unit}}} & \boldsymbol{r} \in \Omega_{\text{unit}}(\boldsymbol{x}) \\ 0 & \text{elsewhere} \end{cases} . \tag{5.4}$$

The weighting function (5.4) for the volume average can be expressed as a box filter of the form

$$m_V(-\boldsymbol{y}) \triangleq \frac{1}{V_{\text{unit}}} \prod_{j=1}^{\mathrm{n}_j} \operatorname{rect}\left(\frac{\boldsymbol{y} \cdot \boldsymbol{l}^{(j)}}{\|\boldsymbol{l}^{(j)}\|^2} \right), \tag{5.5}$$

which shows that the volume average is fully separable with respect to the basis vectors $\boldsymbol{l}^{(j)}/\|\boldsymbol{l}^{(j)}\|^2$ over the interval $y_j \triangleq \frac{\boldsymbol{y}\cdot\boldsymbol{l}^{(j)}}{\|\boldsymbol{l}^{(j)}\|^2} \in I_j = \left[-\frac{1}{2}, \frac{1}{2}\right]$.

The class of filters with $m = m_G * m_V$ satisfies

$$\phi(\boldsymbol{x}) = \phi\left(\boldsymbol{x} + \boldsymbol{l}^{(j)}\right) \quad \Rightarrow \quad \begin{cases} \langle\phi\rangle_m = \langle\langle\phi\rangle\rangle_{m_G} = \langle\phi\rangle = \text{constant} \\ \langle\widetilde{\phi}\rangle_m = \langle\widetilde{\phi}\rangle = 0 \end{cases}, \tag{5.6}$$

for any spatially periodic distribution ϕ. In particular, for any distribution $\boldsymbol{\phi}$ being spatially periodic over the fluid region holds:

$$\boldsymbol{\phi} = \begin{cases} \boldsymbol{\phi}_f(\boldsymbol{x}) = \boldsymbol{\phi}_f\left(\boldsymbol{x} + \boldsymbol{l}^{(j)}\right) & \text{in } \Omega_f \\ 0 & \text{in } \Omega_s \end{cases} \quad \Rightarrow \quad \langle\boldsymbol{\phi}\rangle_m^f = \langle\boldsymbol{\phi}\rangle^f = \text{constant}\,. \tag{5.7}$$

For this type of weighting function, the weighted porosity thus equals the true physical porosity of the solid structures:

$$\epsilon_{fm} = \epsilon_f = \text{constant}\,. \tag{5.8}$$

When ϕ_f is spatially periodic, the filter property (5.7) respects the length-scale constraint (2.91), because

$$\ell_{\boldsymbol{\phi}} \leq r_m = O\left(\|\boldsymbol{l}^{(j)}\|\right) \qquad \text{and} \qquad \mathscr{L}_{\boldsymbol{\phi}} = \infty\,, \tag{5.9}$$

so that $\langle \boldsymbol{\phi} \rangle_m^f$ is a macro-scale quantity.

A special case within this class are the filters based on the weighting function of Quintard and Whitaker [3], which has the form $m = m_C * m_V * m_V$. The function m_C here removes all C^1 discontinuities of $m_V * m_V$ in order that $m = m_C * m_V * m_V \in C^\infty$. For most numerical purposes, the differentiability of the weighting function is not of concern and the function m_C can be approximated as $m_C \simeq 1$. In that case, the filter operator of Quintard and Whitaker is based on the weighting function $m = m_V * m_V$.

The filter with the weighting function $m = m_V * m_V$ is equivalent a double volume average:

$$\langle \boldsymbol{\phi} \rangle_m|_{\boldsymbol{x}} = \frac{1}{V_{\text{unit}}} \int_{\boldsymbol{r_2} \in \Omega_{\text{unit}}(\boldsymbol{x})} \frac{1}{V_{\text{unit}}} \int_{\boldsymbol{r_1} \in \Omega_{\text{unit}}(\boldsymbol{r_2})} \boldsymbol{\phi}(\boldsymbol{r_1})\, d\Omega(\boldsymbol{r_1})\, d\Omega(\boldsymbol{r_2})\,, \tag{5.10}$$

or in compact notation: $\langle \boldsymbol{\phi} \rangle_m = \langle\langle \boldsymbol{\phi} \rangle\rangle$. It is interesting to note that although the averaging window of m_V corresponds to the unit cell domain, the weighting function $m_V * m_V$ has support over a filter window of twice the extent of Ω_{unit}. Therefore $\langle \boldsymbol{\phi} \rangle_m$ represents a weighted average within a characteristic filter radius $r_m \simeq 2\|\boldsymbol{l}^{(j)}\|$.

The double volume average (5.10) can also be calculated as a single integral via the expression for the overall weighting function $m = m_V * m_V$. For a beam-shaped unit cell spanned by the lattice vectors $\boldsymbol{l}^{(1)}$, the expression for $m = m_V * m_V$ is[1]

$$m(-\boldsymbol{y}) = \begin{cases} \frac{1}{V_{\text{unit}}^2} \prod_{j=1}^{\text{n}_j} \dfrac{\|\boldsymbol{l}^{(j)}\|^2 - |\boldsymbol{y} \cdot \boldsymbol{l}^{(j)}|}{\|\boldsymbol{l}^{(j)}\|^2} & \text{if } |\boldsymbol{y} \cdot \boldsymbol{l}^{(j)}| \leq \|\boldsymbol{l}^{(j)}\|^2 \\ 0 & \text{otherwise} \end{cases}, \tag{5.11}$$

The weighting function (5.11) is visualized in Figure 5.8 for a two-dimensional rectangular unit cell spanned by the vectors $\boldsymbol{l}^{(1)}$ and $\boldsymbol{l}^{(2)}$. We note that expression (5.11) follows directly from (5.5) and the fact that

$$\text{rect}\,(x) * \text{rect}\,(x) = \int_{\mathbb{R}} \text{rect}\,(x - r)\,\text{rect}\,(r)\, dr = \text{rect}\left(\frac{x}{2}\right)(1 - |x|)\,, \tag{5.12}$$

where the integration space $\mathbb{R}$ could have been replaced by the finite interval $(x - r) \in [-\frac{1}{2}, \frac{1}{2}]$.

[1] In our paper [57], the form was given for the case when $\boldsymbol{l}^{(j)}$ are mutually orthogonal.

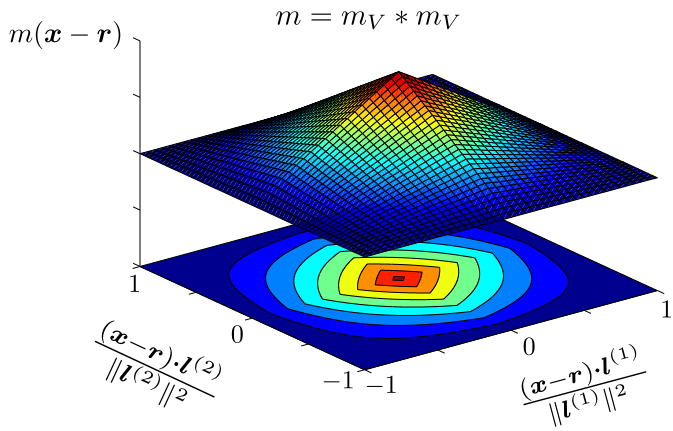

Figure 5.8: Two-dimensional representation of the weighting function $m = m_V * m_V$ for a rectangular unit cell spanned by the lattice vectors $\boldsymbol{l}^{(1)}$ and $\boldsymbol{l}^{(2)}$.

A third way for evaluating the double volume average (5.10) is through consecutive one-dimensional convolutions products. This third evaluation method relies on the fact that the filter with the weighting function (5.11) is fully separable with respect to the basis vectors $\boldsymbol{l}^{(j)}/\|\boldsymbol{l}^{(j)}\|^2$. In its fully separable form, the weighting function $m = m_V * m_V$ is given by

$$m'_j(-y_j) = \frac{1-|y_j|}{\sqrt[n_j]{V^2_{\text{unit}}}}\,\text{rect}\left(\frac{y_j}{2}\right) \quad \text{where} \quad y_j \triangleq \frac{\boldsymbol{y}\cdot\boldsymbol{l}^{(j)}}{\|\boldsymbol{l}^{(j)}\|^2} \in I_j = [-1,1]\,. \tag{5.13}$$

It was shown by Quintard and Whitaker [3] that for $m = m_V * m_V$, the spatial moments of the periodic solid structures are constant:

$$\langle \boldsymbol{y}^{\otimes n}\gamma_f\rangle_m \quad \text{or} \quad \langle \boldsymbol{y}^{\otimes n}\gamma_s\rangle_m = \begin{cases} \text{constant} & \text{if } n \text{ is even} \\ 0 & \text{if } n \text{ is odd} \end{cases}, \tag{5.14}$$

as equation (5.1) is exact. Therefore, a filter based on $m = m_C * m_V * m_V$ is idempotent with respect to a linear distribution with gradient $\boldsymbol{c}$ over the fluid domain:

$$\boldsymbol{\phi} = \begin{cases} \boldsymbol{\phi}_f(\boldsymbol{x}) = \boldsymbol{c}\cdot\boldsymbol{x} & \text{in } \Omega_f \\ 0 & \text{in } \Omega_s \end{cases} \quad \Rightarrow \quad \langle\boldsymbol{\phi}\rangle^f_m = \boldsymbol{c}\cdot\boldsymbol{x}\,. \tag{5.15}$$

Strictly speaking, we cannot call $\langle \boldsymbol{\phi} \rangle_m^f$ a macro-scale quantity in that case, because $\langle \boldsymbol{\phi} \rangle_m^f$ varies over the same scale as $\boldsymbol{\phi}$: $\mathscr{L}_\phi = \ell_\phi$ and $r_m \simeq 2\|\boldsymbol{l}^{(j)}\|$. Furthermore, because of (5.14), the geometrical tensors in the expression for the surface filter (2.64) become zero:

$$\boldsymbol{G}_m^{(n)} = 0\,. \tag{5.16}$$

The weighting function $m = m_C * m_V * m_V$ thus simplifies the geometrical decomposition of the surface filter;

$$\langle \boldsymbol{n}_{fs}(\boldsymbol{\phi}_f - \boldsymbol{\phi}_s)\delta_{fs} \rangle_m = \langle \boldsymbol{n}_{fs}(\widetilde{\boldsymbol{\phi}}_f - \widetilde{\boldsymbol{\phi}}_s)\delta_{fs} \rangle_m\,. \tag{5.17}$$

In summary, a surface filter based on $m = m_C * m_V * m_V$ passes only the small-scale deviations fields in periodic solid structures and not the corresponding macro-scale fields.

5.7 Periodically Developed Flow

As we expect the forced flow in a device with spatially periodic solid structures to attain, after a short entrance region, a periodically developed character, we can assume that the flow is periodically developed over the largest part of Ω. In the periodically developed region of Ω, there exists a unit cell over which the velocity distribution at any time t varies in a periodic pattern:

$$\boldsymbol{u}(\boldsymbol{x}, t) = \boldsymbol{u}\left(\boldsymbol{x} + \boldsymbol{l}^{(j)}, t\right)\,. \tag{5.18}$$

As illustrated in Figure 5.9, the pressure distribution in periodically developed flow consists of a part that varies linearly in space with a constant gradient $\nabla \mathrm{P}$, and a portion $p^\star$ that behaves in a periodic fashion from one unit cell to another [10]:

$$p(\boldsymbol{x}, t) = \nabla \mathrm{P} \cdot (\boldsymbol{x} - \boldsymbol{x}_0)\gamma_f + p^\star(\boldsymbol{x}, t)\,, \tag{5.19}$$

with

$$p^\star(\boldsymbol{x}, t) = p^\star\left(\boldsymbol{x} + \boldsymbol{l}^{(j)}, t\right)\,. \tag{5.20}$$

We remark that both p and $p^\star$ are zero in Ω_s and that $\boldsymbol{x}_0$ is some point at the onset of the periodically developed flow region. The constant pressure gradient $\nabla \mathrm{P}$ represents the constant pressure drop over each unit cell.

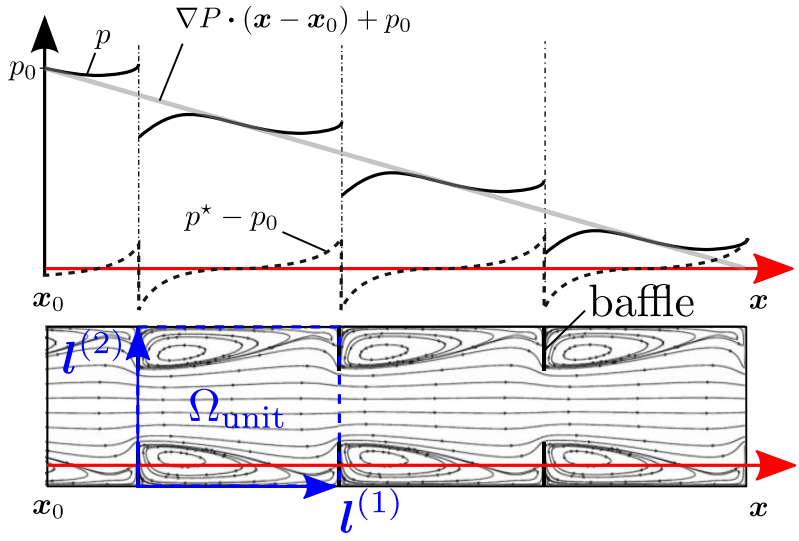

Figure 5.9: Illustration of the streamlines and the pressure profile in steady periodically developed flow through an array of parallel channels with periodic baffles, inspired by [58].

Postulating the form of equations (5.18) and (5.19), we have assumed spatial periodicity of $\boldsymbol{u}$ and $p^\star$ at any time t. This assumption is valid for the unsteady periodically developed flow regime as long as the Reynolds number is sufficiently low (cf. §5.3) and time-periodic flow phenomena such as time-periodic vortex shedding in the array of solid structures occur.

The equations which govern the velocity and pressure in the periodically developed flow regime are found by restricting the flow equations (3.1) and (3.2) to the fluid domain and by decomposing the pressure according to equation (5.19):

$$\begin{aligned} \nabla \cdot \boldsymbol{u}_f &= 0\,, \\ \rho_f \frac{\partial \boldsymbol{u}_f}{\partial t} + \rho_f \boldsymbol{u}_f \cdot \nabla \boldsymbol{u}_f &= -\nabla p_f^\star - \nabla \mathrm{P} + \nabla \cdot \boldsymbol{\tau}_f + \boldsymbol{f}_f\,. \end{aligned} \tag{5.21}$$

In the periodically developed flow regime, the appropriate boundary con-

ditions on the fluid domain of the unit cell $\Omega_f \cap \Omega_{\text{unit}}$ are

$$\begin{aligned} \boldsymbol{u}_f(\boldsymbol{x},t) &= \boldsymbol{u}_f\left(\boldsymbol{x}+\boldsymbol{l}^{(j)},t\right) \\ p^\star(\boldsymbol{x},t) &= p_f^\star\left(\boldsymbol{x}+\boldsymbol{l}^{(j)},t\right) \end{aligned} \qquad \text{and} \qquad \boldsymbol{u}_f = 0 \ \text{ on } \Gamma_{fs}\cap\Omega_{\text{unit}}\,, \quad (5.22)$$

where $j = \{1,\ldots,\mathrm{n}_j\}$. We remark that the value of $\langle\overline{p^\star}\rangle$ over the unit cell, which determines the pressure level $p_0 \triangleq p(\boldsymbol{x}_0,t_0) = p^\star(\boldsymbol{x}_0,t_0)$ at the onset of the periodically developed region (see Figure 5.9), must be imposed to find a unique solution for $p^\star$.

The periodic flow equations (5.21) and (5.22) relate the constant pressure gradient ∇P to the volume-averaged velocity $\langle\boldsymbol{u}\rangle$ over the unit cell at any time, because $\boldsymbol{u}_f$ and $p_f^\star$ depend uniquely on ∇P through these equations:

$$\langle\boldsymbol{u}\rangle = \langle\boldsymbol{u}\rangle\big(\mu_f,\rho_f,\boldsymbol{f},\nabla P,\Gamma_{fs}\cap\Omega_{\text{unit}},t\big)\,. \quad (5.23)$$

This relationship between the constant pressure gradient and velocity also depends on the fluid viscosity and density, the presence of a body force as well as the boundary shape of the solid structure within the unit cell. It is reasonable to assume that the functional relationship (5.23) is a one-to-one mapping: different pressure gradients lead to different volume-averaged velocity vectors and vice versa.

5.8 Macro-scale Description of Periodically Developed Flow

If the weighting function is chosen to be of the form $m = m_G * m_V$ with $\bar{\Omega} = \Omega_{\text{unit}}$ for m_V as in (5.4) and $m_G \in C^\infty$, the filtered velocity and weighted porosity are spatially constant in the periodically developed regime:

$$\langle\boldsymbol{u}\rangle_m = \langle\boldsymbol{u}\rangle \qquad \text{and} \qquad \epsilon_{fm} = \epsilon_f\,, \quad (5.24)$$

due to the periodicity of the velocity distribution and fluid indicator (cf. (5.4) and (5.8)). This choice of weighting function thus ensures that $\langle\boldsymbol{u}\rangle_m^f$ is a macro-scale quantity, because $\langle\langle\boldsymbol{u}^f\rangle_m^f\rangle_m^f = \langle\boldsymbol{u}\rangle_m^f = \langle\boldsymbol{u}\rangle^f$. Moreover, any filter based on $m = m_G * m_V$ automatically respects the velocity scale constraint (3.23) as

$$\ell_{\boldsymbol{u}} \le r_m = O\left(\|\boldsymbol{l}^{(j)}\|\right) \qquad \text{and} \qquad \mathscr{L}_{\boldsymbol{u}} = \infty. \quad (5.25)$$

The filtered pressure in periodically developed flow is given by

$$\langle p\rangle_m^f = \nabla \mathrm{P} \cdot \langle (\boldsymbol{r} - \boldsymbol{x}_0)\gamma_f \rangle_m^f + \langle p^\star \rangle_m^f \tag{5.26}$$

$$= \nabla \mathrm{P} \cdot \langle \boldsymbol{y} \rangle_m^f + \nabla \mathrm{P} \cdot (\boldsymbol{x} - \boldsymbol{x}_0) + \langle p^\star \rangle_m^f \,, \tag{5.27}$$

as $\boldsymbol{y} \triangleq \boldsymbol{r} - \boldsymbol{x}$. In addition, the pressure deviation part $\widetilde{p}$ satisfies

$$\widetilde{p}(\boldsymbol{x}, t) = p^\star(\boldsymbol{x}, t) - \langle p^\star \rangle_m^f \gamma_f - \nabla \mathrm{P} \cdot \langle \boldsymbol{y} \rangle_m^f \gamma_f \,. \tag{5.28}$$

From (5.26) and (5.28), we learn that the filter must suppress the first spatial moment of the solid structures, i.e. $\langle \boldsymbol{y} \rangle_m^f \simeq 0$, in order that $\langle \widetilde{p} \rangle_m \simeq 0$ and the filtered pressure be truly a macro-scale quantity. This property is realized with the aid of $m_G = m_C * m_V$ and $m_C \in C^\infty$, because then we have $\langle \langle p \rangle_m^f \rangle_m^f = \langle p \rangle_m^f$ and $\langle \widetilde{p} \rangle_m = 0$, as $\langle \boldsymbol{y} \rangle_m^f = 0$ by (5.14). The weighting function m_C is still of arbitrary choice.

It is concluded that the appropriate filter for the velocity and pressure in the periodically developed flow regime is based on a double volume-average, i.e. $m = m_C * m_V * m_V$, due to the idempotence property of this filter with respect to periodic and linear functions (cf. (5.7) and (5.15)).

In the periodically developed flow regime, the macro-scale pressure gradient is given by[2]

$$\nabla \langle p \rangle_m^f = \left(\boldsymbol{I} + \nabla \langle \boldsymbol{y} \rangle_m^f \right) \cdot \nabla \mathrm{P} + \nabla \langle p^\star \rangle_m^f \,. \tag{5.29}$$

For a filter based on $m = m_G * m_V$ with $m_G \in C^\infty$ and $\bar{\Omega} = \Omega_{\mathrm{unit}}$ for m_V, $\langle p^\star \rangle_m^f$ is constant over space due to the periodicity of $p^\star$. For this type of filter, the gradient of the filtered pressure thus becomes

$$\nabla \langle p \rangle_m^f = \left(\boldsymbol{I} - \boldsymbol{G}_m'^{(1)} \right) \cdot \nabla \mathrm{P} \,. \tag{5.30}$$

On the other hand, the weighting function $m = m_C * m_V * m_V$ with $m_C \in C^\infty$, not only defines the true macro-scale velocity and macro-scale pressure, but also recovers the constant physical pressure gradient for the macro-scale flow:

$$\nabla \langle p \rangle_m^f = \nabla \mathrm{P} \,, \tag{5.31}$$

as $\boldsymbol{G}_m'^{(1)} = \nabla \langle \boldsymbol{y} \rangle_m^f = 0$ in (5.30). Therefore, the macro-scale pressure $\langle p \rangle_m^f$ varies linearly over the part of the device domain where the flow

[2] In our paper [2] this inner product was erroneously changed.

is periodically developed (cf. (5.26)), just like in fully developed channel flow. This important analogy is however only recovered by defining the macro-scale velocity and macro-scale pressure through the double volume average introduced by Quintard and Whitaker.

Would one define the macro-scale pressure through a simple volume average or any other filter with $m_G \neq m_C * m_V$, the macro-scale pressure would consist of a linear pressure variation over space as well as a spatially periodic term $\nabla \mathrm{P} \cdot \langle \boldsymbol{y} \rangle_m^f$ contributed by the interaction of the volume-averaging operator with the geometry of the solid structures (see (5.30)). In that case, equation (5.30) reveals that the simple volume average or another filter with $m_G \neq m_C * m_V$ must ensure that the gradient of the first spatial moment is negligible for the solid structures under consideration, because then $\boldsymbol{I} \gg \boldsymbol{G}_m'^{(1)}$ and $\langle \widetilde{p} \rangle_m^f \simeq 0$. Otherwise, the filter would not respect the pressure constraint of (3.23) and thus not define a true macro-scale pressure. Whether this condition is fulfilled, depends on the specific geometry of the solid structures and the weighting function m_G that one chooses. Of course, if $m_G = m_C * m_V$, the condition is certainly fulfilled.

Lastly, from the expressions for the pressure and velocity distributions and their filtered counterparts for periodically developed flow, it follows that the deviation quantities are also spatially periodic if $m = m_G * m_V$ and $m_G \in C^\infty$:

$$\widetilde{\boldsymbol{u}}_f(\boldsymbol{x}, t) = \widetilde{\boldsymbol{u}}_f\left(\boldsymbol{x} + \boldsymbol{l}^{(j)}, t\right), \qquad \widetilde{p}_f(\boldsymbol{x}, t) = \widetilde{p}_f\left(\boldsymbol{x} + \boldsymbol{l}^{(j)}, t\right), \quad (5.32)$$

where $j = \{1, \ldots, \mathrm{n}_j\}$.

For flow through a porous medium, the deviation velocity $\widetilde{\boldsymbol{u}}_f$ and pressure $\widetilde{p}_f$ are often assumed to approximately satisfy periodic boundary conditions over the REV. For the periodically developed flow regime in periodic solid structures on the contrary, the periodic boundary conditions (5.32) on the unit cell domain are exact. In the next sections, we will show that the exactness of the periodic boundary conditions allows an exact reconstruction of the micro-scale details, $\widetilde{\boldsymbol{u}}_f$ and $\widetilde{p}_f$, from knowledge of the macro-scale flow and vice versa, for any filter of the form $m = m_G * m_V$ with $\bar{\Omega} = \Omega_{\mathrm{unit}}$.

From the foregoing discussion, it is concluded that with a filter of the form $m = m_G * m_V$, the periodically developed flow regime can be completely characterized at the macro-scale level by the filtered velocity $\langle \boldsymbol{u} \rangle_m^f = \langle \boldsymbol{u} \rangle^f$

and the macro-scale pressure gradient $\nabla\langle p\rangle_m^f = \left(\boldsymbol{I} - \boldsymbol{G}_m^{\prime(1)}\right)\cdot\nabla\mathrm{P}$ if $\boldsymbol{G}_m^{\prime(1)} \ll \boldsymbol{I}$. While the macro-scale velocity is constant, the macro-scale gradient $\nabla\langle p\rangle_m^f$ is space-dependent if the geometrical tensor $\boldsymbol{G}_m^{\prime(1)}$ varies over the unit cell domain. The relation between the macro-scale velocity $\langle \boldsymbol{u}\rangle_m^f$ and the macro-scale pressure gradient $\nabla\langle p\rangle_m^f$ can be correlated explicitly at any time by solving the periodically developed flow equations (5.21) and (5.22) on a unit cell for an applied pressure gradient $\nabla\mathrm{P}$. The relationship (5.23) then becomes equivalent to

$$\langle \boldsymbol{u}\rangle_m^f = \langle \boldsymbol{u}\rangle_m^f \left(\mu_f, \rho_f, \boldsymbol{f}, \nabla\langle p\rangle_m^f \text{ or } \nabla\mathrm{P}, \Gamma_{fs} \cap \Omega_{\text{unit}}, t\right) . \tag{5.33}$$

5.9 Closure for Periodically Developed Flow

We will show now that for any filter based on $m = m_G * m_V$ with $\bar{\Omega} = \Omega_{\text{unit}}$ for m_V, the closure terms in the periodically flow regime can be obtained from the macro-scale momentum equation.

In the part of Ω over which the unsteady periodically flow regime extends, macro-scale mass conservation is trivially satisfied when $m = m_G * m_V$ and the macro-scale momentum equation (3.17) reduces to

$$\rho_f \frac{\partial\langle \boldsymbol{u}\rangle_m^f}{\partial t} = -\nabla\langle p\rangle_m^f + \boldsymbol{b}_{fs}^{\prime} + \langle \boldsymbol{f}\rangle_m^f . \tag{5.34}$$

Here we made use of the fact that the filtered velocity and the momentum dispersion source $\boldsymbol{M}^{\prime}$ are spatially constant for $m = m_G * m_V$ with $\bar{\Omega} = \Omega_{\text{unit}}$ for m_V. The fact that $\boldsymbol{M}^{\prime}$ is spatially constant in that case follows from the observation that for this weighting function, the following expression holds exactly:

$$\boldsymbol{M}^{\prime} = \langle \widetilde{\boldsymbol{u}}\widetilde{\boldsymbol{u}}\rangle_m^f . \tag{5.35}$$

Because the unsteady periodically developed regime is characterized by time-periodic flow phenomena, the macro-scale momentum equation (5.34) can be averaged over a time period to find that

$$\nabla\langle p\rangle_m^f = \overline{\boldsymbol{b}_{fs}^{\prime}} + \langle \bar{\boldsymbol{f}}\rangle_m^f . \tag{5.36}$$

For steady periodically developed flow, the former macro-scale momentum equation becomes

$$\nabla\langle p\rangle_m^f = \boldsymbol{b}_{fs}^{\prime} + \langle \boldsymbol{f}\rangle_m^f . \tag{5.37}$$

In case no gravitational body force is present, the macro-scale interfacial force thus equals the macro-scale pressure gradient, so that the pressure drop over each unit cell is directly caused by the pressure and shear stress contributions at the solid-fluid interface.

Through knowledge of the relation (5.33) between the macro-scale pressure gradient and the macro-scale velocity relation, the previous macro-scale momentum equations can be used to determine the weighted interfacial force $\boldsymbol{b}'_{fs}$ for unsteady (cf. (5.34)) and steady (cf. (5.37)) periodically developed flow, in function of the macro-scale velocity $\langle \boldsymbol{u} \rangle^f_m$:

$$\boldsymbol{b}'_{fs} = \boldsymbol{b}'_{fs} \left(\mu_f, \rho_f, \boldsymbol{f}, \langle \boldsymbol{u} \rangle^f_m, \Gamma_{fs} \cap \Omega_{\text{unit}}, \boldsymbol{x}, t \right) . \tag{5.38}$$

For steady periodically developed flow the time parameter t plays no role. Similarly, solving the periodically developed flow equations on a unit cell allows to correlate the momentum dispersion source in function of $\langle \boldsymbol{u} \rangle^f_m$:

$$\boldsymbol{M}' = \boldsymbol{M}' \left(\mu_f, \rho_f, \boldsymbol{f}, \langle \boldsymbol{u} \rangle^f_m, \Gamma_{fs} \cap \Omega_{\text{unit}}, t \right) . \tag{5.39}$$

In general, for an arbitrary filter operator with $m = m_G * m_V$, the closure term $\boldsymbol{b}'_{fs}$ may vary over each point $\boldsymbol{x}$ of the unit cell domain Ω_{unit}. The possible space dependence of $\boldsymbol{b}'_{fs}$ is related to the fact that the macro-scale gradient $\nabla \langle p \rangle^f_m$ in (5.34) and (5.37) varies over Ω_{unit} if $\boldsymbol{G}'^{(1)}_m$ is not constant. Depending on the particular choice of weighting function m_G for filtering, the possible space dependence of $\boldsymbol{b}'_{fs}$ might impair the practical closure of the spatially averaged flow equations.

If however the filter operator guarantees that $\boldsymbol{b}'_{fs}$ and $\boldsymbol{M}'$ depend directly on $\langle \boldsymbol{u} \rangle^f_m$ in a manner that both closure terms are spatially constant for periodically developed flow, the closure relations (5.38) and (5.39) can be correlated with a reduced parameter set, no longer containing $\boldsymbol{x}$. When we remember that $\boldsymbol{M}'$ is already spatially constant for periodically developed flow by choosing $\bar{\Omega} = \Omega_{\text{unit}}$ for m_V, the remaining question is how the filter operator, or more precisely its weighting function m_G, should be chosen in order to ensure that also the closure term $\boldsymbol{b}'_{fs}$ is spatially constant for periodically developed flow, i.e. $\boldsymbol{b}'_{fs} = \boldsymbol{b}'_{fs}(t)$. In the next section, we will prove that the weighting function $m = m_C * m_V * m_V$ which defines the true macro-scale velocity and macro-scale pressure in the developed regime, automatically ensures that $\boldsymbol{b}'_{fs} = \boldsymbol{b}'_{fs}(t)$.

5.10 Choice of Weighting Function for Periodically Developed Flow

Initially, the normalized weighting function m was assumed to have derivatives of all orders (cf. (2.12)). Afterwards, the form $m = m_G * m_V$ was chosen for the weighting function, in a manner that the support of m_V matches with a unit cell of the periodic solid structures: $\bar{\Omega} = \Omega_{\text{unit}}$. This second restriction on m makes the filter suitable for defining the macro-scale velocity (cf. (5.24)) and makes it possible to obtain the closure terms by solving the periodically developed flow equations on a unit cell of the device domain (cf. §5.9). Furthermore, we have shown that the weighting function should be based on $m_G = m_C * m_V$ to define a meaningful macro-scale pressure, or at least that m_G respects $\langle \boldsymbol{y} \rangle_m^f \simeq 0$ and $\boldsymbol{G}_m'^{(1)} \ll \boldsymbol{I}$ (cf. §5.7).

In order to easily correlate the closure functions of (5.34) and (5.37), the weighting function must ensure that both closure terms are constant over the unit cell domain. A deeper analysis in accordance to [3] actually reveals that $\boldsymbol{b}'_{fs}$ is constant when the filter enforces $\boldsymbol{b}'_{fs}$ to depend directly on the periodic deviation pressure $\widetilde{p}_f$ and deviation velocity $\widetilde{\boldsymbol{u}}_f$ as follows:

$$\begin{aligned} \boldsymbol{b}'_{fs} &= \epsilon_{fm}^{-1} \langle \boldsymbol{n}_{fs} \cdot (-p_f \boldsymbol{I} + \boldsymbol{\tau}_f)\, \delta_{fs} \rangle_m \\ &\Rightarrow \qquad \boldsymbol{b}'_{fs} = \epsilon_{fm}^{-1} \langle \boldsymbol{n}_{fs} \cdot (-\widetilde{p}_f \boldsymbol{I} + \widetilde{\boldsymbol{\tau}}_f)\, \delta_{fs} \rangle_m \,. \end{aligned} \tag{5.40}$$

In general, using the decomposition of p and $\boldsymbol{\tau}$ according to (2.60), the weighted interfacial force, defined by (3.22), can be expressed as

$$\begin{aligned} \boldsymbol{b}'_{fs} = \epsilon_{fm}^{-1} \langle \boldsymbol{n}_{fs} \cdot \left(-\langle p \rangle_m^f \boldsymbol{I} + \langle \boldsymbol{\tau} \rangle_m^f \right) \delta_{fs} \rangle_m \\ + \epsilon_{fm}^{-1} \langle \boldsymbol{n}_{fs} \cdot (-\widetilde{p}_f \boldsymbol{I} + \widetilde{\boldsymbol{\tau}}_f)\, \delta_{fs} \rangle_m \,. \end{aligned} \tag{5.41}$$

If the macro-scale pressure $\langle p \rangle_m^f$ and macro-scale viscous stress tensor $\langle \boldsymbol{\tau} \rangle_m^f$ are represented by their Taylor series expansion about the centroid $\boldsymbol{x}$ of the filter window $\bar{\Omega}(\boldsymbol{x})$, equation (5.41) results in [3]

$$\begin{aligned} \boldsymbol{b}'_{fs} = -\sum_{n=0}^{\infty} \boldsymbol{G}'^{(n)}_m \underbrace{\cdot\cdot}_{n\text{-times}} \nabla^{\otimes n} \langle p \rangle_m^f + \sum_{n=0}^{\infty} \boldsymbol{G}'^{(n)}_m \underbrace{\cdot\cdot}_{(n+1)\text{-times}} \nabla^{\otimes n} \langle \boldsymbol{\tau} \rangle_m^f \\ + \epsilon_{fm}^{-1} \langle \boldsymbol{n}_{fs} \cdot (-\widetilde{p}_f \boldsymbol{I} + \widetilde{\boldsymbol{\tau}}_f)\, \delta_{fs} \rangle_m \,, \end{aligned} \tag{5.42}$$

[3] In our paper [2], the minus sign was erroneously missing.

which corresponds to (2.64). From the result (5.42), it is concluded that a weighting function m is suited for filtering $\boldsymbol{f}_{fs}$, when the geometrical tensors $\boldsymbol{G}_m^{\prime(n)}$ are zero:

$$\boldsymbol{b}'_{fs} = \epsilon_{fm}^{-1} \langle \boldsymbol{n}_{fs} \cdot (-\widetilde{p}_f \boldsymbol{I} + \widetilde{\boldsymbol{\tau}}_f)\, \delta_{fs} \rangle_m \qquad \Leftrightarrow \qquad \boldsymbol{G'}_m^{(n)} = 0\,. \tag{5.43}$$

As this property is always satisfied when $m_G = m_C * m_V$, but depends on the topology of the solid structures for any other form of m_G, the weighting function of Quintard and Whitaker $m = m_C * m_V * m_V$ is thus the most appropriate weighting function for the periodically developed flow regime.

With the weighting function of Quintard and Whitaker, the weighted interfacial force is also given by

$$\boldsymbol{b}'_{fs} = \epsilon_{fm}^{-1} \langle \boldsymbol{n}_{fs} \cdot \left(-p^\star_f \boldsymbol{I} + \widetilde{\boldsymbol{\tau}}_f\right) \delta_{fs} \rangle_m\,. \tag{5.44}$$

The last equality holds, because $\widetilde{p}$ and $p^\star$ differ from each other only in the spatially constant value $\langle p^\star \rangle_m^f = \langle p^\star \rangle^f$ when $m = m_C * m_V * m_V$ (see (5.28)). Similarly, $\widetilde{\boldsymbol{u}}$ and $\boldsymbol{u}$ are equal up to $\langle \boldsymbol{u} \rangle_m^f = \langle \boldsymbol{u} \rangle^f$ (cf. 5.24)).

Lastly, we note that if we drop the condition that $m \in C^\infty$ and choose $m_C = 1$, the weighted interfacial force reduces to

$$\boldsymbol{b}'_{fs} = \epsilon_{fm}^{-1} m_V * \left[\frac{1}{V} \int_{\boldsymbol{r} \in \bar{\Gamma}_{fs}(\boldsymbol{x})} \boldsymbol{n}_{fs} \cdot (-\widetilde{p}_f(\boldsymbol{r},t) \boldsymbol{I} + \widetilde{\boldsymbol{\tau}}_f(\boldsymbol{r},t))\; d\Gamma(\boldsymbol{r}) \right], \tag{5.45}$$

which holds by definition of the Dirac distribution. Under the additional assumption that the flow deviation quantities are periodic, the integral in the former equation is constant over space, which simplifies the former expression to

$$\boldsymbol{b}'_{fs} = \epsilon_f^{-1} \frac{1}{V} \int_{\boldsymbol{r} \in \bar{\Gamma}_{fs}(\boldsymbol{x})} \boldsymbol{n}_{fs} \cdot (-\widetilde{p}_f(\boldsymbol{r},t) \boldsymbol{I} + \boldsymbol{\tau}_f(\boldsymbol{r},t))\; d\Gamma(\boldsymbol{r})\,. \tag{5.46}$$

This expression for the interfacial force is often incorrectly postulated to be exact in the VAT framework, although it is only valid if $m = m_C * m_V * m_V$ and the deviation fields are exactly periodic (cf. (5.32)), as derived here for periodically developed flow.

Because of (5.44), the last result (5.46) implies that the weighted interfacial force corresponds to the integral resistance force $\boldsymbol{F}_{fs}$ on the flow, exerted by a single unit of the solid structures:

$$\boldsymbol{b}'_{fs} = \epsilon_f^{-1} \frac{1}{V_{\text{unit}}} \boldsymbol{F}_{fs} \,, \tag{5.47}$$

with

$$\boldsymbol{F}_{fs} \triangleq \int_{\boldsymbol{r} \in (\Gamma_{fs} \cap \Omega_{\text{unit}})} \boldsymbol{n}_{fs}(\boldsymbol{r}) \cdot \left(-p_f^\star(\boldsymbol{r},t) \boldsymbol{I} + \boldsymbol{\tau}_f(\boldsymbol{r},t) \right) d\Gamma(\boldsymbol{r}) \,. \tag{5.48}$$

Therefore, in the periodically developed regime, correlations for the drag and lift forces, which are the components of $\boldsymbol{F}_{fs}$ respectively parallel and orthogonal to $\langle \boldsymbol{u} \rangle$, can be used to determine the weighted interfacial force. This approach was proposed in studies like [36, 49, 50], although these studies assumed they correlated the interfacial force for the volume-averaged equations instead of the macro-scale flow equations based on the filter $m = m_C * m_V * m_V$.

5.11 Local Closure Problem for Periodically Developed Flow

In Section 5.9, a practical closure strategy for an arbitrary filter with $m = m_G * m_V$ satisfying (3.23) was presented, which relies on solving the periodically developed flow equations for an imposed constant pressure gradient $\nabla \mathrm{P}$ to find $\langle \boldsymbol{u} \rangle$ (or for an imposed value of $\langle \boldsymbol{u} \rangle$ to find $\nabla \mathrm{P}$) and post-processing the space dependent interfacial force $\boldsymbol{b}'_{fs}$ via the macro-scale momentum equations. Hereby, the value of $\langle \overline{p^\star} \rangle$ over the unit cell domain, which is just like $p_0 \triangleq p(\boldsymbol{x}_0, t)$ not known without solving the entire pressure distribution through DNS, can be chosen arbitrary, because $\boldsymbol{b}'_{fs}$ is invariant with respect to the absolute pressure level p_0: $\langle \boldsymbol{n}_{fs} \cdot (-p_0 \boldsymbol{I}) \, \delta_{fs} \rangle_m = -p_0 \nabla \epsilon_{fm} = 0$.

The previous section proposed the particular weighting function $m = m_C * m_V * m_V$ for filtering, which greatly simplifies this closure strategy. Indeed, with this weighting function, the constant interfacial force can be post-processed directly from the solution fields $\boldsymbol{u}_f$ and $p^\star$ of the periodic flow equations through (5.44).

This section explores the possibility of obtaining closure for a filter of the form $m = m_G * m_V$ by solving the closure problem of (3.34) and (3.35), which for unsteady periodically developed flow becomes equivalent to

$$\nabla \cdot \boldsymbol{u}_f = 0\,, \tag{5.49}$$

$$\rho_f \frac{\partial \widetilde{\boldsymbol{u}}_f}{\partial t} + \rho_f \boldsymbol{u}_f \cdot \nabla \boldsymbol{u}_f = -\nabla \widetilde{p}_f + \nabla \cdot \boldsymbol{\tau}_f - \left\{ \boldsymbol{b}'_{fs} \right\}_f + \widetilde{\boldsymbol{f}}_f\,, \tag{5.50}$$

as $\nabla \boldsymbol{u}_f = \nabla \widetilde{\boldsymbol{u}}_f$ and $\nabla \epsilon_{fm} = 0$. The appropriate boundary conditions for this local closure problem are of course still given by (5.22). Note that the sum of equations (5.34) and (5.50) in Ω_f again yields (5.21).

For an arbitrary filter with $m = m_G * m_V$, equations (5.49) and (5.50) are still coupled to the macro-scale flow equation (5.34) as the interfacial force term, $\boldsymbol{b}'_{fs} = \epsilon_{fm}^{-1} \langle \boldsymbol{n}_{fs} \cdot (-p_f \boldsymbol{I} + \boldsymbol{\tau}_f)\, \delta_{fs} \rangle_m$, contains an integral form of the unknowns $\boldsymbol{u}_f$, $\langle p \rangle_m^f$ and $\widetilde{p}_f$ over the whole fluid-solid interface Γ_{fs}.

This dependence of $\boldsymbol{b}'_{fs}$ on the full pressure and velocity distributions for an arbitrary filter makes this closure problem of little interest. First, it abandons the possibility of obtaining a closure relation without solving the macro-scale flow. Second, it requires solving equations (5.49) and (5.50) over the entire fluid domain Ω_f. Lastly, the dependence on the full pressure and velocity distributions causes spatial variations of $\boldsymbol{b}'_{fs}$ as discussed before.

On the other hand, when for periodically developed flow the filter ensures that $\boldsymbol{b}'_{fs} = \epsilon_{fm}^{-1} \langle \boldsymbol{n}_{fs} \cdot (-\widetilde{p}_f \boldsymbol{I} + \widetilde{\boldsymbol{\tau}}_f)\, \delta_{fs} \rangle_m$, equations (5.49) and (5.50) transform into a local closure problem that can be solved a priori on a unit cell of the device domain, independently of the macro-scale flow equations. This local closure problem relates $\boldsymbol{b}'_{fs}$ again to the solution of $\boldsymbol{u}_f$ and $\widetilde{p}_f$ on Ω_{unit}. Unfortunately, in that case, equation (5.50) becomes a complex integro-differential equation, in which the constant closure term $\boldsymbol{b}'_{fs}$ has to be calculated iteratively as a boundary integral around the solid boundary in the unit cell domain.

In the end, even when the appropriate filter function $m = m_C * m_V * m_V$ is used, it remains rather difficult to solve the closure problem for unsteady periodically developed flow in order to correlate $\boldsymbol{b}'_{fs}$ in function of $\langle \boldsymbol{u} \rangle_m^f$ (cf. (5.38)). Instead, it is easier to solve the periodic flow equations (5.21) and (5.22) on a unit cell for an imposed pressure gradient ∇P, and then

determine $\langle \boldsymbol{u} \rangle_m^f$ as well as $\boldsymbol{b}'_{fs}$ by suitable post-processing of the solution fields $\boldsymbol{u}_f$ and $\widetilde{p}_f$.

On the contrary, for steady periodically developed flow, the closure problem does reduce to a very simple form:

$$\nabla \cdot \boldsymbol{u}_f = 0\,, \tag{5.51}$$

$$\rho_f \nabla \cdot \boldsymbol{u}_f \boldsymbol{u}_f = -\nabla \widetilde{p}_f + \nabla \cdot \boldsymbol{\tau}_f - \left\{ \boldsymbol{b}'_{fs} \right\}_f + \widetilde{\boldsymbol{f}}_f\,. \tag{5.52}$$

This steady closure problem allows to easily correlate the closure relation (5.38) for steady periodic flow, at least if we choose $m = m_C * m_V * m_V$. Choosing this weighting function, we only need to solve equations (5.51) and (5.52) for an imposed constant source term $\boldsymbol{b}'_{fs}$ and post-process the corresponding macro-scale velocity $\langle \boldsymbol{u} \rangle_m^f = \langle \boldsymbol{u} \rangle$ from the velocity field $\boldsymbol{u}_f$ on the unit cell. Of course, this closure strategy is fully equivalent to solving the periodically developed flow equations for an imposed pressure gradient, as in that case $\boldsymbol{b}'_{fs} = \nabla \mathrm{P} - \rho_f \boldsymbol{g}$ holds.

5.12 Form of Closure Terms for Steady Periodically Developed Flow

In this section, it is shown that when $m = m_C * m_V * m_V$ and therefore, $\boldsymbol{b}'_{fs} = \epsilon_{fm}^{-1} \langle \boldsymbol{n}_{fs} \cdot (-\widetilde{p}_f \boldsymbol{I} + \widetilde{\boldsymbol{\tau}}_f)\, \delta_{fs} \rangle_m$, the former closure problem for steady periodically developed flow implies that the closure functions (5.38) and (5.39) can be correlated as

$$\boldsymbol{b}'_{fs} = -\mu_f \boldsymbol{K}_m^{-1} \cdot \langle \boldsymbol{u} \rangle_m^f\,, \tag{5.53}$$

$$\boldsymbol{M}' = \langle \boldsymbol{u} \rangle_m^f \cdot \boldsymbol{\Lambda}_m \cdot \langle \boldsymbol{u} \rangle_m^f\,. \tag{5.54}$$

The second-order tensor $\boldsymbol{K}_m^{-1}$ can be called the inverse *weighted permeability* of the solid structure and the fourth-order tensor $\boldsymbol{\Lambda}_m$ represents a *weighted momentum coefficient*. The closure tensors $\boldsymbol{K}_m^{-1}$ and $\boldsymbol{\Lambda}_m$ depend of course on the macro-scale flow direction and magnitude as well as the geometry of the unit cell and the fluid properties, but are spatially constant.

From equations (5.53) and (5.37) it follows that the momentum equation for steady periodically developed flow is also equivalent to

$$-\mu_f \boldsymbol{K}_m^{-1} \cdot \langle \boldsymbol{u} \rangle_m^f = \nabla \mathrm{P} - \rho_f \boldsymbol{g}\,, \tag{5.55}$$

which resembles Darcy's law for flow in porous media. Although $\langle \boldsymbol{u} \rangle_m^f = \langle \boldsymbol{u} \rangle^f$ for periodic flow, the subscript m of the weighted permeability tensor $\boldsymbol{K}_m$ reminds us that this result was governed through use of the weighting function of Quintard and Whitaker [3]. Therefore, it is concluded that for periodic structures, the permeability correlations in literature derived from periodically developed flow equations or experimentally measured pressure drops are compatible within the framework of the weighted spatial averaging technique, but not within the one of the volume averaging technique.

Definition of the Closure Coefficients

The proof of the existence of the closure coefficients $\boldsymbol{K}_m$ and $\boldsymbol{\Lambda}_m$ in (5.53) and (5.54) is analogous to the one given in [55]. It starts with the postulate that there exists a general mapping between the macro-scale velocity and the deviation velocity and pressure for periodically developed flow:

$$\widetilde{\boldsymbol{u}} = \boldsymbol{\Lambda}_{\boldsymbol{u}} \cdot \langle \boldsymbol{u} \rangle_m^f + \widetilde{\boldsymbol{u}}^0\,, \tag{5.56}$$

$$\widetilde{p} = \boldsymbol{\lambda}_p \cdot \langle \boldsymbol{u} \rangle_m^f + \widetilde{p}^0\,. \tag{5.57}$$

Here $\boldsymbol{\Lambda}_{\boldsymbol{u}}$, $\boldsymbol{\lambda}_p$, $\widetilde{\boldsymbol{u}}^0$, $\widetilde{p}^0$ are defined to equal zero in $\Omega_s \cap \Omega_{\mathrm{unit}}$. With a *general* mapping it is understood that the closure variable $\boldsymbol{\Lambda}_{\boldsymbol{u}}$ of the vector-to-vector mapping (5.56) and the closure variable $\boldsymbol{\lambda}_p$ of the vector-to-scalar mapping (5.57) are distributions defined on the unit cell that can depend on the filtered velocity itself, which is the only macro-scale quantity that remains in the local closure problem for periodically developed flow.

It can easily be seen through substitution of (5.56) and (5.57) in (5.51), (5.52), (5.46) and (5.22) that the steady periodic flow equations are satisfied, when the mapping fields are the solution of the following two closure problems in Ω_{unit}, with μ_f constant over $\Omega_f \cap \Omega_{\mathrm{unit}}$:

Closure problem I

$$\nabla^\nu \cdot \boldsymbol{\Lambda_u} = 0\,, \tag{5.58}$$

$$\rho_f \left((\boldsymbol{I} + \boldsymbol{\Lambda_u}) \cdot \langle \boldsymbol{u} \rangle_m^f + \widetilde{\boldsymbol{u}}^0 \right) \cdot \nabla^\nu \boldsymbol{\Lambda_u} = -\nabla^\nu \boldsymbol{\lambda}_p + \mu_f \nabla^\nu \cdot \nabla^\nu \boldsymbol{\Lambda_u} + \epsilon_{fm}^{-1} \langle \boldsymbol{n}_{fs} \cdot \left(\boldsymbol{I} \gamma_f \left\{ \boldsymbol{\lambda}_p \right\}_f - \mu_f \nabla \left\{ \boldsymbol{\Lambda_u} \right\}_f \right) \delta_{fs} \rangle_m\,, \tag{5.59}$$

$$\begin{aligned} \boldsymbol{\Lambda_u}(\boldsymbol{x}) &= \boldsymbol{\Lambda_u}\left(\boldsymbol{x} + \boldsymbol{l}^{(j)}\right) \\ \boldsymbol{\lambda}_p(\boldsymbol{x}) &= \boldsymbol{\lambda}_p\left(\boldsymbol{x} + \boldsymbol{l}^{(j)}\right) \end{aligned} \qquad \boldsymbol{\Lambda_u} = -\boldsymbol{I} \quad \text{on } \Gamma_{fs} \cap \Omega_{\text{unit}}\,, \tag{5.60}$$

and

Closure problem II

$$\nabla \cdot \widetilde{\boldsymbol{u}}^0 = 0\,, \tag{5.61}$$

$$\rho_f \left((\boldsymbol{I}\gamma_f + \boldsymbol{\Lambda_u}) \cdot \langle \boldsymbol{u} \rangle_m^f + \widetilde{\boldsymbol{u}}^0 \right) \cdot \nabla^\nu \widetilde{\boldsymbol{u}}^0 = -\nabla^\nu \widetilde{p}^0 + \mu_f \nabla^\nu \cdot \nabla^\nu \widetilde{\boldsymbol{u}}^0 + \epsilon_{fm}^{-1} \langle \boldsymbol{n}_{fs} \cdot \left(\boldsymbol{I} \widetilde{p}_f^0 - \mu_f \nabla \widetilde{\boldsymbol{u}}_f^0 \right) \delta_{fs} \rangle_m\,, \tag{5.62}$$

$$\begin{aligned} \widetilde{\boldsymbol{u}}^0(\boldsymbol{x}) &= \widetilde{\boldsymbol{u}}^0\left(\boldsymbol{x} + \boldsymbol{l}^{(j)}\right) \\ \widetilde{p}^0(\boldsymbol{x}) &= \widetilde{p}^0\left(\boldsymbol{x} + \boldsymbol{l}^{(j)}\right) \end{aligned} \qquad \widetilde{\boldsymbol{u}}^0 = 0 \quad \text{on } \Gamma_{fs} \cap \Omega_{\text{unit}}\,. \tag{5.63}$$

In Appendix I, it is proven that under the additional constraints

$$\boldsymbol{G'}_m^{(n)} = 0\,, \qquad \langle\, \boldsymbol{\Lambda_u} \rangle_m^f = 0\,, \qquad \langle\, \widetilde{\boldsymbol{u}}^0 \rangle_m^f = 0\,, \tag{5.64}$$

which also impose $\langle \widetilde{\boldsymbol{u}} \rangle_m^f = 0$, it follows that

$$\widetilde{\boldsymbol{u}}^0 = 0\,, \qquad \widetilde{p}^0 = \text{constant}\,. \tag{5.65}$$

The proof presented in Appendix I was already given by Whitaker [55] from a closure problem which implicitly assumes that $\boldsymbol{G}_m^{'(n)} = 0$, which is not guaranteed by the volume-averaging technique. An analogue derivation of this proof starting from the periodically developed flow equations, was published in our work [2].

Consequently, through this proof, the weighted permeability tensor in (5.53) is uniquely defined by closure problem I as

$$\boldsymbol{K}_m^{-1} \triangleq \frac{1}{\mu_f}\epsilon_{fm}^{-1}\langle \boldsymbol{n}_{fs}\cdot(\boldsymbol{I}\boldsymbol{\lambda}_p - \mu_f\nabla\boldsymbol{\Lambda}_{\boldsymbol{u}})\,\delta_{fs}\rangle_m\,. \tag{5.66}$$

Furthermore, closure problem I determines the weighted momentum coefficient in (5.54) as

$$\boldsymbol{\Lambda}_m \triangleq \langle \boldsymbol{\Lambda}_{\boldsymbol{u}}^{\intercal}\boldsymbol{\Lambda}_{\boldsymbol{u}}\rangle_m^f\,. \tag{5.67}$$

Although the permeability representation (5.66) defined here is unique, it must be emphasized that it is not necessarily the only valid representation, because simultaneous satisfaction of closure problem I and II imposes a stronger condition to the deviation fields than the original periodically developed flow equations.

In [55] it is shown that the tensor $\boldsymbol{K}_m^{-1}$ can be decomposed as follows

$$\begin{aligned}\boldsymbol{b}'_{fs} &= -\mu_f\boldsymbol{\mathcal{K}}_m^{-1}\cdot\langle\boldsymbol{u}\rangle_m - \mu_f\boldsymbol{\mathcal{K}}_m^{-1}\cdot\boldsymbol{\mathcal{F}}_m\cdot\langle\boldsymbol{u}\rangle_m\\ &= -\mu_f\boldsymbol{\mathcal{K}}_m^{-1}\cdot\epsilon_{fm}^{-1}\langle\boldsymbol{u}\rangle_m^f - \mu_f\boldsymbol{\mathcal{K}}_m^{-1}\cdot\boldsymbol{\mathcal{F}}_m\cdot\epsilon_{fm}^{-1}\langle\boldsymbol{u}\rangle_m^f\,,\end{aligned} \tag{5.68}$$

where $\boldsymbol{\mathcal{F}}_m$ is the *weighted Forchheimer tensor* and $\boldsymbol{\mathcal{K}}_m$ is the *weighted Darcy permeability* $\boldsymbol{\mathcal{K}}_m$, which are defined so that $\boldsymbol{\mathcal{F}}_m$ becomes zero in the case of Stokes flow. The tensor $\boldsymbol{\mathcal{K}}_m$ is symmetric and independent of $\langle\boldsymbol{u}\rangle_m^f$.

In summary, we have shown in this section that the closure terms in the periodically developed flow regime can be represented by spatially independent *effective parameters*: a permeability tensor and a momentum coefficient tensor. As these effective parameters are defined identically to the effective parameters in the work of Whitaker [55] for flow through porous media, the permeability (and Forchheimer tensor) correlations for porous media, e.g. [59, 60], can be used to determine the interfacial force in periodically developed flow. Furthermore, for developed flow through periodic solid structures, these correlations are exact, even though they hold only approximatively for flow through porous media.

Finally, we would like to remark that the relationship between the macroscale velocity vector and the effective parameters is more difficult to correlate numerically than the interfacial force, as it requires solving closure problem I. Therefore, we believe that knowledge of the interfacial force itself is more of interest, rather than its representation through a permeability tensor.

5.13 Periodically Developed Planar Flow

Unit Cell for a Domain Bounded by Planar Surfaces
Let us consider planar flow through a three-dimensional domain Ω which is partly bounded by two parallel planar surfaces, like in Figure 3.2, and suppose that the solid structures are placed in a periodic configuration between these two planar surfaces. Then, the concept of a unit cell $\Omega_{\text{unit}}(\boldsymbol{x})$ as defined by (5.2) does not exist, when the shape of the array of solid structures changes non-periodically in the direction $\boldsymbol{e}^{(3)}$ perpendicular to both planar surfaces. The reason is that even at any centroid $\boldsymbol{x}$ far from Γ, one cannot identify a third lattice vector parallel to $\boldsymbol{e}^{(3)}$ for which the solid distribution is spatially periodic:

$$\nexists \boldsymbol{l}^{(3)} \in \mathbb{R}^3 \left(\gamma_f \left(\boldsymbol{x} + \boldsymbol{l}^{(3)} \right) = \gamma_f \left(\boldsymbol{x} \right) \rightarrow \boldsymbol{l}^{(3)} \neq 0 \, , \boldsymbol{l}^{(3)} \times \boldsymbol{e}^{(3)} = 0 \right) . \quad (5.69)$$

Yet, it is still possible to define a local unit cell domain $\Omega_{\text{unit}}(\boldsymbol{x})$ in accordance to (5.2) for all positions $\boldsymbol{x}$ lying in the middle plane parallel to both planar surfaces, $\Omega_{x_3=0}$, if we redefine the third lattice vector as

$$\boldsymbol{l}^{(3)} \triangleq l_3 \boldsymbol{e}^{(3)} \, , \quad (5.70)$$

where l_3 is the distance between the two planar surfaces. In that case, the unit cell domain is thus given by

$$\Omega_{\text{unit}}(\boldsymbol{x}_{1,2}) \triangleq \left\{ \boldsymbol{r} \, | \, \exists \, c_j \in \left(-\frac{1}{2}, \frac{1}{2} \right) \Leftrightarrow \boldsymbol{r} = \boldsymbol{x}_{1,2} + \sum_{j=1}^{2} c_j \boldsymbol{l}^{(j)} + c_3 l_3 \boldsymbol{e}^{(3)} \right\} . \quad (5.71)$$

In (5.71), it is understood that $\boldsymbol{l}^{(1)} \cdot \boldsymbol{e}^{(3)} = \boldsymbol{l}^{(2)} \cdot \boldsymbol{e}^{(3)} = \boldsymbol{l}^{(3)} \times \boldsymbol{e}^{(3)} = 0$. When the shape of the array of solid structures changes non-periodically in the direction $\boldsymbol{e}^{(3)}$ perpendicular to both planar surfaces, one can expect the planar flow to become periodically developed over this type of unit cell (5.71). An example of such a unit cell for a channel of a plate-fin heat exchanger is depicted in Figure 5.10.

When the shape of the periodically placed solid structures does change periodically in the direction $\boldsymbol{e}^{(3)}$ perpendicular to both planar surfaces or does not change at all along $\boldsymbol{e}^{(3)}$ (cf. (3.45)), also the concept of a unit cell as defined by (5.2) does exist. One will even be able to find multiple lattice vectors $\boldsymbol{l}^{(3)}$ parallel to $\boldsymbol{e}^{(3)}$, for which the fluid-solid distribution is

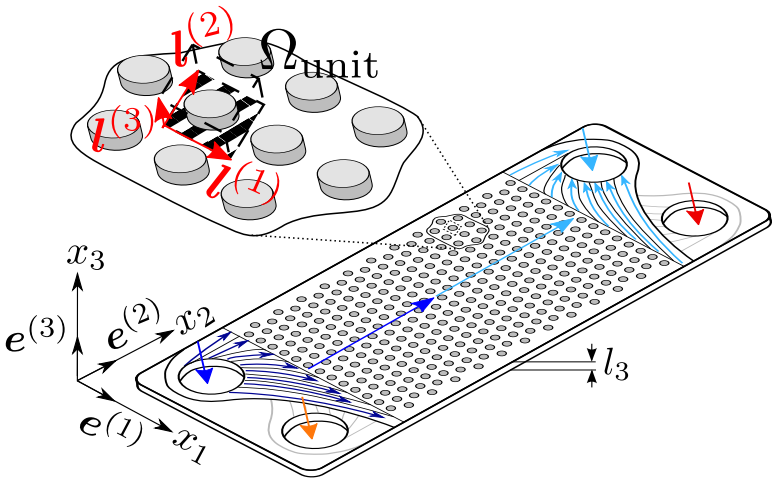

Figure 5.10: Example of a unit cell (dashed lines) and its lattice vectors in a channel of a plate-fin heat exchanger (cf. Figure 1.2).

spatially periodic. However, if the distance l_3 between the planar surfaces is small, planar flow will rarely if ever become periodically developed over such a unit cell. Instead, planar flow can mostly be expected to become periodically developed over a unit cell as defined by (5.71).

Periodically Developed Planar Flow

With the alternative definition (5.71) for the unit cell, periodically developed planar flow is described as in §5.7, except that the flow quantities in planar flow are only periodic with respect to the two lattice vectors $\boldsymbol{l}^{(1)}$ and $\boldsymbol{l}^{(2)}$ at any position $\boldsymbol{x}$. For periodically developed planar flow through a plate channel with height l_3, the flow quantities are the solution of equations (5.21) on the fluid region of the unit cell (5.71) for the following boundary conditions:

$$\begin{aligned} \boldsymbol{u}_f(\boldsymbol{x},t) &= \boldsymbol{u}_f\left(\boldsymbol{x}+\boldsymbol{l}^{(j)},t\right), \\ p_f^\star(\boldsymbol{x},t) &= p_f^\star\left(\boldsymbol{x}+\boldsymbol{l}^{(j)},t\right) \end{aligned} \quad \text{and} \quad \begin{aligned} \boldsymbol{u}_f(\boldsymbol{x},t) &= 0 \quad \boldsymbol{x}\in\Gamma_{fs}\cap\Omega_{\text{unit}}, \\ \boldsymbol{u}_f(\boldsymbol{x},t) &= 0 \quad \boldsymbol{x}\in\Gamma_{fw}\cap\Omega_{\text{unit}}, \end{aligned} \tag{5.72}$$

where $j=\{1,2\}$ and $\boldsymbol{x}\in\Gamma_{fw}\cap\Omega_{\text{unit}} \Leftrightarrow x_3=\pm\frac{l_3}{2}$.

The boundary conditions (5.72) for planar periodically developed flow incorporate the no-slip condition (3.59) at the planar surfaces:

$$\boldsymbol{u}_f\left(\boldsymbol{x}_{1,2}-\frac{1}{2}\boldsymbol{l}^{(3)},t\right)=\boldsymbol{u}_f\left(\boldsymbol{x}_{1,2}+\frac{1}{2}\boldsymbol{l}^{(3)},t\right)=0\,, \tag{5.73}$$

where $\boldsymbol{l}^{(3)}\triangleq l_3\boldsymbol{e}^{(3)}$.

In periodically developed planar flow, the planar velocity $\boldsymbol{v}$ and planar pressure $\mathcal{P}$, as well as the closure terms φ_3 and $\boldsymbol{\Psi}_3$, can be governed by integrating the velocity and pressure solution of (5.21) on a unit cell, in accordance with (3.41) and (3.42).

It should be noted that if the solid structures have the same shape along $\boldsymbol{e}^{(3)}$ and if $\nabla\mathrm{P}\cdot\boldsymbol{e}^{(3)}=0$, the planar velocity and planar pressure can also be obtained approximately by solving the following equations on a two-dimensional subspace of the unit cell, $\Omega_{\mathrm{unit}}\cap\Omega_{x_3=0}$:

$$\begin{aligned}\nabla\cdot\boldsymbol{v}_f&=\{\varphi_3\}_f\,,\\ \rho_f\frac{\partial\boldsymbol{v}_f}{\partial t}+\rho_f\nabla\cdot(\boldsymbol{v}_f\boldsymbol{v}_f)&=-\nabla\mathcal{P}_f^\star-\nabla\mathrm{P}+\nabla\cdot\mu\big[\nabla\boldsymbol{v}_f+(\nabla\boldsymbol{v}_f)^\intercal\big]\\&\quad+\big\{\langle\boldsymbol{f}_{1,2}\rangle_3\big\}_f+\{\boldsymbol{\Psi}_3\}_f\,.\end{aligned} \tag{5.74}$$

with $\{\varphi_3\}_f\simeq 0$ and $\boldsymbol{\Psi}_3\simeq\big(1-\langle\zeta_{\boldsymbol{u}}^2\rangle_3\big)\rho_f\nabla^\nu\cdot(\boldsymbol{v}\boldsymbol{v})+\mu\boldsymbol{v}\left\langle\frac{\partial^2\zeta_{\boldsymbol{u}}}{\partial x_3^2}\right\rangle_3$. These flow equations are to be solved for the boundary conditions

$$\begin{aligned}&\boldsymbol{v}_f(\boldsymbol{x},t)=\boldsymbol{v}_f\left(\boldsymbol{x}+\boldsymbol{l}^{(j)},t\right)\,,\\&\mathcal{P}_f^\star(\boldsymbol{x},t)=\mathcal{P}_f^\star\left(\boldsymbol{x}+\boldsymbol{l}^{(j)},t\right)\end{aligned}\qquad\text{and}\qquad\boldsymbol{u}_f=0\;\;\boldsymbol{x}\in\Gamma_{fs,x_3=0}\cap\Omega_{\mathrm{unit}}\,. \tag{5.75}$$

Bulk Velocity in Periodically Developed Planar Flow

To continue our discussion on periodically developed planar flow, we remark that planar flow through channels without solid structures is often described by means of a bulk flow velocity [10], which determines the mass flow rate through the channel. For channels with spatially periodic solid structures, an analogous bulk velocity can be defined, at least if the main flow direction over time $\boldsymbol{e}_s\triangleq\langle\overline{\boldsymbol{u}}\rangle/\|\langle\overline{\boldsymbol{u}}\rangle\|$ is aligned with one of the vectors $\boldsymbol{l}^{(k)}$ of the unit cell of (5.2) or (5.71):

$$u_b(\boldsymbol{x},t)\triangleq\frac{1}{A^\star}\int_{\boldsymbol{r}\in\bar{\Gamma}^*(\boldsymbol{x})}\boldsymbol{u}(\boldsymbol{r},t)\cdot\boldsymbol{l}^{(k)}\,d\Gamma^*(\boldsymbol{r})\,. \tag{5.76}$$

In (5.76), $A^\star$ corresponds to the cross-sectional area of one side of the unit cell:

$$A^\star \triangleq \int_{\boldsymbol{r}\in\bar{\Gamma}^*(\boldsymbol{x})} d\Gamma^*(\boldsymbol{r}) \tag{5.77}$$

where

$$\bar{\Gamma}^*(\boldsymbol{x}) \triangleq \left\{ \boldsymbol{r} \,|\, \exists\, c_j \in \left[-\frac{1}{2},\frac{1}{2}\right] \Leftrightarrow \boldsymbol{r} = \boldsymbol{x} + \sum_{\substack{j=1\\ j\neq k}}^{\mathrm{n}_j} c_j \boldsymbol{l}^{(j)} \right\}, \tag{5.78}$$

Due to the periodicity of the flow velocity in the periodically developed regime, $u_b(\boldsymbol{x},t)$ is a spatially constant vector, so that we have

$$\langle \boldsymbol{u} \rangle|_{(\boldsymbol{x},t)} = \boldsymbol{e}_s \int_{1/2}^{-1/2} u_b\left(\boldsymbol{x} + c_k \boldsymbol{l}^{(k)}, t\right) dc_k = u_b(t)\boldsymbol{e}_s\,. \tag{5.79}$$

Therefore, the volume-averaged velocity of the unit cell domain $\langle \boldsymbol{u} \rangle$ has a very important physical interpretation: it is the bulk flow velocity which determines the mass flow rate of an incompressible planar flow through a channel.

Macro-Scale Description of Periodically Developed Planar Flow
The macro-scale description of periodically developed planar flow is just like we explained in §5.7, with the difference that for planar flow, the weighting function m_V is based on a unit cell as in (5.71) instead of (5.2). In that case, the volume averaging operator of (5.4) is a partly separable filter with respect to $\boldsymbol{e}^{(3)}$ at $x_3 = 0$:

$$\begin{aligned} &\langle \boldsymbol{\phi} \rangle = \langle \langle \boldsymbol{\phi} \rangle_{1,2} \rangle_3 = \langle \langle \boldsymbol{\phi} \rangle_3 \rangle_{1,2} \\ &\quad \text{with} \qquad m_3'(-y_3) = \frac{1}{l_3}\,\mathrm{rect}\,(y_3) \\ &\qquad\qquad m_{1,2}(-\boldsymbol{y}_{1,2}) = \left\| \boldsymbol{l}^{(1)} \times \boldsymbol{l}^{(2)} \right\|^{-1} \prod_{j=1}^{2} \mathrm{rect}\left(\frac{\boldsymbol{y}_{1,2} \cdot \boldsymbol{l}^{(j)}}{\|\boldsymbol{l}^{(j)}\|^2} \right). \end{aligned} \tag{5.80}$$

The integration intervals (cf. (2.27)) for the above filter are $I_3 = \left[-\frac{l_3}{2}, \frac{l_3}{2}\right]$ and $\bar{\Omega}_{1,2} = \Omega_{\mathrm{unit}}(\boldsymbol{x}_{1,2}) = \left\{ \boldsymbol{y}_{1,2} = c_1 \boldsymbol{l}^{(1)} + c_2 \boldsymbol{l}^{(2)} | c_j \in I_3 \right\}$.

Also, the double volume-averaging operator with $m = m_V * m_V$ is in that case a partly separable filter with respect to $\boldsymbol{e}^{(3)}$ and for the unit cell (5.71) at $x_3 = 0$ it takes the form

$$\begin{aligned} \langle\boldsymbol{\phi}\rangle_m &= \langle\langle\boldsymbol{\phi}\rangle\rangle = \langle\langle\boldsymbol{\phi}\rangle_{1,2}\rangle_3 = \langle\langle\boldsymbol{\phi}\rangle_3\rangle_{1,2} \\ \text{with} \qquad m_3'(-y_3) &= \frac{1}{l_3}\,\mathrm{rect}\,(y_3) \\ m_{1,2}(-\boldsymbol{y}_{1,2}) &= \prod_{j=1}^{2} \frac{\|\boldsymbol{l}^{(j)}\|^2 - |\boldsymbol{y}_{1,2}\cdot\boldsymbol{l}^{(j)}|}{\|\boldsymbol{l}^{(1)}\times\boldsymbol{l}^{(2)}\|\|\boldsymbol{l}^{(j)}\|^2}\,\mathrm{rect}\left(\frac{\boldsymbol{y}_{1,2}\cdot\boldsymbol{l}^{(j)}}{2\|\boldsymbol{l}^{(j)}\|^2}\right). \end{aligned} \tag{5.81}$$

The integration intervals (cf. (2.27)) for the double volume average are $I_3 = \left[-\frac{l_3}{2}, \frac{l_3}{2}\right]$ and $\bar{\Omega}_{1,2} = \left\{\boldsymbol{y}_{1,2}|\ |\boldsymbol{y}_{1,2}\cdot\boldsymbol{l}^{(j)}| \le \|\boldsymbol{l}^{(j)}\|^2\right\}$.

Because the filters (5.80) and (5.81) are separable, the macro-scale velocity and pressure equal the macro-scale planar velocity and pressure when $\boldsymbol{u}\cdot\boldsymbol{e}^{(3)} = 0$ (cf. (3.75) and (3.76)).

We remark that for both of the former separable filters (5.80) and (5.81), two closure terms are zero in the planar flow equations, $\boldsymbol{\Psi}_3^{\mathrm{II}} = \varphi_3 = 0$, because m_3 is independent of y_3 and because the no-slip condition (3.59) holds (see also (D.5), (D.17) and (D.18)).

5.14 Macro-Scale Flow through a Cylindrical Tube Array

In this part, the macro-scale description of periodically developed flow is illustrated for the steady flow through an array of N cylindrical tubes. This case study serves to underline the importance of the filter technique from the former sections, for adequate modelling of realistic heat transfer devices with periodic solid structures.

In this case study, the flow field is considered to be two-dimensional with the main flow direction along the x-axis of the reference frame, while the y-axis is perpendicular to the main flow. The device domain and its geometrical parameters are depicted in Figure 5.11. The geometrical parameters are the cylinder diameter d, the horizontal and vertical cylinder

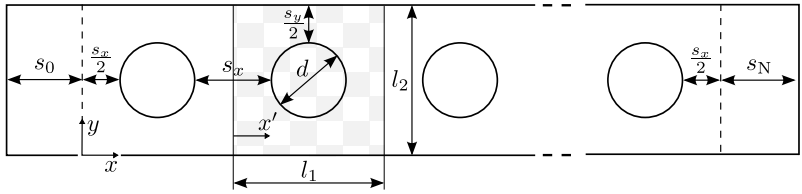

Figure 5.11: Device Domain, geometry of cylinder array and unit cell.

spacing s_x and s_y, the positions of the first and last cylinder, s_0 and s_N respectively, and the lattice sizes l_1, l_2 of a periodic unit cell. Table 5.1 summarizes the values for the parameters of the device domain and unit cell in this case study, as well as the flow parameters.

Geometry array		**Regime**	
s_x/d	1	Re	10
s_y/d	1		
s_0/d	1		
s_N/d	1		
N	5		

Table 5.1: Flow through a Cylindrical Tube Array: Case study parameters.

As boundary condition at the inlet and outlet of the device domain, the total pressure drop Δp over the tube array in the main stream direction is specified. At the solid cylinder boundaries, the no slip condition is imposed. On the other domain boundaries, symmetry boundary conditions for the velocity and pressure distributions are specified.

The pressure and velocity distributions are filtered assuming periodicity over the symmetry boundaries. Upstream of the entrance, the flow velocity and pressure are taken equal to the inlet conditions, while downstream of the outlet of the device domain, they are assumed to stay equal to the outlet conditions. This extension of the velocity and pressure avoids the commutation error of §2.15 and makes it possible to use the discrete filtering technique of [2]. As a consequence of this extension, all filtered quantities vary only in the x-direction over the cylinder array.

Figure 5.12 shows the volume-averaged fluid indicator, denoted by $\epsilon_f \triangleq \langle \gamma_f \rangle$, which represents in matter of fact the local porosity of the cylinder array. Also the weighted porosity ϵ_{fm} is visible in Figure 5.12. Both the weighted porosity ϵ_{fm} and local porosity ϵ_f equal the constant porosity of the unit cell over the largest part of the domain:

$$\epsilon_{fm} \simeq \epsilon_f \simeq 1 - \frac{\pi d^2}{4 l_1 l_2}\,, \tag{5.82}$$

as the solid structures are spatially periodic everywhere, apart from the cylinders near the inlet and outlet region.

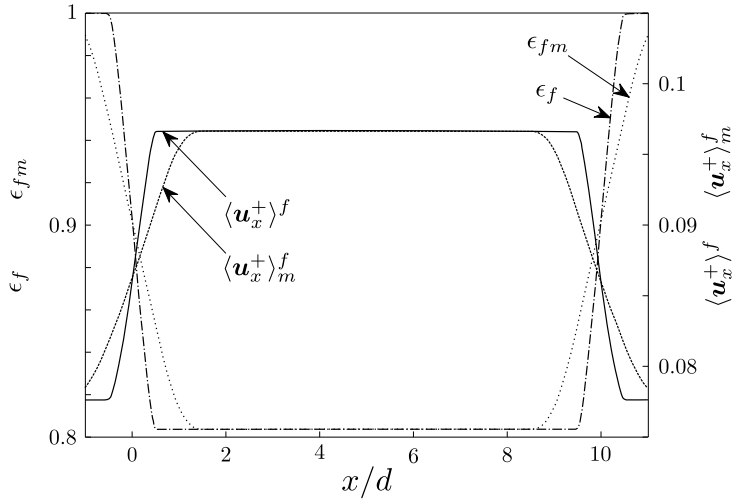

Figure 5.12: Filtered fluid indicator and filtered dimensionless velocity in streamwise direction.

The difference between ϵ_{fm} and ϵ_f near the entrance and outlet regions translates into a difference between the intrinsic weighted average velocity $\langle \boldsymbol{u}^+ \rangle_m^f$ and the intrinsic volume averaged velocity $\langle \boldsymbol{u}^+ \rangle^f$ in Figure 5.12. This difference near the inlet and outlet is not present between the superficially averaged velocities $\langle \boldsymbol{u}^+ \rangle_m^f$ and $\langle \boldsymbol{u}^+ \rangle^f$. The superficially averaged velocities are both quasi constant and equal over the entire domain. This is a consequence of the fact that hydraulic entrance effects disappear quickly downstream for the low Reynolds number in this case study:

$\mathrm{Re} \triangleq \frac{\rho_f U_{\mathrm{ref}}\, d}{\mu} = 10$, causing the laminar flow to become periodically developed already after the first cylinder.

We note that the dimensionless velocity distribution in Figure 5.12 is defined as $\boldsymbol{u}^+ \triangleq \frac{\boldsymbol{u}}{U_{\mathrm{ref}}}$, where $U_{\mathrm{ref}} \triangleq \sqrt{\frac{\Delta p}{\rho_f}}$ and consists only of a component along the x-axis after filtering.

In terms of the filtered velocity and porosity, the weighted spatial averaging technique and volume averaging technique yield similar results, because both filter techniques respect (5.7). On the contrary, the effect of the weighting function on the pressure distribution is more pronounced.

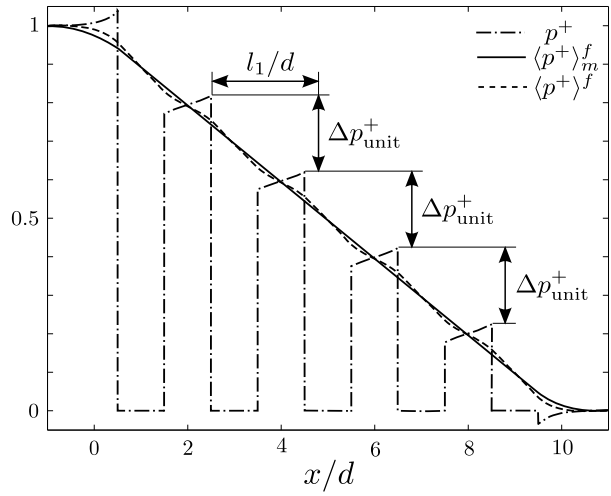

Figure 5.13: Filtered dimensionless pressure distributions at the centreline of the cylinder array.

Figure 5.13 shows the dimensionless pressure profile $p^+ \triangleq \frac{p}{\Delta p}$ at the centreline of the device domain. It illustrates how the pressure builds up strongly in front of each cylinder, as the flow in this zone is blocked by the cylinder. Immediately after each cylinder, the pressure seems to rise again. Nevertheless, a very short wake zone exists behind each cylinder, where the pressure is low and pressure gradients are small. This wake zone is nearly invisible in this low Reynolds number flow regime.

The pressure within the solid cylinders is arbitrary set to zero, as in (2.5). This convention simplifies the mathematical form and physical interpretation of the spatially averaged flow equations.

Figure 5.13 exposes that as soon as the flow is periodically developed after the first cylinder, the (dimensionless) pressure drop $\Delta p^{+}_{\text{unit}}$ over each cylinder unit is the same. The pressure distribution then contains a part that varies linearly in the stream direction with a constant gradient $\nabla \mathrm{P} = \frac{-\Delta p_{\text{unit}}}{l_1} \boldsymbol{e}_x$.

Also the volume averaged pressure $\langle p^{+} \rangle^f$ and the filtered pressure $\langle p^{+} \rangle^f_m$ with $m = m_V * m_V$ are compared in Figure 5.13. It is clear that the gradient of the weighted average pressure $\nabla \langle p \rangle^f_m$ equals the constant physical pressure gradient $\nabla \mathrm{P}$ where the flow is periodically developed. The gradient of the volume averaged pressure $\nabla \langle p^{+} \rangle^f$, on the other hand, is not free of small-scale fluctuations. The volume averaged pressure profile $\langle p^{+} \rangle^f$ oscillates around the smooth profile of $\langle p^{+} \rangle^f_m$. The small-scale pressure fluctuations of $\langle p^{+} \rangle^f$ are present because the volume averaging filter does not smooth away the contributions of the geometrical tensors in (5.42).

The amplitude of these small-scale pressure oscillations for fully periodic flow is determined by the first spatial moment of the cylinder array:

$$\frac{\langle p \rangle^f - \langle p \rangle^f_m}{\nabla P \cdot \boldsymbol{e}_x} = \langle (\boldsymbol{r} - \boldsymbol{x})\, \gamma_f \rangle^f \cdot \boldsymbol{e}_x \,. \tag{5.83}$$

This first spatial moment varies over the unit cell domain as

$$\langle (\boldsymbol{r} - \boldsymbol{x})\, \gamma_f \rangle^f \cdot \boldsymbol{e}_x = \begin{cases} \frac{1-\epsilon_f}{\epsilon_f} x' & x' \in \left[0, \frac{l_1 - d}{2}\right] \\ \frac{1-\epsilon_f}{\epsilon_f} \left(x' + \frac{\xi \sqrt{1-\xi^2} - \arccos(\xi)}{\pi} l_1 \right) & x' \in \left[\frac{l_1 - d}{2}, \frac{l_1 + d}{2}\right] \\ \frac{1-\epsilon_f}{\epsilon_f} (x' - l_1) & x' \in \left[\frac{l_1 + d}{2}, l_1\right] \end{cases} \tag{5.84}$$

where $\xi \triangleq \frac{2}{d} \left(\frac{l_1}{2} - x' \right)$.

From the expressions for the first spatial moment, it can be concluded that the small-scale pressure oscillations introduced by the volume averaging technique will increase with decreasing porosity. For structures similar to closely packed cylinders, the volume averaging technique thus requires a fine mesh resolution when an accurate discrete representation of $\langle p \rangle^f$ is desired. The opposite is true for the weighting function $m = m_V * m_V$.

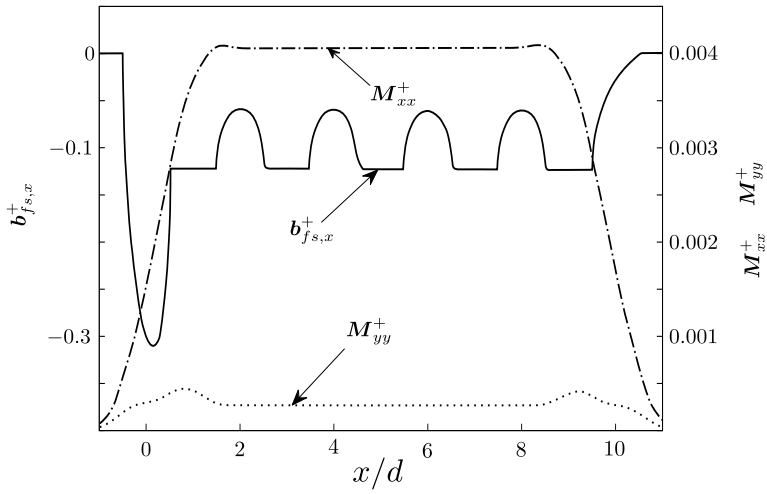

Figure 5.14: Dimensionless closure terms in case $m = m_V$: $\boldsymbol{b}^+_{fs,x}$ (solid line), $\boldsymbol{M}^+_{xx}$ (dash-dot line) and $\boldsymbol{M}^+_{yy}$ (dotted line).

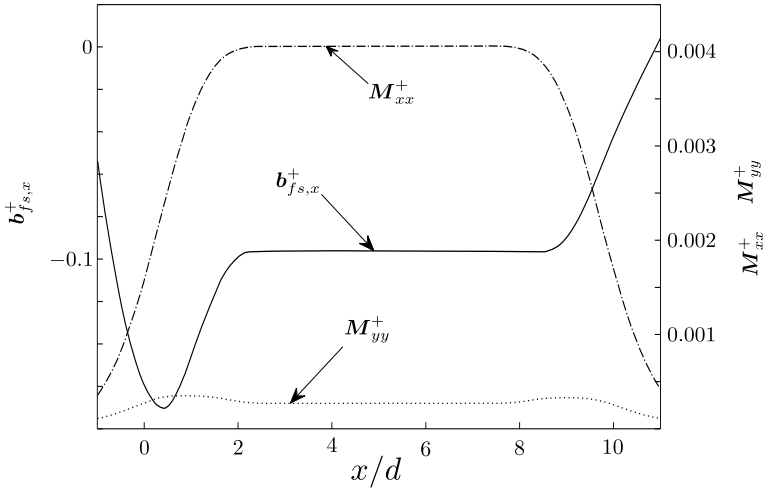

Figure 5.15: Dimensionless closure terms in case $m = m_V * m_V$: $\boldsymbol{b}^+_{fs,x}$ (solid line), $\boldsymbol{M}^+_{xx}$ (dash-dot line) and $\boldsymbol{M}^+_{yy}$ (dotted line).

The double volume average suppresses the effect of spatial moments on $\langle p \rangle_m^f$ for any type of structure and therefore allows a coarser mesh over the part of the system domain where the results of DNS are determined by the physics of periodically developed flow.

In case the volume averaging technique is chosen for the macro-scale description, the dimensionless closure terms for the spatially averaged flow equations are shown in Figure 5.14. The volume averaged interfacial force $\boldsymbol{b}_{fs}^{+} \triangleq \frac{\boldsymbol{b}'_{fs} d}{\rho_f U_{\text{ref}}^2}$ is directed along the x-axis and the volume averaged momentum dispersion source $\boldsymbol{M}^{+} \triangleq \frac{\boldsymbol{M}'}{U_{\text{ref}}^2}$ is a diagonal tensor with components $\boldsymbol{M}_{xx}^{+}$ and $\boldsymbol{M}_{yy}^{+}$, because the macro-flow is directed along the x-axis and the centreline of the tube array is a symmetry-line of the flow. Figure 5.14 reveals the major shortcoming of the volume averaging technique for modelling flow in periodic solid structures. Indeed, the interfacial force term is not constant over the unit cell domain, even where the flow is periodically developed.

On the contrary, the weighted averaging technique of Quintard and Whitaker, does yield constant closure terms for periodically developed flow, as illustrated by Figure 5.15. The value of the weighted momentum dispersion source in the periodically developed flow regime equals that of the volume averaged momentum dispersion source in Figure 5.14. Moreover, the value of the weighted interfacial force in Figure 5.15 corresponds to the volume averaged value of the volume averaged interfacial force in Figure 5.14.

Finally, Figure 5.16 and Figure 5.17 show the velocity and pressure deviation profiles in the neighbourhood of the third cylinder, which are obtained through direct numerical simulation of the flow field in the full tube array. As expected, these profiles of $\boldsymbol{u}^{+}$ and $\tilde{p}^{+}$ for $m = m_V * m_V$ match perfectly with the profiles that are governed from solving the closure problem (5.49) and (5.50) for the imposed constant weighted interfacial force $\boldsymbol{b}_{fs,x}^{+}$ in the periodic flow regime, because the flow is indeed periodically developed in the region of this cylinder. If the volume averaging technique would have been chosen, we should have imposed the space dependent volume averaged interfacial force in order to recover the corresponding pressure deviation field for the volume averaged pressure. This pressure deviation field would have looked different from $\tilde{p}^{+}$ in Figure 5.17.

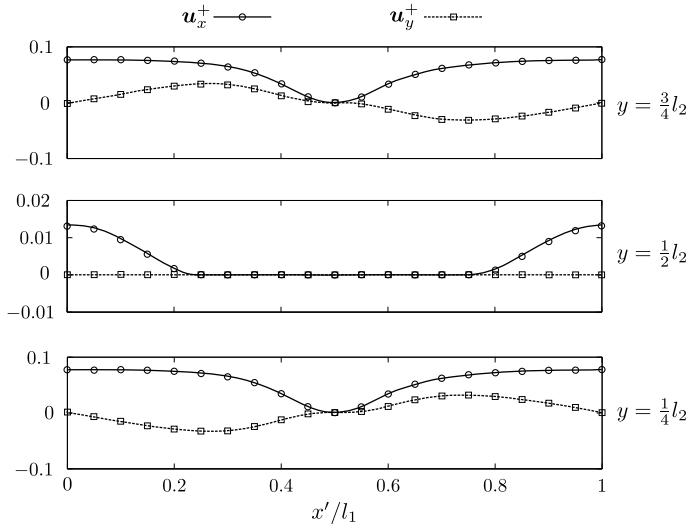

Figure 5.16: Comparison of velocity profiles around third cylinder (solid and dashed lines) with unit cell simulation (circle and square markers).

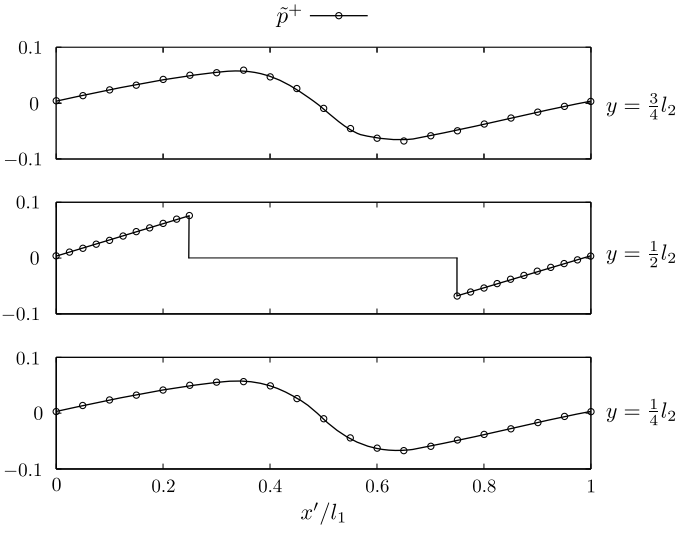

Figure 5.17: Comparison of pressure deviation profiles around third cylinder (solid lines) with unit cell simulation (circle markers).

5.15 Conclusions

The volume averaging technique (VAT) complicates the determination of the closure terms for periodically developed flow, as it leads to a space dependent volume-averaged pressure gradient and interfacial force. The reason for this space dependence lies in the spatial moments of the solid structure, which interact with the volume filter. Nevertheless, the space dependence of the closure terms and volume-averaged pressure gradient has been disregarded by previous studies and VAT is often erroneously employed to describe the macro-scale flow in heat transfer devices with periodic structures.

The spatial averaging technique with the weighting function of Quintard and Whitaker [3] on the other hand strongly simplifies the closure problem. For periodically developed flow, it leads to a spatially constant weighted interfacial force and momentum dispersion source. The weighted interfacial force can be post-processed from the correlation between the constant pressure gradient and volume averaged velocity on a periodic unit cell. In addition, the weighted interfacial force can be represented through a spatially constant permeability tensor.

To the authors' knowledge, the spatially averaged form of the full Navier-Stokes equations, as well as the choice of the averaging technique in light of periodically developed flow, have thus far not been presented that explicitly.

Bibliography

[1] G. Buckinx and M. Baelmans, "Towards a general spatial averaging procedure for multi-scale modeling in heat transfer devices with repetitive fin structures," in *Proceedings of the 15th International Heat Transfer Conference, IHTC-15*, no. 1234, (Kyoto), August 2014.

[2] G. Buckinx and M. Baelmans, "Multi-scale modelling of flow in periodic solid structures through spatial averaging," *Journal of Computational Physics*, vol. 291, pp. 34–51, 2015.

[3] M. Quintard and S. Whitaker, "Transport in ordered and disordered porous media II: Generalized volume averaging," *Transport in Porous Media*, vol. 14, no. 2, pp. 179–206, 1994.

[4] N. Tatsuo, M. Shinichiro, A. Shingho, and K. Yuji, "Flow observations and mass transfer characteristics in symmetrical wavy-walled channels at moderate reynolds numbers for steady flow," *International Journal of Heat and Mass Transfer*, vol. 33, no. 5, pp. 835 – 845, 1990.

[5] D. Koch and A. Ladd, "Moderate Reynolds number flows through periodic and random arrays of aligned cylinders," *Journal of Fluid Mechanics*, vol. 349, pp. 31–66, 1997.

[6] G. Comini, C. Nonino, and S. Savino, "Effect of aspect ratio on convection enhancement in wavy channels," *Numerical Heat Transfer, Part A: Applications*, vol. 44, no. 1, pp. 21–37, 2003.

[7] Shah, R.K. and London, A.L., *Advances in Heat Transfer: laminar flow forced convection in ducts : a source book for compact heat exchanger analytical data*. New York: Academic Press, Inc., 1978.

[8] V. O'Brien, "Pulsatile fully developed flow in rectangular channels," *Journal of the Franklin Institute*, vol. 300, no. 3, pp. 225 – 230, 1975.

[9] S. Ray, B. Ünsal, F. Durst, O. Ertunc, and O. Bayoumi, "Mass flow rate controlled fully developed laminar pulsating pipe flows," *Journal of Fluids Engineering*, vol. 127, no. 3, pp. 405–418, 2005.

[10] S. V. Patankar, C. H. Liu, and E. M. Sparrow, "Fully Developed Flow and Heat Transfer in Ducts Having Streamwise-Periodic Variations of Cross-Sectional Area," *Journal of Heat Transfer*, vol. 99, no. 2, p. 180, 1977.

[11] A. Yutaka, N. Hiroshi, and M. Faghri, "Heat transfer and pressure drop characteristics in a corrugated duct with rounded corners," *International Journal of Heat and Mass Transfer*, vol. 31, no. 6, pp. 1237 – 1245, 1988.

[12] J. Zhang, J. Kundu, and R. M. Manglik, "Effect of fin waviness and spacing on the lateral vortex structure and laminar heat transfer in wavy-plate-fin cores," *International Journal of Heat and Mass Transfer*, vol. 47, pp. 1719–1730, Apr. 2004.

[13] H. Metwally and R. Manglik, "Enhanced heat transfer due to curvature-induced lateral vortices in laminar flows in sinusoidal corrugated-plate channels," *International Journal of Heat and Mass Transfer*, vol. 47, no. 1011, pp. 2283 – 2292, 2004.

[14] R. M. Manglik, J. Zhang, and A. Muley, "Low Reynolds number forced convection in three-dimensional wavy-plate-fin compact channels: fin density effects," *International Journal of Heat and Mass Transfer*, vol. 48, no. 8, pp. 1439 – 1449, 2005.

[15] G.-N. Xie, Q.-W. Wang, M. Zeng, and L.-Q. Luo, "Numerical investigation of heat transfer and fluid flow characteristics inside a wavy channel," *Heat and Mass Transfer*, vol. 43, pp. 603–611, July 2006.

[16] G.-N. Xie, Q.-W. Wang, M. Zeng, and L.-Q. Luo, "Numerical investigation of heat transfer and fluid flow characteristics inside a wavy channel: erratum," *Heat and Mass Transfer*, vol. 43, pp. 721–721, Feb. 2007.

[17] O. P. Arsenyeva, L. L. Tovazhnyanskyy, P. O. Kapustenko, and O. V. Demirskiy, "Heat transfer and friction factor in criss-cross flow channels of plate-and-frame heat exchangers," *Theoretical Foundations of Chemical Engineering*, vol. 46, no. 6, pp. 634–641, 2012.

[18] E. Utriainen and B. Sundén, "Numerical analysis of a primary surface trapezoidal cross wavy duct," *International Journal of Numerical Methods for Heat & Fluid Flow*, vol. 10, no. 6, pp. 634–648, 2000.

[19] E. Utriainen and B. Sundén, "A numerical investigation of primary surface rounded cross wavy ducts," *Heat and Mass Transfer*, vol. 38, no. 7, pp. 537–542, 2002.

[20] G.-Y. Zhou, S.-T. Tu, and H.-G. Ma, "Investigations of heat transfer and friction characteristics of compact cross-corrugated recuperators," *Heat and Mass Transfer*, vol. 50, no. 9, pp. 1301–1310, 2014.

[21] G. Wang and S. Vanka, "Convective heat transfer in periodic wavy passages," *International Journal of Heat and Mass Transfer*, vol. 38, no. 17, pp. 3219 – 3230, 1995.

[22] G. Comini, C. Nonino, and S. Savino, "Effect of space ratio and corrugation angle on convection enhancement in wavy channels," *International Journal of Numerical Methods for Heat & Fluid Flow*, vol. 13, no. 4, pp. 500–519, 2003.

[23] M. Ciofalo, J. Stasiek, and M. Collins, "Investigation of flow and heat transfer in corrugated passages II. Numerical simulations," *International Journal of Heat and Mass Transfer*, vol. 39, no. 1, pp. 165 – 192, 1996.

[24] "Offset fin, n.d. photograph, viewed 13 september 2016, http://ohioheattransfer.com/categories/engineering-solutions-core-designs/engineering-solutions-core-fin-patterns/.."

[25] N. Sahiti, *Thermal and Fluid Dynamic Performance of Pin Fin Heat Transfer Surfaces*. PhD thesis, Der Technischen Fakultät der Universität Erlangen-Nürnberg zur Erlangung des Grades, 2006.

[26] S. Kandlikar, S. Colin, Y. Peles, and et al., "Heat transfer in microchannels 2012 status and research needs," *Journal of Heat Transfer*, vol. 135, no. 9, 2013.

[27] H. Bhowmik and K.-S. Lee, "Analysis of heat transfer and pressure drop characteristics in an offset strip fin heat exchanger," *International Communications in Heat and Mass Transfer*, vol. 36, pp. 259–263, Mar. 2009.

[28] M.-S. Kim, J. Lee, S.-J. Yook, and K.-S. Lee, "Correlations and optimization of a heat exchanger with offset-strip fins," *International Journal of Heat and Mass Transfer*, vol. 54, no. 9-10, pp. 2073–2079, 2011.

[29] D. Soodphakdee, M. Behnia, and D. W. Copeland, "A Comparison of Fin Geometries for Heatsinks in Laminar Forced Convection: Part I - Round, Elliptical, and Plate Fins in Staggered and In-Line Configurations," *The International Journal of Microcircuits and Electronic Packaging*, vol. 24, no. 1, pp. 68–76, 2001.

[30] D. A. Edwards, M. Shapiro, P. Bar-Yoseph, and M. Shapira, "The influence of reynolds number upon the apparent permeability of spatially periodic arrays of cylinders," *Physics of Fluids A*, vol. 2, no. 1, pp. 45–55, 1990.

[31] A. Martin, C. Saltiel, and W. Shyy, "Frictional losses and convective heat transfer in sparse, periodic cylinder arrays in cross flow," *International Journal of Heat Mass Transfer*, vol. 41, pp. 2383–2397, 1998.

[32] T. D. Papathanasiou, B. Markicevic, and E. D. Dendy, "A computational evaluation of the ergun and forchheimer equations for fibrous porous media," *Physics of Fluids*, vol. 13, no. 10, pp. 2795–2804, 2001.

[33] C. K. Ghaddar, "On the permeability of unidirectional fibrous media: A parallel computational approach," *Physics of Fluids*, vol. 7, no. 11, pp. 2563–2586, 1995.

[34] G. Hellström and S. Lundström, "Flow through porous media at moderate reynolds number," in *Proceedings, 4th International Scientific Colloquium Modelling for Material Processing*, pp. 129–134, International Scientific Colloquium Modelling for Material Processing, Riga, June 8-9, 2006, 2006.

[35] A. Tamayol and M. Bahrami, "Transverse permeability of fibrous porous media," *Physical Review E*, vol. 83, p. 046314, Apr 2011.

[36] S. A. Mattis, C. N. Dawson, C. E. Kees, and M. W. Farthing, "Numerical modeling of drag for flow through vegetated domains and porous structures," *Advances in Water Resources*, vol. 39, pp. 44 – 59, 2012.

[37] A. Nakayama, F. Kuwahara, T. Umemoto, and T. Hayashi, "Heat and fluid flow within an anisotropic porous medium," *Journal of Heat Transfer*, vol. 124, pp. 746–753, 2002.

[38] A. Nakayama, F. Kuwahara, and T. Hayashi, "Numerical modelling for three-dimensional heat and fluid flow through a bank of cylinders in yaw," *Journal of Fluid Mechanics*, vol. 498, pp. 139–159, 2004.

[39] A. Alshare, P. Strykowski, and T. Simon, "Modeling of unsteady and steady fluid flow, heat transfer and dispersion in porous media using unit cell scale," *International Journal of Heat and Mass Transfer*, vol. 53, pp. 2294–2310, 2010.

[40] R. Manglik, O. Huzayyin, and M. Jog, "Fin effects in flow channels of plate-fin compact heat exchanger cores," *Journal of Thermal Science and Engineering Applications*, vol. 3, no. 4, 2011.

[41] S. G. Kandlikar and W. J. Grande, "Evolution of microchannel flow passages & thermohydraulic performance and fabrication technology," in *Proceedings of IMECE2002, ASME International Mechanical Engineering Congress & Exposition, November 17-22, 2002, New Orleans, Louisiana*, no. 32043, 2002.

[42] P.-S. Lee and S. V. Garimella, "Thermally developing flow and heat transfer in rectangular microchannels of different aspect ratios," *International Journal of Heat and Mass Transfer*, vol. 49, no. 1718, pp. 3060 – 3067, 2006.

[43] W. M. Kays and A. L. London, *Compact Heat Exchangers.* Krieger Pub Co, 1998.

[44] R. K. Shah and D. P. Sekuli, *Fundamentals of Heat Exchanger Design.* Hoboken, NJ, USA: John Wiley & Sons, Inc., July 2003.

[45] S. Kim, D. Kim, and D. Lee, "On the local thermal equilibrium in microchannel heat sinks," *International Journal of Heat and Mass Transfer*, vol. 43, no. 10, pp. 1735 – 1748, 2000.

[46] C.-H. Chen, "Forced convection heat transfer in microchannel heat sinks," *International Journal of Heat and Mass Transfer*, vol. 50, no. 1112, pp. 2182 – 2189, 2007.

[47] T.-M. Jeng and S.-C. Tzeng, "A semi-empirical model for estimating permeability and inertial coefficient of pin-fin heat sinks," *International Journal of Heat and Mass Transfer*, vol. 48, no. 15, pp. 3140 – 3150, 2005.

[48] T.-M. Jeng, "A porous model for the square pin-fin heat sink situated in a rectangular channel with laminar side-bypass flow," *International Journal of Heat and Mass Transfer*, vol. 51, no. 910, pp. 2214 – 2226, 2008.

[49] A. Horvat and I. Catton, "Numerical technique for modeling conjugate heat transfer in an electronic device heat sink," *International Journal of Heat and Mass Transfer*, vol. 46, pp. 2155–2168, 2003.

[50] A. Horvat and B. Mavko, "Hierarchic modeling of heat transfer processes in heat exchangers," *International Journal of Heat and Mass Transfer*, vol. 48, pp. 361–371, 2005.

[51] A. Alshare, P. Strykowski, and T. Simon, "Simulations of flow and heat transfer in a serpentine heat exchanger having dispersed resistance with porous-continuum and continuum models," *International Journal of Heat and Mass Transfer*, vol. 53, pp. 1088 – 1099, 2010.

[52] I. Catton, "Transport phenomena in heterogeneous media based on volume averaging theory," *Heat Mass Transfer*, vol. 42, pp. 537–551, 2006.

[53] F. Zhou, N. E. Hansen, D. J. Geb, and I. Catton, "Obtaining Closure for Fin-and-Tube Heat Exchanger Modeling Based on Volume Averaging Theory (VAT)," *J. Heat Transfer*, vol. 133, p. 111802, 2011.

[54] F. Zhou and I. Catton, "Obtaining closure for a plane fin heat sink with elliptic scale-roughened surfaces for Volume Averaging Theory (VAT) based modeling," *International Journal of Thermal Sciences*, vol. 71, pp. 264–273, 2013.

[55] S. Whitaker, "The Forchheimer equation: A theoretical development," *Transport in Porous Media*, vol. 25, no. 1, pp. 27–61, 1996.

[56] P. M. Adler, *Porous media: Geometry and transport*. Butterworth-Heinemann, Stoneham, 1992.

[57] G. Buckinx and M. Baelmans, "Macro-scale heat transfer in periodically developed flow through isothermal solids," *Journal of Fluid Mechanics*, vol. 780, pp. 274–298, 009 2015.

[58] C. Kang and K.-S. Yang, "Flow instability in baffled channel flow," *International Journal of Heat and Fluid Flow*, vol. 38, pp. 40 – 49, 2012.

[59] D. Lasseux, A. A. Abbasian Arani, and A. Ahmadi, "On the stationary macroscopic inertial effects for one phase flow in ordered and disordered porous media," *Physics of Fluids*, vol. 23, no. 7, 2011.

[60] C. DeGroot and A. Straatman, "Numerical results for the effective flow and thermal properties of idealized graphite foam," *Journal of Heat Transfer*, vol. 134, no. 4, p. 042603, 2012.

CHAPTER

6

MACRO-SCALE DESCRIPTION OF PERIODICALLY DEVELOPED HEAT TRANSFER IN ISOTHERMAL SOLID STRUCTURES

6.1 Introduction

This chapter gives an exact and physically meaningful macro-scale description of the laminar periodically developed heat transfer regime in isothermal solids. Parts of this chapter are published in [1]. In this chapter, the governing equations for the periodically developed heat transfer regime in isothermal solids are derived. It is shown that the appropriate macro-scale temperature in the periodically developed heat transfer regime is obtained by averaging the temperature with a specific weighting function which is adapted to the temperature decay rate. This matched weighting function allows the representation of the macro-scale interfacial

heat transfer and thermal dispersion source by means of a spatially constant interfacial heat transfer coefficient and thermal dispersion vector, which both can be calculated from the periodic rescaled temperature on a unit cell of the solid structures. Moreover, it is proved that for small temperature decay rates, the matched weighting function yields the same macro-scale description as repeated volume averaging. The theoretical framework of this chapter is applied to a case study, describing the heat transfer between a fluid and an array of solid cylinders at constant temperature.

6.2 Outline

This chapter first gives a qualitative description of (periodically) developed heat transfer in devices with spatially periodic isothermal solid structures. In the next section, Section 4, some historical background information is given on the periodically developed heat transfer under isothermal conditions and its macro-scale description in the literature is re-examined. Subsequently, in Section 5, the definition of the developed heat transfer regime, which has already been given for channel flow [2–4], is extended towards flow through isothermal periodic solids. The generalization of this definition requires a reference temperature with a constant decay rate. Also, the eigenvalue problem which determines the decay rate of the reference temperature is derived. From the knowledge of the decay rate, the appropriate weighting function for the spatially averaged temperature is constructed in Section 6. In Section 7, this weighting function is used to obtain a simple representation of the thermal closure terms in the periodically developed heat transfer regime. The macro-scale description of the periodically developed heat transfer regime in planar flow through isothermal periodic solid structures is treated in Section 8. In the last but one section, the exactness of our macro-scale description is numerically illustrated for laminar flow and heat transfer in an array of cylindrical tubes. Finally, Section 10 summarizes the main conclusions in this chapter.

6.3 Developed Heat Transfer in Devices under Isothermal Conditions

In a heat transfer device of which the spatially periodic structures and solid walls have the same constant temperature, a special heat transfer regime occurs after the onset of the periodically developed flow regime. This special regime is called the *periodically developed heat transfer regime*, because it is the result of periodically developed flow in combination with a periodically similar (constant) temperature boundary condition at the fluid-solid interface.

In Figure 6.1, the bottom picture gives an impression of the temperature distribution in a channel with cylindrical pin fins at a constant temperature. In the illustration, the fluid enters the channel at a temperature higher (red colour) than that of the cylindrical pin fins, so that the fluid cools down (blue colour) towards the outlet. Where the flow is periodically developed, the temperature distribution does not seem to be characterized by any periodical patterns at first sight. Nevertheless, when the temperature distribution is rescaled with an appropriate reference temperature, periodical patterns in the temperature distribution do become visible in the periodically developed flow region. The rescaled temperature is depicted in the top picture of Figure 6.1. Where the rescaled temperature varies in a periodic fashion from one pin fin to another, we can recognize the periodically developed heat transfer regime. The periodically developed heat transfer regime does not necessarily coincide with the entire periodically developed flow region, but often covers a large part of it.

The periodically developed heat transfer regime is a generalization of the *fully developed heat transfer regime*, which occurs in fully developed flow through ducts subject to a constant wall temperature [2]. The fully developed heat transfer regime in ducts at a constant wall temperature is characterized by the fact that the bulk temperature of the fluid varies exponentially in the streamwise direction from cross section to cross section. Therefore, the heat flux at the wall is directly proportional to the difference between the fluid bulk temperature and the constant wall temperature, at least if the mass flow rate through the duct remains constant. The latter observation has lead to the concept of a *heat transfer coefficient*, which is the constant of proportionality between the wall heat flux and the temperature difference between the bulk fluid and the wall.

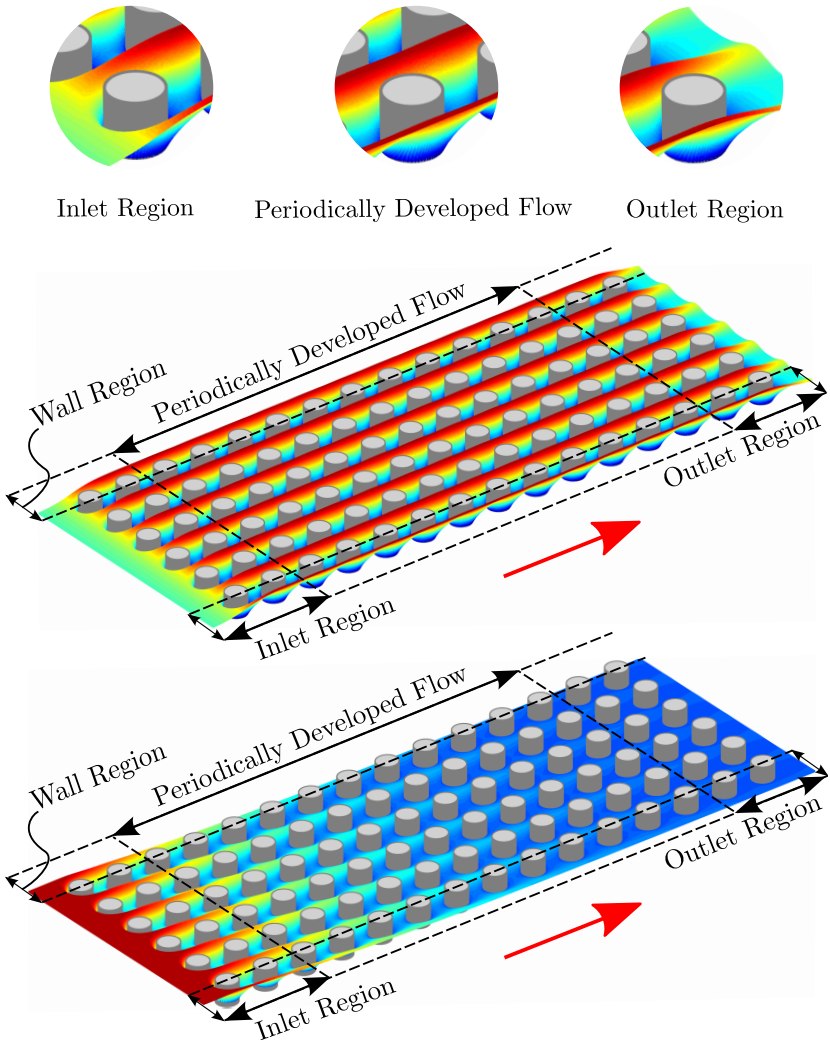

Figure 6.1: Temperature distribution (bottom picture) and rescaled temperature distribution (top picture) in the inlet region, outlet region, wall region and periodically developed flow region within the channel of Figure 5.1 from §5.3. The fins have a constant temperature.

6.4 Historical Background

Developed Heat Transfer in Isothermal Solid Structures
The laminar fully developed heat transfer regime in ducts with a constant cross-sectional shape and constant wall temperature has been studied intensively in the literature, since the pioneering work [5] of Nusselt in 1910. As we mentioned, the regime is described by means of two quantities: the fluid bulk-averaged temperature T_b and the heat transfer coefficient h. In the literature, e.g. [2, 6], these quantities are defined as

$$T_b \triangleq \frac{1}{A_c u_m} \int_{A_c} uT dA \qquad \text{and} \qquad h \triangleq \frac{q_p''}{T_w - T_b} .$$

Here, u_m is the average of the normal velocity component u over the local cross-section A_c of the duct, while q_p'' and T_w are respectively the average heat flux and wall temperature along the periphery of A_c. Mathematically, the fully developed heat transfer regime in isothermal ducts is defined as the regime for which the rescaled temperature at a cross section is invariant, i.e. independent of the coordinate x along the main flow direction:

$$\frac{\partial}{\partial x}\left(\frac{T - T_w}{T_b - T_w}\right) = 0 \qquad \text{or} \qquad \frac{\frac{d}{dx}(T_b - T_w)}{T_b - T_w} = \lambda = \text{constant} .$$

The solutions for the (bulk) temperature and the constant heat transfer coefficient in the fully developed regime in ducts with a constant wall temperature were reviewed in the book of Shah and London [2]. Correlations for the heat transfer coefficient in the fully developed regime in isothermal rectangular ducts, which are of interest for micro heat exchangers, have also been presented, for instance, by Lee et al. [7].

In 1977, Patankar, Liu and Sparrow [3] generalized the steady laminar fully developed heat transfer regime to two-dimensional or axisymmetric duct flows with a periodically varying cross section. In their study, the term *periodically developed heat transfer* was adopted for this generalized regime. To describe the steady periodically developed heat transfer regime in isothermal ducts, Patankar et al. introduced two temperature variables θ and λ, both being periodic in the main flow direction x over the period length L of the duct:

$$\theta(x, y) \triangleq \frac{T(x, y) - T_w}{T_b(x) - T_w} \qquad \text{and} \qquad \lambda(x) \triangleq \frac{\frac{d}{dx}(T_b - T_w)}{T_b - T_w} .$$

The variable $\lambda(x) = \lambda(x + L)$ must be calculated iteratively such that θ satisfies

$$\int_{A_c} \theta |u| \, dy = \int_{A_c} |u| \, dy$$

at every local cross section $A_c(x)$. Because Patankar et al. have kept the same definition of h as for ducts with a constant cross section, the heat transfer coefficient varies from cross section to cross section in the periodically developed heat transfer regime: $h(x) = h(x + L)$.

The steady periodically developed heat transfer regime in isothermal corrugated fins was investigated by Yutaka et al. in 1988 [8]. In the work of Yutaka et al., the average heat transfer coefficient over the streamwise direction was correlated. Similar results for wavy fins can be found in the studies [9–11] of Zhang, Manglik, Metwally around 2004. Also in the work of Xie et al. [12, 13], the characteristics of the steady periodically developed heat transfer regime in isothermal wavy fins have been investigated, although under the assumption that the temperature T itself is periodic. Therefore, these results are not consistent with the model equations of Patankar et al. [3]. Correlations for the steady periodically developed heat transfer regime in isothermal cross-corrugated fins have been presented by Zhou et al. in 2014 [14]. However, in the work of Zhou et al., the heat transfer coefficient is based on the volume-averaged temperature at the center of the fin unit, instead of the local bulk temperature.

The unsteady periodically developed heat transfer regime in isothermal wavy fins was described in the work of Wang and Vanka in 1995 [15]. Wang and Vanka recognized that in the unsteady periodically developed heat regime, the bulk temperature and hence the variables θ and λ from Patankar's temperature equation [3] must become time-dependent. As a number of other terms from Patankar's equation were disregarded by Wang and Vanka, it is not clear whether their results truly represent unsteady solutions for the periodically developed heat transfer regime. Unsteady developed solutions in corrugated (or wavy) fins at a constant temperature were investigated by Comini et al. [16, 17]. In the latter studies, however, the bulk temperature was assumed to be time-independent.

As the time-dependence of the bulk temperature complicates the formalism of Patankar for unsteady periodically developed heat transfer in wavy channels, Stalio and Piller [4] proposed an equivalent temperature simi-

larity θ in 2006:

$$\theta(x,y,z) \triangleq \frac{T(x,y,z)}{\mathrm{e}^{-\lambda_L x}} .$$

Stalio and Piller thus suggested to use an exponential reference temperature with a constant decay rate λ_L instead of the bulk temperature. The constant decay rate of this reference temperature corresponds to the streamwise average of the decay rate of the time-averaged bulk temperature $\overline{T}_b$:

$$\lambda_L \triangleq \frac{1}{L}\int_{x_0}^{x_0+L} \lambda(x)\,dx \qquad \text{with} \qquad \lambda(x) \triangleq \frac{\frac{d}{dx}\left(\overline{T}_b - T_w\right)}{\overline{T}_b - T_w} .$$

Whereas Patankar et al. described the steady periodically developed heat transfer regime in isothermal ducts in terms of the rescaled temperature variables θ and λ, Karimian and Straatman [18] in 2007 proposed a description in terms of the temperature T itself. In the description of Karimian and Straatman, the temperature $T_{i,1}$ at the inlet and the temperature $T_{i,2}$ at the outlet of the duct unit are coupled by a periodic boundary condition of the form

$$T_{i,1} = T_w - r_h\,(T_w - T_{i,2}) \qquad \text{with} \qquad r_h \triangleq \frac{T_w - T_{b,2}}{T_w - T_{b,1}} .$$

The temperature ratio r_h over the duct unit needs to be calculated iteratively from the specified bulk temperature at the inlet and the unknown bulk temperature at the outlet section of the duct. Although the formulation of Karimian and Straatman is much more simple than that of Patankar et al., it is based on the assumption that streamwise heat conduction can be neglected in the energy balance for a duct section.

Macro-Scale Modelling of Heat Transfer in Isothermal Solids —
The majority of the macro-scale models for convective heat transfer in spatially periodic solid structures are heuristic VAT models for convective heat transfer in porous media. That means that these macro-scale models contain a volume-averaged temperature equation for the fluid, in which the closure terms are only partly taken into account via heuristically defined closure coefficients. These closure coefficients or effective properties are governed approximatively from numerical heat transfer experiments on a unit cell of the solid structures. In a few studies, the numerical experiments have been conducted on a unit cell with solid structures at a constant temperature in a periodically developed flow.

In the work of Martin et al. from 1998 [19], the macro-scale heat transfer between a periodically developed flow and an array of isothermal cylinders was modelled through an interfacial heat transfer coefficient h_{fs}, which is the effective property defined as

$$h_{fs} \triangleq \frac{\frac{1}{V}\int_{A_{fs}} q_{fs}\, dA}{(\langle T\rangle^f - \langle T\rangle^s)}\,.$$

The interfacial heat transfer coefficient in [19] was calculated by evaluating the integral of the heat flux q_{fs} as well as the volume-averaged temperature difference $\langle T\rangle^f - \langle T\rangle^s$ at the centroid of the unit cell. The temperature field itself on the unit cell was calculated by solving the energy equation for the fluid under the assumption that no heat transfer takes place over the boundaries of the unit cell.

The idea that the interfacial heat transfer coefficient for the macro-scale temperature equation can be evaluated directly from the temperature field on a unit cell also appears in the work of Kuwahara, Shirota and Nakayama from 2001 [20]. In the latter study, the heat transfer between a periodically developed flow and an array of isothermal square rods was investigated. Kuwahara et al. took the interfacial heat transfer coefficient h_{fs} to be equal to the streamwise-averaged heat transfer coefficient for the bulk temperature difference in the developed regime. As a matter of fact, Kuwahara et al. implicitly assumed that

$$h_{fs} \simeq \frac{1}{L}\int_{x_0}^{x_0+L} h(x)\, dx = \frac{1}{L}\int_{x_0}^{x_0+L} \frac{q_{fs}}{T_b - T_s}\, dx\,,$$

where $T_s = \langle T\rangle^s$ is the constant temperature of the solid squares. This assumption allowed them to determine the interfacial heat transfer coefficient by resolving the periodically developed temperature field on a unit cell of the rod array, following Patankar's approach [3].

As Patankar's original description of the periodically developed heat transfer regime is only applicable to two-dimensional ducts, it cannot be used for arrays of three-dimensional solid structures. Furthermore, the reformulations of Patankar's description by [4, 18] are only applicable to arrays of solid structures in which the main flow direction is aligned with a symmetry plane of the array. Therefore, Nakayama, Kuwahara et al. [21, 22] have formulated a set of boundary conditions for the steady periodically developed heat transfer regime in isothermal solid structures,

which should be applicable to cases where the volume-averaged velocity of the fluid is directed under different angles with respect to the three-dimensional structures. These boundary conditions were used to determine the temperature field on a unit cell of an array of squares and to obtain the interfacial heat transfer coefficient at the centroid of the unit cell. Unfortunately, we have found that their generalization does not describe a valid temperature similarity for the periodically developed regime and even violates energy conservation over the unit cell.

Apart from the foregoing heuristic VAT models, also more rigorous closure models for porous media have been used to model macro-scale convective heat transfer in spatially periodic solid structures. The closure equations of the two-equation model (cf. §4.3) for macro-scale heat convection in a cylinder array were first numerically solved by Quintard, Kaviany and Whitaker [23] in 1997. The numerical results of Quintard et al. include the interfacial heat transfer coefficient, the thermal dispersion coefficients, as well as the convective coefficients for arrays of staggered and in-line solid cylinders. The closure coefficients are given for different solid-to-fluid conductivity ratios and different cell Peclet numbers.

The closure equations of the two-equation model [23] were also solved by DeGroot and Straatman [24] to simulate the macro-scale temperature field in a channel with a block of graphite foam inside. Although a graphite foam is a porous medium, its geometry closely resembles a periodic configuration of idealized graphite foam cells. Therefore, DeGroot and Straatman first correlated the effective properties of the flow in an idealized unit cell via the closure equations of [23]. Afterwards, they used these correlations to determine the closure terms in the volume-averaged temperature equation, which they solved numerically with a finite-volume method [25, 26].

When the solid-to-fluid conductivity is high, the closure equations of the two-equation model [23] can be simplified into the equivalent closure problem derived by DeGroot and Straatman [27] in 2011. This equivalent closure problem was derived under the assumption that the temperature T_s of the solid is constant. It is based on the following representation of the temperature deviation part:

$$\widetilde{T}_f = \boldsymbol{b} \cdot \nabla \langle T \rangle^f + \psi \left(T_s - \langle T \rangle^f \right) .$$

DeGroot and Straatman solved the periodic closure variables $\boldsymbol{b}$ and ψ on a unit cell numerically to determine the interfacial heat transfer coeffi-

cient and thermal dispersion coefficient which appear in the macro-scale temperature equation for a flow through an array of isothermal cylinders. The thermal dispersion coefficient in the equivalent closure problem of [27] is defined as

$$\boldsymbol{K}_d \triangleq -\rho_f c_f \langle \widetilde{\boldsymbol{u}}\boldsymbol{b} \rangle^f \qquad \text{so that} \qquad \rho_f c_f \nabla \cdot \langle \widetilde{\boldsymbol{u}}\widetilde{T} \rangle^f \simeq -\boldsymbol{K}_d \cdot \nabla \langle T \rangle^f .$$

The hypothesis that the thermal dispersion source can be related to the macro-scale temperature gradient by means of a thermal dispersion coefficient had already been suggested by Nakayama et al. [28] in 2006, on the basis of the characteristics of fully developed heat transfer in isothermal ducts.

Open Research Questions in the Literature

From the preceding literature survey, we conclude that a correct and general description of the (un)steady periodically developed heat transfer regime in three-dimensional isothermal solid structures has not been given yet. It remains thus an open question how the temperature similarity of Patankar [3] can be generalized towards unsteady flows with an arbitrary direction in three-dimensional arrays of solid structures.

To answer this first question, we will reconsider in the next section, §6.5, whether the bulk temperature is effectively an appropriate reference temperature in the periodically developed regime. In addition, we will reconsider whether cross-sectional averaging is an appropriate method to describe the periodically developed regime.

Our literature review also reveals that the macro-scale models for heat transfer in spatially periodic structures contain three levels of approximation. The first level of approximation is the introduction of VAT models for porous media which neglect the exact form of the closure terms for spatially periodic structures (cf. §4.6). The second level of approximation is the representation of these inexact closure terms by effective parameters which are assumed to be constant over space (and time). The third level of approximation is the lack of distinction between the effective parameters for the volume-averaged transport equations and the cross-sectional average quantities that characterize the periodically developed regime.

While the (length-scale) constraints that justify the first and second level of approximation have been discussed in the light of the more rigorous closure models for porous media [23, 27], it has not been shown whether these constraints are fulfilled in the periodically developed heat transfer regime

in isothermal solids. Therefore, the suitability of the volume-averaging technique and the former closure models for the periodically developed regime requires a critical re-evaluation. A re-evaluation is especially necessary, because the different levels of approximation have not lead to a clear physical interpretation of the volume-averaged quantities. Hence, the appropriate macro-scale description of the periodically developed heat transfer regime is still an open problem in the literature. Therefore, we will address this second problem in Section 6.6, where we will determine the weighting function to accomplish a meaningful macro-scale description which is fully consistent with DNS results.

Also for the heuristic VAT models, the second level of approximation has never been validated. On the contrary, in the heuristic models, the space-and-time independence of the closure coefficients is just postulated. For instance, the heurstic VAT models of Martin, Nakayama, Kuwahara and their co-worker [19, 21, 22] all postulate that the interfacial heat transfer coefficient is constant. Nevertheless, the observations from [29] clearly illustrate the spatial dependence of the interfacial heat transfer coefficient for the volume-averaged temperature in an array of solid squares. Moreover, also the derivations of [23, 27] contradict the existence of constant closure coefficients for the heuristic VAT models. A third important question is thus whether it is theoretically possible to develop a macro-scale description which allows us to represent the closure terms in the periodically developed regime by a spatially constant heat transfer coefficient and thermal dispersion coefficient. This question will be answered in Section 6.7.

The third level of approximation only arises in the heuristic VAT models for spatially periodic structures, but not in the more rigorous closure models for porous media [23, 27]. In the heuristic VAT models [19, 21, 22], the heat transfer coefficient defined by Patankar et al. [3] is not distinguished from the interfacial heat transfer coefficient in the macro-scale equation. However, both heat transfer coefficients are completely different quantities, just like the fluid bulk temperature and the volume-averaged fluid temperature are completely different quantities. We believe that this type of approximation is a misconception that has been introduced in some studies, because a comprehensive macro-scale description of the periodically developed regime in isothermal solid structures was still absent. The difference between both heat transfer coefficients is illustrated in the case study of Section 6.9.

6.5 Periodically Developed Heat Transfer in Isothermal Solids

The appropriate definition of the periodically developed heat transfer regime is that there exists a *periodic similarity* in the temperature distribution over some part of the domain as a result of the periodically developed flow field in that part of the domain. For a system domain composed of periodic solid structures, this periodic similarity implies that the profiles of the temperature distribution contained within different unit cells (cf. (5.2)) of the solid structures can be brought together by a suitable mathematical transformation or scaling.

In the case where the solid structures have a temperature T_s which is constant over the solid domain and no viscous dissipation nor volumetric heat generation occurs, we can seek for a suitable temperature scaling for the steady periodically developed heat transfer regime by adopting the transformation of Patankar et al. [3] for periodic heat transfer in ducts with a uniform wall temperature. Accordingly, we introduce the rescaled temperature

$$\theta \triangleq \frac{T - T_s}{T_{\mathrm{ref}} - T_s}\,, \tag{6.1}$$

where T_{ref} is a local reference temperature yet to be determined.

For periodically developed flow, the flow field varies in a periodic fashion from one unit cell to another:

$$\boldsymbol{u}(\boldsymbol{x}, t) = \boldsymbol{u}\left(\boldsymbol{x} + \boldsymbol{l}^{(j)}, t\right)\,. \tag{6.2}$$

Therefore, we postulate the existence of a suitable reference temperature T_{ref} such that the temperature transformation of (6.1) yields a periodic rescaled temperature which is similar for every unit cell (5.2):

$$\theta(\boldsymbol{x}, t) = \theta\left(\boldsymbol{x} + \boldsymbol{l}^{(j)}, t\right)\,. \tag{6.3}$$

The occurrence of the periodic similarity in the temperature distribution expressed by equation (6.3) thus serves as the definition for the periodically developed heat transfer regime when the solid temperature is constant. Just like we have assumed the periodically developed velocity field to be time-periodic, also the rescaled temperature θ is assumed to be time-periodic here.

When the rescaled temperature θ is substituted into the temperature equation (4.5), the following equation results:

$$\rho\frac{\partial^{\nu}(c\theta)}{\partial t}+\rho\nabla^{\nu}\cdot(\boldsymbol{u}c\theta)=\nabla^{\nu}\cdot(k\,\nabla^{\nu}\theta)+(\dot{q}+\dot{q}_{\mathrm{visc}})\,(T_{\mathrm{ref}}-T_s)^{-1}+\sigma_T\,, \quad (6.4)$$

where

$$\sigma_T \triangleq -\rho\theta\frac{\partial^{\nu}(cT_{\mathrm{ref}})}{\partial t}\,(T_{\mathrm{ref}}-T_s)^{-1}+(2k\nabla^{\nu}\theta-\rho c\boldsymbol{u}\theta)\cdot\boldsymbol{\lambda}_T+ k\theta\boldsymbol{\lambda}_T\cdot\boldsymbol{\lambda}_T+\theta\nabla^{\nu}\cdot(k\boldsymbol{\lambda}_T) \quad (6.5)$$

and

$$\boldsymbol{\lambda}_T \triangleq \frac{\nabla^{\nu}(T_{\mathrm{ref}}-T_s)}{T_{\mathrm{ref}}-T_s}\,. \quad (6.6)$$

The derivation of (6.4) and (6.5) can be found in Appendix J. As we assume that there are no temperature changes due to viscous dissipation and volumetric heat sources, the corresponding terms in equation (6.4) are zero:

$$\dot{q}=\dot{q}_{\mathrm{visc}}=0\,. \quad (6.7)$$

Mathematically, a periodic solution for θ from (6.4) is possible under the condition that the fluid properties are space independent and the local reference temperature satisfies

$$\boldsymbol{\lambda}_T(\boldsymbol{x},t)=\boldsymbol{\lambda}_T\left(\boldsymbol{x}+\boldsymbol{l}^{(j)},t\right)\,, \quad (6.8)$$

as in that case the source term in the rescaled temperature equation is also periodic:

$$\sigma_T(\boldsymbol{x},t)=\sigma_T\left(\boldsymbol{x}+\boldsymbol{l}^{(j)},t\right)\,. \quad (6.9)$$

Because $\theta_s=0$, it suffices to determine θ_f by resolving equation (6.4) on the fluid domain of the unit cell. The appropriate boundary conditions for θ_f in $\Omega_f\cap\Omega_{\mathrm{unit}}$ are thus

$$\theta_f(\boldsymbol{x},t)=0 \qquad \boldsymbol{x}\in\Gamma_{fs}\cap\Omega_{\mathrm{unit}} \quad \text{and} \quad \theta_f(\boldsymbol{x},t)=\theta_f\left(\boldsymbol{x}+\boldsymbol{l}^{(j)},t\right)\,, \quad (6.10)$$

where $j=\{1,\ldots,\mathrm{n}_j\}$.

We remark that the time-and-volume-averaged value of the rescaled temperature over the unit cell domain, $\langle\bar{\theta}\rangle$, must be imposed in order to find a unique solution for (6.4). Otherwise, θ would be only determined up to an arbitrary constant $\theta(\boldsymbol{x}_0, t_0)$, which depends on the fluid temperature $T_f(\boldsymbol{x}_0, t_0)$ and reference temperature $T_{\mathrm{ref}}(\boldsymbol{x}_0, t_0)$ at some point and time instant in the periodically developed heat transfer regime.

In the periodically developed regime for isothermal solids, the rescaled temperature depends on the constant fluid properties, the velocity field and $\boldsymbol{\lambda}_T$ via (6.4) as well as the unit cell geometry via (6.10):

$$\theta = \theta\left(\rho_f, c_f, k_f, \boldsymbol{u}, \boldsymbol{\lambda}_T, \Gamma_{fs} \cap \Omega_{\mathrm{unit}}, \boldsymbol{x}, t\right) . \tag{6.11}$$

When the flow is periodically developed, it follows from (5.21), (5.22) and (5.23) that the functional dependence of the velocity field is given by the following parameter set:

$$\boldsymbol{u} = \boldsymbol{u}\left(\rho_f, \mu_f, \boldsymbol{f}, \langle\boldsymbol{u}\rangle, \Gamma_{fs} \cap \Omega_{\mathrm{unit}}, \boldsymbol{x}, t\right) , \tag{6.12}$$

where $\boldsymbol{f}$ represents a spatially periodic body force over the unit cell domain. In conclusion, by equation (6.11) it holds that

$$\theta = \theta\left(\rho_f, c_f, k_f, \mu_f, \langle\boldsymbol{u}\rangle, \boldsymbol{f}, \boldsymbol{\lambda}_T, \Gamma_{fs} \cap \Omega_{\mathrm{unit}}, \boldsymbol{x}, t\right) . \tag{6.13}$$

Choice of Reference Temperature

If a suitable reference temperature can be found which satisfies equation (6.8), θ represents a periodic similarity between the temperature profiles within different unit cells. For periodically developed heat transfer in ducts with streamwise-periodic variations of cross-sectional area, Patankar et al. [3] suggested that any temperature in the local cross section of the duct could be chosen as T_{ref} in order to have periodicity of θ.

For the periodically developed heat transfer regime in solid structures, one can also make use of a cross-sectional reference temperature, at least if the flow has a main direction which coincides with one of the lattice vectors. Suppose the main flow is directed along $\boldsymbol{l}^{(k)}$: a convenient choice of cross-sectional reference temperature could be the modified bulk temperature T_b, which is defined by

$$T_b - T_s \triangleq \frac{\displaystyle\int_{\boldsymbol{r}\in\bar{\Gamma}^*(\boldsymbol{x})} (T(\boldsymbol{r}) - T_s)\, |\boldsymbol{u}\cdot\boldsymbol{l}^{(k)}|\, d\Gamma^*(\boldsymbol{r})}{\displaystyle\int_{\boldsymbol{r}\in\bar{\Gamma}^*(\boldsymbol{x})} |\boldsymbol{u}\cdot\boldsymbol{l}^{(k)}|\, d\Gamma^*(\boldsymbol{r})} \tag{6.14}$$

and based on the local cross section

$$\bar{\Gamma}^*(\boldsymbol{x}) \triangleq \left\{ \boldsymbol{r} \,|\, \exists\, c_j \in \left(-\frac{1}{2}, \frac{1}{2}\right) \Leftrightarrow \boldsymbol{r} = \boldsymbol{x} + \sum_{\substack{j=1 \\ j\neq k}}^{3} c_j \boldsymbol{l}^{(j)} \right\} . \tag{6.15}$$

As shown by Patankar, $\boldsymbol{\lambda}_T$ will not be constant over space if $T_{\mathrm{ref}} = T_b$.

While the choice of a cross-sectional reference temperature seems suited to flow through ducts, it seems not to be for flow through periodic solid structures. First, it is not straightforward to identify an appropriate local cross section for a periodic solid structure if the main flow is not aligned with one of the lattice vectors. Second, with the aim of simplifying the rescaled temperature equation (6.4), it is more interesting to choose a reference temperature such that $\boldsymbol{\lambda}_T$ is a spatially constant vector,

$$\boldsymbol{\lambda}_T = \lambda_T \boldsymbol{e}_\lambda \,. \tag{6.16}$$

For that reason we propose

$$T_{\mathrm{ref}}(\boldsymbol{x}) = A_0 \exp\left(\lambda_T\, \boldsymbol{x} \cdot \boldsymbol{e}_\lambda\right) + T_s \,, \tag{6.17}$$

where the arbitrary constant A_0 has the unit of the temperature T. The same form of reference temperature was also used by Stalio and Piller [4] in their study of unsteady periodic flow and heat transfer in converging-diverging wavy channels. This reference temperature represents, apart from the offset T_s, the exponential envelope of the physical temperature T, for which θ acts like a modulated carrier signal.

Any reference temperature of the form

$$T_{\mathrm{ref}}(\boldsymbol{x}, t) = A(\boldsymbol{x}, t) \exp\left(\lambda_T\, \boldsymbol{x} \cdot \boldsymbol{e}_\lambda\right) + T_s \tag{6.18}$$

with

$$A(\boldsymbol{x}, t) = A\left(\boldsymbol{x} + \boldsymbol{l}^{(j)}, t\right) , \tag{6.19}$$

will also lead to a periodic rescaled temperature θ and to a constant temperature ratio[1] over the unit cell [18, 22, 29],

$$\frac{T\left(\boldsymbol{x} + \boldsymbol{l}^{(j)}, t\right) - T_s}{T(\boldsymbol{x}, t) - T_s} = \exp\left(\lambda_T \boldsymbol{e}_\lambda \cdot \boldsymbol{l}^{(j)}\right) \triangleq \tau_T^{(j)} \,. \tag{6.20}$$

[1]Equation (6.20) shows that $\tau_T^{(j)}$ shows that the temperature ratio from [22] is wrong, because $T(\boldsymbol{x} + \boldsymbol{l}^{(1)} + \boldsymbol{l}^{(2)} + \boldsymbol{l}^{(3)}) - T_s = (T(\boldsymbol{x}) - T_s) \sum_{j=1}^{3} \boldsymbol{\lambda}_T \cdot \boldsymbol{l}^{(j)}$.

However, for any reference temperature different from (6.17), $\boldsymbol{\lambda}_T(\boldsymbol{x}, t)$ will always vary periodically over space.

If one opts for a filtered temperature as reference, i.e.

$$T_{\text{ref}} = \langle T \rangle_m \,, \tag{6.21}$$

the appropriate weighting function m should be constructed such that θ and $\boldsymbol{\lambda}_T$ can be made periodic. This is, for instance, the case, if $m = m_V$ or $m = m_V * m_V$ and the filter window of m_V matches with a unit cell of the domain, $\bar{\Omega} = \Omega_{\text{unit}}$ as in (5.4). In the next section, §6.6, we will derive the weighting function m for which $\boldsymbol{\lambda}_T$ and hence $\tau_T^{(j)}$ are constant.

Reference Temperature Eigenvalue Problem

When the decay rate of the reference temperature $\boldsymbol{\lambda}_T$ is constant over space, its value can be governed by averaging equation (6.4) both over space and time, under absence of heat sources:

$$\rho_f c_f \frac{\partial \langle \bar{\theta} \rangle_m}{\partial t} + \rho_f \nabla \cdot \langle \overline{\boldsymbol{u} c \theta} \rangle_m = \nabla \cdot k_f \, \nabla \langle \bar{\theta} \rangle_m + \langle \boldsymbol{n}_{fs} \cdot k_f \nabla \bar{\theta}_f \delta_{fs} \rangle_m + \langle \overline{\sigma_T} \rangle_m \,, \tag{6.22}$$

with

$$\langle \overline{\sigma_T} \rangle_m = \left(2 k_f \nabla \langle \bar{\theta} \rangle_m - \rho_f \langle \overline{\boldsymbol{u} c \theta} \rangle_m \right) \cdot \boldsymbol{\lambda}_T + k_f \langle \bar{\theta} \rangle_m \boldsymbol{\lambda}_T \cdot \boldsymbol{\lambda}_T \,, \tag{6.23}$$

because $\boldsymbol{\lambda}_T$ is assumed constant. Note that in (6.22), we made use of the fact that $\theta_f = 0$ at the fluid-solid interface, because $T_f = T_s$ at Γ_{fs} according to (4.9).

If one chooses a weighting function of the form $m = m_G * m_V$, where $m_G \in C^\infty$ is an arbitrary weighting function and the filter window of m_V matches a unit cell of the domain, i.e. $\bar{\Omega} = \Omega_{\text{unit}}$, all the weighted averages of periodic terms in (6.22) reduce to their constant volume-averaged value. Hence, if $m = m_G * m_V$, equations (6.22) and (6.23) reduce to a quadratic equation for the temperature decay rate:

$$\langle \boldsymbol{n}_{fs} \cdot k_f \nabla \bar{\theta}_f \delta_{fs} \rangle - \left(\rho_f c_f \langle \overline{\boldsymbol{u} \theta} \rangle \cdot \boldsymbol{e}_\lambda \right) \lambda_T + k_f \langle \bar{\theta} \rangle \lambda_T^2 = 0 \,. \tag{6.24}$$

From physical considerations, only the negative decay rate $\lambda_T < 0$ of equation (6.24) makes sense. Because $\langle \overline{\boldsymbol{u}} \rangle_m = \langle \overline{\boldsymbol{u}} \rangle = \| \langle \overline{\boldsymbol{u}} \rangle \| \boldsymbol{e}_s$ is a constant vector when $m = m_G * m_V$, the reference temperature must decay exponentially in the main flow direction, so $\boldsymbol{e}_\lambda = \boldsymbol{e}_s$. Moreover, equation

(6.24) shows that the decay rate only determines the rescaled temperature up to the constant $\langle\bar{\theta}\rangle$.

In fact, equation (6.24) might be called the eigenvalue problem for periodically developed heat transfer in isothermal solid structures, as it resembles an analogue of the eigenvalue problem [2] for the fluid bulk temperature in fully developed heat transfer in ducts with a constant wall temperature.

In summary, when $\boldsymbol{\lambda}_T$ is constant, its value corresponds to the negative root of (6.24), which is directly determined by the velocity field $\boldsymbol{u}$ and rescaled temperature θ within the unit cell. Therefore, the decay rate $\boldsymbol{\lambda}_T$ can be left out of the functional relationship (6.13):

$$\theta = \theta\left(\rho_f, c_f, k_f, \mu_f, \langle\boldsymbol{u}\rangle, \Gamma_{fs} \cap \Omega_{\text{unit}}, \boldsymbol{x}, t\right) . \tag{6.25}$$

Consequently, the decay rate itself depends on the fluid properties, the volume-averaged velocity and the geometry of the unit cell domain:

$$\boldsymbol{\lambda}_T = \boldsymbol{\lambda}_T\left(\rho_f, c_f, k_f, \mu_f, \langle\boldsymbol{u}\rangle, \Gamma_{fs} \cap \Omega_{\text{unit}}\right) . \tag{6.26}$$

6.6 Choice of Weighting Function for Periodically Developed Heat Transfer in Isothermal Solids

Up to this point, the question of how to choose the weighting function for the spatially averaged temperature has been left unanswered. Nevertheless, in the previous sections several restrictions have been imposed on the weighting function. First of all, the weighting function is required to be normalized and infinitely derivable. Second, the weighting function should respect the length scale constraints of (4.28).

Let us again propose a weighting function of the form $m = m_G * m_V$, where $m_G \in C^\infty$ and the filter window of m_V matches with a unit cell of the domain, $\bar{\Omega} = \Omega_{\text{unit}}$. This weighting function m satisfies

$$\boldsymbol{\phi}(\boldsymbol{x}) = \boldsymbol{\phi}\left(\boldsymbol{x} + \boldsymbol{l}^{(j)}\right) \qquad \Rightarrow \qquad \langle\boldsymbol{\phi}\rangle_m = \langle\boldsymbol{\phi}\rangle = \text{constant}\,, \tag{6.27}$$

for any spatially periodic distribution $\boldsymbol{\phi}$.

Consequently, if $m = m_G * m_V$, the weighted porosity equals the constant physical porosity or void fraction, $\epsilon_{fm} = \epsilon_f \triangleq \langle \gamma_f \rangle$. By equation (6.2) this weighting function also yields a spatially constant filtered velocity $\langle \boldsymbol{u} \rangle_m^f = \langle \boldsymbol{u} \rangle^f$ for periodically developed flow. Hence, the weighting function m respects the velocity scale constraint of (4.28), as it leads to the order of magnitude estimates $\ell_{\boldsymbol{u}} \leq r_m = O\left(\left\| \boldsymbol{l}^{(j)} \right\|\right)$ and $\mathcal{L}_{\boldsymbol{u}} = \infty$.

In order that $m = m_G * m_V$ would also satisfy the temperature scale constraint of (4.28), we will choose m_G in a manner such that for the overall weighting function m it additionally holds that[2]:

$$\langle \boldsymbol{\phi} \mathrm{e}^{\boldsymbol{\lambda}_T \cdot \boldsymbol{r}} \rangle_m = \langle \boldsymbol{\phi} \rangle \mathrm{e}^{\boldsymbol{\lambda}_T \cdot \boldsymbol{x}} \,, \tag{6.28}$$

where $\boldsymbol{\phi}$ is any arbitrary distribution and $\boldsymbol{\lambda}_T$ is the constant temperature decay rate vector given by (6.16).

The above property of the weighting function ensures that the spatially averaged temperature remains unaltered after repeatedly averaging:

$$\langle T \rangle_m = A_0 \langle \theta \mathrm{e}^{\boldsymbol{\lambda}_T \cdot \boldsymbol{r}} \rangle_m + T_s = A_0 \langle \theta \rangle \mathrm{e}^{\boldsymbol{\lambda}_T \cdot \boldsymbol{x}} + T_s = \langle \langle T \rangle_m \rangle_m \,. \tag{6.29}$$

The scale constraint $r_m \ll \mathcal{L}_T$ is then automatically satisfied because $\langle \widetilde{T} \rangle_m = 0$ and $\langle \langle T \rangle_m^f \rangle_m^f = \langle T \rangle_m^f$ by (6.29). The fact that this overall weighting function suppresses the temperature deviation field after filtering can also be seen from the expression

$$\widetilde{T} = A_0 \widetilde{\theta} \mathrm{e}^{\boldsymbol{\lambda}_T \cdot \boldsymbol{x}} = \frac{\widetilde{\theta}}{\langle \theta \rangle} \epsilon_{fm} \left(\langle T \rangle_m^f - T_s \right) \,, \tag{6.30}$$

by remarking that $\langle \widetilde{\theta} \rangle = 0$. As a comment, we add that because the exponential temperature envelope in (6.30) equals

$$A_0 \mathrm{e}^{\boldsymbol{\lambda}_T \cdot \boldsymbol{x}} = \langle \theta \rangle^{-1} \left(\langle T \rangle_m - T_s \right) = \langle \theta \rangle^{-1} \epsilon_f \left(\langle T \rangle_m^f - T_s \right) \,, \tag{6.31}$$

$\widetilde{\theta}$ plays the role of a closure variable (or mapping) as in the theory for porous media [23, 27], which links the deviation temperature to the macro-scale temperature.

[2]The expression $\langle \boldsymbol{\phi} \mathrm{e}^{\boldsymbol{\lambda}_T \cdot \boldsymbol{r}} \rangle_m$ is actually an abuse of notation and should be interpreted as $\boldsymbol{\phi}(\boldsymbol{r}) e^{\boldsymbol{\lambda}_T \cdot \boldsymbol{r}}$ appearing as a function of the integration variable $\boldsymbol{r}$ within the integral operator $\langle \, \rangle_m$.

Furthermore, if the weighting function m is chosen to have the properties (6.27) and (6.28), the length scale for the filtered temperature can be estimated by $\mathcal{L}_T = \mathcal{O}\left(\lambda_T^{-1}\right)$, because

$$\frac{\nabla\langle T\rangle_m^f}{\langle T\rangle_m^f - T_s} = \frac{\nabla\langle T\rangle_m}{\langle T\rangle_m - T_s} = \boldsymbol{\lambda}_T\,. \tag{6.32}$$

On the other hand, according to (6.30), the length scale for the deviation temperature can be estimated by $\ell_T = \mathcal{O}(\ell_\theta)$. This confirms that the weighting function with the former properties also satisfies $\ell_T \ll \mathcal{L}_T$.

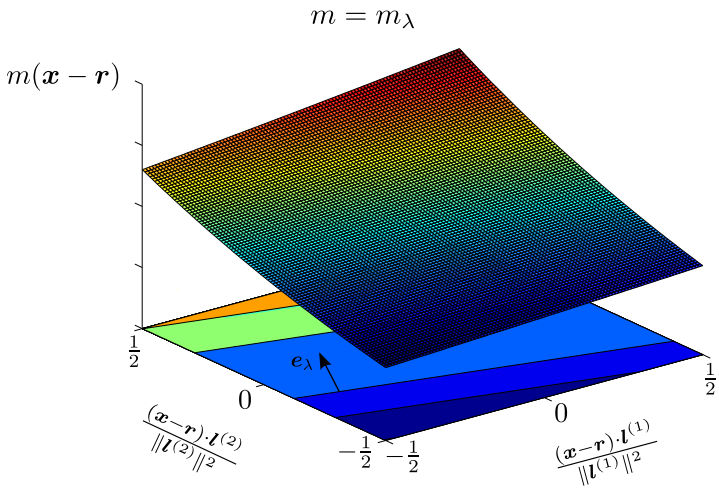

Figure 6.2: Two-dimensional representation of the weighting function $m = m_\lambda$ for a rectangular unit cell spanned by the lattice vectors $\boldsymbol{l}^{(1)}$ and $\boldsymbol{l}^{(2)}$.

It is readily verified that the overall weighting function m satisfying both (6.27) and (6.28) is given by $m = m_G * m_V = m_C * m_\lambda * m_V$, where m_C is arbitrary and

$$m_\lambda(-\boldsymbol{y}) \triangleq \begin{cases} \beta(\boldsymbol{\lambda}_T)\exp\left(-\boldsymbol{y}\cdot\boldsymbol{\lambda}_T\right) & \boldsymbol{r}\in\bar{\Omega}_{\text{unit}}(\boldsymbol{x}) \\ 0 & \text{elsewhere} \end{cases}\,. \tag{6.33}$$

This weighting function is depicted in Figure 6.2.

The normalization factor β for m_λ is derived in Appendix K and depends on the temperature decay rate:

$$\beta(\boldsymbol{\lambda}_T) \triangleq \frac{1}{V_{\text{unit}}} \prod_{j=1}^{\text{n}_j} \frac{\boldsymbol{\lambda}_T \cdot \boldsymbol{l}^{(j)}}{2 \sinh\left(\frac{\boldsymbol{\lambda}_T \cdot \boldsymbol{l}^{(j)}}{2}\right)} \ , \tag{6.34}$$

with V_{unit} given by equation (5.3).

The appropriate filter operator $\langle\ \rangle_m$ for the periodically developed heat transfer regime in isothermal periodic solid structures is thus a matched filter, because its kernel $m = m_C * m_\lambda * m_V$ matches the decay rate λ_T of the exponentially decreasing temperature envelope. Moreover, if we set $\langle\theta\rangle = 1$, the reference temperature proposed in the previous section is found by averaging the full-scale temperature distribution T with this matched filter:

$$T_{\text{ref}} = \langle T \rangle_m \qquad \Leftrightarrow \qquad \langle\theta\rangle = \langle\bar{\theta}\rangle = 1\,. \tag{6.35}$$

In Appendix L, it is shown that the matched weighting function $m = m_\lambda * m_V$ is a fully separable filter with respect to the basis vectors $\boldsymbol{l}^{(j)}/\|\boldsymbol{l}^{(j)}\|^2$. Its separable form is given by

$$m'_j(-y_j) = \sqrt[\text{n}_j]{\frac{1}{V_{\text{unit}}}} \left(\frac{\text{e}^{-\lambda_j} - \text{e}^{-\lambda_j|y_j|}}{\text{e}^{\lambda_j} - 1}\right) \exp\left(-\frac{1}{2}\lambda_j y_j (1 + \operatorname{sgn} y_j)\right),$$
$$\text{where} \qquad y_j \triangleq \frac{\boldsymbol{y} \cdot \boldsymbol{l}^{(j)}}{\|\boldsymbol{l}^{(j)}\|^2} \in [-1, 1] \qquad \text{and} \qquad \lambda_j \triangleq \boldsymbol{\lambda}_T \cdot \boldsymbol{l}^{(j)} \tag{6.36}$$

When the decay rate is sufficiently small, i.e.

$$\max_j \left(\boldsymbol{\lambda}_T \cdot \boldsymbol{l}^{(j)}\right) \ll 1\,, \tag{6.37}$$

the overall weighting function $m = m_C * m_\lambda * m_V$ can be approximated as $m \simeq m_C * m_V * m_V$, which is the appropriate weighting function for the pressure and velocity in the periodically developed flow regime (see §5.10). Theoretically m_C should be chosen such that $(m_C * m_V * m_V) \in C^\infty$, because $(m_V * m_V) \in C^0$. For numerical purposes one can take $m_C \simeq 1$, as differentiability of the weighting function is seldom of concern. In that case we have for $\lambda_T \to 0$:

$$m \simeq m_V * m_V\,. \tag{6.38}$$

So, for small eigenvalues of (6.24), the filter operator need only be customised to the spatial periodicity of the solid structures, which is determined by the lattice vectors.

In the limit of (6.37), the double volume filter can be further approximated by a single volume filter, $\langle\langle\boldsymbol{\phi}\rangle\rangle \simeq \langle\boldsymbol{\phi}\rangle$. The approximation $\langle\langle T\rangle\rangle \simeq \langle T\rangle$ requires at least that terms involving the volume-averaged spatial moments $\langle(\boldsymbol{r}-\boldsymbol{x})^{\otimes n}\rangle$, which vary periodically over the unit cell, are negligible. Depending on the type of solid structures, the influence of the spatial moments on the volume-averaged temperature might be considerable, so that the idempotence of the volume-averaging operator might be violated and $\langle T\rangle$ might not be a macro-scale temperature. Moreover, the idempotence of the volume average is difficult to check from an a priori analysis, i.e. without information from DNS. Therefore, it is recommended to use a double volume filter, i.e. $m = m_V * m_V$, whenever the temperature decay rate is expected to be small.

6.7 Closure for Periodically Developed Heat Transfer in Isothermal Solids

Because the weighting function $m = m_C * m_\lambda * m_V$ defines a macro-scale temperature as reference temperature for which θ is periodic, the closure problem can be strongly simplified in the periodically developed heat transfer regime. Indeed, the relationship between the closure terms and the macro-scale temperature becomes very simple, as the macro-scale temperature $\langle T\rangle_m$ can be moved outside the averaging operator $\langle\,\rangle_m$ due to the filter property (6.28).

The thermal dispersion source, for instance, can be expressed as

$$\mathcal{D} = \langle\widetilde{\boldsymbol{u}}\widetilde{T}\rangle_m = \frac{\langle\widetilde{\boldsymbol{u}}\theta\rangle}{\langle\theta\rangle}\left(\langle T\rangle_m - T_s\right) = \epsilon_f \frac{\langle\widetilde{\boldsymbol{u}}\theta\rangle}{\langle\theta\rangle}\left(\langle T\rangle_m^f - T_s\right)\,, \tag{6.39}$$

by virtue of (6.29), (6.30) and (6.31). Note that $\mathcal{D} = \mathcal{D}_{\text{approx}} \triangleq \langle\widetilde{\boldsymbol{u}}\widetilde{T}\rangle_m$ is exact, because $\langle\widetilde{\boldsymbol{u}}\rangle_m = 0$ and $\langle\widetilde{T}\rangle_m = 0$. Hence, if $\langle\theta\rangle = 1$, the thermal dispersion source $\mathcal{D}$ and its approximative form $\mathcal{D}_{\text{approx}}$ can both be represented by the same spatially constant dispersion vector coefficient

$$\boldsymbol{k}_d = \boldsymbol{k}_{d,\text{approx}} = \langle\widetilde{\boldsymbol{u}}\theta\rangle = \langle\widetilde{\boldsymbol{u}}\widetilde{\theta}\rangle\,. \tag{6.40}$$

The dispersion vector coefficients $\boldsymbol{k}_d$ and $\boldsymbol{k}_{d,\text{approx}}$ in (6.40) are defined by

$$\boldsymbol{\mathcal{D}} \triangleq \epsilon_{fm} \boldsymbol{k}_d \left(\langle T \rangle_m^f - T_s \right) \tag{6.41}$$

and

$$\boldsymbol{\mathcal{D}}_{\text{approx}} \triangleq \epsilon_{fm} \boldsymbol{k}_{d,\text{approx}} \left(\langle T \rangle_m^f - T_s \right) \tag{6.42}$$

respectively. From (6.32) and (6.41) it follows that the dispersion vector coefficient $\boldsymbol{k}_d$ and the thermal dispersion tensor $\boldsymbol{K}_d$ of [27] are related via the relation

$$\boldsymbol{K}_d = -\rho_f c_f \lambda_T^{-1} \boldsymbol{k}_d \boldsymbol{\lambda_T} \,, \tag{6.43}$$

at least in the periodically developed heat transfer regime.

The interfacial heat transfer term is related to the macro-scale temperature as follows:

$$\begin{aligned} \langle \boldsymbol{n}_{fs} \cdot k_f \nabla T_f \delta_{fs} \rangle_m &= \langle \boldsymbol{n}_{fs} \cdot k_f \frac{\nabla \theta_f}{\langle \theta \rangle} \left(\langle T \rangle_m - T_s \right) \delta_{fs} \rangle_m \\ &\quad + \langle \boldsymbol{n}_{fs} \cdot k_f \frac{\theta_f}{\langle \theta \rangle} \nabla \langle T \rangle_m \delta_{fs} \rangle_m \\ &= \frac{\langle \boldsymbol{n}_{fs} \cdot k_f \nabla \theta_f \delta_{fs} \rangle}{\langle \theta \rangle} \left(\langle T \rangle_m - T_s \right) \\ &= \epsilon_f \frac{\langle \boldsymbol{n}_{fs} \cdot k_f \nabla \theta_f \delta_{fs} \rangle}{\langle \theta \rangle} \left(\langle T \rangle_m^f - T_s \right) \,, \end{aligned} \tag{6.44}$$

where we have used the fact that $\theta_f = 0$ at the fluid-solid interface, because $T_f = T_s$ at Γ_{fs} according to (4.9). Therefore, the convective heat transfer coefficient defined by

$$\langle q_{fs} \delta_{fs} \rangle_m \triangleq \epsilon_{fm} h_{fs} \left(\langle T \rangle_m^f - \langle T \rangle_m^s \right) \,, \tag{6.45}$$

equals

$$h_{fs} = -\langle \boldsymbol{n}_{fs} \cdot k_f \nabla \theta_f \delta_{fs} \rangle \,, \tag{6.46}$$

if $\langle \theta \rangle = 1$ in the periodically developed regime[3].

Finally, the thermal tortuosity is given by

$$\langle \boldsymbol{n}_{fs} T_f \delta_{fs} \rangle_m = \langle \boldsymbol{n}_{fs} \delta_{fs} \rangle_m T_s = -T_s \nabla \epsilon_{fm} \tag{6.47}$$

[3]Note that in [1], we erroneously changed the sign convention for h_{fs}.

and hence vanishes for a periodic solid structure as $\epsilon_{fm} = \epsilon_f$ is constant.

From the previous expressions, we conclude that the weighting function $m = m_C * m_\lambda * m_V$ ensures that the closure terms, at least for the periodically developed heat transfer regime in periodic solid structures, have a representation based on a constant interfacial heat transfer coefficient and a constant dispersion vector. Both constant closure coefficients follow from the rescaled temperature distribution on a unit cell. Accordingly, the functional dependence of the interfacial heat transfer coefficient is given by

$$h_{fs} = h_{fs}\left(\rho_f, c_f, k_f, \mu_f, \langle \boldsymbol{u} \rangle, \boldsymbol{f}, \Gamma_{fs} \cap \Omega_{\text{unit}}, t\right) . \tag{6.48}$$

The thermal dispersion vector $\boldsymbol{k}_d$ has a similar functional dependence when $m = m_C * m_\lambda * m_V$.

In absence of a body force and for a fixed flow direction as well as fixed unit cell geometry with characteristic reference length L_{ref}, the relationship (6.48) can also be expressed as a dimensionless correlation between the time-averaged Nusselt number $(\overline{h_{fs}} L_{\text{ref}}^2/k_f)$, the Reynolds number based on the volume-averaged velocity $(\rho_f \left\| \langle \overline{\boldsymbol{u}} \rangle \right\| L_{\text{ref}}/\mu_f)$, the Prandtl number $(\mu_f c_f/k_f)$ and the Strouhal number $L_{\text{ref}}/(\tau \left\| \langle \overline{\boldsymbol{u}} \rangle \right\|)$. The thermal dispersion vector $\boldsymbol{k}_d$ has a functional dependence similar to that of the interfacial heat transfer coefficient and thus also varies with the Reynolds number and Prandtl number when $m = m_C * m_\lambda * m_V$.

With the weighting function $m = m_C * m_\lambda * m_V$, the time-averaged macro-scale temperature equation (4.17) poses the following relationship between the closure coefficients $\boldsymbol{k}_d$ and h_{fs} and the temperature decay rate:

$$\rho_f c_f \langle \overline{\boldsymbol{u}} \rangle^f \cdot \boldsymbol{\lambda}_T = k_f \boldsymbol{\lambda}_T \cdot \boldsymbol{\lambda}_T - \overline{h_{fs}} - \rho_f c_f \overline{\boldsymbol{k}_d} \cdot \boldsymbol{\lambda}_T . \tag{6.49}$$

This relationship follows from the macro-scale energy equation, (4.17), after substitution of the definitions of $\boldsymbol{\lambda}_T$ and the closure coefficients. Relation (6.49) is completely equivalent to the rescaled temperature eigenvalue problem (6.24). It shows that the rescaled macro-scale temperature gradient $\boldsymbol{\lambda}_T$, projected in the direction of the time-averaged macro-scale flow velocity $\langle \overline{\boldsymbol{u}} \rangle$, is caused by an imbalance between macro-scale conduction effects, thermal dispersion and convective macro-scale heat transfer at the fluid-solid interface. Because equation (6.49) is the only mechanism for inducing a macro-scale temperature gradient, it explains why the vector $\boldsymbol{\lambda}_T$ has solely a component along the time-averaged macro-scale flow direction $\boldsymbol{e}_s$ in the developed regime.

By (6.49), the negative eigenvalue for the reference temperature or macro-scale temperature decay rate is also given by[4]

$$\lambda_T = \frac{\rho_f c_f \left(\left\| \langle \overline{\boldsymbol{u}} \rangle^f \right\| + \overline{\boldsymbol{k}_d} \cdot \boldsymbol{e}_s \right)}{2k_f} \left(1 + \sqrt{1 + \frac{4k_f \overline{h_{fs}}}{\left(\rho_f c_f \left(\left\| \langle \overline{\boldsymbol{u}} \rangle^f \right\| + \overline{\boldsymbol{k}_d} \cdot \boldsymbol{e}_s \right) \right)^2}} \right) . \tag{6.50}$$

In order that λ_T be a real negative number, the discriminant of equation (6.49) must be greater than or equal to zero. Therefore, in order to have at least one physically possible solution, the closure coefficients must satisfy

$$\rho_f c_f \left(\left\| \langle \overline{\boldsymbol{u}} \rangle^f \right\| + \overline{\boldsymbol{k}_d} \cdot \boldsymbol{e}_s \right) \geq \sqrt{4k_f \overline{h_{fs}}} \, . \tag{6.51}$$

In the special case when macro-scale conduction effects and thermal dispersion are negligible in (6.49), one finds that the constant exponent of the macro-scale temperature equals

$$\lambda_T \simeq \frac{-\overline{h_{fs}}}{\rho_f c_f \left\| \langle \overline{\boldsymbol{u}} \rangle^f \right\|} \, . \tag{6.52}$$

This constant exponent was introduced as the decay rate of the steady volume-averaged temperature in the study of Kuwahara, Nakayama et al. [21, 22], although our analysis shows that it requires the macro-scale temperature to be based on the weighting function $m = m_C * m_\lambda * m_V$.

6.8 Periodically Developed Planar Heat Transfer in Isothermal Solids

Periodically Developed Planar Heat Transfer Regime

Let us consider again periodically developed planar flow through a plate channel, like in Section 5.13, where it was explained that this type of flow is the periodic solution of equations (5.21) and (5.72) on a unit cell (5.71). In addition, let us deal with the case where the walls of the plate channel have the same constant temperature as the spatially periodic solid structures in the channel or the case where there is no heat flux at the boundary between the fluid and the wall.

[4]Note that in [1], the equations corresponding to (6.49) and (6.50) contain some typos.

In that case, we have $T_{wt} = T_s$, or $T_{wb} = T_s$ and/or $q_{wt} = 0$ or $q_{wb} = 0$ in (4.59) and (4.60). From a physical point, this means that each of the channel walls is either thermally insulated or made of a material with a very high conductivity just like the solid structures are assumed to have a very high thermal conductivity.

Furthermore, we still assume that there are no volumetric heat sources present and that viscous dissipation in the flow can be neglected: $\dot{q} = \dot{q}_{\text{visc}} = 0$.

Under these conditions, there can exist a reference temperature with a constant decay rate as in (6.17) and thus also a rescaled temperature θ which is periodic over the same unit cell (5.71) as the velocity field. In the latter case, we speak of the *periodically developed planar heat transfer regime*. The rescaled temperature θ in the periodically developed planar heat transfer regime is described by equation (6.4) and satisfies the boundary conditions

$$\begin{aligned} &\theta_f(\boldsymbol{x},t) = 0 \qquad \boldsymbol{x} \in \Gamma_{fs} \cap \Omega_{\text{unit}} \qquad \text{and} \qquad \theta_f(\boldsymbol{x},t) = \theta_f\left(\boldsymbol{x} + \boldsymbol{l}^{(j)}, t\right), \\ &\theta_f(\boldsymbol{x},t) = 0 \qquad \text{or} \qquad \boldsymbol{e}^{(3)} \cdot \nabla\theta_f = 0 \qquad \boldsymbol{x} \in \Gamma_{fw} \cap \Omega_{\text{unit}} \end{aligned} \tag{6.53}$$

where $j = \{1, 2\}$ and $\boldsymbol{x} \in \Gamma_{fw} \cap \Omega_{\text{unit}} \Leftrightarrow x_3 = \pm\frac{l_3}{2}$.

Macro-Scale Temperature

In the periodically developed planar heat transfer regime, the appropriate reference temperature $T_{\text{ref}} = \langle T \rangle_m$ for the rescaled temperature θ is also based on a weighting function of the form $m = m_C * m_\lambda * m_V$, as in §6.6. However, the difference is that the filter window of m_V and m_λ corresponds to the unit cell (5.71) instead of (5.2). Therefore, the macro-scale description of §6.7 remains valid for the periodically developed heat transfer regime in planar flow through isothermal solids, when we re-interpret the unit cell as the one defined by (5.2).

When the solid structures have a shape which is symmetric with respect to the middle plane $\Omega_{x_3=0}$ of the channel, the vector $\boldsymbol{\lambda}_T$ is expected to have no component in the direction $\boldsymbol{e}^{(3)}$ perpendicular to $\Omega_{x_3=0}$. Also when the bottom and top plate of the channel are separated over a relatively small distance l_3, it is very likely that $\boldsymbol{\lambda}_T \cdot \boldsymbol{e}^{(3)} = 0$, because then the overall flow direction usually remains parallel to both plates, $\boldsymbol{e}_s \cdot \boldsymbol{e}^{(3)} = 0$.

If $\boldsymbol{\lambda}_T \cdot \boldsymbol{e}^{(3)} = 0$, the filter $m = m_C * m_\lambda * m_V$ with the unit cell (5.71) as filter window, is separable with respect to $\boldsymbol{e}^{(3)}$.

$$\langle\boldsymbol{\phi}\rangle = \langle\langle\boldsymbol{\phi}\rangle_{1,2}\rangle_3 = \langle\langle\boldsymbol{\phi}\rangle_3\rangle_{1,2}$$

$$\text{with} \qquad m_3'(-y_3) = \frac{1}{l_3}\,\mathrm{rect}\,(y_3)\,,$$

$$m_{1,2}(-\boldsymbol{y}_{1,2}) = \left[\beta(\boldsymbol{\lambda}_T)\mathrm{e}^{-\boldsymbol{y}_{1,2}\cdot\boldsymbol{\lambda}_T}\prod_{j=1}^{2}\mathrm{rect}\left(\frac{\boldsymbol{y}_{1,2}\cdot\boldsymbol{l}^{(j)}}{\|\boldsymbol{l}^{(j)}\|^2}\right)\right] * \left[\prod_{j=1}^{2}\mathrm{rect}\left(\frac{\boldsymbol{y}_{1,2}\cdot\boldsymbol{l}^{(j)}}{\|\boldsymbol{l}^{(j)}\|^2}\right)\right]. \tag{6.54}$$

This separable filter has a filter window coinciding with $I_3 = \left[-\frac{l_3}{2}, \frac{l_3}{2}\right]$ and $\bar{\Omega}_{1,2} = \left\{\boldsymbol{y}_{1,2} = c_1\boldsymbol{l}^{(1)} + c_2\boldsymbol{l}^{(2)} | c_j \in [-1,1]\right\}$.

For the separable filter of (6.54), the macro-scale temperature and macro-scale planar temperature are equal (cf. (4.76)):

$$\langle\mathcal{T}\rangle_m = \langle T\rangle_m \qquad \Leftrightarrow \qquad \boldsymbol{\lambda}_T \cdot \boldsymbol{e}^{(3)} = 0\,. \tag{6.55}$$

This fact can also be verified from the expression for the planar temperature. Given that $\boldsymbol{e}_\lambda \cdot \boldsymbol{e}^{(3)} = \boldsymbol{e}_s \cdot \boldsymbol{e}^{(3)} = 0$, the planar temperature (4.49) in $\Omega_{x_3=0}$ equals

$$\mathcal{T} = A_0\langle\theta\rangle_3\mathrm{e}^{\boldsymbol{\lambda}_T\cdot\boldsymbol{x}} + T_s \qquad \Leftrightarrow \qquad \boldsymbol{\lambda}_T \cdot \boldsymbol{e}^{(3)} = 0\,, \tag{6.56}$$

where $\boldsymbol{x} = \boldsymbol{x}_{1,2}$ as $\langle\,\rangle_3$ is evaluated at $(\boldsymbol{x}_{1,2}, x_3 = 0, t)$.

Hence, when the planar temperature is filtered with the weighting function $m_{1,2}$ of (5.80), we find indeed that

$$\langle\mathcal{T}\rangle_{1,2} = A_0\langle\theta\rangle\mathrm{e}^{\boldsymbol{\lambda}_T\cdot\boldsymbol{x}} + T_s \qquad \Leftrightarrow \qquad \boldsymbol{\lambda}_T \cdot \boldsymbol{e}^{(3)} = 0\,, \tag{6.57}$$

which is identical to (6.29).

Periodically Developed Planar Closure Terms

Equation (6.55) implies the following periodic similarity for the planar temperature:

$$\langle\theta\rangle_3 = \frac{\mathcal{T} - T_s}{\langle T\rangle_m - T_s} = \frac{\mathcal{T} - T_s}{\langle\mathcal{T}\rangle_m - T_s}\,. \tag{6.58}$$

With (6.58), the closure terms for the planar temperature equation (4.53) can be governed from the rescaled temperature on the unit cell. The first closure term in the planar temperature equation is given by

$$\frac{\psi_3^{\mathrm{I}}}{\mathcal{T}-T_s} = \rho\frac{1}{\langle\theta\rangle_3}\nabla^\nu\cdot(\boldsymbol{v}c\langle\theta\rangle_3 - \langle\boldsymbol{u}_{1,2}c\theta\rangle_3) + \frac{1}{\langle\theta\rangle_3}(\boldsymbol{v}c\langle\theta\rangle_3 - \langle\boldsymbol{u}_{1,2}c\theta\rangle_3)\cdot\boldsymbol{\lambda}_T\,, \tag{6.59}$$

while the second closure term equals

$$\frac{\psi_3^{\mathrm{II}}}{\mathcal{T}-T_s} = -\rho\frac{\langle\nabla_3^\nu\cdot(\boldsymbol{u}_3c\theta)\rangle_3}{\langle\theta\rangle_3} + \rho c\varphi_3\frac{T_s}{\mathcal{T}-T_s} = 0\,. \tag{6.60}$$

The second closure term is zero, just like $\varphi_3 = 0$, due to the no-slip condition (3.59) when m_3' is independent of y_3 (cf. (D.5)). Furthermore, the third closure term has the form

$$\frac{\psi_3^{\mathrm{III}}}{\mathcal{T}-T_s} = \frac{\langle\nabla_3^\nu\cdot(k\nabla_3^\nu\theta)\rangle_3}{\langle\theta\rangle_3} \triangleq -h_w\,. \tag{6.61}$$

Because $m_3'(-y_3) = \frac{1}{l_3}$, the heat transfer coefficient h_w can be split as

$$h_w = h_{wb} + h_{wt}\,, \tag{6.62}$$

where

$$h_{wt} \triangleq -k_f\frac{1}{\langle\theta\rangle_3}\,\frac{1}{l_3}\frac{\partial\theta}{\partial x_3}\bigg|_{x_3=\frac{l_3}{2}} \quad\text{and}\quad h_{wb} \triangleq k_f\frac{1}{\langle\theta\rangle_3}\,\frac{1}{l_3}\frac{\partial\theta}{\partial x_3}\bigg|_{x_3=-\frac{l_3}{2}}\,. \tag{6.63}$$

Then, it holds that

$$q_{wt} = h_{wt}\,(T_s-\mathcal{T}) \qquad\text{and}\qquad q_{wb} = h_{wb}\,(T_s-\mathcal{T})\,, \tag{6.64}$$

in accordance with (4.59) and (4.60). Both heat transfer coefficients h_{wt} and h_{wb} depend on the spatial coordinate $\boldsymbol{x}_{1,2}$.

Periodically Developed Planar Macro-Scale Closure Terms By equation (6.55) we also have

$$\langle T\rangle_m - T_s = \langle\mathcal{T}\rangle_m - T_s = \frac{\langle\theta\rangle}{\langle\theta\rangle_3}(\mathcal{T}-T_s)\,. \tag{6.65}$$

Therefore, the first closure term in the macro-scale planar temperature equation is given by

$$\begin{aligned}\langle\psi_3^{\mathrm{I}}\rangle_m &= \epsilon_{fm}\langle\psi_3^{\mathrm{I}}\rangle_m^f \\ &= \left(c_f\langle\boldsymbol{v}\langle\theta\rangle_3\rangle - c_f\langle\langle\boldsymbol{u}_{1,2}\theta\rangle_3\rangle\right)\cdot\boldsymbol{\lambda}_T\left(\langle\mathcal{T}\rangle_m - T_s\right) . \end{aligned} \tag{6.66}$$

This expression follows from (6.59), (6.65) and (6.28).

The third closure term in the macro-scale planar temperature equation is given by

$$\begin{aligned}\langle\psi_3^{\mathrm{III}}\rangle_m &= \epsilon_{fm}\langle\psi_3^{\mathrm{III}}\rangle_m^f \\ &= \langle h_w\langle\theta\rangle_3\rangle\left(T_s - \langle\mathcal{T}\rangle_m\right) . \end{aligned} \tag{6.67}$$

This result is obtained from (6.61), (6.65) and (6.28).

In analogy with (6.24), the temperature decay rate of the macro-scale planar temperature satisfies the relationship

$$\langle\boldsymbol{n}_{fs}\cdot k_f\{\nabla\langle\bar{\theta}\rangle_3\}_f\delta_{fs}\rangle - \rho_f c_f\langle\langle\overline{\boldsymbol{u}_{1,2}}\theta\rangle_3\rangle\cdot\boldsymbol{\lambda}_T + k_f\lambda_T^2 - \langle\overline{h_w\langle\theta\rangle_3}\rangle = 0 . \tag{6.68}$$

where, if equation (3.45) holds,

$$-\langle\boldsymbol{n}_{fs}\cdot k_f\{\nabla\langle\bar{\theta}\rangle_3\}_f\delta_{fs}\rangle = \langle h_{fs}\rangle_3 \qquad \Leftrightarrow \qquad \boldsymbol{n}_{fs}(\boldsymbol{x}_{1,2}) . \tag{6.69}$$

For clarity, we precise that the volume-averaging operator $\langle\ \rangle$ in (6.66)-(6.69) is defined as in (5.5), but with $\mathrm{n}_j = 2$.

Separable Form of the Rescaled Temperature

When we neglect the thermal conduction in $\Omega_{x_3=0}$, i.e. $\nabla_{1,2}^{\nu}\cdot\nabla_{1,2}^{\nu}T \simeq 0$ everywhere except at Γ_{fs} and assume that the velocity is given by equation (3.62), the rescaled temperature can be shown to be a separable function of the coordinate x_3:

$$\theta(\boldsymbol{x},t) \simeq \langle\theta\rangle_3|_{(\boldsymbol{x}_{1,2},t)}\,\zeta_\theta(x_3) . \tag{6.70}$$

The proof of this form is included in Appendix M and also holds when $\nabla_{1,2}^{\nu}\cdot\nabla_{1,2}^{\nu}T \neq 0$ and $\zeta_{\boldsymbol{u}} = 1$.

The function $\zeta_\theta(x_3)$ is the solution of the differential equation

$$\frac{d^2\zeta_\theta}{dx_3^2} + \lambda_\theta\zeta_{\boldsymbol{u}}(x_3)\zeta_\theta(x_3) = 0 . \tag{6.71}$$

The eigenvalue λ_θ in (6.71) is a constant determined by the following boundary conditions (6.72)

$$\frac{d\zeta_\theta}{dx_3} = 0 \qquad \text{or} \qquad \zeta_\theta = 0 \qquad \text{at} \qquad x_3 = \pm\frac{l_3}{2}\,. \tag{6.72}$$

The boundary condition $\frac{d\zeta_\theta}{dx_3} = 0$ at $x_3 = \frac{l_3}{2}$ holds if $q_{wt} = 0$. The boundary condition $\frac{d\zeta_\theta}{dx_3} = 0$ at $x_3 = -\frac{l_3}{2}$ holds if $q_{wb} = 0$. In the other case, $T = T_s$ holds, so that $\zeta_\theta = 0$.

With the separable form of θ from (6.70), the closure terms can be simplified to

$$\psi_3^{\mathrm{I}} \simeq \rho\,(1 - \langle\zeta_\theta\zeta_{\boldsymbol{u}}\rangle_3)\,\nabla^\nu\cdot(\boldsymbol{v}c\mathcal{T}) \tag{6.73}$$

and

$$\psi_3^{\mathrm{III}} \simeq \langle\nabla_3^\nu\cdot(k\nabla_3^\nu\zeta_\theta)\rangle_3\,(\mathcal{T} - T_s)\,. \tag{6.74}$$

Furthermore, the heat transfer coefficients (6.63) at the wall surfaces are given by

$$h_{wt} \simeq -k_f\,\frac{1}{l_3}\frac{d\zeta_\theta}{dx_3}\bigg|_{x_3=\frac{l_3}{2}} \qquad \text{and} \qquad h_{wb} \simeq k_f\,\frac{1}{l_3}\frac{d\zeta_\theta}{dx_3}\bigg|_{x_3=-\frac{l_3}{2}}\,. \tag{6.75}$$

The above heat transfer coefficients are space-and-time independent.

With the last three expressions, the closure terms for the macro-scale planar temperature equations become

$$\langle\psi_3^{\mathrm{I}}\rangle_m \simeq \rho_f\,(1 - \langle\zeta_\theta\zeta_{\boldsymbol{u}}\rangle_3)\left(\nabla\cdot\left(\epsilon_{fm}\langle\boldsymbol{v}\rangle_m^f c_f\langle\mathcal{T}\rangle_m^f\right) + \nabla\cdot(c_f\boldsymbol{\mathcal{D}})\right), \tag{6.76}$$

$$\langle\psi_3^{\mathrm{III}}\rangle_m \simeq (h_{wt} + h_{wb})\,(T_s - \langle\mathcal{T}\rangle_m)\,. \tag{6.77}$$

The eigenvalue problem (6.68) for the temperature decay rate is then equivalent to

$$-\langle\overline{h_{fs}}\rangle_3 - h_{wt} - h_{wb} - \rho_f c_f\langle\zeta_\theta\zeta_{\boldsymbol{u}}\rangle_3\langle\overline{\boldsymbol{v}\langle\theta\rangle_3}\rangle\cdot\boldsymbol{\lambda}_T + k_f\lambda_T^2 \simeq 0\,. \tag{6.78}$$

The last term $k_f\lambda_T^2$ should be neglected when $\nabla_{1,2}^\nu\cdot\nabla_{1,2}^\nu T \simeq 0$ is assumed everywhere except at Γ_{fs}. If the thermal dispersion vector $\boldsymbol{k}_d \simeq \langle\zeta_\theta\zeta_{\boldsymbol{u}}\rangle_3\langle\widetilde{\boldsymbol{v}}\overline{\langle\theta\rangle_3}\rangle$ can be neglected, we thus find that the temperature decay rate of the planar macro-scale temperature equals

$$\lambda_T \simeq -\frac{\langle\overline{h_{fs}}\rangle_3 + h_{wt} + h_{wb}}{\rho_f c_f\langle\zeta_\theta\zeta_{\boldsymbol{u}}\rangle_3\|\langle\overline{\boldsymbol{v}}\rangle\|}\,, \tag{6.79}$$

which is the equivalent of (6.52) for two-dimensional planar flow.

6.9 Macro-Scale Heat Transfer in an Array of Isothermal Cylinders

In the following case study, the weighted spatial averaging technique is applied to describe the steady macro-scale heat transfer through an array of N solid cylinders at constant temperature. This simple case study provides some illustrations which reveal the main characteristics of the periodically developed heat transfer regime in isothermal periodic solid structures.

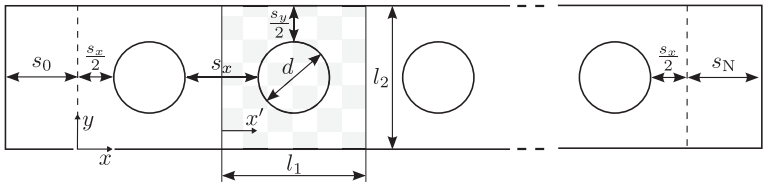

Figure 6.3: Geometry of cylinder array and unit cell.

The geometrical parameters of the cylinder array in Figure 6.3 consist of the cylinder diameter d, the horizontal and vertical cylinder spacing s_x and s_y, as well as the positions of the first and last cylinder, s_0 and s_N respectively. A two-dimensional unit cell of the array with lattice sizes l_1 and l_2 and local axis x' is indicated by the checker-board pattern in Figure 6.3. The values for all the case parameters are summarized in Table 6.1.

System domain		**Unit cell**		**Regime**	
s_0/d	1	s_x/d	1	Re	100
s_N/d	1	s_y/d	1	Pr	1
N	15				

Table 6.1: Heat Transfer in an Array of Isothermal Cylinders: Case study parameters.

The flow field through the array is considered two-dimensional and the main flow direction is along the x-axis of the global reference frame. The y-axis is therefore perpendicular to the main flow. The total pressure drop Δp over the array between in- and outlet is specified as boundary

condition. At the boundaries of the solid cylinders, the velocity field satisfies the no-slip condition. Furthermore, the inlet temperature T_{in} is prescribed and a zero gradient condition is set for the temperature at the outlet. At the other domain boundaries, symmetry boundary conditions for the velocity, pressure and temperature distributions are imposed.

For numerically solving the steady Navier-Stokes flow and temperature equations with the finite-volume method, the gradient operator is discretized according to the least-square gradient scheme of [30], while the Laplacian operator is discretized using the approach of [31]. A linear face interpolation scheme is used for the discrete divergence operator. The unstructured finite-volume mesh for the cylinder array consists of a series of N square mesh blocks, each centred around a single cylinder. Every mesh block is composed of a nearly orthogonal elliptic mesh of about 100 000 quadrilateral cells for the fluid region and a triangular Delaunay mesh of about 6 000 cells for the cylindrical solid region. The mesh for the solid region is used to apply the discrete spatial filter operator proposed by [32] on the discrete flow and temperature distributions.

All distributions in this case study are filtered assuming periodicity over the symmetry boundaries, so that the filtered quantities vary only in the x-direction over the cylinder array. The one-dimensional nature of the filtered results facilitates their graphical representation and interpretation.

Figure 6.4 presents the dimensionless temperature profile at the centreline of the cylinder array. The dimensionless temperature $T^+ \triangleq (T-T_s)/(T_{\text{in}}-T_s)$ is defined such that it becomes zero in the solid domain. Figure 6.4 shows that the fluid temperature decreases in front of each cylinder, as the bulk fluid transfers heat towards the cylinders, which maintain a temperature $T_s^+ = 0$ lower than the bulk fluid temperature T_b^+ (cf. (6.14)). In the wake zone after each cylinder, the heat transfer is lower than in front of the cylinder, due to a lower fluid velocity in this region and the existence of a recirculation zone. Therefore, the fluid temperature rises again in the wake zone behind each cylinder.

In this laminar flow regime at a moderate Reynolds number, $\text{Re} \triangleq \rho_f U_{\text{ref}} d / \mu_f = 100$ where $U_{\text{ref}} \triangleq \sqrt{\Delta p/\rho_f}$, the flow field is affected by entrance effects only over a short distance from the inlet. As a result, the flow is periodically developed already after the second cylinder. Also the heat transfer regime is periodically developed downstream from the second cylinder. The simultaneous development of the flow and temperature

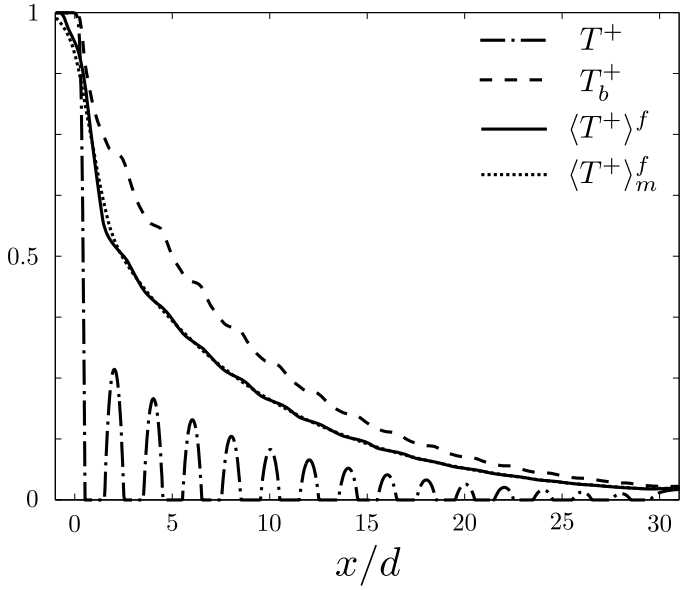

Figure 6.4: Filtered dimensionless temperature distributions at the centreline $y = \frac{l_2}{2}$ of the cylinder array.

fields can be explained by noting that the relative scales of momentum diffusion and thermal diffusion are equal in this case: $\mathrm{Pr} = 1$.

The onset of the periodically developed heat transfer regime is reflected by the exponentially decreasing profile of the filtered temperature $\langle T^+ \rangle_m^f$ in Figure 6.4, for $x/d > 4$. The intrinsically filtered temperature $\langle T^+ \rangle_m^f$ in Figure 6.4 is calculated with the matched weighting function $m = m_\lambda * m_V$. In this specific case, the decay rate λ_T of the filtered temperature is rather small, $\lambda_T l_1 \ll 1$, so that the weighting function $m = m_V * m_V$ would have yielded nearly the same curve for $\langle T^+ \rangle_m^f$ as the matched filter in Figure 6.4. On the other hand, the difference between the intrinsically volume-averaged temperature $\langle T^+ \rangle^f$ and filtered temperature $\langle T^+ \rangle_m^f$ is more pronounced. The profile of the volume-averaged temperature wiggles around the profile of $\langle T^+ \rangle_m^f$ in Figure 6.4, due to the fact that the decay rate of $\langle T^+ \rangle^f$ in the developed regime varies periodically over the array.

The reference temperature decay rate (cf. (6.6)) in the periodically developed regime is shown in Figure 6.5 for four different reference tempera-

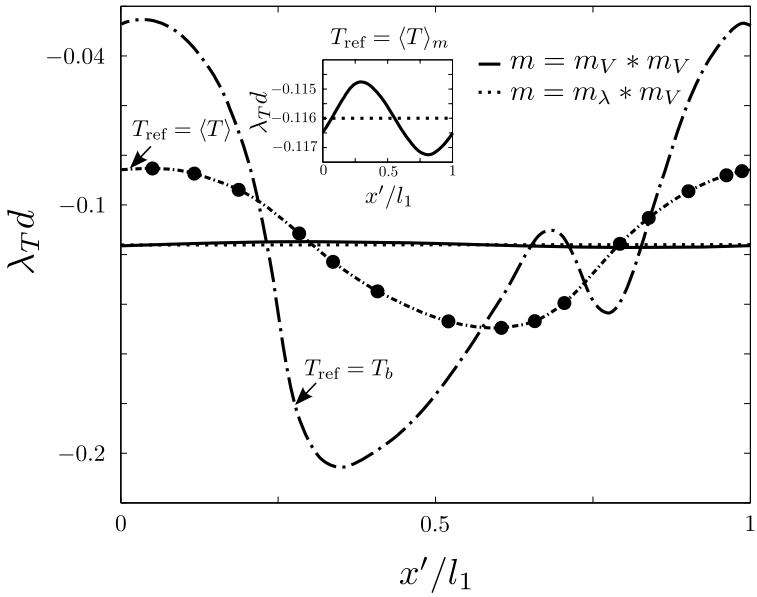

Figure 6.5: Variation of the decay rate over the unit cell domain for different reference temperatures.

tures T_{ref} over the unit cell domain. The appropriate reference temperature for the periodically developed heat transfer regime is the macro-scale temperature $\langle T \rangle_m$ obtained by filtering the temperature with the matched filter $m = m_\lambda * m_V$, because this macro-scale temperature has the same constant decay rate as the physical temperature envelope. The reference temperature $T_{\text{ref}} = \langle T \rangle_m$ with $m = m_V * m_V$ is obtained by volume-averaging the temperature twice. From Figure 6.5 we observe that in this numerical experiment, the physically meaningful constant temperature decay rate can be determined in good approximation by averaging the temperature distribution twice with a simple volume filter. On the contrary, by applying a single volume averaging filter, we find a volume averaged temperature $\langle T \rangle$ with a distinctly spatially varying decay rate. This makes it difficult to assign a physical meaning to the volume-averaged temperature $\langle T \rangle$ in the periodically developed heat transfer regime. Lastly, Figure 6.5 illustrates that for the same reason also the bulk temperature T_b complicates the description of the developed regime in periodic isothermal solids.

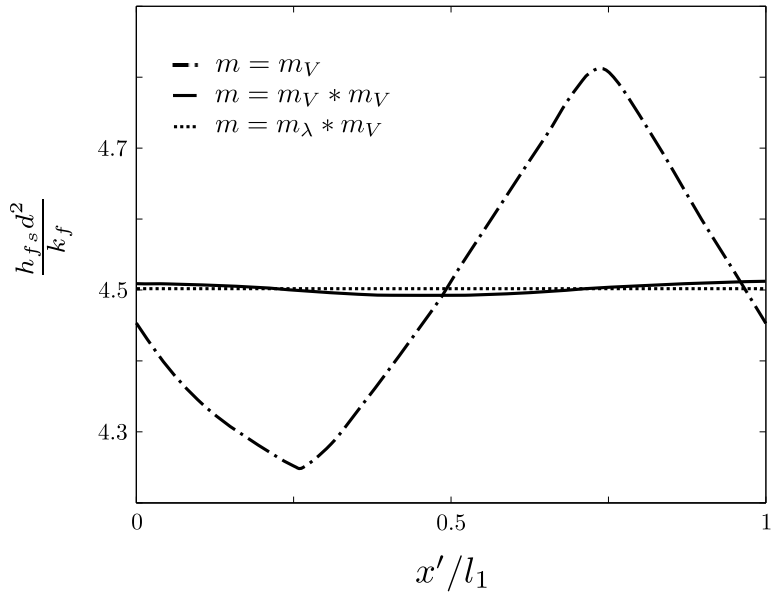

Figure 6.6: Variation of the interfacial heat transfer coefficient over the unit cell domain for different weighting functions.

The value of the interfacial heat transfer coefficient depends in the first place on the weighting function of the filtered temperature (cf. (6.45)). In Figure 6.6, the heat transfer coefficient h_{fs} for the volume-averaged temperature varies clearly in the main flow direction over the unit cell domain. The fact the heat transfer coefficient for the volume-averaged temperature is a function of the position of the averaging window $\bar{\Omega}(\boldsymbol{x}) = \Omega_{\text{unit}}(\boldsymbol{x})$, was also remarked by Teruel et al. [29]. Teruel et al. pragmatically suggested to use a double averaging procedure in order to obtain a constant h_{fs}. Their pragmatic solution is also justified in this specific case, because the heat transfer coefficient for the double-averaged temperature $\langle T \rangle_m$ with $m = m_V * m_V$ in Figure 6.6, deviates less than a percent from its mean value. However, as illustrated in Figure 6.6, a truly constant heat transfer coefficient in the periodically developed regime is theoretically only ensured by the matched weighting function $m = m_\lambda * m_V$.

The interfacial heat transfer coefficient $h_{fs}(m_V)$ for the volume-average filter and the spatially constant heat transfer coefficient $h_{fs}(m_\lambda * m_V)$ for

the matched filter are related to each other as

$$h_{fs}(m_V) = h_{fs}(m_\lambda * m_V) + \frac{\displaystyle\sum_{n=1}^{\infty} \frac{1}{n!} \langle \boldsymbol{n}_{fs} \cdot \nabla\theta_f \left(\boldsymbol{y} \cdot \boldsymbol{\lambda}_T\right)^n \delta_{fs} \rangle}{\displaystyle\sum_{n=1}^{\infty} \frac{1}{n!} \langle \theta \left(\boldsymbol{y} \cdot \boldsymbol{\lambda}_T\right)^n \delta_{fs} \rangle} . \tag{6.80}$$

So for small decay rates (6.37), we have $|\boldsymbol{y} \cdot \boldsymbol{\lambda}_T| \leq |\boldsymbol{l}^{(j)} \cdot \boldsymbol{\lambda}_T| \ll 1$ and

$$h_{fs}(m_V) \simeq h_{fs}(m_\lambda * m_V) + \frac{\langle \boldsymbol{n}_{fs} \cdot \nabla\theta_f \left(\boldsymbol{y} \cdot \boldsymbol{\lambda}_T\right) \delta_{fs} \rangle}{\langle \theta \left(\boldsymbol{y} \cdot \boldsymbol{\lambda}_T\right) \delta_{fs} \rangle} . \tag{6.81}$$

The second term on the right-hand side of the last result explains the difference between $h_{fs}(m_V)$ and $h_{fs}(m_\lambda * m_V)$ in Figure 6.6.

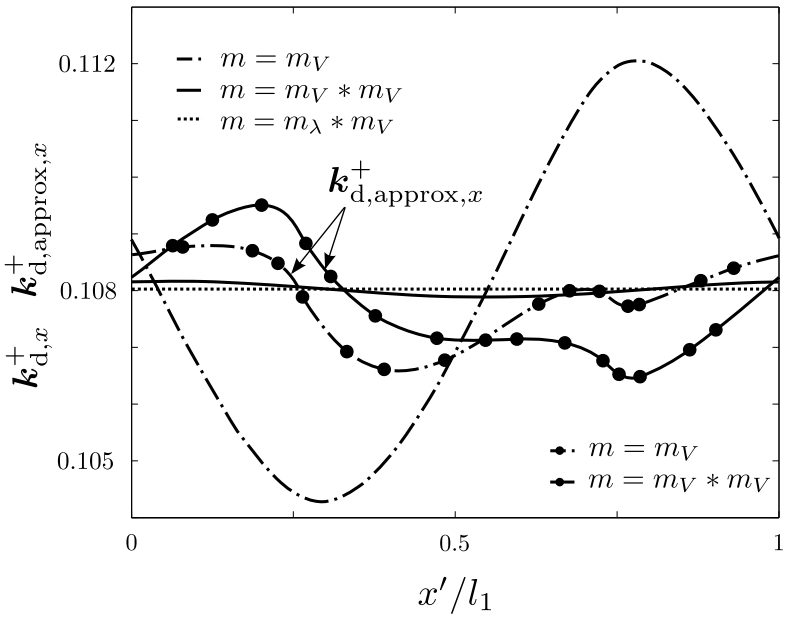

Figure 6.7: Variation of the streamwise component of the dispersion vector over the unit cell domain for different weighting functions.

The matched weighting function also yields a constant dispersion coefficient in the developed heat transfer regime. The constant dimensionless dispersion coefficient for $m = m_\lambda * m_V$ can be calculated in two ways, either as $\boldsymbol{k}_\mathrm{d}^+ \triangleq \boldsymbol{k}_\mathrm{d}/U_\mathrm{ref}$ or as $\boldsymbol{k}_{\mathrm{d,\ approx}}^+ \triangleq \boldsymbol{k}_{\mathrm{d,\ approx}}/U_\mathrm{ref}$, and is shown in Figure 6.7. The equality $\boldsymbol{k}_\mathrm{d} = \boldsymbol{k}_{\mathrm{d,\ approx}}$ holds exactly because the thermal dispersion equals $\boldsymbol{D} = \langle\widetilde{\boldsymbol{u}}\widetilde{T}\rangle_m$ for this filter. For the volume filter and double volume filter, $\boldsymbol{D} \simeq \langle\widetilde{\boldsymbol{u}}\widetilde{T}\rangle_m$ holds only approximately. The difference between $\boldsymbol{k}_\mathrm{d}$ and $\boldsymbol{k}_{\mathrm{d,\ approx}}$ is mostly ignored in the context of the volume-averaging technique. Figure 6.7 confirms that the relative discrepancies between $\boldsymbol{k}_\mathrm{d}$ and $\boldsymbol{k}_{\mathrm{d,\ approx}}$ for $m = m_V$ or $m = m_V * m_V$ are at most one percent in this case. Nevertheless, one should be careful not to generalize the validity of $\boldsymbol{k}_\mathrm{d} \simeq \boldsymbol{k}_{\mathrm{d,\ approx}}$ towards different solid structures or even other flow and heat transfer regimes with a different Re and Pr .

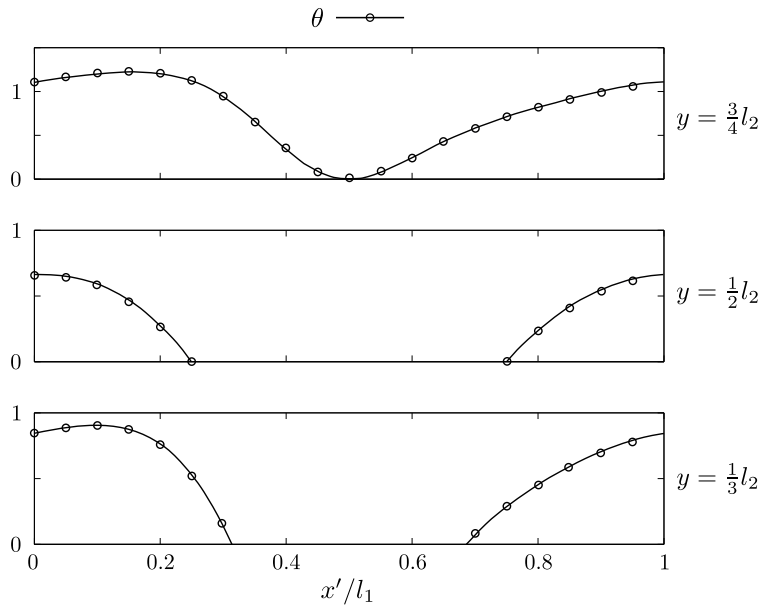

Figure 6.8: Comparison of rescaled temperature profiles around eighth cylinder (solid lines) with unit cell simulation (circle markers).

The final illustration, Figure 6.8, gives the profiles of the rescaled temperature θ within the unit cell of which the centroid coincides with the center of the eighth cylinder. The profiles obtained by DNS of the temperature

field equations, cf. (4.5), are in agreement with the profiles retrieved by solving the rescaled temperature equations (6.4) and (6.10) on the unit cell domain. Figure 6.8 demonstrates that when the reference temperature for the rescaled temperature corresponds to the macro-scale temperature based on the matched weighting function, a perfect reconstruction of the micro-scale temperature field is possible. The reconstruction requires only the knowledge of the unit cell geometry, as well as parameters of the flow and heat transfer regime, Pr and Re.

6.10 Conclusions

For the periodically developed heat transfer regime in isothermal periodic solid structures, the appropriate macro-scale temperature is obtained by averaging the temperature with a weighting function which matches the constant decay rate of the exponential temperature envelope. This macro-scale temperature defines a scaling factor which maps the temperature profiles within different unit cells of the solid structures into the same periodic rescaled temperature.

With the aid of the matched weighting function, the closure terms can be represented by a constant interfacial heat transfer coefficient and constant dispersion vector, which are governed from the rescaled temperature distribution on a single unit cell. For small temperature decay rates, spatial averaging with a matched weighting function yields the same result as a double volume-average. On the contrary, a single volume-average as used in the volume-averaging technique (VAT) unavoidably leads to a spatially varying heat transfer coefficient and dispersion vector in the periodically developed regime. The space dependence of the heat transfer coefficient for the volume-averaged temperature has been often erroneously disregarded by previous studies.

To the authors' knowledge, no profound mathematical treatment of the periodically developed heat transfer regime in periodic isothermal solids nor its macro-scale description have been presented before.

Bibliography

[1] G. Buckinx and M. Baelmans, "Macro-scale heat transfer in periodically developed flow through isothermal solids," *Journal of Fluid Mechanics*, vol. 780, pp. 274–298, 009 2015.

[2] Shah, R.K. and London, A.L., *Advances in Heat Transfer: laminar flow forced convection in ducts : a source book for compact heat exchanger analytical data*. New York: Academic Press, Inc., 1978.

[3] S. V. Patankar, C. H. Liu, and E. M. Sparrow, "Fully Developed Flow and Heat Transfer in Ducts Having Streamwise-Periodic Variations of Cross-Sectional Area," *Journal of Heat Transfer*, vol. 99, no. 2, p. 180, 1977.

[4] E. Stalio and M. Piller, "Direct numerical simulation of heat transfer in converging-diverging wavy channels," *Journal of Heat Transfer*, vol. 129, no. 7, pp. 769–777, 2006.

[5] W. Nusselt, "Die abhängigkeit der wärmeübergangszahl von der rohrlänge," *Zeitschrift Vereins Deutscher Ingenieure*, vol. 28, pp. 1154–1158, 1910.

[6] W. M. Kays and A. L. London, *Compact Heat Exchangers*. Krieger Pub Co, 1998.

[7] P.-S. Lee and S. V. Garimella, "Thermally developing flow and heat transfer in rectangular microchannels of different aspect ratios," *International Journal of Heat and Mass Transfer*, vol. 49, no. 1718, pp. 3060 – 3067, 2006.

[8] A. Yutaka, N. Hiroshi, and M. Faghri, "Heat transfer and pressure drop characteristics in a corrugated duct with rounded corners," *International Journal of Heat and Mass Transfer*, vol. 31, no. 6, pp. 1237 – 1245, 1988.

[9] J. Zhang, J. Kundu, and R. M. Manglik, "Effect of fin waviness and spacing on the lateral vortex structure and laminar heat transfer in wavy-plate-fin cores," *International Journal of Heat and Mass Transfer*, vol. 47, pp. 1719–1730, Apr. 2004.

[10] H. Metwally and R. Manglik, "Enhanced heat transfer due to curvature-induced lateral vortices in laminar flows in sinusoidal

corrugated-plate channels," *International Journal of Heat and Mass Transfer*, vol. 47, no. 1011, pp. 2283 – 2292, 2004.

[11] R. M. Manglik, J. Zhang, and A. Muley, "Low Reynolds number forced convection in three-dimensional wavy-plate-fin compact channels: fin density effects," *International Journal of Heat and Mass Transfer*, vol. 48, no. 8, pp. 1439 – 1449, 2005.

[12] G.-N. Xie, Q.-W. Wang, M. Zeng, and L.-Q. Luo, "Numerical investigation of heat transfer and fluid flow characteristics inside a wavy channel," *Heat and Mass Transfer*, vol. 43, pp. 603–611, July 2006.

[13] G.-N. Xie, Q.-W. Wang, M. Zeng, and L.-Q. Luo, "Numerical investigation of heat transfer and fluid flow characteristics inside a wavy channel: erratum," *Heat and Mass Transfer*, vol. 43, pp. 721–721, Feb. 2007.

[14] G.-Y. Zhou, S.-T. Tu, and H.-G. Ma, "Investigations of heat transfer and friction characteristics of compact cross-corrugated recuperators," *Heat and Mass Transfer*, vol. 50, no. 9, pp. 1301–1310, 2014.

[15] G. Wang and S. Vanka, "Convective heat transfer in periodic wavy passages," *International Journal of Heat and Mass Transfer*, vol. 38, no. 17, pp. 3219 – 3230, 1995.

[16] G. Comini, C. Nonino, and S. Savino, "Effect of aspect ratio on convection enhancement in wavy channels," *Numerical Heat Transfer, Part A: Applications*, vol. 44, no. 1, pp. 21–37, 2003.

[17] G. Comini, C. Nonino, and S. Savino, "Effect of space ratio and corrugation angle on convection enhancement in wavy channels," *International Journal of Numerical Methods for Heat & Fluid Flow*, vol. 13, no. 4, pp. 500–519, 2003.

[18] S. M. Karimian and A. G. Straatman, "A thermal periodic boundary condition for heating and cooling processes," *International Journal of Heat and Fluid Flow*, vol. 28, no. 2, pp. 329 – 339, 2007.

[19] A. Martin, C. Saltiel, and W. Shyy, "Frictional losses and convective heat transfer in sparse, periodic cylinder arrays in cross flow," *International Journal of Heat and Mass Transfer*, vol. 41, no. 15, pp. 2383–2397, 1998.

[20] F. Kuwahara, M. Shirota, and A. Nakayama, "A numerical study of interfacial convective heat transfer coefficient in two-energy equation model for convection in porous media," *International Journal of Heat and Mass Transfer*, vol. 44, pp. 1153–1159, 2001.

[21] A. Nakayama, F. Kuwahara, T. Umemoto, and T. Hayashi, "Heat and fluid flow within an anisotropic porous medium," *Journal of Heat Transfer*, vol. 124, no. 4, pp. 746–753, 2002.

[22] A. Nakayama, F. Kuwahara, and T. Hayashi, "Numerical modelling for three-dimensional heat and fluid flow through a bank of cylinders in yaw," *Journal of Fluid Mechanics*, vol. 498, pp. 139–159, 2004.

[23] M. Quintard, M. Kaviany, and S. Whitaker, "Two-medium treatment of heat transfer in porous media: numerical results for effective properties," *Advances in Water Resources*, vol. 20, no. 2-3, pp. 77–94, 1997.

[24] C. DeGroot and A. Straatman, "Numerical results for the effective flow and thermal properties of idealized graphite foam," *Journal of Heat Transfer*, vol. 134, no. 4, p. 042603, 2012.

[25] L. Betchen, A. G. Straatman, and B. E. Thompson, "A nonequilibrium finite-volume model for conjugate fluid/porous/solid domains," *Numerical Heat Transfer, Part A: Applications*, vol. 49, no. 6, pp. 543–565, 2006.

[26] C. T. DeGroot and A. G. Straatman, "A finite-volume model for fluid flow and nonequilibrium heat transfer in conjugate fluid-porous domains using general unstructured grids," *Numerical Heat Transfer, Part B: Fundamentals*, vol. 60, no. 4, pp. 252–277, 2011.

[27] C. T. DeGroot and A. G. Straatman, "Closure of non-equilibrium volume-averaged energy equations in high-conductivity porous media," *International Journal of Heat and Mass Transfer*, vol. 54, no. 23-24, pp. 5039–5048, 2011.

[28] A. Nakayama, F. Kuwahara, and Y. Kodama, "An equation for thermal dispersion flux transport and its mathematical modelling for heat and fluid flow in a porous medium," *Journal of Fluid Mechanics*, vol. 563, pp. 81–96, 2006.

[29] F. Teruel and L. Díaz, "Calculation of the interfacial heat transfer coefficient in porous media employing numerical simulations," *International Journal of Heat and Mass Transfer*, vol. 60, pp. 406–412, 2013.

[30] A. Haselbacher and J. Blazek, "Accurate and Efficient Discretisation of Navier–Stokes Equations on Mixed Grids," *AIAA Journal*, vol. 38, no. 11, pp. 2094–2102, 2000.

[31] P. Traoré, Y. M. Ahipo, and C. Louste, "A robust and efficient finite volume scheme for the discretization of diffusive flux on extremely skewed meshes in complex geometries," *Journal of Computational Physics*, vol. 228, pp. 5148–5159, 2009.

[32] G. Buckinx and M. Baelmans, "Multi-scale modelling of flow in periodic solid structures through spatial averaging," *Journal of Computational Physics*, vol. 291, pp. 34–51, 2015.

CHAPTER

7

MACRO-SCALE DESCRIPTION OF PERIODICALLY DEVELOPED CONJUGATE HEAT TRANSFER

7.1 Introduction

This chapter treats the macro-scale description of the periodically developed conjugate heat transfer regime, in which heat transfer takes place between an incompressible viscous flow and spatially periodic solid structures, through a spatially periodic interfacial heat flux. Parts of this chapter are published in [1]. The macro-scale temperature of the fluid and the solid structures is defined through a spatial averaging operator with a specific weighting function. It is shown that a double volume average is necessary in order to have a linearly changing macro-scale temperature in response to a constant macro-scale heat flux. Furthermore, with the aid of a double volume average, the thermal dispersion source, the thermal tortuosity and the interfacial heat transfer coefficient all become spatially

constant in the developed regime. That way, these closure terms of the macro-scale temperature equations can be exactly determined from the periodic temperature part on a unit cell of the solid structures without taking the spatial moments of the solid into account. The theoretical derivations of this chapter are illustrated for a case study, describing the heat transfer between a fluid flow and an array of solid squares with a uniform volumetric heat source.

7.2 Outline

This chapter starts with a qualitative description of the periodically developed conjugate heat transfer regime in heat transfer devices with spatially periodic solid structures. In Section 4, the historical background on the description of this regime and its macro-scale treatment in the literature are discussed. In Section 5, the general characteristics of the periodically developed conjugate heat transfer regime are given. It is also discussed how the temperature gradient in the periodically developed conjugate heat transfer regime can be determined. The question how to choose the weighting function which defines a physically meaningful macro-scale temperature in the periodically developed conjugate heat transfer regime, is answered in Section 6. It is concluded that the weighting function of Quintard and Whitaker [2, 3] or a double volume-average filter should be chosen. Subsequently, Section 7 treats the exact form of the closure terms in the spatially averaged temperature equations for the double volume-average, as well as for the single volume-average filter. It is shown that for the double volume-average filter, the interfacial heat transfer coefficient, tortuosity and thermal dispersion are spatially constant. The macro-scale treatment of the planar periodically developed conjugate heat transfer regime is expounded in Section 8. In Section 9, all theoretical derivations are illustrated for a two-dimensional flow through an array of solid squares. Finally, in Section 10, the most important conclusions of this chapter are summarized.

7.3 Developed Heat Transfer in Devices under Imposed Heat Flux Conditions

When the solid walls of a heat transfer device are exposed to a uniform external heat flux, the spatially periodic structures typically acquire the same interfacial heat flux distribution in the periodically developed flow regime. In the latter case, we speak of the *periodically developed conjugate heat transfer regime*. The adjective *conjugate* refers to the fact that in the latter regime, the temperature of the fluid and the solid structures are coupled by the heat transfer mechanisms in both the fluid and the solid.

At the bottom of Figure 7.1, an impression is given of the temperature distribution in a plate-fin channel with square pin fins. The red and orange colours indicate the highest temperatures, while the yellow, green and blue colours gradually indicate the lower temperatures. In the figure, the top and bottom channel walls are exposed to a constant heat source so that heat transfer takes place from the channel walls towards the coolant flow and the pin fins. The coolant flow enters the channel at a low temperature (blue colour) to get heated up (red colour) towards the outlet of the channel, while being in contact with the channel walls and pin fins.

When the temperature distribution is filtered with a double volume-average filter, the temperature deviation part can be visualized as in Figure 7.1. The illustration at the top of Figure 7.1 reveals that the temperature deviation part is spatially periodic where the flow is periodically developed. In this chapter, we will show that this feature characterizes the periodically developed conjugate heat transfer regime.

The periodically developed conjugate heat transfer regime can be regarded as a generalization of the *fully developed heat transfer regime* in ducts of a constant cross section with walls subject to a constant heat flux. The fully developed heat transfer regime in ducts with a constant wall heat flux is characterized by the fact that the bulk temperature of the fluid varies linearly in the streamwise direction from cross section to cross section. Therefore, the heat transfer coefficient which relates the wall heat flux to the difference between the fluid bulk temperature and the perimeter-averaged wall temperature at each cross section is constant.

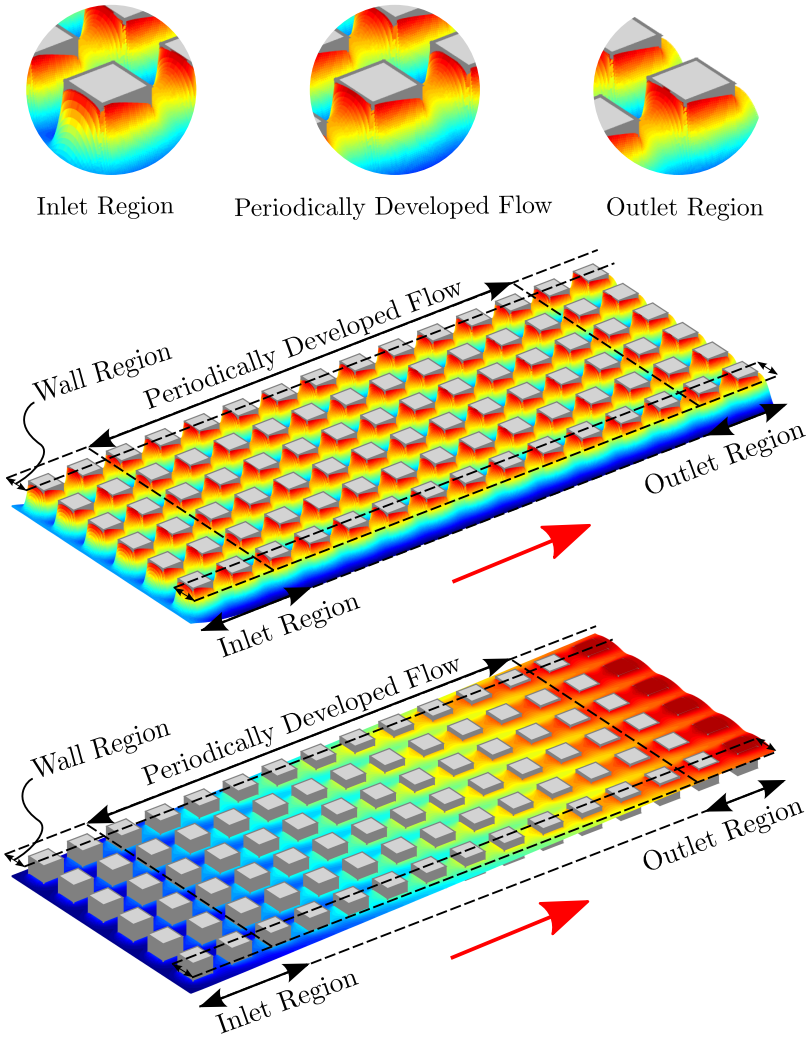

Figure 7.1: Temperature distribution (bottom picture) and temperature deviation part (top picture) in the inlet region, outlet region, wall region and periodically developed flow region within a channel with square pin fins. The channel walls are exposed to a uniform external heat flux.

7.4 Historical Background

Developed Heat Transfer under an Imposed Heat Flux
It has been known for at least a century that the bulk temperature varies streamwise linearly in the laminar fully developed regime in ducts with a constant cross-sectional shape and constant wall heat flux. The constant gradient of the bulk temperature depends on the mass flow rate $\dot{m}$ and the heat capacity c of the fluid, as well as the perimeter P of the duct and the heat flux q''_w [4, 5]:

$$T_b(x) = T_b(0) + \frac{q''_w P}{\dot{m}c} x \,.$$

A review of the solutions for the temperature and the constant heat transfer coefficient $h \triangleq q''_w/(T_w - T_b)$ in the fully developed regime in ducts with a constant wall heat flux was given by Shah and London [4] around 1980. Correlations for the heat transfer coefficient in rectangular ducts under a uniform heat flux were also presented in the work of Lee et al. [6] from 2006.

In the previous chapter, it was already mentioned that Patankar et al. [7] gave a generalization of the steady laminar fully developed heat transfer regime in 1977. This generalization has been called the periodically developed heat transfer regime and occurs in duct flows with a periodically varying cross section. In the steady periodically developed heat transfer regime, the temperature consists of a linear part and a periodic part,

$$T(x,y) = \frac{q''_w L}{\dot{m}c} x + \widehat{T}(x,y) \qquad \text{with} \qquad \widehat{T}(x,y) = \widehat{T}(x+L,y) \,,$$

when the rate of heat addition q''_w to the fluid is constant along the period length L of the duct.

By solving the equations of Patankar et al. numerically, Utriainen and Sunden obtained the heat transfer coefficient $h \triangleq q''_w/\overline{T_w - T_b}$, based on the mean wall-to-bulk temperature difference $\overline{T_w - T_b}$ for a cross section, in cross-wavy and cross-corrugated fins with a uniform wall heat flux [8, 9]. Solutions of the steady periodically developed heat transfer regime for other channel-like solid structures under constant heat flux conditions seem to be absent in the literature.

Apart from the formulation of Patankar, which describes the steady periodically developed heat transfer regime in terms of the periodic tem-

perature variable $\widehat{T}$, also formulations exist in terms of the temperature field itself. Karimian and Straatman [10] proposed the following boundary conditions to determine the inlet and outlet temperatures $T_{i,1}$ and $T_{i,2}$ of a duct unit:

$$T_{i,1} = T_{\mathrm{ref}} - r_c \left(T_{\mathrm{ref}} - T_{i,2}\right) \qquad \text{with} \qquad r_h \triangleq \frac{T_{\mathrm{ref}} - T_{b,2}}{T_{\mathrm{ref}} - T_{b,1}} \,.$$

Here, T_{ref} is a reference temperature that can be assumed as $T_{\mathrm{ref}} = 0$ and $T_{b,1}$ is the prescribed bulk temperature of the fluid at the inlet.

The descriptions of the steady periodically developed heat transfer regime by the previous authors [7, 10] are strictly speaking only applicable to duct flows. A more general case than duct flow is when the solid structures form an array which is not necessarily aligned with the main flow direction. The latter case was treated in the work of Alshare et al. [11] in 2010. In the work of Alshare et al., the fluid temperature over a two-dimensional unit cell of the array was calculated via the boundary conditions

$$T(l, y) = T(0, y) + \frac{\dot{S}_{\mathrm{gen}}}{\rho_f c_f \|\langle \boldsymbol{u} \rangle\|} l \cos\alpha \,,$$
$$T(x, h) = T(x, 0) + \frac{\dot{S}_{\mathrm{gen}}}{\rho_f c_f \|\langle \boldsymbol{u} \rangle\|} h \sin\alpha \,.$$

These boundary conditions specify a temperature gradient over the unit cell, in the direction α of the volume-averaged velocity $\langle \boldsymbol{u} \rangle$, which depends on the rate of heat generation $\dot{S}_{\mathrm{gen}}$. The authors do not clarify whether the heat generation $\dot{S}_{\mathrm{gen}}$ is a separate uniform volumetric heat source or corresponds to the imposed uniform interfacial heat flux.

In the preceding studies, the heat flux at the interface between the fluid and the duct wall or solid structures was assumed to be constant and known. Therefore, the solid temperature was not resolved in the periodically developed heat transfer regime. In the more general case, the heat flux at the fluid-solid interface may no longer be constant, but spatially periodic and dependent on the temperature fields of the fluid and the solid. That means that the solid temperature must also be determined, so that we speak of periodically developed conjugate heat transfer.

A description of the steady periodically developed conjugate heat transfer regime was given by Lopez Penha et al. [12] in 2012. Because Lopez Penha et al. considered the main flow direction to be parallel to the array

of solid structures, the governing equations for the fluid temperature in their work are identical to those of Patankar et al. [7]. Lopez Penha et al. assumed the solid structures to be exposed to a constant volumetric heat source, so that the solid temperature is given by

$$T_s = \alpha x + \widehat{T}_s \, .$$

Here $\widehat{T}_s$ is the part of the solid temperature that is periodic over the unit cell and α is the constant temperature gradient which follows from the constant volumetric heat source $\dot{q}_s$ in the solid:

$$\alpha = \frac{(1-\epsilon_f)\dot{q}_s}{\rho_f c_f \| \langle \boldsymbol{u} \rangle^f \|} \, .$$

Macro-Scale Modelling of Heat Transfer for Imposed Heat Flux
In our literature review on the macro-scale modelling of the periodically developed heat transfer regime in isothermal solid structures (cf. §6.4), we distinguished three levels of approximation. The same three levels of approximation are also present in the literature on the macro-scale modelling of periodically developed heat transfer in solid structures with an imposed heat flux.

The first and second level of approximation refer to the fact that the existing macro-scale descriptions are based on VAT equations in which the approximate closure terms are inexactly represented by space-independent effective parameters. For instance, in the studies of Kuwahara, Nakayama and Koyama [13, 14] from 1996 and 1999, the approximate thermal dispersion source is represented by an apparent conductivity tensor $\boldsymbol{K}_{\mathrm{d}}$:

$$-\rho_f c_f \langle \widetilde{\boldsymbol{u}} \widetilde{T} \rangle \triangleq \boldsymbol{K}_{\mathrm{d}} \cdot \nabla \langle T \rangle \, .$$

However, this apparent conductivity tensor $\boldsymbol{K}_{\mathrm{d}}$ was not calculated in [13, 14]. Instead, the tensor $\boldsymbol{K}_{\mathrm{d}}$ was replaced by a scalar dispersion coefficient $k_{\mathrm{d},YY}$ defined as

$$k_{\mathrm{d},YY} \triangleq -\rho_f c_f \, \langle \widetilde{\boldsymbol{u}} \, (T - \langle T \rangle|_{\boldsymbol{x}}) \rangle|_{\boldsymbol{x}} \cdot \frac{\nabla \mathrm{T}}{\|\nabla \mathrm{T}\|^2} \, ,$$

where $\nabla \mathrm{T}$ is the temperature gradient over the unit cell in the steady periodically developed conjugate heat transfer regime. The notation $\langle \, \rangle|_{\boldsymbol{x}}$ does not appear in the original studies [13, 14], but is used here to remind us that the scalar dispersion coefficient $k_{\mathrm{d},YY}$ is treated as space-independent and is evaluated as a volume-average at the centroid $\boldsymbol{x}$ of the unit cell.

The expression of $k_{\mathrm{d},YY}$ reflects that the volume-averaged temperature in [13, 14] is treated as constant over the unit cell:

$$\langle T\rangle|_{\boldsymbol{r}} \simeq \langle T\rangle|_{\boldsymbol{x}} \,.$$

It also reflects that Kuwahara, Nakayama and Koyama assumed local thermal equilibrium to be valid, which means that

$$\langle T\rangle|_{\boldsymbol{x}} \simeq \langle T\rangle^f\big|_{\boldsymbol{x}} \simeq \langle T\rangle^s|_{\boldsymbol{x}} \,.$$

Similar to the thermal dispersion source, the thermal tortuosity term in the work of Kuwahara, Nakayama and Koyama [13, 14] is represented by the apparent conductivity tensor $\boldsymbol{K}_{\mathrm{tor}}$:

$$\langle \boldsymbol{n}_{fs} T \delta_{fs}\rangle \triangleq \frac{1}{k_f - k_s} \boldsymbol{K}_{\mathrm{tor}} \cdot \nabla \langle T\rangle \,.$$

The apparent conductivity tensor $\boldsymbol{K}_{\mathrm{tor}}$ in [13, 14] was assumed to have a component $K_{\mathrm{tor},YY}$ normal or parallel to the main flow direction, depending on whether the temperature gradient over the unit cell is normal or parallel to the main flow direction. This component was approximated as

$$K_{\mathrm{tor},YY} \simeq k_{\mathrm{tor},YY} \triangleq (k_f - k_s)\, \langle \boldsymbol{n}_{fs} T \delta_{fs}\rangle|_{\boldsymbol{x}} \cdot \frac{\nabla \mathrm{T}}{\|\nabla \mathrm{T}\|^2} \,.$$

Both of the effective parameters $k_{\mathrm{d},YY}$ and $k_{\mathrm{tor},YY}$ were numerically calculated by Kuwahara, Nakayama and Koyama for the steady periodically developed conjugate heat transfer regime in an array of solid squares. Their values are given for different porosities, fluid-to-solid conductivity ratios, Prandtl numbers and Peclet numbers.

The previous levels of approximation and definitions of the effective parameters from [13, 14] were adopted in the work of Alshare, Strykowski and Simon [15] in 2010. Alshare, Strykowski and Simon not only correlated the dispersion and tortuosity coefficients in an array of solid squares for a range of flow angles, porosities and Reynolds numbers, but also investigated the interfacial heat transfer coefficient in the periodically developed heat transfer regime for a constant imposed interfacial heat flux. The interfacial heat transfer coefficient in the work of Alshare et al. was treated as constant over the unit cell and was evaluated at the centroid of the unit cell:

$$h_{fs} \simeq \frac{\langle \boldsymbol{n}_{fs} \cdot k_f \nabla T_f \delta_{fs}\rangle|_{\boldsymbol{x}}}{\langle T\rangle^s|_{\boldsymbol{x}} - \langle T\rangle^f\,|_{\boldsymbol{x}}} \,.$$

The correlations for the heat transfer, dispersion and tortuosity coefficients from [15] were applied and validated in a numerical VAT model for the macro-scale velocity and temperature fields in a serpentine heat exchanger [11]. Alshare, Strykowski and Simon have discussed in depth the accuracy of this VAT model in comparison to direct numerical simulation.

In both of the latter studies by Alshare et al. [11, 15], also the third level of approximation can be recognized, which is the lack of distinction between the quantities in the volume-averaged transport equations and the quantities that characterize the periodically developed regime. In the studies of Alshare et al., for example, the gradient of the intrinsically volume-averaged fluid temperature is taken equal to the temperature gradient over the unit cell in the periodically developed conjugate heat transfer regime:

$$\nabla \langle T \rangle^f \simeq \nabla \mathrm{T} \,,$$

so that the approximate macro-scale temperature equation in [11, 15] actually reads

$$\rho_f c_f \| \langle \boldsymbol{u} \rangle \| \frac{d \langle T \rangle^f}{dX} \simeq \rho_f c_f \langle \boldsymbol{u} \rangle \cdot \nabla \mathrm{T} = \dot{S}_{\mathrm{gen}} \,.$$

The former approximation does however make sense under the assumption of local thermal equilibrium, because then it holds that

$$\langle T \rangle^f \simeq \langle T \rangle \qquad \text{and} \qquad \nabla \langle T \rangle = \nabla \mathrm{T} \,, \tag{7.1}$$

as it was correctly suggested in the studies of Kuwahara, Nakayama and Koyama [13, 14].

Another example which illustrates that the third level of approximation is common in the literature, can be found in the work of Lopez Penha et al. [12]. In the work of Lopez Penha et al., the interfacial heat transfer coefficient for the volume-averaged temperature equations is not distinguished from the heat transfer coefficient for the periodic temperature part in the periodically developed conjugate heat transfer regime:

$$h_{fs} \simeq \frac{\langle \boldsymbol{n}_{fs} \cdot k_f \nabla \widehat{T} \delta_{fs} \rangle \Big|_{\boldsymbol{x}}}{\langle \widehat{T} \rangle^s \,|_{\boldsymbol{x}} - \langle \widehat{T} \rangle^f \,|_{\boldsymbol{x}}} \,.$$

We remark that all of the three levels of approximations have not been identified as approximations in the above studies. Consequently, wherever

we have used the approximation sign $\simeq$ in this literature survey, there appears an equality sign in the cited studies.

Open Research Questions in the Literature

It seems that a description of the unsteady periodically developed heat transfer regime in spatially periodic solid structures with a uniform or spatially periodic interfacial heat flux has not been given yet. Neither has it been explained how the temperature gradient in the (un)steady periodically developed regime can be determined in the general case. By the general case, we mean the situation when also viscous dissipation, heat conduction and heat sources in the flow are possibly present and when the flow is not necessarily aligned with the solid array. Therefore, we will first give a complete description of the periodically developed conjugate heat transfer in the next section.

Our examination of the literature has brought to light that the existing macro-scale descriptions of the periodically developed heat transfer regime under an imposed interfacial heat flux contain three levels of approximation. As the accuracy and necessity of these levels of approximation have not been addressed, the question arises whether a macro-scale description can be developed free from any approximations. We will give a positive answer to this question in Section 6 and Section 7, where we develop an exact macro-scale description of the periodically developed heat transfer regime for the class of volume-average filters from §5.6.

Furthermore, we establish that the literature does not give a unifying description of the fully developed heat transfer regime and the periodically developed heat transfer regime together. Another question of interest is thus whether we can define a macro-scale temperature for both regimes which represents the same overall characteristics of the temperature field, whether the flow channels contain spatially periodic solid structures or not. Preferably, these overall characteristics would be in agreement with our physical intuition: we expect the macro-scale temperature to vary linearly in the streamwise direction like the bulk temperature does in the fully developed regime. In Section 6 and 7, we will determine the weighting function so that the macro-scale temperature plays a role similar to that of the bulk temperature. Moreover, in Section 9, we will illustrate the analogies between the fully developed heat transfer regime and the periodically developed heat transfer regime for this weighting function. It will be shown that an important analogy is the existence of a spatially constant heat transfer coefficient.

7.5 Periodically Developed Conjugate Heat Transfer

The periodically developed heat transfer regime in solid structures is characterized by the occurrence of a similarity between the profiles of the temperature distribution contained within different unit cells (5.2) of the solid structures. The periodically developed heat transfer regime is the result of a flow field which varies in a periodic fashion from one unit cell to another at any time t:

$$\boldsymbol{u}(\boldsymbol{x},t) = \boldsymbol{u}\left(\boldsymbol{x}+\boldsymbol{l}^{(j)},t\right) . \tag{7.2}$$

In that case also the viscous dissipation is a spatially periodic term:

$$\dot{q}_{\mathrm{visc}}(\boldsymbol{x},t) = \dot{q}_{\mathrm{visc}}\left(\boldsymbol{x}+\boldsymbol{l}^{(j)},t\right) . \tag{7.3}$$

We will assume that all time-dependent quantities in the periodically developed regime have a time-periodic behaviour, characterized by the same time period τ, so that no initial conditions need to be specified for further analysis. Furthermore, for the periodically developed regime to occur, we consider it necessary that all material properties of the fluid and solid are constant.

In the periodically developed *conjugate* heat transfer regime, the similarity between the temperature profiles within different unit cells is attributed to the fact that the temperature distribution consists of a part that varies linearly in space with a constant gradient $\nabla\mathrm{T}$, and a periodic part $T^\star$ that is similar for every unit cell [7, 12]:

$$T(\boldsymbol{x},t) = \nabla\mathrm{T}\cdot(\boldsymbol{x}-\boldsymbol{x}_0) + T^\star(\boldsymbol{x},t)\,, \quad \text{with} \quad T^\star(\boldsymbol{x},t) = T^\star\left(\boldsymbol{x}+\boldsymbol{l}^{(j)},t\right) . \tag{7.4}$$

The term *conjugate* heat transfer regime is used, because the former similarity occurs when the fluid and solid are subject to a spatially periodic volumetric heat source,

$$\dot{q}(\boldsymbol{x},t) = \dot{q}\left(\boldsymbol{x}+\boldsymbol{l}^{(j)},t\right) , \tag{7.5}$$

and a spatially periodic interfacial heat flux,

$$q_{fs}(\boldsymbol{x},t) = q_{fs}\left(\boldsymbol{x}+\boldsymbol{l}^{(j)},t\right) \qquad \text{for} \qquad \boldsymbol{x}\in\Gamma_{fs}\,, \tag{7.6}$$

which cause a coupling between the fluid temperature and solid temperature at the interface Γ_{fs}.

In the periodically developed conjugate heat transfer regime, the periodic part $T^\star$ of the temperature field can be governed by solving the temperature equation for T on a single unit cell, for an imposed temperature gradient $\nabla\mathrm{T}$. The governing equation for $T^\star$ in Ω_{unit} is given by[1]

$$\rho\frac{\partial^\nu\left(cT^\star\right)}{\partial t}+\rho\nabla\cdot\left(\boldsymbol{u}cT^\star\right)=\nabla^\nu\cdot\left(k\,\nabla^\nu T^\star\right)+\dot{q}_{\mathrm{visc}}+\dot{q}-\rho c\boldsymbol{u}\cdot\nabla\mathrm{T} \quad (7.7)$$

with the periodic boundary conditions

$$T^\star(\boldsymbol{x},t)=T^\star\left(\boldsymbol{x}+\boldsymbol{l}^{(j)},t\right)\qquad\text{where}\qquad j=\{1,\ldots,\mathrm{n}_j\}\,. \quad (7.8)$$

In order to solve (7.7) and (7.8) numerically, one should employ a discretization procedure which is able to cope with discontinuous transport coefficients [12, 16], as the distributions ρ, k and c are discontinuous at the fluid-solid interface within the unit cell domain.

The need for such a discretization procedure can be circumvented by decomposing (7.7) into a set of two coupled equations which are to be solved separately on the fluid and solid region. The first of both equations determines the periodic temperature part $T_f^\star$ and is the restriction of (7.7) to the fluid region $\Omega_f\cap\Omega_{\mathrm{unit}}$ of the unit cell:

$$\rho_f\frac{\partial\left(c_fT_f^\star\right)}{\partial t}+\rho_f\nabla\cdot\left(\boldsymbol{u}_fc_fT_f^\star\right)=\nabla\cdot\left(k_f\,\nabla T_f^\star\right)+\dot{q}_{\mathrm{visc}}+\dot{q}_f-\rho_fc_f\boldsymbol{u}_f\cdot\nabla\mathrm{T}\,. \quad (7.9)$$

The second equation follows by restricting (7.7) to the solid region $\Omega_s\cap\Omega_{\mathrm{unit}}$ of the unit cell:

$$\rho_s\frac{\partial\left(c_sT_s^\star\right)}{\partial t}=\nabla\cdot\left(k_s\,\nabla T_s^\star\right)+\dot{q}_s\,. \quad (7.10)$$

The former equations are coupled by the following boundary conditions at the interface Γ_{fs}:

$$\begin{aligned}&T_f^\star=T_s^\star\,,\\&q_{fs}=-\boldsymbol{n}_{fs}\cdot k_f\,\left(\nabla T_f^\star+\nabla\mathrm{T}\right)=-\boldsymbol{n}_{fs}\cdot k_s\,\left(\nabla T_s^\star+\nabla\mathrm{T}\right)\,,\end{aligned} \quad (7.11)$$

[1] In [1], the symbol ∇ instead of ∇^ν was erroneously written.

which impose the continuity of the temperature T and the interfacial heat flux q_{fs} at the interface. In addition, (7.9) and (7.10) are subject to the periodic boundary conditions

$$T_f^\star(\boldsymbol{x},t) = T_f^\star\left(\boldsymbol{x}+\boldsymbol{l}^{(j)},t\right), \qquad T_s^\star(\boldsymbol{x},t) = T_s^\star\left(\boldsymbol{x}+\boldsymbol{l}^{(j)},t\right), \tag{7.12}$$

where $j = \{1,\ldots,\mathrm{n}_j\}$. The discretization of (7.9) and (7.10) is no longer hampered by the presence of discontinuous transport coefficients. Instead, a proper discretization of the coupling boundary conditions of (7.11) is required.

The governing equations for the periodically developed conjugate heat transfer regime, (7.7) and (7.8), or equivalently, (7.9)-(7.12), show that the periodic temperature similarity has the following functional dependence:

$$T^\star = T^\star\left(\rho, c, k, \mu_f, \Gamma_{fs}\cap\Omega_{\mathrm{unit}}, \boldsymbol{u}, \dot{q}, \nabla\mathrm{T}, \boldsymbol{x}, t\right). \tag{7.13}$$

Hence, the periodic temperature part $T^\star$ in the periodically developed conjugate heat transfer regime is reconstructible from the knowledge of the material properties of fluid and solid, the geometry of the unit cell, the periodically developed velocity field, the periodic heat source and the temperature gradient over the unit cell. As the periodically developed flow field $\boldsymbol{u}$ is reconstructible from the spatially constant volume-averaged velocity $\langle\boldsymbol{u}\rangle$ over the unit cell domain (cf. (5.23)), $\boldsymbol{u}$ can be replaced by $\langle\boldsymbol{u}\rangle$ in (7.13).

It must be remarked that the governing equations for the periodically developed conjugate heat transfer regime determine the periodic temperature part $T^\star$ only up to a constant. A unique solution for $T^\star$ is found by imposing for instance its time-and-volume-averaged value over the unit cell domain, so that

$$\langle\overline{T^\star}\rangle = \text{constant}. \tag{7.14}$$

As a matter of fact, the constant value of $\langle\overline{T^\star}\rangle$ is determined by the upstream temperature conditions just before the point where the heat transfer regime becomes periodically developed. Therefore, different values of $\langle\overline{T^\star}\rangle$ correspond to situations in which the fluid and solid posses a different average energy level over a unit cell, after the onset of the periodically developed regime.

Finally, we add that (7.9), (7.11) and (7.12) also allow us to investigate the fluid temperature in the periodically developed regime for an imposed interfacial heat flux q_{fs}. In the latter case, the solid temperature $T_s^\star$ is no longer resolved and (7.14) may be replaced by $\langle \overline{T^\star} \rangle^f = \text{constant}$, to find a unique solution for $T_f^\star$. The functional dependence of the fluid temperature for an imposed interfacial heat flux looks like

$$T_f^\star = T_f^\star \left(\rho_f, c_f, k_f, \mu_f, \Gamma_{fs} \cap \Omega_{\text{unit}}, \langle \boldsymbol{u} \rangle, q_{fs}, \dot{q}_f, \nabla \mathrm{T}, \boldsymbol{x}, t \right) . \tag{7.15}$$

Temperature Gradient for Developed Conjugate Heat Transfer
The temperature gradient $\nabla \mathrm{T}$ in the periodically developed conjugate heat transfer regime is directly determined by the volumetric heat source and the viscous dissipation, through the relationship

$$\frac{\partial}{\partial t} \langle \rho c T^\star \rangle + \rho_f c_f \langle \boldsymbol{u} \rangle \cdot \nabla \mathrm{T} = \langle \dot{q} \rangle + \langle \dot{q}_{\text{visc}} \rangle , \tag{7.16}$$

which expresses an energy balance for the unit cell. The former energy balance is found after volume-averaging (7.7) over the unit cell domain, taking $\bar{\Omega} = \Omega_{\text{unit}}$ for m_V. After averaging (7.16) over time and assuming time-periodicity of flow and temperature, we get

$$\nabla \mathrm{T} = \frac{\langle \bar{\dot{q}} \rangle + \langle \bar{\dot{q}}_{\text{visc}} \rangle}{\rho_f c_f \| \langle \overline{\boldsymbol{u}} \rangle \|} \boldsymbol{e}_s . \tag{7.17}$$

Here, it was taken into account that by (7.16), the constant temperature gradient can have only a component along the direction of the time-and-volume-averaged velocity vector $\langle \overline{\boldsymbol{u}} \rangle \triangleq \| \langle \overline{\boldsymbol{u}} \rangle \| \boldsymbol{e}_s$. For a steady flow, one can replace $\langle \overline{\boldsymbol{u}} \rangle = \langle \boldsymbol{u} \rangle$ in (7.17), which shows that the equality above is similar to the expression for the unit cell gradient derived by Lopez Penha et al. [12] in search of a steady solution of the temperature equation (7.7). In this way, (7.17) generalizes their result towards time-periodic developed flow fields of which the volume-averaged velocity $\langle \boldsymbol{u} \rangle$ changes over time, as considered in [17, 18].

It is interesting to note that the temperature gradient is also determined by the interfacial heat flux q_{fs} via the energy balance for the fluid within the unit cell,

$$\rho_f c_f \epsilon_f \frac{\partial \langle T^\star \rangle^f}{\partial t} + \rho_f c_f \langle \boldsymbol{u} \rangle \cdot \nabla \mathrm{T} = - \langle q_{fs} \delta_{fs} \rangle + \epsilon_f \langle \dot{q} \rangle^f + \epsilon_f \langle \dot{q}_{\text{visc}} \rangle^f . \tag{7.18}$$

This energy balance for the fluid within the unit cell domain follows from multiplying each term of (7.7) with γ_f, before averaging each term over the unit cell domain. In (7.18), we have made use of the equality $\langle \boldsymbol{n}_{fs} \cdot (k_f \nabla T_f^\star) \delta_{fs} \rangle = -\langle q_{fs} \delta_{fs} \rangle$, which will proven in §7.7. After time-averaging (7.18), we thus also have[2]

$$\nabla \mathrm{T} = \frac{\epsilon_f \langle \overline{\dot{q}} \rangle^f + \epsilon_f \langle \overline{\dot{q}}_{\mathrm{visc}} \rangle^f - \langle \overline{q}_{fs} \delta_{fs} \rangle}{\rho_f c_f \| \langle \overline{\boldsymbol{u}} \rangle \|} \boldsymbol{e}_s \,. \tag{7.19}$$

The time-averaged energy balances of (7.17) and (7.19) allow the calculation of the unit cell temperature gradient from all the parameters that determine $T^\star$. Consequently, $\nabla \mathrm{T}$ can be left out the functional relationship (7.13) for the periodic temperature part. Likewise, when the solid temperature is not resolved, but just the functional dependence of the fluid temperature $T_f^\star$ for an imposed heat flux is of interest, (7.19) relates $\nabla \mathrm{T}$ to q_{fs}, so that $\nabla \mathrm{T}$ can be left out the functional relationship (7.15) for $T_f^\star$. This leads to the conclusion that the full-scale temperature field T and all the closure terms in the periodically developed conjugate heat transfer regime are entirely determined by the parameter set

$$\{\rho, c, k, \mu_f, \Gamma_{fs} \cap \Omega_{\mathrm{unit}}, \langle \boldsymbol{u} \rangle, \dot{q}, \boldsymbol{x}, t\} \,,$$

or the parameter set

$$\{\rho_f, c_f, k_f, \mu_f, \Gamma_{fs} \cap \Omega_{\mathrm{unit}}, \langle \boldsymbol{u} \rangle, \dot{q}, q_{fs}, \boldsymbol{x}, t\} \,,$$

if the heat flux is known.

In this section, the relationship between the unit cell temperature gradient and the heat sources has been found via the simple volume-averaging technique. The results (7.17) and (7.19) could also have been derived using a more general filter of the form $m = m_G * m_V$, where m_G is an arbitrary function, as long as $\bar{\Omega} = \Omega_{\mathrm{unit}}$ for m_V. In the next section, we will show that the appropriate weighting function for the periodically developed conjugate heat transfer regime indeed has the form $m = m_G * m_V$, so that the relations (7.17) and (7.19) remain consistent with the following analysis.

[2] In [1], the minus sign before the term $\langle \overline{q}_{fs} \delta_{fs} \rangle$ was erroneously missing.

7.6 Choice of Weighting Function for Periodically Developed Conjugate Heat Transfer

The appropriate filter for the periodically developed conjugate heat transfer regime should at least define a physically meaningful macro-scale temperature for this regime. To construct the appropriate filter, we first explore for which type of filter, the filtered temperature $\langle T\rangle_m$ represents an averaged impression of the original temperature T which remains unaltered after successive averaging. In other words, we first require the filter to respect that $\langle\langle T\rangle_m\rangle_m \simeq \langle T\rangle_m$ in order to have a meaningful averaged temperature. In general, the requirement $\langle\langle T\rangle_m\rangle_m \simeq \langle T\rangle_m$ is fulfilled when the filter suppresses the gradients and other higher order derivatives of the filtered temperature distribution, as can be seen from the Taylor series (2.59) for the double filtered temperature,

$$\langle\langle T\rangle_m\rangle_m\big|_{(\boldsymbol{x},t)} = \langle T\rangle_m\big|_{(\boldsymbol{x},t)} + \sum_{n=1}^{\infty} \frac{1}{n!}\, \langle \boldsymbol{y}^{\otimes n}\rangle_m\big|_{\boldsymbol{x}} \underbrace{\cdot\cdot}_{n-\text{times}} \nabla^{\otimes n}\langle T\rangle_m\big|_{(\boldsymbol{x},t)} \,. \tag{7.20}$$

After substitution of (7.4), the former Taylor series becomes

$$\begin{aligned}\langle\langle T\rangle_m\rangle_m\big|_{(\boldsymbol{x},t)} = {} & \langle T\rangle_m\big|_{(\boldsymbol{x},t)} + \langle \boldsymbol{y}\rangle_m\big|_{\boldsymbol{x}} \cdot \nabla \mathrm{T} \\ & + \sum_{n=1}^{\infty} \frac{1}{n!}\, \langle \boldsymbol{y}^{\otimes n}\rangle_m\big|_{\boldsymbol{x}} \underbrace{\cdot\cdot}_{n-\text{times}} \nabla^{\otimes n}\langle T^\star\rangle_m\big|_{(\boldsymbol{x},t)} \,. \end{aligned} \tag{7.21}$$

This result shows that the appropriate filter for the periodically developed conjugate heat transfer regime should be based on a weighting function of the form $m = m_G * m_V$, where the filter window of m_V coincides with the unit cell domain and $m_G \in C^\infty$ is an arbitrary weighting function, because then $\langle\langle T\rangle_m\rangle_m = \langle T\rangle_m$ holds exactly. Indeed, for any filter based on $m = m_G * m_V$ with $\bar{\Omega} = \Omega_{\text{unit}}$ for m_V, it holds that $\langle \boldsymbol{y}\rangle_m\big|_{\boldsymbol{x}} = 0$, because $\boldsymbol{x}$ corresponds to the geometrical centroid of the averaging window. Furthermore, this form of the filter invokes that the last term in (7.21) vanishes as $\langle T^\star\rangle_m$ is constant, because of (5.6).

With the appropriate filter form $m = m_G * m_V$, the superficially averaged temperature in the periodically developed conjugate heat transfer regime,

$$\langle T\rangle_m = \nabla \mathrm{T} \cdot (\langle \boldsymbol{y}\rangle_m + (\boldsymbol{x} - \boldsymbol{x}_0)) + \langle T^\star\rangle_m \,, \tag{7.22}$$

varies linearly over space as $\langle \boldsymbol{y} \rangle_m = 0$ and the filtered temperature gradient,

$$\begin{aligned} \nabla \langle T \rangle_m &= (\nabla \langle \boldsymbol{y} \rangle_m + \boldsymbol{I}) \cdot \nabla \mathrm{T} + \nabla \langle T^\star \rangle_m \\ &= \nabla \mathrm{T} + \nabla \langle T^\star \rangle_m \,, \end{aligned} \tag{7.23}$$

becomes equal to the constant temperature gradient: $\nabla \langle T \rangle_m = \nabla \mathrm{T}$.

In order to have also a meaningful intrinsically averaged temperature of the fluid and solid, we need to ensure that the filter in addition respects that $\langle \langle T \rangle_m^f \rangle_m^f \simeq \langle T \rangle_m^f$ and $\langle \langle T \rangle_m^s \rangle_m^s \simeq \langle T \rangle_m^s$. Because the intrinsically averaged fluid temperature in the periodically developed conjugate heat transfer regime is given by

$$\langle T \rangle_m^f = \nabla \mathrm{T} \cdot \left(\langle \gamma_f \boldsymbol{y} \rangle_m^f + (\boldsymbol{x} - \boldsymbol{x}_0) \right) + \langle T^\star \rangle_m^f \tag{7.24}$$

and the intrinsically averaged solid temperature is given by

$$\langle T \rangle_m^s = \nabla \mathrm{T} \cdot \left(\langle \gamma_s \boldsymbol{y} \rangle_m^s + (\boldsymbol{x} - \boldsymbol{x}_0) \right) + \langle T^\star \rangle_m^s \,, \tag{7.25}$$

the requirements $\langle \langle T \rangle_m^f \rangle_m^f = \langle T \rangle_m^f$ and $\langle \langle T \rangle_m^s \rangle_m^s = \langle T \rangle_m^s$ are satisfied exactly, if the filter operator suppresses the first-order spatial moments of the solid structures, which means that $\langle \gamma_f \boldsymbol{y} \rangle_m^f = \langle \gamma_s \boldsymbol{y} \rangle_m^s = 0$. This filter property is achieved by choosing m_G of the form $m_G = m_C * m_V$, where m_C is yet to determine, because with the overall weighting function $m = m_C * m_V * m_V$, the filter ensures that all odd spatial moments of the solid structures vanish (see also (5.14)):

$$\langle \gamma_f \boldsymbol{y}^{\otimes n} \rangle_m = 0 \qquad \text{and} \qquad \langle \gamma_s \boldsymbol{y}^{\otimes n} \rangle_m = 0 \qquad \text{if } n \text{ is odd} \,. \tag{7.26}$$

Due to the property that $\langle \langle T \rangle_m^f \rangle_m^f = \langle T \rangle_m^f$ and $\langle \langle T \rangle_m^s \rangle_m^s = \langle T \rangle_m^s$, the appropriate filter guarantees that the temperature changes occurring over the smallest length-scales, which are contained within the temperature deviation part $\widetilde{T}$, are filtered away: $\langle \widetilde{T} \rangle_m = 0$. The fact that $\langle \widetilde{T} \rangle_m = 0$ for the weighting function $m = m_C * m_V * m_V$ is easily verified from the expression for the temperature deviation in the periodically developed conjugate heat transfer regime,

$$\widetilde{T} = T^\star - \langle T^\star \rangle_m^f \gamma_f - \langle T^\star \rangle_m^s \gamma_s - \nabla \mathrm{T} \cdot \left(\langle \gamma_f \boldsymbol{y} \rangle_m^f \gamma_f + \langle \gamma_s \boldsymbol{y} \rangle_m^s \gamma_s \right) \,, \tag{7.27}$$

which proves that $\langle \widetilde{T} \rangle_m = 0$ is a direct consequence of (7.26).

Another consequence of (7.26) is that the intrinsically averaged temperature of the fluid and solid have the same constant gradient $\nabla\langle T\rangle_m^f = \nabla\langle T\rangle_m^s = \nabla \mathrm{T}$ as the superficially averaged temperature. Thus, the appropriate filter with $m = m_C * m_V * m_V$ leads to a linearly varying filtered temperature of the fluid and solid and a spatially constant filtered interfacial heat flux $\langle q_{fs}\rangle_m = \langle q_{fs}\rangle$ in the periodically developed conjugate heat transfer regime. As this resembles an analogy with developed channel flow in which the fluid bulk temperature varies linearly in the main flow direction when the heat flux from the solid wall is constant, we argue that the weighting function $m = m_C * m_V * m_V$ is also needed to have a filtered temperature of which the physical interpretation is clear.

Although the former filter based on $m = m_C * m_V * m_V$ guarantees that the filtered temperatures $\langle T\rangle_m$, $\langle T\rangle_m^f$ and $\langle T\rangle_m^s$ do not change after successive filtering and have a clear physical interpretation, we still need to determine m_C in order that $\langle T\rangle_m$, $\langle T\rangle_m^f$ and $\langle T\rangle_m^s$ can be justifiably called macro-scale temperatures. This means that m_C should be chosen so that $\langle T\rangle_m$, $\langle T\rangle_m^f$ and $\langle T\rangle_m^s$ do not change significantly over length-scales smaller than the spatial periods $\|\boldsymbol{l}^j\|$ of the solid structures. We will show now that we can choose m_C arbitrarily. We start by noting that for any m_C, it holds that $\langle\widetilde{T}\rangle_m = 0$, which on its turn implies that the order-of-magnitude estimates r_m and $\mathscr{L}_T$ satisfy $\mathscr{L}_T \gg r_m$ by definition:

$$\begin{aligned}\langle\widetilde{T}\rangle_m &= \sum_{n=1}^{\infty}\frac{1}{n!}\langle\gamma_f \boldsymbol{y}^{\otimes n}\rangle_m \underbrace{\cdot\cdot}_{n\text{-times}} \nabla^{\otimes n}\langle T\rangle_m^f + \sum_{n=1}^{\infty}\frac{1}{n!}\langle\gamma_s \boldsymbol{y}^{\otimes n}\rangle_m \underbrace{\cdot\cdot}_{n\text{-times}} \nabla^{\otimes n}\langle T\rangle_m^s \\ &= \mathcal{O}\left(\frac{\epsilon_{fm} r_m \langle T\rangle_m^f}{\mathscr{L}_T}\right) + \mathcal{O}\left(\frac{\epsilon_{sm} r_m \langle T\rangle_m^s}{\mathscr{L}_T}\right). \end{aligned} \tag{7.28}$$

As the characteristic size r_m of the filter window for $m = m_C * m_V * m_V$ has at least the same order-of-magnitude as the size of the unit cell domain, i.e. $r_m \geq O\left(\|\boldsymbol{l}^j\|\right)$, we see that any m_C defines a macro-scale temperature, because $\mathscr{L}_T \gg \|\boldsymbol{l}^j\|$ for any m_C. Actually, we may think of $\mathscr{L}_T$ as the distance over which the macro-scale temperature has a linear profile, thus the distance over which the periodically developed regime extends in Ω in the streamwise direction $\boldsymbol{e}_s$. Secondly, we note that for any m_C, the temperature deviation $\widetilde{T}$ is periodic over the unit cell domain, just like the periodic temperature part $T^\star$, as $\widetilde{T}$ and $T^\star$ are equal apart from the offset $-\langle T^\star\rangle_m^f\gamma_f - \langle T^\star\rangle_m^s\gamma_s$ in (7.27). Accordingly, the characteristic length-scale for $\widetilde{T}$ is smaller than the spatial periods of the unit cell: $\ell_T = \ell_{T^\star} \leq \max\|\boldsymbol{l}^j\|$. Therefore, $\langle\widetilde{T}\rangle_m = 0$ indeed implies that all tem-

perature changes over a length-scale smaller than the spatial periods $\|\boldsymbol{l}^j\|$ are suppressed by the filter.

From the foregoing analysis, it is concluded that the filter operator which defines the appropriate macro-scale temperature in the periodically developed conjugate heat transfer regime is based on any weighting function of the form $m = m_C * m_V * m_V$. The former weighting function was originally proposed by Quintard and Whitaker for the macro-scale description of hydrostatic equilibrium and Stokes flow in ordered media [2, 3]. In the previous chapters, this weighting function has also been shown to be the appropriate filter kernel for periodically developed flow as well as an approximation for the matched filter kernel in the periodically developed heat transfer regime in isothermal solids.

Since m_C is a weighting function of arbitrary choice, it can be freely chosen to simplify the form of the closure terms in the periodically developed regime. In the next section it will be shown that m_C does not affect the form of the closure terms, so that we will set it to $m_C = 1$. In that case, the overall weighting function finally becomes $m = m_V * m_V$, which has the analytical representation (5.11). Theoretically, m_C must be chosen such that $m = m_C * m_V * m_V \in C^\infty$, while $m_C = 1$ gives rise to an overall weighting function $m = m_V * m_V \in C^0$. Nonetheless, $m_C = 1$ is acceptable as m_C does not have any effect on the final macro-scale temperatures.

The preceding discussion reveals that the macro-scale description of the developed conjugate heat transfer regime in spatially periodic solid structures requires a filter other than the simple volume-average filter based on $m_G = 1$, that is used in the VAT theory for porous media. However, under some conditions, a filter of the form $m = m_G * m_V$ with $m_G \neq m_C * m_V$ can still be used to obtain an approximation of the physically meaningful macro-scale temperature that is found via $m = m_C * m_V * m_V$. When $m_G \neq m_C * m_V$, we have $\nabla\langle T\rangle_m^f = (\boldsymbol{I} - \boldsymbol{A}_m) \cdot \nabla \mathrm{T}$ and $\nabla\langle T\rangle_m^s = (\boldsymbol{I} - \boldsymbol{B}_m) \cdot \nabla \mathrm{T}$ with $\boldsymbol{A}_m = \epsilon_{fm}^{-1} \boldsymbol{G}_m^{(1)}$ and $\boldsymbol{B}_m = -\epsilon_{sm}^{-1} \boldsymbol{G}_m^{(1)}$, as ϵ_{fm} and ϵ_{sm} are constant by (5.1) and (5.6). This means that a filter based on $m = m_G * m_V$ still yields an approximately linearly varying macro-scale temperature of the fluid and solid under the condition that $\boldsymbol{I} \gg \boldsymbol{A}_m$ and $\boldsymbol{I} \gg \boldsymbol{B}_m$, or $\boldsymbol{G}_m^{(1)} \simeq 0$.

Whether the gradient of the first spatial moment is small for this form of filter, i.e. $\boldsymbol{G}_m^{(1)} \simeq 0$, depends entirely on the specific shape of the fluid-solid interface. How small $\boldsymbol{G}_m^{(1)}$ should be for a specific configuration of solid structures if $m_G \neq m_C * m_V$, is a question of which the answer is subjective, as it depends on what one considers to be a meaningful approximation of the linear macro-scale temperature for $m = m_C * m_V * m_V$. Furthermore, if such an approximation is considered to be meaningful as long as $\langle\langle T\rangle_m^f\rangle_m^f \simeq \langle T\rangle_m^f$ and $\langle\langle T\rangle_m^s\rangle_m^s \simeq \langle T\rangle_m^s$, then a quantitative criterion should be specified to measure how small the spatial moments of the solid structures should be, i.e. to quantify the approximations $\langle\gamma_f \boldsymbol{y}\rangle_m^f \simeq \langle\gamma_s \boldsymbol{y}\rangle_m^s \simeq 0$ in (7.27). Fortunately, such a (subjective) criterion to quantify the former approximations is not needed for the appropriate weighting function $m = m_C * m_V * m_V$.

7.7 Closure for Periodically Developed Conjugate Heat Transfer

Now that the appropriate filter for the macro-scale temperature in the periodically developed conjugate heat transfer regime has been determined, we will derive the form of the closure terms for this filter and compare it with the form for the volume-average filter. Starting with the thermal dispersion source of (4.18), we find by (7.4) that

$$\begin{aligned}\mathcal{D} = \langle \boldsymbol{u} T^\star\rangle_m - \epsilon_{fm}\langle \boldsymbol{u}\rangle_m^f \langle T^\star\rangle_m^f + \langle \boldsymbol{u}(\boldsymbol{r}-\boldsymbol{x}_0)\rangle_m \cdot \nabla \mathrm{T} \\ - \epsilon_{fm}\langle \boldsymbol{u}\rangle_m^f \left(\langle\gamma_f \boldsymbol{y}\rangle_m^f + (\boldsymbol{x}-\boldsymbol{x}_0)\right) \cdot \nabla \mathrm{T}\,. \end{aligned} \tag{7.29}$$

For a weighting function of the form $m = m_G * m_V$ with $\bar{\Omega} = \Omega_{\mathrm{unit}}$ for m_V, we have $\boldsymbol{u} = \langle \boldsymbol{u}\rangle_m^f \gamma_f + \widetilde{\boldsymbol{u}}$ with $\langle \boldsymbol{u}\rangle_m^f = \langle \boldsymbol{u}\rangle^f = $ constant and $\langle\widetilde{\boldsymbol{u}}\rangle_m = \langle\widetilde{\boldsymbol{u}}\rangle = 0$, by virtue of (6.2) and (5.6). Hence, for this form of filter, the thermal dispersion source simplifies to

$$\mathcal{D} = \langle \widetilde{\boldsymbol{u}} T^\star\rangle_m + \langle \widetilde{\boldsymbol{u}}(\boldsymbol{r}-\boldsymbol{x}_0)\rangle_m \cdot \nabla \mathrm{T} = \langle \widetilde{\boldsymbol{u}} T^\star\rangle_m + \langle \widetilde{\boldsymbol{u}}\boldsymbol{y}\rangle_m \cdot \nabla \mathrm{T}\,, \tag{7.30}$$

because $\langle \widetilde{\boldsymbol{u}}(\boldsymbol{x}-\boldsymbol{x}_0)\rangle_m = \langle\widetilde{\boldsymbol{u}}\rangle_m(\boldsymbol{x}-\boldsymbol{x}_0) = 0$. The thermal dispersion source $\mathcal{D}$ is thus in general not spatially constant for this filter, but it depends on the moment of the velocity deviation field, $\langle\widetilde{\boldsymbol{u}}\boldsymbol{y}\rangle_m$, which varies spatially periodic over the unit cell domain. Also the approximation for the thermal dispersion source,

$$\mathcal{D}_{\mathrm{approx}} \triangleq \langle \widetilde{\boldsymbol{u}}\widetilde{T}\rangle_m = \langle \widetilde{\boldsymbol{u}} T^\star\rangle_m + \langle \widetilde{\boldsymbol{u}}\langle\gamma_f \boldsymbol{y}\rangle_m\rangle_m \cdot \nabla \mathrm{T}\,, \tag{7.31}$$

is in general not spatially constant for a filter with $m = m_G * m_V$, as this form of filter does not necessarily ensure that $\langle \widetilde{\boldsymbol{u}} \langle \gamma_f \boldsymbol{y} \rangle_m \rangle_m = 0$. Besides, for this filter, the approximation $\boldsymbol{\mathcal{D}} \simeq \boldsymbol{\mathcal{D}}_{\text{approx}}$ is only permitted if the moment of the deviation velocity is sufficiently small, $\langle \widetilde{\boldsymbol{u}} \boldsymbol{y} \rangle_m \simeq 0$, a condition which might be violated for some periodically developed flow fields.

In the case that the filter is based on $m = m_C * m_V * m_V$, the moment of the velocity deviation field is exactly zero, i.e. $\langle \widetilde{\boldsymbol{u}} \boldsymbol{y} \rangle_m = 0$ by analogy with (7.26), and the thermal dispersion source does become spatially constant:

$$\boldsymbol{\mathcal{D}} = \boldsymbol{\mathcal{D}}_{\text{approx}} = \langle \widetilde{\boldsymbol{u}} T^\star \rangle_m \,. \tag{7.32}$$

The equality $\boldsymbol{\mathcal{D}} = \boldsymbol{\mathcal{D}}_{\text{approx}}$ is a consequence of the fact that $T^\star$ and $\widetilde{T}$ are equal up to a constant for $m = m_C * m_V * m_V$, according to (7.27) and (7.26).

The thermal tortuosity in the periodically developed conjugate heat transfer regime is obtained after substitution of (7.4) into (4.26):

$$\langle \boldsymbol{n}_{fs} T_f \delta_{fs} \rangle_m = \left(\boldsymbol{G}_m^{(0)} (\boldsymbol{x} - \boldsymbol{x}_0) + \boldsymbol{G}_m^{(1)} \right) \cdot \nabla \mathrm{T} + \langle \boldsymbol{n}_{fs} T_f^\star \delta_{fs} \rangle_m \,, \tag{7.33}$$

where we again made use of the geometrical tensors of (2.65). Although $\boldsymbol{G}_m^{(0)} = -\nabla \epsilon_{fm} = 0$ for any weighting function $m = m_G * m_V$ with $\bar{\Omega} = \Omega_{\text{unit}}$ for m_V, we have in general $\boldsymbol{G}_m^{(1)} \neq 0$, as $\boldsymbol{G}_m^{(1)}$ is spatially periodic over the unit cell domain for this form of weighting function. On the contrary, the weighting function $m = m_C * m_V * m_V$ does have the property that $\boldsymbol{G}_m^{(0)} = \boldsymbol{G}_m^{(1)} = 0$ by (7.26) and therefore yields the following spatially constant thermal tortuosity term,

$$\langle \boldsymbol{n}_{fs} T_f \delta_{fs} \rangle_m = \langle \boldsymbol{n}_{fs} T_f^\star \delta_{fs} \rangle_m = \langle \boldsymbol{n}_{fs} T_s^\star \delta_{fs} \rangle_m \,. \tag{7.34}$$

The interfacial heat transfer term in the periodically developed heat transfer regime follows from substitution of (2.65) and (7.4) into (4.25) which results in

$$\begin{aligned} \langle q_{fs} \delta_{fs} \rangle_m &= -\langle \boldsymbol{n}_{fs} \cdot (k_f \nabla T_f) \delta_{fs} \rangle_m \\ &= -\boldsymbol{G}_m^{(0)} \cdot k_f \nabla \mathrm{T} - \langle \boldsymbol{n}_{fs} \cdot (k_f \nabla T_f^\star) \delta_{fs} \rangle_m \,. \end{aligned} \tag{7.35}$$

For any weighting function of the form $m = m_G * m_V$ with $\bar{\Omega} = \Omega_{\text{unit}}$ for m_V, (5.6) is applicable, so the last term of (7.35) is constant and $\boldsymbol{G}_m^{(0)} = -\nabla\epsilon_f = 0$ for this weighting function. In the periodically developed conjugate heat transfer regime, the interfacial heat transfer term is thus a constant scalar, whether the filter is based on $m = m_G * m_V$ or $m = m_C * m_V * m_V$:

$$\langle q_{fs}\delta_{fs}\rangle_m = -\langle \boldsymbol{n}_{fs} \cdot (k_f \nabla T_f^\star)\delta_{fs}\rangle_m = -\langle \boldsymbol{n}_{fs} \cdot (k_s \nabla T_s^\star)\delta_{fs}\rangle_m \,. \quad (7.36)$$

Nevertheless, only for the weighting function $m = m_C * m_V * m_V$, the interfacial heat transfer coefficient defined by

$$\langle q_{fs}\delta_{fs}\rangle_m \triangleq \epsilon_{fm} h_{fs} \left(\langle T\rangle_m^f - \langle T\rangle_m^s \right) \quad (7.37)$$

is spatially constant because of (7.24), (7.25) and (7.26). In that case, the interfacial heat transfer coefficient satisfies[3]

$$h_{fs} = \epsilon_{fm}^{-1} \frac{\langle q_{fs}\delta_{fs}\rangle_m}{\langle T^\star\rangle_m^f - \langle T^\star\rangle_m^s} \,, \quad (7.38)$$

where $\langle q_{fs}\delta_{fs}\rangle_m$ is given by (7.36).

The interfacial heat transfer coefficient of (7.38) was introduced as the heat transfer coefficient for the volume-averaged fluid and solid temperature in the studies [15] and [12], although we have shown that it requires the macro-scale temperature to be defined through the weighting function $m = m_C * m_V * m_V$. This constant heat transfer coefficient depends on the same parameters as the periodic temperature, except the position vector $\boldsymbol{x}$. For solid structures with a single geometric parameter L_{ref}, the functional dependence of the heat transfer coefficient in the steady regime can be reduced to a dimensionless correlation between the Nusselt number ($h_{fs}L_{\text{ref}}^2/k_f$), the Reynolds number based on the volume-averaged velocity ($\rho_f \|\langle \boldsymbol{u}\rangle\| L_{\text{ref}}/\mu_f$), the flow direction $\boldsymbol{e}_s$, the Prandtl number of the fluid ($\mu_f c_f/k_f$) and the conductivity ratio k_f/k_s, at least if the heat source is spatially constant. For the unsteady periodically developed conjugate heat transfer regime, the time-averaged Nusselt number depends additionally on the fluid-to-solid heat capacity ratio ($\rho_f c_f/(\rho_s c_s)$) as well as the Strouhal number ($L_{\text{ref}}/(\tau\|\langle \boldsymbol{u}\rangle\|)$).

In summary, the interfacial heat transfer term is spatially constant in the periodically conjugate heat transfer regime for any filter based on the

[3]This heat transfer coefficient differs from the one defined in [1] by the factor ϵ_{fm}.

weighting function for volume-averaging. The filter based on the weighting function of Quintard and Whitaker, which is in essence equivalent to a double volume average, ensures in addition that the interfacial heat transfer coefficient as well as the thermal tortuosity and dispersion are spatially constant in the periodically developed conjugate heat transfer regime, irrespective of the specific shape of the periodic solid structures.

The fact that these closure terms become spatially constant for the double volume-average filter indicates that there is no development any more from a macro-scale point of view. Therefore the double volume-average filter gives a macro-scale description in agreement with the physical interpretation of what it is called a developed regime, i.e. a regime in which the velocity and temperature profiles become similar for every unit cell and hence do not change from a macro-scale point of view. The physical interpretation of the closure terms for the simple volume-average filter is less clear, because the closure terms vary over the unit cell domain in the developed regime. The spatial gradients of these closure terms are mainly caused by the geometrical properties, the spatial moments, of the fluid-solid interface and they are not related to changes of the real macro-scale quantities like the averaged flow velocity $\langle \boldsymbol{u} \rangle$ or the constant temperature gradient $\nabla \mathrm{T}$.

7.8 Periodically Developed Planar Conjugate Heat Transfer

Periodically Developed Planar Conjugate Heat Transfer Regime
In periodically developed planar flow (cf. §5.13) through a plate channel with walls subject to a periodic heat flux, the *periodically developed planar conjugate heat transfer regime* usually occurs sufficiently far from the channel boundaries. By a periodic heat flux (cf. (4.59) and (4.60)), it is understood that

$$q_{wt}(\boldsymbol{x}, t) = q_{wt}\left(\boldsymbol{x} + \boldsymbol{l}^{(j)}, t\right) \qquad \text{at} \qquad x_3 = \frac{l_3}{2}\,, \tag{7.39}$$

$$q_{wb}(\boldsymbol{x}, t) = q_{wb}\left(\boldsymbol{x} + \boldsymbol{l}^{(j)}, t\right) \qquad \text{at} \qquad x_3 = -\frac{l_3}{2}\,, \tag{7.40}$$

for $j = \{1, 2\}$, as we take $\boldsymbol{l}^{(1)} \cdot \boldsymbol{e}^{(3)} = \boldsymbol{l}^{(2)} \cdot \boldsymbol{e}^{(3)} = \boldsymbol{l}^{(3)} \times \boldsymbol{e}^{(3)} = 0$.

The periodically developed planar conjugate heat transfer regime is characterized by a periodic temperature part $T^\star$ and a constant temperature gradient $\nabla \mathrm{T}$ just as in (7.4) and (7.7). However, in the periodically developed planar conjugate heat transfer regime, the periodic temperature part $T^\star$ is not entirely periodic as in (7.8). Instead, $T^\star$ satisfies the following boundary conditions over the unit cell (5.71):

$$\begin{aligned} T^\star(\boldsymbol{x},t) &= T^\star\left(\boldsymbol{x}+\boldsymbol{l}^{(j)},t\right) && \text{for} \quad j=\{1,2\}\,, \\ q_{wt}(\boldsymbol{x},t) &= k\frac{\partial T^\star}{\partial x_3}+\boldsymbol{e}^{(3)}\cdot k\nabla \mathrm{T} && \text{at} \quad x_3=\frac{l_3}{2}\,, \\ q_{wb}(\boldsymbol{x},t) &= -k\frac{\partial T^\star}{\partial x_3}-\boldsymbol{e}^{(3)}\cdot k\nabla \mathrm{T} && \text{at} \quad x_3=-\frac{l_3}{2}\,. \end{aligned} \tag{7.41}$$

When $\nabla \mathrm{T}\cdot\boldsymbol{e}^{(3)}=0$, the planar temperature consists of linear contribution and a periodic term:

$$\mathcal{T}(\boldsymbol{x},t)=\nabla \mathrm{T}\cdot(\boldsymbol{x}-\boldsymbol{x}_0)+\mathcal{T}^\star(\boldsymbol{x},t)\,, \tag{7.42}$$

where

$$\mathcal{T}^\star(\boldsymbol{x},t)=\mathcal{T}^\star\left(\boldsymbol{x}+\boldsymbol{l}^{(j)},t\right)\,. \qquad \text{and} \qquad \mathcal{T}^\star=\langle T^\star\rangle_3\,. \tag{7.43}$$

In analogy with (7.19), it follows from (4.53) that the temperature gradient in the periodically developed planar conjugate heat transfer regime is given by

$$\nabla \mathrm{T}=\frac{\langle\langle\overline{\dot{q}}\rangle_3\rangle+\langle\langle\overline{\dot{q}}_{\mathrm{visc}}\rangle_3\rangle+\langle\psi_3\rangle}{\rho_f c_f\|\langle\overline{\boldsymbol{v}}\rangle\|}\boldsymbol{e}_s\,, \tag{7.44}$$

In analogy with (7.19), the temperature gradient in the periodically developed planar conjugate heat transfer regime also given by

$$\nabla \mathrm{T}=\frac{\epsilon_f\langle\langle\overline{\dot{q}}\rangle_3\rangle^f+\epsilon_f\langle\langle\overline{\dot{q}}_{\mathrm{visc}}\rangle_3\rangle^f-\langle\langle\overline{q}_{fs}\rangle_3\delta_{fs}\rangle}{\rho_f c_f\|\langle\overline{\boldsymbol{v}}\rangle\|}\boldsymbol{e}_s\,, \tag{7.45}$$

where

$$\langle\langle\overline{q}_{fs}\rangle_3\delta_{fs}\rangle=-\langle\boldsymbol{n}_{fs}\cdot(k_f\,\nabla\mathcal{T}_f^\star)\delta_{fs}\rangle\,, \tag{7.46}$$

because we have assumed that $\boldsymbol{n}_{fs}\cdot\boldsymbol{e}^{(3)}=0$ when planar flow occurs (cf. (3.48)).

Periodically Developed Planar Closure Terms

With (7.4), the first closure term (4.56) in the planar temperature becomes

$$\psi_3^{\mathrm{I}} = \rho\nabla^\nu \cdot (\boldsymbol{v}cT^\star - \langle \boldsymbol{u}_{1,2}cT^\star\rangle_3) - \rho_f c_f \left(\nabla^\nu \cdot \langle \boldsymbol{u}_{1,2}\boldsymbol{y}\rangle_3\right) \cdot \nabla \mathrm{T} \,. \tag{7.47}$$

The second planar thermal closure term (4.57) then becomes

$$\psi_3^{\mathrm{II}} = \rho_f c_f \varphi_3 \nabla \mathrm{T} \cdot (\boldsymbol{x} - \boldsymbol{x}_0) - \rho\langle \nabla_3^\nu \cdot (\boldsymbol{u}_3 cT^\star)\rangle_3 \,, \tag{7.48}$$

at least if $\nabla \mathrm{T} \cdot \boldsymbol{e}^{(3)} = 0$. When $m_3 = \frac{1}{l_3}$, we have $\psi_3^{\mathrm{II}} = 0$ due to the no-slip condition (3.59) (see also (F.7)).

With (7.4) the third planar thermal closure term can be expressed as

$$\psi_3^{\mathrm{III}} = \langle \nabla_3^\nu \cdot (k\nabla_3^\nu T^\star)\rangle_3 \,. \tag{7.49}$$

When $m_3 = \frac{1}{l_3}$, the third planar thermal closure term is known from the boundary conditions (see Appendix F):

$$\psi_3^{\mathrm{III}} = \frac{1}{l_3}\left(q_{wt} + q_{wb}\right) \,. \tag{7.50}$$

From equations (7.47) - (7.49), it is concluded that in the periodically developed planar conjugate heat transfer regime, the three closure terms for the planar temperature equation can be calculated from the periodic temperature part (7.13) on a unit cell.

Macro-Scale Description

The macro-scale description of the periodically developed planar conjugate heat transfer regime is completely analogous to the macro-scale description of the periodically developed conjugate heat transfer regime (see §7.6 and §7.7). The only modification required for the macro-scale description of the periodically developed planar conjugate heat transfer regime is to use the unit cell (5.71) as filter window for the weighting function m_V. Therefore, the appropriate filters for the periodically developed planar conjugate heat transfer regime are the same as for periodically developed planar flow and given by (5.80) and (5.81).

Because the filters (5.80) and (5.81) are separable, the macro-scale temperature and the macro-scale planar temperature are equal (cf. (4.76)). For these filters we thus also have

$$\langle T^\star\rangle_m^f = \langle \mathcal{T}^\star\rangle_m^f \qquad \text{and} \qquad \langle T^\star\rangle_m^s = \langle \mathcal{T}^\star\rangle_m^s \,. \tag{7.51}$$

In addition, due to the separability of these filters, the interfacial heat transfer and thermal tortuosity satisfy (4.77) and (4.78) respectively. Consequently, when $\nabla \mathrm{T} \cdot \boldsymbol{e}^{(3)} = 0$ and (7.4) holds, the interfacial heat transfer and thermal tortuosity are respectively given by

$$\langle \boldsymbol{n}_{fs} \cdot k_f \nabla T_f \delta_{fs} \rangle_m = \langle \boldsymbol{n}_{fs} \cdot k_f \nabla \mathcal{T}_f^\star \delta_{fs} \rangle_m \tag{7.52}$$

and

$$\langle \boldsymbol{n}_{fs} T_f \delta_{fs} \rangle_m = \langle \boldsymbol{n}_{fs} \mathcal{T}_f^\star \delta_{fs} \rangle_m \,. \tag{7.53}$$

It must be emphasized that (7.53) only holds for the double volume-average filter of (5.81), as in that case the geometric tensors are zero (cf. (7.34)). On the other hand, (7.52) is valid for both the volume-average filter of (5.80) and the double volume-average of (5.81) (cf. (7.36)).

From (7.51) and (7.52) it follows that the heat transfer coefficient of (7.38) satisfies

$$h_{fs} = \epsilon_{fm}^{-1} \frac{\langle q_{fs} \delta_{fs} \rangle_m}{\langle \mathcal{T}^\star \rangle_m^f - \langle \mathcal{T}^\star \rangle_m^s} \,, \tag{7.54}$$

if $\nabla \mathrm{T} \cdot \boldsymbol{e}^{(3)} = 0$, because the geometric tensors are zero for the double volume-average of (5.81).

For the double volume-average filter of (5.81), the first planar macro-scale thermal closure term is given by

$$\begin{aligned} \langle \psi_3^{\mathrm{I}} \rangle_m &= \epsilon_{fm} \langle \psi_3^{\mathrm{I}} \rangle_m^f \\ &= \rho \nabla^\nu \cdot \left(\langle \boldsymbol{v} c T^\star \rangle_m - \langle \langle \boldsymbol{u}_{1,2} c T^\star \rangle_3 \rangle_m \right) - \rho_f c_f \left(\nabla \cdot \langle \langle \boldsymbol{u}_{1,2} \boldsymbol{y} \rangle_3 \rangle_m \right) \cdot \nabla \mathrm{T} \\ &= 0 \,, \end{aligned} \tag{7.55}$$

as $\langle \langle \boldsymbol{u}_{1,2} \boldsymbol{y} \rangle_3 \rangle_m = 0$ for the weighting function m of (5.81).

The second planar macro-scale thermal closure term vanishes for the double volume-average filter of (5.81):

$$\langle \psi_3^{\mathrm{II}} \rangle_m = 0 \,, \tag{7.56}$$

because $\psi_3^{\mathrm{II}} = 0$ when $m_3 = \frac{1}{l_3}$.

Finally, the third planar macro-scale thermal closure term is just equal to

$$\psi_3^{\mathrm{III}} = \frac{1}{l_3} \left(\langle q_{wt} \rangle_m + \langle q_{wb} \rangle_m \right) \,. \tag{7.57}$$

7.9 Macro-Scale Conjugate Heat Transfer in an Array of Solid Squares

In the following case study, a macro-scale description is given of the heat transfer between an array of solid squares having a uniform volumetric heat source and an incompressible fluid in which no volumetric heat generation takes place. This case study serves to support illustratively the theoretical derivations of the previous parts and exposes the essential features of the periodically developed conjugate heat transfer regime in solid structures.

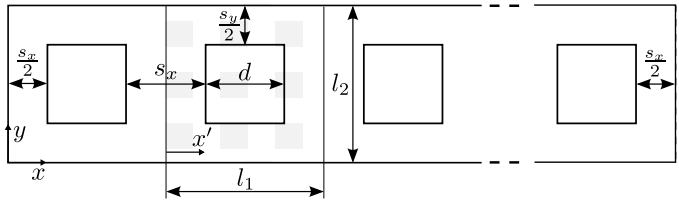

Figure 7.2: Geometry of the square array and unit cell.

A single row of the two-dimensional array is depicted in Figure 7.2 and consists of N identical squares with side length d, which are separated from each other by a distance s_x along the horizontal axis x. On the same figure, s_y indicates the distance between two adjacent rows of the array. The checker-board pattern in Figure 7.2 corresponds to a two-dimensional unit cell of the array with the lattice sizes l_1 and l_2 and coordinate axis x'. The values of all the parameters for this case study are summarized in table 1.

Geometry array		**Regime**	
s_x/d	1	Re	100
s_y/d	1	Pr	1
N	15	k_s/k_f	100
		$\dot{q}_s^+$	1

Table 7.1: Conjugate Heat Transfer in an Array of Solid Squares: Case study parameters.

The velocity field through the single row of solid squares in Figure 7.2 is computed for an imposed pressure drop Δp between the inlet at $x = 0$ and the outlet at $x = \mathrm{N}l_1$. The velocity field satisfies the no-slip condition at the boundaries of the solid squares. The temperature distribution over the single row of squares is calculated for a prescribed inlet temperature T_{in} and a zero temperature gradient at the outlet. At the solid boundaries, the continuity of the temperature field as well as the interfacial heat flux is imposed. As the velocity field and temperature distribution are resolved on only a single row of the array, they both are assumed to satisfy symmetry boundary conditions at $y = 0$ and $y = l_2$. Viscous dissipation is not considered and the uniform volumetric heat source in the solid is chosen such that $\dot{q}_s^+ \triangleq \dot{q}_s d^2/(k_s \Delta T_{\mathrm{ref}}) = 1$, as we define $\Delta T_{\mathrm{ref}} \triangleq \dot{q}_s d^2/k_s$.

For numerically solving the steady Navier-Stokes flow and temperature equations, the finite-volume method is applied with the same discretization schemes as in §6.9. The finite-volume mesh for the square array in this case study consists of 937 500 quadrilateral cells of nearly equal size. For calculating the filtered flow and temperature distributions, the spatial filter operator is discretized by a number of 360 000 sample points following the approach of Buckinx and Baelmans [17]. Furthermore, all distributions are filtered assuming periodicity over the symmetry boundaries, so that the filtered quantities vary only in the direction of the unit vector $\boldsymbol{e}_x$ along the x-axis of the square array.

Figure 7.3 shows the dimensionless temperature of the fluid and solid, $T^+ \triangleq (T - T_{\mathrm{in}})/\Delta T_{\mathrm{ref}}$, at the centreline of the square array. The fluid temperature rises in streamwise direction in front of each solid, as the solid conducts the heat from its internal heat source towards the fluid. In the immediate region after each solid, the presence of a wake with flow recirculation and less advective heat transport leads to a locally decreasing fluid temperature. Within the solid squares, the dimensionless temperature profile flattens, because the solid has a much higher heat conductivity than the fluid: $k_s/k_f = 100$, which explains why the temperature gradients within the solid region are much smaller than in the fluid region.

In this case study, the periodically developed conjugate heat transfer regime sets in after the second solid square at $x/d \simeq 4$, causing the temperature profiles around the third to the second last solid square in Figure 7.3 to become similar. The rapid onset of the periodically developed flow and heat transfer regime near the inlet is a typical observation for laminar

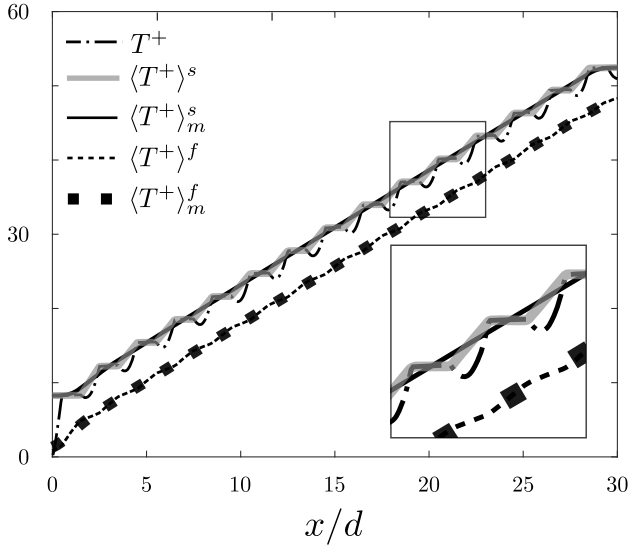

Figure 7.3: Filtered dimensionless temperature distributions at the centreline $y = l_2/2$ of the square array.

incompressible flow of a fluid with $\mathrm{Pr} = 1$ at moderate Reynolds numbers. In this numerical experiment, we have chosen $\mathrm{Re} \triangleq \rho_f U_{\mathrm{ref}}\, d/\mu_f = 100$, where $U_{\mathrm{ref}} \triangleq \sqrt{\Delta p/\rho_f}$.

The fact that the heat transfer regime is periodically developed over the largest part of the square array, also translates into a linearly increasing macro-scale temperature over the entire array, apart from the inlet and outlet region. More precisely, only the profiles of the intrinsically averaged fluid and solid temperature $\langle T^+\rangle^f_m$ and $\langle T^+\rangle^s_m$ on Figure 7.3, which are based on the weighting function $m = m_V * m_V$, have a constant slope in the developed regime. The profiles of the intrinsically volume-averaged fluid and solid temperature $\langle T^+\rangle^f$ and $\langle T^+\rangle^s$ on Figure 7.3 are clearly nowhere exactly linear. However, the difference between $\langle T^+\rangle^f$ and $\langle T^+\rangle^f_m$ as well as the difference between $\langle T^+\rangle^s$ and $\langle T^+\rangle^s_m$ is small, indicating that the first-order volume-averaged spatial moments of the square solids are negligible. The small magnitude of these spatial moments is a consequence

of the relatively high porosity of the square array,

$$\epsilon_f = 1 - \frac{d^2}{l_1 l_2}, \tag{7.58}$$

which equals $\epsilon_f = 0.75$ in this case study. This can be seen from the expression [19, 20] for the first-order spatial moment of the fluid indicator on the unit cell domain:

$$\langle \gamma_f(\boldsymbol{r} - \boldsymbol{x}) \rangle \cdot \boldsymbol{e}_x = \begin{cases} (1-\epsilon_f) x' & x' \in \left[0, \frac{l_1 - d}{2}\right] \\ (1-\epsilon_f) \left[x' - \frac{l_1}{d}\left(x' - \frac{l_1 - d}{2}\right)\right] & x' \in \left[\frac{l_1 - d}{2}, \frac{l_1 + d}{2}\right] \\ (1-\epsilon_f)\left(x' - l_1\right) & x' \in \left[\frac{l_1 + d}{2}, l_1\right] \end{cases} . \tag{7.59}$$

It therefore seems that the simple volume-averaging operator succeeds in yielding a meaningful macro-scale temperature for this case. Nevertheless, we argue that the filter operator based on $m = m_V * m_V$ yields a more physically meaningful macro-scale temperature for the periodically developed conjugate heat transfer regime, and it does that for any porosity ϵ_f and any shape of the solid structures. The first argument is that the double-averaged fluid temperature $\langle T^+ \rangle_m^f$ in a flow through solid structures subject to a periodic heat flux, resembles the linearly increasing fluid temperature in a channel without internal solids, but with walls subject to a constant heat flux [4].

The second argument is that the filter operator based on the weighting function $m = m_V * m_V$ gives rise to an interfacial heat transfer coefficient h_{fs} which is constant over space in the periodically developed regime. This property is illustrated in Figure 7.4 and agrees with the notion that also the heat transfer coefficient in a channel with a constant wall flux is space-independent in the fully developed flow and heat transfer regime [4]. The space-independence of the heat transfer coefficient for the weighting function of Quintard and Whitaker originates from the general principle that the difference between the curves of $\langle T \rangle_m^f$ and $\langle T \rangle_m^s$ is constant in the developed regime, as Figure 7.3 confirms.

On the contrary, Figure 7.4 reveals that the interfacial heat transfer coefficient h_{fs} for the volume-averaged solid and fluid temperature is a function of the position x' within the unit cell. For the weighting function m_V, the heat transfer coefficient h_{fs} thus varies together with the location where

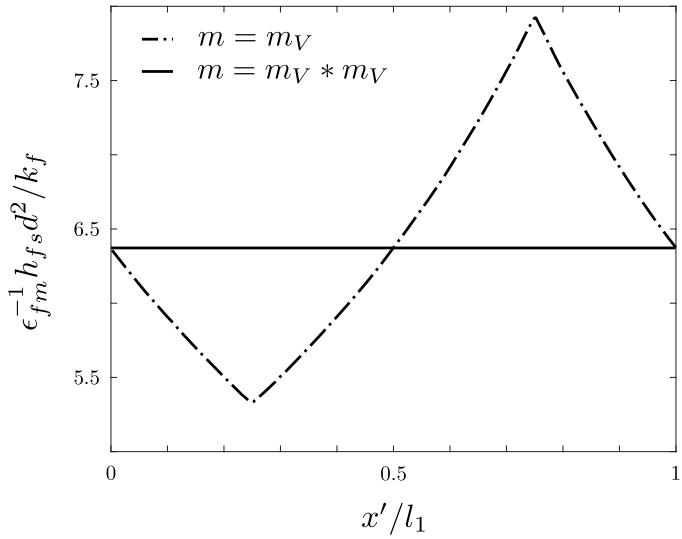

Figure 7.4: Interfacial heat transfer coefficient over the unit cell domain for different weighting functions.

the difference between the volume-averaged temperatures of the fluid and solid, $\langle T \rangle^f - \langle T \rangle^s$, is evaluated.

It is readily verified from (7.38) that the heat transfer coefficient for the weighting function m_V, denoted by $h_{fs}(m_V)$, is related to the spatially constant heat transfer coefficient for the weighting function $m = m_V * m_V$, denoted by $h_{fs}(m_V * m_V)$, through the formula

$$h_{fs}(m_V * m_V) = \left[\left\langle \frac{1}{h_{fs}(m_V)} \right\rangle \right]^{-1} . \tag{7.60}$$

We remark that the relative difference between $h_{fs}(m_V * m_V)$ and $h_{fs}(m_V)$ in Figure 7.4 is locally as much as 20%, to conclude that the weighting function has an important effect on the value of the interfacial heat transfer coefficient.

Figure 7.5 gives the thermal tortuosity for the square array in the periodically developed conjugate heat transfer regime. The thermal tortuosity varies over the unit cell domain for the volume-averaging operator with the weighting function m_V. As visualized in Figure 7.5, the spatial de-

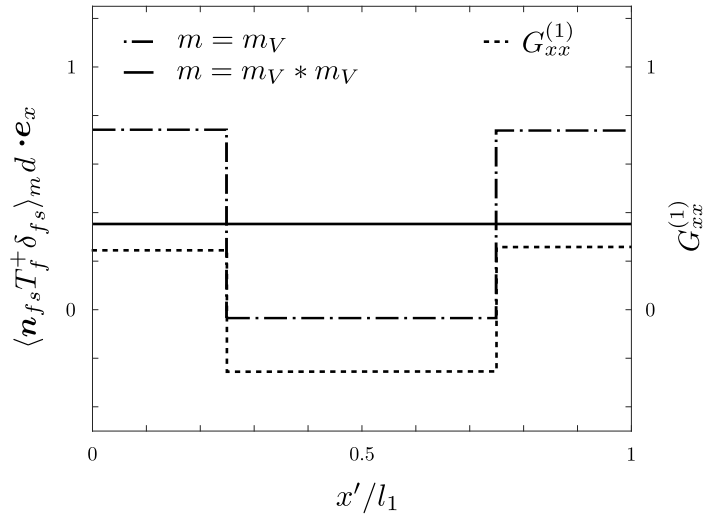

Figure 7.5: Thermal tortuosity for different weighting functions and first geometrical tensor over the unit cell domain.

pendence of the thermal tortuosity for m_V is caused by the non-zero first geometrical tensor, whose component $G^{(1)}_{xx} \triangleq \boldsymbol{G}^{(1)} \cdot \cdot \boldsymbol{e}_x \boldsymbol{e}_x$ is calculated numerically and agrees with its analytical expression

$$G^{(1)}_{xx} \triangleq \frac{\partial}{\partial x} \langle (\boldsymbol{r} - \boldsymbol{x}) \gamma_f \rangle \cdot \boldsymbol{e}_x = \begin{cases} (1 - \epsilon_f) & x' \in \left[0, \frac{l_1 - d}{2}\right] \\ (1 - \epsilon_f)\left(1 - \frac{l_1}{d}\right) & x' \in \left[\frac{l_1 - d}{2}, \frac{l_1 + d}{2}\right] \\ (1 - \epsilon_f) & x' \in \left[\frac{l_1 + d}{2}, l_1\right] \end{cases} . \tag{7.61}$$

In addition, Figure 7.5 demonstrates that the weighting function of Quintard and Whitaker, $m = m_V * m_V$, effectively results in a spatially constant tortuosity term, whose value is the average over the unit cell domain of the tortuosity term for the weighting function m_V.

Figure 7.6 learns us that it is advantageous to define the macro-scale temperature through the double volume-averaging operator of Quintard and Whitaker for yet another reason: similar to the interfacial heat transfer coefficient and the thermal tortuosity, also the thermal dispersion source becomes spatially constant in the developed regime. The thermal dispersion

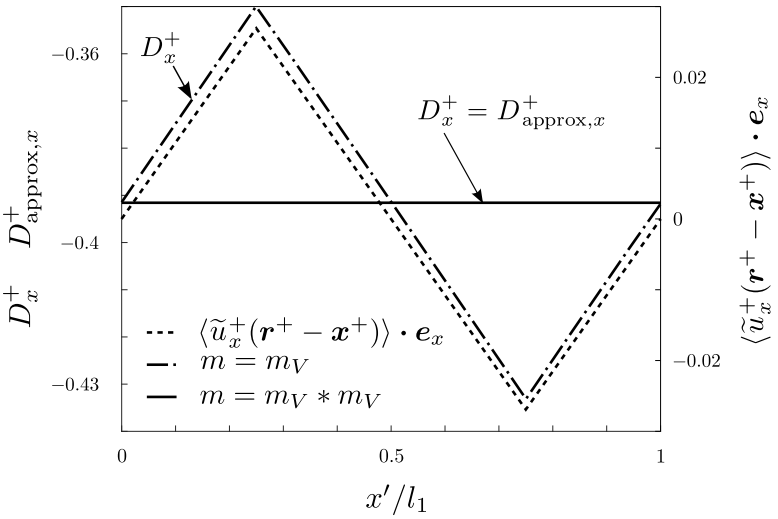

Figure 7.6: Thermal dispersion source for different weighting functions and volume-averaged spatial moment of the deviation velocity over the unit cell domain.

source $D_x^+ \triangleq \boldsymbol{\mathcal{D}} \cdot \boldsymbol{e}_x/(U_{\mathrm{ref}}\,\Delta T_{\mathrm{ref}})$ then equals $D^+_{\mathrm{approx},x} \triangleq \langle \widetilde{\boldsymbol{u}}^+ \widetilde{T}^+\rangle_m \cdot \boldsymbol{e}_x$, with $m = m_V * m_V$.

As Figure 7.6 shows, when the volume-averaged temperature is taken as macro-scale temperature, a dependence of the thermal dispersion source on the unit cell coordinate x' is induced by the non-zero volume-averaged spatial moment of the deviation velocity, $\langle \widetilde{\boldsymbol{u}}^+(\boldsymbol{r}^+ - \boldsymbol{x}^+)\rangle \cdot\cdot\, \boldsymbol{e}_x\boldsymbol{e}_x \triangleq \langle \widetilde{u}_x(\boldsymbol{r} - \boldsymbol{x})\rangle \cdot \boldsymbol{e}_x/(U_{\mathrm{ref}}\,d)$.

We emphasize that all the closure terms for the single and double volume-average filter in Figures 7.4 to 7.6 have been numerically calculated first from the filtered temperature and velocity distributions through their definitions (4.25)-(4.27). Afterwards, we have verified that these values agree with the exact closure equations of Section 7. To this end, we solved the periodic temperature part on the unit cell domain, via (7.9)-(7.12) and (7.17). The unit cell closure equations of Section 7 depend upon the velocity field on the unit cell domain, which was numerically reconstructed from the constant filtered velocity field $\langle \boldsymbol{u}\rangle_m = \langle \boldsymbol{u}\rangle_m$ in the developed regime via the exact closure equations of [17].

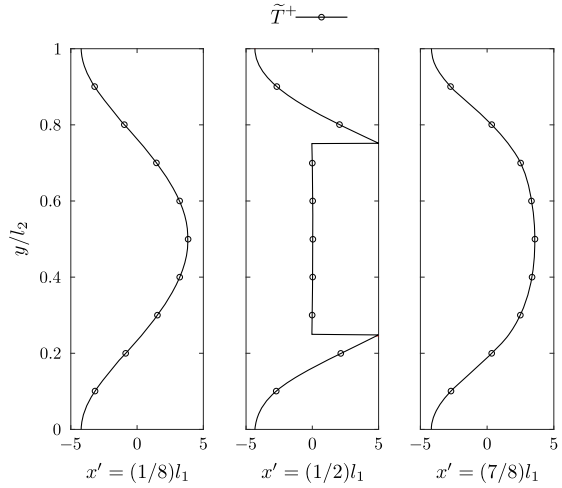

Figure 7.7: Comparison of deviation temperature profiles around the eighth solid square (solid lines) with unit cell simulation (circle markers)

The last illustration, Figure 7.7, gives the profiles of the deviation temperature for $m = m_V * m_V$ within the unit cell whose centroid coincides with the centre of the eighth solid square. These profiles are obtained in two ways. First, the deviation temperature profiles are calculated via their definition, (2.60), by filtering the full temperature distribution. Second, the deviation temperature is reconstructed exactly by solving just the periodic temperature part on the unit cell domain, via the equality $\widetilde{T} = T^\star - \langle T^\star \rangle_m^f \gamma_f - \langle T^\star \rangle_m^s \gamma_s$ that follows from (7.27).

The reconstruction of the micro-scale temperature details $\widetilde{T}^+$ in the periodically developed regime requires only knowledge of the unit cell geometry, the parameters of the flow and heat transfer regime, k_s/k_f, Pr and Re, and finally the heat source $\dot{q}^+$. The reconstruction of the deviation part of the volume-averaged temperature would necessitate in addition the calculation of the first-order spatial moments, as well as the first geometrical tensor and the volume-averaged spatial moment of the deviation velocity.

In conclusion, we have illustrated in this case study that both the thermal closure terms and the deviation temperature are exactly predicted in the periodically developed conjugate heat transfer regime by solving the pe-

riodic temperature part on the unit cell domain via the the exact closure equations of §7.7. In principle, also the filtered temperature distributions in figure 7.3, which are obtained by filtering the DNS results, thus could have been exactly reconstructed in the developed region $x/d \simeq 4 \ldots 26$, if the exact boundary conditions for the filtered temperature equations (4.19) and (4.20) were known. However, the temperature conditions at the onset of the periodically developed regime, $\langle T \rangle_m^f \big|_{\boldsymbol{x}_0}$ and $\langle T \rangle_m^s \big|_{\boldsymbol{x}_0}$, which determine the constant $\langle \overline{T^\star} \rangle$, are in general unknown for every spatial averaging operator, whether a traditional volume-average or a double volume average is chosen.

7.10 Conclusions

In the periodically developed conjugate heat transfer regime, all the solid structures have the same interfacial heat flux distribution, so that the closure terms can be governed by resolving the periodic part of the temperature field on a unit cell of the solid structures. For a simple volume-average filter, as in the volume-averaging technique (VAT), the closure terms in the periodically developed regime vary with the position within the unit cell. Nevertheless, the spatial dependence of the closure terms for the volume-averaged temperature has been neglected by previous studies. On the other hand, for a double volume-average filter based on the weighting function of Quintard and Whitaker, the thermal dispersion source, the thermal tortuosity as well as the interfacial heat transfer coefficient and macro-scale temperature temperature gradient are all spatially constant. It is therefore concluded that the appropriate filter for the macro-scale temperature in the periodically developed conjugate heat transfer regime is equivalent to a double volume average. To the authors' knowledge, the correct form of the closure terms and an appropriate definition of the macro-scale temperature in the periodically developed heat transfer regime have not been given before.

Bibliography

[1] G. Buckinx and M. Baelmans, "Macro-scale conjugate heat transfer in periodically developed flow through solid structures," *Journal of*

Fluid Mechanics, vol. 804, pp. 298–322, 2016.

[2] M. Quintard and S. Whitaker, "Transport in ordered and disordered porous media I: The cellular average and the use of weighting functions," *Transport in Porous Media*, vol. 14, no. 2, pp. 163–177, 1994.

[3] M. Quintard and S. Whitaker, "Transport in ordered and disordered porous media II: Generalized volume averaging," *Transport in Porous Media*, vol. 14, no. 2, pp. 179–206, 1994.

[4] Shah, R.K. and London, A.L., *Advances in Heat Transfer: laminar flow forced convection in ducts : a source book for compact heat exchanger analytical data*. New York: Academic Press, Inc., 1978.

[5] W. M. Kays and A. L. London, *Compact Heat Exchangers*. Krieger Pub Co, 1998.

[6] P.-S. Lee and S. V. Garimella, "Thermally developing flow and heat transfer in rectangular microchannels of different aspect ratios," *International Journal of Heat and Mass Transfer*, vol. 49, no. 1718, pp. 3060 – 3067, 2006.

[7] S. Patankar, C. Liu, and E. Sparrow, "Fully developed flow and heat transfer in ducts having streamwise-periodic variations of cross-sectional area," *Journal of Heat Transfer*, vol. 99, no. 2, p. 180, 1977.

[8] E. Utriainen and B. Sundén, "Numerical analysis of a primary surface trapezoidal cross wavy duct," *International Journal of Numerical Methods for Heat & Fluid Flow*, vol. 10, no. 6, pp. 634–648, 2000.

[9] E. Utriainen and B. Sundén, "A numerical investigation of primary surface rounded cross wavy ducts," *Heat and Mass Transfer*, vol. 38, no. 7, pp. 537–542, 2002.

[10] S. M. Karimian and A. G. Straatman, "A thermal periodic boundary condition for heating and cooling processes," *International Journal of Heat and Fluid Flow*, vol. 28, no. 2, pp. 329 – 339, 2007.

[11] A. Alshare, P. Strykowski, and T. Simon, "Simulations of flow and heat transfer in a serpentine heat exchanger having dispersed resistance with porous-continuum and continuum models," *International Journal of Heat and Mass Transfer*, vol. 53, no. 5-6, pp. 1088 – 1099, 2010.

[12] D. Lopez Penha, S. Stolz, J. Kuerten, M. Nordlund, A. Kuczaj, and B. Geurts, "Fully-developed conjugate heat transfer in porous media with uniform heating," *International Journal of Heat and Fluid Flow*, vol. 38, pp. 94–106, 2012.

[13] F. Kuwahara, A. Nakayama, and H. Koyama, "A numerical study of thermal dispersion in porous media," *Journal of Heat Transfer*, vol. 118, pp. 756–761, 1996.

[14] F. Kuwahara and A. Nakayama, "Numerical determination of thermal dispersion coefficients using a periodic porous structure," *Journal of Heat Transfer*, vol. 121, pp. 160–163, 1999.

[15] A. Alshare, P. Strykowski, and T. Simon, "Modeling of unsteady and steady fluid flow, heat transfer and dispersion in porous media using unit cell scale," *International Journal of Heat and Mass Transfer*, vol. 53, no. 9-10, pp. 2294–2310, 2010.

[16] C. Schroeder, A. Stomakhin, R. Howes, and J. Teran, "A second order virtual node algorithm for Navier–Stokes flow problems with interfacial forces and discontinuous material properties," *Journal of Computational Physics*, vol. 265, pp. 221 – 245, 2014.

[17] G. Buckinx and M. Baelmans, "Multi-scale modelling of flow in periodic solid structures through spatial averaging," *Journal of Computational Physics*, vol. 291, pp. 34–51, 2015.

[18] C. Ghaddar, "On the permeability of unidirectional fibrous media: A parallel computational approach," *Physics of Fluids*, vol. 7, no. 11, pp. 2563–2586, 1995.

[19] M. Quintard and S. Whitaker, "Transport in ordered and disordered porous media IV: Computer generated porous media for three-dimensional systems," *Transport in Porous Media*, vol. 15, no. 1, pp. 51–70, 1994.

[20] B. Wood, "Technical note: Revisiting the geometric theorems for volume averaging," *Advances in Water Resources*, vol. 62, pp. 340–352, 2013.

CHAPTER

8

CONCLUSIONS AND SUGGESTIONS FOR FURTHER RESEARCH

8.1 Conclusions

The main goal of this work is the development of a physically meaningful and exact macro-scale description of the flow and heat transfer in spatially periodic solid structures like fin arrays and tube bundles, which are commonly applied in compact heat transfer devices. The presented macro-scale description allows us to extract the physically relevant overall features of the very detailed flow and temperature fields in a heat transfer device through a filtering operation. That way, the detailed local information originating from a real-life or DNS experiment can be reduced to a limited amount of overall data involving only the macro-scale (i.e. filtered) flow and temperature. Moreover, the presented macro-scale description enables us to exactly determine the macro-scale quantities from a numerical experiment on a single unit cell of the solid structures only, at least in the periodically developed flow and heat transfer regimes.

In the periodically developed flow regime, the flow velocity varies in a periodic fashion from one unit cell of the solid structures to another. In this regime, the macro-scale quantities are obtained by filtering the flow velocity and pressure with a double volume-average filter over the unit cell. The macro-scale flow velocity is in that case spatially constant and directly proportional to the mass flow rate through the device. The macro-scale pressure on the other hand decreases linearly in the main flow direction. Its constant gradient corresponds to the pressure drop over each unit cell. Therefore, the relationship between the macro-scale flow velocity and the constant macro-scale pressure gradient can be governed by solving the periodically developed flow equations on a unit cell. Also the closure terms which affect the macro-scale flow, i.e. the interfacial force, as well as the momentum dispersion source are both space-independent when the flow is periodically developed and can be governed from a unit cell experiment. With the double volume-average filter, the interfacial force agrees exactly with the resistance force (drag and lift) exerted by a single solid structure on the flow. Furthermore, its time-averaged value equals the constant macro-scale pressure gradient. If the flow is steady, the interfacial force can be represented by means of a space-independent permeability tensor.

When the flow is periodically developed and the solid structures are all at the same constant temperature, the periodically developed heat transfer regime sets in. The periodically developed heat transfer regime in isothermal solid structures is characterized by an exponentially varying macro-scale fluid temperature in the main flow direction and a spatially periodic rescaled temperature. The macro-scale fluid temperature is obtained by filtering the fluid temperature with a filter that is matched to the decay rate of the macro-scale fluid temperature. The rescaled temperature which is similar for each unit cell, equals the ratio of the difference between the fluid and solid temperatures to the difference between the fluid and solid macro-scale temperatures. Via the governing equations for the rescaled temperature on a unit cell, the decay rate of the macro-scale temperature can be correlated with respect to the macro-scale flow velocity. With the aid of the matched filter, the macro-scale interfacial heat transfer can be represented by means of space-independent heat transfer coefficient. The matched filter also defines a space-independent dispersion coefficient to represent the thermal dispersion source. Both the heat transfer coefficient and the dispersion coefficient can be calculated from the rescaled temperature on a unit cell.

When the flow is periodically developed and the spatially periodic solid structures have the same interfacial heat flux, we speak of the periodically developed conjugate heat transfer regime. In the latter regime, the macro-scale temperature is obtained by filtering the temperature with a double volume-average filter. The macro-scale temperature of the fluid and solid then varies linearly in the main flow direction with a constant macro-scale temperature gradient. The constant macro-scale temperature gradient corresponds to the temperature difference over each unit cell of the solid structures. Therefore, the macro-scale temperature gradient is directly related to the time-averaged interfacial heat flux and volumetric heat sources within the unit cell, as well as the macro-scale velocity. Through the double volume-average filter, the macro-scale interfacial heat transfer can again be represented by means of space-independent heat transfer coefficient. This heat transfer coefficient can be determined by solving the equations for the periodic deviation temperature on a unit cell. With the double volume-average filter, also the thermal tortuosity is space-independent and obtainable from the periodic part of the temperature on a unit cell.

The presented macro-scale description has been developed mainly from the filter technique introduced by Quintard and Whitaker in the field of porous media [1–3]. Further, it starts with an extension of the periodically developed regimes, for which the basis has been provided by Patankar et al. [4]. As the presented macro-scale description is rigorously derived by filtering of the Navier-Stokes flow and temperature equations and is based on exact regime solutions of the Navier-Stokes equations, it is fully consistent with DNS results. That makes this macro-scale description a valuable alternative for the existing macro-scale models for heat transfer devices. After all, the existing macro-scale models for heat transfer devices are based on heuristic approaches or inexact VAT models and contain many approximations which are either not justified or difficult to verify. Moreover, while the existing macro-scale models for heat transfer devices with spatially periodic solid structures are difficult to interpret, the macro-scale description from this work does give a clear physical interpretation to all macro-scale quantities.

8.2 Suggestions for Further Research

In this work, the foundations have been set out for the macro-scale modelling of real heat transfer devices with spatially periodic solid structures. As such, this work can serve as a starting point for further research. To guide further research, some research questions and recommendations are given here.

Macro-Scale Models for Single-Fluid Heat Exchangers
The periodically developed heat transfer regimes considered in this work are limiting cases for real heat transfer devices. For instance, the periodically developed heat transfer regime in isothermal solids would only occur when the thermal conductivity of the solid wall and solid structures is infinitely high. On the other hand, the periodically developed conjugate heat transfer regime only occurs when the solid walls of the heat transfer device are subject to a truly constant heat source. Nevertheless, both limiting cases are of theoretical and practical interest to model real heat transfer devices. To date, one-dimensional single-fluid heat exchanger models, which are based on the assumption of either a constant solid temperature or a constant heat source, are still successfully applied to model real heat sinks [5].

We have shown in [6] that the one-dimensional single-fluid heat exchanger model for a constant solid temperature can be derived from our treatment of the planar periodically developed heat transfer regime in channels with isothermal solids. More specifically, we have shown that the temperature in the one-dimensional single-fluid heat exchanger model actually corresponds to the macro-scale temperature defined by the matched filter from Chapter 6. Consequently, the constant heat transfer coefficient appearing in the single-fluid heat exchanger model, whose existence was postulated but not proven yet, can be defined and calculated as the interfacial heat transfer coefficient from Chapter 6.

It still has to be shown how our treatment of the planar periodically developed conjugate heat transfer regime can be used to define the temperature and constant heat transfer coefficient in the one-dimensional single-fluid heat exchanger model for a constant heat source. Furthermore, it would be interesting to investigate whether the separable form of the rescaled temperature of §6.8 is a good approximation for the one-dimensional single-fluid heat exchanger model for a constant solid temperature. The reason

is that with the separable form of the rescaled temperature, the need for three-dimensional flow and heat transfer simulations can be omitted, as the variation perpendicular to the planar flow no longer has to be resolved.

Macro-Scale Models for Two-Fluid Heat Exchangers

The well-known correlations for the effectiveness (ϵ) and the number of transfer units (NTU) of counter-flow and cross-flow heat exchangers [7–9] are still the most widely applied models for two-fluid heat exchangers. These ϵ-NTU models are based on the assumption that the temperature distribution in a counter-flow heat exchanger is one-dimensional and two-dimensional in a cross-flow heat exchanger. Furthermore, these ϵ-NTU models incorporate a constant heat transfer coefficient to represent the heat transfer from the hot flow to the cold flow. As the temperature distribution in a heat exchanger with spatially periodic structures is three-dimensional and the local heat transfer coefficient at the separating wall between the two flows is space-dependent, it is not clear whether the ϵ-NTU models can be theoretically reconciled with DNS experiments of the Navier-Stokes flow and temperature equations.

The spatial averaging technique of Chapter 2 might allow us to develop an ϵ-NTU model for counter-flow heat exchangers that is in full agreement with DNS results. We believe that it is possible to discover a temperature similarity in a counter-flow heat exchanger which occurs when both flows are periodically developed. We expect that this temperature similarity will be spatially periodic over a domain consisting of two neighbouring unit cells: one in the channel of the hot flow and the other in the channel of the cold flow. From this temperature similarity it should be possible to develop a macro-scale description of the heat transfer between the hot flow and the cold flow. In addition, because the macro-scale temperatures of the hot and cold flow in a counter-flow heat exchanger are expected to change exponentially in the streamwise direction of each flow, we believe that some type of matched filter like in Chapter 6 is necessary to define the macro-scale temperature of the hot and cold flow.

Macro-Scale Description of Turbulent Developed Regimes

In this work, only the laminar periodically developed flow and heat transfer regimes have been treated. To the author's knowledge, a mathematical description of the turbulent developed flow and heat transfer regimes in periodic solid structures has not been presented yet, nor experimentally verified. Nevertheless, the existence of turbulent developed regimes in periodic solid structures seems generally accepted in the literature [7–9].

Given that the turbulent periodically developed regimes exist, an important question is which similarities characterize them. One may ask oneself whether the similarities which define the laminar periodically developed regimes remain valid for turbulent flow, although in a time-averaged sense.

To obtain time-averaged statistics in fully developed turbulent flow in channels without solid structures, Reynolds time-averaging has been applied [10]. Therefore, a combination of Reynolds time-averaging and spatial averaging might be a means to develop a macro-scale description of the turbulent developed flow and heat transfer regimes in periodic solid structures. We expect that such a macro-scale description would be more or less equivalent to the LES models for channel flow, with the difference that the filter window is much larger than in LES. Another difference would be that such a macro-scale description requires a model for the closure terms like the interfacial force and interfacial heat transfer, which do not appear in the current LES models, because the commutation error near boundaries is usually neglected [11].

Closure Correlations for the Periodically Developed Regimes — The literature reviews from the preceding chapters indicate that the closure terms in the periodically developed flow and heat transfer regimes have not been investigated in a systematic way. Even for the most well-studied geometries like solid cylinders and squares, the available data for the interfacial force only covers a limited range of flow angles, Reynolds numbers and porosities. Furthermore, the momentum dispersion source in the periodically developed regime has not been investigated at all.

To extend the data from the literature, we have numerically calculated both the interfacial force and the momentum dispersion source in steady periodically developed flow through equidistant cylinders [12]. Our database currently covers seven different porosity values, the entire range of flow angles with a resolution of five degrees, as well as the entire range of Reynolds numbers for which the flow remains steady with a resolution of five. However, this data is only available in the form of a lookup table and should still be correlated in the form of analytical formulas to be useful in practise.

In the literature, no correlations for the closure terms in the periodically developed heat transfer regime in isothermal solid structures have been presented, as this regime was not yet mathematically described prior to this work. Nonetheless, the development of correlations for the heat trans-

fer coefficient, the temperature decay rate and the thermal dispersion coefficient in developed flow around isothermal cylinders is technologically relevant for a variety of heat transfer devices. The development of these correlations is thus a topic for further research.

Macro-Scale Description for Non-Periodic Solid Structures The closure models given in this work are only valid for the periodically developed flow and heat transfer regimes, hence for spatially periodic solid structures with a constant porosity. When a configuration of spatially periodic solid structures is perturbed into a non-periodic configuration, periodically developed flow and heat transfer will no longer occur. Moreover, in non-periodic solid structures also gradients of the weighted porosity will arise unavoidably for the filters from this work. Nevertheless, the closure models for the periodically developed regimes might still be applicable as a local approximation of the true closure terms in a non-periodic configuration. For example, the relation between the local interfacial force and the local macro-scale velocity and the local macro-scale pressure gradient in a non-periodic configuration of solids might still be nearly the same as in the periodically developed flow regime, if the gradients of the weighted porosity are not too large.

To explore this idea, we have started a perturbation analysis of the generalized Navier-Stokes flow equations and the macro-scale flow equations. Unfortunately, our work [13] is far from completed yet and many questions remain unanswered. One unsolved research problem is how the weighting function should be chosen for filtering non-periodic distributions. In a non-periodic configuration of solids there exists no such thing as a unit cell. Therefore, it is not clear what the averaging domain should be in order to make a comparison with the periodically developed flow regime.

Optimal Configuration of Non-Periodic Solid Structures As explained above, it is not known whether the closure models for the periodically developed regimes can also be applied locally to model the macro-scale flow and heat transfer in non-periodic solid structures. However, it is certainly worth investigating whether a macro-scale flow and heat transfer model based on these closure models can be used to optimize the size or position of individual non-periodic solid structures in a heat transfer device. The objective for the optimization could be for instance improving the power density of the device. This optimization problem is probably best solved with a gradient-based optimization algorithm in combination with the adjoint method.

Currently, we are exploring this idea for a heat sink consisting of long, highly conductive pin fins on a base plate. The interfacial force and momentum dispersion source in the macro-scale flow equations for the flow through the pin fins are modelled via the lookup tables from [12]. Further research is needed to include the macro-scale heat transfer in the optimization model. Finally, also the outcome of this optimization method and the physical interpretation of its underlying macro-scale model will require a careful examination.

Bibliography

[1] M. Quintard and S. Whitaker, "Transport in ordered and disordered porous media I: The cellular average and the use of weighting functions," *Transport in Porous Media*, vol. 14, no. 2, pp. 163–177, 1994.

[2] M. Quintard and S. Whitaker, "Transport in ordered and disordered porous media II: Generalized volume averaging," *Transport in Porous Media*, vol. 14, no. 2, pp. 179–206, 1994.

[3] M. Quintard and S. Whitaker, "Transport in ordered and disordered porous media III: Closure and comparison between theory and experiment," *Transport in Porous Media*, vol. 15, no. 1, pp. 31–49, 1994.

[4] S. V. Patankar, C. H. Liu, and E. M. Sparrow, "Fully Developed Flow and Heat Transfer in Ducts Having Streamwise-Periodic Variations of Cross-Sectional Area," *Journal of Heat Transfer*, vol. 99, no. 2, p. 180, 1977.

[5] R. Knight, J. Goodling, and D. Hall, "Optimal thermal design of forced convection heat sinks-analytical," *ASME. J. Electron. Packag.*, vol. 113, no. 3, 1991.

[6] G. Buckinx and M. Baelmans, "Macro-scale modelling of heat sinks with highly conductive periodically arranged fins," in *Massarotti, N. (Ed.), Nithiarasu, P. (Ed.), Joshi, Y. (Ed.), Fourth International Conference on Computational Methods for Thermal Problems. Georgia Tech, Atlanta, USA, 6-8 July 2016.*, no. 1234, (Kyoto), August 2016.

[7] W. M. Kays and A. L. London, *Compact Heat Exchangers*. Krieger Pub Co, 1998.

[8] R. K. Shah and D. P. Sekuli, *Fundamentals of Heat Exchanger Design*. Hoboken, NJ, USA: John Wiley & Sons, Inc., July 2003.

[9] Shah, R.K. and London, A.L., *Advances in Heat Transfer: laminar flow forced convection in ducts : a source book for compact heat exchanger analytical data*. New York: Academic Press, Inc., 1978.

[10] J. Kim, P. Moin, and R. Moser, "Turbulence statistics in fully developed channel flow at low reynolds number," *Journal of Fluid Mechanics*, vol. 177, pp. 133–166, 04 1987.

[11] A. Dunca, V. John, and W. J. Layton, "The commutation error of the space averaged navier-stokes equations on a bounded domain," *Journal of Mathematical Fluid Mechanics*, vol. 1, no. 3, pp. 273–283, 2003.

[12] G. Buckinx, "Interfacial force and momentum dispersion in steady periodically developed flow through cylinders (unpublished work)," *KU Leuven*, 2016.

[13] G. Buckinx, "Macro-scale flow in non-periodic solid structures – a perturbation analysis (unpublished work)," *KU Leuven*, 2016.

APPENDIX

A

VAT AND HOMOGENIZATION: AN INTRODUCTORY EXAMPLE

In this appendix, the main features of the volume-averaging technique and asymptotic homogenization are illustrated for a one-dimensional steady heat conduction problem. The analysis here is inspired by the treatise of Davit et al.[1], which gives an illustrative comparison of VAT and homogenization for a general time-dependent diffusion problem.

[1]Y. Davit, C. G. Bell, H. M. Byrne, L. A. C. Chapman, L. S. Kimpton, G. E. Lang, K. H. L. Leonard, J. M. Oliver, N. C. Pearson, R. J. Shipley, S. L. Waters, J. P. Whiteley, B. D. Wood, and M. Quintard, "Homogenization via formal multiscale asymptotics and volume averaging: How do the two techniques compare?," *Advances in Water Resources*, vol. 62, Part B, pp. 178 – 206, 2013

A.1 One-Dimensional Steady Heat Conduction Problem

The one-dimensional steady heat conduction problem for a continuum medium Ω is:

$$-\frac{d}{dx}\left(k(x)\frac{d}{dx}T\right) = \dot{q} \qquad \text{with} \qquad x \in \Omega = [0, L]\,. \tag{A.1}$$

We consider the following boundary conditions:

$$T|_{x=0} = T_0 \qquad \text{and} \qquad T|_{x=L} = T_L\,. \tag{A.2}$$

This problem describes for instance the temperature T in a thin heterogeneous rod of length L, which is subject to a heat source $\dot{q}$ and whose end points are kept at different temperatures. To obtain a non-dimensional form, we define the following dimensionless parameters

$$T^+ \triangleq \frac{T - T_L}{T_0 - T_L}\,, \qquad x^+ \triangleq \frac{x}{L}\,, \qquad q^+ \triangleq \frac{\dot{q}L^2}{k_{\text{ref}}} \quad \text{and} \quad k^+ \triangleq \frac{k}{k_{\text{ref}}}\,. \tag{A.3}$$

After substitution of the dimensionless parameters, the conduction problem becomes equivalent to

$$\boxed{\begin{aligned} -\frac{d}{dx^+}\left(k^+(x^+)\frac{d}{dx^+}T^+\right) = \dot{q}^+ \quad &\text{with} \quad x^+ \in \Omega^+ = [0,1]\,, \\ T^+|_{x^+=0} = 1 \quad &\text{and} \quad T^+|_{x^+=1} = 0\,. \end{aligned}} \tag{A.4}$$

Formally, the problem of interest, (A.4), can also be represented using operator notation as

$$\mathcal{A}^+T^+ = \dot{q}^+ \quad \text{with the operator} \quad \mathcal{A}^+ \triangleq -\frac{d}{dx^+}\left(k^+(x^+)\frac{d}{dx^+}\right)\,. \tag{A.5}$$

We assume that the thermally conducting medium is periodically heterogeneous, so that its conduction coefficient k is periodic over a length scale ℓ:

$$k(x) = k(x + \ell)\,. \tag{A.6}$$

The domain Ω_{unit} over which the conductivity and hence the medium are assumed to be periodic, is called the *unit cell*:

$$\Omega_{\text{unit}}(x) \triangleq \{\forall r \in [(x - \ell/2, x + \ell/2]\}\,. \tag{A.7}$$

The average conductivity over the unit cell is taken as reference conductivity of the medium: $k_{\text{ref}} \triangleq \frac{1}{\ell}\int_0^\ell k(x)\,dx$.

Further, we assume the length scale ℓ over which the conductivity changes is much smaller than the domain size L. In that case, the conduction problem can be called a multi-scale problem characterised by the small parameter

$$\varepsilon \triangleq \frac{\ell}{L} \ll 1\,. \tag{A.8}$$

Rather than to determine the temperature T by solving (A.4) directly, we now wish to describe the temperature variation within the medium in some *macro-scale sense*. By *macro-scale sense*, it is understood that we can somehow mathematically describe the overall temperature profile over the domain Ω without the temperature details that manifest themselves over the smallest length scale ℓ.

A.2 Application of the Volume-Averaging Technique

The volume-averaging technique will allow us to derive a model for the volume-averaged temperature distribution. For the one-dimensional conduction problem under consideration, the volume-average corresponds to a moving average over the period ℓ of $k(x)$. The unit cell will thus serve as an REV of the medium. The volume-averaged temperature is expected to represent the overall temperature profile, containing no detailed temperature changes over a length scale smaller than ℓ.

Assumptions
The VAT method requires five important assumptions to be made:

(**A**1) The temperature can be decomposed in a spatially averaged part and a deviation part:

$$T^+ = \langle T^+\rangle + \widetilde{T}^+ \qquad \text{with} \qquad \langle T^+\rangle \triangleq \frac{1}{\varepsilon}\int_{x^+-\varepsilon/2}^{x^++\varepsilon/2} T^+(r^+)\,dr^+\,, \tag{A.9}$$

where the average temperature is sufficiently constant over the local averaging domain $\bar{\Omega}(x) = \Omega_{\text{unit}}(x)$, so that

$$\langle\langle T^+\rangle\rangle \simeq \langle T^+\rangle \qquad \text{and} \qquad \langle\widetilde{T}^+\rangle \simeq 0\,. \tag{A.10}$$

(**A**2) More or less consistent with (A.10) of (**A**1), it is assumed that the gradient of the average temperature can be moved outside the averaging operator $\langle\ \rangle$, e.g.:

$$\frac{d}{dx^+}\left\langle k^+\frac{d}{dx^+}\langle T^+\rangle\right\rangle \simeq \frac{d}{dx^+}\left(\langle k^+\rangle\frac{d}{dx^+}\langle T^+\rangle\right). \tag{A.11}$$

(**A**3) As a third approximation, the product of the deviation part of the conductivity and the second-order derivative of the averaged temperature is assumed to be negligible:

$$\frac{d}{dx^+}\left(\widetilde{k}^+\frac{d}{dx^+}\langle T^+\rangle\right) \simeq \left(\frac{d}{dx^+}\widetilde{k}^+\right)\frac{d}{dx^+}\langle T^+\rangle\,. \tag{A.12}$$

(**A**4) There exists a periodic mapping which relates the deviation temperature to the averaged temperature. For the linear heat conduction problem, this periodic mapping is expressed by

$$\widetilde{T}^+ = \zeta(x^+)\frac{d}{dx^+}\langle T^+\rangle \qquad \text{with} \qquad \zeta(x^+) = \zeta(x^+ + \varepsilon)\,. \tag{A.13}$$

The closure mapping field $\zeta(x^+)$ is assumed to be periodic over the averaging domain, which corresponds to the unit cell domain $\bar{\Omega}^+_{\text{unit}}(x^+) \triangleq \{\forall r^+ \in (x^+ - \varepsilon/2, x^+ + \varepsilon/2)\}$.

(**A**5) The heat source has no deviation part

$$\dot{\widetilde{q}}^+ = \dot{q}^+ - \langle\dot{q}^+\rangle = 0\,. \tag{A.14}$$

Approximations like (**A**1)-(**A**3), which are necessary to obtain a simplified VAT model of practical use, are typically called *length-scale constraints*. They are called that way, because the length scales of the problem, like ℓ and L in this case, are often used to estimate the order of magnitude of the terms that are neglected through these approximations. Hence, these approximations introduce negligible errors as long as the magnitude of the

neglected terms is small, or as long as the length scales of the problem satisfy some constraints.

The standard volume-averaging technique as applied by Whitaker and Quintard[2] typically proceeds through the following four steps.

Step 1: Average Continuum Equation
If we average the heat conduction problem (A.4), the macro-scale equation for the volume-averaged temperature is obtained:

$$\boxed{-\frac{d}{dx^+}\left(\langle k^+\rangle \frac{d}{dx^+}\langle T^+\rangle\right) = \langle \dot{q}^+\rangle + C_T\,,} \tag{A.15}$$

where the closure term C_T is defined as

$$C_T \equiv -\frac{d}{dx^+}\left(\langle k^+\rangle \frac{d}{dx^+}\langle T^+\rangle\right) + \frac{d}{dx^+}\left\langle k^+ \frac{d}{dx^+}T^+\right\rangle . \tag{A.16}$$

Note that the order of the derivative operator and the averaging operator can be interchanged when the temperature and heat conduction coefficient are continuous functions.

Step 2: Set up and Simplify Closure Equation
For solving the macro-scale equation, the closure term C_T must be modelled as well. By subtracting the macro-scale equation (A.15) from the original problem (A.4), we find the equation for the closure term:

$$-\frac{d}{dx^+}\left(k^+\frac{d}{dx^+}T^+\right) + \frac{d}{dx^+}\left(\langle k^+\rangle \frac{d}{dx^+}\langle T^+\rangle\right) = \dot{\tilde{q}} - C_T \tag{A.17}$$

This closure equation needs to be solved simultaneously with the macro-scale equation (A.15) in order to determine the closure term C_T.

After applying the spatial decomposition of (**A**1), the closure equation (A.17) becomes equivalent to

$$-\frac{d}{dx^+}\left(\widetilde{k}^+\frac{d}{dx^+}\langle T^+\rangle\right) - \frac{d}{dx^+}\left(k^+\frac{d}{dx^+}\widetilde{T}^+\right) = \dot{\tilde{q}} - C_T\,, \tag{A.18}$$

where

$$C_T = -\frac{d}{dx^+}\left(\langle k^+\rangle \frac{d}{dx^+}\langle T^+\rangle\right) + \frac{d}{dx^+}\left\langle k^+\frac{d}{dx^+}\langle T^+\rangle\right\rangle + \frac{d}{dx^+}\left\langle k^+\frac{d}{dx^+}\widetilde{T}^+\right\rangle . \tag{A.19}$$

[2]S. Whitaker, *The Method of Volume Averaging (Theory and Applications of Transport in Porous Media)*. Kluwer Academic Publishers, Boston, 1999

With the approximation of (**A**3), the closure equation can be simplified into

$$\boxed{-\left(\frac{d}{dx^+}\widetilde{k}^+\right)\frac{d}{dx^+}\langle T^+\rangle - \frac{d}{dx^+}\left(k^+\frac{d}{dx^+}\widetilde{T}^+\right) \simeq \dot{\widetilde{q}} - C_T\,.} \tag{A.20}$$

The second approximation (**A**2) allows to simplify the expression for the closure term C_T in the former closure problem:

$$\boxed{C_T \simeq \frac{d}{dx^+}\left\langle k^+\frac{d}{dx^+}\widetilde{T}^+\right\rangle\,.} \tag{A.21}$$

In this simplified form, the closure term C_T depends only on the deviation temperature $\widetilde{T}^+$, but not on the average temperature. The assumption that the closure terms can be expressed as a function of the just the deviation quantities, is very common in VAT. Although this assumption is difficult to verify a priori, it seems to be a good approximation for many problems of interest.

Step 3: Set up Unit Cell (REV) Problem for Closure
The simplified closure problem (A.20) is still as complex and expensive to solve as the original heat conduction problem, because its solution contains all high-resolution temperature details $\widetilde{T}^+$ over the entire domain Ω^+. By substituting the periodic closure mapping of (**A**4), the closure equation is transformed into a problem which needs to be solved just on the unit cell domain (the REV):

$$\boxed{\begin{aligned} -\frac{d\widetilde{k}^+}{dx^+} &= -\frac{d}{dx^+}\left(k^+\frac{d}{dx^+}\zeta(x^+)\right) \qquad \forall x^+ \in \Omega^+_{\text{unit}} = [0,\varepsilon]\,, \\ \zeta(0) &= \zeta(\varepsilon)\,, \\ \langle\zeta\rangle &= \int_0^\varepsilon \zeta(x^+)\,dx^+ = 0\,. \end{aligned}} \tag{A.22}$$

The integral constraint $\langle\zeta\rangle = 0$ ensures that $\langle\widetilde{T}^+\rangle \simeq 0$ and invokes a unique solution for ζ.

Finally, by (A.21), the closure term C_T follows from the solution for the closure mapping function on the unit cell domain:

$$C_T \simeq \frac{d}{dx^+}\left\langle k^+\frac{d\zeta}{dx^+}\right\rangle\frac{d}{dx^+}\langle T^+\rangle\,. \tag{A.23}$$

Step 4: Assemble Macro-Scale Equation
If we substitute the expression for the closure term from the unit cell problem (A.23) into the macro-scale problem (A.15), we find

$$\boxed{-\frac{d}{dx^+}\left(k^+_{\text{eff}}\frac{d}{dx^+}\langle T^+\rangle\right) = \langle \dot{q}^+\rangle\,,} \tag{A.24}$$

where the effective conductivity, which determines the volume-averaged temperature, is given by

$$\boxed{k^+_{\text{eff}} = \left\langle k^+\left(1+\frac{d\zeta}{dx^+}\right)\right\rangle\,.} \tag{A.25}$$

The macro-scale temperature equation obtained via VAT is easier to solve than the original temperature equation (A.4), because it contains a constant instead of spatially varying conductivity coefficient. Moreover, the effective conductivity (A.25) can be determined by solving just a single detailed experiment on a unit cell of the medium (A.22) instead of the entire medium. Therefore, we say that (A.24) is a reduced model for (A.4).

A.3 Application of Asymptotic Homogenization

The method of asymptotic homogenization will allow us to derive a model for the temperature distribution of the one-dimensional conduction problem (A.4) in the limit of

$$\varepsilon \triangleq \frac{\ell}{L} \to 0\,. \tag{A.26}$$

Assumptions
The method of asymptotic homogenization for the one-dimensional heat conduction problem is based on four important assumptions:

> (**A**1) The dimensionless heat conduction coefficient varies periodically over the unit cell of the medium and thus depends solely on the micro-scale coordinate y^+:
>
> $$k^+ = k^+(y^+) \qquad \text{where} \qquad y^+ \triangleq \frac{x^+}{\varepsilon}\,.$$

(**A**2) The temperature distribution can be represented by a series approximation of the form

$$T^+(x^+) = \sum_{i=0}^{\infty} T_i^+ \left(x^+, \frac{x^+}{\varepsilon} \right) \varepsilon^i \triangleq \sum_{i=0}^{\infty} T_i^+ \left(x^+, y^+ \right) \varepsilon^i \,,$$

where the variables x^+ and y^+ are assumed to be independent of each-other.

(**A**3) It is assumed that the temperature can be represented by a sequence of terms which are periodic in the micro-scale coordinate:

$$T_i^+ \left(x^+, y^+ \right) = T_i^+ \left(x^+, y^+ + 1 \right) \,.$$

Hence, the interval of periodicity for the micro-scale coordinate, which we call the *unit cell* domain, is given by $y^+ \in \Omega^+_{\text{unit}} = [0, 1]$ and corresponds to $x \in [0, \ell]$.

(**A**4) The source term depends only on the macro-scale coordinate x^+:

$$\dot{q}^+ = \dot{q}^+(x^+) \,.$$

The asymptotic temperature solution T_0^+ is the temperature profile for $\varepsilon = 0$ and is expected to be independent of the micro-scale coordinate y^+. Therefore, we can call T_0^+ the macro-scale temperature. Our goal is thus to find a model equation for the macroscopic temperature solution T_0^+, which, we hope, is easier to solve than the original heat conduction problem. We will show that this in fact possible through the following steps.

Step 1: Decompose Operator of Continuum Equation
By (**A**2), the temperature is transformed into a new functional of the independent coordinates x^+ and y^+. Therefore, also the operator $\mathcal{A}^+$ of (A.5) must be decomposed according the chain rule for differentiation,

$$\frac{d}{dx^+} = \frac{\partial}{\partial x^+} + \varepsilon^{-1} \frac{\partial}{\partial y^+} \,. \tag{A.27}$$

The application of the chain rule of (A.27) together with (**A**1) yields the following two-scale decomposition of the operator $\mathcal{A}^+$:

$$\mathcal{A}^+ = \varepsilon^{-2} \mathcal{A}_0^+ + \varepsilon^{-1} \mathcal{A}_1^+ + \mathcal{A}_2^+ \,, \tag{A.28}$$

where

$$\mathcal{A}_0^+ \triangleq -\frac{\partial}{\partial y^+}\left(k^+(y^+)\frac{\partial}{\partial y^+}\right) \tag{A.29}$$

$$\mathcal{A}_1^+ \triangleq -\frac{\partial}{\partial x^+}\left(k^+(y^+)\frac{\partial}{\partial y^+}\right) - \frac{\partial}{\partial y^+}\left(k^+(y^+)\frac{\partial}{\partial x^+}\right) \tag{A.30}$$

$$\mathcal{A}_2^+ \triangleq -\frac{\partial}{\partial x^+}\left(k^+(y^+)\frac{\partial}{\partial x^+}\right) \tag{A.31}$$

In operator notation, the heat conduction problem is thus written as

$$\mathcal{A}^+T^+ = \underbrace{\varepsilon^{-2}\mathcal{A}_0^+T^+}_{\substack{\text{derivatives}\\ \text{w.r.t. } y^+}} + \underbrace{\varepsilon^{-1}\mathcal{A}_1^+T^+}_{\substack{\text{cross-derivatives}\\ \text{w.r.t. } x^+ \text{and } y^+}} + \underbrace{\mathcal{A}_2^+T^+}_{\substack{\text{derivatives}\\ \text{w.r.t. } x^+}} = \dot{q}^+ . \tag{A.32}$$

Step 2: Set up Asymptotic Sub-Problems
When the two-scale temperature expansion of (**A**2) is inserted in the heat conduction equation with the decomposed operator of (A.32) and all terms containing equal powers of ε are equated, the following three nested sub-problems are retrieved:

$$O\left(\varepsilon^{-2}\right), \qquad \mathcal{A}_0^+T_0^+ = 0 \tag{A.33}$$

$$O\left(\varepsilon^{-1}\right), \qquad \mathcal{A}_0^+T_1^+ = -\mathcal{A}_1^+T_0^+ \tag{A.34}$$

$$O\left(\varepsilon^{0}\right), \qquad \mathcal{A}_0^+T_2^+ = -\mathcal{A}_1^+T_1^+ - \mathcal{A}_2^+T_0^+ + \dot{q}^+ . \tag{A.35}$$

Note that we restrict our analysis only to powers of ε up to order one, $O\left(\varepsilon^0\right) = O(1)$, as we are looking for an asymptotic solution for the temperature when $\varepsilon \to 0$.

Step 3: Analyse and Simplify Asymptotic Sub-Problems
From the sub-problem for $O\left(\varepsilon^{-2}\right)$ and the form of the operator $\mathcal{A}_0^+$ together with the periodicity of T^+ in y^+, we find that the asymptotic solution T_0^+ indeed depends only on the macro-scale coordinate x^+:

$$T_0^+(x^+, y^+) = T_0^+(x^+) . \tag{A.36}$$

Consequently, because of (A.36), the sub-problem for $O\left(\varepsilon^{-1}\right)$ is simplified into

$$\mathcal{A}_1^+T_0^+ = -\frac{\partial}{\partial y^+}\left(k^+(y^+)\frac{dT_0^+}{dx^+}\right) . \tag{A.37}$$

Step 4: Set up Unit Cell Problem
We now proceed to the sub-problem for $O\left(\varepsilon^{-1}\right)$. The sub-problem (A.34) shows that T_1^+ depends on the asymptotic solution $T_0^+(x^+)$. Let us propose a linear relationship of the form

$$T_1^+ = \chi(y^+)\frac{dT_0^+}{dx^+} \quad \text{with} \quad \chi(y^+) = \chi(y^+ + 1)\,. \tag{A.38}$$

This form is motivated by the linearity of the operator $\mathcal{A}_1^+$ and represents a temperature T_1^+ which is a separable function with respect to both coordinates x^+ and y^+. After substitution of this form into the sub-problem (A.34), we find that $\chi(y^+)$ is the periodic solution of

$$\boxed{\begin{aligned} -\frac{d}{dy^+}\left(k^+(y^+)\frac{d\chi}{dy^+}\right) &= \frac{dk^+}{dy^+} \qquad \forall y^+ \in \Omega^+_{\text{unit}} = (0,1)\,, \\ \chi(0) &= \chi(1)\,, \\ \langle\chi\rangle_y \triangleq \int_0^1 \chi(y^+)\,dy^+ &= 0\,. \end{aligned}} \tag{A.39}$$

Note that we impose the additional integral constraint $\langle\chi\rangle_y = 0$, because the boundary value problem (A.39) determines the periodic solution $\chi(y^+)$ only up to an arbitrary constant. This differential equation yields the solution of the subproblem for $O\left(\varepsilon^{-1}\right)$ on the unit cell domain. Therefore, (A.39) is called *the unit cell problem.*

Step 5: Derive Macro-Scale Equation
In order to solve the third sub-problem for $O\left(\varepsilon^0\right) = O(1)$, the fifth step consists of averaging (A.35) over the unit cell domain. By (**A**4) this yields the following equation:

$$\langle\mathcal{A}_0^+T_2^+\rangle_y + \langle\mathcal{A}_1^+T_1^+\rangle_y + \langle\mathcal{A}_2^+T_0^+\rangle_y = \dot{q}^+\,. \tag{A.40}$$

Using the fact that T_i^+ is periodic in y^+, we have

$$\langle\mathcal{A}_0^+T_2^+\rangle_y = 0 \qquad \text{and} \qquad \langle\mathcal{A}_1^+T_1^+\rangle_y = -\frac{\partial}{\partial x^+}\left\langle\left(k^+(y^+)\frac{\partial T_1^+}{\partial y^+}\right)\right\rangle_y\,. \tag{A.41}$$

It follows that (A.35) reduces to

$$-\frac{\partial}{\partial x^+}\left\langle\left(k^+(y^+)\frac{\partial T_1^+}{\partial y^+}\right)\right\rangle_y - \frac{\partial}{\partial x^+}\left\langle\left(k^+(y^+)\frac{dT_0^+}{dx^+}\right)\right\rangle_y = \dot{q}^+\,, \tag{A.42}$$

If we substitute the expression (A.38) for the first asymptotic perturbation T_1^+, we find the following equation for the macro-scale temperature:

$$\boxed{-\frac{d}{dx^+}\left(k_{\text{eff}}^+ \frac{d}{dx^+} T_0^+\right) = \dot{q}^+ \qquad \text{with} \qquad x^+ \in \Omega^+ = [0,1]\ ,} \tag{A.43}$$

where the constant k_{eff}^+ represents the effective thermal conductivity of the heterogeneous medium and is defined by

$$k_{\text{eff}}^+ \triangleq \left\langle k^+ \left(1 + \frac{d\chi}{dy^+}\right)\right\rangle_y . \tag{A.44}$$

After a single integration of the unit cell problem with respect to y^+, it follows for χ that

$$k^+ \frac{d\chi}{dy^+} = \left[\left\langle \frac{1}{k^+}\right\rangle_y\right]^{-1} - k^+ , \tag{A.45}$$

so that the effective conductivity can be calculated by averaging the locally varying conductivity over one periodic unit:

$$\boxed{k_{\text{eff}}^+ = \left[\left\langle \frac{1}{k^+}\right\rangle_y\right]^{-1} .} \tag{A.46}$$

The effective conductivity above is denoted by the same symbol as the effective conductivity in (A.44), because both effective parameters are equal. Indeed, because $\langle k^+ \rangle$ is constant, we have

$$-\frac{d\widetilde{k}^+}{dx^+} = -\frac{dk^+}{dx^+} \tag{A.47}$$

Therefore, it is readily seen from a comparison of (A.23) and (A.39) that both unit cell problems are equivalent and that $\chi = \zeta$. Hence, because $\dot{q}^+ = \langle \dot{q}^+ \rangle$ by (**A**4), it is concluded that also $T_0^+ = \langle T^+ \rangle$ in this case.

In summary, the method of asymptotic homogenization and the volume-averaging technique yield the same macro-scale description and same type of model reduction for the one-dimensional conduction problem under study.

Illustration for A Composite Medium

Figure A.1 gives the temperature distribution in a medium composed of two alternating materials α and β, which occupy the same volume within the medium and whose conductivities are k_α and k_β respectively. No heat source is assumed to be present in the composite medium. The conductivity k of the composite medium in the first unit cell $x \in [0, \ell]$ is given by

$$k(x) = \begin{cases} k_\beta & x \in \left[\frac{1}{4}\ell, \frac{3}{4}\ell\right] \\ k_\alpha & \text{elsewhere} \end{cases} . \tag{A.48}$$

Although the former conductivity is not a continuous function, the volume-averaging technique and the method of asymptotic homogenization can still be applied to this problem.

Figure A.1 shows that the temperature distribution T_ε^+ in the medium, which is the solution of the one-dimensional heat conduction problem (A.4), depends on the spatial period $\varepsilon \triangleq \ell/L$ between the two materials. For larger spatial periods, e.g. $\varepsilon = 1/3$, the temperature distribution T_ε^+ clearly exhibits a sawtooth-like profile. For smaller spatial periods, e.g. $\varepsilon = 1/10$, the temperature distribution T_ε^+ tends to a linear profile, although temperature wiggles with a frequency of ε^{-1} are still present. In the limit of $\varepsilon = 0$, both materials succeed each other in space at a very high spatial frequency and we retrieve the macro-scale temperature T_0^+. The macro-scale temperature T_0^+ does not show any temperature wiggles with a high spatial frequency, but reflects the overall temperature profile for $\varepsilon = 1/3$, $\varepsilon = 1/10$ and other values of ε. The overall temperature T_0^+ has a linear profile everywhere, except near the boundaries $x^+ = 0$ and $x^+ = 1$, where the macro-scale equation (A.43) is not valid, because the medium has no periodic composition, nor conductivity over the boundaries.

The asymptotic temperature profile T_0^+ agrees with the volume-average of the temperature distribution T_ε^+ for any period ε, except near the boundaries, where $\langle T_\varepsilon^+ \rangle = \langle T^+ \rangle$ depends on how the averaging operator for the volume-average is defined near the boundary.

The effective conductivity of the composite medium is known from the geometry and thermal properties of the unit cell (REV) and equals

$$k_{\text{eff}} = \left(\frac{1}{2} \frac{1}{k_\alpha} + \frac{1}{2} \frac{1}{k_\beta} \right)^{-1} = \frac{2 k_\alpha k_\beta}{k_\alpha + k_\beta} . \tag{A.49}$$

Because no heat sources are present, the effective conductivity of the composite medium does not influence the macro-scale temperature.

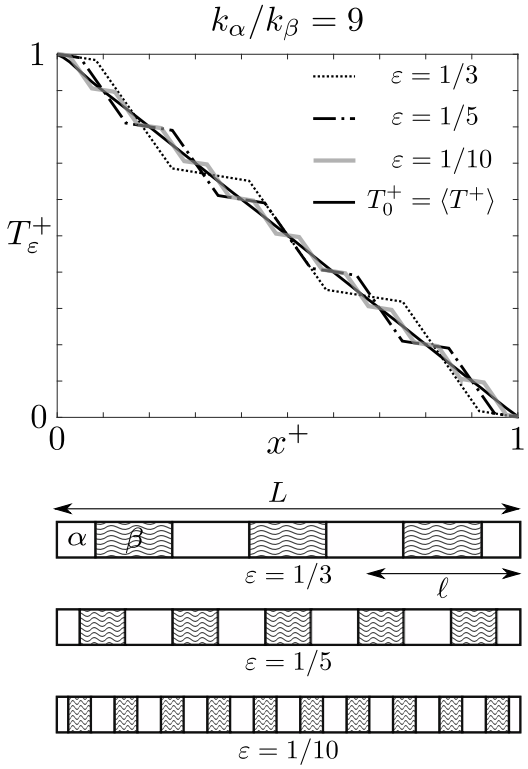

Figure A.1: Temperature distribution in a one-dimensional medium composed of two materials with conductivities k_α and k_β, which succeed each other over a spatial period ε.

APPENDIX

B

SPATIAL AVERAGING OF THE GENERALIZED FLOW EQUATIONS

In this appendix, each of the terms of the generalized Navier-Stokes equations (3.1) and (3.2) is spatially averaged over the entire system domain Ω, in order to obtain the macro-scale flow equations (3.13) and (3.14).

Averaging of Continuity Equation

Averaging the divergence of the velocity distribution in the usual sense and applying the spatial averaging gradient theorem (2.48) yields:

$$\langle \nabla^{\nu} \cdot \boldsymbol{u} \rangle_m = \nabla \cdot \langle \boldsymbol{u} \rangle_m + \underbrace{\langle \boldsymbol{n}_{fs} \cdot \boldsymbol{u}_f \delta_{fs} \rangle_m}_{=0, \text{ by Eq. (3.6)}} \tag{B.1}$$

$$= \nabla \cdot \langle \boldsymbol{u} \rangle_m \,. \tag{B.2}$$

As indicated in the first step of the derivation (B.1), the integral over the fluid-solid interface is zero due to the no-slip condition (3.6) on Γ_{fs}. This result leads directly from (3.1) to (3.13).

Averaging of Momentum Equation

The local time derivative of the velocity distribution is averaged using the theorem (2.54):

$$\left\langle \frac{\partial^\nu \boldsymbol{u}}{\partial t} \right\rangle_m = \frac{\partial \langle \boldsymbol{u} \rangle_m}{\partial t} \,. \tag{B.3}$$

In order to average the convective acceleration term, we apply the spatial averaging gradient theorem (2.48):

$$\langle \nabla^\nu \cdot (\boldsymbol{u}\boldsymbol{u}) \rangle_m = \nabla \cdot \langle \boldsymbol{u}\boldsymbol{u} \rangle_m + \underbrace{\langle \boldsymbol{n}_{fs} \cdot \boldsymbol{u}_f \boldsymbol{u}_f \delta_{fs} \rangle_m}_{=0, \text{ by Eq. (3.6)}} \tag{B.4}$$

$$= \nabla \cdot \langle \boldsymbol{u}\boldsymbol{u} \rangle_m \,. \tag{B.5}$$

Now we make use of the spatial decomposition of the velocity distribution (2.60) with $\boldsymbol{u}_s = \widetilde{\boldsymbol{u}}_s = 0$:

$$\nabla \cdot \langle \boldsymbol{u}\boldsymbol{u} \rangle_m = \nabla \cdot \langle \langle \boldsymbol{u} \rangle_m^f \langle \boldsymbol{u} \rangle_m^f \gamma_f + \langle \boldsymbol{u} \rangle_m^f \gamma_f \widetilde{\boldsymbol{u}} + \widetilde{\boldsymbol{u}} \langle \boldsymbol{u} \rangle_m^f \gamma_f + \widetilde{\boldsymbol{u}}\widetilde{\boldsymbol{u}} \rangle_m \tag{B.6}$$

$$\simeq \nabla \cdot \big(\epsilon_{fm} \langle \boldsymbol{u} \rangle_m^f \langle \boldsymbol{u} \rangle_m^f + \underbrace{\langle \boldsymbol{u} \rangle_m^f \langle \widetilde{\boldsymbol{u}} \rangle_m + \langle \widetilde{\boldsymbol{u}} \rangle_m \langle \boldsymbol{u} \rangle_m^f}_{\langle \widetilde{\boldsymbol{u}} \rangle_m \approx 0,\, r_m \ll \mathscr{L}_{\boldsymbol{u}}} + \langle \widetilde{\boldsymbol{u}}\widetilde{\boldsymbol{u}} \rangle_m \big) \tag{B.7}$$

$$\simeq \nabla \cdot \big(\epsilon_{fm} \langle \boldsymbol{u} \rangle_m^f \langle \boldsymbol{u} \rangle_m^f + \epsilon_{fm} \langle \widetilde{\boldsymbol{u}}\widetilde{\boldsymbol{u}} \rangle_m^f \big) \,. \tag{B.8}$$

Upon taking the spatial average, possible variations of the intrinsically averaged velocity within $\bar{\Omega}$ can be sometimes neglected, as in (B.7) and (B.8). This approximation is justified when the support of the filter has a characteristic length-scale r_m which is small compared to the length-scale $\mathscr{L}_{\boldsymbol{u}}$ over which the filtered velocity changes (see §2.13 and (2.84)). With this approximation, two contributions to the inertial term remain in (B.8): one due to the average velocity and another that depends on the deviation velocity.

Before averaging the shear stress tensor, we first remark that the velocity gradient equals the velocity gradient in the usual sense, due to the no-slip condition at the fluid-solid interface, so that also

$$\langle \nabla^\nu \boldsymbol{u} \rangle_m = \nabla \langle \boldsymbol{u} \rangle_m + \underbrace{\langle \boldsymbol{n}_{fs} \boldsymbol{u}_f \delta_{fs} \rangle_m}_{=0, \text{ by Eq. (3.6)}} \tag{B.9}$$

$$= \nabla \langle \boldsymbol{u} \rangle_m \,. \tag{B.10}$$

The viscous term itself is averaged as follows:

$$\langle \nabla^\nu \cdot \boldsymbol{\tau} \rangle_m = \nabla \cdot \langle \boldsymbol{\tau} \rangle_m + \langle \boldsymbol{n}_{fs} \cdot \boldsymbol{\tau}_f \delta_{fs} \rangle_m \tag{B.11}$$

$$= \nabla \cdot \langle \boldsymbol{\tau} \rangle_m + \langle \boldsymbol{n}_{fs} \cdot \mu_f \left(\nabla \boldsymbol{u}_f + (\nabla \boldsymbol{u}_f)^\intercal \right) \delta_{fs} \rangle_m \,, \tag{B.12}$$

because $\nabla^\nu \boldsymbol{u} = \nabla \boldsymbol{u}_f$ in Ω_f and $\nabla^\nu \boldsymbol{u} = 0$ in Ω_s.

If the fluid viscosity μ_f, which might be function of the space coordinate $\boldsymbol{x}$, can be treated as constant within the averaging window $\bar{\Omega}(\boldsymbol{x})$ at each position, the filtered viscous stress tensor is given by

$$\langle \boldsymbol{\tau} \rangle_m = \mu_f \langle \boldsymbol{S} \rangle_m \quad \text{with} \quad \langle \boldsymbol{S} \rangle_m = \nabla \langle \boldsymbol{u} \rangle_m + (\nabla \langle \boldsymbol{u} \rangle_m)^\intercal \,, \tag{B.13}$$

as a consequence of (3.3), (2.93) and (B.9). The intrinsically averaged viscous stress tensor then satisfies

$$\langle \boldsymbol{\tau} \rangle_m^f = \mu_f \langle \boldsymbol{S} \rangle_m^f \tag{B.14}$$

$$= \mu_f \boldsymbol{S}'_m + \mu_f \epsilon_{fm}^{-1} \nabla \epsilon_{fm} \langle \boldsymbol{u} \rangle_m^f + \mu_f \langle \boldsymbol{u} \rangle_m^f \nabla \epsilon_{fm} \epsilon_{fm}^{-1} \,, \tag{B.15}$$

with $\boldsymbol{S}'_m \triangleq \nabla \langle \boldsymbol{u} \rangle_m^f + (\nabla \langle \boldsymbol{u} \rangle_m^f)^\intercal$. The deviation stress tensor then satisfies

$$\widetilde{\boldsymbol{\tau}} = \mu_f \widetilde{\boldsymbol{S}}_m - \mu_f \epsilon_{fm}^{-1} \nabla \epsilon_{fm} \langle \boldsymbol{u} \rangle_m^f \gamma_f - \mu_f \langle \boldsymbol{u} \rangle_m^f \nabla \epsilon_{fm} \epsilon_{fm}^{-1} \gamma_f \,, \tag{B.16}$$

with $\widetilde{\boldsymbol{S}}_m \triangleq \nabla \widetilde{\boldsymbol{u}} + (\nabla \widetilde{\boldsymbol{u}})^\intercal$.

When the fluid viscosity is really spatially independent, averaging of the viscous term can be done through substitution of (B.13) in (B.12):

$$\langle \nabla^\nu \cdot \boldsymbol{\tau} \rangle_m = \mu_f \nabla^2 \langle \boldsymbol{u} \rangle_m + \mu_f \underbrace{\nabla \cdot (\nabla \langle \boldsymbol{u} \rangle_m)^\intercal}_{=0, \text{ by Eq. (B.1)}} + \langle \boldsymbol{n}_{fs} \cdot \boldsymbol{\tau}_f \delta_{fs} \rangle_m \tag{B.17}$$

$$= \mu_f \nabla^2 \langle \boldsymbol{u} \rangle_m + \langle \boldsymbol{n}_{fs} \cdot \mu \left(\nabla \boldsymbol{u}_f + (\nabla \boldsymbol{u}_f)^\intercal \right) \delta_{fs} \rangle_m \,, \tag{B.18}$$

A second way proceeds by averaging (3.15), which yields

$$\langle \nabla^\nu \cdot \boldsymbol{\tau} \rangle_m = \mu_f \langle \nabla^{\nu\,2} \cdot \boldsymbol{u} \rangle_m \tag{B.19}$$

$$= \mu_f \nabla \cdot \langle \nabla^\nu \boldsymbol{u} \rangle_m + \langle \boldsymbol{n}_{fs} \cdot \mu_f \nabla \boldsymbol{u}_f \delta_{fs} \rangle_m \tag{B.20}$$

$$= \mu_f \nabla^2 \langle \boldsymbol{u} \rangle_m + \langle \boldsymbol{n}_{fs} \cdot \mu_f \nabla \boldsymbol{u}_f \delta_{fs} \rangle_m \,, \tag{B.21}$$

because of (2.48) and (B.9). The last term of (B.18) and (B.21) are thus equal, due to the no-slip condition (3.6):

$$\langle \boldsymbol{n}_{fs} \cdot \mu \left(\nabla \boldsymbol{u}_f + (\nabla \boldsymbol{u}_f)^\intercal \right) \delta_{fs} \rangle_m = \langle \boldsymbol{n}_{fs} \cdot \mu_f \nabla \boldsymbol{u}_f \delta_{fs} \rangle_m \,. \tag{B.22}$$

Finally, for the pressure gradient, the following result is directly derived from the spatial averaging gradient theorem (2.48):

$$\langle \nabla^{\nu} \cdot p\boldsymbol{I} \rangle_m = \nabla \langle p \rangle_m + \langle \boldsymbol{n}_{fs} \cdot p_f \boldsymbol{I} \delta_{fs} \rangle_m \,. \tag{B.23}$$

Here, the averaging procedure again leaves an integral over the interfacial surface that is contained within the averaging domain $\bar{\Omega}$. At every point in space this integral amounts to the pressure force exerted by the solid on the flow, measured in a small neighbourhood around that point, corresponding to the averaging domain around that point. In the same way, averaging of the force due to viscous stresses gave rise to a viscous force from the averaged flow field and a viscous interfacial force in (B.12).

When the spatial average of the momentum equation is taken and all the previous terms are substituted, the result is (3.14).

Intrinsically Averaged Momentum Equation

The intrinsically averaged momentum equation (3.17) is obtained after dividing the superficially averaged momentum equation (3.14) by ϵ_{fm}, expressing each superficially averaged flow quantity in terms of its intrinsic average: $\langle \boldsymbol{\phi} \rangle_m = \epsilon_{fm}^{-1} \langle \boldsymbol{\phi} \rangle_m^f$, and finally applying the chain rule for differentiation on each term of the form $\nabla \cdot (\epsilon_{fm}^{-1} \langle \boldsymbol{\phi} \rangle_m^f)$. For the viscous stress term for instance, the second step requires to substitute expression (B.14) in the term (B.13) of (3.14).

The transition from the porosity-dependent term of (3.18) to (3.21) under the assumption that the viscosity μ_f is constant, is clarified as follows. When μ_f is constant, the last two terms of (3.18) equal

$$\begin{aligned}
&\nabla \cdot \mu_f \left(\epsilon_{fm}^{-1} \nabla \epsilon_{fm} \langle \boldsymbol{u} \rangle_m^f + \langle \boldsymbol{u} \rangle_m^f \nabla \epsilon_{fm} \epsilon_{fm}^{-1} \right) && \text{(B.24)} \\
&= \mu_f \epsilon_{fm}^{-1} \nabla^2 \epsilon_{fm} \langle \boldsymbol{u} \rangle_m^f + \mu_f \nabla \epsilon_{fm} \cdot \nabla \left(\epsilon_{fm}^{-1} \langle \boldsymbol{u} \rangle_m^f \right) \\
&\qquad + \mu_f \nabla \cdot \left(\epsilon_{fm}^{-1} \langle \boldsymbol{u} \rangle_m^f \right) \nabla \epsilon_{fm} + \mu_f \epsilon_{fm}^{-1} \langle \boldsymbol{u} \rangle_m^f \cdot \nabla \nabla \epsilon_{fm} && \text{(B.25)} \\
&= \mu_f \epsilon_{fm}^{-1} \nabla^2 \epsilon_{fm} \langle \boldsymbol{u} \rangle_m^f - \mu_f \epsilon_{fm}^{-2} \nabla \epsilon_{fm} \cdot \nabla \epsilon_{fm} \langle \boldsymbol{u} \rangle_m^f \\
&\qquad + \mu_f \epsilon_{fm}^{-1} \nabla \epsilon_{fm} \cdot \nabla \langle \boldsymbol{u} \rangle_m^f - \mu_f \epsilon_{fm}^{-2} \nabla \epsilon_{fm} \cdot \langle \boldsymbol{u} \rangle_m^f \nabla \epsilon_{fm} \\
&\qquad + \mu_f \nabla \cdot \langle \boldsymbol{u} \rangle_m^f \epsilon_{fm}^{-1} \nabla \epsilon_{fm} + \mu_f \epsilon_{fm}^{-1} \langle \boldsymbol{u} \rangle_m^f \cdot \nabla \nabla \epsilon_{fm} \,. && \text{(B.26)}
\end{aligned}$$

When we add the second term of (3.18), which is given by (B.14), to the

former result (B.26), we find

$$\begin{aligned}
&\epsilon_{fm}^{-1}\nabla\epsilon_{fm}\cdot\langle\boldsymbol{\tau}\rangle_m^f+\nabla\cdot\mu_f\left(\epsilon_{fm}^{-1}\nabla\epsilon_{fm}\langle\boldsymbol{u}\rangle_m^f+\langle\boldsymbol{u}\rangle_m^f\nabla\epsilon_{fm}\epsilon_{fm}^{-1}\right)\\
&=\mu_f\epsilon_{fm}^{-1}\nabla^2\epsilon_{fm}\langle\boldsymbol{u}\rangle_m^f+2\mu_f\epsilon_{fm}^{-1}\nabla\epsilon_{fm}\cdot\nabla\langle\boldsymbol{u}\rangle_m^f\\
&\quad+\mu_f\nabla\cdot\langle\boldsymbol{u}\rangle_m^f\epsilon_{fm}^{-1}\nabla\epsilon_{fm}+\mu_f\epsilon_{fm}^{-1}\langle\boldsymbol{u}\rangle_m^f\cdot\nabla\nabla\epsilon_{fm}\\
&\quad+\mu_f\nabla\langle\boldsymbol{u}\rangle_m^f\cdot\epsilon_{fm}^{-1}\nabla\epsilon_{fm} \qquad \text{(B.27)}\\
&=\mu_f\epsilon_{fm}^{-1}\nabla^2\epsilon_{fm}\langle\boldsymbol{u}\rangle_m^f+2\mu_f\epsilon_{fm}^{-1}\nabla\epsilon_{fm}\cdot\nabla\langle\boldsymbol{u}\rangle_m^f-\mu_f\nabla\cdot\left(\nabla\langle\boldsymbol{u}\rangle_m^f\right)^{\mathsf{T}}. \qquad \text{(B.28)}
\end{aligned}$$

When the last result is substituted in (3.18), (3.21) is found. For the last step in (B.28), the following identity was used:

$$\begin{aligned}
\nabla\cdot\left(\nabla\langle\boldsymbol{u}\rangle_m^f\right)^{\mathsf{T}}&=\nabla\cdot\left(\nabla\left(\epsilon_{fm}^{-1}\langle\boldsymbol{u}\rangle_m\right)\right)^{\mathsf{T}} && \text{(B.29)}\\
&=\nabla\cdot\left(-\epsilon_{fm}^{-2}\nabla\epsilon_{fm}\langle\boldsymbol{u}\rangle_m+\epsilon_{fm}^{-1}\nabla\langle\boldsymbol{u}\rangle_m\right)^{\mathsf{T}} && \text{(B.30)}\\
&=\nabla\cdot\left(-\epsilon_{fm}^{-1}\langle\boldsymbol{u}\rangle_m^f\nabla\epsilon_{fm}+\epsilon_{fm}^{-1}\left(\nabla\langle\boldsymbol{u}\rangle_m\right)^{\mathsf{T}}\right) && \text{(B.31)}\\
&=\epsilon_{fm}^{-2}\nabla\epsilon_{fm}\cdot\langle\boldsymbol{u}\rangle_m^f\nabla\epsilon_{fm}-\epsilon_{fm}^{-1}\nabla\cdot\left(\langle\boldsymbol{u}\rangle_m^f\nabla\epsilon_{fm}\right)\\
&\quad-\epsilon_{fm}^{-2}\nabla\epsilon_{fm}\cdot\left(\nabla\langle\boldsymbol{u}\rangle_m\right)^{\mathsf{T}}+\underbrace{\epsilon_{fm}^{-1}\nabla\cdot\left(\nabla\langle\boldsymbol{u}\rangle_m\right)^{\mathsf{T}}}_{=0,\text{ by Eq. (B.1)}} && \text{(B.32)}\\
&=\epsilon_{fm}^{-2}\nabla\epsilon_{fm}\cdot\langle\boldsymbol{u}\rangle_m^f\nabla\epsilon_{fm}-\epsilon_{fm}^{-1}\nabla\cdot\langle\boldsymbol{u}\rangle_m^f\nabla\epsilon_{fm}\\
&\quad-\epsilon_{fm}^{-1}\langle\boldsymbol{u}\rangle_m^f\cdot\nabla\nabla\epsilon_{fm}-\epsilon_{fm}^{-2}\nabla\langle\boldsymbol{u}\rangle_m\cdot\nabla\epsilon_{fm} && \text{(B.33)}\\
&=\epsilon_{fm}^{-2}\nabla\epsilon_{fm}\cdot\langle\boldsymbol{u}\rangle_m^f\nabla\epsilon_{fm}-\epsilon_{fm}^{-1}\nabla\cdot\langle\boldsymbol{u}\rangle_m^f\nabla\epsilon_{fm}\\
&\quad-\epsilon_{fm}^{-1}\langle\boldsymbol{u}\rangle_m^f\cdot\nabla\nabla\epsilon_{fm}-\epsilon_{fm}^{-2}\nabla\epsilon_{fm}\langle\boldsymbol{u}\rangle_m^f\cdot\nabla\epsilon_{fm}\\
&\quad-\epsilon_{fm}^{-1}\nabla\langle\boldsymbol{u}\rangle_m^f\cdot\nabla\epsilon_{fm} && \text{(B.34)}\\
&=-\epsilon_{fm}^{-1}\nabla\cdot\langle\boldsymbol{u}\rangle_m^f\nabla\epsilon_{fm}-\epsilon_{fm}^{-1}\langle\boldsymbol{u}\rangle_m^f\cdot\nabla\nabla\epsilon_{fm}\\
&\quad-\epsilon_{fm}^{-1}\nabla\langle\boldsymbol{u}\rangle_m^f\cdot\nabla\epsilon_{fm}. && \text{(B.35)}
\end{aligned}$$

The intrinsically averaged momentum equation for a constant viscosity (3.20) and the gradient dependent term of (3.21) can also be recovered directly from (3.14) after substitution of (3.15) and applying the chain rule for the gradient of a product term.

APPENDIX

C

DERIVATION OF THE GLOBAL CLOSURE PROBLEM FOR THE MACRO-SCALE FLOW EQUATIONS

In this appendix, the global closure problem of (3.34) and (3.35)) is derived. The global closure problem is found by subtracting the filtered flow equations (3.16 and (3.17) from the original flow equations (3.1) and (3.2) on the f-region.

Continuity Equation for Closure Problem
From the continuity equation (3.1) we have

$$\nabla^\nu \cdot \boldsymbol{u} - \nabla \cdot \langle \boldsymbol{u} \rangle_m^f = (\nabla \cdot \langle \boldsymbol{u} \rangle_m^f)\gamma_f + \nabla^\nu \cdot \widetilde{\boldsymbol{u}} - \nabla \cdot \langle \boldsymbol{u} \rangle_m^f \tag{C.1}$$

$$= \nabla \cdot \widetilde{\boldsymbol{u}}_f \qquad \text{in } \Omega_f\,, \tag{C.2}$$

where we have made use of (2.62).

Momentum Equation for Closure Problem

The difference between the acceleration terms of (3.2) and (3.17) is

$$\frac{\partial^\nu \boldsymbol{u}}{\partial t} - \frac{\partial \langle \boldsymbol{u} \rangle_m^f}{\partial t} = \frac{\partial \langle \boldsymbol{u} \rangle_m^f}{\partial t}\gamma_f + \frac{\partial^\nu \tilde{\boldsymbol{u}}}{\partial t} - \frac{\partial \langle \boldsymbol{u} \rangle_m^f}{\partial t} \tag{C.3}$$

$$= \frac{\partial \tilde{\boldsymbol{u}}_f}{\partial t} \qquad \text{in } \Omega_f\,. \tag{C.4}$$

The subtraction of the convective inertial terms in Ω_f gives as result

$$\begin{aligned}
&\nabla^\nu \cdot (\boldsymbol{u}\boldsymbol{u}) - \nabla \cdot \left(\langle \boldsymbol{u} \rangle_m^f \langle \boldsymbol{u} \rangle_m^f \right) \\
&= \nabla^\nu \cdot (\langle \boldsymbol{u} \rangle_m^f \langle \boldsymbol{u} \rangle_m^f \gamma_f + \langle \boldsymbol{u} \rangle_m^f \gamma_f \tilde{\boldsymbol{u}} + \tilde{\boldsymbol{u}} \langle \boldsymbol{u} \rangle_m^f \gamma_f + \tilde{\boldsymbol{u}}\tilde{\boldsymbol{u}}) \\
&\quad - \nabla \cdot \left(\langle \boldsymbol{u} \rangle_m^f \langle \boldsymbol{u} \rangle_m^f \right) && \text{(C.5)} \\
&= \nabla \cdot \left(\langle \boldsymbol{u} \rangle_m^f \langle \boldsymbol{u} \rangle_m^f \right) \gamma_f + \nabla \cdot \left(\langle \boldsymbol{u} \rangle_m^f \tilde{\boldsymbol{u}} + \tilde{\boldsymbol{u}} \langle \boldsymbol{u} \rangle_m^f \right) \gamma_f + \nabla^\nu \cdot (\tilde{\boldsymbol{u}}\tilde{\boldsymbol{u}}) \\
&\quad - \nabla \cdot \left(\langle \boldsymbol{u} \rangle_m^f \langle \boldsymbol{u} \rangle_m^f \right) && \text{(C.6)} \\
&= \nabla \cdot \left(\left\{ \langle \boldsymbol{u} \rangle_m^f \right\}_f \widetilde{\boldsymbol{u}}_f + \widetilde{\boldsymbol{u}}_f \left\{ \langle \boldsymbol{u} \rangle_m^f \right\}_f \right) + \nabla \cdot (\widetilde{\boldsymbol{u}}_f \widetilde{\boldsymbol{u}}_f) \qquad \text{in } \Omega_f && \text{(C.7)} \\
&= \nabla \cdot (\boldsymbol{u}_f \widetilde{\boldsymbol{u}}_f) + \nabla \cdot \left(\widetilde{\boldsymbol{u}}_f \left\{ \langle \boldsymbol{u} \rangle_m^f \right\}_f \right) \qquad \text{in } \Omega_f && \text{(C.8)} \\
&= \boldsymbol{u}_f \cdot \nabla \widetilde{\boldsymbol{u}}_f + \nabla \cdot \left(\widetilde{\boldsymbol{u}}_f \left\{ \langle \boldsymbol{u} \rangle_m^f \right\}_f \right) \qquad \text{in } \Omega_f\,, && \text{(C.9)}
\end{aligned}$$

where the last identity holds by virtue of (3.1).

The difference between the true pressure gradient and the filtered pressure gradient follows directly through application of 2.62):

$$\nabla^\nu p - \nabla \langle p \rangle_m^f = \nabla \langle p \rangle_m^f \gamma_f + \nabla^\nu \widetilde{p} - \nabla \langle p \rangle_m^f \tag{C.10}$$

$$= \nabla \widetilde{p}_f \qquad \text{in } \Omega_f\,. \tag{C.11}$$

It can easily be seen that the difference of the viscous terms yields

$$\begin{aligned}
\boldsymbol{S} - \boldsymbol{S}'_m &= \nabla^\nu \boldsymbol{u} + (\nabla^\nu \boldsymbol{u})^\intercal - \nabla \langle \boldsymbol{u} \rangle_m^f - (\nabla \langle \boldsymbol{u} \rangle_m^f)^\intercal && \text{(C.12)} \\
&= (\nabla \langle \boldsymbol{u} \rangle_m^f)\gamma_f + (\nabla \langle \boldsymbol{u} \rangle_m^f)^\intercal \gamma_f + \nabla^\nu \widetilde{\boldsymbol{u}} + (\nabla^\nu \widetilde{\boldsymbol{u}})^\intercal \\
&\quad - \nabla \langle \boldsymbol{u} \rangle_m^f - (\nabla \langle \boldsymbol{u} \rangle_m^f)^\intercal && \text{(C.13)} \\
&= \nabla \widetilde{\boldsymbol{u}}_f + (\nabla \widetilde{\boldsymbol{u}}_f)^\intercal \qquad \text{in } \Omega_f && \text{(C.14)} \\
&\triangleq \left\{ \widetilde{\boldsymbol{S}}_m \right\}_f \qquad \text{in } \Omega_f\,. && \text{(C.15)}
\end{aligned}$$

Lastly, we have

$$\boldsymbol{f} - \langle \boldsymbol{f} \rangle_m^f = \langle \boldsymbol{f} \rangle_m^f - \boldsymbol{f}\gamma_f + \widetilde{\boldsymbol{f}} = \widetilde{\boldsymbol{f}}_f \qquad \text{in } \Omega_f\,. \tag{C.16}$$

APPENDIX

D

DERIVATION OF THE PLANAR FLOW EQUATIONS

In this appendix, the planar flow equations (3.51) and (3.52) are derived for a Cartesian vector basis and for a general vector basis.

D.1 Derivation for Cartesian Vector Basis

To derive the planar flow equations, we will first describe the flow with respect to an orthonormal Cartesian vector basis in $\mathbb{R}^3$:

$$\boldsymbol{u}(\boldsymbol{x},t) = u_1\boldsymbol{e}^{(1)} + u_2\boldsymbol{e}^{(2)} + u_3\boldsymbol{e}^{(3)}\,, \tag{D.1}$$

where the position vector satisfies

$$\forall \boldsymbol{x} \in \Omega : \boldsymbol{x} = x_1\boldsymbol{e}^{(1)} + x_2\boldsymbol{e}^{(2)} + x_3\boldsymbol{e}^{(3)} \Leftrightarrow x_3 \in I_3 = \left[-\frac{l_3}{2}, \frac{l_3}{2}\right]\,. \tag{D.2}$$

Continuity Equation for Planar Flow

With the coordinates of (D.2), the continuity equation (3.1) becomes[1]

$$\frac{\partial u_1}{\partial x_1} + \frac{\partial u_2}{\partial x_2} + \frac{\partial u_3}{\partial x_3} = 0\,. \tag{D.3}$$

After multiplication with a weighting function $m_3'(-x_3)$ and integration over the interval $x_3 \in I_3$, the continuity equation takes the form (3.51):

$$\frac{\partial \langle u_1 \rangle_3}{\partial x_1} + \frac{\partial \langle u_2 \rangle_3}{\partial x_2} = \varphi_3\,, \tag{D.4}$$

where the operator $\langle\ \rangle_3$ is evaluated at the coordinates $(x_1, x_2, x_3 = 0, t)$. The source term $\varphi_3(x_1, x_2)$ in the continuity equation for planar flow is defined as

$$\begin{aligned}\varphi_3 &\triangleq -\left\langle \frac{\partial u_3}{\partial x_3} \right\rangle_3 \triangleq -\int_{-\frac{l_3}{2}}^{\frac{l_3}{2}} m_3'(-x_3) \frac{\partial u_3}{\partial x_3}\, dx_3 \\ &= -m_3'(-x_3)\, u_3 \Big|_{x_3=-\frac{l_3}{2}}^{x_3=\frac{l_3}{2}} + \int_{-\frac{l_3}{2}}^{\frac{l_3}{2}} \frac{\partial m_3'(-x_3)}{\partial x_3} u_3\, dx_3\,,\end{aligned} \tag{D.5}$$

as follows after integration by parts. If $m_3(-x_3)$ and $u_3(x_1, x_2, x_3)$ are even functions of x_3, the integral in the right hand side of the last expression vanishes. In vector form, the source term $\varphi_3(x_1, x_2)$ is defined as

$$\varphi_3 \triangleq -\langle (\boldsymbol{e}^{(3)} \cdot \nabla)(\boldsymbol{u} \cdot \boldsymbol{e}^{(3)}) \rangle_3\,. \tag{D.6}$$

Momentum Equation for Planar Flow

With the coordinates of (D.2), the momentum equation (3.2) becomes

$$\begin{aligned}\rho_f \left(\frac{\partial u_1}{\partial t} + \frac{\partial u_1^2}{\partial x_1} + \frac{\partial u_2 u_1}{\partial x_2} + \frac{\partial u_3 u_1}{\partial x_3} \right) &= -\frac{\partial p}{\partial x_1} + f_1 \\ + \frac{\partial}{\partial x_1}\left[2\mu_f \frac{\partial u_1}{\partial x_1} \right] + \frac{\partial}{\partial x_2}\left[\mu_f \left(\frac{\partial u_1}{\partial x_2} + \frac{\partial u_2}{\partial x_1} \right) \right] &+ \frac{\partial \tau_{1,3}}{\partial x_3}\,,\end{aligned} \tag{D.7}$$

$$\begin{aligned}\rho_f \left(\frac{\partial u_2}{\partial t} + \frac{\partial u_1 u_2}{\partial x_1} + \frac{\partial u_2^2}{\partial x_2} + \frac{\partial u_3 u_2}{\partial x_3} \right) &= -\frac{\partial p}{\partial x_2} + f_2 \\ + \frac{\partial}{\partial x_1}\left[\mu_f \left(\frac{\partial u_1}{\partial x_2} + \frac{\partial u_2}{\partial x_1} \right) \right] + \frac{\partial}{\partial x_2}\left[2\mu_f \frac{\partial u_2}{\partial x_2} \right] &+ \frac{\partial \tau_{2,3}}{\partial x_3}\,.\end{aligned} \tag{D.8}$$

[1] Note that all spatial derivatives of this velocity distribution exist, as $\boldsymbol{u}$ is continuous in Ω as well as $\Omega_{x_3=0}$.

The shear stress components in this momentum equation are defined as $\tau_{j,k} \triangleq \boldsymbol{\tau} \cdot\cdot \boldsymbol{e}^{(j)}\boldsymbol{e}^{(k)}$:

$$\tau_{1,3} = \mu\left(\frac{\partial u_3}{\partial x_1} + \frac{\partial u_1}{\partial x_3}\right), \tag{D.9}$$

$$\tau_{2,3} = \mu\left(\frac{\partial u_2}{\partial x_3} + \frac{\partial u_3}{\partial x_2}\right). \tag{D.10}$$

After multiplying with a weighting function $m_3'(-x_3)$ and integrating over the interval $x_3 \in I_3$, the two-dimensional form of the momentum equations is retrieved, under the assumption that the viscosity is approximately constant over the interval $x_3 \in I_3$:

$$\begin{aligned}\rho_f \left(\frac{\partial \langle u_1\rangle_3}{\partial t} + \frac{\partial \langle u_1\rangle_3^2}{\partial x_1} + \frac{\partial \langle u_2\rangle_3\langle u_1\rangle_3}{\partial x_2}\right) &= -\frac{\partial \langle p\rangle_3}{\partial x_1} + \langle f_1\rangle_3 \\ &+ \frac{\partial}{\partial x_1}\left[2\mu_f \frac{\partial \langle u_1\rangle_3}{\partial x_1}\right] + \frac{\partial}{\partial x_2}\left[\mu_f\left(\frac{\partial \langle u_1\rangle_3}{\partial x_2} + \frac{\partial \langle u_2\rangle_3}{\partial x_1}\right)\right] + \boldsymbol{\Psi}_3 \cdot \boldsymbol{e}^{(1)},\end{aligned} \tag{D.11}$$

$$\begin{aligned}\rho_f \left(\frac{\partial \langle u_2\rangle_3}{\partial t} + \frac{\partial \langle u_1\rangle_3\langle u_2\rangle_3}{\partial x_1} + \frac{\partial \langle u_2\rangle_3^2}{\partial x_2}\right) &= -\frac{\partial \langle p\rangle_3}{\partial x_2} + \langle f_2\rangle_3 \\ &+ \frac{\partial}{\partial x_1}\left[\mu_f\left(\frac{\partial \langle u_1\rangle_3}{\partial x_2} + \frac{\partial \langle u_2\rangle_3}{\partial x_1}\right)\right] + \frac{\partial}{\partial x_2}\left[2\mu_f \frac{\partial \langle u_2\rangle_3}{\partial x_2}\right] + \boldsymbol{\Psi}_3 \cdot \boldsymbol{e}^{(2)}.\end{aligned} \tag{D.12}$$

Here, the operator $\langle\ \rangle_3$ is again evaluated at the coordinates $(x_1, x_2, x_3 = 0, t)$. The vector term $\boldsymbol{\Psi}_3$ in these momentum equations consists of three contributions:

$$\boldsymbol{\Psi}_3 \triangleq \boldsymbol{\Psi}_3^{\mathrm{I}} + \boldsymbol{\Psi}_3^{\mathrm{II}} + \boldsymbol{\Psi}_3^{\mathrm{II}}. \tag{D.13}$$

The first contribution is given by

$$\begin{aligned}\boldsymbol{\Psi}_3^{\mathrm{I}} \cdot \boldsymbol{e}^{(1)} \triangleq &\rho_f \frac{\partial}{\partial x_1}\left[\langle u_1\rangle_3^2 - \langle u_1^2\rangle_3\right] \\ &+ \rho_f \frac{\partial}{\partial x_2}\left[\langle u_2\rangle_3\langle u_1\rangle_3 - \langle u_2 u_1\rangle_3\right],\end{aligned} \tag{D.14}$$

$$\begin{aligned}\boldsymbol{\Psi}_3^{\mathrm{I}} \cdot \boldsymbol{e}^{(2)} \triangleq &\rho_f \frac{\partial}{\partial x_1}\left[\langle u_1\rangle_3\langle u_2\rangle_3 - \langle u_1 u_2\rangle_3\right] \\ &+ \rho_f \frac{\partial}{\partial x_2}\left[\langle u_2\rangle_3^2 - \langle u_2^2\rangle_3\right],\end{aligned} \tag{D.15}$$

or in vector form, with the aid of (3.41):

$$\boldsymbol{\Psi}_3^{\mathrm{I}} \triangleq \rho_f \nabla^\nu \cdot \big(\boldsymbol{v}\boldsymbol{v} - \langle \Big(\boldsymbol{u} - \boldsymbol{u}\cdot\boldsymbol{e}^{(3)}\boldsymbol{e}^{(3)}\Big)\Big(\boldsymbol{u} - \boldsymbol{u}\cdot\boldsymbol{e}^{(3)}\boldsymbol{e}^{(3)}\Big)\rangle_3\big)\,. \tag{D.16}$$

The second contribution consists of

$$\begin{aligned}\boldsymbol{\Psi}_3^{\mathrm{II}}\cdot\boldsymbol{e}^{(1)} &\triangleq -\left\langle \frac{\partial u_3 u_1}{\partial x_3}\right\rangle_3 \triangleq -\int_{-\frac{l_3}{2}}^{\frac{l_3}{2}} m_3'(-x_3)\frac{\partial u_3 u_1}{\partial x_3}\,dx_3 \\ &= -m_3'(-x_3)\,u_3u_1\Big|_{x_3=-\frac{l_3}{2}}^{x_3=\frac{l_3}{2}} + \int_{-\frac{l_3}{2}}^{\frac{l_3}{2}} \frac{\partial m_3'(-x_3)}{\partial x_3} u_3u_1\,dx_3\,, \end{aligned}\tag{D.17}$$

$$\begin{aligned}\boldsymbol{\Psi}_3^{\mathrm{II}}\cdot\boldsymbol{e}^{(2)} &\triangleq -\left\langle \frac{\partial u_3 u_2}{\partial x_3}\right\rangle_3 \triangleq -\int_{-\frac{l_3}{2}}^{\frac{l_3}{2}} m_3'(-x_3)\frac{\partial u_3 u_2}{\partial x_3}\,dx_3 \\ &= -m_3'(-x_3)\,u_3u_2\Big|_{x_3=-\frac{l_3}{2}}^{x_3=\frac{l_3}{2}} + \int_{-\frac{l_3}{2}}^{\frac{l_3}{2}} \frac{\partial m_3'(-x_3)}{\partial x_3} u_3u_2\,dx_3\,, \end{aligned}\tag{D.18}$$

where we used integration by parts. In vector form $\boldsymbol{\Psi}_3^{\mathrm{II}}$ becomes

$$\boldsymbol{\Psi}_3^{\mathrm{II}} \triangleq -\langle(\boldsymbol{e}^{(3)}\cdot\nabla)\big(\boldsymbol{u}\cdot\boldsymbol{e}^{(3)}\Big(\boldsymbol{u} - \boldsymbol{u}\cdot\boldsymbol{e}^{(3)}\boldsymbol{e}^{(3)}\Big)\big)\rangle_3\,. \tag{D.19}$$

The third part $\boldsymbol{\Psi}_3^{\mathrm{III}}$ is defined as

$$\begin{aligned}\boldsymbol{\Psi}_3^{\mathrm{III}}\cdot\boldsymbol{e}^{(1)} &\triangleq \left\langle \frac{\partial \tau_{1,3}}{\partial x_3}\right\rangle_3 \triangleq \int_{-\frac{l_3}{2}}^{\frac{l_3}{2}} m_3'(-x_3)\frac{\partial \tau_{1,3}}{\partial x_3}\,dx_3 \\ &= m_3'(-x_3)\,\tau_{1,3}\Big|_{x_3=-\frac{l_3}{2}}^{x_3=\frac{l_3}{2}} - \int_{-\frac{l_3}{2}}^{\frac{l_3}{2}} \frac{\partial m_3'(-x_3)}{\partial x_3}\tau_{1,3}\,dx_3\,, \end{aligned}\tag{D.20}$$

$$\begin{aligned}\boldsymbol{\Psi}_3^{\mathrm{III}}\cdot\boldsymbol{e}^{(2)} &\triangleq \left\langle \frac{\partial \tau_{2,3}}{\partial x_3}\right\rangle_3 \triangleq \int_{-\frac{l_3}{2}}^{\frac{l_3}{2}} m_3'(-x_3)\frac{\partial \tau_{2,3}}{\partial x_3}\,dx_3 \\ &= m_3'(-x_3)\,\tau_{2,3}\Big|_{x_3=-\frac{l_3}{2}}^{x_3=\frac{l_3}{2}} - \int_{-\frac{l_3}{2}}^{\frac{l_3}{2}} \frac{\partial m_3'(-x_3)}{\partial x_3}\tau_{2,3}\,dx_3\,, \end{aligned}\tag{D.21}$$

or

$$\boldsymbol{\Psi}_3^{\mathrm{III}} \triangleq \langle(\boldsymbol{e}^{(3)}\cdot\nabla)(\tau_{1,3}\boldsymbol{e}^{(1)} + \tau_{2,3}\boldsymbol{e}^{(2)})\rangle_3\,. \tag{D.22}$$

Note that the first term on the right hand side of (D.21) can be forced to vanish if the weighting function satisfies

$$m_3'(-x_3) = 0 \qquad \text{at } x_3 = \pm\tfrac{l_3}{2}\,. \tag{D.23}$$

The two-dimensional form of the momentum equation can finally be written in vector form as (3.52).

D.2 General Derivation

The planar flow equations (3.51) and (3.52) can also be derived from the orthogonal decomposition of the velocity field and gradient operator,

$$\begin{aligned} \boldsymbol{u} &= \boldsymbol{u}_{1,2} + \boldsymbol{u}_3 \qquad \text{with} \qquad \boldsymbol{u}_3 \triangleq \boldsymbol{u} \cdot \boldsymbol{e}^{(3)} \boldsymbol{e}^{(3)} , \\ \nabla^\nu &= \nabla^\nu_{1,2} + \nabla^\nu_3 \qquad \text{with} \qquad \nabla^\nu_3 \triangleq \boldsymbol{e}^{(3)} \boldsymbol{e}^{(3)} \cdot \nabla^\nu , \end{aligned} \tag{D.24}$$

as given in (3.43) and (3.44). Because of their orthogonality, the gradient operators $\nabla^\nu_{1,2}$ and ∇^ν_3 satisfy

$$\nabla^\nu_{1,2} \cdot \nabla^\nu_3 = \nabla^\nu_3 \cdot \nabla^\nu_{1,2} = 0 . \tag{D.25}$$

Continuity Equation for Planar Flow

With the former orthogonal decomposition, the continuity equation (3.1) becomes

$$\nabla^\nu_{1,2} \cdot \boldsymbol{u}_{1,2} + \underbrace{\nabla^\nu_{1,2} \cdot \boldsymbol{u}_3 + \nabla^\nu_3 \cdot \boldsymbol{u}_{1,2}}_{=0, \text{ by Eq. (D.24)}} + \nabla^\nu_3 \cdot \boldsymbol{u}_3 = 0 , \tag{D.26}$$

where the underbraced dot product terms are zero, due to the orthogonality of the gradient operator part with respect to the velocity part. After taking the one-dimensional convolution product (3.41) of each term, we find that

$$\nabla^\nu_{1,2} \cdot \langle \boldsymbol{u}_{1,2} \rangle_3 = -\langle \nabla^\nu_3 \cdot \boldsymbol{u}_3 \rangle_3 \triangleq \varphi_3 , \tag{D.27}$$

which is the planar continuity as in (3.52).

Momentum Equation for Planar Flow

The time derivative of the velocity field of (3.2) is decomposed as

$$\frac{\partial^\nu \boldsymbol{u}}{\partial t} = \frac{\partial^\nu \boldsymbol{u}_{1,2}}{\partial t} + \frac{\partial^\nu \boldsymbol{u}_3}{\partial t} , \tag{D.28}$$

so through the application of the one-dimensional convolution product of (3.41), we have

$$\frac{\partial^\nu \langle \boldsymbol{u} \rangle_3}{\partial t} = \frac{\partial^\nu \langle \boldsymbol{u}_{1,2} \rangle_3}{\partial t} + \frac{\partial^\nu \langle \boldsymbol{u}_3 \rangle_3}{\partial t} . \tag{D.29}$$

The orthogonal decomposition of the advective acceleration term of (3.2) leads to

$$\begin{aligned}\nabla^\nu\cdot(\boldsymbol{u}\boldsymbol{u}) = \nabla^\nu_{1,2}\cdot(\boldsymbol{u}_{1,2}\boldsymbol{u}_{1,2}) + \nabla^\nu_{1,2}\cdot(\boldsymbol{u}_{1,2}\boldsymbol{u}_3) + \underbrace{\nabla^\nu_{1,2}\cdot(\boldsymbol{u}_3\boldsymbol{u}_{1,2})}_{=0,\text{ by Eq. (D.24)}}\\ + \underbrace{\nabla^\nu_{1,2}\cdot(\boldsymbol{u}_3\boldsymbol{u}_3) + \nabla^\nu_3\cdot(\boldsymbol{u}_{1,2}\boldsymbol{u}_{1,2}) + \nabla^\nu_3\cdot(\boldsymbol{u}_{1,2}\boldsymbol{u}_3)}_{=0,\text{ by Eq. (D.24)}}\\ + \nabla^\nu_3\cdot(\boldsymbol{u}_3\boldsymbol{u}_{1,2}) + \nabla^\nu_3\cdot(\boldsymbol{u}_3\boldsymbol{u}_3)\,. \end{aligned} \tag{D.30}$$

When the convolution product operator $\langle\,\rangle_3$ is applied on this result, we get

$$\begin{aligned}\langle\nabla^\nu\cdot(\boldsymbol{u}\boldsymbol{u})\rangle_3 &= \nabla^\nu_{1,2}\cdot\langle\boldsymbol{u}_{1,2}\boldsymbol{u}_{1,2}\rangle_3 + \langle\nabla^\nu_{1,2}\cdot(\boldsymbol{u}_{1,2}\boldsymbol{u}_3)\rangle_3\\ &\quad + \langle\nabla^\nu_3\cdot(\boldsymbol{u}_3\boldsymbol{u}_{1,2})\rangle_3 + \langle\nabla^\nu_3\cdot(\boldsymbol{u}_3\boldsymbol{u}_3)\rangle_3\\ &= \nabla^\nu_{1,2}\cdot(\langle\boldsymbol{u}_{1,2}\rangle_3\langle\boldsymbol{u}_{1,2}\rangle_3) - \boldsymbol{\Psi}^{\mathrm{I}}_3 - \boldsymbol{\Psi}^{\mathrm{II}}_3\\ &\quad + \langle\nabla^\nu_{1,2}\cdot(\boldsymbol{u}_{1,2}\boldsymbol{u}_3)\rangle_3 + \langle\nabla^\nu_3\cdot(\boldsymbol{u}_3\boldsymbol{u}_3)\rangle_3\,, \end{aligned} \tag{D.31}$$

where

$$\boldsymbol{\Psi}^{\mathrm{I}}_3 \triangleq \nabla^\nu_{1,2}\cdot(\langle\boldsymbol{u}_{1,2}\rangle_3\langle\boldsymbol{u}_{1,2}\rangle_3) - \nabla^\nu_{1,2}\cdot\langle\boldsymbol{u}_{1,2}\boldsymbol{u}_{1,2}\rangle_3 \tag{D.32}$$

and

$$\boldsymbol{\Psi}^{\mathrm{II}}_3 \triangleq -\langle\nabla^\nu_3\cdot(\boldsymbol{u}_3\boldsymbol{u}_{1,2})\rangle_3\,. \tag{D.33}$$

The viscous stress term of (3.2) has the following decomposition:

$$\begin{aligned}\nabla^\nu\cdot\boldsymbol{\tau} = \nabla^\nu_{1,2}\cdot\mu\left(\nabla^\nu_{1,2}\boldsymbol{u}_{1,2} + \left(\nabla^\nu_{1,2}\boldsymbol{u}_{1,2}\right)^{\mathsf{T}}\right) + \nabla^\nu_{1,2}\cdot\mu\left(\nabla^\nu_{1,2}\boldsymbol{u}_3\right)\\ + \underbrace{\nabla^\nu_{1,2}\cdot\mu\left(\nabla^\nu_{1,2}\boldsymbol{u}_3\right)^{\mathsf{T}} + \nabla^\nu_{1,2}\cdot\mu\left(\nabla^\nu_3\boldsymbol{u}_{1,2}\right)}_{=0,\text{ by Eq. (D.25)}} + \nabla^\nu_{1,2}\cdot\mu\left(\nabla^\nu_3\boldsymbol{u}_{1,2}\right)^{\mathsf{T}}\\ + \underbrace{\nabla^\nu_{1,2}\cdot\mu\left(\nabla^\nu_3\boldsymbol{u}_3 + (\nabla^\nu_3\boldsymbol{u}_3)^{\mathsf{T}}\right) + \nabla^\nu_3\cdot\mu\left(\nabla^\nu_{1,2}\boldsymbol{u}_{1,2} + \left(\nabla^\nu_{1,2}\boldsymbol{u}_{1,2}\right)^{\mathsf{T}}\right)}_{=0,\text{ by Eq. (D.25)}}\\ + \underbrace{\nabla^\nu_3\cdot\mu\left(\nabla^\nu_{1,2}\boldsymbol{u}_3\right)}_{=0,\text{ by Eq. (D.25)}} + \nabla^\nu_3\cdot\mu\left(\nabla^\nu_{1,2}\boldsymbol{u}_3\right)^{\mathsf{T}} + \nabla^\nu_3\cdot\mu\left(\nabla^\nu_3\boldsymbol{u}_{1,2}\right)\\ + \underbrace{\nabla^\nu_3\cdot\mu\left(\nabla^\nu_3\boldsymbol{u}_{1,2}\right)^{\mathsf{T}}}_{=0,\text{ by Eq. (D.25)}} + \nabla^\nu_3\cdot\mu\left(\nabla^\nu_3\boldsymbol{u}_3 + (\nabla^\nu_3\boldsymbol{u}_3)^{\mathsf{T}}\right)\,. \end{aligned} \tag{D.34}$$

Therefore, the one-dimensional convolution of the viscous stress term is given by

$$\begin{aligned}\langle \nabla^\nu \cdot \boldsymbol{\tau} \rangle_3 = \nabla^\nu_{1,2} \cdot \mu \left(\nabla^\nu_{1,2} \langle \boldsymbol{u}_{1,2} \rangle_3 + \left(\nabla^\nu_{1,2} \langle \boldsymbol{u}_{1,2} \rangle_3 \right)^\intercal \right) + \boldsymbol{\Psi}^{\mathrm{III}}_3 \\ + \langle \nabla^\nu_{1,2} \cdot \mu \left(\nabla^\nu_{1,2} \boldsymbol{u}_3 + (\nabla^\nu_3 \boldsymbol{u}_{1,2})^\intercal \right) \rangle_3 \\ + \langle \nabla^\nu_3 \cdot \mu \left(\nabla^\nu_3 \boldsymbol{u}_3 + (\nabla^\nu_3 \boldsymbol{u}_3)^\intercal \right) \rangle_3 \,, \end{aligned} \tag{D.35}$$

where

$$\boldsymbol{\Psi}^{\mathrm{III}}_3 \triangleq \langle \nabla^\nu_3 \cdot \mu \left(\nabla^\nu_3 \boldsymbol{u}_{1,2} + \left(\nabla^\nu_{1,2} \boldsymbol{u}_3 \right)^\intercal \right) \rangle_3 \tag{D.36}$$

and

$$(\nabla^\nu_3 \boldsymbol{u}_3)^\intercal = \nabla^\nu_3 \boldsymbol{u}_3 \,. \tag{D.37}$$

Lastly, the one-dimensional convolution of the pressure gradient is given by

$$\langle \nabla^\nu p \rangle_3 = \nabla^\nu_{1,2} \langle p \rangle_3 + \langle \nabla^\nu_3 p \rangle_3 \,. \tag{D.38}$$

If we introduce the decomposition of the body force,

$$\boldsymbol{f} = \boldsymbol{f}_{1,2} + \boldsymbol{f}_3 \qquad \text{with} \qquad \boldsymbol{f}_3 \triangleq \boldsymbol{f} \cdot \boldsymbol{e}^{(3)} \boldsymbol{e}^{(3)} \,. \tag{D.39}$$

and collect all of the convolution terms of the momentum equation that are orthogonal to $\boldsymbol{u}_{1,2}$, we end up with

$$\begin{aligned}\rho_f \left(\frac{\partial^\nu \langle \boldsymbol{u}_3 \rangle_3}{\partial t} + \langle \nabla^\nu_{1,2} \cdot (\boldsymbol{u}_{1,2} \boldsymbol{u}_3) \rangle_3 + \langle \nabla^\nu_3 \cdot (\boldsymbol{u}_3 \boldsymbol{u}_3) \rangle_3 \right) = -\langle \nabla^\nu_3 p \rangle_3 \\ + \langle \nabla^\nu_{1,2} \cdot \mu \left(\nabla^\nu_{1,2} \boldsymbol{u}_3 + (\nabla^\nu_3 \boldsymbol{u}_{1,2})^\intercal \right) \rangle_3 + 2 \langle \nabla^\nu_3 \cdot \mu \nabla^\nu_3 \boldsymbol{u}_3 \rangle_3 + \boldsymbol{f}_3 \,. \end{aligned} \tag{D.40}$$

The convolution terms of the momentum equation that are parallel to $\boldsymbol{u}_{1,2}$ form the planar momentum equation (3.52).

APPENDIX

E

CLOSURE TERMS FOR MACRO-SCALE PLANAR FLOW

This appendix clarifies the relationship between the closure terms in the macro-scale momentum equation for planar flow (3.74) and the closure terms in the macro-scale equation for three-dimensional flow (3.14).

Momentum Dispersion in Planar flow

The momentum dispersion source of (3.14) can be decomposed as

$$\boldsymbol{M} \triangleq \boldsymbol{M}_{1,2;1,2} + \boldsymbol{M}_{1,2;3} + \boldsymbol{M}_{3;1,2} + \boldsymbol{M}_{3;3} \tag{E.1}$$

by introducing the following definitions in accordance with (D.24):

$$\begin{aligned}
\boldsymbol{M}_{1,2;1,2} &\triangleq \langle \boldsymbol{u}_{1,2}\boldsymbol{u}_{1,2}\rangle_m - \epsilon_{fm}\langle \boldsymbol{u}_{1,2}\rangle_m\langle \boldsymbol{u}_{1,2}\rangle_m \\
\boldsymbol{M}_{1,2;3} &\triangleq \langle \boldsymbol{u}_{1,2}\boldsymbol{u}_{3}\rangle_m - \epsilon_{fm}\langle \boldsymbol{u}_{1,2}\rangle_m\langle \boldsymbol{u}_{3}\rangle_m \\
\boldsymbol{M}_{3;1,2} &\triangleq \langle \boldsymbol{u}_{3}\boldsymbol{u}_{1,2}\rangle_m - \epsilon_{fm}\langle \boldsymbol{u}_{3}\rangle_m\langle \boldsymbol{u}_{1,2}\rangle_m \\
\boldsymbol{M}_{3;3} &\triangleq \langle \boldsymbol{u}_{3}\boldsymbol{u}_{3}\rangle_m - \epsilon_{fm}\langle \boldsymbol{u}_{3}\rangle_m\langle \boldsymbol{u}_{3}\rangle_m \,.
\end{aligned} \tag{E.2}$$

When the gradient operator is decomposed in accordance with (D.24), we find

$$\nabla \cdot \boldsymbol{M} = \nabla_{1,2} \cdot \boldsymbol{M}_{1,2;1,2} + \nabla_{1,2} \cdot \boldsymbol{M}_{1,2;3} + \underbrace{\nabla_{1,2} \cdot \boldsymbol{M}_{3;1,2} + \nabla_{1,2} \cdot \boldsymbol{M}_{3;3}}_{=0} + \underbrace{\nabla_3 \cdot \boldsymbol{M}_{1,2;1,2} + \nabla_3 \cdot \boldsymbol{M}_{1,2;3}}_{=0} + \nabla_3 \cdot \boldsymbol{M}_{3;1,2} + \nabla_3 \cdot \boldsymbol{M}_{3;3} \,, \tag{E.3}$$

or equivalently,

$$\begin{aligned} \nabla \cdot \boldsymbol{M} = {} & \nabla_{1,2} \cdot \langle \boldsymbol{u}_{1,2} \boldsymbol{u}_{1,2} \rangle_m - \nabla_{1,2} \cdot (\epsilon_{fm} \langle \boldsymbol{u}_{1,2} \rangle_m \langle \boldsymbol{u}_{1,2} \rangle_m) \\ & + \nabla_{1,2} \cdot \langle \boldsymbol{u}_{1,2} \boldsymbol{u}_3 \rangle_m - \nabla_{1,2} \cdot (\epsilon_{fm} \langle \boldsymbol{u}_{1,2} \rangle_m \langle \boldsymbol{u}_3 \rangle_m) \\ & + \underbrace{\nabla_{1,2} \cdot \langle \boldsymbol{u}_3 \boldsymbol{u}_{1,2} \rangle_m - \nabla_{1,2} \cdot (\epsilon_{fm} \langle \boldsymbol{u}_3 \rangle_m \langle \boldsymbol{u}_{1,2} \rangle_m)}_{=0} \\ & + \underbrace{\nabla_{1,2} \cdot \langle \boldsymbol{u}_3 \boldsymbol{u}_3 \rangle_m - \nabla_{1,2} \cdot (\epsilon_{fm} \langle \boldsymbol{u}_3 \rangle_m \langle \boldsymbol{u}_3 \rangle_m)}_{=0} \\ & + \underbrace{\nabla_3 \cdot \langle \boldsymbol{u}_{1,2} \boldsymbol{u}_{1,2} \rangle_m - \nabla_3 \cdot (\epsilon_{fm} \langle \boldsymbol{u}_{1,2} \rangle_m \langle \boldsymbol{u}_{1,2} \rangle_m)}_{=0} \\ & + \underbrace{\nabla_3 \cdot \langle \boldsymbol{u}_{1,2} \boldsymbol{u}_3 \rangle_m - \nabla_3 \cdot (\epsilon_{fm} \langle \boldsymbol{u}_{1,2} \rangle_m \langle \boldsymbol{u}_3 \rangle_m)}_{=0} \\ & + \nabla_3 \cdot \langle \boldsymbol{u}_3 \boldsymbol{u}_{1,2} \rangle_m - \nabla_3 \cdot (\epsilon_{fm} \langle \boldsymbol{u}_3 \rangle_m \langle \boldsymbol{u}_{1,2} \rangle_m) \\ & + \nabla_3 \cdot \langle \boldsymbol{u}_3 \boldsymbol{u}_3 \rangle_m - \nabla_3 \cdot (\epsilon_{fm} \langle \boldsymbol{u}_3 \rangle_m \langle \boldsymbol{u}_3 \rangle_m) \,. \end{aligned} \tag{E.4}$$

The divergence of the momentum dispersion source has the following contributions that are parallel to $\boldsymbol{u}_{1,2}$:

$$\begin{aligned} \{\nabla \cdot \boldsymbol{M}\}_{1,2} &= \nabla_{1,2} \cdot \boldsymbol{M}_{1,2;1,2} + \nabla_3 \cdot \boldsymbol{M}_{3;1,2} \\ &= \nabla_{1,2} \cdot \langle \boldsymbol{u}_{1,2} \boldsymbol{u}_{1,2} \rangle_m - \nabla_{1,2} \cdot (\epsilon_{fm} \langle \boldsymbol{u}_{1,2} \rangle_m \langle \boldsymbol{u}_{1,2} \rangle_m) \\ &\quad + \nabla_3 \cdot \langle \boldsymbol{u}_3 \boldsymbol{u}_{1,2} \rangle_m - \nabla_3 \cdot (\epsilon_{fm} \langle \boldsymbol{u}_3 \rangle_m \langle \boldsymbol{u}_{1,2} \rangle_m) \end{aligned} \tag{E.5}$$

The divergence of the momentum dispersion source has the following contributions that are orthogonal to $\boldsymbol{u}_{1,2}$:

$$\begin{aligned} \{\nabla \cdot \boldsymbol{M}\}_3 &= \nabla_{1,2} \cdot \boldsymbol{M}_{1,2;3} + \nabla_3 \cdot \boldsymbol{M}_{3;3} \\ &= \nabla_{1,2} \cdot \langle \boldsymbol{u}_{1,2} \boldsymbol{u}_3 \rangle_m - \nabla_{1,2} \cdot (\epsilon_{fm} \langle \boldsymbol{u}_{1,2} \rangle_m \langle \boldsymbol{u}_3 \rangle_m) \\ &\quad + \nabla_3 \cdot \langle \boldsymbol{u}_3 \boldsymbol{u}_3 \rangle_m - \nabla_3 \cdot (\epsilon_{fm} \langle \boldsymbol{u}_3 \rangle_m \langle \boldsymbol{u}_3 \rangle_m) \,. \end{aligned} \tag{E.6}$$

If the filter operator is separable w.r.t. the unit vector $\boldsymbol{e}^{(3)}$ parallel to $\boldsymbol{u}_3$, i.e. $\langle\ \rangle_m = \langle\langle\ \rangle_3\rangle_{1,2}$ as in (2.32) and $\langle\ \rangle_3$ is evaluated at the coordinates $(\boldsymbol{x}_{1,2}, x_3 = 0, t)$ as in (3.41), we have

$$\begin{aligned}\{\nabla\cdot\boldsymbol{M}\}_{1,2} &= \nabla_{1,2}\cdot\langle\boldsymbol{u}_{1,2}\boldsymbol{u}_{1,2}\rangle_m - \nabla_{1,2}\cdot(\epsilon_{fm}\langle\boldsymbol{v}\rangle_{1,2}\langle\boldsymbol{v}\rangle_{1,2}) \\ &\quad + \nabla_3\cdot\langle\boldsymbol{u}_3\boldsymbol{u}_{1,2}\rangle_m - \nabla_3\cdot(\epsilon_{fm}\langle\boldsymbol{u}_3\rangle_m\langle\boldsymbol{v}\rangle_{1,2}) \qquad \text{(E.7)} \\ &= -\langle\boldsymbol{\Psi}_3^{\mathrm{I}}\rangle_{1,2} - \langle\boldsymbol{\Psi}_3^{\mathrm{II}}\rangle_{1,2} - \nabla_{1,2}\cdot(\epsilon_{fm}\langle\boldsymbol{v}\rangle_{1,2}\langle\boldsymbol{v}\rangle_{1,2}) \\ &\quad + \langle\nabla^\nu\cdot(\boldsymbol{v}\boldsymbol{v})\rangle_{1,2} - \nabla_3\cdot(\epsilon_{fm}\langle\boldsymbol{u}_3\rangle_m\langle\boldsymbol{v}\rangle_{1,2}) \qquad \text{(E.8)} \\ &= -\langle\boldsymbol{\Psi}_3^{\mathrm{I}}\rangle_{1,2} - \langle\boldsymbol{\Psi}_3^{\mathrm{II}}\rangle_{1,2} + \nabla_{1,2}\cdot\boldsymbol{\mathcal{M}} \\ &\quad - \nabla_3\cdot(\epsilon_{fm}\langle\boldsymbol{u}_3\rangle_m\langle\boldsymbol{v}\rangle_{1,2})\ . \qquad \text{(E.9)}\end{aligned}$$

Because $\langle\boldsymbol{\Psi}_3^{\mathrm{I}}\rangle_3 = \boldsymbol{\Psi}_3^{\mathrm{I}}$, $\langle\boldsymbol{\Psi}_3^{\mathrm{II}}\rangle_3 = \boldsymbol{\Psi}_3^{\mathrm{II}}$ and $\langle\boldsymbol{v}\rangle_3 = \boldsymbol{v}$, we can notate the last result as

$$\begin{aligned}\{\nabla\cdot\boldsymbol{M}\}_{1,2} = &-\langle\boldsymbol{\Psi}_3^{\mathrm{I}}\rangle_m - \langle\boldsymbol{\Psi}_3^{\mathrm{II}}\rangle_m + \nabla\cdot\boldsymbol{\mathcal{M}} \\ &- \nabla_3\cdot(\epsilon_{fm}\langle\boldsymbol{u}_3\rangle_m\langle\boldsymbol{v}\rangle_m)\ . \qquad \text{(E.10)}\end{aligned}$$

In step (E.8), we have used the definition of $\boldsymbol{\Psi}_3^{\mathrm{I}}$ (cf. (D.32)) which leads to

$$\begin{aligned}\langle\boldsymbol{\Psi}_3^{\mathrm{I}}\rangle_{1,2} &= \langle\nabla_{1,2}^\nu\cdot(\langle\boldsymbol{u}_{1,2}\rangle_3\langle\boldsymbol{u}_{1,2}\rangle_3)\rangle_{1,2} - \nabla_{1,2}\cdot\langle\langle\boldsymbol{u}_{1,2}\boldsymbol{u}_{1,2}\rangle_3\rangle_{1,2} \qquad \text{(E.11)} \\ &= \langle\nabla_{1,2}^\nu\cdot(\boldsymbol{v}\boldsymbol{v})\rangle_{1,2} - \nabla_{1,2}\cdot\langle\boldsymbol{u}_{1,2}\boldsymbol{u}_{1,2}\rangle_m\,. \qquad \text{(E.12)}\end{aligned}$$

In addition, step (E.8) rests on the result

$$\begin{aligned}\langle\boldsymbol{\Psi}_3^{\mathrm{II}}\rangle_{1,2} &= -\langle\langle\nabla_3^\nu\cdot(\boldsymbol{u}_3\boldsymbol{u}_{1,2})\rangle_3\rangle_{1,2} \qquad \text{(E.13)} \\ &= -\nabla_3\cdot\langle\boldsymbol{u}_3\boldsymbol{u}_{1,2}\rangle_m\,, \qquad \text{(E.14)}\end{aligned}$$

which follows from (D.33). The intermediate results (E.12) and (E.14) hold because we have assumed the filter to be separable and $\boldsymbol{v}$ to satisfy the equations (3.49) and (3.50).

Interfacial Force in Planar flow

The interfacial force of (3.14) can be decomposed in accordance with (D.24) as follows:

$$\begin{aligned}\boldsymbol{b}_{fs} = &-\langle\boldsymbol{n}_{fs}\cdot p_f\boldsymbol{I}\delta_{fs}\rangle_m + \langle\boldsymbol{n}_{fs}\cdot\mu_f\left\{\nabla_{1,2}\boldsymbol{u}_{1,2} + (\nabla_{1,2}\boldsymbol{u}_{1,2})^{\intercal}\right\}_f\delta_{fs}\rangle_m \\ &+ \langle\boldsymbol{n}_{fs}\cdot\mu_f\left\{\nabla_{1,2}\boldsymbol{u}_3 + (\nabla_3\boldsymbol{u}_{1,2})^{\intercal}\right\}_f\delta_{fs}\rangle_m\,. \qquad \text{(E.15)}\end{aligned}$$

This result is based on the assumption that $\boldsymbol{n}_{fs} \cdot \boldsymbol{e}^{(3)} = 0$ when planar flow occurs (cf. (3.48)).

For a separable filter $\langle\ \rangle_m = \langle\langle\ \rangle_3\rangle_{1,2}$ with $\langle\ \rangle_3$ evaluated at the coordinates $(\boldsymbol{x}_{1,2}, x_3 = 0, t)$, we therefore find that

$$\begin{aligned}\boldsymbol{b}_{fs} = &-\langle \boldsymbol{n}_{fs} \cdot \langle p_f \rangle_3 \boldsymbol{I} \delta_{fs} \rangle_{1,2} + \langle \boldsymbol{n}_{fs} \cdot \mu_f \left(\nabla \boldsymbol{v}_f + (\nabla \boldsymbol{v}_f)^{\intercal} \right) \delta_{fs} \rangle_{1,2} \\ &+ \langle \boldsymbol{n}_{fs} \cdot \mu_f \left\{ \nabla_{1,2} \boldsymbol{u}_3 + (\nabla_3 \boldsymbol{u}_{1,2})^{\intercal} \right\}_f \delta_{fs} \rangle_m \,, \end{aligned} \tag{E.16}$$

because of (3.45) and (3.50). The part of the interfacial parallel to the planar flow velocity $\boldsymbol{v}$ is thus given by

$$\boldsymbol{b}_{fs} = -\langle \boldsymbol{n}_{fs} \cdot \mathcal{P}_f \boldsymbol{I} \delta_{fs} \rangle_{1,2} + \langle \boldsymbol{n}_{fs} \cdot \mu_f \left(\nabla \boldsymbol{v}_f + (\nabla \boldsymbol{v}_f)^{\intercal} \right) \delta_{fs} \rangle_{1,2} \tag{E.17}$$

$$= \langle \boldsymbol{n}_{fs} \cdot \left(-\mathcal{P}_f \boldsymbol{I} + \boldsymbol{\mathfrak{T}}_f \right) \delta_{fs} \rangle_{1,2} \,, \tag{E.18}$$

in agreement with (3.74).

Macro-Scale Velocity in Planar flow

The relationship between the macro-scale velocity and planar macro-scale velocity is clarified as follows. The macro-scale velocity satisfies

$$\langle \boldsymbol{u} \rangle_m = \langle \boldsymbol{u}_{1,2} \rangle_m + \langle \boldsymbol{u}_3 \rangle_m \,, \tag{E.19}$$

so that for a separable filter $\langle\ \rangle_m = \langle\langle\ \rangle_3\rangle_{1,2}$ with $\langle\ \rangle_3$ evaluated at the coordinates $(\boldsymbol{x}_{1,2}, x_3 = 0, t)$, it follows that

$$\langle \boldsymbol{u} \rangle_m = \langle \boldsymbol{v} \rangle_{1,2} + \langle \boldsymbol{u}_3 \rangle_m \,. \tag{E.20}$$

By equation (3.47) it must then hold that

$$\langle \gamma_f \rangle_m = \langle \gamma_f \rangle_{1,2} \,, \tag{E.21}$$

so that also

$$\langle \boldsymbol{u} \rangle_m^f = \langle \boldsymbol{v} \rangle_{1,2}^f + \langle \boldsymbol{u}_3 \rangle_m^f \,. \tag{E.22}$$

Because $\langle \boldsymbol{v} \rangle_3 = \boldsymbol{v}$ under the assumption of (3.41), we can notate the last result as

$$\langle \boldsymbol{u} \rangle_m^f = \langle \boldsymbol{v} \rangle_m^f + \langle \boldsymbol{u}_3 \rangle_m^f \,. \tag{E.23}$$

APPENDIX

F

DERIVATION OF THE PLANAR TEMPERATURE EQUATIONS

In this appendix, the planar temperature equation (4.53) is derived for a Cartesian vector basis as well as for a general vector basis.

F.1 Derivation for Cartesian Vector Basis

Fluid Temperature Equation for Planar Flow
With the velocity decomposition of (D.1) and the Cartesian coordinates of (D.2), the temperature equation of the fluid (4.7) becomes

$$\rho_f \left(\frac{\partial \left(c_f T_f \right)}{\partial t} + \frac{\partial \left(u_1 c_f T_f \right)}{\partial x_1} + \frac{\partial \left(u_2 c_f T_f \right)}{\partial x_2} + \frac{\partial \left(u_3 c_f T_f \right)}{\partial x_3} \right) = \frac{\partial}{\partial x_1} \left(k_f \frac{\partial T_f}{\partial x_1} \right) + \frac{\partial}{\partial x_2} \left(k_f \frac{\partial T_f}{\partial x_2} \right) + \frac{\partial}{\partial x_3} \left(k_f \frac{\partial T_f}{\partial x_3} \right) + \dot{q}_{\mathrm{visc},f} + \dot{q}_f \,. \tag{F.1}$$

When the former fluid temperature equation is multiplied with the scalar function $m_3'(-x_3)$ and subsequently integrated over $x_3 \in I_3$, we find

$$\rho_f \left(\frac{\partial \left(c_f \langle T_f \rangle_3 \right)}{\partial t} + \frac{\partial \left(c_f \langle u_1 \rangle_3 \langle T_f \rangle_3 \right)}{\partial x_1} + \frac{\partial \left(c_f \langle u_2 \rangle_3 \langle T_f \rangle_3 \right)}{\partial x_2} \right) = \frac{\partial}{\partial x_1} \left(k_f \frac{\partial \langle T_f \rangle_3}{\partial x_1} \right) + \frac{\partial}{\partial x_2} \left(k_f \frac{\partial \langle T_f \rangle_3}{\partial x_2} \right) + \langle \dot{q}_{\mathrm{visc},f} \rangle_3 + \langle \dot{q}_f \rangle_3 + \{ \psi_3 \}_f \ , \tag{F.2}$$

because we assumed the specific heat capacity c_f and the conductivity k_f to be approximately constant over the integration interval. The operator $\langle \ \rangle_3$ is defined by (2.26) and is evaluated at the coordinates $(x_1, x_2, x_3 = 0, t)$.

The scalar term $\{ \psi_3 \}_f$ in the integrated energy equation consists of three contributions:

$$\{ \psi_3 \}_f \triangleq \left\{ \psi_3^{\mathrm{I}} \right\}_f + \left\{ \psi_3^{\mathrm{II}} \right\}_f + \left\{ \psi_3^{\mathrm{III}} \right\}_f \ , \tag{F.3}$$

where

$$\left\{ \psi_3^{\mathrm{I}} \right\}_f \triangleq \rho_f \frac{\partial}{\partial x_1} \left[c_f \left(\langle u_1 \rangle_3 \langle T_f \rangle_3 - \langle u_1 T_f \rangle_3 \right) \right] + \rho_f \frac{\partial}{\partial x_2} \left[c_f \left(\langle u_2 \rangle_3 \langle T_f \rangle_3 - \langle u_2 T_f \rangle_3 \right) \right] \tag{F.4}$$

and

$$\left\{ \psi_3^{\mathrm{II}} \right\}_f \triangleq - \int_{-\frac{l_3}{2}}^{\frac{l_3}{2}} m_3'(-x_3) \frac{\partial \left(u_3 c_f T_f \right)}{\partial x_3} \, dx_3 \, . \tag{F.5}$$

and

$$\left\{ \psi_3^{\mathrm{III}} \right\}_f \triangleq \int_{-\frac{l_3}{2}}^{\frac{l_3}{2}} m_3'(-x_3) \frac{\partial}{\partial x_3} \left(k_f \frac{\partial T_f}{\partial x_3} \right) \, dx_3 \, . \tag{F.6}$$

Using integration by parts, we find eventually that

$$\left\{ \psi_3^{\mathrm{II}} \right\}_f = -m_3'(-x_3) \ \left(u_3 c_f T_f \right) \Big|_{x_3 = -\frac{l_3}{2}}^{x_3 = \frac{l_3}{2}} + \int_{-\frac{l_3}{2}}^{\frac{l_3}{2}} \frac{\partial m_3'(-x_3)}{\partial x_3} \left(u_3 c_f T_f \right) \, dx_3 \, . \tag{F.7}$$

as well as

$$\left\{\psi_3^{\mathrm{III}}\right\}_f = m_3'(-x_3)\left(k_f\frac{\partial T_f}{\partial x_3}\right)\Bigg|_{x_3=-\frac{l_3}{2}}^{x_3=\frac{l_3}{2}} - \int_{-\frac{l_3}{2}}^{\frac{l_3}{2}} \frac{\partial m_3'(-x_3)}{\partial x_3}\left(k_f\frac{\partial T_f}{\partial x_3}\right) dx_3\,. \tag{F.8}$$

Solid Temperature Equation for Planar Flow

With the equations (D.1) and (D.2), the temperature equation of the solid (4.8) becomes

$$\rho_s\frac{\partial\left(c_sT_s\right)}{\partial t} = \frac{\partial}{\partial x_1}\left(k_s\frac{\partial T_s}{\partial x_1}\right) + \frac{\partial}{\partial x_2}\left(k_s\frac{\partial T_s}{\partial x_2}\right) + \frac{\partial}{\partial x_3}\left(k_s\frac{\partial T_s}{\partial x_3}\right) + \dot{q}_s\,. \tag{F.9}$$

Applying the planar averaging operator $\langle\ \rangle_3$ on this equation for c_s and k_s constant in the x_3-direction, yields directly the planar temperature equation for the solid:

$$\begin{aligned}\rho_s\frac{\partial\left(c_s\langle T_s\rangle_3\right)}{\partial t} = {}& \frac{\partial}{\partial x_1}\left(k_s\frac{\partial\langle T_s\rangle_3}{\partial x_1}\right) + \frac{\partial}{\partial x_2}\left(k_s\frac{\partial\langle T_s\rangle_3}{\partial x_2}\right)\\ & + \frac{\partial}{\partial x_3}\left(k_s\frac{\partial\langle T_s\rangle_3}{\partial x_3}\right) + \langle\dot{q}_s\rangle_3 + \left\{\psi_3^{\mathrm{III}}\right\}_s\,,\end{aligned} \tag{F.10}$$

where

$$\begin{aligned}\left\{\psi_3^{\mathrm{III}}\right\}_s &= \int_{-\frac{l_3}{2}}^{\frac{l_3}{2}} m_3'(-x_3)\frac{\partial}{\partial x_3}\left(k_s\frac{\partial T_s}{\partial x_3}\right) dx_3\\ &= m_3'(-x_3)\left(k_s\frac{\partial T_s}{\partial x_3}\right)\Bigg|_{x_3=-\frac{l_3}{2}}^{x_3=\frac{l_3}{2}} - \int_{-\frac{l_3}{2}}^{\frac{l_3}{2}} \frac{\partial m_3'(-x_3)}{\partial x_3}\left(k_s\frac{\partial T_s}{\partial x_3}\right) dx_3\,.\end{aligned} \tag{F.11}$$

Therefore, we define $\left\{\psi_3^{\mathrm{I}}\right\}_s \triangleq 0$ and $\left\{\psi_3^{\mathrm{II}}\right\}_s \triangleq 0$.

F.2 General Derivation

The planar temperature equation can also be obtained directly from the generalized temperature equation (4.5), if one uses the orthogonal decomposition of the velocity (D.24) and the gradient operator (D.25) and one applies the convolution operator $\langle\ \rangle_3$ on each term.

For instance, for the local time derivative of the thermal energy this procedure gives

$$\left\langle \rho \frac{\partial^{\nu}\left(cT\right)}{\partial t} \right\rangle_3 = \rho \frac{\partial\left(c\langle T\rangle_3\right)}{\partial t}\,. \tag{F.12}$$

The same procedure applied to the advection term of the thermal energy yields

$$\begin{aligned}
\langle \rho \nabla^{\nu}\cdot(\boldsymbol{u}cT)\rangle_3 &= \rho\nabla^{\nu}_{1,2}\cdot\langle \boldsymbol{u}_{1,2}cT\rangle_3 + \rho\underbrace{\langle\nabla^{\nu}_{1,2}\cdot(\boldsymbol{u}_3cT)\rangle_3}_{=0,\text{ by Eq. (D.24)}} \\
&\quad + \rho\underbrace{\langle\nabla^{\nu}_{3}\cdot(\boldsymbol{u}_{1,2}cT)\rangle_3}_{=0,\text{ by Eq. (D.24)}} + \rho\langle\nabla^{\nu}_{3}\cdot(\boldsymbol{u}_3cT)\rangle_3 && \text{(F.13)}\\
&= \rho\nabla^{\nu}_{1,2}\cdot\langle \boldsymbol{u}_{1,2}cT\rangle_3 + \rho\langle\nabla^{\nu}_{3}\cdot(\boldsymbol{u}_3cT)\rangle_3 && \text{(F.14)}\\
&= \rho\nabla^{\nu}_{1,2}\cdot(\langle \boldsymbol{u}_{1,2}\rangle_3 c\langle T\rangle_3) - \psi^{\mathrm{I}}_3 - \psi^{\mathrm{II}}_3\,, && \text{(F.15)}
\end{aligned}$$

because of

$$\psi^{\mathrm{I}}_3 \triangleq \rho\nabla^{\nu}_{1,2}\cdot(\langle \boldsymbol{u}_{1,2}\rangle_3 c\langle T\rangle_3) - \rho\nabla^{\nu}_{1,2}\cdot\langle \boldsymbol{u}_{1,2}cT\rangle_3 \tag{F.16}$$

and because of

$$\psi^{\mathrm{II}}_3 \triangleq -\rho\langle\nabla^{\nu}_{3}\cdot(\boldsymbol{u}_3cT)\rangle_3\,. \tag{F.17}$$

For the thermal conduction term, the same procedure results in

$$\begin{aligned}
\langle \nabla^{\nu}\cdot(k\nabla^{\nu}T)\rangle_3 &= \nabla^{\nu}_{1,2}\cdot\left(k\nabla^{\nu}_{1,2}\langle T\rangle_3\right) + \underbrace{\langle\nabla^{\nu}_{1,2}\cdot(k\nabla^{\nu}_{3}T)\rangle_3}_{=0,\text{ by Eq. (D.24)}} \\
&\quad + \underbrace{\langle\nabla^{\nu}_{3}\cdot\left(k\nabla^{\nu}_{1,2}T\right)\rangle_3}_{=0,\text{ by Eq. (D.24)}} + \langle\nabla^{\nu}_{3}\cdot(k\nabla^{\nu}_{3}T)\rangle_3 && \text{(F.18)}\\
&= \nabla^{\nu}_{1,2}\cdot\left(k\nabla^{\nu}_{1,2}\langle T\rangle_3\right) + \psi^{\mathrm{III}}_3\,, && \text{(F.19)}
\end{aligned}$$

where

$$\psi^{\mathrm{III}}_3 \triangleq \langle\nabla^{\nu}_{3}\cdot(k\nabla^{\nu}_{3}T)\rangle_3\,. \tag{F.20}$$

The one-dimensional convolution product of the viscous source and the volumetric heat source are simply $\langle\dot{q}\rangle_3$ and $\langle\dot{q}_{\mathrm{visc}}\rangle_3$.

APPENDIX

G

SPATIAL AVERAGING OF THE GENERALIZED TEMPERATURE EQUATION

In this appendix, the generalized thermal energy equation (4.5) is spatially averaged over the system domain Ω.

Averaging of Temperature Equation

First, the local time derivative of the internal energy is spatially averaged under the assumption that the heat capacity distribution can be treated as quasi-constant over the fluid and solid within an averaging domain (see (2.93)):

$$\left\langle \rho \frac{\partial^{\nu}(cT)}{\partial t} \right\rangle_m = \frac{\partial \langle \rho c T \rangle_m}{\partial t} \tag{G.1}$$

$$= \rho_f \epsilon_{fm} \frac{\partial \left(c_f \langle T \rangle_m^f \right)}{\partial t} + \rho_s \epsilon_{sm} \frac{\partial \left(c_s \langle T \rangle_m^s \right)}{\partial t} . \tag{G.2}$$

Averaging the convective derivative of the internal energy distribution goes as follows:

$$\langle \rho \nabla^\nu \cdot (\boldsymbol{u} cT) \rangle_m = \rho_f \langle \nabla^\nu \cdot (\boldsymbol{u} cT) \rangle_m \tag{G.3}$$

$$\langle \nabla^\nu \cdot (\boldsymbol{u} cT) \rangle_m = \nabla \cdot \langle \boldsymbol{u} cT \rangle_m + \underbrace{\langle \boldsymbol{n}_{fs} \cdot \boldsymbol{u}_f c_f T_f \delta_{fs} \rangle_m}_{=0, \text{ by Eq. (3.6)}} \tag{G.4}$$

$$= \nabla \cdot \langle \boldsymbol{u} cT \rangle_m \tag{G.5}$$

$$= \nabla \cdot c_f \langle \boldsymbol{u} T \rangle_m \,. \tag{G.6}$$

Here the heat capacity c was treated as quasi-constant over the fluid domain (see also (2.93)). The result of the last equation can be further approximated:

$$\langle \boldsymbol{u} T \rangle_m = \langle \langle \boldsymbol{u} \rangle_m^f \gamma_f T + \tilde{\boldsymbol{u}} T \rangle_m \tag{G.7}$$

$$\simeq \langle \boldsymbol{u} \rangle_m^f \langle T \gamma_f \rangle_m + \langle \tilde{\boldsymbol{u}} T \rangle_m \tag{G.8}$$

$$\simeq \epsilon_{fm} \langle \boldsymbol{u} \rangle_m^f \langle T \rangle_m^f + \langle \tilde{\boldsymbol{u}} \langle T \rangle_m^f + \tilde{\boldsymbol{u}} \tilde{T} \rangle_m \tag{G.9}$$

$$\simeq \epsilon_{fm} \langle \boldsymbol{u} \rangle_m^f \langle T \rangle_m^f + \langle T \rangle_m^f \langle \tilde{\boldsymbol{u}} \rangle_m + \langle \tilde{\boldsymbol{u}} \tilde{T} \rangle_m \tag{G.10}$$

$$\simeq \epsilon_{fm} \langle \boldsymbol{u} \rangle_m^f \langle T \rangle_m^f + \langle \tilde{\boldsymbol{u}} \tilde{T} \rangle_m \,. \tag{G.11}$$

By analogy with the derivation of the spatially averaged momentum equation (cf. (B.6)), variations of the intrinsic spatially averaged velocity and temperature within $\bar{\Omega}$ are neglected in the approximation above. This approximation is justified when the characteristic scale for the support of the averaging operator,r_m, is small compared to the length scales $\mathcal{L}_{\boldsymbol{u}}$ and $\mathcal{L}_T$, over which the gradients of the spatially averaged velocity and temperature are significant.

Averaging of the thermal conduction term yields

$$\langle \nabla^\nu \cdot (k \nabla^\nu T) \rangle_m = \nabla \cdot \langle k \nabla^\nu T \rangle_m + \underbrace{\langle \boldsymbol{n}_{fs} \cdot (k_f \nabla T_f - k_s \nabla T_s) \delta_{fs} \rangle_m}_{=0, \text{ by Eq. (4.10)}} \tag{G.12}$$

$$= \nabla \cdot \langle k \nabla^\nu T \rangle_m \tag{G.13}$$

$$= \nabla \cdot k_f \epsilon_{fm} \langle \nabla^\nu T \rangle_m^f + \nabla \cdot k_s \epsilon_{sm} \langle \nabla^\nu T \rangle_m^s \,. \tag{G.14}$$

It is assumed that gradients in k_f and k_s over the fluid and solid regions respectively are sufficiently small, so that (2.93) can be applied. The

spatial averages of the temperature gradients in the usual sense are given by the spatial averaging theorem:

$$\epsilon_{fm}\langle\nabla^{\nu}T\rangle_m^f \triangleq \langle\nabla^{\nu}T\gamma_f\rangle_m \tag{G.15}$$
$$= \nabla\langle T\gamma_f\rangle_m + \langle \boldsymbol{n}_{fs}T_f\delta_{fs}\rangle_m \tag{G.16}$$
$$= \nabla\big(\epsilon_{fm}\langle T\rangle_m^f\big) + \langle \boldsymbol{n}_{fs}T_f\delta_{fs}\rangle_m \tag{G.17}$$

$$\epsilon_{sm}\langle\nabla^{\nu}T\rangle_m^s \triangleq \langle\nabla^{\nu}T\gamma_s\rangle_m \tag{G.18}$$
$$= \nabla\langle T\gamma_s\rangle_m - \langle \boldsymbol{n}_{fs}T_s\delta_{fs}\rangle_m \tag{G.19}$$
$$= \nabla\big(\epsilon_{sm}\langle T\rangle_m^f\big) - \langle \boldsymbol{n}_{fs}T_s\delta_{fs}\rangle_m\,. \tag{G.20}$$

Finally, through combination of the former results the spatially smoothed generalized energy conservation equation (4.17) is retrieved.

APPENDIX

H

DERIVATION OF THE GLOBAL CLOSURE PROBLEM FOR THE MACRO-SCALE TEMPERATURE EQUATIONS

This appendix presents a derivation of the global closure problem for the macro-scale temperature equations. The closure equations (4.40) and (4.41) are found after subtraction of the filtered temperature equations (4.21) and (4.22) from the generalized temperature equation (4.5).

Closure Equation for the Fluid Temperature

The difference between the internal energy of the fluid-solid continuum (cf. (4.5)) and the macro-scale internal energy of the fluid (cf. (4.21)) equals

$$\rho \frac{\partial^{\nu}\left(cT\right)}{\partial t} - \rho_f \frac{\partial\left(c_f \langle T\rangle_m^f\right)}{\partial t} = \rho_f \frac{\partial\left(c_f \widetilde{T}_f\right)}{\partial t} \qquad \text{in } \Omega_f\,. \tag{H.1}$$

When we subtract the advection of internal energy of the fluid-solid continuum (cf. (4.5)) from the advection of internal energy of the fluid at the macro-scale level (cf. (4.21)), we find

$$\begin{aligned}
&\rho\nabla^{\nu}\cdot(\boldsymbol{u}cT)-\rho_f\nabla\cdot\left(c_f\langle\boldsymbol{u}\rangle_m^f\langle T\rangle_m^f\right)-\rho_f\nabla\cdot\left(c_f\boldsymbol{\mathcal{D}}'\right)\\
&=\rho\nabla^{\nu}\cdot\left(\langle\boldsymbol{u}\rangle_m^f c\,\langle T\rangle_m^f\gamma_f+\langle\boldsymbol{u}\rangle_m^f c\widetilde{T}\gamma_f+\widetilde{\boldsymbol{u}}c\,\langle T\rangle_m^f+\widetilde{\boldsymbol{u}}c\widetilde{T}\right)\\
&\qquad-\rho_f\nabla\cdot\left(c_f\langle\boldsymbol{u}\rangle_m^f\langle T\rangle_m^f\right)-\rho_f\nabla\cdot\left(c_f\boldsymbol{\mathcal{D}}'\right) &\text{(H.2)}\\
&=\rho_f\nabla\cdot\left(\left\{\langle\boldsymbol{u}\rangle_m^f\right\}_f c_f\widetilde{T}_f+\widetilde{\boldsymbol{u}}_f c_f\left\{\langle T\rangle_m^f\right\}_f+\widetilde{\boldsymbol{u}}_f c_f\widetilde{T}_f\right)\\
&\qquad-\rho_f\nabla\cdot\left(c_f\boldsymbol{\mathcal{D}}'_f\right)\qquad\text{in }\Omega_f &\text{(H.3)}\\
&=\rho_f\nabla\cdot\left(\boldsymbol{u}_f c_f\widetilde{T}_f+\widetilde{\boldsymbol{u}}_f c_f\left\{\langle T\rangle_m^f\right\}_f\right)\\
&\qquad-\rho_f\nabla\cdot\left(c_f\boldsymbol{\mathcal{D}}'_f\right)\qquad\text{in }\Omega_f &\text{(H.4)}
\end{aligned}$$

The difference between the conduction term in the fluid-solid continuum (cf. (4.5)) and the macro-scale conduction term in the fluid (cf. (4.21)) is

$$\nabla^{\nu}\cdot(k\,\nabla^{\nu}T)-\nabla\cdot k_f\nabla\langle T\rangle_m^f=\nabla\cdot k_f\nabla\widetilde{T}_f\qquad\text{in }\Omega_f\,. \tag{H.5}$$

Further, we define the deviation part of the viscous dissipation term as

$$\widetilde{\dot{q}}_{\mathrm{visc},f}\triangleq\boldsymbol{\tau}_f\cdot\cdot\nabla\boldsymbol{u}_f-\left\{\langle\boldsymbol{\tau}\cdot\cdot\nabla^{\nu}\boldsymbol{u}\rangle_m^f\right\}_f. \tag{H.6}$$

The results (H.1), (H.4), (H.5) and (H.6) show the origin of the terms in the closure equation for the fluid temperature (4.40).

Closure Equation for the Solid Temperature

The origin of the terms in (4.41)is explained in analogous way. We just remark that the difference between the internal energy term of (4.5)) and the macro-scale internal energy term of (4.22) equals

$$\rho\frac{\partial^{\nu}(cT)}{\partial t}-\rho_s\frac{\partial\left(c_s\langle T\rangle_m^s\right)}{\partial t}=\rho_s\frac{\partial\left(c_s\widetilde{T}_s\right)}{\partial t}\qquad\text{in }\Omega_s \tag{H.7}$$

and that the difference between the conduction terms in (4.5)) and (4.22) is given by

$$\nabla^{\nu}\cdot(k\,\nabla^{\nu}T)-\nabla\cdot k_s\nabla\langle T\rangle_m^f=\nabla\cdot k_s\nabla\widetilde{T}_s\qquad\text{in }\Omega_s\,. \tag{H.8}$$

APPENDIX

I

PROOF FOR THE CLOSURE MAPPING FOR STEADY PERIODICALLY DEVELOPED FLOW

The proof for the closure mapping (5.65) starts by taking the dot product of each term in (5.62) and spatially averaging each of the terms with the weighting function m_V. For the first term this gives

$$\rho_f \langle \left(\boldsymbol{u} \cdot \nabla^\nu \widetilde{\boldsymbol{u}}^0 \right) \cdot \widetilde{\boldsymbol{u}}^0 \rangle^f = \rho_f \langle \nabla^\nu \cdot \left(\boldsymbol{u} \left(\frac{1}{2} \widetilde{\boldsymbol{u}}^0 \cdot \widetilde{\boldsymbol{u}}^0 \right) \right) \rangle^f \tag{I.1}$$

$$= \rho_f \nabla \cdot \langle \boldsymbol{u} \left(\frac{1}{2} \widetilde{\boldsymbol{u}}^0 \cdot \widetilde{\boldsymbol{u}}^0 \right) \rangle^f + \rho_f \epsilon_f^{-1} \langle \boldsymbol{n}_{fs} \cdot \boldsymbol{u}_f \left(\frac{1}{2} \widetilde{\boldsymbol{u}}_f^0 \cdot \widetilde{\boldsymbol{u}}_f^0 \right) \delta_{fs} \rangle \tag{I.2}$$

$$= 0 \, .$$

Here, we used the fact that both $\boldsymbol{u} = \left((\boldsymbol{I} + \boldsymbol{\Lambda}_{\boldsymbol{u}}) \cdot \langle \boldsymbol{u} \rangle_m^f + \widetilde{\boldsymbol{u}}^0\right)$ and $\widetilde{\boldsymbol{u}}^0$ are solenoidal in (I.1). The first term in (I.3) is zero by periodicity of $\boldsymbol{u}$ and $\widetilde{\boldsymbol{u}}^0$, while the second term vanishes due to the no-slip boundary condition on the interface boundary.

Following the same reasoning for the second term, we find

$$
\begin{aligned}
-\langle \nabla^\nu \widetilde{p}^0 \cdot \widetilde{\boldsymbol{u}}^0 \rangle^f &= -\langle \nabla^\nu \cdot \left(\widetilde{p}^0 \widetilde{\boldsymbol{u}}^0 \right) \rangle^f && \text{(I.3)} \\
&= -\nabla \cdot \langle \widetilde{p}^0 \widetilde{\boldsymbol{u}}^0 \rangle_m^f + \epsilon_f^{-1} \langle \boldsymbol{n}_{fs} \cdot \left(\widetilde{p}_f^0 \widetilde{\boldsymbol{u}}_f^0 \right) \delta_{fs} \rangle && \text{(I.4)} \\
&= 0 \,.
\end{aligned}
$$

Spatial averaging the dot product of the viscous term in (5.62) with $\widetilde{\boldsymbol{u}}^0$ leads to

$$
\begin{aligned}
\langle \mu \left(\nabla^\nu \cdot \nabla^\nu \widetilde{\boldsymbol{u}}^0 \right) \cdot \widetilde{\boldsymbol{u}}^0 \rangle^f &= \langle \mu \nabla^\nu \cdot \left(\left(\nabla^\nu \widetilde{\boldsymbol{u}}^0 \right) \cdot \widetilde{\boldsymbol{u}}^0 \right) \rangle^f \\
&\quad - \langle \mu \left(\nabla^\nu \widetilde{\boldsymbol{u}}^0 \right)^\mathsf{T} \cdot\cdot \left(\nabla^\nu \widetilde{\boldsymbol{u}}^0 \right) \rangle^f && \text{(I.5)} \\
&= \nabla \cdot \langle \mu \left(\nabla^\nu \widetilde{\boldsymbol{u}}^0 \right) \cdot \widetilde{\boldsymbol{u}}^0 \rangle^f \\
&\quad + \epsilon_{fm}^{-1} \langle \boldsymbol{n}_{fs} \cdot \mu \left(\left(\nabla^\nu \widetilde{\boldsymbol{u}}^0 \right) \cdot \widetilde{\boldsymbol{u}}^0 \right) \delta_{fs} \rangle \\
&\quad - \langle \mu \left(\nabla^\nu \widetilde{\boldsymbol{u}}^0 \right)^\mathsf{T} \cdot\cdot \left(\nabla^\nu \widetilde{\boldsymbol{u}}^0 \right) \rangle^f && \text{(I.6)} \\
&= -\langle \mu \left(\nabla^\nu \widetilde{\boldsymbol{u}}^0 \right)^\mathsf{T} \cdot\cdot \left(\nabla^\nu \widetilde{\boldsymbol{u}}^0 \right) \rangle^f && \text{(I.7)}
\end{aligned}
$$

Lastly, for the term containing the surface filter, this procedure yields

$$
\begin{aligned}
&\langle \epsilon_{fm}^{-1} \langle \boldsymbol{n}_{fs} \cdot \left(\boldsymbol{I} \widetilde{p}_f^0 - \mu_f \nabla \widetilde{\boldsymbol{u}}_f^0 \right) \delta_{fs} \rangle_m \cdot \widetilde{\boldsymbol{u}}^0 \rangle^f = \\
&\qquad \epsilon_{fm}^{-1} \langle \boldsymbol{n}_{fs} \cdot \left(\boldsymbol{I} \widetilde{p}_f^0 - \mu_f \nabla \widetilde{\boldsymbol{u}}_f^0 \right) \delta_{fs} \rangle_m \cdot \langle \widetilde{\boldsymbol{u}}^0 \rangle^f \,, && \text{(I.8)}
\end{aligned}
$$

because ϵ_{fm} is constant and the surface filter is constant as well due to the periodicity of $\widetilde{p}_f^0$ and $\widetilde{\boldsymbol{u}}_f^0$.

If the former results are assembled, it holds by (5.62) that

$$
0 = -\langle \mu \left(\nabla^\nu \widetilde{\boldsymbol{u}}^0 \right)^\mathsf{T} \cdot\cdot \left(\nabla^\nu \widetilde{\boldsymbol{u}}^0 \right) \rangle^f + \epsilon_{fm}^{-1} \langle \boldsymbol{n}_{fs} \cdot \left(\boldsymbol{I} \widetilde{p}_f^0 - \mu_f \nabla \widetilde{\boldsymbol{u}}_f^0 \right) \delta_{fs} \rangle_m \cdot \langle \widetilde{\boldsymbol{u}}^0 \rangle^f \,,
$$

for which the only possible solution consists of $\widetilde{\boldsymbol{u}}^0 = 0$ under the constraints of (5.64). Moreover, as $\widetilde{\boldsymbol{u}}^0 = 0$ via the former derivation, we retrieve from closure problem II:

$$0 = -\nabla^\nu \widetilde{p}^0 + \epsilon_{fm}^{-1} \langle \boldsymbol{n}_{fs} \cdot \boldsymbol{I} \widetilde{p}_f^0 \delta_{fs} \rangle_m \,. \tag{I.9}$$

Therefore, if $\langle \boldsymbol{n}_{fs} \cdot \boldsymbol{I} \widetilde{p}_f^0 \delta_{fs} \rangle_m$ is constant by periodicity of $\widetilde{p}^0$, $\widetilde{p}^0$ must satisfy

$$\widetilde{p}^0 = \begin{cases} \widetilde{p}_f^0 = \boldsymbol{\alpha} \cdot \boldsymbol{x} + \text{constant} & \text{in } \Omega_f \cap \Omega_{\text{unit}} \\ 0 & \text{in } \Omega_s \cap \Omega_{\text{unit}} \end{cases} , \tag{I.10}$$

where the constant vector $\boldsymbol{\alpha} = 0$, because $\widetilde{p}^0$ is periodic.

Finally, we note that substitution of (5.56) and (5.57) into the definition of the closure terms (3.22) proves the representation of the closure terms used in (5.53) and (5.54) under the constraint $\boldsymbol{G}_m^{\prime(n)} = 0$.

APPENDIX

J

SIMILARITY TRANSFORMATION OF TEMPERATURE EQUATION

This appendix shows the derivation of the rescaled temperature equation (6.4).

Similarity Transformation of Temperature Equation

Starting from the definition of the rescaled temperature θ, equation (6.1), one finds easily through application of the chain rule for differentiation:

$$\frac{\partial \theta}{\partial t} = \frac{\partial T}{\partial t}\left(T_{ref} - T_s\right)^{-1} - \left(T - T_s\right)\left(T_{ref} - T_s\right)^{-2}\frac{\partial T_{ref}}{\partial t} \tag{J.1}$$

$$= \frac{\partial T}{\partial t}\left(T_{ref} - T_s\right)^{-1} - \theta\left(T_{ref} - T_s\right)^{-1}\frac{\partial T_{ref}}{\partial t}\,. \tag{J.2}$$

In the same way, using the definition of $\boldsymbol{\lambda}_T$, equation (6.6), one finds for the advective derivative of the rescaled temperature:

$$\boldsymbol{u}\cdot\nabla\theta = \boldsymbol{u}\cdot\nabla T\left(T_{ref} - T_s\right)^{-1} - \left(T - T_s\right)\left(T_{ref} - T_s\right)^{-2}\boldsymbol{u}\cdot\nabla T_{ref} \tag{J.3}$$

$$= \boldsymbol{u}\cdot\nabla T\left(T_{ref} - T_s\right)^{-1} - \theta\boldsymbol{u}\cdot\boldsymbol{\lambda}_T\,. \tag{J.4}$$

The heat conduction term is given by

$$\begin{aligned}\nabla \cdot (k\nabla\theta) &= \nabla \cdot (k\nabla T)\,(T_{ref} - T_s)^{-1} - (k\nabla T) \cdot (T_{ref} - T_s)^{-2}\,\nabla T_{ref} \\ &\quad - \nabla \cdot \Big(k\,(T - T_s)\,(T_{ref} - T_s)^{-2}\,\nabla T_{ref}\Big) \qquad \text{(J.5)} \\ &= \nabla \cdot (k\nabla T)\,(T_{ref} - T_s)^{-1} - (k\nabla T)\,(T_{ref} - T_s)^{-1} \cdot \boldsymbol{\lambda}_T \\ &\quad - \nabla \cdot (k\boldsymbol{\lambda}_T\theta) \qquad \text{(J.6)} \\ &= \nabla \cdot (k\nabla T)\,(T_{ref} - T_s)^{-1} - k\nabla\theta \cdot \boldsymbol{\lambda}_T - k\theta\boldsymbol{\lambda}_T \cdot \boldsymbol{\lambda}_T \\ &\quad - \nabla \cdot (k\boldsymbol{\lambda}_T\theta) \qquad \text{(J.7)} \\ &= \nabla \cdot (k\nabla T)\,(T_{ref} - T_s)^{-1} - 2k\nabla\theta \cdot \boldsymbol{\lambda}_T - k\theta\boldsymbol{\lambda}_T \cdot \boldsymbol{\lambda}_T \\ &\quad - \theta\nabla \cdot (k\boldsymbol{\lambda}_T)\ , \qquad \text{(J.8)}\end{aligned}$$

where we made use of the following relationship

$$\nabla T\,(T_{ref} - T_s)^{-1} = \nabla\theta + \theta\boldsymbol{\lambda}_T\,. \qquad \text{(J.9)}$$

APPENDIX

K

DERIVATION OF THE NORMALIZATION FACTOR FOR THE MATCHED WEIGHTING FUNCTION

In this appendix, the normalization factor β (cf. (6.34)) for the matched weighting function m_λ is derived.

Normalization Condition

The normalization condition for the matched weighting function of (6.33) is

$$\int_{\boldsymbol{r}\in\Omega_{\mathrm{unit}}(\boldsymbol{x})} m_\lambda(\boldsymbol{x}-\boldsymbol{r})\, d\Omega(\boldsymbol{r}) = 1\,. \tag{K.1}$$

The integration domain of the former integral contains all points within the unit cell domain (cf. (5.2)), which are located by the integration variable

$$\boldsymbol{r} = \boldsymbol{x} + \sum_{j=1}^{\mathrm{n}_j} c_j \boldsymbol{l}^{(j)} \qquad \text{where } c_j \in \left[-\tfrac{1}{2}, \tfrac{1}{2}\right]. \tag{K.2}$$

Hence, the integration domain can also be parametrized with respect to the variables c_j:

$$d\Omega(c_j) = \begin{cases} \left| \left(\frac{\partial \boldsymbol{r}}{\partial c_1} \times \frac{\partial \boldsymbol{r}}{\partial c_2} \right) \right| dc_1\, dc_2 & \text{if } d = 2 \\ \left\| \frac{\partial \boldsymbol{r}}{\partial c_1} \cdot \left(\frac{\partial \boldsymbol{r}}{\partial c_2} \times \frac{\partial \boldsymbol{r}}{\partial c_3} \right) \right\| dc_1\, dc_2\, dc_3 & \text{if } d = 3 \end{cases} . \tag{K.3}$$

With the aid of equation (5.3), the integration domain is thus given by

$$d\Omega(c_j) = V_{\text{unit}} \prod_{j=1}^{\mathrm{n}_j} dc_j \, . \tag{K.4}$$

The normalization condition (K.1) therefore requires that

$$\beta^{-1} = V_{\text{unit}} \prod_{j=1}^{\mathrm{n}_j} \int_{-1/2}^{1/2} \exp\left[- \left(\boldsymbol{\lambda}_T \cdot \boldsymbol{l}^{(j)} \right) c_j \right] dc_j \, . \tag{K.5}$$

The result of this integral is given by (6.34). When the decay rate vector $\boldsymbol{\lambda}_T$ is orthogonal with respect to one of the lattice vectors, their scalar product is zero, $\boldsymbol{\lambda}_T \cdot \boldsymbol{l}^{(k)} = 0$. In that case, the appropriate value of the normalization factor is given by the limit

$$\lim_{\boldsymbol{\lambda}_T \cdot \boldsymbol{l}^{(k)} \to 0} \beta = \frac{1}{V_{\text{unit}}} \prod_{\substack{j=1 \\ j \neq k}}^{\mathrm{n}_j} \frac{\boldsymbol{\lambda}_T \cdot \boldsymbol{l}^{(j)}}{2 \sinh\left(\frac{\boldsymbol{\lambda}_T \cdot \boldsymbol{l}^{(j)}}{2} \right)} \, . \tag{K.6}$$

APPENDIX

L

SEPARABLE FORM OF THE MATCHED WEIGHTING FUNCTION

In this appendix, the separable form of the weighting function m_λ (6.36) is derived.

Separable Form of The Matched Weighting Function
The derivation starts with the expression for the following one-dimensional convolution product in $\mathbb{R}$:

$$
\begin{aligned}
\left(\mathrm{e}^{ax}\,\mathrm{rect}\,(x)\right) * \mathrm{rect}\,(x) &= \int_{\mathbb{R}} \mathrm{rect}\,(x-r)\left(\mathrm{e}^{ar}\,\mathrm{rect}\,(r)\right)\,dr \\
&= \begin{cases} \frac{\mathrm{e}^{-\frac{1}{2}a}}{a}\left(\mathrm{e}^{a}-\mathrm{e}^{ax}\right) & \text{if } 0 < x < 1\,, \\ \frac{\mathrm{e}^{-\frac{1}{2}a}}{a}\left(\mathrm{e}^{a}-\mathrm{e}^{-ax}\right)\mathrm{e}^{ax} & \text{if } -1 < x \leq 0 \end{cases} \\
&= \frac{\mathrm{e}^{-\frac{1}{2}a}}{a}\left(\mathrm{e}^{a}-\mathrm{e}^{a|x|}\right)\mathrm{e}^{\frac{1}{2}ax(1-\operatorname{sgn}x)} \quad -1 < x < 1 \quad \cdot
\end{aligned}
\tag{L.1}
$$

We emphasize that in (L.1), the convolution product $*$ corresponds to a shifted integration over $x \in (-\infty, +\infty)$.

The next step consists of decomposing the position vector $\boldsymbol{y}$ within the averaging domain with respect to the basis of lattice vectors in the unit cell:

$$\boldsymbol{y} = \sum_{j=1}^{\mathrm{n}_j} c_j \boldsymbol{l}^{(j)} \qquad \text{where } c_j \in \left[-\tfrac{1}{2}, \tfrac{1}{2}\right]. \tag{L.2}$$

A similar decomposition of the rescaled temperature gradient $\boldsymbol{\lambda}_T$ gives

$$\boldsymbol{\lambda}_T \triangleq \sum_{j=1}^{\mathrm{n}_j} \frac{\lambda_j}{\|\boldsymbol{l}^{(j)}\|^2} \boldsymbol{l}^{(j)}. \tag{L.3}$$

With the latter decompositions, the weighting functions m_V and m_λ can be written as

$$m_V(c_j) = \prod_{j=1}^{\mathrm{n}_j} \sqrt[\mathrm{n}_j]{\frac{1}{V_{\mathrm{unit}}}}\, \mathrm{rect}(c_j) \tag{L.4}$$

and

$$m_\lambda(c_j) = \prod_{j=1}^{\mathrm{n}_j} \sqrt[\mathrm{n}_j]{\frac{1}{V_{\mathrm{unit}}}}\, \mathrm{e}^{\lambda_j c_j}\, \mathrm{rect}(c_j) \tag{L.5}$$

respectively.

With (L.4) and (L.5), the convolution product $m_V * m_\lambda$ can thus be written as

$$m_V * m_\lambda = V_{\mathrm{unit}} \prod_{j=1}^{\mathrm{n}_j} \left[\sqrt[\mathrm{n}_j]{\frac{1}{V_{\mathrm{unit}}}}\, \mathrm{rect}(c_j) \right] * \left[\sqrt[\mathrm{n}_j]{\frac{1}{V_{\mathrm{unit}}}}\, \mathrm{e}^{\lambda_j c_j}\, \mathrm{rect}(c_j) \right], \tag{L.6}$$

where the first convolution product $*$ corresponds to a shifted integration over $\boldsymbol{y} \in \mathbb{R}^d$ and the second over $c_j \in (-\infty, +\infty)$. The leading factor V_{unit} in (L.6) arises due to the transformation of the integration domain with respect to the coordinates c_j of the position vector $\boldsymbol{y}$:

$$d\Omega(c_j) = V_{\mathrm{unit}} \prod_{j=1}^{\mathrm{n}_j} dc_j, \tag{L.7}$$

as shown in (K.4).

The derivation ends by applying (L.1) to (L.6) to retrieve (6.36).

APPENDIX

M

SEPARABLE FORM OF THE RESCALED TEMPERATURE

In this appendix, the separable form of the rescaled temperature θ in (6.70) is proven.

The proof starts with the substitution of the separable form for θ of (6.70) in the rescaled temperature (6.4), which yields

$$\begin{aligned}\rho_f \frac{\partial^\nu \left(c\langle\theta\rangle_3\right)}{\partial t}\zeta_\theta + \rho_f \nabla^\nu_{1,2}\cdot\left(\boldsymbol{u}_{1,2}c\langle\theta\rangle_3\right)\zeta_\theta + \rho_f\nabla^\nu_3\cdot\left(\boldsymbol{u}_3 c\zeta_\theta\right)\langle\theta\rangle_3 = \\ \nabla^\nu_{1,2}\cdot\left(k\nabla^\nu_{1,2}\langle\theta\rangle_3\right)\zeta_\theta + \nabla^\nu_3\cdot\left(k\nabla^\nu_3\zeta_\theta\right)\langle\theta\rangle_3 + 2k\boldsymbol{\lambda}_T\cdot\nabla^\nu_{1,2}\langle\theta\rangle_3\zeta_\theta \\ -\rho c\boldsymbol{\lambda}_T\cdot\boldsymbol{u}_{1,2}c\langle\theta\rangle_3\zeta_\theta + k\langle\theta\rangle_3\zeta_\theta\lambda_T^2\,. \qquad \text{(M.1)}\end{aligned}$$

The result (M.1) holds under the assumption that $\boldsymbol{\lambda}_T\cdot\boldsymbol{e}^{(3)} = 0$. We have derived it via the orthogonal decompositions (D.24) and (D.25).

When the separable form (3.62) for the velocity is substituted in the last

equation (M.1) and we apply time-averaging, we obtain

$$\rho_f \nabla^\nu_{1,2} \cdot \left(\overline{\boldsymbol{v} c \langle\theta\rangle_3} \right) \zeta_\theta \zeta_{\boldsymbol{u}} = \nabla^\nu_{1,2} \cdot \left(k \nabla^\nu_{1,2} \overline{\langle\theta\rangle_3} \right) \zeta_\theta + \nabla^\nu_3 \cdot \left(k \nabla^\nu_3 \zeta_\theta \right) \overline{\langle\theta\rangle_3} + 2k \boldsymbol{\lambda}_T \cdot \nabla^\nu_{1,2} \overline{\langle\theta\rangle_3} - \rho c \boldsymbol{\lambda}_T \cdot \overline{\boldsymbol{v} c \langle\theta\rangle_3} \zeta_\theta \zeta_{\boldsymbol{u}} + k \overline{\langle\theta\rangle_3} \zeta_\theta \lambda_T^2 \,. \tag{M.2}$$

If we now assume that $\nabla^\nu_{1,2} \cdot \left(k \nabla^\nu_{1,2} T \right) = 0$, we find thus that

$$\rho_f \nabla^\nu_{1,2} \cdot \left(\overline{\boldsymbol{v} c \langle\theta\rangle_3} \right) \zeta_\theta \zeta_{\boldsymbol{u}} + \rho c \boldsymbol{\lambda}_T \cdot \overline{\boldsymbol{v} c \langle\theta\rangle_3} \zeta_\theta \zeta_{\boldsymbol{u}} = \nabla^\nu_3 \cdot \left(k \nabla^\nu_3 \zeta_\theta \right) \overline{\langle\theta\rangle_3} \,. \tag{M.3}$$

Because the terms $\nabla^\nu_3 \cdot (k \nabla^\nu_3 \zeta_\theta)$, ζ_θ and $\zeta_{\boldsymbol{u}}$ depend solely on x_3, while all other terms of (M.3) depend solely on $\boldsymbol{x}_{1,2}$, we must have

$$\frac{\nabla^\nu_3 \cdot (k \nabla^\nu_3 \zeta_\theta)}{\zeta_\theta \zeta_{\boldsymbol{u}}} = \text{constant} \,, \tag{M.4}$$

or

$$\frac{d^2 \zeta_\theta}{dx_3^2} + \lambda_\theta \zeta_{\boldsymbol{u}}(x_3) \zeta_\theta(x_3) = 0 \,, \tag{M.5}$$

where λ_θ is a constant.

When $\zeta_{\boldsymbol{u}} = 1$ and $\nabla^\nu_{1,2} \cdot \left(k \nabla^\nu_{1,2} T \right) \neq 0$ in (M.2), the same reasoning can be repeated to find that

$$\frac{d^2 \zeta_\theta}{dx_3^2} + \lambda_\theta \zeta_\theta(x_3) = 0 \,. \tag{M.6}$$

CURRICULUM VITAE

Geert Jacques Maria Buckinx
Born April 14, 1988 in Tongeren (Belgium)

Education

2011–now	Doctoral Programme in Engineering KU Leuven Supervisor: *Prof. dr. ir. Martine Baelmans*
2009–2011	Master of Engineering: Energy KU Leuven Graduated Magna Cum Laude Thesis: *Analysis and Optimization of High-Performance Cross-Flow Micro Heat Exchangers*
2006–2009	Bachelor of Mechanical Engineering (option Electrical Engineering) KU Leuven Graduated Cum Laude

2000–2006 Secondary school
ASO Latin - Mathematics
Heilig Grafinstituut Bilzen

Professional Experience

2011–now Research assistant
Department of Mechanical Engineering
KU Leuven

2009 Iaeste Internship
Company: *Turbomotores Ecuatorianos*
Quito, Ecuador

Research Projects

2011–2012 IWT SBO Project 60830
High Performance Micro-Cooling for Electronic Components (Hypercool-IT)

Grants

2012–now Doctoral Grant Strategic Basic Research (121079)
Institute for the Promotion of Innovation through Science and Technology in Flanders (IWT Vlaanderen)

LIST OF PUBLICATIONS

Articles in International Journals

1. G. Buckinx and M. Baelmans, "Macro-scale conjugate heat transfer in periodically developed flow through solid structures," *Journal of Fluid Mechanics*, vol. 804, pp. 298–322, 2016

2. G. Buckinx and M. Baelmans, "Macro-scale heat transfer in periodically developed flow through isothermal solids," *Journal of Fluid Mechanics*, vol. 780, pp. 274–298, 2015

3. G. Buckinx and M. Baelmans, "Multi-scale modelling of flow in periodic solid structures through spatial averaging," *Journal of Computation Physics*, vol. 291, pp. 34–51, 2015

4. G. Buckinx, F. Rogiers, and M. Baelmans, "Thermal design and optimization of small-scale high effectiveness cross-flow heat exchangers," *International Journal of Heat and Mass Transfer*, vol. 60, pp. 210 – 220, 2013

Articles in International Conference Proceedings

1. G. Buckinx and M. Baelmans, "Macro-scale modelling of heat sinks with highly conductive periodically arranged fins," in *Massarotti, N. (Ed.), Nithiarasu, P. (Ed.), Joshi, Y. (Ed.), Fourth International Conference on Computational Methods for Thermal Problems. Georgia Tech, Atlanta, USA, 6-8 July 2016.*, no. 1234, (Kyoto), August 2016

2. G. Buckinx and M. Baelmans, "Towards a general spatial averaging procedure for multi-scale modeling in heat transfer devices with repetitive fin structures," in *Proceedings of the 15th International Heat Transfer Conference, IHTC-15*, no. 1234, (Kyoto), August 2014

FACULTY OF ENGINEERING SCIENCE
DEPARTMENT OF MECHANICAL ENGINEERING
THERMAL AND FLUIDS ENGINEERING:
Celestijnenlaan 300A box 2421
B-3001 Leuven